

SYSTEM HYDRODYNAMICS TO REDUCE FOULING OF AIR-SPARGED IMMERSED FLAT-SHEET MICROFILTRATION MEMBRANES

by

Martin Louis Hamann

*Thesis submitted in partial fulfilment
of the requirements for the Degree*

of

MASTER OF SCIENCE IN ENGINEERING
(CHEMICAL ENGINEERING)

in the Department of Process Engineering
at the University of Stellenbosch



Supervised by

Prof Steven Bradshaw
Prof Ed Jacobs

STELLENBOSCH

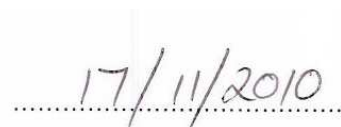
DECEMBER 2010

Declaration

I, the undersigned, hereby declare that the work contained in this thesis is my own original work and that I have not previously in its entirety or in part submitted it at any university for a degree.

A handwritten signature in black ink, appearing to read 'M. M. M.', written over a horizontal dotted line.

Signature

A handwritten date '17/11/2010' in black ink, written over a horizontal dotted line.

Date

Abstract

Immersed membrane systems hold many operational and environmental advantages in biological treatment of wastewater. However, immersed membrane filtration have only found application in niche markets to date because of higher capital and operating costs associated with membrane fouling. But with capital costs on the decline as membranes become less expensive, immersed membrane systems are increasingly considered as an attractive alternative to conventional treatment processes. Operating costs remain high however, since energy intensive techniques such as air-sparging are required to limit membrane fouling. Improving the air-scouring efficiency of air-sparged immersed membranes can significantly reduce operating costs and unlock the immersed membrane system technology to wider application.

The aim of this study was to identify factors that will improve air-scouring efficiency in order to produce guidelines that will help in the development of an immersed microfiltration membrane system with a resulting lower operating cost. Although, the research was done on a flat-sheet microfiltration membrane, the guidelines obtained can be used for the development of any immersed microfiltration membrane arrangement.

An airlift reactor set-up was chosen for this study. Six system hydrodynamic factors were evaluated in a factorial design to determine their effects on the cross-flow velocity profile. They were the downcomer area to riser area ratio, top clearance distance, bottom clearance distance, aeration intensity, water depth and air sparger location. It was found that the air-scouring efficiency was increased by generating a cross-flow velocity profile with increased magnitude and uniformity, but absolute uniformity of the cross-flow velocity profile was found to be a prerequisite for optimisation of air-scouring efficiency. Downcomer area to riser area ratio was found to be 99.9% significant in determining the magnitude of the cross-flow velocity profile.

Two models were developed to respectively predict the relative magnitude and uniformity of the cross-flow velocity profile. By using these two models, a methodology was developed to design an airlift reactor set-up that would produce system hydrodynamics with an improved air-scouring efficiency.

Opsomming

Gesonke membraanstelsels beskik oor talle bedryfs- en omgewingsvoordele in biologiese behandeling van afvalwater. Maar weens die hoër kapitaal- en bedryfskoste wat gepaardgaan met membraanbevuiling, kon gesonke membraanstelsels tot op hede nog net toepassing in nismarkte vind. Maar soos kapitaalkoste daal met al hoe goedkoper membrane beskikbaar, word gesonke membraanstelsels al hoe aanlokliker as 'n alternatief vir konvensionele behandelingsprosesse. Bedryfskoste bly egter hoog aangesien energie-intensiewe tegnieke soos lugborreling benodig word om membraanbevuiling te vertraag. Deur die effektiwiteit van die skropaksie wat lugborreling aan gesonke membrane bied te verbeter, kan 'n beduidende besparing in bedryfskoste teweeggebring word om sodoende die uitgebreide toepassing van gesonke membraanstelsel tegnologie moontlik te maak.

Hierdie studie het ten doel gehad die identifisering van faktore wat lugskropaksie effektiwiteit kan verbeter en om riglyne op te stel vir die ontwikkeling van 'n gesonke mikrofiltrasie membraanstelsel met gevolglik laer bedryfskoste. Alhoewel hierdie navorsing 'n plat-blad mikrofiltrasie membraan gebruik het, kan die riglyne steeds vir enige gesonke mikrofiltrasie membraanuitleg gebruik word.

Daar is besluit op 'n lugligter-reaktor opstelling vir hierdie studie. Ses stelselhidrodinamika faktore is geëvalueer in 'n faktoriale ontwerp om hul effekte op die kruisvloeiselheidsprofiel te bepaal. Hulle was die afvloe-area tot opvloe-area verhouding, topruimte-afstand, bodemuimte-afstand, belugtingsintensiteit, waterdiepte en belugterligging. Daar is bevind dat die lugskropaksie effektiwiteit verhoog word wanneer 'n kruisvloeiselheidsprofiel geskep word met 'n verhoogde grootte en gelykvormigheid, maar die absolute gelykvormigheid van die kruisvloeiselheidsprofiel is gevind om 'n voorvereiste te wees vir optimale effektiwiteit. Afvloe-area tot opvloe-area verhouding is gevind om 99.9% beduidend te wees in die bepaling van die selheidsprofiel se grootte.

Twee modelle is ontwikkel om afsonderlik die relatiewe grootte en gelykvormigheid van die kruisvloeiselheidsprofiel te voorspel. Die modelle is in 'n metodologie vervat vir die ontwerp van 'n lugligter opstelling met stelselhidrodinamika wat verbeterde lugskropaksie effektiwiteit sal skep.

Acknowledgements

I thank the Lord for the insight and strength He gave me to finish this study when completion seemed impossible. I also wish to express my sincere gratitude and appreciation to the following people for their contributions towards the successful completion of this study:

- My supervisor, Ed Jacobs, for the opportunity to be part of the MBR research programme. Without his guidance and motivation this thesis would never have seen the light of day.
 - My supervisor, Steven Bradshaw, for his continued belief in me and his willingness to help.
 - Minnaar Pienaar, for enrolling me yet one more time.
 - Deon Koen (University of Stellenbosch, Department of Chemistry and Polymer Science), for his assistance and advice in the workshop and laboratory.
 - Helen Divey (University of Cape Town, Department of Chemical Engineering), for measuring the bentonite particle size distribution.
 - Jianxin Li (University of Stellenbosch, Department of Chemistry and Polymer Science), for lending me his ultrasonic equipment and helping me with the UTDR data interpretation.
 - Joos van der Merwe (University of Stellenbosch, Department of Geology), for helping me develop a suitable bentonite suspension preparation method.
 - All my Sasol colleagues for their interest and continued encouragement, especially to Ronél Augustyn, Michael van Niekerk, Doep Du Plessis, Estelle Marais and Deon Nieuwenhuis.
 - Alan Anderson, my spiritual brother. Thank you for all the support. I regret not attending your wedding because of this thesis.
 - My parents for their countless sacrifices.
 - My wife, Jolene, for her unconditional love and support through all these years and to my daughter, Annika, for lighting up my day with a single smile.
-

Table of contents

DECLARATION	I
ABSTRACT	II
OPSOMMING	III
ACKNOWLEDGEMENTS	IV
TABLE OF CONTENTS	V
LIST OF FIGURES	VIII
LIST OF TABLES	XI
LIST OF ABBREVIATIONS	XII
INTRODUCTION	1
1.1 Background.....	1
1.2 Aim of study.....	4
1.3 Layout of thesis.....	5
MEMBRANE FOULING BACKGROUND	6
2.1 Introduction	6
2.2 Mass transport	7
2.2.1 Concentration polarisation.....	8
2.2.2 Back-transport	9
Brownian diffusion.....	10
Shear-induced diffusion	11
Inertial lift.....	12
Surface transport.....	13
2.3 Membrane fouling mechanisms.....	14
2.3.1 Physico-chemical fouling mechanisms	14
2.3.2 Biofouling mechanisms	16

2.3.3	Membrane fouling modelling	17
2.4	Membrane fouling amelioration	22
2.4.1	Feed pretreatment	22
2.4.2	Membrane material selection	23
2.4.3	Back-transport promotion	23
	Surface hydrodynamics	23
	Permeate flux destabilisation	23
	Sub-critical flux operation	24
AIR-SCOURING OF IMMersed MEMBRANES		27
3.1	Introduction	27
3.2	Scouring action of rising bubbles	28
3.3	Airlift reactors	30
3.3.1	Liquid velocity	31
3.3.2	Airlift reactor application for immersed membrane fouling control	32
FOULING QUANTIFICATION FOR AIR-SCOURING EVALUATION		33
4.1	Introduction	33
4.2	Fouling quantification methods	35
4.3	Flux-step method for indirect fouling quantification	37
4.3.1	Background	37
4.3.2	Experimental set-up	40
4.3.3	Method	42
4.3.4	Results	44
4.4	Ultrasound for direct fouling quantification	49
4.4.1	Background	49
4.4.2	Experimental set-up	55
	Ultrasonic measurement system	55
	A_d/A_r ratios	60
	Constant aeration intensity	60
	Constant permeate flux	61
4.4.3	Method	61
4.4.4	Results	62
	Reflected waveforms	62
	Membrane fouling	66
SYSTEM HYDRODYNAMIC EFFECTS OF AIRLIFT REACTOR FACTORS		68
5.1	Introduction	68
5.2	Design of experiments	71
5.2.1	Full factorial designs	73
5.2.2	Screening designs	73
5.3	Screening of system hydrodynamic factors	75
5.3.1	Experimental set-up	75
5.3.2	Method	77
	Linear liquid velocity measurement	77
	Response calculation	78

Design of experiment	80
Effects calculation	84
Significance of effects	85
5.3.3 Results.....	86
Area under the velocity profile	86
Average gradient of the velocity profile.....	86
5.4 Validation of system hydrodynamic factors	88
5.4.1 Experimental set-up	88
5.4.2 Method.....	88
5.4.3 Results.....	90
CONCLUSIONS	92
6.1 Introduction	92
6.2 Air-scouring efficiency.....	93
6.3 System hydrodynamic factors	94
REFERENCES	95
MODEL FOULANT PREPARATION.....	110
A.1 Introduction	110
A.2 Model foulant selection	111
A.3 Suspension preparation.....	113
A.4 Turbidity calibration.....	114
MEMBRANE ELEMENT CONSTRUCTION.....	115
B.1 Introduction	115
B.2 Membrane material.....	116
B.3 Membrane element production	117
FLUX-STEP EXPERIMENTAL DATA	127
UTDR EXPERIMENTAL DATA.....	133
Determining speed of sound in bentonite cake layer	133
SCREENING DESIGN EXPERIMENTAL DATA.....	134
MODEL VALIDATION EXPERIMENTAL DATA	152

List of figures

Figure 1.1: Equivalent wastewater treatment processes: (a) conventional activated sludge process and (b) MBR process replacing all the conventional process steps in one treatment step.....	3
Figure 1.2: The two MBR process configurations for solids/liquid separation: (a) sidestream operation and (b) immersed operation.	3
Figure 1.3: Thesis flow diagram indicating the logical unfolding of information and results necessary to reach sensible conclusions.	5
Figure 2.1 Mass transport operations for pressure-driven cross-flow membrane filtration.	8
Figure 2.2: Illustration of the particle size dependency of membrane fouling. A minimum back-diffusivity exists with deposition of material at a relative low TMP.	12
Figure 2.3: Physico-chemical fouling mechanisms [Belfort et al., 1993].	15
Figure 2.4: Stages of biofilm growth on a clean membrane.	16
Figure 2.5: Contribution of each hydraulic resistance to the TMP for a hypothetical microfiltration process at constant permeate flux where the feed could be changed from pure water to a particulate suspension.	21
Figure 2.6: Critical flux hypothesis for microfiltration: (a) strong form and (b) weak form. Above the critical flux in both cases TMP continuous to increase at constant permeate flux and displays TMP hysteresis when permeate flux is reduced to below the critical flux.	25
Figure 2.7: Hypothetical TMP profile of incremented constant permeate fluxes from sub-critical to above critical fluxes.	26
Figure 2.8: Hypothetical TMP profiles of constant permeate fluxes when the feed was switched from pure water to a particulate suspension. Above critical flux cake layer formation commences and continues at a constant rate.	26
Figure 3.1: Aeration regimes inside a tube: (a) bubble flow; (b) slug flow; (c) churn flow; (d) annular flow; and (e) mist flow [Judd et al., 2001].	28
Figure 3.2: Slug flow inside an inside-out tubular membrane. A rising air slug scours the membrane surface by first subjecting it to a negative shear stress ($\tau_{L\text{Film}}$) and then by a positive shear stress ($\tau_{L\text{Slug}}$) [Laborie et al., 1998; Cabassud et al., 2001].	29
Figure 3.3: Air-sparging of immersed outside-in flat-sheet membranes.	29
Figure 3.4: Liquid flow patterns: (a) chaotic liquid circulation cells in a bubble column; (b) clearly defined liquid flow in an airlift reactor: upwards in the gassed riser and downwards in the ungassed downcomers [Chisti and Moo-Young, 1987; Choi et al., 1996].	30
Figure 4.1: The typical TMP profile of a flux-step experiment where the permeate flux was incremented five times with an arbitrary chosen permeate flux J from below critical flux to above critical flux at a time increment of t . In this case a permeate flux of $2J$ was still below the critical flux, whereas a permeate flux of $3J$ was above the critical flux with a resulting continued increase in TMP.	38
Figure 4.2: The rates of stabilised TMP increase of each permeate flux increment as derived from the typical TMP profile of a flux-step experiment as shown in Figure 4.1. The critical flux is found where $d\text{TMP}/dt$ changes from zero to a positive value,	

	which in this case, lies between the flux-step experiment's second and third permeate flux increment.	40
Figure 4.3:	Set-up for the flux-step experiment: (a) main equipment and (b) detail of airlift reactor.	41
Figure 4.4:	The presence of a region of stagnant bubbles in the riser section during aeration. This region promotes localised fouling where it crosses the immersed membrane.	45
Figure 4.5:	Membrane fouling rate at different aeration intensities. The intermediate aeration intensity (580 L/(m ² ·min)) produced the highest scouring ability. Between an aeration intensity of 580 and 1 100 L/(m ² ·min) the region of stagnant bubbles develop to cross the immersed membrane and promote localised fouling.....	47
Figure 4.6:	Membrane fouling rate at different permeate fluxes. An increase in the permeate flux will lead to an increase in the fouling rate (dTMP/dt), if above the critical flux. However, at the correct aeration intensity the fouling rate at any permeate flux can be greatly reduced. Under and over aeration may accelerate the fouling rate as is shown in this graph.....	47
Figure 4.7:	Reflection of wave energy at media interfaces. Two cases are shown here: (a) material 2 has a higher acoustic impedance than material 1, but the difference is slight to produce a low energy reflected wave in phase with the incident wave; (b) material 2 has a lower acoustic impedance than material 1 and the difference is significant to produce a high energy reflected wave out of phase with the incident wave.....	51
Figure 4.8:	Hypothetical oscilloscope waveforms to explain UTDR for fouling quantification. (Notice that only one side of the immersed membrane was considered here.).....	54
Figure 4.9:	The experimental set-up for the UTDR experiment for the direct fouling quantification of immersed membrane fouling. Besides the ultrasonic equipment, the equipment set-up is identical to the equipment set-up described in Section 4.3.2 for the flux-step experiment.....	56
Figure 4.10:	A photograph of one of the membrane elements that were used in the ultrasound experiment with its membrane spacer material and the Panametrics Videoscan V120-RB transducer.	57
Figure 4.11:	Section of the side view of the riser section to show the location of the immersed ultrasonic transducer. The transducer was positioned halfway the depth of the membrane element's flat-sheet surface.	59
Figure 4.12(a):	Typical waveform translation of a clean membrane.....	63
Figure 4.12(b):	Typical waveform translation of internal fouling.	64
Figure 4.12(c):	Typical waveform translation of cake layer formation.	65
Figure 4.13:	The arrival time differences at the relative positions after 20 hours of membrane filtration in a 1.0 g/L bentonite suspension.	67
Figure 5.1:	Typical hydrodynamic field patterns that were observed in the riser section of an airlift reactor: (a) fast rising liquid and bubbles in the middle with churning liquid and stagnant bubbles on the sides; (b) uniformly fast rising liquid and bubbles across the riser section; and (c) fast rising liquid and bubbles on the sides with churning liquid and stagnant bubbles in the middle.....	68
Figure 5.2:	The six aspects of airlift reactor design that were investigated to determine their influences on the velocity profile in the riser section.....	70
Figure 5.3:	A basic explanation of DOE for a hypothetical system. (a) Three factors, A, B and C, were identified as possibly having an impact on the response and needed to be investigated. An experimental error is present in the system and contributes to the value of the response. (b) Two levels were chosen for each factor, which are the only values where the factors are maintained during the designed experiment. Note that the levels of factor C are attributes. Each factor's high level is indicated by "+1" and their corresponding low level is indicated by "-1". (c) Factors A and B, as well as their interaction AB, were found to have a significant effect on the response, since they managed to change the response value to	

	outside of its inherent variation. Factor C and all other interactions are insignificant and can be ignored in future optimisation studies.	72
Figure 5.4:	Experimental set-up for the screening of system hydrodynamic factors: (a) PVC tank with one half of the front containing a clear PVC sheet and (b) the baffle plate framework which could be changed to create different airlift reactor configurations when slotted inside the PVC tank.....	76
Figure 5.5:	Velocity profile quantification: (a) hypothetical pathways of PP pieces when entering the riser section in the different subsections and (b) hypothetical plotted average linear liquid velocities calculated for each subsection to compile a velocity profile across the riser section. The magnitude of the velocity profile is indicated by the area under the profile and the uniformity is indicated by the average gradient of the profile.	79
Figure 5.6:	Average membrane fouling rates for the different configurations. Although not shown for the sake of clarity, the variability in the fouling rate increased with an increase in absolute velocity profile gradient and was therefore the highest for configuration 4.	91
Figure A.1:	Particle size distribution of the bentonite used in this study.....	112
Figure A.2:	Regressed calibration curve for bentonite suspensions.	114
Figure B.1:	A photograph of three membrane elements under construction.	117
Figure B.2(a):	Membrane curtain is cut from the membrane material.	118
Figure B.2(b):	Membrane curtain contains the selected number of filter tubes and the inactive tube remains on the sides.....	118
Figure B.2(c):	Stainless steel mesh strips are inserted into the filter tubes to act as spacer material. The membrane curtain is then slotted inside a slit cut into a PVC pipe...	119
Figure B.2(d):	Bottom end of membrane element sealed off.	120
Figure B.2(e):	Construction of the permeate collector.	121
Figure B.2(f):	Sealing of membrane curtain entrance at permeate collector.	121
Figure B.2(g):	The mould set-up around the permeate collector.....	122
Figure B.2(h):	The flow of the injected resin through the injection tube, into the PVC pipe and around the permeate collector.	123
Figure B.2(i):	The set resin around the permeate collector. Note how the silicon rubber plug and the silicon rubber sealing at the membrane curtain entrance keeps the permeate collector empty.....	123
Figure B.2(j):	The finished membrane element product. The resin filled parts of the bottom sealed pipe and the top permeate collector have been sawn off.	124
Figure B.2(k):	Cross-section through the middle of a completed membrane element.....	125
Figure B.3:	Detail measurements of the polyethylene mould blocks: (a) blocks A and B connected to form the total mould; (b) one block A; and (c) both blocks B. Note that drawings are not to scale and that measurements are given in millimetres.	126

List of tables

Table 4.1:	The three chosen aeration intensities for the flux-step experiment. (Notice the relative large deviation in the compressor's air flow rate to achieve the high aeration intensity.)	43
Table 4.2:	The random order in which the trials were conducted to minimise the risk of unknown influences on the results.	43
Table 4.3:	Panametrics Videoscan ultrasonic transducers that were evaluated for the monitoring of fouling layer formation [Koen, 2000b]	57
Table 4.4:	The three airlift reactor geometries and the flat-sheet membrane sizes used in the UTDR experiment.	60
Table 5.1:	Plackett-Burman design for 7 factors (factors A, B, C, D, E, F and G) and 8 treatments. Each factor is completely confounded with three interactions, but is opposite in sign. The "+" and "-" signs in each treatment indicate the required high or low level of the corresponding factor for the specific treatment.	74
Table 5.2:	Values of the levels at which each factor was evaluated.	80
Table 5.3:	The treatments for the experimental design of the base, reflection and full factorial treatments. The "+" and "-" signs indicate the setting of the levels. The order indicates the randomisation of the treatments and their replicates. The shaded treatments indicate treatments that were already covered in the base and reflection treatments.	82
Table 5.4:	The treatments (from the full factorial section of Table 5.3) used in the full factorial designs to determine the effects of the interactions. The "+" and "-" signs indicate the levels of the respective factors in the same order as the name of the interaction. The numbers of the shown treatments refer to numbers 1 to 22 mentioned in the full factorial section of Table 5.3.	83
Table 5.5:	The decision limits for the significance of effects.	85
Table 5.6:	Different airlift reactor configurations chosen to validate their predicted velocity profile areas and gradients as predicted by Equations 5.7 and 5.8. The "+1" and "-1" indicate the respective high and low levels of the specific factor as is explained in Table 5.2. Configuration 1 represents the configuration with the most uniform velocity profile and configuration 2 represents the configuration with the highest velocity profile area.	89
Table 5.7:	The random order in which the treatments were conducted to minimise the risk of unknown influences on the results. The configuration numbers correlate with the configurations listed in Table 5.6.	90

List of abbreviations

A_d/A_r	total downcomer cross-sectional area to riser cross-sectional area ratio
CSV	comma separated value (Microsoft Excel file format)
df	degrees of freedom
DL	decision limits
DOE	design of experiments
EPS	extracellular polymeric substances
MBR	membrane bioreactor
OD	outer diameter
PP	polypropylene
PVC	polyvinyl chloride
TMP	transmembrane pressure
UTDR	ultrasonic time-domain reflectometry

Chapter 1

Introduction

1.1 Background

In biological treatment of wastewater, membranes provide absolute separation of solids and liquids [Günder and Krauth, 1998]. This ability offers membrane systems a superior operating envelope compared to conventional treatment systems that have to rely on clarification for solids/liquid separation. Since the hydraulic retention time is completely decoupled from the sludge retention time in a membrane system, the sludge age can be set to any value by the operator, the system can be operated at very high mixed liquor suspended solids concentrations, slow-growing microorganisms such as nitrifying bacteria can be accommodated and waste sludge production can be reduced [Judd, 2008]. Besides improved operability, membrane systems, by the nature of the exclusivity of their solids/liquid separation, can produce on-specification treated water in a single process step; thereby eliminating conventional downstream treatment steps to reduce plant footprint [Günder and Krauth, 1998; Gander et al., 2000]. The most widely used membrane system for solids/liquid separation in wastewater treatment processes is the membrane bioreactor (MBR) [Stephenson et al., 2000a]. Figure 1.1 illustrates the simplification that an MBR system introduces to a wastewater treatment process to achieve similar, or even better, product results when compared to a conventional activated sludge system.

However, membrane fouling [Meng et al., 2009] still remains the main obstacle for the wider application of MBR technology, since membrane fouling is responsible for considerable capital cost and operating cost components. For the two different MBR configurations, sidestream and immersed [Gander et al., 2000; Van't Oever, 2005; Pearce, 2008] shown in Figure 1.2, there is a trade-off between cost and performance to address membrane fouling. In a sidestream configuration the membranes are external to the bioreactor and the wastewater is pumped across the membranes at high cross-flow velocities to reduce fouling. The cross-flow pumping results in high operating costs, but the membranes can be allowed to operate at high permeate flows. In an immersed configuration the membranes are immersed in the wastewater and only a moderate cross-flow can be induced across the membranes by vigorously aerating the water beneath the membranes. Also, immersed membranes have to revert to much lower permeate flows to reduce

membrane fouling and therefore require larger membrane surfaces to produce the same permeate rate than a sidestream configuration. Gander et al. [2000] have found that the sidestream configuration has a higher total energy cost, up to two orders of magnitude higher, than the total energy cost of operating an immersed configuration.

With a continued decrease in membrane cost over the last two decades [Churchouse and Wildgoose, 1999; Judd, 2008] and with lower energy requirements than sidestream configurations, immersed MBRs have become the most popular MBR configuration for solids/liquids separation in wastewater treatment processes. With environmental regulations becoming increasingly more stringent and demand for additional hydraulic capacity increases on existing conventional activated sludge processes, the opportunity exists to retrofit these wastewater treatment plants with immersed MBRs [Ahn et al., 1999; Tiranuntakul et al., 2005].

Although an immersed MBR usually has a lower operating cost than a sidestream MBR, the major portion of the immersed MBR's operating cost is for coarse bubble aeration to limit fouling of the immersed membranes [Gander et al., 2000; Judd, 2008]. In the view of rising energy prices, it is therefore imperative that immersed MBRs, and especially those for retrofitted systems, are designed and operated as optimally as possible to improve their fouling behaviour and reduce the operating cost of aeration [Verrecht et al., 2008].

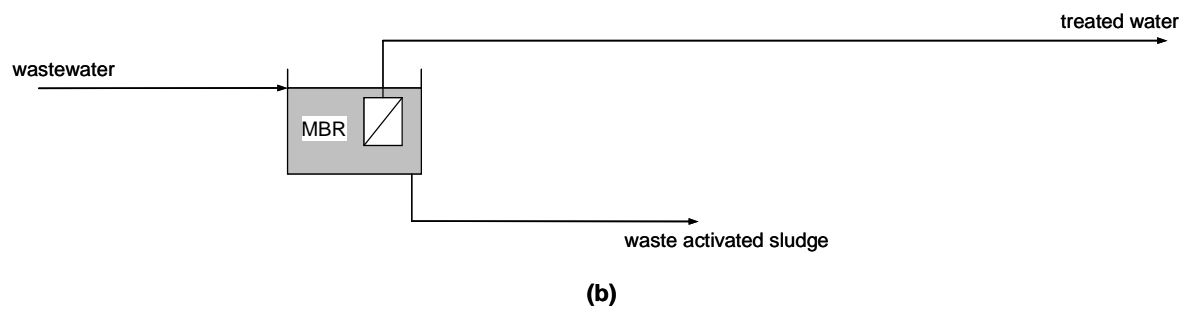
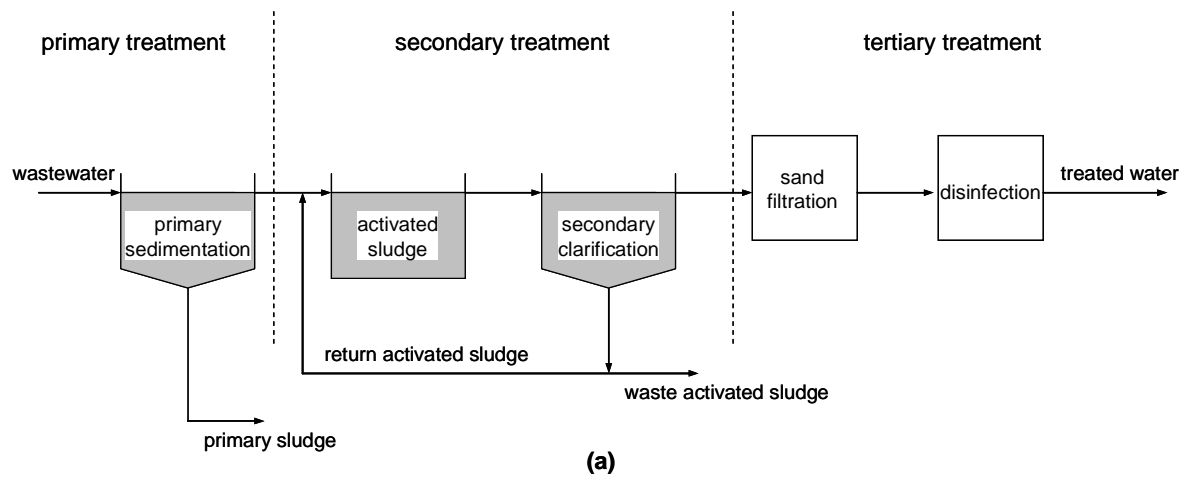


Figure 1.1: Equivalent wastewater treatment processes: (a) conventional activated sludge process and (b) MBR process replacing all the conventional process steps in one treatment step.

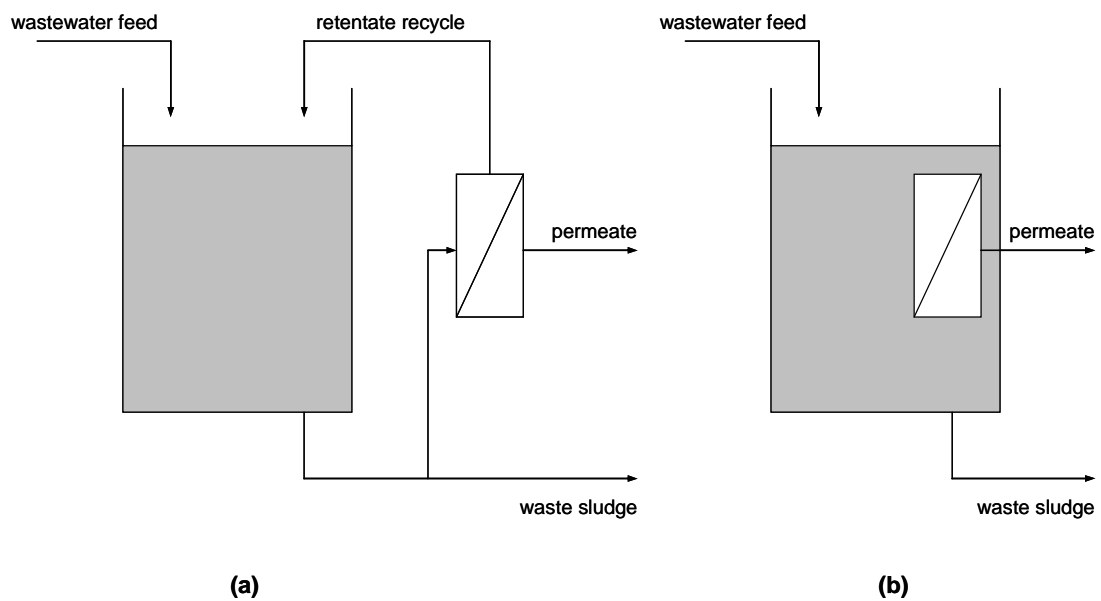


Figure 1.2: The two MBR process configurations for solids/liquid separation: (a) sidestream operation and (b) immersed operation.

1.2 Aim of study

Immersed MBR systems hold very promising opportunities, but their widespread application is still hindered by their high operating and capital costs as a result of membrane fouling. With membrane costs declining, the capital cost of immersed MBR systems will eventually compare better with conventional activated sludge systems. But with increasing energy prices, immersed MBR systems will remain unfavourable because of their air-scouring (or other abatement techniques) requirements, unless this can be improved. There is consequently an incentive to improve on the air-scouring efficiencies of immersed MBR systems.

The aim of this study is to identify factors that will improve air-scouring efficiency of an immersed microfiltration membrane and to suggest the directions for further optimisation. Optimisation of these factors, physical parameters and operating parameters is beyond the scope of this study and should be addressed in future optimisation studies.

1.3 Layout of thesis

This thesis covers many different fields of science and information is therefore required to be unfolded in a logical manner. Results in one chapter are used as inputs in the next chapters. All the results of the previous chapters are discussed in Chapter 6 for a holistic approach.

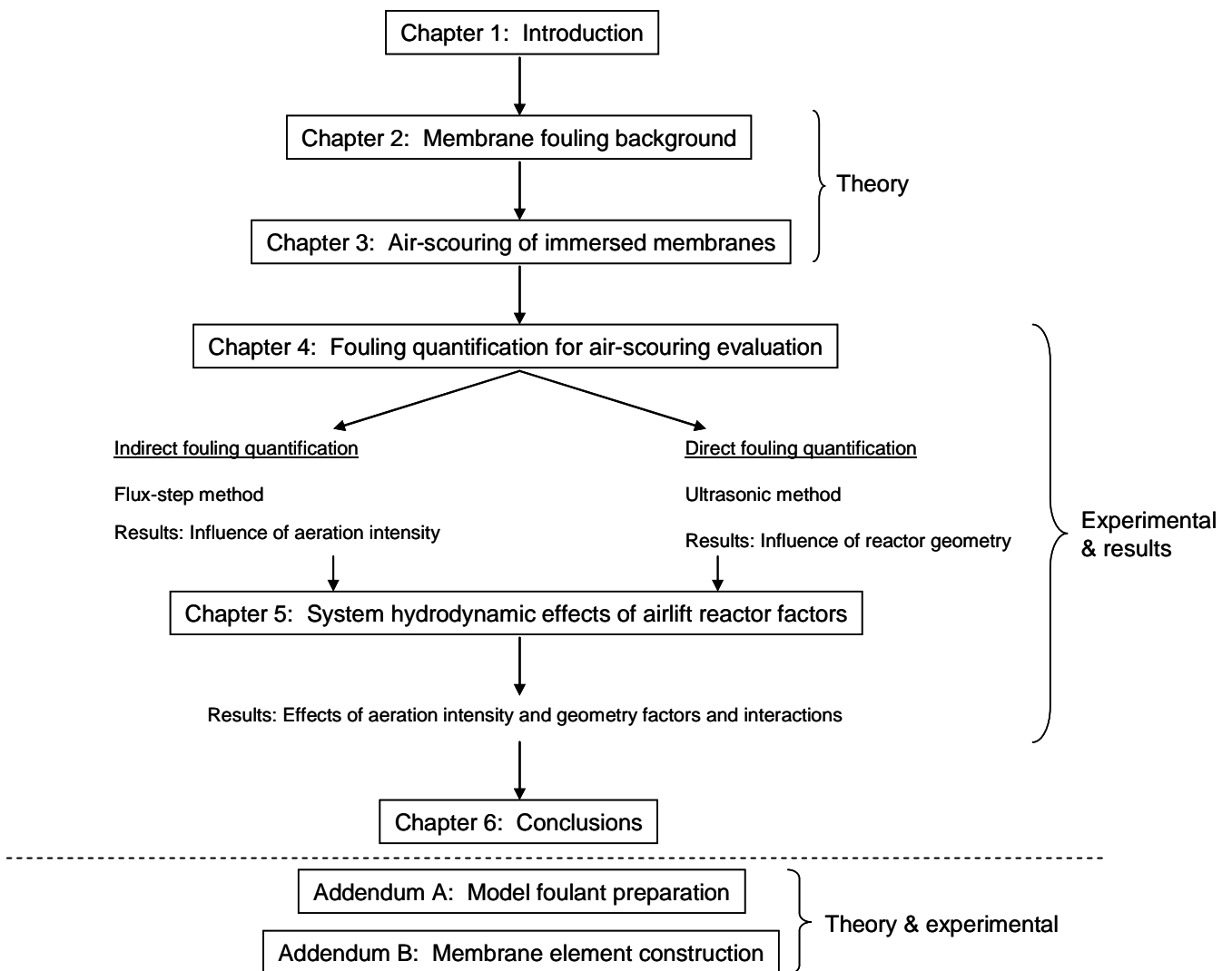


Figure 1.3: Thesis flow diagram indicating the logical unfolding of information and results necessary to reach sensible conclusions.

Chapter 2

Membrane fouling background

2.1 Introduction

Membrane fouling refers to the collective processes responsible for the undesirable accumulation of deposit on the membrane surface and inside the membrane pores to increase the hydraulic resistance to mass transport through the membrane during filtration operations. While the immediate manifestation of membrane fouling is a declining specific permeate flux (unit permeate flux per unit driving force), the long term results may include irreversible fouling and membrane damage to shorten membrane lifetime [Al-Ahmad et al., 2000]. Membrane fouling is the single most important impediment to the widespread large-scale application of membrane filtration for wastewater treatment, since large capital investments and high operating costs are necessitated to reduce fouling or to treat its detrimental consequences in order to maintain an adequate throughput.

Membrane fouling forms a mechanistic part of membrane filtration and can never be completely eliminated. It is therefore important to understand the causes of membrane fouling and the conditions that will suppress it to enable the design and operation of a membrane system with a more favourable fouling behaviour; and therefore with a more viable water treatment production. This chapter will focus on the membrane fouling encountered in microfiltration for wastewater treatment applications.

2.2 Mass transport

During microfiltration the driving force for mass transport through the membrane is an applied pressure differential across the membrane which is known as the transmembrane pressure (TMP) [Belfort et al. (1994)]. The TMP can either be created by applying a vacuum on the permeate side of the membrane or by increasing the pressure on the feed side.

Figure 2.1 illustrates the mass transport operations for pressure-driven cross-flow membrane filtration. The TMP driving force creates a convective fluid flow which follows the pressure gradient from the high pressure at the bulk of the feed stream to the low pressure on the permeate side of the membrane. Any other material present in the fluid is consequently also carried to the membrane where the membrane pore size differentiates the larger material, which is retained on the high pressure side of the membrane, from the smaller material passing through the membrane. Close to the membrane surface the cross-flow may be assumed to be laminar, but because of wall friction the cross-flow velocity is zero at the membrane surface. A velocity boundary layer is therefore created to form a relative stagnant film across the membrane surface in which back-transport is limited to diffusion, a relatively slow mass transport process. With the consequent accumulation of rejected material near the membrane surface a concentration boundary layer develops in the stagnant film with an increased concentration of this material near the membrane surface compared to the lower uniform concentration in the bulk; a phenomenon known as concentration polarisation. Back-transport mechanisms facilitate the removal of retained material from near the membrane surface back to the bulk, but if the convective permeation flux is greater than the back-transport flux, the material is likely to be deposited on the membrane surface. Conversely, with a back-transport flux greater than the permeation flux, the likelihood of material deposition is limited.

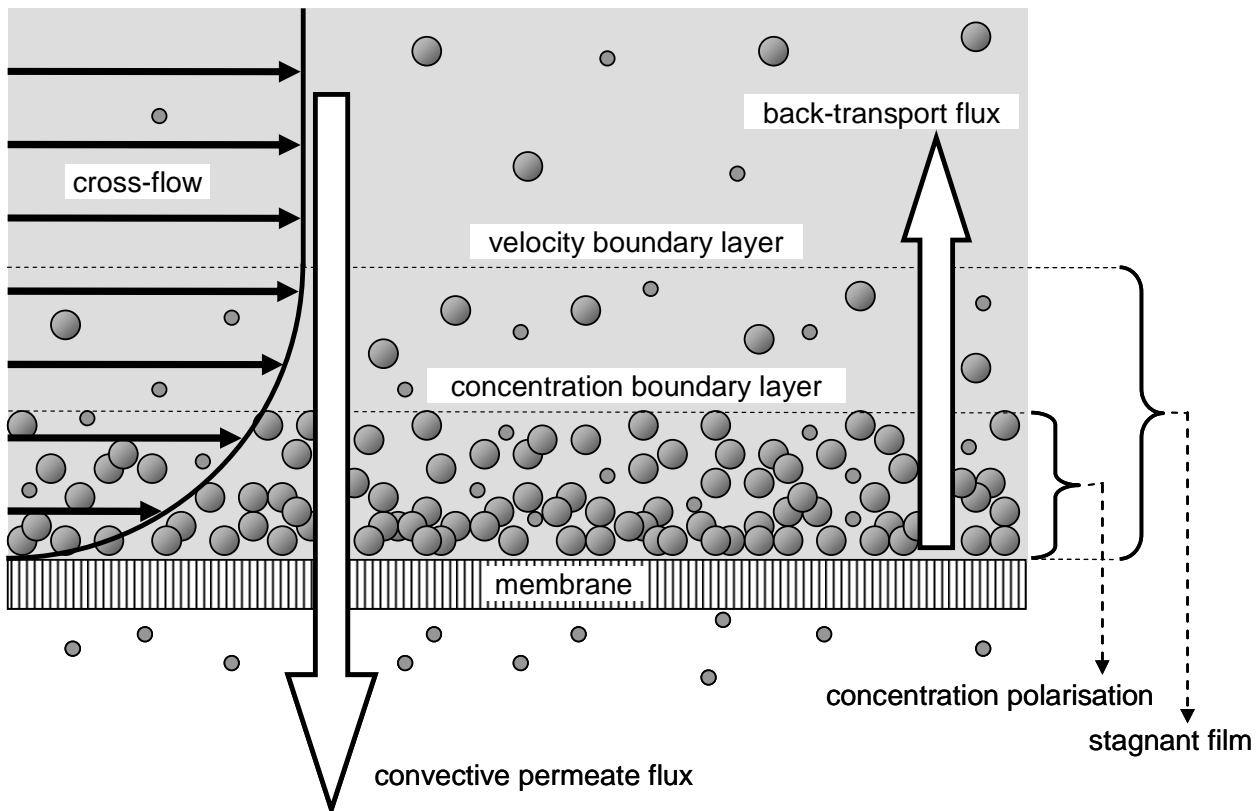


Figure 2.1 Mass transport operations for pressure-driven cross-flow membrane filtration.

Because microfiltration is based on size exclusion at the membrane surface, the accumulation of material near the membrane is an inevitable result of this separation process. Arguably, it can be viewed therefore that concentration polarisation and the relative size of the back-transport flux to the permeation flux determines the extent of membrane fouling.

2.2.1 Concentration polarisation

Concentration polarisation describes the tendency of material to accumulate at the membrane surface and can be ascribed to two phenomena associated with membrane filtration: permselectivity of membranes and the existence of a stagnant film near the membrane surface in cross-flow operations [Matthiasson and Sivik, 1980].

Concentration polarisation itself usually represents a resistance against permeate flux, since the osmotic pressure of the retained material reduces the effective TMP driving force [Belfort et al., 1994]. However, for microfiltration operations the resistance induced by concentration polarisation is negligible, since the retained particles are relatively large with small osmotic pressures [Bai and

Leow, 2002]. But even though it may act as an additional resistance against permeation, it is important to note that concentration polarisation is not a fouling mechanism, since it is a reversible result of membrane separation and will disappear once membrane filtration is stopped. However, concentration polarisation provides the conditions in which fouling can occur.

The transition from concentration polarisation to membrane fouling may be quite different and complex for reverse osmosis, ultrafiltration and microfiltration operations, but in each filtration operation concentration polarisation ultimately leads to an increase in TMP at constant permeate flux operation or decrease in permeate flux at constant TMP operation. For reverse osmosis the presence of a concentration boundary layer at the membrane surface increases the propensity for scaling [Lee and Lueptow, 2003]. In ultrafiltration operations, concentration polarisation promotes the precipitation of slightly soluble solutes and particle-particle interactions to form a gel layer on the membrane [Chen et al., 1997; Bacchin et al., 2002]. The effect of concentration polarisation to promote membrane fouling tends to be severe for microfiltration operations, since the permeate fluxes are usually high, while the diffusive back-transport is slow for particles [Wakeman and Williams; 2002]. Consequently, the close proximity of the retained particles to the membrane surface leads to the formation of a cake layer.

Since material retention will always occur in microfiltration operations, concentration polarisation can never be completely removed. The extent of concentration polarisation should therefore be kept to a minimum to limit membrane fouling by operating at low permeate fluxes to reduce the driving force and improving turbulence on the feed side of the membrane to enhance back-transport.

2.2.2 Back-transport

Particle back-transport mechanisms can be divided into two classes: diffusive and convective hydrodynamic shear forces [Silva et al., 2000]. Most of the proposed models in the literature for back-transport are primarily based on diffusion mechanisms, but in microfiltration and ultrafiltration systems with hydrodynamic shear forces at the membrane surface the back-transport of particles are predominantly caused by these convective forces and the effect of diffusion may be neglected [Shulz et al., 1989; Sayed Razavi et al., 1996]. The proposed models for diffusive back-transport include Brownian diffusion and shear-induced diffusion, whereas convective hydrodynamic back-transport mechanisms may be explained by inertial lift and surface transport [Belfort et al., 1994; Tardieu et al., 1998].

Brownian diffusion

Consider the cross-flow membrane filtration of a fluid containing only true solutes. Initially the rate at which solute species are introduced to the stagnant film is determined by the convective permeation flux and the degree of solute retention of the membrane. Diffusion is the only mechanism for back-transport in the stagnant film and the back-diffusion of solute to the bulk will increase with the increase of solute in the stagnant film. At steady-state operation the build-up of solute in the stagnant film is counteracted by a Brownian diffusive flux of solute away from the membrane.

When assuming a 100% retention of solute by the membrane and a constant stagnant film thickness, Brownian back-diffusion for steady-state membrane filtration can be defined by the film model as [Stephenson et al., 2000b]:

$$J = k \ln\left(\frac{C_m}{C_b}\right) \quad (2.1)$$

with $k = \frac{D_B}{\delta}$ (2.2)

where J = permeate flux (m/s)
 D_B = Brownian diffusion coefficient (m²/s)
 δ = stagnant film thickness (m)
 C_m = solute concentration at membrane surface (volume fraction)
 C_b = solute concentration in bulk (volume fraction)
 k = mass transfer coefficient (m/s)

The Brownian diffusion coefficient for solutes can be estimated from the Stokes-Einstein equation [Field, 1993]:

$$D_B = \frac{\kappa T}{6\pi\mu r_p} \quad (2.3)$$

where κ = Boltzmann constant = 1.380×10^{-23} (J/K)
 T = absolute temperature (K)
 μ = absolute viscosity (Pa.s)
 r_p = particle or solute radius (m)

It is evident from Equation 2.1 that the film model predicts the permeate flux to be mass transfer limited and independent of TMP under steady-state conditions. The permeate flux therefore

benefits from improved back-transport which is obtained by a higher mass transfer coefficient (Equation 2.2) and an increased concentration driving force from the membrane surface to the bulk. Equation 2.3 shows the inverse relationship between a solute's radius and its Brownian diffusion coefficient and explains why larger Brownian diffusion coefficients are exhibited by solutes of smaller radii to increase back-transport from the membrane surface. In addition, as is shown by Equation 2.2, back-transport is enhanced by a thinner stagnant film. The stagnant film thickness again is dependent on the system hydrodynamics, and any technique to increase the fluid shear rate at the membrane surface will decrease the stagnant film's thickness to increase back-transport and maintain the system at a higher permeate flux [Porter, 1972; Reed and Belfort, 1982].

Although film theory provides acceptable permeate flux predictions when true solutes accumulate near the membrane surface, it was found, however, that the predictions for colloidal and particulate suspensions were 1 to 2 orders of magnitude smaller than the experimental permeate fluxes [Porter, 1972; Reed and Belfort, 1982]. This gross under-prediction of the permeate flux, the so-called flux paradox [Green and Belfort, 1980], can be explained by the small Brownian diffusivity of larger materials. The inaccuracy of the film model to predict the permeate fluxes for the ultrafiltration of colloids and the microfiltration of particles, suggests that other back-transport mechanisms also play a role during these operations.

Shear-induced diffusion

Unlike Brownian diffusion, a perikinetic effect, where diffusion is facilitated by the random bombarding motion of fluid molecules, shear-induced diffusion is an orthokinetic effect, meaning that the diffusion is caused by velocity gradients. When considering a particle in a suspension which is subjected to a shear flow, the particle will interact with other particles to cause a succession of displacements across the fluid streamlines. The particle displacement of the resulting random behaviour will, however, in the absence of a concentration gradient, have a zero mean. In the presence of a concentration gradient, the particle will experience more interactions from the high concentration side, compared to the low concentration side, and a resulting force will consequently displace the particle to streamlines down the concentration gradient [Eckstein et al., 1977; Leighton and Acrivos, 1987; Davis and Leighton, 1987]. Following on the early work of Eckstein et al. [1977], Leighton and Acrivos [1986] estimated shear-induced diffusivities from:

$$D_s = \frac{1}{3} r_p^2 \gamma \varphi^2 \left(1 + \frac{1}{2} e^{8.8\varphi} \right) \quad \text{for } \varphi < 0.5 \quad (2.4)$$

where D_s = shear-induced diffusion coefficient (m^2/s)
 r_p = particle radius (m)
 γ = fluid shear rate (s^{-1})
 φ = volumetric particle concentration (dimensionless)

Equation 2.4 shows the direct proportionality between the shear-induced diffusion coefficient and the square of the particle diameter and the shear rate. Brownian diffusion, on the other hand, is inversely proportional to the particle diameter and independent of shear rate (Equation 2.3). As a result, Brownian diffusion is the dominant back-diffusion mechanism for sub-micrometre particles in a low shear field, whereas shear-induced diffusion is important in typical cross-flow microfiltration operations to remove micrometre-size and larger particles from the membrane surface [Howell, 1995]. From the particle size dependency of these two back-diffusion mechanisms, it can be shown that a minimum back-diffusivity exists, as shown in Figure 2.2.

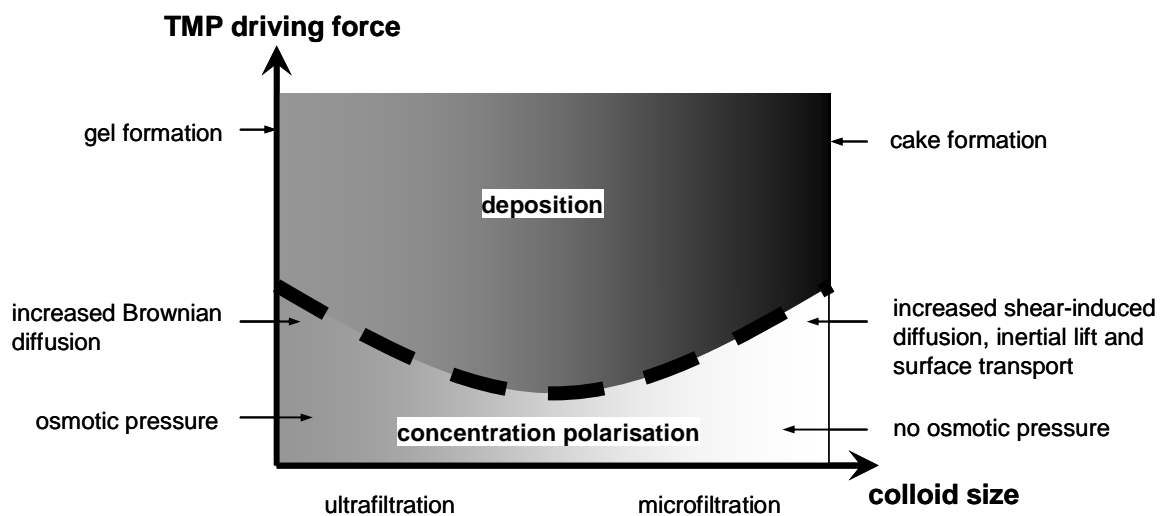


Figure 2.2: Illustration of the particle size dependency of membrane fouling. A minimum back-diffusivity exists with deposition of material at a relative low TMP.

Inertial lift

For tubular membranes the inertial lift model describes that, under lift and drag forces, neutrally buoyant particles in a laminar flow field will move away from both the membrane tube wall and the tube axis to reach equilibrium at a radial position [Green and Belfort, 1980; Belfort, 1989]. This phenomenon is also known in the literature as the tubular pinch effect [Porter, 1972]. Inertial lift

was first observed and published by Segré and Silberberg [1961] who worked with dilute suspensions of rigid spheres. Although a number of studies followed to investigate inertial lift, it was not until Porter [1972] first suggested that inertial lift could explain the flux paradox with Brownian diffusion as back-transport model, that inertial lift was investigated as an augmenting back-transport mechanism in tubular membranes. The study of inertial lift has also been extended to membrane systems containing slits [Altena and Belfort, 1984; Otis et al., 1986; Drew et al., 1991].

The lift forces, such as slip-spin and slip-shear forces [Porter, 1972], arise from nonlinear interactions of particles with the surrounding flow field. When these lift forces are stronger than the permeation drag force, it is proposed that the particles will not deposit on the membrane surface, but will migrate away from the membrane wall. Numerous models have been developed to determine the corresponding lift velocity of a particle in a given system, which must exceed the permeate velocity if the particle is to be carried away from the membrane [Cox and Brenner, 1968; Ho and Leal, 1974; Vasseur and Cox, 1976]. The derived expression for the lift velocity varies from system to system, but summarised, for both a tube and a slit, it applies that the lift velocity is increased for suspensions with larger particles at high cross-flow velocities [Green and Belfort, 1980; Altena and Belfort, 1984].

Surface transport

Surface transport models consider the possibility of particles deposited on the membrane surface to slide or roll tangentially across the membrane surface with the cross-flow. Surface transport can be described by two approaches: continuum and single-particle models.

In the continuum approach [Leonard and Vassilieff, 1984; Davis and Birdsell, 1987; Romero and Davis, 1988, 1990] particles retained at the membrane surface either remain as a stagnant cake layer on the membrane surface or they may, at high enough shear rates, move along the membrane surface in a flowing cake layer.

Single particle models consider the forces acting on a single spherical particle on the membrane or the stagnant cake surface to determine if the particle will adhere to the surface or be transported along the surface [Lu and Ju, 1989; Stamatakis and Tien, 1993].

Quantitative predictions of surface transport are difficult, but like shear-induced diffusion and inertial lift, surface transport is promoted by increases in the cross-flow velocity and the particle sizes.

2.3 Membrane fouling mechanisms

Depending on the concentration polarisation and back-transport conditions, the fouling behaviour of microfiltration membranes differs from system to system. The parameters that determine the concentration polarisation and back-transport are: particles' sizes, surface charges and concentrations; membrane material and its pore size distribution; hydrodynamic conditions at the membrane surface; temperature; pH and TMP driving force [Kawakatsu et al., 1993; Hwang et al., 1996; Bowen and Sharif, 1998; Bai and Leow, 2002; Le-Clech et al., 2003b; Trussell et al., 2007].

2.3.1 Physico-chemical fouling mechanisms

A polarised particle that is not being back-transported to the bulk has one of several destinations. Firstly, the particle may permeate through the membrane, given that the particle is smaller than the membrane pore size and that no attractive forces between the particle and the membrane material exist. In this scenario the particle leaves the membrane unimpeded, but other possibilities exist in which the particle can foul the membrane to reduce its permeability and thereby increase the hydraulic resistance to permeation. Depending on the relative sizes of the particle and available membrane pore, as well as prevailing surface charges, possible physico-chemical fouling mechanisms are adsorption, pore-blocking and cake layer formation [Belfort et al., 1993; Kawakatsu et al., 1993]. These three fouling mechanisms and their possible effects on the pore size distribution and the TMP versus permeate flux relation are shown schematically in Figure 2.3 for a membrane with a typical pore size distribution.

In the presence of attractive forces between the particle and the membrane, the particle may interact with the membrane through adsorption. The particle can adsorb to the membrane surface (the upstream side of the membrane) or, when small enough, adsorb to the membrane on the inside of an accessible pore to constrict it (Figure 2.3(a)). Continued adsorption of other particles inside the pores will result in a loss of pores from the pore size distribution to reduce the cross-sectional area available for permeation. The TMP therefore has to compensate for the reduced permeability and is consequently higher, compared to pure water filtration, when a constant permeate flux is required.

If the particle approaches a membrane pore of similar size, pore-blocking may occur when entering it to bridge the pore's entrance partially or even completely (Figure 2.3(b)). Pore-blocking affects

the pore size distribution and the TMP versus permeate flux relation in a similar way as adsorption, perhaps more severe, since a single particle suffices to completely block a membrane pore.

The surface filtration mechanism of sieving occurs when the particle is too large to enter a membrane pore (Figure 2.3(c)). The subsequent deposition of large particles on the membrane surface or other already deposited material forms a growing cake layer. The deposited cake layer acts as an additional filter, or so-called dynamic membrane, and reduces the effective pore sizes. The cake continues to acquire higher hydraulic resistances as the cake layer grows and the effective pore sizes decline with filtration time and TMP through particle compaction, particle rearrangement and deposition of smaller particles in the pores of the cake. The permeate flux is observed to change, with increased cake hydraulic resistance, from being pressure-controlled to being mass transfer-controlled, independent of TMP, as is shown in Figure 2.3(c) [Belfort et al., 1993; Hwang et al., 1996].

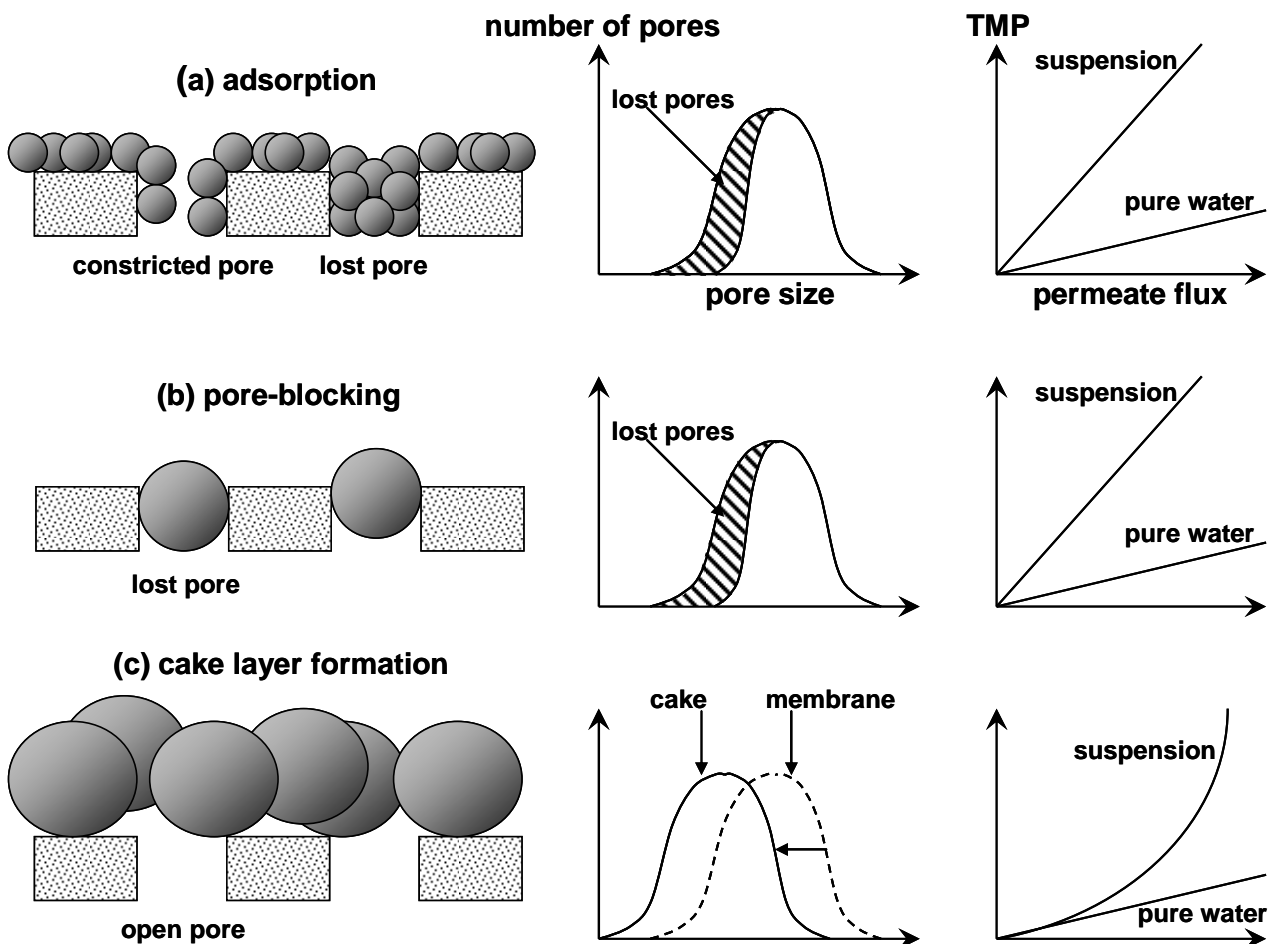


Figure 2.3: Physico-chemical fouling mechanisms [Belfort et al., 1993].

2.3.2 Biofouling mechanisms

Membrane biofouling arises from biofilm formation [Jacobs et al., 1996] on the surface and in the pores of the membrane to impose an extra hydraulic resistance [McDonogh et al., 1994; Aryal et al., 2009]. Biofilm comprises microbial cells embedded in a highly hydrated matrix of excreted extracellular polymeric substances (EPS) [Baker and Dudley, 1998]. It is widely documented that EPS mainly constitutes biofouling [Hodgson et al., 1993; Baker and Dudley, 1998; Nagaoka et al., 1998, 2000]. EPS serves as a binding material for the adhesion of the micro-organisms to the membrane surface and the cohesion of the biofilm [Flemming et al., 1997], thereby significantly increasing the energy requirement for biofilm removal. Complex biofilms, typical to industrial membrane operations, are often closely associated with entrapped particles [Al-Ahmad et al., 2000]. These deposits can even be more detrimental to membrane operation, since they may form more rapidly and be more tightly bound than biofilm on its own [Characklis, 1990].

The process of biofilm formation on a clean membrane surface is postulated to follow a number of steps [Flemming and Schaule, 1988; Lynch and Edyvean, 1988; Marshall and Blainey, 1991] and are shown in Figure 2.4:

1. Immediately upon immersion of the clean membrane in a bio-phase, dissolved organic material is adsorbed onto the membrane surface to form a conditioned layer.
2. Microbial cells transported to the membrane surface attach to the conditioned layer.
3. Growth and metabolism (start of EPS production) of the attached micro-organisms.
4. Limitation of biofilm growth by fluid shear forces and nutrient limitation at the base of the biofilm to attain a steady-state thickness.

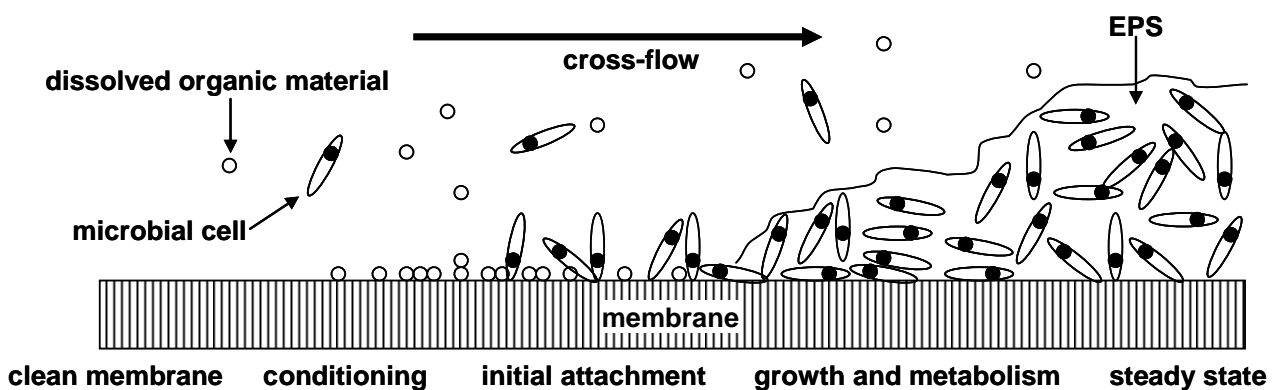


Figure 2.4: Stages of biofilm growth on a clean membrane.

Membrane biofouling, although inherently different from the physico-chemical attachment mechanisms of non-living particles, is nevertheless also considered to foul membranes by

constricting and blocking pores; and the formation of a cake layer on the membrane surface [Shimizu et al., 1997; Lim and Bai, 2003].

2.3.3 Membrane fouling modelling

Resistance models offer the simplest way to account for membrane fouling in the dynamic modelling of membrane performances [Kawakatsu et al., 1993; Piron et al., 1995; Chen et al., 1997; Tansel et al., 2000; Ghosh, 2002]. The starting point in the development of these models follows Darcy's law which can be written as:

$$J = \frac{\Delta P - \sigma \Delta \Pi}{\mu R_t} \quad (2.5)$$

where J = permeate flux (m/s)

ΔP = transmembrane pressure (TMP) (Pa)

σ = osmotic reflection coefficient (dimensionless)

$\Delta \Pi$ = transmembrane osmotic pressure (Pa)

μ = absolute viscosity of the fluid (Pa.s)

R_t = total hydraulic resistance (m⁻¹)

In Equation 2.5 the driving force for permeation is the effective TMP which is the applied TMP, ΔP , minus the resulting transmembrane osmotic pressure, $\sigma \Delta \Pi$. The osmotic reflection coefficient, σ , is a measure of the leakiness of the membrane to the osmotic components and varies from one for a fully retentive membrane to zero for a fully permeable membrane. The transmembrane osmotic pressure, $\Delta \Pi$, resembles a pressure resistance that has to be overcome for permeation to occur and results from the difference in osmotic potential on both sides of the membrane during concentration polarisation as mentioned in Section 2.2.1.

The total hydraulic resistance, R_t , is defined as the sum of a series of resistances:

$$R_t = R_m + R_i + R_c \quad (2.6)$$

where R_m = membrane resistance (m⁻¹)

R_i = internal fouling (adsorption and pore-blocking) resistance (m⁻¹)

R_c = cake resistance (m⁻¹)

The membrane resistance states the intrinsic resistance of an unfouled membrane and is the benchmark for the minimum in the total hydraulic resistance. During membrane operation, fouling mechanisms will increase this minimum hydraulic resistance by depositing material internally

through adsorption and pore-blocking and externally through cake layer formation. Adsorption and pore-blocking resistances are usually lumped together as internal fouling resistance since it is very hard to quantitatively and qualitatively tell the resulting fouling apart. Instead of distinguishing between internal fouling and cake resistances, some sources refer to the fouling resistances as either being reversible or irreversible [Field et al., 1995; Krstić et al., 2002; Vyas et al., 2002]. This distinction is made on a quantitative basis for a specific cleaning process after a certain membrane operation time by comparing the calculated total hydraulic resistance values from Equation 2.5 at the start of operation, at the end of operation and after subsequent cleaning as follows:

$$R_{irre} = (R_t)_{clean} - R_m \quad (2.7)$$

$$R_{re} = (R_t)_{end} - (R_t)_{clean} \quad (2.8)$$

where R_{irre} = irreversible fouling resistance (m^{-1})
 $(R_t)_{clean}$ = total hydraulic resistance after cleaning (m^{-1})
 R_m = membrane resistance and equal to R_t for an unfouled membrane (m^{-1})
 R_{re} = reversible fouling resistance (m^{-1})
 $(R_t)_{end}$ = total hydraulic resistance at the end of membrane operation (m^{-1})

The specific cleaning process is therefore only able to remove the reversible fouling resistance, but by improving the cleaning process for the same membrane operation, the ratio of R_{re} to R_{irre} may be increased. Generally the removal of the cake layer requires considerably less energy compared to the removal of internal fouling, hence cake layer formation is often reversible, while internal fouling is usually irreversible [Wakeman and Williams, 2002].

Particles and large colloids exhibit negligible osmotic pressures and can be ignored in MF operations. Therefore, when substituting Equation 2.6 into Equation 2.5, the resistance model for microfiltration becomes:

$$J = \frac{\Delta P}{\mu (R_m + R_i + R_c)} \quad (2.9)$$

and when microfiltration is operated at a constant flux and the fluid viscosity assumed to be constant, the required TMP to compensate for an increasing total hydraulic resistance can be calculated from:

$$\Delta P(t) = J\mu [R_m(t) + R_i(t) + R_c(t)] \quad (2.10)$$

Although the membrane resistance, R_m , is usually considered as a constant, a time dependency was included for the term in Equation 2.10, since membrane compaction or a loss of integrity may increase or decrease the membrane resistance respectively with time.

As indicated in Equation 2.10, the evolution of the TMP increase is the result of various resistances working together, but the relative importance of each of the resistances may change with time. When constant flux permeation is started with an unfouled membrane, the initial TMP only depends on R_m , since R_i and R_c are zero. Since it is possible that membrane pores can be completely blocked by the first particles to reach the membrane, the subsequent internal fouling can be a very quick process to cause a rapid TMP increase [Bai and Leow, 2002]. Internal fouling can however be ignored if the suspended particles are larger than the membrane pores. As more particles are deposited on the membrane surface, a cake layer starts to form which offers an additional growing resistance, R_c , and, for a flat membrane, it can be calculated from [Belfort et al., 1994]:

$$R_c = \hat{R}_c \delta_c \quad (2.11)$$

where \hat{R}_c = specific cake resistance per unit cake thickness (m^{-2})

δ_c = cake thickness (m)

The initial impact of cake layer formation on the total hydraulic resistance does not seem to be as drastic, compared with internal fouling [Lim and Bai, 2003]. This may be explained by the relative permeability of a cake layer, as opposed to pore-blocking, and the fact that the cake layer thickness is limited by the prevailing shear stress at the cake surface [Benkahla et al., 1995]. After a steady-state cake thickness is attained, the further gradual increase in R_c can mainly be ascribed, as is evident from Equation 2.11, to the increase in the specific cake resistance of the cake layer. According to Porter [1977] the specific cake resistance can be described by:

$$\hat{R}_c = \alpha_o (\Delta P)^s \rho_s \Phi_c \quad (2.12)$$

where α_o = constant dependent on the size and shape of the cake particles

s = compressibility exponent of the cake

ρ_s = mass density of solids in the cake (kg/m^3)

Φ_c = solid volume fraction in the cake

The constant, α_o , increases with a decrease in particle size; and the solid volume fraction, Φ_c , increases as smaller particles are entrapped in the cake. It has been documented elsewhere that a cake layer of smaller particles or a cake layer capturing smaller particles exhibits increased

specific cake resistances [Bai and Leow, 2002; Lim and Bai, 2003]. Cake layers may also be compressed with increasing TMP to raise the specific cake resistance [Kawakatsu et al., 1993]. The compressibility exponent, s , varies from zero for a perfectly incompressible cake to one for a perfectly compressible cake. In practice the compressibility of cakes usually ranges between 0.1 and 0.8 [Porter, 1977].

In general, microfiltration can initially be characterised by a membrane resistance limited, followed by an internal fouling resistance limited and eventually a cake resistance limited process [Lim and Bai, 2003]. Although filtration models have been developed for each resistance limited process [Suki et al., 1986; Belfort et al., 1993; Silva et al., 2000], the exact behaviour of each resistance remains very system specific and must be empirically determined.

Consider the TMP-time profile of a hypothetical cross-flow microfiltration process in Figure 2.5 showing the contributions of each resistance limited process on the TMP required to produce a constant permeate flux. No fouling occurs while pure water is filtrated and the hydraulic resistance remains the constant resistance imposed by the membrane. In this process the feed is instantaneously switched from pure water to a particulate suspension capable of fouling the membrane internally and depositing a cake layer externally. With the onset of suspension filtration, internal fouling is the resistance limited process and the TMP initially rises rapidly, where after the gradient decreases as cake layer formation becomes the resistance limited process. Cake layer thickening and specific cake resistance behaviour will determine the rate of cake resistance increase, which tends to be linear at a constant permeate flux [Tardieu et al., 1998, 1999; Ghosh, 2002; Guibert et al., 2002]. Although the rate by which internal fouling increases the hydraulic resistance is usually much more rapid than that of cake layer formation, the latter is the resistance limited process for most of the microfiltration time and is therefore eventually responsible for the majority of the total hydraulic resistance and the resulting TMP increase. Filtration at higher constant permeate fluxes will accelerate both the rates of internal fouling resistance and cake layer resistance increases.

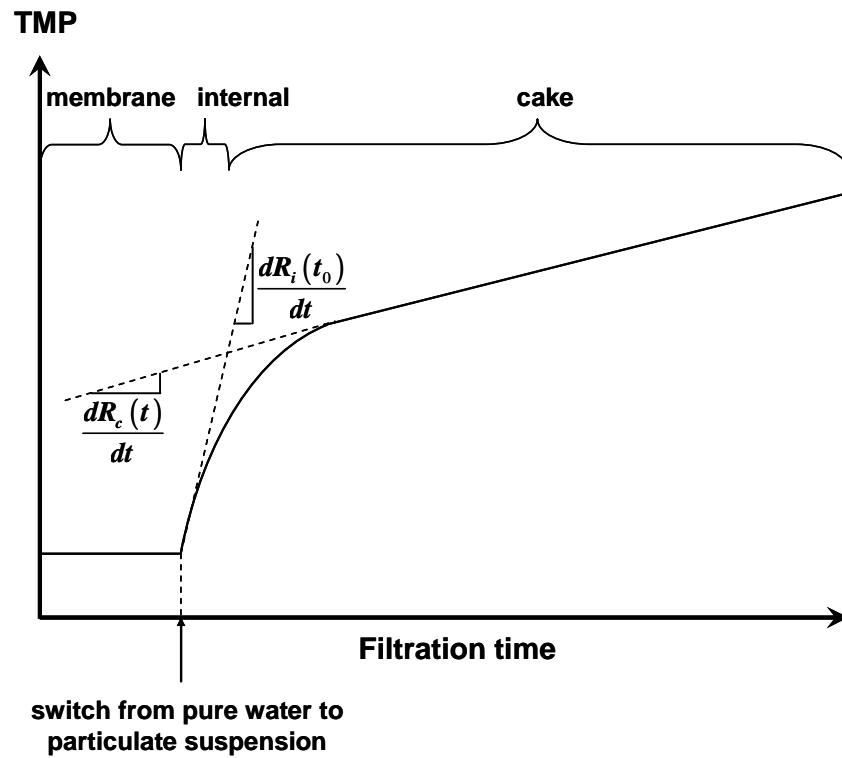


Figure 2.5: Contribution of each hydraulic resistance to the TMP for a hypothetical microfiltration process at constant permeate flux where the feed could be changed from pure water to a particulate suspension.

2.4 Membrane fouling amelioration

Membrane fouling manifests as an increasing TMP during constant permeate flux operations or as a decreasing permeate flux during constant TMP operations. In both cases a critical point will be reached where membrane operation becomes uneconomical; either because of too high operating costs to maintain an escalating TMP in the former case or because of inadequate throughput in the latter case. Also, for certain systems, the resulting high TMP and bio-deterioration of bio-susceptible membranes when biofouling is present, can cause severe membrane damage. These undesirable situations necessitate a disruption of membrane operation to perform a membrane cleaning or replacement operation, depending on the irreversibility of the fouling and the integrity of the membranes. Clearly the frequency and the extent of these membrane cleaning and replacement operations have to be minimised for reduced downtime, operating (cleaning chemicals) and capital (replaced membranes) costs. Although the prevention of fouling can probably never be achieved, the viability of a membrane process will ultimately be determined by its ability to limit fouling to:

- extend the period of economical membrane operation and thereby reduce the frequency of membrane cleaning and replacement;
- reduce membrane damage and increase membrane lifespan;
- require a less severe cleaning regime with resulting cost savings and an extended membrane lifespan; and
- reduce product water consumption for cleaning or backwashing of membranes.

Membrane fouling amelioration strategies during membrane operation can be grouped into three approaches [Ridgway and Safarik, 1991; Fane et al., 2000; Wakeman and Williams, 2002; Leiknes, 2003]:

- feed pretreatment;
- membrane material selection; and
- back-transport promotion.

2.4.1 Feed pretreatment

In feed pretreatment the foulants are either removed or treated to prevent them from reaching and depositing on the membrane surface. Physical processes include prefiltration, centrifugation and heating followed by settling, while chemical processes include precipitation, coagulation and flocculation [Mietton and Ben Aim, 1992], or dosing of proprietary chemicals as anti-scalants or disinfectants.

2.4.2 Membrane material selection

For systems where surface chemistry plays a significant part in membrane fouling, the choice of membrane material may greatly determine the extent of fouling during operation and the ability to remove foulants during cleaning [Matthiasson, 1983; Ma et al., 2001]. Physical membrane properties that may also be important are porosity and surface roughness [Ridgway and Safarik, 1991; Sadr Ghayeni et al., 1998; Pasmore et al., 2001; Vrijenhoek et al., 2001].

2.4.3 Back-transport promotion

Back-transport of material from the membrane to the bulk may be improved by the hydrodynamic conditions at the membrane surface, destabilisation of the permeate flux and by limiting the transport of foulants to the membrane by operating at a sub-critical flux.

Surface hydrodynamics

By applying a cross-flow, and thereby exerting a shear stress, a thin concentration boundary layer is maintained across the membrane surface on the feed side to increase back-transport of fouling material to the bulk. Increased shear stress is obtained at higher cross-flow velocities. The shear stress may also be created by relative movement of the membrane to the fluid [Engler and Wiesner, 2000; Fyles and Lycon, 2000; Lee and Lueptow, 2003].

When the applied shear is coupled with fluid instabilities to induce turbulence, the concentration and velocity boundary layers at the membrane surface are disturbed to convectively augment back-transport through a scouring action [Winzeler and Belfort, 1993]. Various methods are employed to generate turbulence: placing inserts in flow channels [Gupta et al., 1995; Schwinge et al., 2000; Krstic et al., 2002], air or gas sparging [Cui and Wright, 1994; Cabassud et al., 1997, 2001; Mercier et al., 1997; Laborie et al., 1998; Li et al., 1998b; Serra et al., 1999; Mercier-Bonin et al., 2001; Chang and Judd, 2002], pulsatile feed flow [Finnigan and Howell, 1989; Mackley and Sherman, 1994] and vibration of the membrane [Bian et al., 2000; Al Akoum et al., 2002].

Permeate flux destabilisation

Destabilisation strategies strive to overcome the binding energy of adsorbed material and to destroy cake layer structures and thereby leaving the detached material at the disposal of back-transport mechanisms.

In permeate flux destabilisation the TMP is switched in cycles between a positive and negative value to change the direction of permeation through the membrane from forward filtration (production stage) to reverse filtration (cleaning stage) respectively. Optimal values for the frequency, duration, flow rate and negative TMP for flow reversal will depend on the system and type of flow reversal, such as backwashing [Serra et al., 1999; Hwang et al., 2009] or a more rapid backpulsing [Redkar et al., 1996; Jones et al., 1999; Héran and Elmaleh, 2000; Mores et al., 2000; Ma et al., 2001].

In a strategy called relaxation or crossflushing [Ma et al., 2001; Wu et al., 2008a], the TMP, and therefore permeation, is stopped intermittently, while cross-flow is continued across the membrane. In the absence of the TMP driving force the cake layer decompresses, and may even detach from the membrane surface to be sheared off by the cross-flow.

Sub-critical flux operation

For a certain cross-flow velocity it can be concluded from the back-transport models described in Section 2.2.2 and the force models proposed by Lu and Ju [1989], Bacchin et al. [1995] and Vigneswaran et al. [2000] that the net force on a particle, normal to the membrane surface, will depend on the particle's size. Shear-induced diffusion, inertial lift and surface transport back-transport mechanisms are amplified as particle size increases in the micrometre range. The stronger back-transport force on a larger particle must at least be balanced out by a higher convective permeate flux in order for the particle to reach the membrane surface for possible deposition. The permeate flux with a drag force equal to the back-transport force for a certain particle is the critical flux for that particle. Therefore, for given hydrodynamics, the permeate flux will determine which particle sizes will be deposited - incrementing the permeate flux will lead to the successive deposition of increasing particle sizes [Howell, 1995; Tardieu et al., 1998]. On the other hand, by improving the surface hydrodynamics, with an increased cross-flow velocity for example, the particle back-transport is augmented to consequently raise the critical flux needed for each particle size to reach the membrane surface. Ultimately, it is therefore theoretically possible, when operating a membrane system below its lowest particle critical flux, to experience no membrane fouling. Although the consequent lower permeate fluxes of sub-critical flux operation may necessitate a larger membrane area, it provides a possible solution for long-term non-fouling membrane operation. Pollice et al. [2005] have however still found biofouling to occur at sub-critical fluxes.

The critical flux concept was introduced by Field et al. [1995] and the existence of the critical flux has since been experimentally confirmed by other researchers [Chen et al., 1997; Li et al., 1998a;

Defrance and Jaffrin, 1999a, 1999b; Fradin and Field, 1999; Wu et al., 1999; Kwon et al., 2000; Vigneswaran et al., 2000; Vyas et al., 2002]. Translated for constant permeate flux operation, Field et al. [1995] hypothesised that for microfiltration there exists a critical permeate flux on start-up below which no increase in TMP with time is observed, but above this permeate flux fouling occurs with a consequent continuous increase in TMP.

Defrance and Jaffrin [1999a] described stable TMP operation at sub-critical fluxes for their system with pore-blocking, adsorption and concentration polarisation as quasi-steady resistance values. However, when the critical flux for the system is exceeded, cake formation commences and the TMP rises rapidly without stabilisation. These findings explain the expansion of the critical flux concept to include a weak and strong form of the critical flux hypothesis for microfiltration [Fradin and Field, 1999; Ognier et al., 2004] and is explained in Figure 2.6. In its strong form the sub-critical flux of a membrane operation is equivalent to the pure water permeate flux and requires the same TMP, since no fouling has occurred and no additional hydraulic resistance has to be overcome. However, in its weak form the sub-critical flux has to account for internal fouling and requires a slightly higher TMP than the TMP for the same pure water permeate flux. In both cases the sub-critical flux varies linearly with the corresponding TMP without any hysteresis. In reality this will only strictly be applicable to completely reversible fouling, whereas irreversible fouling will always demonstrate some degree of hysteresis. Nevertheless, above the critical flux the TMP exhibits a significant hysteresis when the permeate flux is reduced, even when reduced to below the critical flux.

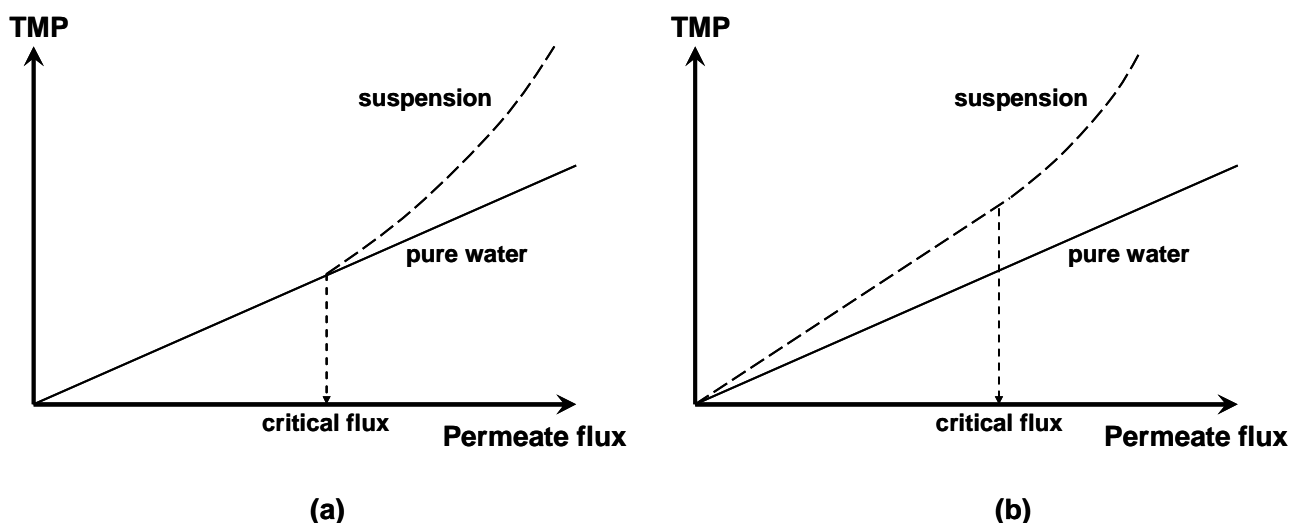


Figure 2.6: Critical flux hypothesis for microfiltration: (a) strong form and (b) weak form. Above the critical flux in both cases TMP continues to increase at constant permeate flux and displays TMP hysteresis when permeate flux is reduced to below the critical flux.

Figure 2.7 shows the hypothetical TMP profile when a permeate flux is incremented from A to E which is from sub-critical to above critical. Figure 2.8 shows the TMP profiles of these constant permeate fluxes A to E for a hypothetical microfiltration process where the feed could be switched from pure water to a particulate suspension capable of internal fouling and cake layer formation.

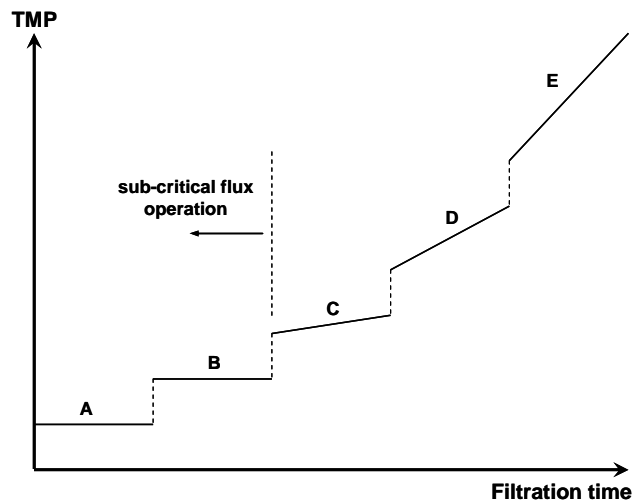


Figure 2.7: Hypothetical TMP profile of incremented constant permeate fluxes from sub-critical to above critical fluxes.

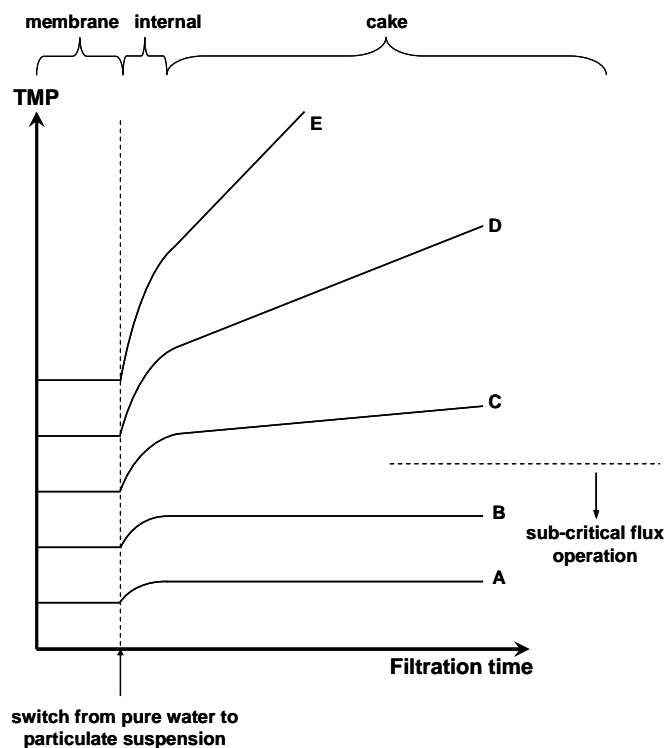


Figure 2.8: Hypothetical TMP profiles of constant permeate fluxes when the feed was switched from pure water to a particulate suspension. Above critical flux cake layer formation commences and continues at a constant rate.

Chapter 3

Air-scouring of immersed membranes

3.1 Introduction

Improved surface hydrodynamics, as mentioned in Section 2.4.3, provide a means to arrest membrane fouling. When a cross-flow is applied across the membrane, the shear stresses exerted at the membrane surface should limit concentration polarisation and restrict particle deposition by improving back-transport. The side-stream membrane configuration especially lends itself to the utilisation of a high shear rate cross-flow, since the feed is pumped at high velocities through an external unit across the membrane surfaces. The shear rate at the membrane surface may even be further increased by the introduction of turbulence promoters in the external unit [Krstić et al., 2002]. For immersed membrane systems, however, the physical design usually rules out the possibility for the feed to be pumped across the membrane surfaces and immersed membranes consequently have to rely on other methods to generate cross-flow.

A popular technique to provide flow across the surface of immersed MBR membranes is to sparge the membranes with gas, usually air, from a diffuser located at the bottom of the reactor. Besides fine-bubble aeration for the respiratory support of biomass in aerobic MBRs, coarse-bubble aeration is also typically employed in an attempt to control membrane fouling [Gander et al., 2000; Chang and Judd, 2002]. The rising bubbles induce a moderate cross-flow and, when intimately in contact with the membranes, are able to scour the membrane surfaces [Bouhabila et al., 1998]. Depending on the membrane configuration, it is even possible to shake the membranes [Ueda et al., 1997; Günder and Krauth, 1998; Suda et al., 1998; Wicaksana et al., 2006] to loosen and remove deposited material.

3.2 Scouring action of rising bubbles

The ability of air, when introduced on the feed side of inside-out tubular membranes, to remove deposited material from the membrane surface has been investigated by Judd et al. [2001], Cabassud et al. [1997, 2001], Mercier et al. [1997] and Laborie et al. [1998]. A number of aeration regimes, depending on the supplied air flow rate, can be produced inside a tube, ranging from fine bubbles, in which the liquid is the continuous medium, to mist, in which the air is the continuous medium (Figure 3.1).

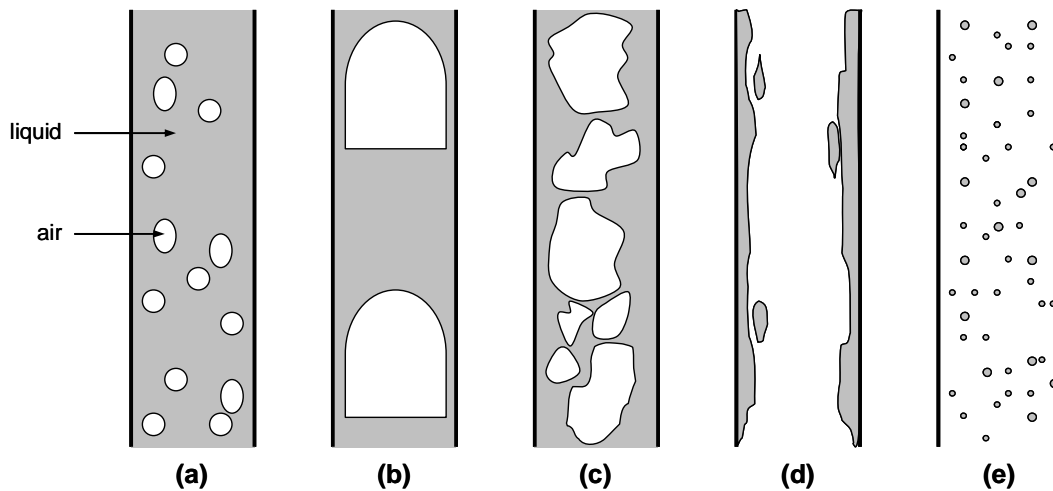


Figure 3.1: Aeration regimes inside a tube: (a) bubble flow; (b) slug flow; (c) churn flow; (d) annular flow; and (e) mist flow [Judd et al., 2001].

In the slug flow aeration regime, an intermediate state where the flow can be described as successively moving pockets of air and liquid, the scouring action of the air was found to be the most effective. The key to this pronounced effect of slug flow lies in the rapid alternation of shear stresses at the membrane surface. An air slug is an almost cylindrical air bubble which occupies most of the cross-sectional tube area with only a thin liquid film separating it from the membrane wall. As an air slug rises the liquid ahead of the air slug is forced down into the liquid film where it accelerates as it moves downwards. The liquid is then injected into the relative stagnant liquid slug behind the air slug to create a highly agitated mixing zone in the air slug's wake. Consequently, with the passing of an air slug, a point on the membrane surface is first subjected to a negative shear stress ($\tau_{L\text{Film}}$), induced by the liquid film around the air slug, to be followed by a positive shear stress ($\tau_{L\text{Slug}}$), induced by the liquid slug (Figure 3.2). This exposure to a fast falling liquid film and a changing shear rate at the membrane surface is responsible for the superior scouring action and

the consequent reduced fouling observed in inside-out vertically installed tubular membranes operating with slug flow aeration regimes.

Mercier-Bonin et al. [2000] have shown that the successes of slug flow in inside-out tubular membranes to reduce fouling can be repeated to a certain degree by injecting air together with the feed when operating inside-out flat-sheet membranes. It is therefore conceivable that the scouring performance of air bubbles inside inside-out membranes may be emulated between immersed outside-in flat-sheet membranes; provided that they are closely packed to allow the bubble diameters to be comparable to the channel widths between the membranes [Zhang et al., 2009] as shown in Figure 3.3.

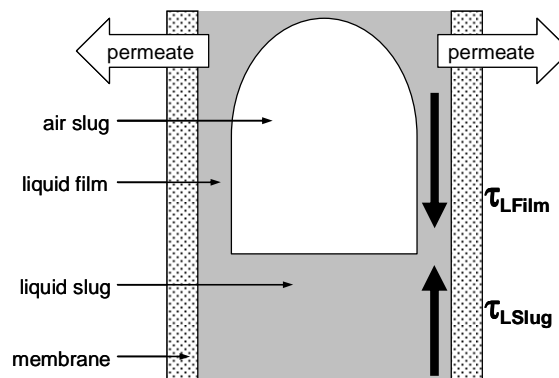


Figure 3.2: Slug flow inside an inside-out tubular membrane. A rising air slug scours the membrane surface by first subjecting it to a negative shear stress (τ_{LFilm}) and then by a positive shear stress (τ_{LSlug}) [Laborie et al., 1998; Cabassud et al., 2001].

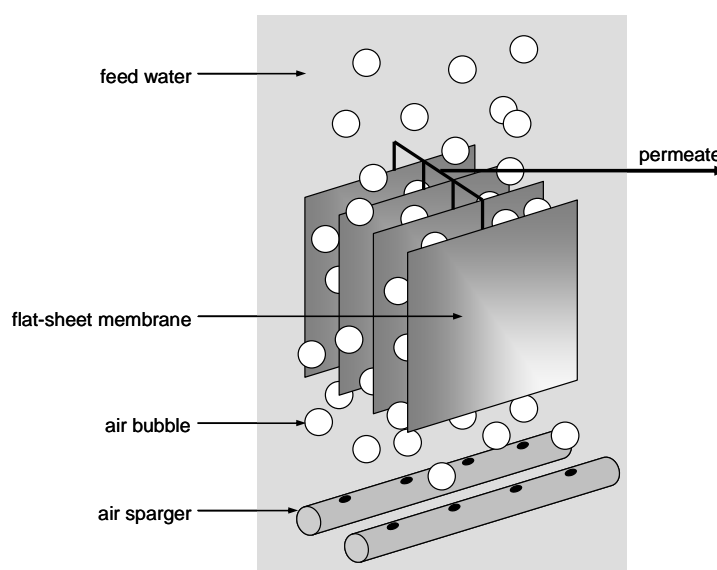


Figure 3.3: Air-sparging of immersed outside-in flat-sheet membranes.

3.3 Airlift reactors

An airlift reactor is a pneumatic agitator in which bubbling gas, usually air, produces the required mixing of the contained suspension. Airlift reactors are therefore ideal for gas-liquid-solid-contact bioprocesses, since these processes demand constant and mild shear throughout the reactor, as well as aseptic operation – all aspects which cannot be guaranteed by the intrusion of mechanical stirring [Chisti and Moo-Young, 1987; Chisti, 1989a]. Unlike a bubble column (Figure 3.4(a)), which is simply an air-sparged tank, an airlift reactor (Figure 3.4(b)) is divided into two distinct, but connected, zones of which one is sparged with air. The subsequent difference in gas hold-ups, and therefore the difference in bulk densities, between the two regions, generates liquid motion between the zones. The denser liquid in the ungasged zone (the downcomer) flows downwards to displace the less dense liquid in the gassed zone (the riser) upwards. Because of these regions of different liquid densities, airlift reactors, as opposed to bubble columns, display a more clearly defined liquid flow with higher linear liquid velocities for the same sparging energy input [Choi et al., 1996].

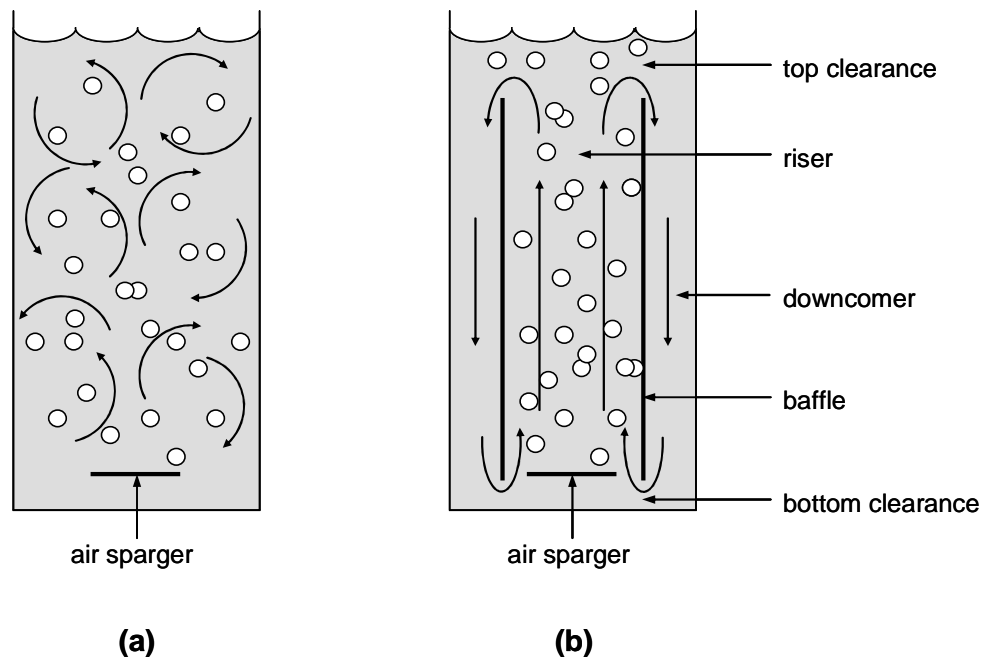


Figure 3.4: Liquid flow patterns: (a) chaotic liquid circulation cells in a bubble column; (b) clearly defined liquid flow in an airlift reactor: upwards in the gassed riser and downwards in the ungasged downcomers [Chisti and Moo-Young, 1987; Choi et al., 1996].

3.3.1 Liquid velocity

The gas-induced liquid circulation velocity is one of the most important characteristic parameters of airlift reactor design and determines the gas hold-up behaviour, mass and heat transfer, extent of mixing and the ability of the reactor to suspend solids [Chisti and Moo-Young, 1993; Contreras et al., 1998]. Nevertheless, the accurate extrapolation of riser and downcomer liquid velocities from studied airlift reactors to any other airlift reactor system, in terms of geometry and operating conditions, has eluded researchers up to now [Chisti, 1989b; Livingston and Zhang, 1993; Merchuk and Berzin, 1995; García-Calvo and Letón, 1996; Al-Masry and Abasaeed, 1998; Couvert et al., 2001]. Numerous empirical correlations have been proposed for the estimation of liquid velocities, but their applicability tends to be restricted to the systems they were derived from. On the other hand, over-simplified assumptions have rendered developed models, based on energy [Chisti and Moo-Young, 1988; Merchuk and Berzin, 1995; García-Calvo and Letón, 1996; Hwang and Cheng, 1997] and momentum balances [Siegel et al., 1986; Dhaouadi et al., 1996; Couvert et al., 2001; Van Baten et al., 2003], incomplete and unable to predict liquid velocities over the full range of airlift reactor geometries and scales. Also, most of the published work on liquid velocities in airlift reactors has been focussed on simple two-phase air-water systems.

Despite these shortcomings in attaining a liquid velocity prediction method relevant to any airlift reactor system, the observed trends are invaluable for the design of airlift reactors that require an enhanced liquid circulation. Unfortunately however, airlift reactor parameters seem to form intricate interactions to affect the circulation velocity equivocally [Siegel et al., 1986; Livingston and Zhang, 1993; Lu et al., 2000], and the influence of system parameters in isolation should therefore be regarded with discretion.

Increasing the sparging rate of gas in the riser causes the riser liquid velocity to increase, although a limit seems to exist beyond which an increase in the sparging rate does not effect the riser liquid velocity [Siegel et al., 1986; Livingston and Zhang, 1993; Hwang and Cheng, 1997; Al-Masry and Abasaeed, 1998; Lu et al., 2000; Couvert et al., 2001]. Like gas sparging, the ratio of the total cross-sectional areas of the downcomer sections to the riser sections, has been found to have a significant effect on the riser liquid velocity [Siegel et al., 1986; Chisti et al., 1988; Livingston and Zhang, 1993; Al-Masry and Abasaeed, 1998; Lu et al., 2000]. An increase in this ratio reduces the downcomer liquid velocity relative to the riser liquid velocity, enabling more gas to escape the downward drag in the downcomer, and thereby effectively increasing the bulk density difference between the downcomer and riser regions for enhanced riser liquid velocity. The size and nature of the top [Siegel et al., 1986; Chisti and Moo-Young, 1993; Livingston and Zhang, 1993; Couvert et al., 1999] and bottom clearances [Chisti et al., 1988; Livingston and Zhang, 1993; Merchuk and

Berzin, 1995; Choi et al., 1996; Couvert et al., 1999], interconnecting the riser and downcomer sections, not only determine the degree of resistance presented against liquid circulation, but, in the case of the top clearance, also the extent of gas separation to provide ungasged fluid to the downcomer for increased liquid circulation, as mentioned before. The riser liquid velocity also seems to benefit from an increase in the riser height [Siegel et al., 1986; Chisti et al., 1988; Chisti and Moo-Young, 1993; Livingston and Zhang, 1993; Lu et al., 1995; Hwang and Cheng, 1997; Lu et al., 2000].

3.3.2 Airlift reactor application for immersed membrane fouling control

The scouring action that a rising bubble exerts on nearby surfaces, as explained in Section 3.2, is enhanced when superimposed on the rising liquid cross-flow, since both the shear stresses and the rate of shear stress reversal at the surfaces are increased. This technique has been successfully applied for fouling control of immersed membranes installed in the riser sections of airlift reactors [Churchouse and Wildgoose, 1999; Liu et al., 2000, 2003; Chang and Judd, 2002; Guibert et al., 2002; Shim et al., 2002].

Increasing the riser liquid velocity will therefore also increase the rising bubbles' ability to scour the immersed membranes and remove deposited material from the membrane surfaces. Experimental results of membranes immersed in risers of airlift bioreactors have indeed shown that the riser liquid velocity could be increased, as discussed in Section 3.3.1, by adopting airlift reactor geometries with higher ratios of downcomer to riser cross-sectional areas, larger bottom clearances, increased liquid depths and by intensifying air sparging in the riser; and that these increased cross-flow velocities led to decreased membrane fouling rates [Liu et al., 2000, 2003; Shim et al., 2002]. Optimised airlift reactors to generate fast riser velocities for increased bubble scouring are therefore ideal to be used in the control of immersed membrane fouling.

Chapter 4

Fouling quantification for air-scouring evaluation

4.1 Introduction

In Chapter 3 the scouring action of air bubbles rising close to membrane surfaces and the viability of sparged air as a method to control immersed membrane fouling were described and explained. Indeed, the application of air-sparging to successfully limit fouling in immersed membrane systems has been extensively documented [Shimizu et al., 1996; Ueda et al., 1997; Bouhabila et al., 1998; Ozaki and Yamamoto, 2001; Chang and Judd, 2002; Guibert et al., 2002; Cui et al., 2003; Le-Clech et al., 2003b]. Despite these numerous accounts, however, the quantitative influence of the applied air on the fouling dynamics has remained unclear.

As explained in Chapter 3, air-scouring is enhanced when more and faster rising bubbles sweep the membrane surface. It therefore seems logical to hypothesise that an increase in the sparged air flow rate will increase the supplied air's ability to scour and reduce immersed membrane fouling. Bouhabila et al. [2001] have confirmed this hypothesis and reported to have found that an increase in the air flow rate has enabled their MBR to operate stably at higher constant fluxes, because of reduced fouling.

Ueda et al. [1997], Silva et al. [2000], Chang and Fane [2001] however, have found that, for a given system, a critical aeration value exists after which an increase in the air flow rate had no effect on the air's scouring ability. Scouring efficiency is defined as the amount of deposited material removed from the membrane surface per volume supplied sparged air in a given time. Therefore, operating at a higher sparged air flow rate than a system's critical aeration value will reduce the sparged air's scouring efficiency, since the increased aeration does not benefit further material removal from the membrane surface. A lower scouring efficiency consequently translates into higher operating costs. Nonetheless, without increasing the air flow rate, Ueda et al. [1997] found that when aeration was intensified from fewer diffusers and the membranes rearranged, the scouring efficiency was increased. Chang and Fane [2001] managed to show that less densely

spaced hollow fibre membranes with smaller diameters positioned in wider channels are less prone to foul than high density hollow fibre membranes with larger diameters in smaller channels at the same air flow rate.

The above-mentioned findings conclude that the hypothesis of increased air-scouring with an increased air flow rate has to be rejected. Although the hypothesis may appear to be true in certain cases, air flow rate is not necessarily the only factor that governs the scouring ability of the sparged air, but geometrical factors also seem to play a significant role. Studies of membranes immersed in airlift reactors have confirmed the importance of geometrical factors to provide ideal system hydrodynamics for efficient air-scouring [Liu et al., 2000, 2003; Shim et al., 2002].

Since membrane air-scouring dominates the operating costs of immersed membrane processes, typically more than 90% for MBRs [Gander et al., 2000], a drive exists to optimise reactor design for higher air-scouring efficiencies [Liu et al., 2000]. In order to evaluate the air-scouring efficiencies of different reactor designs it is necessary to measure some tangible and comparable process output. If the membrane fouling can be quantified, it can be used as a tool to indicate the immersed membrane process's air-scouring efficiency.

4.2 Fouling quantification methods

Methods to quantify membrane fouling may either be direct or indirect. With direct fouling quantification an aspect of the fouling condition on the membrane is measured, whereas indirect fouling quantification refers to the measurement of a membrane fouling consequent as an indicator of the actual fouling behaviour. Naturally, direct fouling quantification is able to provide a membrane fouling diagnosis of far greater accuracy than indirect fouling quantification, but unfortunately the implementation thereof is usually limited by its costly, localised, invasive and sometimes even destructive nature. With indirect fouling quantification methods, on the other hand, it may be possible to obtain a fairly reliable, but inexpensive, indication of the fouling process as a whole in real-time without interfering in the filtration process. Accordingly, indirect fouling quantification is widely favoured as the method for long-term, continuous and holistic monitoring of membrane fouling.

Direct fouling quantification methods include the measurement of the cake layer thickness with light adsorption [Hamachi and Mietton-Peuchot, 1999, 2002], visual techniques [Chang et al., 2002] and ultrasound [Li et al., 2003], as well as the measurement of the cake layer mass by gathering and weighing cake after filtration experiments [Fradin and Field, 1999] or during membrane autopsies [Fane et al., 2000; Vrouwenvelder and Van der Kooij, 2001] and the use of thermogravimetric techniques [Tay et al., 2003].

For indirect fouling quantification researchers have mainly relied on the Darcian resistance model equation, as explained in Section 2.3.3, to predict the membrane fouling resistance [Kwon et al., 2000]. By using Equations 2.6 and 2.9, the microfiltration resistance model equation can be simplified to:

$$J = \frac{\Delta P}{\mu R_t} \quad (4.1)$$

where J = permeate flux (m/s)
 ΔP = transmembrane pressure (TMP) (Pa)
 μ = absolute viscosity of the fluid (Pa.s)
 R_t = total hydraulic resistance (m⁻¹)

Assuming the absolute viscosity of the fluid to be a constant, it is possible, by using Equation 4.1, to estimate the total hydraulic resistance from a single process variable. By setting the filtration

process at a constant permeate flux and measuring the TMP or filtrating at a constant TMP and measuring the permeate flux, the total hydraulic resistance, now the only unknown, can be calculated. The fouling hydraulic resistance is found by subtracting the clean membrane hydraulic resistance from the calculated process total hydraulic resistance (Section 2.3.3). Both TMP and permeate flux are easily measurable variables, hence the popularity of this fouling quantification technique.

Other indirect membrane fouling quantification techniques include the measuring of the decline in the feed's solids concentration [Kwon et al., 2000; McCarthy et al., 2002] and the use of fouling indices to indicate the membrane fouling potential [Rabie et al., 2001].

4.3 Flux-step method for indirect fouling quantification

In Section 4.1 it was hypothesised that an increase in the sparged air flow rate will increase the scouring ability of the air, thereby enabling the immersed membranes to filtrate at a low fouling rate. Although evidence exist in the literature that an increase in the air flow rate may not always affect the air's scouring ability (Section 4.1), and effectively reduce the air-scouring efficiency, it was decided to investigate the influence of an increasing air flow rate on an immersed flat-sheet membrane's fouling rate. As a first approach the indirect fouling quantification technique, the flux-step method, was used for its simplicity and holistic fouling indication. In addition, the flux-step method has been widely used and is regarded as a reliable technique to quantify membrane fouling propensity [Bouhabila et al., 1998; Defrance and Jaffrin, 1999a; Tardieu et al., 1999; Guibert et al., 2002; Le-Clech et al., 2003a, 2003b; Wu et al., 2008b].

4.3.1 Background

The flux-step method uses Equation 4.1 and the critical flux concept, as explained in Section 2.4.3, to characterise a membrane system's ability to resist fouling. The membrane system's permeate flux is incremented with an arbitrary chosen constant at constant time intervals while the resulting TMP is recorded as an indication of the change in the total hydraulic resistance. Figure 4.1 shows the typical TMP results of a flux-step experiment where the permeate flux was incremented from below critical flux to above critical flux.

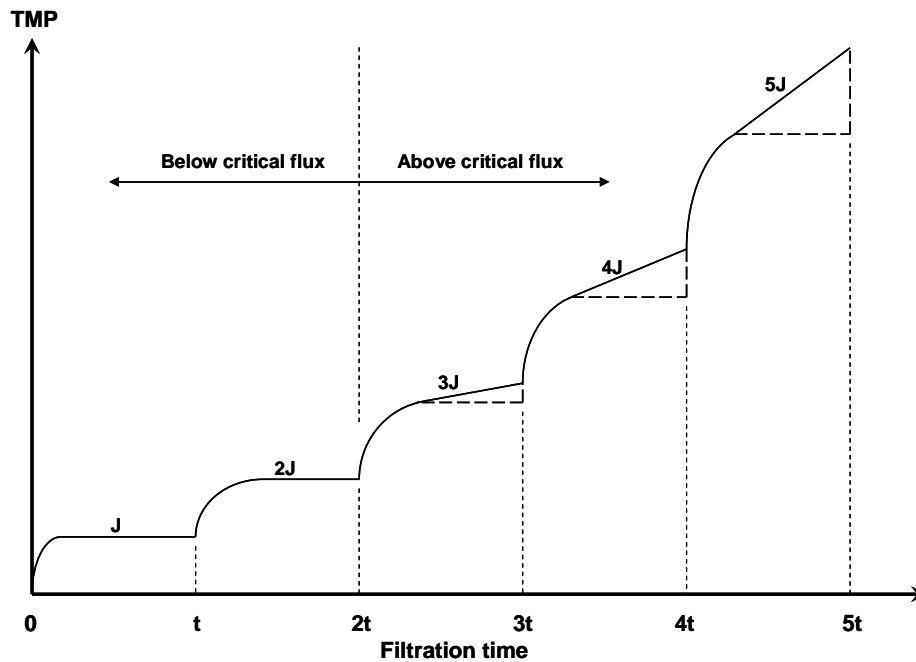


Figure 4.1: The typical TMP profile of a flux-step experiment where the permeate flux was incremented five times with an arbitrary chosen permeate flux J from below critical flux to above critical flux at a time increment of t . In this case a permeate flux of $2J$ was still below the critical flux, whereas a permeate flux of $3J$ was above the critical flux with a resulting continued increase in TMP.

Internal fouling is the only possible fouling mechanism if the initial permeate fluxes are below the critical flux and the total hydraulic resistance will therefore rise sharply, but quickly attain an equilibrium value after the permeate flux is stepped up each time. The TMP will concomitantly exhibit the same behaviour as predicted by Equation 4.1 for constant permeate flux filtration and stabilise at a constant value. However, when the permeate flux is incremented to a value above the critical flux for the system, cake layer formation commences and continues to increase the total hydraulic resistance (Section 2.3). To achieve a constant permeate flux, the compensating TMP also has to increase continuously at a constant rate [Tardieu et al., 1998, 1999; Ghosh, 2002; Guibert et al., 2002].

From Figure 4.1 it can also be seen that the successive permeate fluxes above the critical flux reveals increasing rates of TMP growth. Stabilised TMP growth is obtained once the TMP rate of change has reached a constant value and occurs when cake layer formation becomes the resistance limited process (Section 2.3.3). Mathematically the stabilised TMP profile for Figure 5.1 can be explained as:

$$\left(\frac{\partial TMP}{\partial t}\right)_J = \left(\frac{\partial TMP}{\partial t}\right)_{2J} = 0 \quad \text{for the sub-critical fluxes } J \text{ and } 2J; \text{ and as}$$

$$0 < \left(\frac{\partial TMP}{\partial t}\right)_{3J} < \left(\frac{\partial TMP}{\partial t}\right)_{4J} < \left(\frac{\partial TMP}{\partial t}\right)_{5J} \quad \text{for permeate fluxes of } 3J, 4J \text{ and } 5J.$$

The critical flux of a membrane system can be estimated from a graph of the stabilised rates of TMP increase plotted against the associated permeate fluxes. The permeate flux at which the stabilised rate of TMP increase changes from zero to a positive value indicates the critical flux. See Figure 4.2, which uses the hypothetical stabilised rates of TMP increase derived from Figure 4.1 to estimate the critical flux.

The smaller the permeate flux increments the more accurate the critical flux estimation. It is also important to keep the periods between permeate flux increments long enough to ensure that internal fouling has stabilised, thereby eliminating its influence on the rate of TMP increase.

Once the critical fluxes for different sparged immersed membrane systems have been determined, they can be compared to establish which system is better designed or operated to achieve superior air-scouring of the membrane surfaces. The higher the critical flux of a membrane system, the better the air-scouring for improved back-transport and the less susceptible the membrane is to membrane fouling.

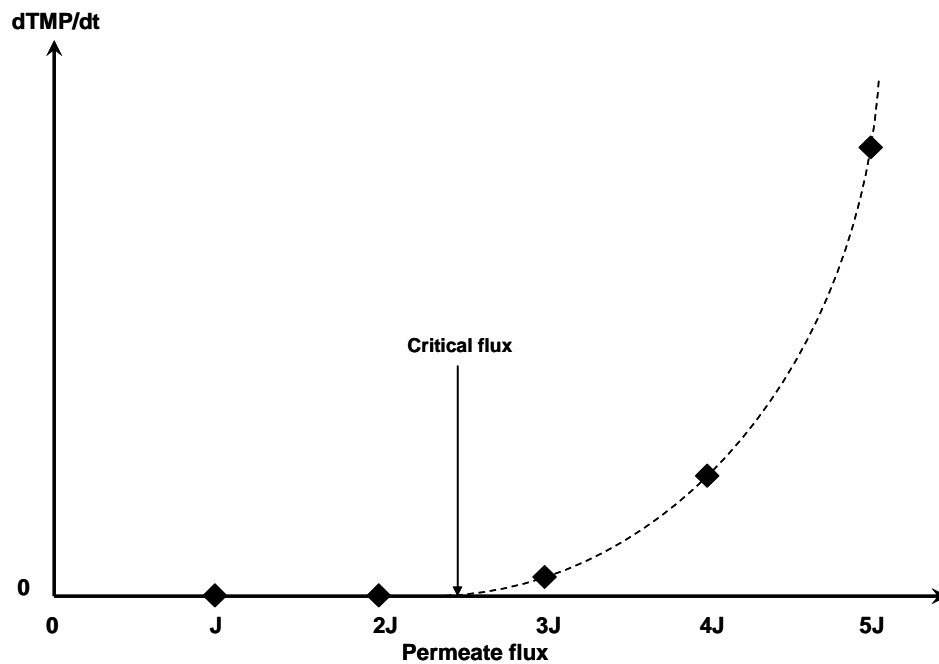


Figure 4.2: The rates of stabilised TMP increase of each permeate flux increment as derived from the typical TMP profile of a flux-step experiment as shown in Figure 4.1. The critical flux is found where $dTMP/dt$ changes from zero to a positive value, which in this case, lies between the flux-step experiment's second and third permeate flux increment.

4.3.2 Experimental set-up

An airlift reactor design, as explained in Section 3.3, was adopted for this flux-step study to determine the effect of air flow rate on the sparged air's ability to scour immersed membranes. Only a single flat-sheet membrane element was immersed and studied in the airlift reactor. With the reactor walls close to the membrane element the set-up represented the basic unit of a membrane module consisting of several flat-sheets [Ozaki and Yamamoto, 2001]. The air-scouring and fouling behaviours observed on the flat-sheet will therefore predict the behaviours found in a module of similar flat-sheet membranes immersed in a scaled-up airlift reactor. The experimental set-up for the flux-step experiment is shown in Figure 4.3.

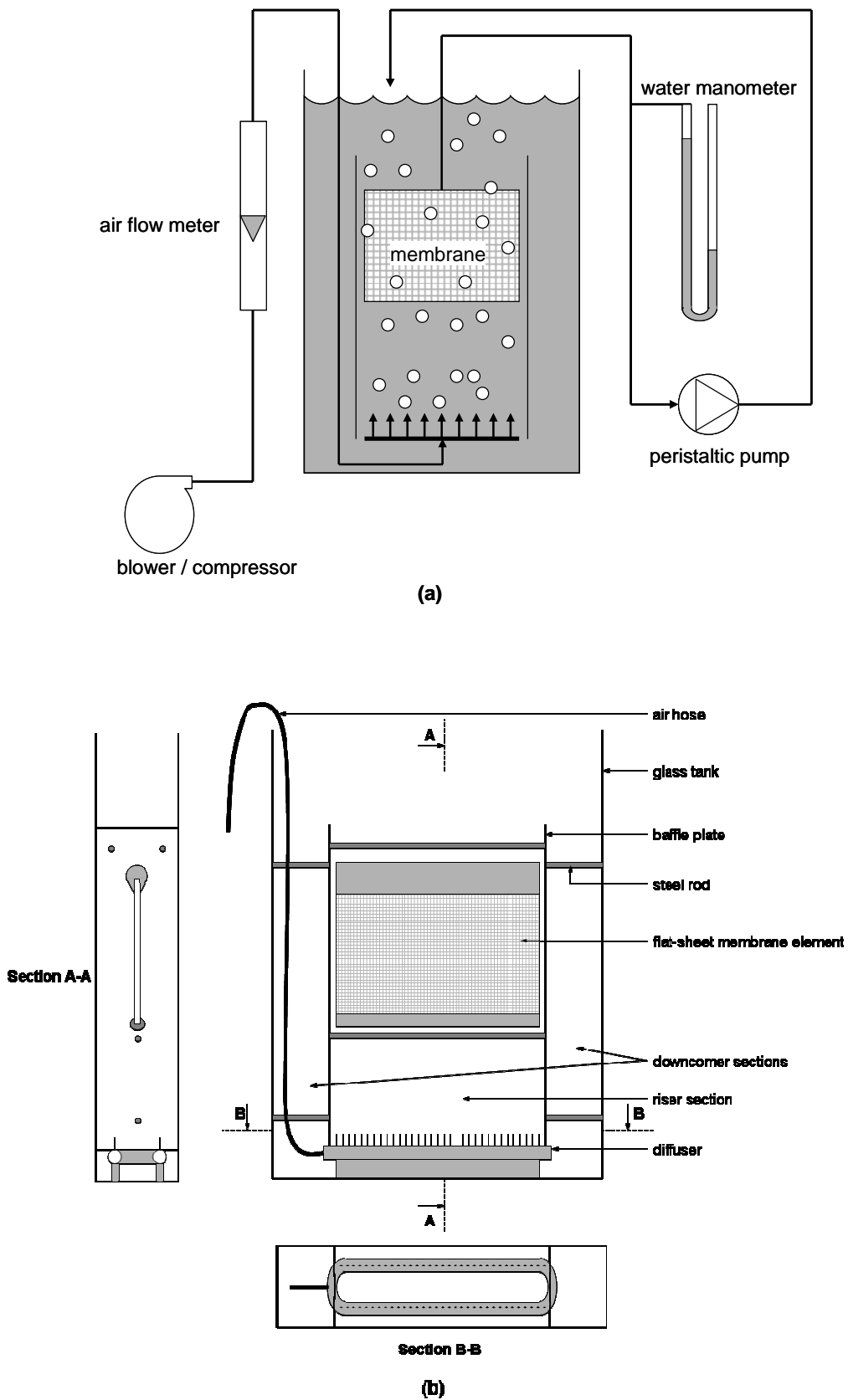


Figure 4.3: Set-up for the flux-step experiment: (a) main equipment and (b) detail of airlift reactor.

The flat-sheet membrane element used in this study was fabricated according to the method explained in Addendum B and had a total active surface area of 0.12 m². The membrane element was firmly secured inside a framework of two Perspex baffle-plates and seven steel rods. The framework, containing the membrane element, fitted tightly into a rectangular glass tank, and the baffle-plates divided the tank into a riser and two downcomer sections. The resulting airlift reactor had a cross-sectional downcomer area to riser area (A_d/A_r) ratio of 0.31. The membrane element was located in the riser and occupied the width of the riser. A double-pipe diffuser was located at the bottom of the tank and stretched the width of the riser. With the baffle-plates resting on the diffuser, it was unable to move during operation and could therefore provide a stable hydrodynamic field for the duration of an experimental trial. Equal size bubbles were obtained by fitting the diffuser with 0.6 mm inner diameter capillary membrane stubs from where the air could escape.

The airlift reactor was filled with a model foulant of ocean bentonite suspended in RO water. For each trial a fresh batch of 60 L suspension was prepared, as explained in Addendum A, with a bentonite concentration of 1.0 g/L.

A very steady air flow was fed to the diffuser at the bottom of the airlift reactor by a blower for relative low air flow rates. Unfortunately the blower was unable to deliver the required higher air flow rates at this high static head of 870 mm water and a compressor, although providing a fluctuating air flow, had to be used. The supplied air flow rate was measured with an air flow meter. A variable speed peristaltic pump, connected to the immersed flat-sheet membrane element, produced the necessary constant permeate flux. The TMP created was measured with a water-filled manometer. Pressure fluctuations caused by the operation of the peristaltic pump was assumed to be negligible in destabilising the concentration boundary layer at the membrane surface, since the deviation was less than 1% of the measured TMP. The permeate was pumped back to the tank to operate at a bentonite concentration which was assumed to remain constant.

4.3.3 Method

The influence of the sparged air flow rate on the scouring ability was studied at three different aeration intensities in the riser. Aeration intensity is defined as the supplied air flow rate per cross-sectional riser area. The lowest aeration intensity was chosen where the supplied air flow rate was just sufficient to provide bubbling along the full length of the diffuser. The highest aeration intensity was set at a value that compares well and even exceeds the maximum aeration intensities used in similar studies by other researchers (Ueda et al. [1997] used 612 L/(m²·min); Liu et al. [2000] used 926 L/(m²·min); Bouhabila et al. [2001] used 60 L/(m²·min); and Shim et al. [2002] used

1 136 L/(m²·min)). An intermediate air flow rate was chosen for an intermediate aeration intensity. A summary of the three chosen aeration intensities is given in Table 4.1.

Table 4.1: The three chosen aeration intensities for the flux-step experiment. (Notice the relative large deviation in the compressor's air flow rate to achieve the high aeration intensity.)

	Equipment	Air flow rate (L/min)	Cross-sectional riser area (m ²)	Aeration intensity (L/(m ² ·min))
Low aeration intensity	Blower	6.0 ± 0.5	0.0516	110 ± 10
Intermediate aeration intensity	Blower	30.0 ± 0.5	0.0516	580 ± 10
High aeration intensity	Compressor	58.0 ± 8.0	0.0516	1 100 ± 160

These three aeration intensities were respectively used in three treatments, filtrating RO water only, as well as in three treatments with replication, filtrating the bentonite suspension. The experiment to quantify fouling at different air flow rates with the flux-step method therefore consisted of nine trials. These nine trials were conducted in a random order, as shown in Table 4.2, to reduce experimental error. No need existed to replicate the three treatments with RO water filtration, since, regardless of the aeration intensity, no fouling should occur and were therefore replicates per se.

Table 4.2: The random order in which the trials were conducted to minimise the risk of unknown influences on the results.

	RO water	Bentonite suspension (1.0 g/L)
Low aeration intensity	1	2, 8
Intermediate aeration intensity	7	3, 4
High aeration intensity	5	6, 9

For each treatment, subjected to a certain aeration intensity, the permeate flux was incremented with 5 L/(m²·h) from an initial permeate flux of 5 L/(m²·h) to a permeate flux of 25 L/(m²·h). Each permeate flux was maintained for a period of two hours to ensure that internal fouling has

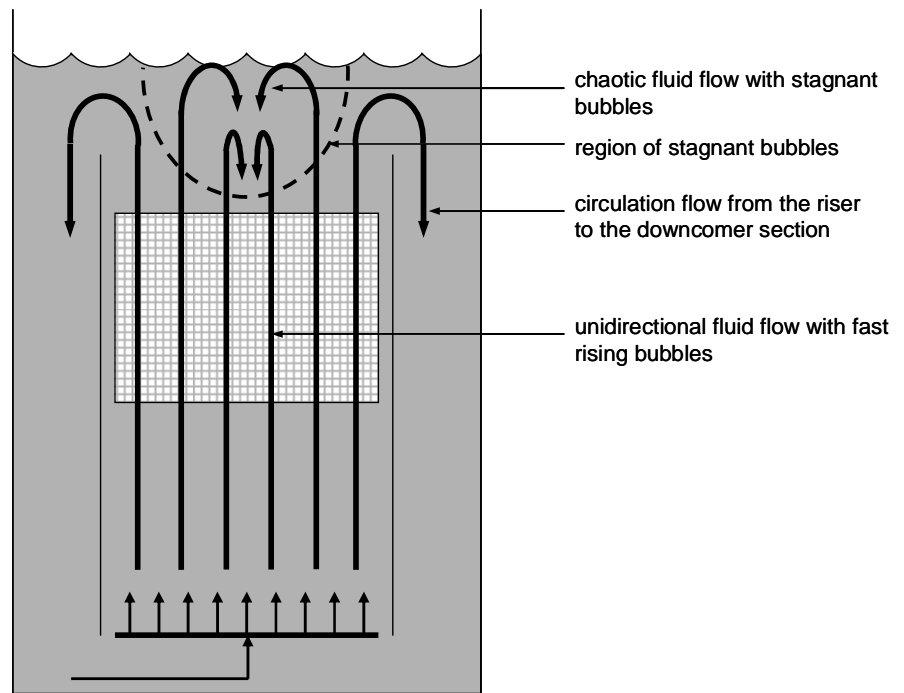
stabilised and that any subsequent fouling could be attributed to cake layer formation alone. During these two hour periods the TMP was regularly recorded and the permeate flux, air flow rate and suspension temperature measured to confirm they stay relatively constant. The permeate flux did not vary more than $0.8 \text{ L}/(\text{m}^2 \cdot \text{h})$ from the intended permeate flux and the treatments were conducted at suspension temperatures of $20 \pm 3^\circ\text{C}$.

A simple backwash procedure, prior to an experimental trial, proved to be adequate in restoring the original hydraulic resistance of the membrane, therefore removing all particles within, as well as on the membrane surface.

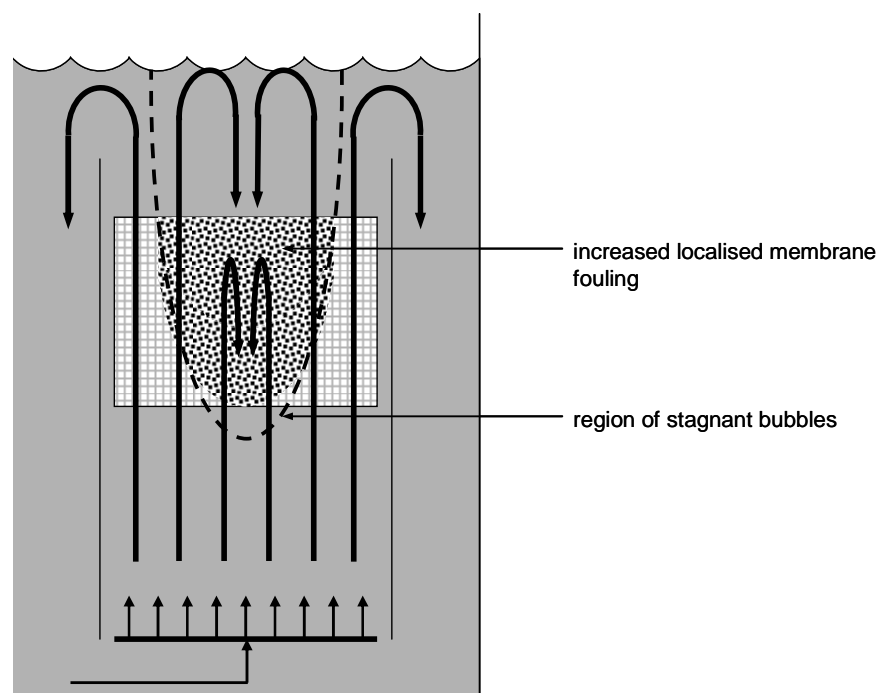
4.3.4 Results

An interesting visual observation was made from the three treatments in the flux-step experiment. With each treatment a region of trapped air bubbles was observed in the riser section. The bubbles trapped in this region moved in short erratic distances and were therefore not truly stagnant, but compared to the fast and unidirectional rising of the bubbles outside of this region, they appeared very stagnant. In the treatment with the low aeration intensity this region of fairly stagnant bubbles was located at the top of the riser section, but as the aeration intensity was increased, the region grew towards the bottom of the riser section. This phenomenon is depicted in Figure 4.4.

As described in Section 3.3, an increase in the air flow will lead to an increased air holdup in the riser section and therefore an increased difference in density between the riser and the downcomer sections with a consequent higher liquid circulation velocity. But as the liquid circulation velocity increases, more air bubbles are entrained into the downcomer sections, and when the downward liquid velocity exceeds the rise velocity of the air bubbles in the downcomers, the air holdup in the downcomer sections starts to increase. At this critical circulation velocity the difference in density between the riser and downcomer sections, the driving force for the circulation, starts to diminish to the extent that any further increases in the air supplied to the riser section will lead to very little to no increases in the induced liquid circulation velocity [Couvert et al., 1999, 2001]. But except for the induced circulation, water is also transported to the top of the riser section through the drag of the rising air bubbles. Therefore, at high air flow rates supplied to the riser section and a consequent relative low liquid circulation velocity, the resistance for the water to enter the downcomer sections becomes too high and a portion of the water starts to circulate from the top towards the bottom of the riser section. This downward flow of circulating water in the riser section force balances the rising bubbles – therefore the visual effect of a region of trapped and stagnant bubbles in the riser section.



(a) Relative low aeration intensity



(b) Relative high aeration intensity

Figure 4.4: The presence of a region of stagnant bubbles in the riser section during aeration. This region promotes localised fouling where it crosses the immersed membrane.

For the low and intermediate aeration intensity treatments of this experiment the region of stagnant bubbles was located above the immersed membrane in the riser section (Figure 4.4(a)). The fluid flow across the membrane surface was unaffected by the circulation of water inside the riser section and was therefore fast and unidirectional. This improved the scouring ability of the sparged air and allowed for uniform membrane fouling.

However, for the high aeration intensity the region of stagnant bubbles grew towards the bottom of the riser section as a result of increased circulation inside the riser section (Figure 4.4(b)). The region even crossed the immersed membrane and therefore affected the fluid flow behaviour across the membrane surface. Across the edges of the membrane the fluid flow was very fast and unidirectional, but across the middle, which was situated in the region of stagnant bubbles, the fluid flow was slow and chaotic. The scouring ability of the slow moving bubbles in this region was very poor, since, visually it seemed as if all the membrane fouling occurred where the region of stagnant bubbles crossed the membrane surface. With the whole membrane surface subjected to a constant permeate flux, the region of stagnant bubbles, unable to remove particles from the membrane surface, will actually promote localised membrane fouling.

In the flux-step experiment the rate of membrane fouling is manifested in the increase of TMP with time ($dTMP/dt$). During the flux-step experiment, the TMP data of only the last hour of each two hour permeate flux period was used to determine the fouling rates. This was to ensure that the calculated fouling rates accounted for cake layer formation only. The TMP increase for each permeate flux at each of the three aeration intensities was therefore found to be a linear function with time, since fouling rate is a constant when cake layer formation is the only fouling mechanism. These derived fouling rates are represented in two ways in Figures 4.5 and 4.6. The three aeration intensity treatments were replicated and the deviation shown in Figures 4.5 and 4.6. Experimental data can be found in Addendum C.

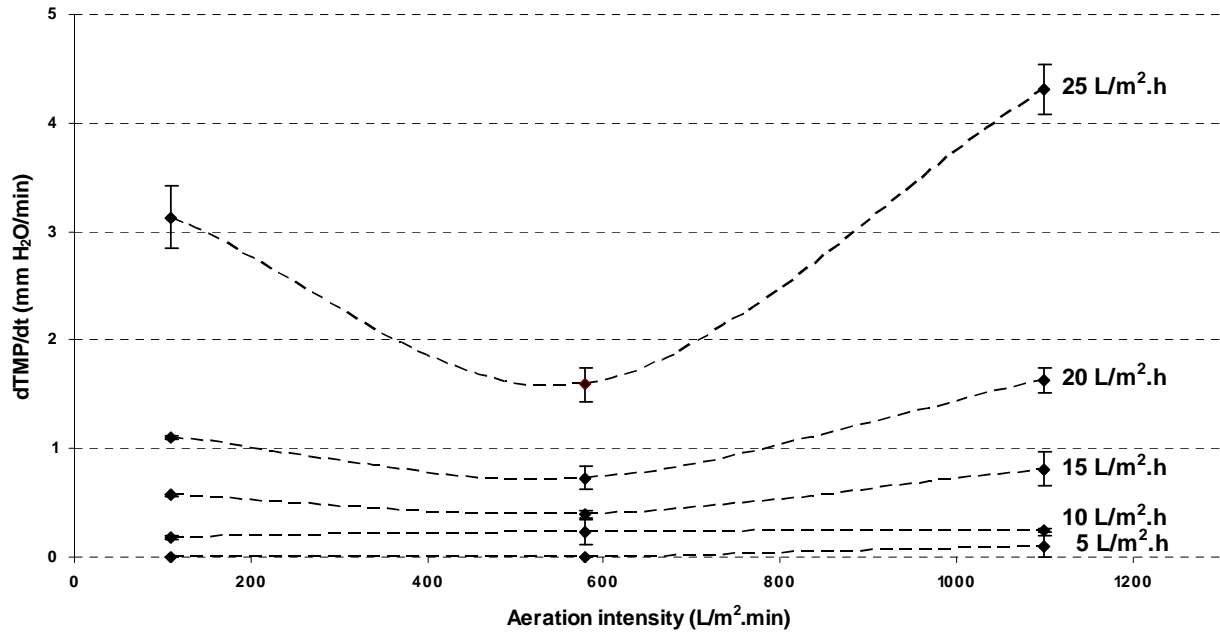


Figure 4.5: Membrane fouling rate at different aeration intensities. The intermediate aeration intensity (580 L/(m².min)) produced the highest scouring ability. Between an aeration intensity of 580 and 1 100 L/(m².min) the region of stagnant bubbles develop to cross the immersed membrane and promote localised fouling.

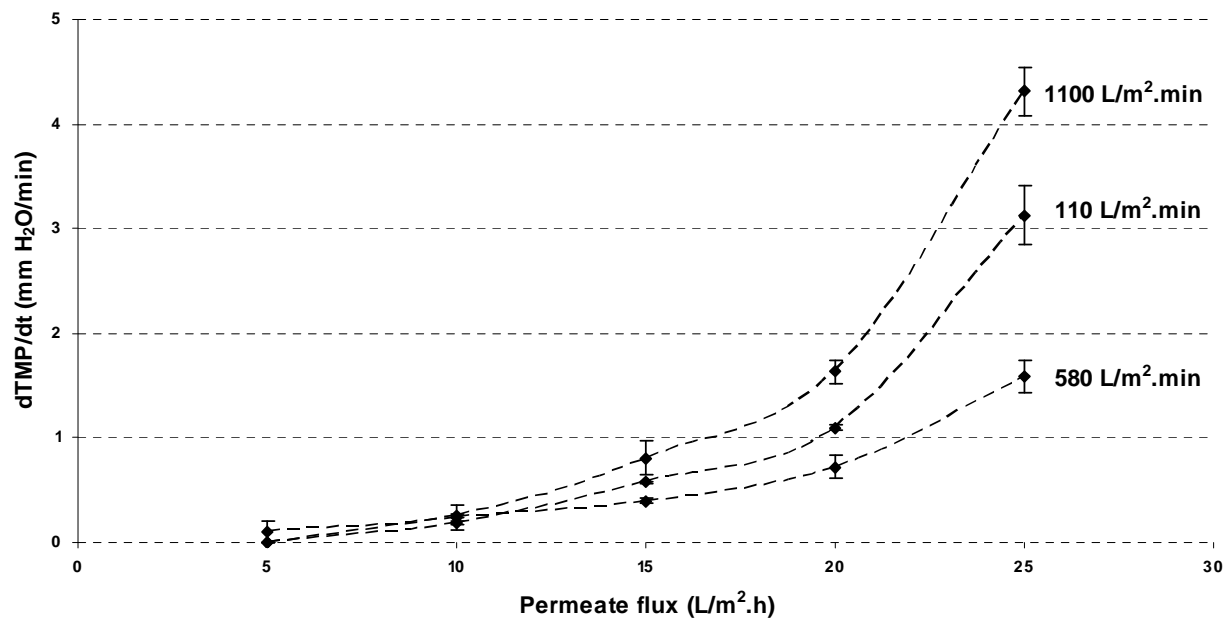


Figure 4.6: Membrane fouling rate at different permeate fluxes. An increase in the permeate flux will lead to an increase in the fouling rate (dTMP/dt), if above the critical flux. However, at the correct aeration intensity the fouling rate at any permeate flux can be greatly reduced. Under and over aeration may accelerate the fouling rate as is shown in this graph.

For the configuration used in this flux-step experiment, it can be seen from Figures 4.5 and 4.6 that an increase in the aeration intensity from 110 L/(m²·min) to 580 L/(m²·min) increased the scouring ability of the sparged air and reduced the fouling rate. It is also evident that sub-critical flux operation was achieved for this configuration at a permeate flux of 5 L/(m²·h) at aeration intensities of 110 L/(m²·min) and 580 L/(m²·min). However, when the aeration intensity was increased from 580 L/(m²·min) to 1 100 L/(m²·min), the fouling rate for each flux increased. Even the critical flux was reduced to a value below 5 L/(m²·h). This paradoxical decrease in scouring ability with an increase in aeration intensity can be explained by the formation of a region of stagnant bubbles that encompassed a significant portion of the immersed membrane.

4.4 Ultrasound for direct fouling quantification

In Section 4.3.4 it was showed that by increasing the aeration intensity, in an attempt to improve the scouring ability of the sparged air, that, on the contrary, the membrane fouling rate might be increased. In this case the increased aeration intensity produced a hydrodynamic stagnant region in the riser section of the airlift reactor which promoted localised fouling where it crossed the membrane element. It is therefore important to understand the system hydrodynamics in an airlift reactor, since this will dictate the scouring ability of the sparged air and the consequent fouling behaviour of the immersed membrane system. Section 3.3.1 lists that both sparged air flow rate (aeration intensity) and reactor geometry determine the system hydrodynamics in an airlift reactor.

The flux-step method used in Section 4.3 indicated the effect of aeration intensity on the overall membrane fouling rate, but being an indirect fouling quantification method, was not able to correlate the aeration intensity with the visually observed localised bentonite deposition. However, realising the presence of complex hydrodynamic fields in an airlift reactor from this experiment, it was felt that the use of a direct fouling quantification method would add more value if the influence of reactor geometry on the membrane fouling behaviour was also investigated. A direct fouling quantification method would be able to measure the fouling profile across the membrane surface, which would describe the reigning system hydrodynamics as created by the reactor geometry.

It was decided to use an ultrasonic technique, ultrasonic time-domain reflectometry (UTDR), as the direct fouling quantification method to investigate the influence of the airlift reactor geometry on the fouling of an immersed membrane. UTDR enables the measurement of fouling layer thickness in real-time, in a non-destructive and non-invasive manner [Peterson et al., 1998; Mairal et al., 1999; 2000; Xu et al., 2009]. These qualities made UTDR very favourable, compared to other direct fouling quantification methods, since it allowed for the monitoring of fouling layer growth during membrane filtration and the repeated use of the same membrane. Unfortunately the technique is limited by its localised nature and therefore requires several trials at different locations to provide for a fouling profile.

4.4.1 Background

When ultrasonic wave energy propagates through a composite structure of material layers with different acoustic impedances, a portion of the energy will be reflected and the remaining energy

will be transmitted at each successive media interface. The acoustic impedance of a medium is defined as [Li et al., 2003]:

$$W = V_m \rho \quad (4.2)$$

where W = acoustic impedance (kg/s.m²)
 V_m = sound velocity in medium (m/s)
 ρ = medium's density (kg/m³)

The proportioning of the reflected and transmitted wave energy at each interface will be dependent on the relative acoustic impedances of the media at the interface. Consider from material 1 an incident ultrasonic wave normal to the interface between material 1 and material 2. The ratio of the reflected wave amplitude to the incident wave amplitude is then given as [Koen, 2000a]:

$$C_r = \frac{W_2 - W_1}{W_2 + W_1} \quad (4.3)$$

where C_r = ratio of reflected wave amplitude to incident wave amplitude
 W_1 = acoustic impedance of material 1 with incident wave (kg/s.m²)
 W_2 = acoustic impedance of material 2 with transmitted wave (kg/s.m²)

Therefore, if material 2 has a greater acoustic impedance than material 1, the ratio C_r will be positive, indicating that the reflected wave will be in phase with the incident wave. Conversely, if the acoustic impedance of material 2 is less than the acoustic impedance of material 1, the consequent negative value of C_r indicates that the reflected wave is out of phase with the incident wave. Important though, is to realise that the larger the difference in the acoustic impedances of the two materials, the higher the proportion of reflected energy at the interface will be, regardless of being in or out of phase with the incident wave.

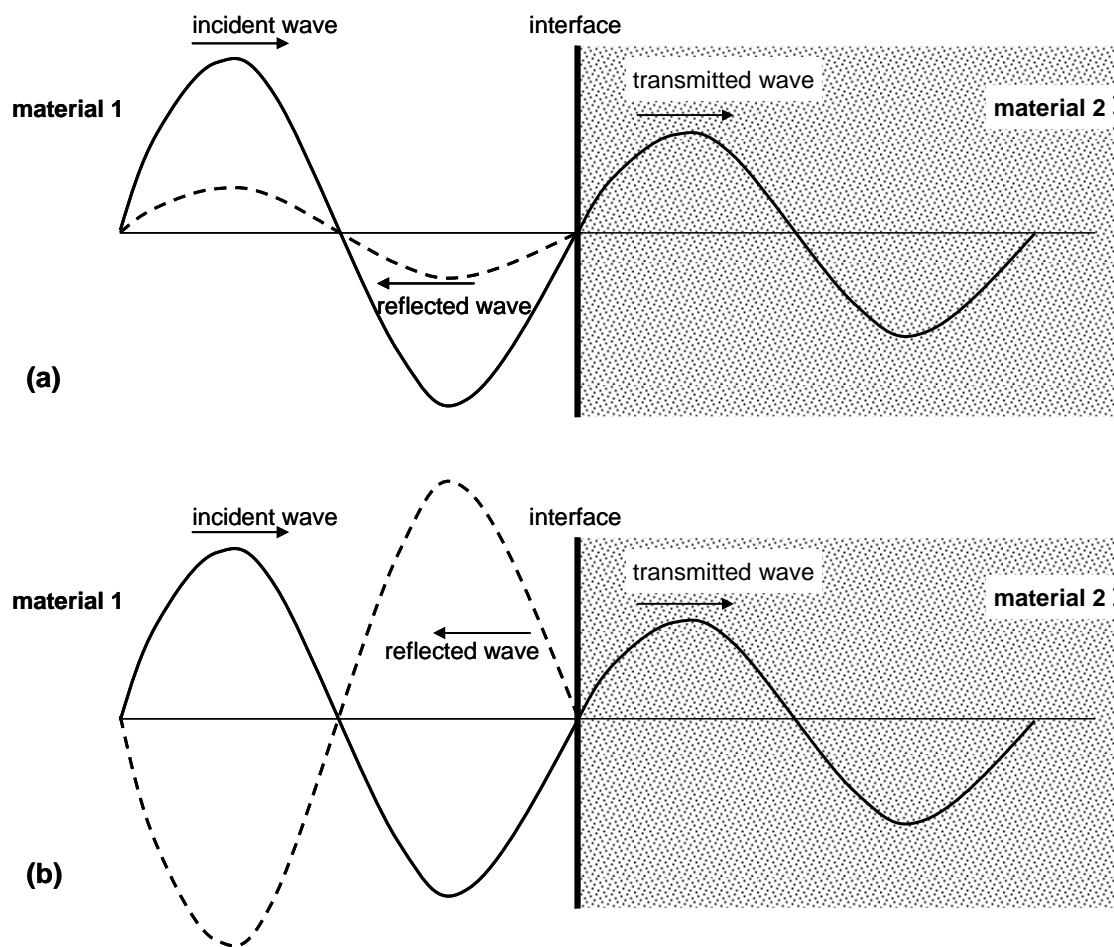


Figure 4.7: Reflection of wave energy at media interfaces. Two cases are shown here: (a) material 2 has a higher acoustic impedance than material 1, but the difference is slight to produce a low energy reflected wave in phase with the incident wave; (b) material 2 has a lower acoustic impedance than material 1 and the difference is significant to produce a high energy reflected wave out of phase with the incident wave.

Equation 4.3 only applies for the case when an ultrasonic wave arrives normal to an absolutely perfect media interface without any scattering, attenuation or any other form of energy dissipation at the interface. Accordingly, Equation 4.3 cannot be used for an accurate prediction of the reflected wave energy, but was given here to highlight the role of an acoustic impedance difference at a media interface on the reflection of wave energy.

The technique of UTDR relies on this phenomenon of wave energy reflection at interfaces of acoustic impedance changes to measure material thicknesses and to differentiate between media along the propagation direction in a composite system. With UTDR it is possible to detect the commencement of a fouling layer on the membrane surface when ultrasonic wave energy is reflected at the surface of the new fouling layer – a new media interface. The fouling layer growth

is measured with the increase in travelling time between the reflected wave energy from the fouling layer surface interface and the reflected wave energy from the fouling layer/membrane surface interface. The utilisation of UTDR to detect and measure the fouling layer thickness on an immersed membrane is explained in Figure 4.8.

As shown in Figure 4.8, a transducer is used to convert a generated electrical signal into an ultrasonic pressure signal and to emit the ultrasonic waves onto the immersed membrane. The reflected ultrasonic waves are also received by the transducer and converted into an electric signal which can be displayed on an oscilloscope. The interpreted electric signal is represented as a waveform of amplitudes against their arrival times. This indicates the amount of wave energy that is reflected at each media interface and the total travel time of the ultrasonic waves from the transducer to the respective interfaces and back to the transducer.

Consider Figure 4.8(a), showing a clean immersed membrane before filtration has started. Ultrasonic waves propagate from the transducer through the water in which the membrane is immersed to meet the clean membrane, the first difference in media density, at the water/membrane interface, A. A fraction of the sent energy is reflected from the interface, received again by the transducer, converted and displayed as peak A of a waveform on the oscilloscope. The remainder of the energy continues to propagate through the membrane to meet the membrane/water interface B where, again, a certain fraction of the energy of incidence is reflected to produce peak B of the displayed waveform. In this case, although the change in impedance at the two interfaces is the same, the difference in amplitude value between peaks A and B is ascribed to the difference in the available incidence energy at each interface.

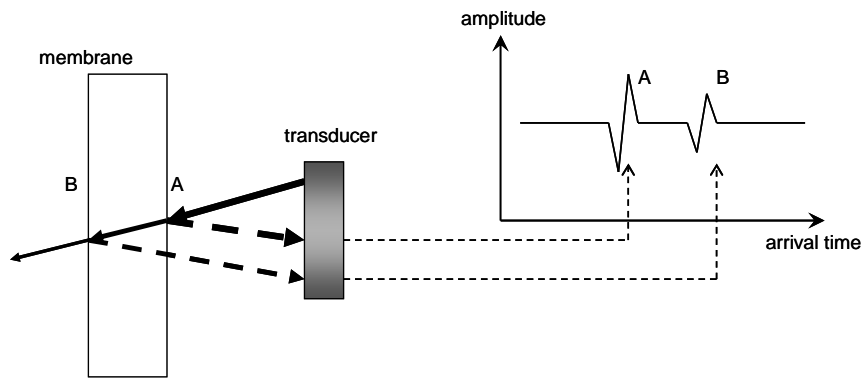
In Figure 4.8(b) the filtration was started and particles have just started to group on the membrane surface to form the first traces of a cake layer. But, as mentioned in Section 2.3, internal fouling is a rapid fouling mechanism and dominates in the early stages of filtration. Therefore, before the proper commencement of a cake layer has started, internal fouling has already impregnated the outer layers of the membrane to solidify it to a certain extent and made it denser as well as smoother. Hence, as internal fouling leads to cake layer formation, the denser membrane surface represents an interface (A') of greater acoustic impedance change with a greater proportion of the incidence energy reflected. Also, the smoother surface means that less of the reflected waves are lost through scattering, but rather reflected back to the transducer. The increase in the reflected wave energy from this interface to the transducer is manifested in the amplitude increase at the arrival time correlating with interface A'. Since more wave energy is reflected at interface A', the transmitted wave energy is reduced and consequently the amount of wave energy to be reflected

at interface B' is also reduced. Therefore the decrease in the amplitude at the arrival time that correlates with interface B'.

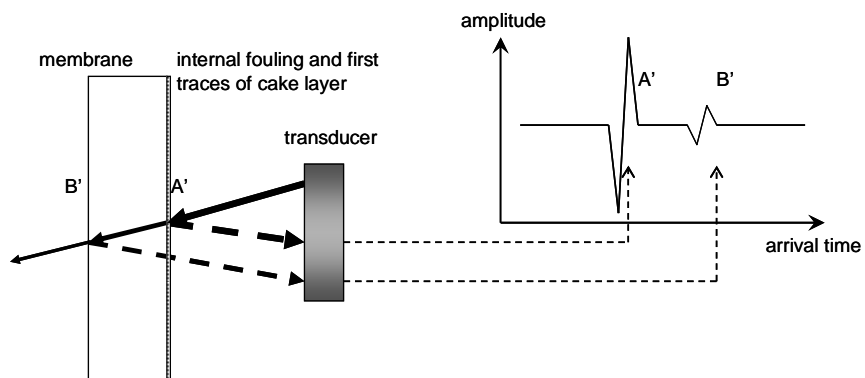
In Figure 4.8(c) membrane filtration has occurred for a significant time and a well established cake layer has formed on the membrane surface. Comparing the displayed waveforms of Figures 4.8(a) and 4.8(c), it can be seen that the presence of the cake layer has resulted in the appearance of a new peak C in the waveform with an earlier arrival time than the water/membrane surface interface A. Peak C represents the energy that is reflected from the new water/cake layer surface interface. The portion of the incident energy that is reflected from this new interface, and therefore the amplitude of peak C, will be determined by the density and the texture of the cake layer surface. The denser the cake layer and the smoother the cake layer surface the greater the portion of the incident wave energy that will be reflected at the water/cake layer surface interface [Koen, 2000b; Li et al., 2002b]. Again, as was the case with cake layer commencement shown in Figure 4.8(b), the subsequent interfaces will receive a reduction in incident wave energy, thereby reducing the wave energy that is reflected at each interface and consequently also the amplitudes of the waveform of the reflected energy. The new water/cake layer interface is closer to the transducer and hence the earlier arrival time of peak C. If the immersed membrane is static the time-domain positions of peaks A'' and B'' will stay unchanged, but the consequent growth in the cake layer will manifest in the movement of peak C to an earlier arrival time. The measured arrival time difference, Δt , between peaks C and A'' will therefore increase as the cake layer thickness increases. Given that the speed of sound through the cake layer is known, the measured arrival time difference between peaks C and A'' can be used to calculate the cake layer thickness with [Li et al., 2002a]:

$$\Delta S = \frac{1}{2} c \Delta t \quad (4.4)$$

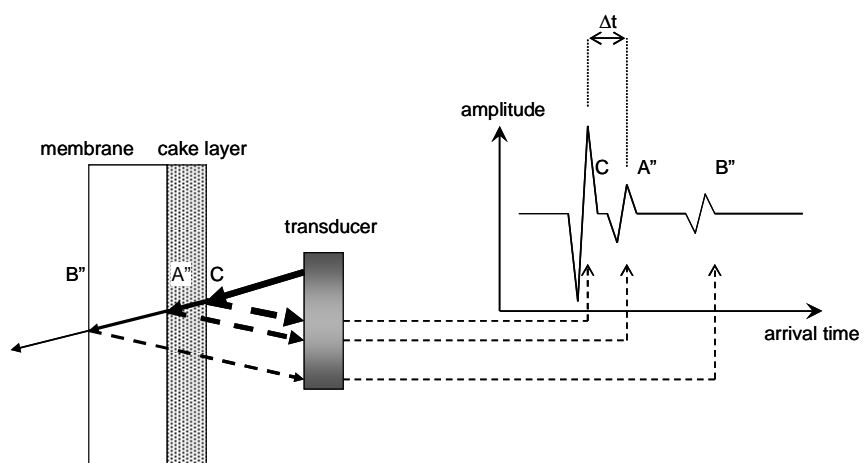
where ΔS = fouling layer thickness (m)
 c = speed of sound in the fouling layer (m/s)
 Δt = arrival time difference (s)



(a) clean membrane



(b) cake layer commencement



(c) cake layer growth

Figure 4.8: Hypothetical oscilloscope waveforms to explain UTDR for fouling quantification. (Notice that only one side of the immersed membrane was considered here.)

Although Figure 4.8 presents oversimplified and hypothetical waveforms, it serves to explain how the technique of UTDR is employed to measure fouling layer thicknesses. UTDR and its application to measure cake layer thickness were discussed here in a very concise and superficial manner; in just enough detail to allow for the comprehension of the experimental work to follow. The technique of UTDR to monitor membrane fouling is described in much greater detail elsewhere [Koen, 2000b; Li, 2002].

4.4.2 Experimental set-up

The experimental set-up for the direct quantification of immersed membrane fouling with UTDR was similar to the experimental set-up for the indirect fouling quantification as described in Section 4.3.2 and shown in Figure 4.3. The only differences were the addition of the ultrasonic measurement system, the study of airlift reactor geometries at three A_d/A_r ratios and the aeration intensity, as well as the permeate flux, set to constants of $1\,100 \pm 160$ L/(m²·min) and 15 ± 0.4 L/(m²·h) respectively.

Ultrasonic measurement system

The ultrasonic measurement system was the only new equipment that was added to the experimental set-up described in Section 4.3.2, and comprised of an ultrasonic transducer, a pulser/receiver, an oscilloscope, a computer and the connecting cables (Figure 4.9).

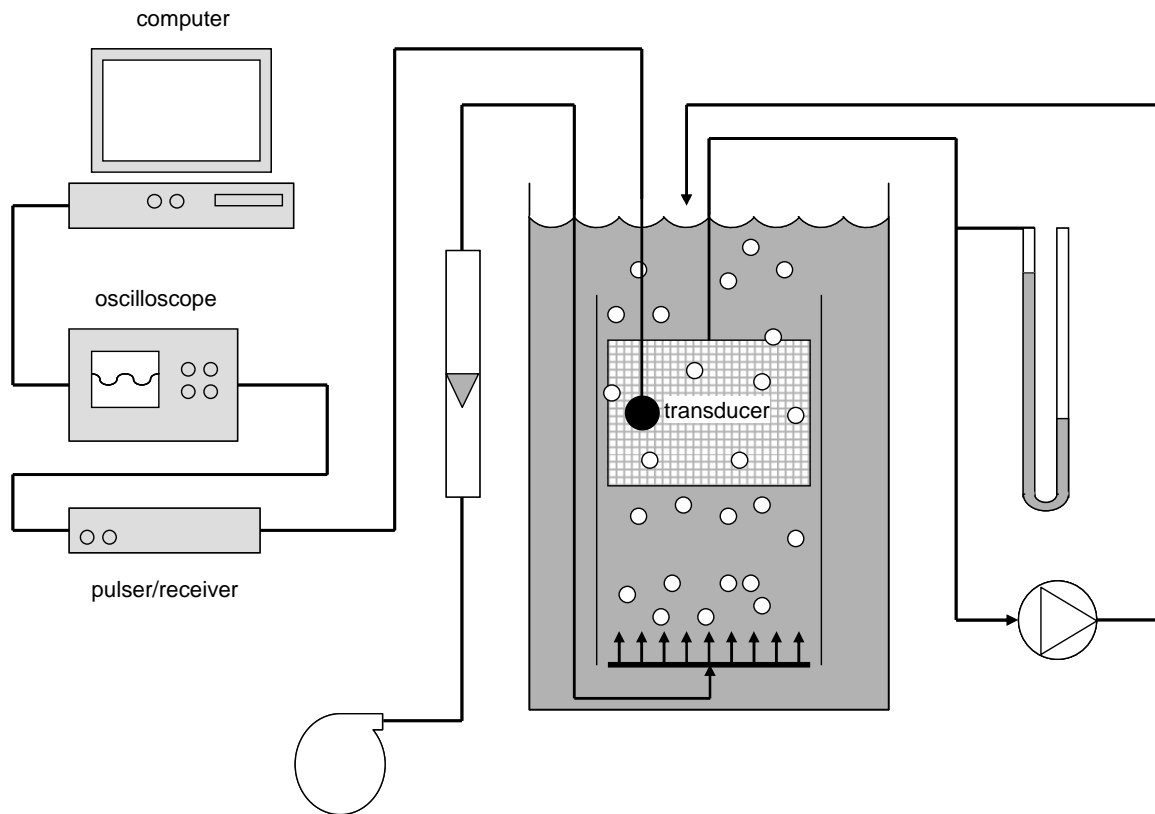


Figure 4.9: The experimental set-up for the UTDR experiment for the direct fouling quantification of immersed membrane fouling. Besides the ultrasonic equipment, the equipment set-up is identical to the equipment set-up described in Section 4.3.2 for the flux-step experiment.

In this study a Panametrics Videoscan ultrasonic transducer was used. The type of transducer to be used must be selected for its application. The transducer can either be selected to enhance the sensitivity or the resolution of the system [Koen, 2000b]. Low ultrasonic frequency transducers enhance the sensitivity of the system to enable it to detect density changes at various depths of the test material, as opposed to high ultrasonic frequency transducers that enhance the resolution of the system to enable it to finely discriminate between density changes near the surface of the test material. Therefore, the higher the frequency of the transducer, the better is the resolution, but with a decrease in penetration depth. For this study of fouling layer monitoring a set of ultrasonic transducers were evaluated, as shown in Table 4.3. The V120-RB 7.5 MHz transducer was found to be the best suited for this application, because it is capable of fairly high resolution at the membrane surface and with adequate sensitivity for the detection of density differences just beneath the membrane surface. The theoretical resolution of the V120-RB transducer in water is given as 48 μm . This is an indication of the smallest detail that can be detected by the transducer in water. The bentonite particle size distribution was measured, as shown in Addendum A, and it

was found that approximately 6% of the particles were larger than 48 μm with the 90th percentile of the particle size distribution at 41.78 μm . It was found that the relative small amount of particles larger than 48 μm did not add significant noise to the reflected energy.

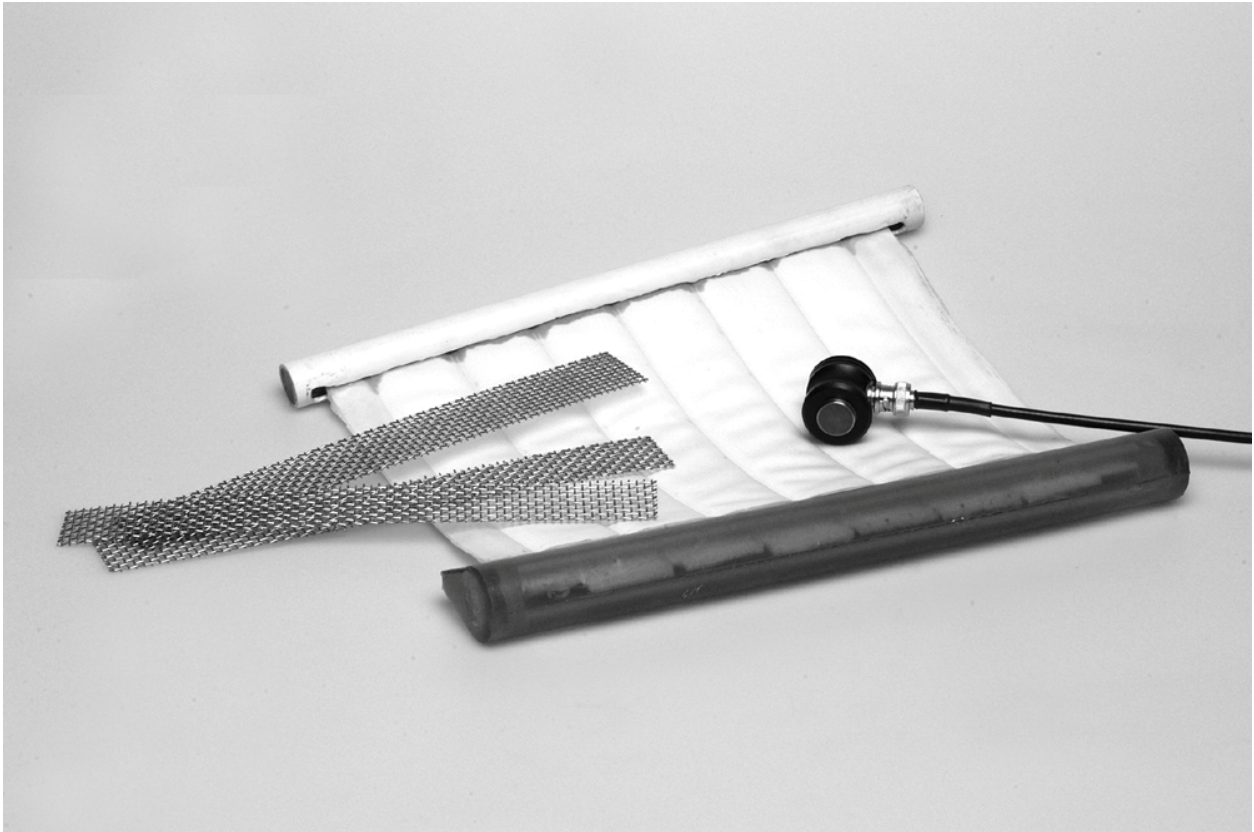


Figure 4.10: A photograph of one of the membrane elements that were used in the ultrasound experiment with its membrane spacer material and the Panametrics Videoscan V120-RB transducer.

Table 4.3: Panametrics Videoscan ultrasonic transducers that were evaluated for the monitoring of fouling layer formation [Koen, 2000b]

Transducer type	Frequency (MHz)	Resolution (μm)
V106-RB	2.25	159
V182-RB	3.5	102
V109-RB	5	72
V120-RB	7.5	48
V111-RB	10	36

The 7.5 MHz ultrasonic transducer was placed inside the riser section of the airlift reactor, as shown in Figure 4.11, so that the bentonite suspension was the only medium between the transducer and the membrane surface. The transducer was positioned to face the one side of the membrane element at halfway the depth of the flat-sheet membrane surface. The different membrane elements used in the experiment only differed with regards to their widths and were placed at the same depth in every trial to ensure that they were subjected to the same water head range (bottom to top of flat-sheet membrane surface). Consequently, the local TMP of the membrane surfaces monitored by the transducer all experienced the same water head contribution. The transducer and the membrane element were tightly secured to remain immovable during aeration. This enabled the transducer to detect the fouling process accurately with UTDR. The transducer was placed at a distance of between 20 mm and 30 mm from the membrane surface so as not to disturb the fluid-flow behaviour near the membrane surface. There was no need to ensure that the distance between the transducer and the membrane surface is the same for all the experimental trials; however, the distance between the transducer and the membrane surface had to remain constant for the duration of an experimental trial.

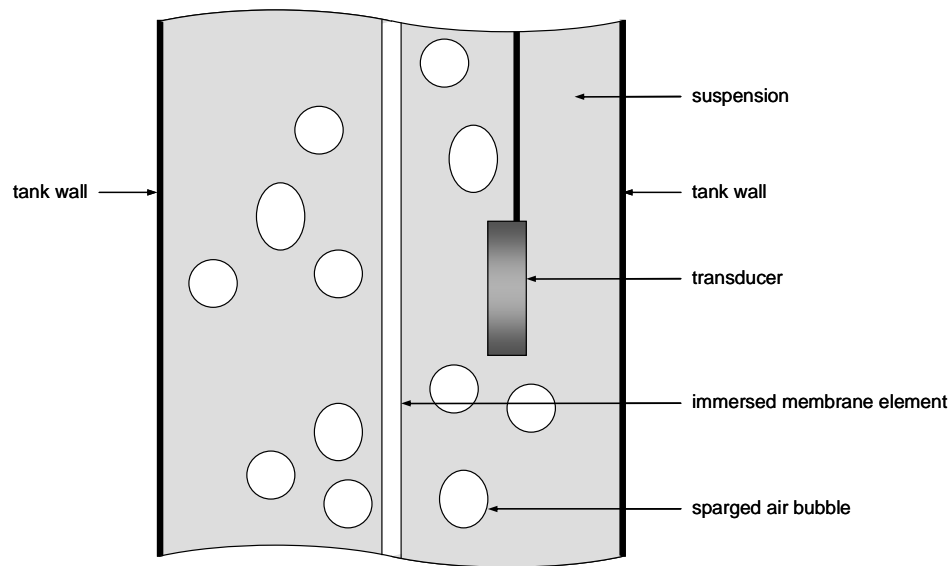


Figure 4.11: Section of the side view of the riser section to show the location of the immersed ultrasonic transducer. The transducer was positioned halfway the depth of the membrane element's flat-sheet surface.

The transducer was connected to a pulser-receiver (Panametrics 5058PR). The pulser-receiver is responsible for generating the high frequency signal, as well as receiving the converted reflected signal from the transducer. An oscilloscope (Hewlett Packard 54602B) was used to observe the reflected signal as a waveform which could be captured as 2 000 time-amplitude value pairs (4 000 data points) and stored on a computer's hard drive. The waveform data was saved in comma-separated (.CSV) form and could be opened in Microsoft Excel for further data processing.

Numerous experiments, together with the chosen 7.5 MHz ultrasonic transducer, were performed to determine the operating settings of the pulser-receiver which would provide for the most sensible visualisation of the reflected waveform on the oscilloscope.

The optimum operating settings of the pulser-receiver was found to be:

- an excitation pulse of 400 V;
- a pulse damping of 50 Ω ;
- with the internal trigger set at a repetition rate of 200 MHz;
- a receiver gain of 40 dB;
- a receiver attenuation of 25 dB;
- with echo pulses selected as normal (0°); and
- with the use of the 0.1 MHz high pass filter.

A_d/A_r ratios

The framework of two Perspex baffle-plates and seven steel rods, as mentioned in Section 4.3.2, could be adjusted by sliding the baffle-plates on the steel rods to create different A_d/A_r ratios inside the airlift reactor. Three A_d/A_r ratios of 0.31, 0.71 and 1.45 were created for this direct fouling quantification study. Since the flat-sheet membrane elements had to stretch the widths of the respective riser sections, a membrane element had to be fabricated for each A_d/A_r ratio airlift reactor, as explained in Addendum B. Except for the differences in the respective membrane elements' widths, the membrane elements all had the same dimensions. The riser and downcomer cross-sectional dimensions, as well as the dimensions of the active membrane area of the membrane element used for each A_d/A_r ratio are given in Table 4.4. Note that the active flat-sheet membrane widths are smaller than the respective occupied riser section widths. This is because the inactive tubes remain on the membrane elements' sides and the permeate collector (see Addendum B) require the remaining space in the riser sections. For each configuration a double-pipe diffuser, with 0.6 mm holes, was located at the bottom of the tank and stretched the width of the respective riser.

Table 4.4: The three airlift reactor geometries and the flat-sheet membrane sizes used in the UTDR experiment.

A_d/A_r ratio	Cross-sectional riser dimensions (mm)	Cross-sectional downcomer dimensions (mm)	Active flat-sheet membrane dimensions (mm)	Total active membrane area (m ²)
0.31	430 x 120	67 x 120	351 x 170	0.12
0.71	330 x 120	117 x 120	234 x 170	0.080
1.45	230 x 120	167 x 120	156 x 170	0.053

Constant aeration intensity

As discussed before, the system hydrodynamics are a function of the aeration intensity and the reactor geometry. A constant aeration intensity, therefore, had to be chosen if the influence of reactor geometry at different A_d/A_r ratios, as the only variable, on the system hydrodynamics were to be investigated. The aeration intensity was set to the highest value that was used in Section 4.3, namely 1 100 L/(m²·min). Although any arbitrary value could have been used for this experiment, this relative high aeration intensity was chosen to establish if the lower than expected scouring efficiency, as was observed in Section 4.3, could be improved by changing the airlift reactor geometry. Depending on the geometry that was investigated, either a compressor or a

blower was used to supply the necessary airflow. A compressor was used when the A_d/A_r ratio of 0.31 was investigated and a blower was used when A_d/A_r ratios of 0.71 and 1.45 were investigated. As explained in Section 4.3.2, the blower was unable to provide the relative high airflow needed to maintain the required aeration intensity at the given head for the large cross-sectional area of the riser section when an A_d/A_r of 0.31 was investigated. A compressor was consequently used with a fairly high deviation of 160 L/m²/min in the resulting aeration intensity. The blower was, however, quite capable of providing the necessary airflow to the smaller riser section geometries to maintain aeration intensities within 10 L/m²/min from the desired 1 100 L/m²/min.

Constant permeate flux

The reigning system hydrodynamics in an airlift reactor determine the scouring ability of the sparged air in the riser section as it sweeps across the immersed membrane surface. In other words, the system hydrodynamics influence the rate of back-transport of retained material from the membrane surface to the bulk. Conversely, the permeate flux determines the rate of material transported to the membrane surface. The net force is therefore manifested as the fouling behaviour of the membrane, and if the fouling behaviour is to be related to the geometry of the airlift reactor, it is imperative that the overall permeate flux is kept constant for comparison sake. The permeate flux was arbitrarily set to 15 ± 0.4 L/(m²·h), an intermediate value used in the flux-step experiment, as described in Section 4.3.

4.4.3 Method

The fouling profiles of the membrane elements used in each of the three airlift reactor geometries were generated by measuring the fouling with the UTDR technique at three locations across the membrane surface. The transducer was positioned to measure the fouling on the one side of the far left, middle and far right filter tubes of each membrane element. The experiment to directly quantify fouling in different airlift reactor geometries with the UTDR technique therefore consisted of nine trials. Each trial lasted 20 hours to ensure sufficient cake layer formation that could provide a sensible fouling profile across the membrane surface.

A simple backwash procedure, prior to an experimental trial, proved to be adequate in restoring the original hydraulic resistance of the membrane, therefore removing all particles within, as well as on the membrane surface. The clean backwashed membrane element was then fitted into a glass tank in the same manner as explained in Section 4.3.2 and the ultrasonic transducer located in the correct position as described in Section 4.4.2. The tank was then filled with RO water and permeation started at the constant flux of 15 ± 0.4 L/(m²·h), but without any aeration. This was

done in order to collapse the filter tubes to present a compressed and steady membrane element to the transducer; providing the reference state of the membrane surface before membrane fouling has commenced. With the membrane element compressed, the transducer was slowly rotated in the horizontal to find the position where it received the strongest reflected signal as viewed on the oscilloscope. The transducer would be tightly set once the point of maximum wave energy reflection has been found. In this position the transducer's surface would be parallel to the compressed membrane surface. The received waveform was saved on the computer hard drive as the reference signal to which the signal of the fouled membrane would be compared.

When the permeation was stopped, the membrane element's filter tubes would relax and slowly expand to a fraction of its original volume before permeation, but on re-commencement of permeation the membrane would quickly assume the stable compressed form and reproduce the reference waveform on the oscilloscope. With permeation still stopped, the fouling agent, a suspension of bentonite in RO water, was then added to the tank to create a particulate suspension. For each trial a fresh batch of 60 L suspension was prepared, as explained in Addendum A, with a bentonite concentration of 1.0 g/L. Aeration of the tank at the chosen constant aeration intensity was subsequently started to ensure a homogeneous suspension. The preparation for a UTDR trial was completed now and permeation could recommence.

Permeation was maintained at $15 \pm 0.4 \text{ L}/(\text{m}^2 \cdot \text{h})$ for all trials, while air was supplied to the specific geometry to produce an aeration intensity of $1\ 100 \pm 160 \text{ L}/(\text{m}^2 \cdot \text{min})$. When sampling the reflected ultrasonic signal from the membrane surface, the aeration was momentarily stopped (less than 10 s), while permeation was allowed to continue. Without the interference of the bubbles the transducer was able to receive a clear reflected ultrasonic signal. If the permeation were stopped during the sampling process the membrane would relax, creating an uneven surface with increased scattering of the reflected signal, thereby complicating data interpretation. It was assumed that the increased fouling in the brief absence of aeration was negligible. Sampling was conducted at suspension temperatures of $25 \pm 2^\circ\text{C}$.

4.4.4 Results

Reflected waveforms

In this UTDR investigation the fouling layer was not found to be a clearly defined layer on the membrane surface with a uniform density, but rather a transition from concentration polarisation to an external cake layer to internal fouling. A differential waveform, which is the difference between the test waveform and the initial reference waveform, was therefore employed to highlight any

density changes [Li et al., 2002a]. These density changes could again indicate the fouling mechanisms that were occurring. In Figure 4.12 real and typical waveforms obtained during the study are shown.

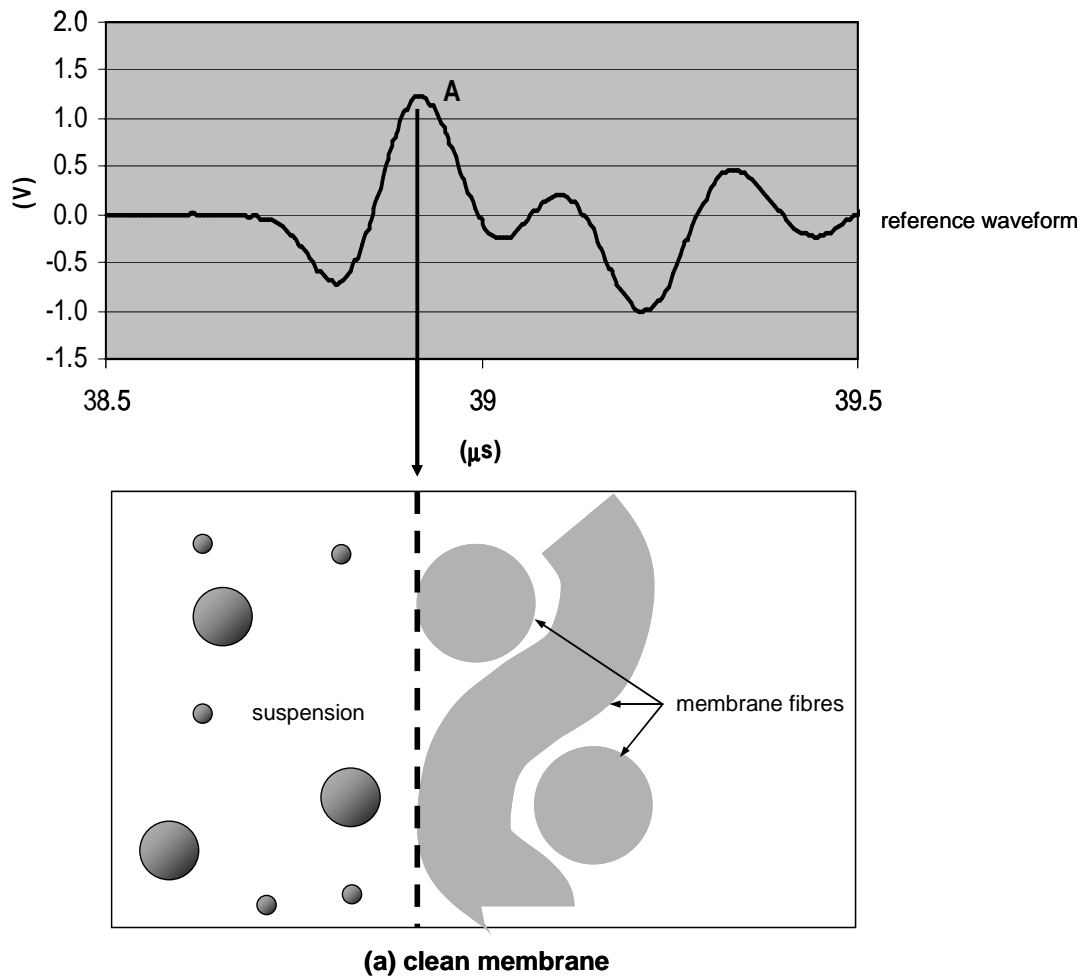


Figure 4.12(a): Typical waveform translation of a clean membrane.

Figure 4.12(a) shows a reflected waveform from a clean membrane at the start of filtration. Peak A represents the membrane surface. This waveform is saved on a computer's hard drive as the reference waveform.

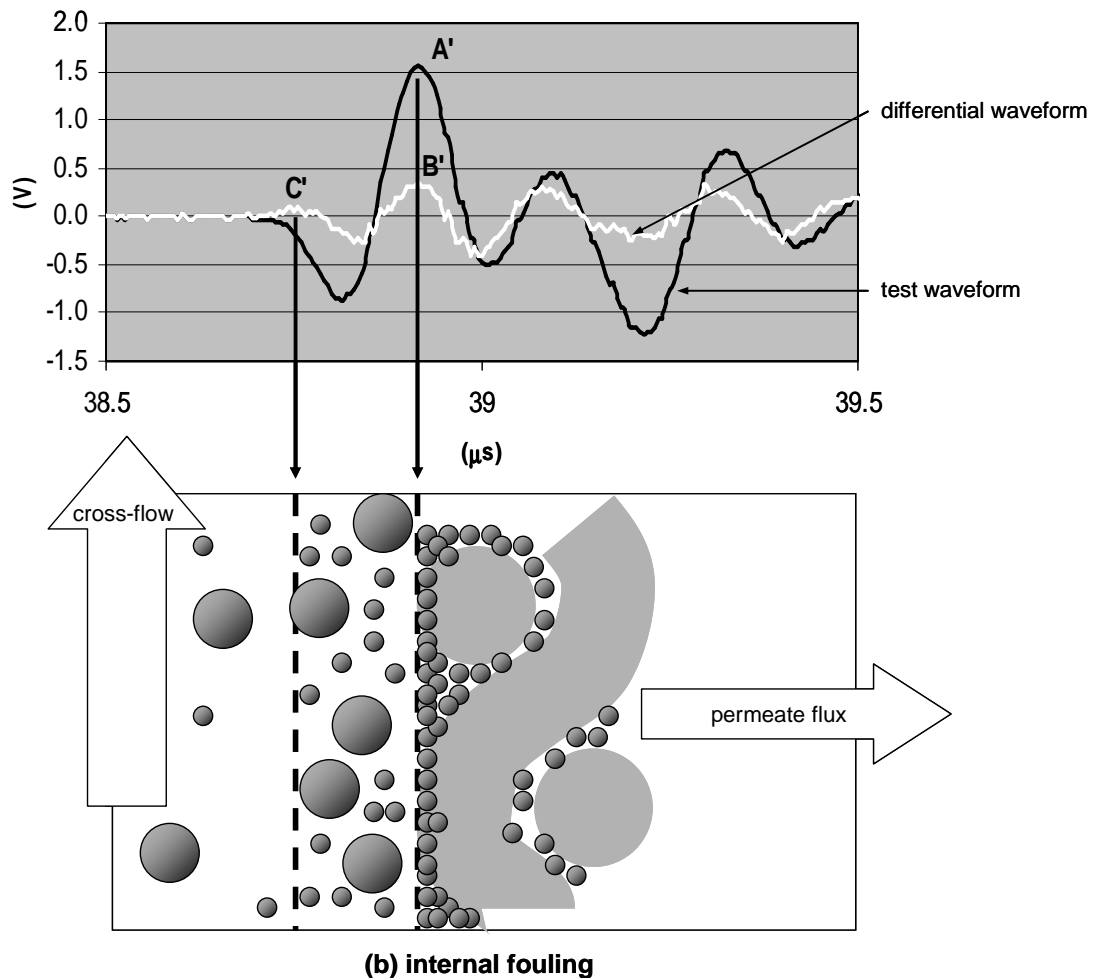


Figure 4.12(b): Typical waveform translation of internal fouling.

When permeation is started, small particles are drawn into the relatively open membrane matrix where they adsorb onto the material and plug the pores (passages between the individual fibres and weave). The membrane quickly densifies with resulting higher acoustic impedance and increased reflection of wave energy. This is depicted in the sudden increase of peak A to form peak A' (Figure 4.12(b)) one minute after start-up. At this stage the differential waveform indicates a difference in density of the membrane surface with peak B' and the existence of concentration polarisation with the appearance of peak C'.

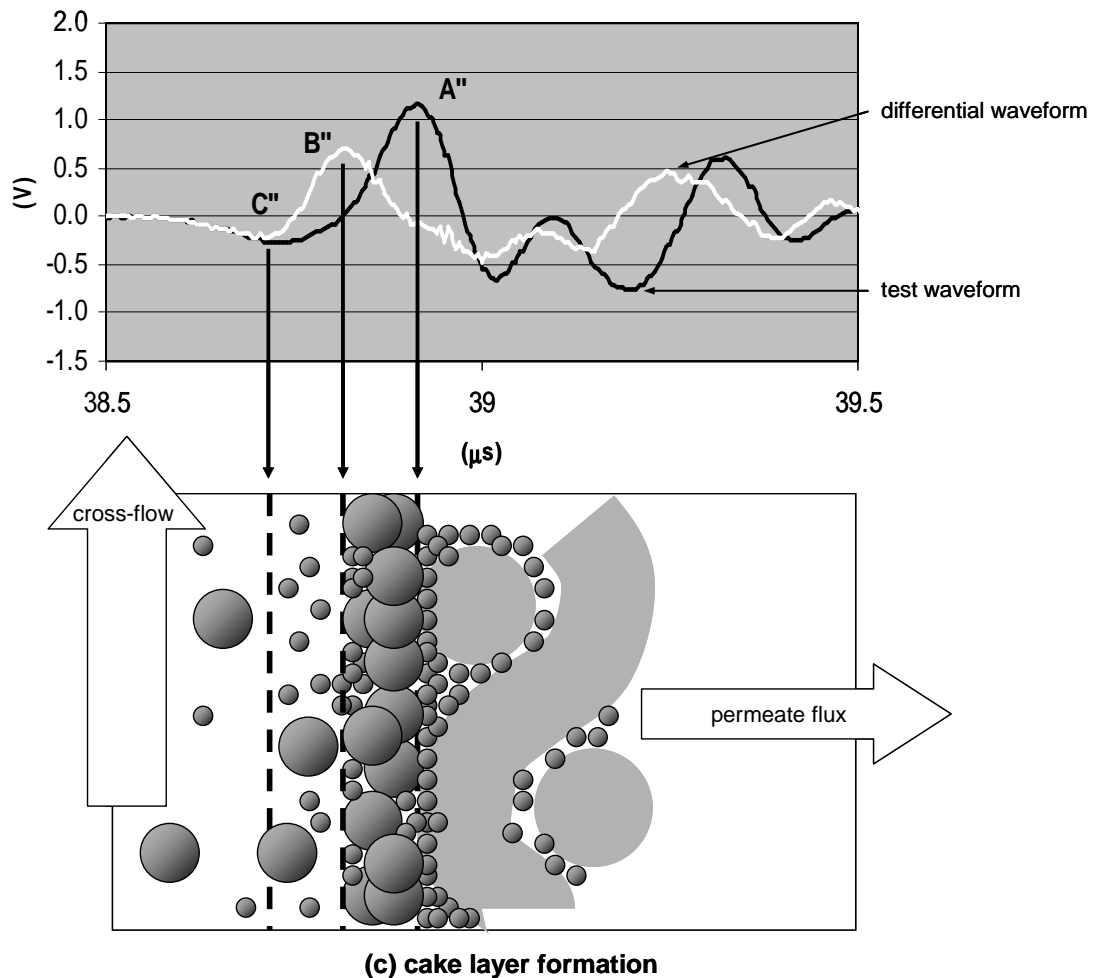


Figure 4.12(c): Typical waveform translation of cake layer formation.

After the initial internal fouling, another fouling mode starts to dominate, namely external fouling where particles are deposited onto the membrane surface to form a cake layer. This cake layer shelters the membrane from the transducer, causing a decrease in peak A'' as the effective reflected energy from the membrane is reduced, as is shown in Figure 4.12(c) which was sampled 25 minutes after start-up. The existence of polarised particles, a cake layer and internal fouling complicated the fouling interpretation of the test waveform, but with the use of the differential waveform the state of fouling inside and on the membrane surface could be determined. The time-domain shift of peak B'' from the membrane surface at peak B' (Figure 4.12(b)) indicates that deposition has occurred. C'' indicates the time-domain position of the concentration boundary

layer (concentration polarisation) where the accumulation of material is responsible for energy reflection.

Membrane fouling

In the configuration with an A_d/A_r ratio of 0.31, it was observed that very high riser cross-flow velocities occurred on the sides, just next to the dividing baffle plates, compared to the very slow, almost stagnant, cross-flow that occurred in the remaining middle of the riser. As the A_d/A_r ratio was increased, the variance in the cross-flow velocity seemed to decrease. Assuming that the density of the cake layer is approximately 2 g/cm^3 (between the density of water of 1 g/cm^3 and the density of bentonite of 3 g/cm^3), velocity of sound in the cake layer was measured to be 2800 m/s (Addendum D). After 20 h of operation the fouling layers in the middle on the membranes had arrival time differences of 90 ns, 105 ns and 130 ns for the airlift reactor configurations with A_d/A_r ratios of 1.45, 0.71 and 0.31 respectively. By using Equation 4.4 these arrival times equate to fouling layer thicknesses of 0.126 mm, 0.147 mm and 0.182 mm respectively. Figure 4.13 shows the calculated fouling layer thickness after 20 h of operation at the various relative positions for the configurations investigated. The thicker fouling layer on the right side (relative position of +1) of the large membrane ($A_d/A_r = 0.31$) can be ascribed to the positioning of the manifold outlet on the right with a significant pressure loss from right to left to produce higher local TMP values on the right side than, for example, the left side (relative position of -1).

By comparing the evolution of the relative height of peak A in each experiment, it was found that for a low A_d/A_r ratio such as 0.31, cake layer formation mainly occurred in the middle of the membrane with internal fouling mainly on the sides. For the higher A_d/A_r ratios the fouling behaviour was more uniform across the whole membrane.

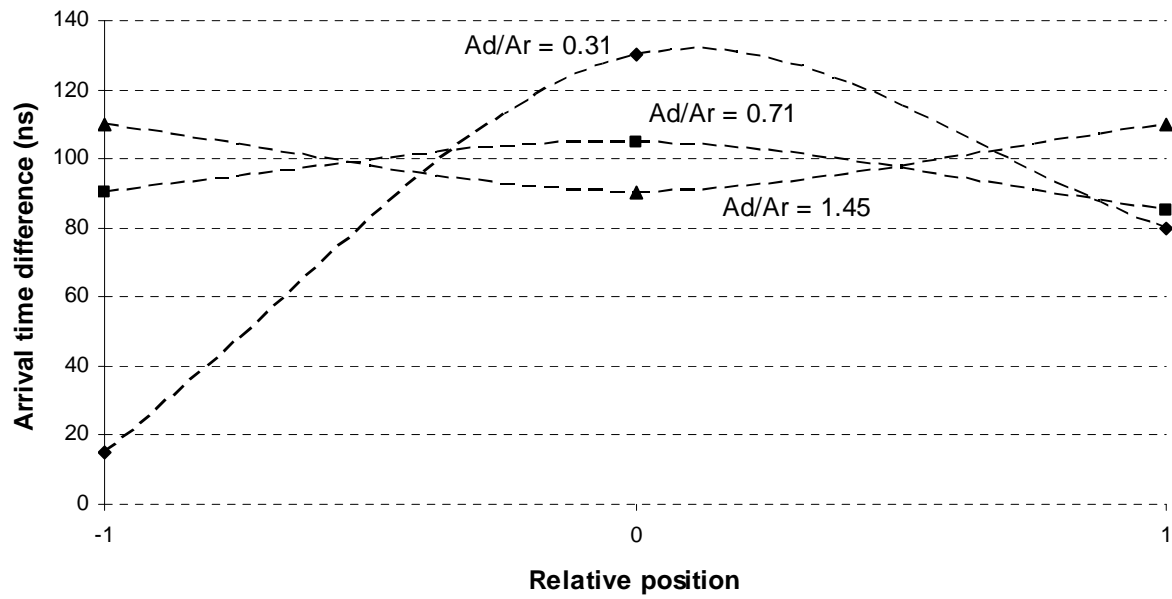


Figure 4.13: The arrival time differences at the relative positions after 20 hours of membrane filtration in a 1.0 g/L bentonite suspension.

Chapter 5

System hydrodynamic effects of airlift reactor factors

5.1 Introduction

The system hydrodynamics of an airlift reactor refer to all the intricate gas-liquid interactions in the various sections of an airlift reactor to create the governing circulation fluid flow. The behaviour of this resulting fluid flow in the riser section of the airlift reactor becomes particularly important if the fast rising liquid and gas bubbles are utilised to limit membrane fouling as was described in Chapter 3. In Chapter 4 it was determined that both the aeration intensity and the geometric configuration of an airlift reactor influence the system hydrodynamics, and are therefore responsible for the fluid flow behaviour that is induced in the riser section. The fluid flow behaviour in the riser section can be described as a hydrodynamic field consisting of fluid flow vectors. The sum of all these fluid flow vectors produces a resultant flow with a velocity profile across the riser section. As was previously observed, typical hydrodynamic fields in airlift reactor riser sections with their respective velocity profiles are shown in Figure 5.1.

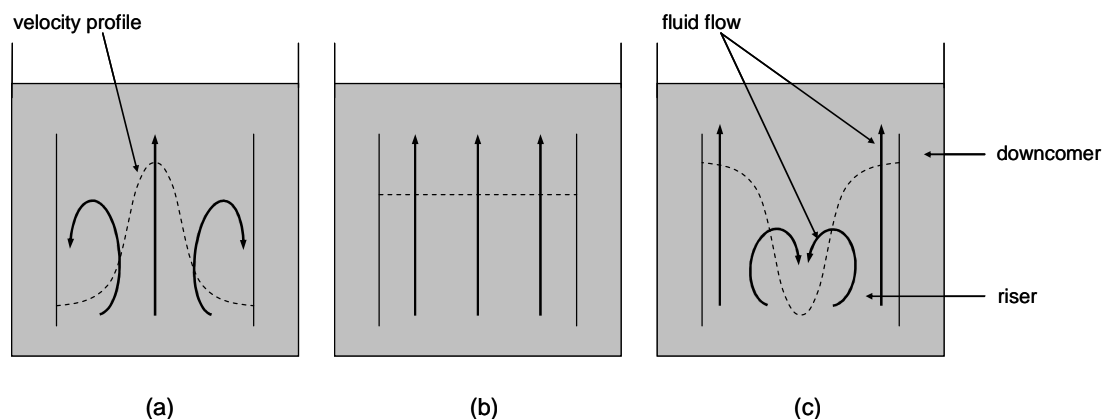


Figure 5.1: Typical hydrodynamic field patterns that were observed in the riser section of an airlift reactor: (a) fast rising liquid and bubbles in the middle with churning liquid and stagnant bubbles on the sides; (b) uniformly fast rising liquid and bubbles across the riser section; and (c) fast rising liquid and bubbles on the sides with churning liquid and stagnant bubbles in the middle.

Because of the two-phase operation of an airlift reactor, there are in reality two velocity profiles in the riser section: the liquid velocity profile and the gas bubble velocity profile superimposed onto the liquid velocity profile. In this study, however, only the liquid velocity profile was investigated since it governs the gas bubble velocity profile. Any further mention of the velocity profile will refer to the liquid velocity profile in the riser section of the airlift reactor.

The presence of a velocity profile in the riser section of the airlift reactor was discussed in Chapter 4. From the findings in Chapter 4 it can be postulated that if an airlift reactor riser section were to be utilised to limit fouling of immersed membranes, the optimal airlift reactor arrangement would be where the aeration intensity and the reactor configuration provide system hydrodynamics such that the velocity profile of the hydrodynamic field in the riser section is maximised and perfectly uniform. The optimised case would be akin to the hydrodynamic field and velocity profile depicted in Figure 5.1(b).

In Section 3.1.1 it was noted that for an airlift reactor the aeration intensity, the ratio of the total cross-sectional areas of the downcomer sections to the riser sections (A_d/A_r), the top clearance distance, the bottom clearance distance and riser section height all seem to influence the liquid velocity in the riser section. In other words, all of these aspects can influence the magnitude of the velocity profile and can be arranged in such a way as to maximise the velocity profile. But if these aspects could also be arranged to simultaneously satisfy the requirement of an uniform velocity profile, then the optimum airlift reactor design for immersed membrane scouring in the riser section would be found. The five airlift reactor aspects mentioned above must therefore be investigated to determine their influences on the velocity profile. Since the top clearance and bottom clearance distances are already considered, it was decided to rather evaluate the influence of the airlift reactor water depth as opposed to the riser section height, since it is related and much simpler to execute during the experiment. Also, it was thought that the air sparger and its introduction of air bubbles at the very bottom of the riser section might contribute to the resistance to the circulation flow in the interconnecting zone from the downcomer section to the riser section. Moving the air sparger to inside the riser section could potentially improve the velocity profile in the riser section.

Bubble size was not considered. In Section 3.2 it was explained how the scouring action of rising bubbles is increased when the bubbles move closer to the membrane surfaces. It was therefore assumed that the optimal bubble size diameter would be equal to the channel width of immersed flat-sheet membranes. The channel width between membrane surfaces was again thought to form part of future optimisation studies and not relevant to this study.

Consequently six aspects of airlift reactor design were identified which could influence the velocity profile. These relationships must be uncovered to enable the design and operation of an airlift reactor with improved system hydrodynamics for a higher scouring efficiency of immersed membranes. The six aspects of airlift reactor design that were investigated are listed and indicated in Figure 5.2.

- 1) downcomer area to riser area ratio (A_d/A_r)
- 2) top clearance distance
- 3) bottom clearance distance
- 4) aeration intensity
- 5) water depth
- 6) air sparger location

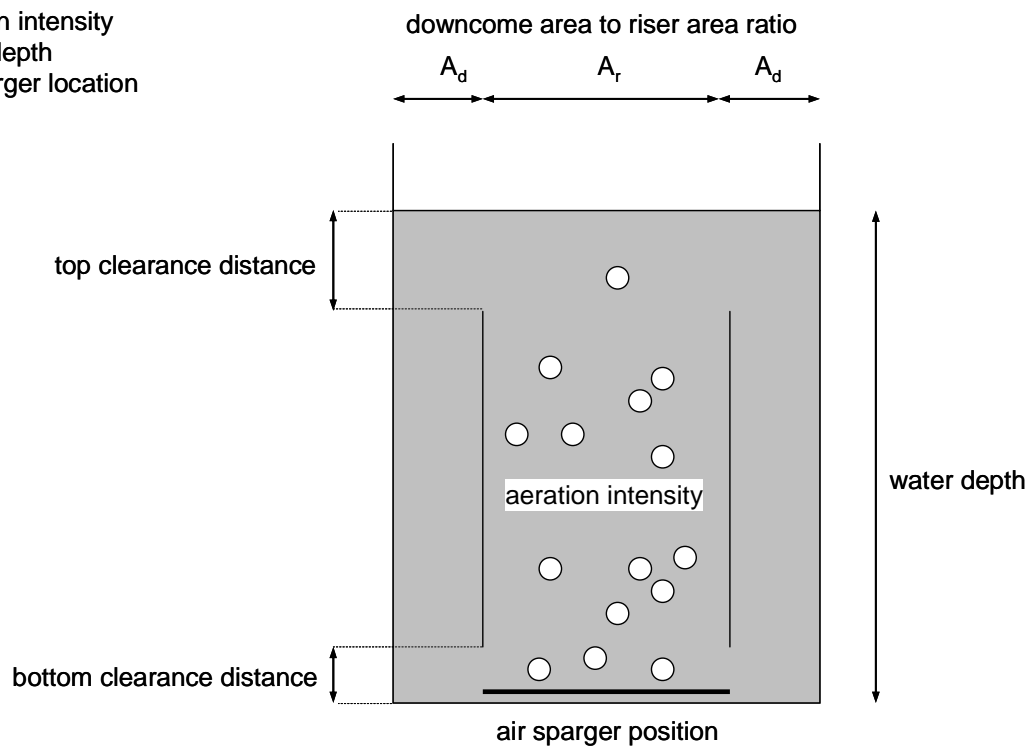


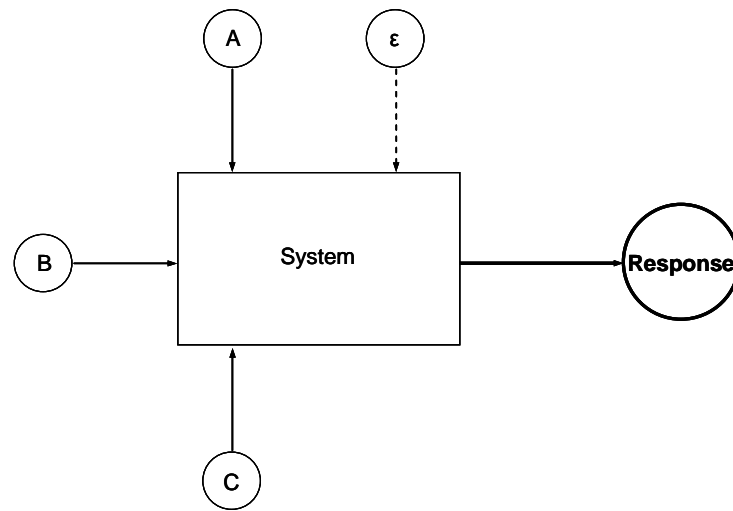
Figure 5.2: The six aspects of airlift reactor design that were investigated to determine their influences on the velocity profile in the riser section.

5.2 Design of experiments

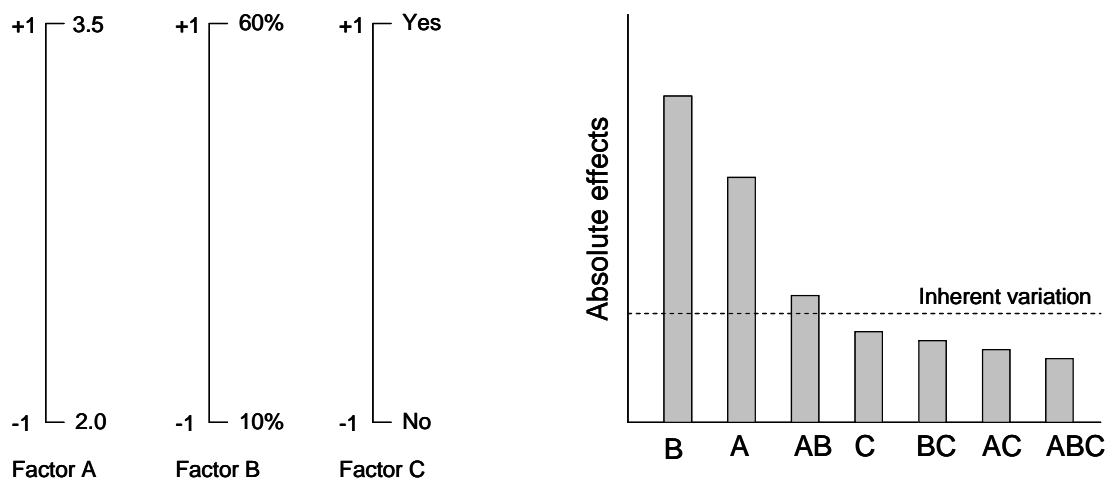
This section only gives a very basic account of design of experiments (DOE) to explain the experimental work and the results that were obtained. Barrentine [1999] provides a good introduction to DOE, but a more fundamental explanation can be found in most statistics textbooks. DOE is a methodology to simultaneously study various system inputs and their interactions with each other to determine their respective effects on a single target output. This is a much more time efficient approach as opposed to testing one system input at a time. Also, by testing system inputs one at a time, the possibility exists that the existence of potential interactions might be overlooked. DOE is therefore ideally suited to investigate multi-factorial systems with potential interactions as a first round tool to optimise these systems.

In DOE the independent system inputs or variables are referred to as factors. For the designed experiment the factors are set at predetermined values which are referred to as levels. Levels do not have to be numeric values, but can also be attributes, i.e. continuous or discrete. In its simplest form a DOE contain factors that are evaluated at only two levels, thereby assuming that the relationships between the factors and the target output are of a linear kind. Factors can be evaluated at more than two levels to capture the potential existence of nonlinear relationships. Sometimes two or more factors together can form an interaction which can influence the target output differently than these factors would individually. The target output in DOE is referred to as the response and it is the result of all the actions of the factors. The impact of a change in a factor or an interaction on the value of the response is referred to as the effect on the response.

In every system there is a certain degree of inherent variation of the response. In other words, if a designed experiment were to be repeated with all the identified factors at the exact same levels, then the response will demonstrate a deviation from the previous experimental trial. The smaller the deviation, the smaller is the experimental error and the more reproducible is the system. The experimental error is a combination of the variation of the factors, the variation of unknown factors and the variation of the response measurement to produce inherent variation of the response. To reduce the impact of experimental error the unique settings of the factor levels, called treatments, must be performed in a randomised fashion. It is therefore important to determine the inherent variation of the response to confirm the significance of factors. If the effect of a factor is indeed higher than the inherent variation of the response, then the factor is regarded to have a significant effect on the response and does not form part of the normal process noise. Figure 5.3 captures the abovementioned concepts for a hypothetical system where DOE was used to determine the effects of all the identified factors and their potential interactions on the system response.



(a)



(b)

(c)

Figure 5.3: A basic explanation of DOE for a hypothetical system. (a) Three factors, A, B and C, were identified as possibly having an impact on the response and needed to be investigated. An experimental error is present in the system and contributes to the value of the response. (b) Two levels were chosen for each factor, which are the only values where the factors are maintained during the designed experiment. Note that the levels of factor C are attributes. Each factor's high level is indicated by "+1" and their corresponding low level is indicated by "-1". (c) Factors A and B, as well as their interaction AB, were found to have a significant effect on the response, since they managed to change the response value to outside of its inherent variation. Factor C and all other interactions are insignificant and can be ignored in future optimisation studies.

The six aspects of airlift reactor design that were identified in Section 5.1 will be used as six factors in the DOE study to establish their effects on the response, the velocity profile in the riser section of the airlift reactor.

5.2.1 Full factorial designs

In full factorial design experiments all the factors are completely considered. The experiment is carried out by studying all possible unique treatments to evaluate all the factors at all their required levels. With a full factorial design experiment the effects of all factors and all interactions can be determined. Also, if factors are evaluated at more than two levels, a full factorial design experiment can tell if the effects on the response are linear or nonlinear. The number of treatments required to perform a full factorial design experiment is calculated by:

$$n = L^f \quad (5.1)$$

where n = number of treatments required
 L = number of levels per factor
 f = number of factors

It is clear that the size of a full factorial design can become enormous with the addition of every extra factor to be considered; even more so if the factors are to be evaluated at many levels. If many factors need to be investigated, it is advisable to first screen the factors and only use the significant factors in subsequent full factorial design experiments with more than two levels for further optimisation.

5.2.2 Screening designs

Screening designs are types of fractional factorial designs which can investigate the same number of factors, but with far less treatments compared to a full factorial design. Unfortunately some of the information is lost when opting for a screening design, but the trade-off in time saved, makes screening designs the recommended starting place when a system with many factors need to be investigated. Subsequent full factorial design experiments can be performed on the screened factors for further optimisation.

With a screening design experiment the factors are evaluated at two levels, and as a result can therefore not give any indication whether the effects are linear or nonlinear. Also, although scarce, the existence of three-factor and higher interactions cannot be detected with screening design experiments. But the main disadvantage of screening designs however, is the confusion of effects

that is created by the confounding of factors and interactions, where the same effect is calculated for factors and interactions. Confounded effects are called aliases and can be between a factor and an interaction or between an interaction and another interaction.

Plackett-Burman designs [Wang et al., 2009] are screening designs that can be used to study $n-1$ factors with n treatments in which n is divisible by four. For example, 7 factors can be studied with 8 treatments. If n is also a power of two, like in the case with 7 factors and 8 treatments, the design is said to be geometric. In geometric designs the confounding of the effects is complete, meaning that they are identical in size, but possibly opposite in sign. Designs are nongeometric if n is divisible by four, but is not a power of two, like in the case with 11 factors and 12 treatments. In nongeometric designs each factor is partially confounded with all interactions that do not contain the factor. The Plackett-Burman design for 7 factors and 8 treatments are shown in Table 5.1. Table 5.1 also shows the aliases, and since this is a geometric design, the confounding is complete. For example, in the case of factor A:

$$E(A) = -E(BD) = -E(CG) = -E(EF)$$

where $E(A)$ = effect of factor A

$E(BD)$ = effect of interaction BD

$E(CG)$ = effect of interaction CG

$E(EF)$ = effect of interaction EF

Table 5.1: Plackett-Burman design for 7 factors (factors A, B, C, D, E, F and G) and 8 treatments. Each factor is completely confounded with three interactions, but is opposite in sign. The “+” and “-” signs in each treatment indicate the required high or low level of the corresponding factor for the specific treatment.

Treatment	A	B	C	D	E	F	G
1	+	-	-	+	-	+	+
2	+	+	-	-	+	-	+
3	+	+	+	-	-	+	-
4	-	+	+	+	-	-	+
5	+	-	+	+	+	-	-
6	-	+	-	+	+	+	-
7	-	-	+	-	+	+	+
8	-	-	-	-	-	-	-
	-BD	-AD	-AG	-AB	-AF	-AE	-AC
	-CG	-CE	-BE	-CF	-BC	-BG	-BF
	-EF	-FG	-DF	-EG	-DG	-CD	-DE

5.3 Screening of system hydrodynamic factors

The six system hydrodynamic factors identified in Section 5.1, with potential effects on the velocity profile in the riser section of an airlift reactor, will be screened in a screening design experiment to determine all the significant factors and two-factor interactions.

5.3.1 Experimental set-up

The configuration of the experimental set-up needed to be flexible to accommodate all the combinations of factor levels that were required for the different treatments of the screening design. Since many treatments needed to be performed, it was important that changing the configuration from one treatment to the next treatment was done in a swift manner to save time. At the same time these changes needed to be accurate to ensure that the correct levels were maintained throughout the experiment. For these reasons an experimental set-up was devised that consisted of many interchangeable parts that could be quickly fitted together and then slotted into the correct positions.

An airlift reactor was constructed within a PVC tank. PVC sheet baffle plates were inserted in the tank to divide it into riser and downcomer sections. The tank contained slots which guided the baffle plates when inserted into the tank, provided stability for the baffle plates during aeration and kept the baffle plates in the correct positions to ensure that the ratio of the downcomer to riser cross-sectional area remained at the right levels. The baffle plates were connected with steel rods for increased stability and to allow for the baffle plates to be easily slid into the correct position to create the required ratio of the downcomer to riser cross-sectional area. Additional PVC sheets could also be fitted on top of these baffle plates, when required, to change the top clearance distance. The baffle plates were supported by steel rod feet, which could also be adjusted, when required, to change the bottom clearance distance. Two air spargers were used in this experiment to fit the two riser sections widths that were created as a result of the two levels of the downcomer to riser ratio factor. The air spargers were identical in design, except for their lengths. Each air sparger was fabricated from a 15 mm (OD) PVC pipe that stretched from baffle plate to baffle plate; containing a single line of 2 mm holes, spaced 50 mm apart, on the top. The baffle plates could support the air sparger at two positions: 200 mm above the bottom of the baffle plates inside the riser section or at the bottom of the tank at the baffle plates' steel rod feet. The relative large holes of the air spargers reduced the pressure drops across them and enabled a blower, even at the relative deep water depths of this experiment, to supply air at constant rates. The air flow rate

was measured with a flow meter and maintained at constant flows to produce the required levels of aeration intensities in the riser section. Tap water was used to fill the airlift reactor. The correct water depth was achieved by making up with tap water or draining the airlift reactor; both which could be done quickly.

The tank housing the airlift reactor was made from grey PVC sheets, but one half of the front side contained a clear PVC sheet to enable visual observation of the hydrodynamic behaviour inside the tank. The use of the clear PVC sheet was restricted to only half of the one side, since the clear PVC sheet had a thickness of 6 mm compared to the grey PVC sheet thickness of 10 mm that consequently limited the ability of the clear PVC sheet to sufficiently withstand the water pressure. Figure 5.4 shows the PVC tank construction and the baffle plate framework that was slotted inside the PVC tank to create the different airlift reactor configurations.

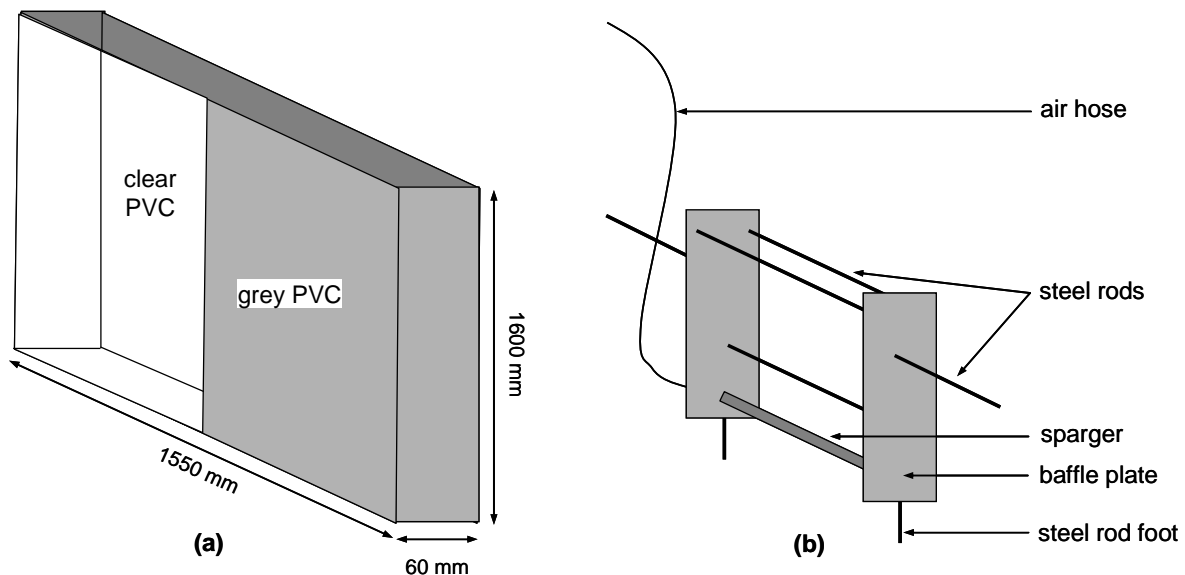


Figure 5.4: Experimental set-up for the screening of system hydrodynamic factors: (a) PVC tank with one half of the front containing a clear PVC sheet and (b) the baffle plate framework which could be changed to create different airlift reactor configurations when slotted inside the PVC tank.

5.3.2 Method

Eventually two facets of the response, the velocity profile in the riser section, must be optimised simultaneously to find the best values of the system hydrodynamic factors for optimised scouring efficiency: magnitude and uniformity. Both these facets can be assessed by measuring the linear liquid velocities across the width of the riser section.

Linear liquid velocity measurement

Linear liquid velocity is a critical operating parameter of airlift reactors and considerable attention has been given to its measurement. However, since the liquid flow behaviour tends to be very complex, it is difficult to measure it directly and usually requires some form of tracer measurement. The tracer is introduced somewhere in the circulation fluid flow path of an airlift reactor and a certain unique property of the tracer is used to detect its arrival some time later downstream in the circulation fluid flow path. The linear liquid velocity can therefore be deduced from the known path distance and the measured travel time of the tracer. Typical tracer measurements include measuring the conductance increase after a salt injection [Hwang and Cheng, 1997; Couvert et al., 1999; Lu et al., 2000]; visually observing colour after a dye injection [Chisty and Moo-Young, 1987; Wongsuchoto et al., 2003]; measuring the pH change after an acid or base injection [Chisty et al., 1988; Livingston and Zhang, 1993; Choi et al., 1996; Couvert et al., 2001]; and measuring the temperature change after a cold or hot stream injection [Dhaouadi et al., 1996].

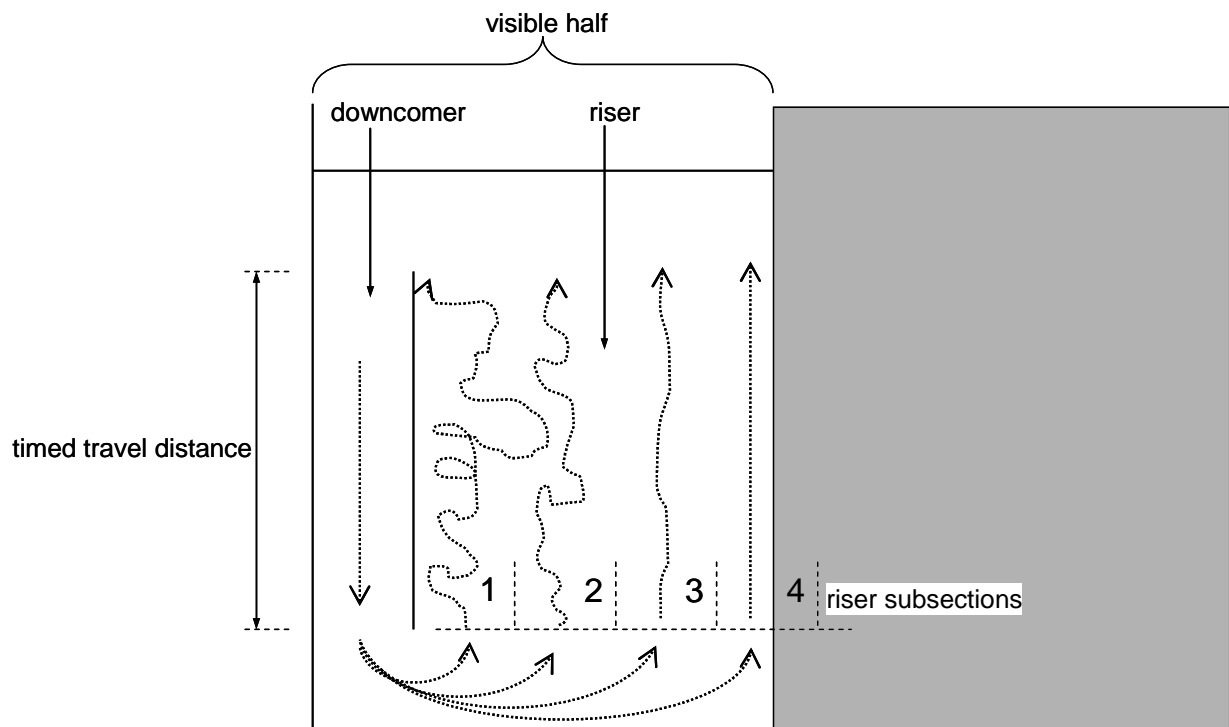
The abovementioned techniques for linear liquid velocity measurement would be impractical, unsafe and expensive in a screening design where numerous measurements would have to be taken in quick succession. Since the relative values, rather than the actual values, of the velocity profiles in the screening design is of importance, it was decided therefore to rather use an indication of the linear liquid velocities to compile velocity profiles. A similar approach was taken by Liu et al. [2003] where the observed velocity of the mixed liquor was assumed as the actual liquid velocity. In this study clearly visible grey polypropylene (PP) pieces of approximately 1 cm^3 with a measured density of 0.97 g/cm^3 that were dragged with the circulation fluid flow were found to work well in this regard.

The PP pieces were added with the tap water in the tank and used as visual tracers to indicate the liquid velocity. With the airlift reactor in operation, the circulation flow would drag the PP pieces down the downcomer sections and again up in the riser section. The PP pieces were well distributed below the riser section to rise up across the whole riser section. The times it took the PP pieces to travel the distance from the bottom of the baffle plate to the top of the baffle plate in

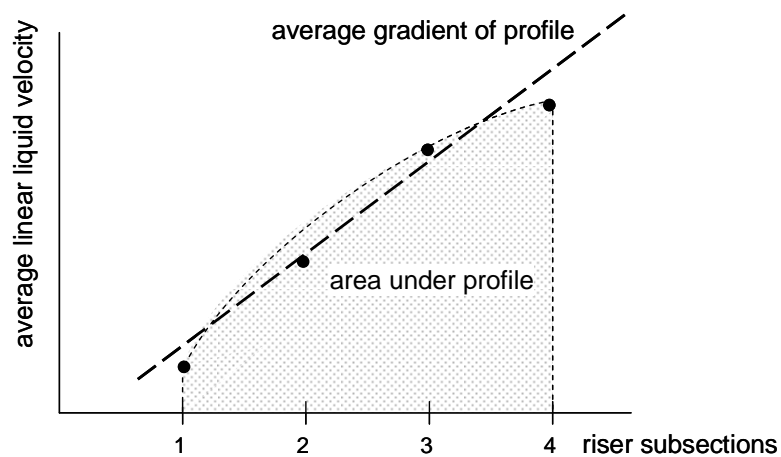
the riser section were measured and converted to linear velocities. This was an inexpensive velocity measurement technique and could be quickly repeated for any number of trials. Although this may not be an accurate measurement of the linear liquid velocities, because of the slight buoyancy of the PP pieces, this technique still produced comparable indications from which the effects of the factors on the hydrodynamics of the system could be calculated.

Response calculation

The baffle plate frameworks that were slotted in the tank were symmetrical - each time creating the riser section in the middle with the downcomer sections on the sides. As a result, one downcomer and exactly one half of the riser section could be seen through the clear PVC sheet that made up one half of the tank's front side. It was assumed that, since the geometry is symmetrical, the hydrodynamic field pattern in the riser section would also be symmetrical and that it would only be necessary to attain a velocity profile of the visible half of the riser section. The width of the entire riser section was divided into seven subsections, stretching from the bottom to the top, with three and a half subsections therefore located in the visible part of the riser section. The calculated linear liquid velocities of the PP pieces were allocated to the specific visible subsection where they entered the riser section, as is explained in Figure 5.5(a). For each subsection an average linear liquid velocity was calculated from 10 measurements. Therefore, 40 measurements were required for each experimental treatment to calculate four average linear liquid velocities from which a velocity profile could be compiled. From the velocity profile, the area under the profile, as well as the average gradient of the profile were calculated as outputs for the effects on velocity profile magnitude and velocity profile uniformity respectively. Figure 5.5 explains this velocity profile quantification procedure. For the velocity profile magnitude in the riser section to be optimised, the area of the integrated velocity profile in the riser section must be maximised, and for the velocity profile uniformity to be optimised, the gradient of the velocity profile in the riser section must be equal to zero. Although the velocity profile was only determined for one half of the riser section, it was assumed that, since the geometry is symmetrical, that the velocity profile magnitude will be exactly the same in the other half and that the velocity uniformity will be the same in the other half, but with an average gradient opposite in sign. Since the riser subsections represent normalised distance to enable comparison of the two riser section widths, the velocity profile area and gradient do not have units and only indicate relative values for the same system.



(a)



(b)

Figure 5.5: Velocity profile quantification: (a) hypothetical pathways of PP pieces when entering the riser section in the different subsections and (b) hypothetical plotted average linear liquid velocities calculated for each subsection to compile a velocity profile across the riser section. The magnitude of the velocity profile is indicated by the area under the profile and the uniformity is indicated by the average gradient of the profile.

Design of experiment

The six factors in the experiment that controls the system hydrodynamics will most probably exhibit nonlinear behaviours, but to reduce the experimental work of the factorial design experiment, the factors were assumed to be linear and that evaluation at two levels would provide for adequate estimations of their effects. Table 5.2 shows the different levels at which each factor were evaluated. The “+1” indicates the high level and the “-1” indicates the low level of the factor. The values of these levels were determined by the physical limitations of the experimental set-up, ease of measuring and practicality for continuously changing the baffle plate framework for the various geometrical arrangements. For simplification the six factors will be referred to by the symbols A to F as is indicated in Table 5.2.

Table 5.2: Values of the levels at which each factor was evaluated.

Factors	Levels	
	- 1	+ 1
A: A_d/A_r	0.5	2
B: Top clearance distance	100 mm	200 mm
C: Bottom clearance distance	30 mm	100 mm
D: Aeration intensity	800 L/(m ² ·min)	1 350 L/(m ² ·min)
E: Water depth	1 100 mm	1 400 mm
F: Air sparger position	Bottom (very bottom of tank below riser section)	Riser section (200 mm above bottom of baffle plates)

From Equation 5.1, a full factorial design of these six factors at two levels would require 64 (2^6) independent experimental treatments, and when replication is included to determine the experimental error, a total amount of 128 ($2^6 + 2^6$) independent experimental treatments would be required. A full factorial design would therefore have consumed a lot of experimental time, and it was decided that a screening design, an 8 treatment Plackett-Burman design with 7 factors [Clauhan et al., 2007; Vatanara et al., 2007; Mukherjee et al., 2008; Dejaegher et al., 2009; Oita et al., 2009], as was shown in Table 5.1, would be utilised. In this case the 7th factor was a so-called dummy factor, since it did not represent any process parameter. Unfortunately, in a screening design the effects could be confounded with each other and is an additional reflection required to

determine the main factor effects. A reflection treatment is an inverse of a base treatment where the factors are evaluated at opposite levels as compared to the levels they were evaluated at in the base treatment. In this case the base and reflection treatments would require 16 independent experimental treatments, and including replication to determine the experimental error, a total of 32 treatments would be required to determine the effects of the factors. These treatments had to be performed in a random order to reduce the experimental error by eliminating the effects of potential unknown factors such as changing water temperature.

It was expected that numerous two-factor interactions would also exist and that their effects should also be determined. Each two-factor interaction was investigated in a two-factor two-level (2^2) full factorial design by only changing the levels of the factors investigated and leaving the other factors unchanged in the six-factor treatment configurations. After carefully examining the unique treatments required to capture all two-factor interactions in the six-factor treatment configurations, it was found that 22 unique six-factor treatment configurations would be required. However, six of these treatments were already captured in the base and reflection treatments to determine the factor effects. Therefore, 16 additional treatments were required, and with replication to determine the experimental error, 32 independent treatments were required to determine the interaction effects. These treatments also had to be randomised to reduce the experimental error. Since only two factors are investigated at a time in these treatments, the levels of the factors not considered were set at the levels which were the easiest to set-up to save time. For this reason factor F, the sparger position, was kept at the “+1” level when not investigated, since it could be quickly installed and removed from the riser section. Similarly, factor E, the water depth, was kept at the “-1” level when not investigated, since a lower water depth made the insertion and removal of the baffle plate framework in and out of the PVC tank much more easier.

Consequently, the total factorial design experiment consisted of 32 independent experimental treatments with 32 replicate treatments; each treatment providing a value for the integrated area under the velocity profile and a value for the average gradient of the velocity profile. Since the same system with the same six-factor configurations were used for all the treatments, it was decided to perform the whole experiment of base, reflection, full factorial and all replication treatments in one randomised experiment to determine the experimental error for all 32 treatments and evaluate all the calculated effects against the same standard error of the effect. For these 32 treatments the degrees of freedom were 32, and for evaluating the effects at a 95% significant level, the tabular t-value of 2.04 from statistical tables was used to determine the experimental errors for both the integrated area under the velocity profile and the average gradient of the velocity profile outputs. The treatments of the whole experimental design are shown in Table 5.3 and the treatments used to perform the full factorial designs are shown in Table 5.4.

Table 5.3: The treatments for the experimental design of the base, reflection and full factorial treatments. The “+” and “-“ signs indicate the setting of the levels. The order indicates the randomisation of the treatments and their replicates. The shaded treatments indicate treatments that were already covered in the base and reflection treatments.

	Treatment	A	B	C	D	E	F	Order
Base	1	+	-	-	+	-	+	4, 18
	2	+	+	-	-	+	-	16, 30
	3	+	+	+	-	-	+	54, 55
	4	-	+	+	+	-	-	6, 9
	5	+	-	+	+	+	-	41, 43
	6	-	+	-	+	+	+	53, 56
	7	-	-	+	-	+	+	7, 8
	8	-	-	-	-	-	-	42, 45
Reflection	9	-	+	+	-	+	-	44, 59
	10	-	-	+	+	-	+	46, 57
	11	-	-	-	+	+	-	1, 31
	12	+	-	-	-	+	+	47, 52
	13	-	+	-	-	-	+	19, 20
	14	+	-	+	-	-	-	3, 17
	15	+	+	-	+	-	-	39, 40
	16	+	+	+	+	+	+	2, 5
Full factorial	17 (1)	-	-	-	-	-	+	10, 24
	(13) (2)	-	+	-	-	-	+	
	18 (3)	-	-	-	+	-	+	12, 25
	19 (4)	-	-	+	-	-	+	13, 15
	20 (5)	-	+	+	-	-	+	11, 14
	(10) (6)	-	-	+	+	-	+	
	21 (7)	-	-	+	-	-	-	26, 51
	22 (8)	-	-	-	+	-	-	27, 58
	23 (9)	-	+	-	-	-	-	28, 64
	24(10)	+	-	-	-	-	+	21, 36
	25(11)	+	+	-	-	-	+	32, 48
	26(12)	+	-	+	-	-	+	33, 37
	(1)(13)	+	-	-	+	-	+	
	(12)(14)	+	-	-	-	+	+	
	27(15)	-	-	-	-	+	+	34, 60
	28(16)	-	+	-	-	+	+	35, 61
29(17)	-	-	-	+	+	+	23, 62	
(7)(18)	-	-	+	-	+	+		
30(19)	+	-	-	-	-	-	29, 49	
(8)(20)	-	-	-	-	-	-		
31(21)	-	+	-	+	-	+	22, 38	
32(22)	-	-	-	-	+	-	50, 63	

Table 5.4: The treatments (from the full factorial section of Table 5.3) used in the full factorial designs to determine the effects of the interactions. The “+” and “-“ signs indicate the levels of the respective factors in the same order as the name of the interaction. The numbers of the shown treatments refer to numbers 1 to 22 mentioned in the full factorial section of Table 5.3.

Interaction	++	+-	-+	--
AB	11	10	2	1
AC	12	10	4	1
AD	13	10	3	1
AE	14	10	15	1
AF	10	19	1	20
BC	5	2	4	1
BD	21	2	3	1
BE	16	2	15	1
BF	2	9	1	20
CD	6	4	3	1
CE	18	4	15	1
CF	4	7	1	20
DE	17	3	15	1
DF	3	8	1	20
EF	15	22	1	20

Effects calculation

A main effect is defined as the difference between the average of all the responses when a factor is evaluated at its high level and the average of all the responses when the same factor is evaluated at its low level. The main effect of factor X is calculated as [Barrentine,1999]:

$$E(X_i) = \bar{Y}_{X_{i+}} - \bar{Y}_{X_{i-}} = \frac{\sum Y_{X_{i+}} - \sum Y_{X_{i-}}}{N} \quad (5.2)$$

where $E(X_i)$ = main effect of factor X_i

$\bar{Y}_{X_{i+}}$ = average of the responses when factor X is at its high level

$\bar{Y}_{X_{i-}}$ = average of the responses when factor X is at its low level

$Y_{X_{i+}}$ = response when factor X is at its high level

$Y_{X_{i-}}$ = response when factor X is at its low level

N = number of treatments per level evaluation

An interaction is defined as one half the difference of the effect of a factor at another factor's high level and this other factor's low level. The interaction effect is calculated as [Barrentine, 1999]:

$$E(X_i X_j) = \frac{1}{2} \left[(\bar{Y}_{X_{i+}} - \bar{Y}_{X_{i-}})_{X_{j+}} - (\bar{Y}_{X_{i+}} - \bar{Y}_{X_{i-}})_{X_{j-}} \right] \quad (5.3)$$

where $E(X_i X_j)$ = effect of interaction $X_i X_j$ between factors X_i and X_j

X_{i+} = condition of factor X_i at its high level

X_{i-} = condition of factor X_i at its low level

X_{j+} = condition of factor X_j at its high level

X_{j-} = condition of factor X_j at its low level

With the main effects and the interaction effects known, a model can be created to calculate and predict the response for any arrangement of factor levels [Barrentime, 1999]:

$$Y = \bar{\bar{Y}} + \frac{1}{2} \sum E(X_i) X_i + \frac{1}{2} \sum E(X_i X_j) X_i X_j \quad (5.4)$$

where Y = the calculated response

$\bar{\bar{Y}}$ = the average of all responses of data

X_i = the level of factor X_i (like -1 or +1)

$X_i X_j$ = the product of the levels of interaction $X_i X_j$ constituent factors (like -1 x -1 = +1)

Significance of effects

The variance for a unique factor treatment was calculated by using the observed responses:

$$S_i^2 = \frac{\sum (Y_i - \bar{Y})^2}{n-1} \quad (5.5)$$

where S_i^2 = variance of the treatment

Y_i = independent response

\bar{Y} = average response for the treatment

n = number of independent treatments performed

The average standard deviation for the effects is calculated by:

$$S_e = \sqrt{\frac{\sum S_i^2}{k}} \quad (5.6)$$

where S_e = average standard deviation for the effects

k = number of unique treatments in the experiment

S_e for the 32 treatments were calculated as

For this experiment the degrees of freedom (df) are calculated by:

$$\begin{aligned} \text{df} &= (\text{number of observations per treatment} - 1) \times (\text{number of treatments}) \\ &= (2 - 1) \times 32 = 32 \end{aligned}$$

For degrees of freedom of 32 the tabular t-value from statistical tables for a significant level of 95% is 2.04. Therefore, the absolute decision limits (DL) for the significance of effects in this experiment is shown in Table 5.5.

Table 5.5: The decision limits for the significance of effects.

	Velocity profile area	Velocity profile gradient
df	32	32
S_e	0.0646	0.0120
DL	0.1318	0.0245

5.3.3 Results

Area under the velocity profile

Factor A and interaction DF were found to be 99.9% and 95% significant respectively in determining the area under the velocity profile. The model to predict the area under the velocity profile includes the average of all the treatments' responses, the determined effects of all the significant factors and interactions, as well as the determined effects of the factors of the significant interactions (hierarchy rule states that the main factors of all significant interaction effects must be included). Using Equation 5.4, the 95% significant model for the prediction of the area under the velocity profile can therefore be written as:

$$Y_{area} = \bar{Y}_{area} + \frac{E(A)}{2}A + \frac{E(D)}{2}D + \frac{E(F)}{2}F + \frac{E(DF)}{2}DF$$

When including the average value of all the treatments' responses and the effects on the area under the velocity profile, as was determined in this experiment, the model can be written as:

$$Y_{area} = 0.6003 + \frac{0.2732}{2}A + \frac{0.0189}{2}D + \frac{-0.0317}{2}F + \frac{0.1710}{2}DF \quad (5.7)$$

Consequently, if Y_{area} has to be maximised for improved fluid flow velocity in the riser section, and considering the +1 and -1 levels of this experiment, A and DF must both be equal to 1. For DF to be equal to 1, the product of D and F must be equal to 1. To counter factor F 's negative effect, F must be equal to -1, and consequently D too. Therefore, only considering the chosen levels, as shown in Table 5.2, the airlift reactor arrangement which would have the highest fluid flow velocity in the riser section would have an A_d/A_r ratio of 2, be operated with an aeration intensity of 800 L/(m²·min) and have the sparger positioned at the bottom of the tank. The other factors did not seem to influence the fluid flow velocity in the riser section. Experimental data can be found in Addendum E.

Average gradient of the velocity profile

Factors C and F , and interactions CF and DF , were found to be 99.9% significant. Interactions AD , BD , BF , CD , DE and EF were found to be 99% significant. As with the area under the velocity profile, using the average of all the treatments' responses and the determined effects on the

average gradients of the velocity profiles, the same procedure can be followed to arrive at the 95% significant model for the prediction of the average gradient of the velocity profile:

$$\begin{aligned}
 Y_{gradient} = & -0.0122 + \frac{0.0136}{2}A + \frac{0.0181}{2}B + \frac{0.0615}{2}C + \frac{-0.0112}{2}D + \frac{0.0226}{2}E + \\
 & \frac{-0.0987}{2}F + \frac{0.0343}{2}AD + \frac{0.0410}{2}BD + \frac{-0.0431}{2}BF + \frac{0.0387}{2}CD + \frac{-0.0817}{2}CF + \\
 & \frac{0.0428}{2}DE + \frac{-0.0813}{2}DF + \frac{-0.0388}{2}EF
 \end{aligned} \tag{5.8}$$

To optimise the uniformity of the fluid flow in the riser section, the average gradient of the velocity profile $Y_{gradient}$ needs to be equal to zero. Using the solver function of Microsoft's Excel, and considering the +1 and -1 levels of this experiment, an optimised average gradient of the velocity profile could be achieved by evaluating the factors at the following levels:

A → +1

B → +1

C → -1

D → -1

E → -1

F → +1

Therefore, only considering the chosen levels, as shown in Table 5.2, the airlift reactor arrangement which would have the most uniform fluid flow in the riser section would have an A_d/A_r ratio of 2, have a top clearance distance of 200 mm, have a bottom clearance distance of 30 mm, be operated with an aeration intensity of 800 L/(m²·min), have a water depth of 1 100 mm and have the sparger positioned inside the riser section (200 mm above the bottom of the baffle plates). Experimental data can be found in Addendum E.

5.4 Validation of system hydrodynamic factors

The models that were developed for calculating the responses on the velocity profile in the riser section (see Section 5.3.3) for the experimental set-up of Section 5.3.1 must be validated.

5.4.1 Experimental set-up

The experimental set-up for validating the effects of the system hydrodynamic factors was the same as the experimental set-up described in Section 5.3.1, but instead of tap water, the PVC tank was filled with a particulate suspension of bentonite. The bentonite suspension of approximately 0.3 g/L was prepared as described in Addendum A. Also, a flat-sheet membrane element was installed in the riser section and was fabricated as explained in Addendum B with an active area of 0.335 m². The membrane element was tightly secured within the baffle plate framework and was located right in the middle of the riser section width. The active membrane area had a width of 429 mm and was wide enough to be exposed to a nonuniform velocity profile in all studied configurations. The water head above the immersed membrane element was kept constant throughout the experiment at 250 mm to ensure that all TMP changes could only be ascribed to membrane fouling. Similar to the flux-step experiment described in Section 4.3.2, a peristaltic pump withdrew permeate and returned it to the tank while a water manometer measured the increase in TMP across the membrane.

5.4.2 Method

Levels for the six factors were chosen to produce four airlift reactor configurations in such a way that the one configuration would produce the maximum velocity profile area according to the prediction of Equation 5.7, one configuration would produce the most uniform velocity profile according to Equation 5.8 and the other two would produce poor velocity profile areas and gradients according to Equations 5.7 and 5.8. The levels were maintained at the same values as explained in Table 5.2.

The flux-step approach, as was applied in Section 4.3, was used to compare the different configurations' abilities to scour the immersed membrane to limit membrane fouling. Two pure water flux treatments were conducted at permeate fluxes incremented by 4 L/(m²·h) from 4 L/(m²·h) to 40 L/(m²·h) to determine the membrane resistance. Thereafter the configurations were evaluated in independent bentonite suspension treatments by incrementing the permeate flux

by 4 L/(m²·h) from 4 L/(m²·h) to 28 L/(m²·h). Each constant permeate flux was maintained for 30 minutes to ensure that internal fouling has stabilised and that any subsequent fouling could be attributed to cake layer formation alone. During these 30 minute periods the TMP was regularly recorded and the permeate flux, air flow rate and suspension temperature measured to confirm they stay relatively constant. The permeate flux did not vary more than 0.4 L/(m²·h) from the intended permeate flux and the treatments were conducted at suspension temperatures of 20 ± 3°C. Table 5.7 shows the order in which the treatments were performed.

The PVC tank in the experiment was much larger than the tank used in the fouling experiments described in Chapter 4 and with the much larger downcomer sections when evaluating the A_d/A_r ratio at 2 (at its +1 level), bentonite would settle in the dead zones of the downcomer sections to reduce the concentration of suspended bentonite. In order to maintain the suspended bentonite at a constant concentration to enable the sensible comparison of membrane fouling data, it was decided to operate at a much lower bentonite concentration of approximately 0.3 g/L (compared to 1.0 g/L in the fouling experiments of Chapter 4) and continuously add bentonite during the experiment. As explained in Addendum A, a suspended bentonite calibration curve was compiled which correlates suspended bentonite concentration with turbidity measured in NTU. From the calibration curve the turbidity of the suspension was maintained at 128 ± 11 NTU by continuously adding small amounts of dry bentonite to ensure that the suspended bentonite concentration remained between 0.31 g/L and 0.37 g/L throughout the experiment.

A simple backwash procedure, prior to an experimental treatment, proved to be adequate in restoring the original hydraulic resistance of the membrane, therefore removing all particles within, as well as on the membrane surface.

Table 5.6: Different airlift reactor configurations chosen to validate their predicted velocity profile areas and gradients as predicted by Equations 5.7 and 5.8. The “+1” and “-1” indicate the respective high and low levels of the specific factor as is explained in Table 5.2. Configuration 1 represents the configuration with the most uniform velocity profile and configuration 2 represents the configuration with the highest velocity profile area.

Configuration	A	B	C	D	E	F	Predicted velocity profile area	Predicted velocity profile gradient
1	+1	+1	-1	-1	-1	+1	0.6261	0.0003
2	+1	-1	+1	-1	+1	-1	0.8288	0.0432
3	+1	-1	-1	-1	-1	+1	0.6261	0.0663
4	-1	-1	+1	+1	-1	+1	0.5428	-0.1438

Table 5.7: The random order in which the treatments were conducted to minimise the risk of unknown influences on the results. The configuration numbers correlate with the configurations listed in Table 5.6.

	Tap water	Bentonite suspension (0.3 g/L)
Configuration 1 (without aeration)	1, 2	
Configuration 1		7, 10
Configuration 2		3, 5
Configuration 3		4, 6
Configuration 4		8, 9

5.4.3 Results

The average stabilised membrane fouling rates for each configuration at each permeate flux is shown in Figure 5.6. Configuration 1 with the predicted most uniform velocity profile had the lowest membrane fouling rate at any of the permeate fluxes and displayed sub-critical flux operation up to a permeate flux of 16 L/(m²·h). Configuration 2 with the highest velocity profile area performed worse than configuration 1, but better than the other at lower permeate fluxes. Experimental data can be found in Addendum F.

From Figure 5.6 it was estimated, using the technique explained in Figure 4.2, that the critical flux in the different configurations was:

Configuration 1 → 16 L/(m²·h)

Configuration 2 → 11 L/(m²·h)

Configuration 3 → 6 L/(m²·h)

Configuration 4 → 4 L/(m²·h)

When considering the critical fluxes of the different configurations, there seems to be an increase in critical flux with an increase in the predicted uniformity of the velocity profile as calculated by Equation 5.8. An increase in the predicted velocity profile area also seems to reduce the membrane fouling rate, especially at lower permeate fluxes. Both Equations 5.7 and 5.8 therefore seems to give a correct indication of the velocity profile and its effect in reducing membrane fouling. The velocity profile uniformity seems to have a much greater impact on the velocity profile's ability to scour the membrane surface, than the velocity profile area.

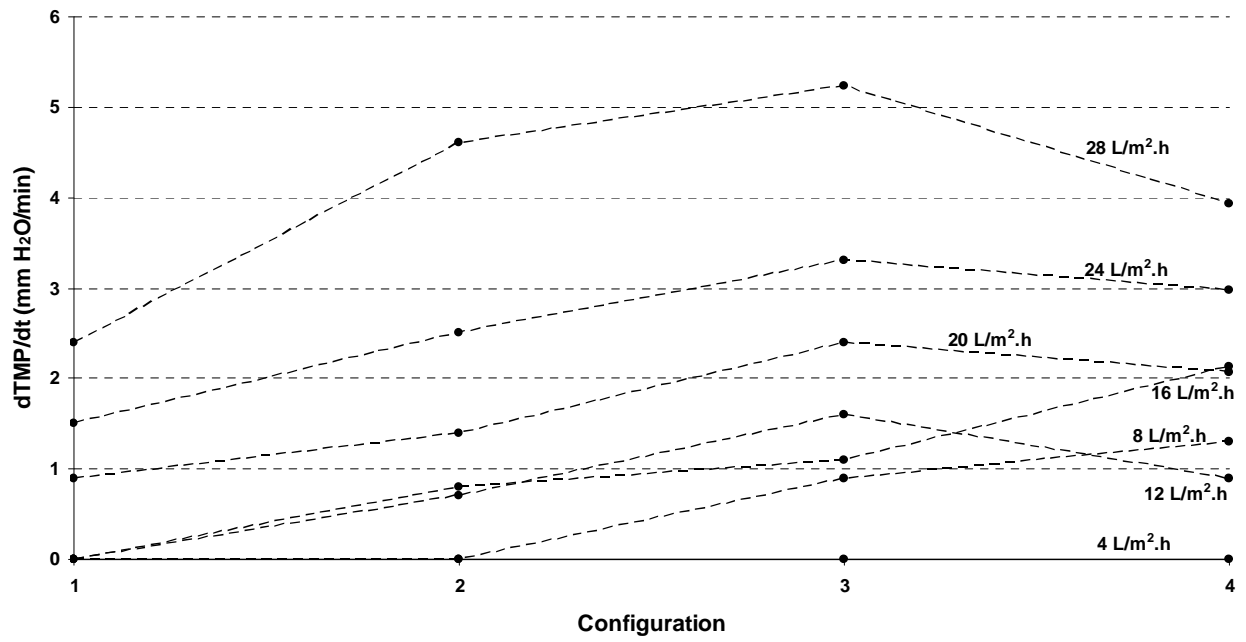


Figure 5.6: Average membrane fouling rates for the different configurations. Although not shown for the sake of clarity, the variability in the fouling rate increased with an increase in absolute velocity profile gradient and was therefore the highest for configuration 4.

Chapter 6

Conclusions

6.1 Introduction

Immersed membrane systems hold many operational and environmental advantages over conventional activated sludge systems, and even sidestream membrane systems. However, except for certain niche applications, immersed membrane systems cannot compete with conventional activated sludge systems when comparing for lowest capital and operating costs. The higher costs associated with immersed membrane systems, as a result of membrane fouling, have made them fairly unattractive in the wastewater treatment field to date. However, the capital layout required for immersed membrane systems has been steadily decreasing over the last two decades, relative to conventional systems, and because of ever-increasingly stringent environmental legislation, immersed membrane systems are more and more considered for new wastewater treatment projects. Retrofitting of existing conventional activated sludge systems with immersed membranes is also becoming more prominent.

Unfortunately operating costs remain high for immersed membrane systems with the largest portion by far dedicated to coarse bubble aeration of the membranes to reduce fouling. In the current climate of worldwide rising energy prices an incentive exists to optimise immersed membrane operation, especially by increasing the air-scouring efficiency. In achieving this, and therefore reducing unit operating cost, immersed membrane systems will develop into a relevant wastewater treatment technology with very unique solutions – perfectly positioned in the global showdown for greener living.

From this study it turned out that air-scouring is not as trivial a matter as was previously believed and that great care must be taken to ensure that the immersed membrane system as a whole is conducive for improved system hydrodynamics for increased air-scouring. Failure to consider system hydrodynamics can promote membrane fouling, even when aeration is increased or intensified.

6.2 Air-scouring efficiency

By nature membrane filtration will always result in membrane fouling, but the fouling rate can be reduced by increasing the efficacy of back-transport mechanisms to remove material from the membrane surface. Air-scouring is usually applied in immersed membrane systems to induce flow across the membrane surfaces to enhance back-transport.

Contrary to what was previously believed, it was found in this study that increasing the air flow rate for an increase in aeration intensity does not necessarily translate to an increase in scouring ability to remove more material from the membrane surfaces. In certain instances an increase in aeration intensity has no effect on the air-scouring ability and could even promote localised fouling. Consequently, by operating immersed membrane systems at increased aeration intensities the resulting low air-scouring efficiencies can seriously jeopardise operating costs of incorrectly designed membrane reactors.

It was found that the air-scouring efficiency is increased by ensuring a uniform cross-flow velocity profile across the membrane surfaces. With a uniform cross-flow velocity profile across the membrane surfaces the same air-scouring ability can be achieved at much lower aeration intensities to significantly increase air-scouring efficiency. A uniform cross-flow velocity profile eliminates localised critical fluxes and selective fouling as permeate flux is increased. With the onset of localised fouling the effective permeate flux for the remaining membrane surface is increased to exceed local critical fluxes and initiate cake layer formation. This vicious cycle is continuously repeated across the whole membrane surface to result in high observed fouling rates. In other words, if localised fouling can be avoided by maintaining a uniform cross-flow velocity profile across the membrane surface, then the membrane will experience only internal fouling until steady state is reached for sub-critical fluxes and slow even cake layer formation for permeate fluxes above the critical flux.

6.3 System hydrodynamic factors

This study highlighted the importance of immersed membranes located in the riser section of an airlift reactor as opposed to simply immerse membranes in bubble reactors. Airlift reactors are capable of providing fast rising and unidirectional bubbles to scour membrane surfaces. Bubble reactors, on the other hand, display chaotic bubble patterns which are less efficient in scouring membrane surfaces.

With the introduction of airlift reactor geometry, the system hydrodynamics of the airlift reactor must be considered if the cross-flow velocity profile in the riser section, and therefore across the membrane surfaces, were to be improved. Six system hydrodynamic factors were investigated in this study and the most important factor identified was the ratio of the total downcomer to riser cross-sectional areas (A_d/A_r). The higher the value of A_d/A_r , the faster is the velocity profile in the riser section.

When designing an airlift reactor with the purpose of air-scouring immersed membranes, the following methodology must be considered to improve air-scouring efficiency:

- choose A_d/A_r as high as physically allowed in the design (higher than the “+1” level used in this study) ;
- opt for placing the air sparger at the very bottom of the tank below the riser section (similar to the “-1” level used in this study); and
- rather operate at lower aeration intensities (similar to the “-1” level used in this study) to also improve air-scouring efficiency.

These steps, according to Equation 5.7 developed in Chapter 5, will provide a fast velocity profile, but not necessarily a uniform velocity profile. As was proven in this study, the uniformity of the velocity profile is critical in avoiding localised membrane fouling with severe fouling rates at higher permeate fluxes. With the values of the three abovementioned system hydrodynamic factors set, the levels of the remaining three factors (top clearance distance, bottom clearance distance and water depth) can be tailored by using Equation 5.8 to achieve a velocity profile with the lowest absolute gradient. The levels can also be extrapolated and evaluated outside of the “-1” to “+1” range.

References

- Ahn, K.-H., Cha, H.-Y. and Song, K.-G. (1999), **Retrofitting municipal sewage treatment plants using an innovative membrane-bioreactor system**, *Desalination*, **124**, pp. 279-286
- Al-Ahmad, M., Abdul Aleem, F.A., Mutiri, A. and Ubaisy, A. (2000), **Biofouling in RO membrane systems part 1: fundamentals and control**, *Desalination*, **132**, pp. 173-179
- Al Akoum, O., Jaffrin, M.Y., Ding, L., Paullier, P. and Vanhoutte, C. (2002), **An hydrodynamic investigation of microfiltration and ultrafiltration in a vibrating membrane module**, *Journal of Membrane Science*, **197**, pp. 37-52
- Alavi Moghaddam, M.R., Satoh, H. and Mino, T. (2001), **Effect of important operation parameters on the performance of coarse pore filtration activated sludge process**, IWA Conference on Water and Wastewater Management in Developing Countries, Kuala Lumpur, Malaysia
- Al-Masry, W.A. and Abasaeed, A.E. (1998), **On the scale-up of external loop airlift reactors: Newtonian systems**, *Chemical Engineering Science*, **53**(24), pp. 4085-4094
- Altena, F.W. and Belfort, G. (1984), **Lateral migration of spherical particles in porous flow channels: application to membrane filtration**, *Chemical Engineering Science*, **39**(2), pp. 343-355
- Aryal, R., Lebegue, J., Vigneswaran, S., Kandasamy, J. and Grasmick, A. (2009), **Identification and characterisation of biofilm formed on membrane bio-reactor**, *Separation and Purification Technology*, **67**, pp. 86-94
- Bacchin, P., Aimar, P. and Sanchez, V. (1995), **Model for colloidal fouling of membranes**, *AIChE Journal*, **41**(2), pp. 368-376
- Bacchin, P., Aimar, P. and Sanchez, V. (1996), **Influence of surface interaction on transfer during colloid ultrafiltration**, *Journal of Membrane Science*, **115**, pp. 49-63
- Bacchin, P., Si-Hassen, D., Starov, V., Clifton, M.J. and Aimar, P. (2002), **A unifying model for concentration polarization, gel-layer formation and particle deposition in cross-flow membrane filtration of colloidal suspensions**, *Chemical Engineering Science*, **57**, pp. 77-91

-
- Bai, R. and Leow, H.F. (2002), **Microfiltration of activated sludge wastewater – the effect of system operation parameters**, *Separation and Purification Technology*, **29**, pp. 189-198
- Baker, J.S. and Dudley, L.Y. (1998), **Biofouling in membrane systems – a review**, *Desalination*, **118**, pp. 81-90
- Barrentine, L.B. (1999), **An Introduction to Design of Experiments**, ASQ Quality Press, Milwaukee, Wisconsin
- Belfort, G. (1989), **Fluid mechanics in membrane filtration: recent developments**, *Journal of Membrane Science*, **40**, pp. 123-147
- Belfort, G., Pimbley, J.M., Greiner, A. and Chung, K.Y. (1993), **Diagnosis of membrane fouling using a rotating annular filter. 1. Cell culture media**, *Journal of Membrane Science*, **77**, pp. 1-22
- Belfort, G., Davis, R.H. and Zydney, A.L. (1994), **Review – The behavior of suspensions and macromolecular solutions in crossflow microfiltration**, *Journal of Membrane Science*, **96**, pp. 1-58
- Benkahla, Y.K., Ould-Dris, A., Jaffrin, M.Y. and Si-Hassen, D. (1995), **Cake growth mechanism in cross-flow microfiltration of mineral suspensions**, *Journal of Membrane Science*, **98**, pp. 107-117
- Bian, R., Yamamoto, K. and Watanabe, Y. (2000), **The effect of shear rate on controlling the concentration polarization and membrane fouling**, *Desalination*, **131**, pp. 225-236
- Bouhabila, E.H., Ben Aïm, R. and Buisson, H. (1998), **Microfiltration of activated sludge using submerged membrane with air bubbling (application to wastewater treatment)**, *Desalination*, **118**, pp. 315-322
- Bouhabila, E.H., Ben Aïm, R. and Buisson, H. (2001), **Fouling characterisation in membrane bioreactors**, *Separation and Purification Technology*, **22-23**, pp. 123-132
- Bowen, W.R. and Sharif, A.O. (1998), **Hydrodynamic and colloidal interactions effects on the rejection of a particle larger than a pore in microfiltration and ultrafiltration membranes**, *Chemical Engineering Science*, **53**(5), pp. 879-890
- Cabassud, C., Laborie, S., Durand-Bourlier, L. and Lainé, J.M. (2001), **Air sparging in ultrafiltration hollow fibres: relationship between flux enhancement, cake characteristics and hydrodynamic parameters**, *Journal of Membrane Science*, **181**, pp. 57-69
- Cabassud, C., Laborie, S. and Lainé, J.M. (1997), **How slug flow can improve ultrafiltration flux in organic hollow fibres**, *Journal of Membrane Science*, **128**, pp. 93-101
- Cauhan, K., Trivedi, U. and Patel, K.C. (2007), **Statistical screening of medium components by Plackett-Burman design for lactic acid production by *Lactobacillus* sp. KCP01 using date juice**, *Bioresource Technology*, **98**, pp. 98-103

-
- Chang, I.-S. and Judd, S.J (2002), **Air sparging of a submerged MBR for municipal wastewater treatment**, *Process Biochemistry*, **37**, pp. 915-920
- Chang, S. and Fane, A.G. (2001), **The effect of fibre diameter on filtration and flux distribution – relevance to submerged hollow fibre modules**, *Journal of Membrane Science*, **184**, pp. 221-231
- Chang, S., Fane, A.G. and Vigneswaran, S. (2002), **Experimental assessment of filtration of biomass with transverse and axial fibres**, *Chemical Engineering Journal*, **87**, pp. 121-127
- Chang, W.-K., Hu, A., Horng, R.-Y. and Tzou, W.-Y. (2007), **Membrane bioreactor with nonwoven fabrics as solid-liquid separation media for wastewater treatment**, *Desalination*, **202**, pp. 122-128
- Characklis, W.G. (1991), **Biofouling: effects and control**, in: Flemming, H.-C. and Geesey, G.G. (eds.), *Biofouling and Biocorrosion in Industrial Water Systems*, Springer-Verlag, Berlin, pp. 7-27
- Chen, V., Fane, A.G., Madaeni, S. and Wenten, I.G. (1997), **Particle deposition during membrane filtration of colloids: transition between concentration polarization and cake formation**, *Journal of Membrane Science*, **125**, pp. 109-122
- Chisti, M.Y. (1989a), **Airlift Bioreactors**, Elsevier Science Publishing Ltd, New York, pp. 1-8
- Chisti, M.Y. (1989b), **Airlift Bioreactors**, Elsevier Science Publishing Ltd, New York, pp. 53-57
- Chisti, M.Y., Halard, B. and Moo-Young, M. (1988), **Liquid circulation in airlift reactors**, *Chemical Engineering Science*, **43**(3), pp. 451-457
- Chisti, M.Y. and Moo-Young, M. (1987), **Airlift reactors: characteristics, applications and design considerations**, *Chemical Engineering Communications*, **60**, pp. 195-242
- Chisti, Y. and Moo-Young, M. (1988), **Prediction of liquid circulation velocity in airlift reactors with biological media**, *Journal of Chemical Technology and Biotechnology*, **42**, pp 211-219
- Chisti, Y. and Moo-Young, M. (1993), **Improve the performance of airlift reactors**, *Chemical Engineering Progress*, **89**(6), pp. 38-45
- Choi, K.H., Chisti, Y. and Moo-Young, M. (1996), **Comparative evaluation of hydrodynamic and gas-liquid mass transfer characteristics in bubble column and airlift slurry reactors**, *Chemical Engineering Journal*, **62**, pp. 223-229
- Churchouse, S. and Wildgoose, D. (1999), **Membrane bioreactors hit the big time – from lab to full-scale application**, 2nd Symposium on Membrane Bioreactors for Wastewater Treatment, Cranfield University, Cranfield, UK

-
- Contreras, A., Chisti, M. and Molina, E. (1998), **A reassessment of relationship between riser and downcomer gas holdups in airlift reactors**, *Chemical Engineering Science*, **53**(24), pp. 4151-4154
- Couvert, A., Bastoul, D., Roustan, M., Line, A. and Chatellier, P. (2001), **Prediction of liquid velocity and gas hold-up in rectangular air-lift reactors of different scales**, *Chemical Engineering and Processing*, **40**, pp. 113-119
- Couvert, A., Roustan, M. and Chatellier, P. (1999), **Two-phase hydrodynamic study of a rectangular air-lift loop reactor with an internal baffle**, *Chemical Engineering Science*, **54**, pp. 5245-5252
- Cox, R.G. and Brenner, H. (1968), **The lateral migration of solid particles in Poiseuille flow – I Theory**, *Chemical Engineering Science*, **23**, pp. 147-173
- Cui, Z.F. and Wright, K.I.T. (1994), **Gas-liquid two-phase cross-flow ultrafiltration of BSA and dextran solutions**, *Journal of Membrane Science*, **90**, pp. 183-189
- Cui, Z.F., Chang, S. and Fane, A.G. (2003), **The use of gas bubbling to enhance membrane processes**, *Journal of Membrane Science*, **221**, pp. 1-35
- Davis, R.H. and Birdsell, S.A. (1987), **Hydrodynamic model and experiments for crossflow microfiltration**, *Chemical Engineering Communications*, **49**, pp. 217-234
- Davis, R.H. and Leighton, D.T. (1987), **Shear-induced transport of a particle layer along a porous wall**, *Chemical Engineering Science*, **42**(2), pp. 275-281
- Defrance, L. and Jaffrin, M.Y. (1999a), **Comparison between filtrations at fixed transmembrane pressure and fixed permeate flux: application to a membrane bioreactor used for wastewater treatment**, *Journal of Membrane Science*, **152**, pp. 203-210
- Defrance, L. and Jaffrin, M.Y. (1999b), **Reversibility of fouling formed in activated sludge filtration**, *Journal of Membrane Science*, **157**, pp. 73-84
- Dejaegher, B., Durand, A. and Vander Heyden, Y. (2009), **Identification of significant effects from an experimental screening design in the absence of effect sparsity**, *Journal of Chromatography B*, **877**(23), pp. 2252-2261
- Dhaouadi, H., Poncin, S., Hornut, J.M., Wild, G. and Oinas, P. (1996), **Hydrodynamics of an airlift reactor: experiments and modeling**, *Chemical Engineering Science*, **51**(11), pp. 2625-2630
- Drew, D.A., Schonberg, J.A. and Belfort, G. (1991), **Lateral inertial migration of a small sphere in fast laminar flow through a membrane duct**, *Chemical Engineering Science*, **46**(12), pp. 3219-3224
- Eckstein, E.C., Bailey, D.G. and Shapiro, A.H. (1977), **Self-diffusion of particles in shear flow of a suspension**, *Journal of Fluid Mechanics*, **79**, pp. 191-208

-
- Engler, J. and Wiesner, M.R. (2000), **Particle fouling of a rotating membrane disk**, *Water Research*, **34**(2), pp. 557-565
- Fane, A.G., Beatson, P. and Li, H. (2000), **Membrane fouling and its control in environmental applications**, *Water Science and Technology*, **41**(10-11), pp. 303-308
- Field, R.W. (1993), **Transport processes in membrane systems**, in: Howell, J.A., Sanchez, V. and Field, R.W. (eds.), *Membranes in Bioprocessing: Theory and Applications*, Chapman & Hall, Cambridge, p. 67
- Field, R.W., Wu, D., Howell, J.A. and Gupta, B.B. (1995), **Critical flux concept for microfiltration fouling**, *Journal of Membrane Science*, **100**, pp. 259-272
- Finnigan, S.M. and Howell, J.A. (1989), **The effect of pulsatile flow on ultrafiltration fluxes in a baffled tubular membrane system**, *Chemical Engineering Research and Design*, **67**, pp. 278-282
- Flemming, H.-C. and Schaule, G. (1988), **Biofouling on membranes – a microbiological approach**, *Desalination*, **70**, pp. 95-119
- Flemming, H.-C., Schaule, G., Griebe, T., Schmitt, J. and Tamachkiarowa, A. (1997), **Biofouling – the Achilles heel of membrane processes**, *Desalination*, **113**, pp. 215-225
- Fradin, B. and Field, R.W. (1999), **Crossflow microfiltration of magnesium hydroxide suspensions: determination of critical fluxes, measurement and modelling of fouling**, *Separation and Purification Technology*, **16**, pp. 25-45
- Fyles, T.M. and Lycon, D.S. (2000), **Fouling reduction using centrifugal membrane separation**, *Journal of Membrane Science*, **176**, pp. 267-276
- Gander, M., Jefferson, B. and Judd, S. (2000), **Aerobic MBRs for domestic wastewater treatment: a review with cost considerations**, *Separation and Purification Technology*, **18**, pp. 119-130
- García-Calvo, E. and Letón, P. (1996), **Prediction of gas hold-up and liquid velocity in airlift reactors using two-phase flow friction coefficients**, *Journal of Chemical Technology and Biotechnology*, **67**, pp. 388-396
- Ghosh, R. (2002), **Study of membrane fouling by BSA using pulsed injection technique**, *Journal of Membrane Science*, **195**, pp. 115-123
- Gourgues, C., Aimar, P. and Sanchez, V. (1992), **Ultrafiltration of bentonite suspensions with hollow fibre membranes**, *Journal of Membrane Science*, **74**, pp. 51-69
- Green, G. and Belfort, G. (1980), **Fouling of ultrafiltration membranes: lateral migration and the particle trajectory model**, *Desalination*, **35**, pp. 129-147
- Guibert, D., Ben Aim, R., Rabie, H. and Côté, P. (2002), **Aeration performance of immersed hollow-fibre membranes in a bentonite suspension**, *Desalination*, **148**, pp. 395-400

-
- Günder, B. and Krauth, K. (1998), **Replacement of secondary clarification by membrane separation – results with plate and hollow fibre modules**, *Water Science and Technology*, **38**(4-5), pp. 383-393
- Gupta, B.B., Howell, J.A., Wu, D. and Field, R.W. (1995), **A helical baffle for crossflow microfiltration**, *Journal of Membrane Science*, **102**, pp. 31-42
- Hamachi, M., Cabassud, M., Davin, A. and Mietton-Peuchot, M. (1999), **Dynamic modelling of crossflow microfiltration of bentonite suspension using recurrent neural networks**, *Chemical Engineering and Processing*, **38**, pp. 203-210
- Hamachi, M. and Mietton-Peuchot, M. (1999), **Experimental investigations of cake characteristics in crossflow microfiltration**, *Chemical Engineering Science*, **54**, pp. 4023-4030
- Hamachi, M. and Mietton-Peuchot, M. (2002), **Analysis of deposit behaviour in crossflow microfiltration by means of thickness measurement**, *Chemical Engineering Journal*, **86**, pp. 251-257
- Héran, M. and Elmaleh, S. (2000), **Cross-flow microfiltration with high frequency reverse flow**, *Water Science and Technology*, **41**(10-11), pp. 337-343
- Ho, B.P. and Leal, L.G. (1974), **Inertial migration of rigid spheres in two-dimensional unidirectional flows**, *Journal of Fluid Mechanics*, **65**, pp. 365-400
- Hodgson, P.H., Leslie, G.L., Schneider, R.P., Fane, A.G., Fell, C.J.D. and Marshall, K.C. (1993), **Cake resistance and solute rejection in bacterial microfiltration: the role of the extracellular matrix**, *Journal of Membrane Science*, **79**, pp. 35-53
- Howell, J.A. (1995), **Sub-critical flux operation of microfiltration**, *Journal of Membrane Science*, **107**, pp. 165-171
- Hwang, K.-J., Chan, C.-S. and Tung, K.-L. (2009), **Effect of backwash on the performance of submerged membrane filtration**, *Journal of Membrane Science*, **330**, pp. 349-356
- Hwang, S.-J., Chang, D.-J. and Chen, C.-H. (1996), **Steady state permeate flux for particle cross-flow filtration**, *Chemical Engineering Journal*, **61**, pp. 171-178
- Hwang, S.-J. and Cheng, Y.-L. (1997), **Gas holdup and liquid velocity in three-phase internal-loop airlift reactors**, *Chemical Engineering Science*, **52**(21/22), pp. 3949-3960
- Jacobs, L., De Bruyn, E.E. and Cloete, T.E. (1996), **The use of biodispersants available for biofouling control in industrial water systems**, WRC Project No. 592/1/97, Water Research Commission of South Africa, South Africa
- Jones, W.F., Valentine, R.L. and Rodgers, V.G.J. (1999), **Removal of suspended clay from water using transmembrane pressure pulsed microfiltration**, *Journal of Membrane Science*, **157**, pp. 199-210

-
- Judd, S. (2008), **The status of membrane bioreactor technology**, *Trends in Biotechnology*, **26**(2), pp. 109-116
- Judd, S.J., Le-Clech, P., Taha, T. and Cui, Z.F. (2001), **Theoretical and experimental representation of a submerged membrane bio-reactor system**, *Membrane Technology*, **135**, pp. 4-9
- Kawakatsu, T., Nakao, S. and Kimura, S. (1993), **Effects of size and compressibility of suspended particles and surface pore size of membrane on flux in crossflow filtration**, *Journal of Membrane Science*, **81**, pp. 173-190
- Koen, L.J. (2000a), **Ultrasonic-time-domain-reflectometry as a real time non-destructive visualisation technique of concentration polarisation and fouling on reverse osmosis membranes**, Master thesis, University of Stellenbosch, Stellenbosch, South Africa, pp. 2-22 – 2-23
- Koen, L.J. (2000b), **Ultrasonic-time-domain-reflectometry as a real time non-destructive visualisation technique of concentration polarisation and fouling on reverse osmosis membranes**, Master thesis, University of Stellenbosch, Stellenbosch, South Africa
- Krstić, D.M., Tekić, M.N., Carić, M.Đ. and Milanović, S.D. (2002), **The effect of turbulence promoter on cross-flow microfiltration of skim milk**, *Journal of Membrane Science*, **208**, pp. 303-314
- Kwon, D.Y., Vigneswaran, S., Fane, A.G. and Ben Aim, R. (2000), **Experimental determination of critical flux in cross-flow microfiltration**, *Separation and Purification Technology*, **19**, pp. 169-181
- Laborie, S., Cabassud, C., Durand-Bourlier, L. and Lainé, J.M. (1998), **Fouling control by air sparging inside hollow fibre membranes – effects on energy consumption**, *Desalination*, **118**, pp. 189-196
- Le-Clech, P., Jefferson, B., Chang, I.S. and Judd, S.J. (2003a), **Critical flux determination by the flux-step method in a submerged membrane bioreactor**, *Journal of Membrane Science*, **227**, pp. 81-93
- Le-Clech, P., Jefferson, B. and Judd, S.J. (2003b), **Impact of aeration, solids concentration and membrane characteristics on the hydraulic performance of a membrane bioreactor**, *Journal of Membrane Science*, **218**, pp. 117-129
- Lee, S. and Lueptow, R.M. (2003), **Control of scale formation in reverse osmosis by membrane rotation**, *Desalination*, **155**, pp. 131-139
- Leighton, D. and Acrivos, A. (1986), **Viscous resuspension**, *Chemical Engineering Science*, **41**(6), pp. 1377-1384
- Leighton, D. and Acrivos, A. (1987), **Measurement of shear-induced self-diffusion in concentrated suspensions of spheres**, *Journal of Fluid Mechanics*, **177**, pp. 109-131

- Leiknes, T. (2003), **Low pressure membrane systems for water and wastewater treatment - emphasis on submerged membrane technology**, 5th WISA-MTD Symposium, Vereeniging, South Africa
- Leonard, E.F. and Vassilieff, C.S. (1984), **The deposition of rejected matter in membrane separation processes**, *Chemical Engineering Communications*, **30**, pp. 209-217
- Li, H., Fane, A.G., Coster, H.G.L. and Vigneswaran, S. (1998a), **Direct observation of particle deposition on the membrane surface during crossflow microfiltration**, *Journal of Membrane Science*, **149**, pp. 83-97
- Li, J. (2002), **Real-time investigation of fouling phenomena in membrane filtrations by a non-invasive ultrasonic technique**, Doctoral thesis, University of Stellenbosch, Stellenbosch, South Africa
- Li, J., Hallbauer, D.K. and Sanderson, R.D. (2003), **Direct monitoring of membrane fouling and cleaning during ultrafiltration using a non-invasive ultrasonic technique**, *Journal of Membrane Science*, **215**, pp. 33-52
- Li, J., Sanderson, R.D., Hallbauer, D.K. and Hallbauer-Zadorozhnaya, V.Y. (2002a), **Measurement and modelling of organic fouling deposition in ultrafiltration by ultrasonic transfer signals and reflections**, *Desalination*, **146**, pp. 177-185
- Li, J., Sanderson, R.D. and Jacobs, E.P. (2002b), **Non-invasive visualization of the fouling of microfiltration membranes by ultrasonic time-domain reflectometry**, *Journal of Membrane Science*, **201**, pp. 17-29
- Li, Q.Y., Ghosh, R., Bellara, S.R., Cui, Z.F. and Pepper, D.S. (1998b), **Enhancement of ultrafiltration by gas sparging with flat sheet membrane modules**, *Separation and Purification Technology*, **14**, pp. 79-83
- Lim, A.L. and Bai, R. (2003), **Membrane fouling and cleaning in microfiltration of activated sludge wastewater**, *Journal of Membrane Science*, **216**, pp. 279-290
- Liu, H., Yang, C., Pu, W. and Zhang, J. (2009), **Formation mechanism and structure of dynamic membrane in the dynamic membrane bioreactor**, *Chemical Engineering Journal*, **148**, pp. 290-295
- Liu, R., Huang, X., Sun, Y.F. and Qian, Y. (2003), **Hydrodynamic effect on sludge accumulation over membrane surfaces in a submerged membrane bioreactor**, *Process Biochemistry*, **39**, pp. 157-163
- Liu, R., Huang, X., Wang, C., Chen, L. and Qian, Y. (2000), **Study on hydraulic characteristics in a submerged membrane bioreactor process**, *Process Biochemistry*, **36**, pp. 249-254
- Livingston, A.G. and Zhang, S.F. (1993), **Hydrodynamic behaviour of three-phase (gas-liquid-solid) airlift reactors**, *Chemical Engineering Science*, **48**(9), pp. 1641-1654

-
- Lu, W.-J., Hwang, S.-J. and Chang, C.-M. (1995), **Liquid velocity and gas holdup in three-phase internal loop airlift reactors with low-density particles**, *Chemical Engineering Science*, **50**(8), pp. 1301-1310
- Lu, W.-M. and Ju, S.-C. (1989), **Selective particle deposition in crossflow filtration**, *Separation Science and Technology*, **24**, pp. 512-540
- Lu, X., Ding, J., Wang, Y. and Shi, J. (2000), **Comparison of the hydrodynamics and mass transfer characteristics of a modified square airlift reactor with common airlift reactors**, *Chemical Engineering Science*, **55**, pp. 2257-2263
- Lynch, J.L. and Edyvean, R.G.J. (1988), **Biofouling in oilfield water systems – a review**, *Biofouling*, **1**, pp. 147-162
- Ma, H., Hakim, L.F., Bowman, C.N. and Davis, R.H. (2001), **Factors affecting membrane fouling reduction by surface modification and backpulsing**, *Journal of Membrane Science*, **189**, pp. 255-270
- Maartens, A., Jacobs, E.P. and Swart, P. (2002), **UF of pulp and paper effluent: membrane fouling prevention and cleaning**, *Journal of Membrane Science*, **209**, pp. 81-92
- Mackley, M.R. and Sherman, N.E. (1994), **Cross-flow filtration with and without cake formation**, *Chemical Engineering Science*, **49**(2), pp. 171-178
- Mairal, A.P., Greenberg, A.R. and Krantz, W.B. (2000), **Investigation of membrane fouling and cleaning using ultrasonic time-domain reflectometry**, *Desalination*, **130**, pp. 45-60
- Mairal, A.P., Greenberg, A.R., Krantz, W.B. and Bond, L.J. (1999), **Real-time measurement of inorganic fouling of RO desalination membranes using ultrasonic time-domain reflectometry**, *Journal of Membrane Science*, **159**, pp. 185-196
- Marshall, K.C. and Blainey, B.L. (1991), **Role of bacterial adhesion in biofilm formation and biocorrosion**, in: Flemming, H.-C. and Geesey, G.G. (eds.), *Biofouling and Biocorrosion in Industrial Water Systems*, Springer-Verlag, Berlin, pp. 29-46
- Matthiasson, E. (1983), **The role of macromolecular adsorption in fouling of ultrafiltration membranes**, *Journal of Membrane Science*, **16**, pp. 23-36
- Matthiasson, E. and Sivik, B. (1980), **Concentration polarisation and fouling**, *Desalination*, **35**, pp. 59-103
- McCarthy, A.A., Walsh, P.K. and Foley, G. (2002), **Experimental techniques for quantifying the cake mass, the cake and membrane resistances and the specific cake resistance during crossflow filtration of microbial suspensions**, *Journal of Membrane Science*, **201**, pp. 31-45
- McDonogh, R., Schaule, G. and Flemming, H.-C. (1994), **The permeability of biofouling layers on membranes**, *Journal of Membrane Science*, **87**, pp. 199-217
-

-
- Meng, F., Chae, S.-R., Drews, A., Kraume, M., Shin, H.-S. and Yang, F. (2009), **Review – Recent advances in membrane bioreactors (MBRs): Membrane fouling and membrane material**, *Water Research*, **43**, pp. 1489-1512
- Merchuk, J.C. and Berzin, I. (1995), **Distribution of energy dissipation in airlift reactors**, *Chemical Engineering Science*, **50**(14), pp 2225-2233
- Mercier, M., Fonade, C. and Lafforgue-Delorme, C. (1997), **How slug flow can enhance the ultrafiltration flux in mineral tubular membranes**, *Journal of Membrane Science*, **128**, pp 103-113
- Mercier-Bonin, M., Daubert, I., Léonard, D., Maranges, C., Fonade, C. and Lafforgue, C. (2001), **How unsteady filtration conditions can improve the process efficiency during cell cultures in membrane bioreactors**, *Separation and Purification Technology*, **22-23**, pp. 601-615
- Mercier-Bonin, M., Lagane, C. and Fonade, C. (2000), **Influence of a gas/liquid two-phase flow on the ultrafiltration and microfiltration performances: case of a ceramic flat sheet membrane**, *Journal of Membrane Science*, **180**, pp. 93-102
- Mietton, M. and Ben Aim, R. (1992), **Improvement of crossflow microfiltration performances with flocculation**, *Journal of Membrane Science*, **68**, pp. 241-248
- Milicic, V. and Bersillon, J.L. (1986), **Anti-fouling techniques in cross-flow microfiltration**, *Filtration and Separation*, **23**, pp. 347-349
- Mores, W.D., Bowman, C.N. and Davis, R.H. (2000), **Theoretical and experimental flux maximization by optimization of backpulsing**, *Journal of Membrane Science*, **165**, pp. 225-236
- Mukherjee, S., Das, P., Sivapathasekaran, C. and Sen, R. (2008), **Enhanced production of biosurfactant by a marine bacterium on statistical screening of nutritional parameters**, *Biochemical Engineering Journal*, **42**, pp. 254-260
- Nagaoka, H., Yamanishi, S. and Miya, A. (1998), **Modeling of biofouling by extracellular polymers in a membrane separation activated sludge system**, *Water Science and Technology*, **38**(4-5), pp. 497-504
- Nagaoka, H., Kono, S., Yamanishi, S. and Miya, A. (2000), **Influence of organic loading rate on membrane fouling in membrane separation activated sludge process**, *Water Science and Technology*, **41**(10-11), pp. 355-362
- Ngo, H.-H., Guo, W. and Xing, W. (2008), **Evaluation of a novel sponge-submerged membrane bioreactor (SSMBR) for sustainable water reclamation**, *Bioresource Technology*, **99**, pp. 2429-2435
- Ognier, S., Wisniewski, C. and Grasmick, A. (2004), **Membrane bioreactor fouling in sub-critical filtration conditions: a local critical flux concept**, *Journal of Membrane Science*, **229**, pp. 171-177

-
- Oita, I., Halewyck, H., Pieters, S., Dejaegher, B., Thys, B., Rombaut, B. and Vander Heyden, Y. (2009), **Improving the capillary electrophoretic analysis of poliovirus using a Plackett-Burman design**, *Journal of Pharmaceutical and Biomedical Analysis*, **50**(4), pp. 655-663
- Otis, J.R., Altena, F.W., Mahar, J.T. and Belfort, G. (1986), **Measurements of single spherical particle trajectories with lateral migration in a slit with one porous wall under laminar flow conditions**, *Experiments in Fluids*, **4**, pp. 1-10
- Ozaki, N. and Yamamoto, K. (2001), **Hydraulic effects on sludge accumulation on membrane surface in crossflow filtration**, *Water Research*, **35**(13), pp. 3137-3146
- Pasmore, M., Todd, P., Smith, S., Baker, D., Silverstein, J., Coons, D. and Bowman, C.N. (2001), **Effects of ultrafiltration membrane surface properties on *Pseudomonas aeruginosa* biofilm initiation for the purpose of reducing biofouling**, *Journal of Membrane Science*, **194**, pp. 15-32
- Pearce, G. (2008), **Introduction to membranes – MBRs: Manufacturers' comparison: part 1**, *Filtration & Separation*, **45**(2), pp. 28-31
- Peterson, R.A., Greenberg, A.R., Bond, L.J. and Krantz, W.B. (1998), **Use of ultrasonic TDR for real-time noninvasive measurement of compressive strain during membrane compaction**, *Desalination*, **116**, pp. 115-122
- Pillay, V.L. (1991), **Modelling of turbulent cross-flow microfiltration of particulate suspensions**, Ph.D. thesis, University of Natal, South Africa
- Piron, E., René, F. and Latrille, E. (1995), **A cross-flow microfiltration model based on integration of the mass transport equation**, *Journal of Membrane Science*, **108**, pp. 57-70
- Pollice, A., Brookes, A., Jefferson, B. and Judd, S. (2005), **Sub-critical flux fouling in membrane bioreactors – a review of recent literature**, *Desalination*, **174**, pp. 221-230
- Porter, M.C. (1972), **Concentration polarization with membrane ultrafiltration**, *Industrial and Engineering Chemistry, Product Research and Development*, **11**(3), pp. 234-248
- Porter, M.C. (1977), **What, when and why of membranes – MF, UF and RO**, *AIChE Symposium Series*, **73**(171), pp. 83-103
- Rabie, H.R., Côté, P. and Adams, N. (2001), **A method for assessing membrane fouling in pilot- and full-scale systems**, *Desalination*, **141**, pp. 237-243
- Redkar, S., Kuberkar, V. and Davis, R.H. (1996), **Modelling of concentration polarization and depolarization with high-frequency backpulsing**, *Journal of Membrane Science*, **121**, pp. 229-242

- Reed, R.H. and Belfort, G. (1982), **Characterization of fouling potential for pressure-driven membrane processes: a new simulated flow cell**, *Water Science and Technology*, **14**, pp. 499-522
- Ridgway, H.F. and Safarik, J. (1991), **Biofouling of reverse osmosis membranes**, in: Flemming, H.-C. and Geesey, G.G. (eds.), *Biofouling and Biocorrosion in Industrial Water Systems*, Springer-Verlag, Berlin, pp. 81-111
- Romero, C.A. and Davis, R.H. (1988), **Global model of crossflow microfiltration based on hydrodynamic particle diffusion**, *Journal of Membrane Science*, **39**, pp. 157-185
- Romero, C.A. and Davis, R.H. (1990), **Transient model of crossflow microfiltration**, *Chemical Engineering Science*, **45**(1), pp. 13-25
- Sadr Ghayeni, S.B., Beatson, P.J., Schneider, R.P. and Fane, A.G. (1998), **Adhesion of waste water bacteria to reverse osmosis membranes**, *Journal of Membrane Science*, **138**, pp. 29-42
- Sayed Razavi, S.K. and Harris, J.L. (1996), **Shear controlled model of the ultrafiltration of soy suspensions**, *Journal of Membrane Science*, **118**, pp. 279-288
- Schwinge, J., Wiley, D.E., Fane, A.G. and Guenther, R. (2000), **Characterization of a zigzag spacer for ultrafiltration**, *Journal of Membrane Science*, **172**, pp. 19-31
- Segré, G. and Silberberg, A. (1961), **Radial particle displacements in Poiseuille flow of suspensions**, *Nature*, **189**, pp. 209-210
- Seminario, L., Rozas, R., Bórques, R. and Toledo, P.G. (2002), **Pore blocking and permeability reduction in cross-flow microfiltration**, *Journal of Membrane Science*, **209**, pp. 121-142
- Serra, C., Durand-Bourlier, L., Clifton, M.J., Moulin, P., Rouch, J.-C. and Aptel, P. (1999), **Use of air sparging to improve backwash efficiency in hollow-fibre modules**, *Journal of Membrane Science*, **161**, pp. 95-113
- Shim, J.K., Yoo, I.-K. and Lee, Y.M. (2002), **Design and operation considerations for wastewater treatment using a flat submerged membrane bioreactor**, *Process Biochemistry*, **38**, pp. 279-285
- Shimizu, Y., Uryu, K., Okuno, Y.-I., Ohtubo, S. and Watanabe, A. (1997), **Effect of particle size distributions of activated sludges on cross-flow microfiltration flux for submerged membranes**, *Journal of Fermentation and Bioengineering*, **83**(6), pp. 583-589
- Shimizu, Y., Uryu, K., Okuno, Y.-I. and Watanabe, A. (1996), **Cross-flow microfiltration of activated sludge using submerged membrane with air bubbling**, *Journal of Fermentation and Bioengineering*, **81**(1), pp. 55-60
- Shulz, G. and Ripperger, S. (1989), **Concentration polarization in crossflow microfiltration**, *Journal of Membrane Science*, **40**, pp. 173-187

-
- Siegel, M.H., Merchuk, J.C. and Schugerl, K. (1986), **Air-lift reactor analysis: interrelationships between riser, downcomer, and gas-liquid separator behavior, including gas recirculation effects**, *AIChE Journal*, **32**(10), pp. 1585-1596
- Silva, C.M., Reeve, D.W., Husain, H., Rabie, H.R. and Woodhouse, K.A. (2000), **Model for flux prediction in high-shear microfiltration systems**, *Journal of Membrane Science*, **173**, pp. 87-98
- Stamatakis, K. and Tien, C. (1993), **A simple model of cross-flow filtration based on particle adhesion**, *AIChE Journal*, **39**(8), pp. 1292-1302
- Stephenson, T., Judd, S., Jefferson, B. and Brindle, K. (2000a), **Membrane bioreactors for wastewater treatment**, IWA Publishing, London
- Stephenson, T., Judd, S., Jefferson, B. and Brindle, K. (2000b), **Membrane bioreactors for wastewater treatment**, IWA Publishing, London, p. 32
- Stewart, D.I., Studds, P.G. and Cousens, T.W. (2003), **The factors controlling the engineering properties of bentonite-enhanced sand**, *Applied Clay Science*, **23**, pp. 97-110
- Suda, K., Shibuya, S., Itoh, Y. and Kohno, T. (1998), **Development of a tank-submerged type membrane filtration system**, *Desalination*, **119**, pp. 151-158
- Suki, A., Fane, A.G. and Fell, C.J.D. (1986), **Modelling fouling mechanisms in protein ultrafiltration**, *Journal of Membrane Science*, **27**, pp. 181-193
- Swart, A.F. (1993), **Considerations in the selection of the operating regimes for microfiltration**, M.Sc.Eng. thesis, University of Natal, South Africa
- Swart, A.F., Brouckaert, C.J. and Buckley, C.A. (1994), **Criteria for selecting the operating regime of the crossflow microfilter or the tubular filter press for clarification of turbid waters**, *Journal of Membrane Science*, **87**, pp. 57-69
- Tansel, B., Bao, W.Y. and Tansel, I.N. (2000), **Characterization of fouling kinetics in ultrafiltration systems by resistances in series model**, *Desalination*, **129**, pp. 7-14
- Tardieu, E., Grasmick, A., Geaugey, V. and Manem, J. (1998), **Hydrodynamic control of bioparticle deposition in a MBR applied to wastewater treatment**, *Journal of Membrane Science*, **147**, pp. 1-12
- Tardieu, E., Grasmick, A., Geaugey, V. and Manem, J. (1999), **Influence of hydrodynamics on fouling velocity in a recirculated MBR for wastewater treatment**, *Journal of Membrane Science*, **156**, pp. 131-140
- Tay, J.-H., Liu, J. and Sun, D.D. (2003), **Quantification of membrane fouling using thermogravimetric method**, *Journal of Membrane Science*, **217**, pp. 17-28

-
- Tiranuntakul, M., Jegatheesan, V., Schneider, P.A. and Fracchia, H.L. (2005), **Performance of an oxidation ditch retrofitted with a membrane bioreactor during the start-up**, *Desalination*, **183**, pp. 417-424
- Trussell, R.S., Merlo, R.P., Hermanowicz, S.W. and Jenkins, D. (2007), **Influence of mixed liquor properties and aeration intensity on membrane fouling in a submerged membrane bioreactor at high mixed liquor suspended solids concentrations**, *Water Research*, **41**, pp. 947-958
- Ueda, T., Hata, K., Kikuoka, Y. and Seino, O. (1997), **Effects of aeration on suction pressure in a submerged membrane bioreactor**, *Water Research*, **31**(3), pp. 489-494
- Van Baten, J.M., Ellenberger, J. and Krishna, R. (2003), **Hydrodynamics of internal air-lift reactors: experiments versus CFD simulations**, *Chemical Engineering and Processing*, **42**, pp. 733-742
- Van der Merwe, J.J. (2003), Personal communication, Department of Geology, University of Stellenbosch, Stellenbosch, South Africa
- Van der Merwe, J.J. (2004), **Parameters affecting accuracy and reproducibility of sedigraph particle size analysis of clays**, Master thesis, University of Stellenbosch, Stellenbosch, South Africa
- Van't Oever, R. (2005), **MBR focus: is submerged best?**, *Filtration & Separation*, **42**(5), pp. 24-27
- Vasseur, P. and Cox, R.G. (1976), **The lateral migration of a spherical particle in two-dimensional shear flows**, *Journal of Fluid Mechanics*, **78**, pp. 385-413
- Vassilieff, C.S., Doneva, T.A. and Ljutov, L.G. (1996), Cross-flow microfiltration of bentonite-in-water dispersions: initial transient effects at low concentration, *Journal of Membrane Science*, **119**, pp. 65-80
- Vatanara, A., Najafabadi, A.R., Gilani, K., Asgharian, R., Darabi, M. and Rafiee-Tehrani, M. (2007), **A Plackett-Burman design for screening of the operation variables in the formation of salbutamol sulphate particles by supercritical antisolvent**, *Journal of Supercritical Fluids*, **40**, pp. 111-116
- Verrecht, B., Judd, S., Guglielmi, G., Brepols, C. and Mulder, J.W. (2008), **An aeration energy model for an immersed membrane bioreactor**, *Water Research*, **42**, pp. 4761-4770
- Vigneswaran, S., Kwon, D.Y., Ngo, H.H. and Hu, J.Y. (2000), **Improvement of microfiltration performance in water treatment: is critical flux a viable solution?**, *Water Science Technology*, **41**(10-11), pp. 309-315
- Vrijenhoek, E.M., Hong, S. and Elimelech, M. (2001), **Influence of membrane surface properties on initial rate of colloidal fouling of reverse osmosis and nanofiltration membranes**, *Journal of Membrane Science*, **188**, pp. 115-128

-
- Vrouwenvelder, J.S. and Van der Kooij, D. (2001), **Diagnosis, prediction and prevention of biofouling of NF and RO membranes**, *Desalination*, **139**, pp. 65-71
- Vyas, H.K., Bennett, R.J. and Marshall, A.D. (2002), **Performance of crossflow microfiltration during constant transmembrane pressure and constant flux operations**, *International Dairy Journal*, **12**, pp. 473-479
- Wakeman, R.J. and Williams, C.J. (2002), **Additional techniques to improve microfiltration**, *Separation and Purification Technology*, **26**, pp. 3-18
- Wang, J. and Wan, W. (2009), **Experimental design methods for fermentative hydrogen production: A review**, *International Journal of Hydrogen Energy*, **34**, pp. 235-244
- Wicaksana, F., Fane, A.G. and Chen, V. (2006), **Fibre movement induced by bubbling using submerged hollow fibre membranes**, *Journal of Membrane Science*, **271**, pp. 186-195
- Winzeler, H.B. and Belfort, G. (1993), **Enhanced performance for pressure-driven membrane processes: the argument for fluid instabilities**, *Journal of Membrane Science*, **80**, pp. 35-47
- Wongsuchoto, P., Charinpanitkul, T. and Pavasant, P. (2003), **Bubble size distribution and gas-liquid mass transfer in airlift contactors**, *Chemical Engineering Journal*, **92**, pp. 81-90
- Wu, D., Howell, J.A. and Field, R.W. (1999), **Critical flux measurement for model colloids**, *Journal of Membrane Science*, **152**, pp. 89-98
- Wu, J., Le-Clech, P., Stuetz, R.M., Fane, A.G. and Chen, V. (2008a), **Effects of relaxation and backwashing conditions on fouling in membrane bioreactor**, *Journal of Membrane Science*, **324**, pp. 26-32
- Wu, Z., Wang, Z., Huang, S., Mai, S., Yang, C., Wang, X. and Zhou, Z. (2008b), **Effects of various factors on critical flux in submerged membrane bioreactors for municipal wastewater treatment**, *Separation and Purification Technology*, **62**, pp. 56-63
- Xu, X., Li, J., Li, H., Cai, Y., Cao, Y., He, B. and Zhang, Y. (2009), **Non-invasive monitoring of fouling in hollow fibre membrane via UTDR**, *Journal of Membrane Science*, **326**, pp. 103-110
- Ye, Y., Le Clech, P., Chen, V. and Fane, A.G. (2005), **Evolution of fouling during crossflow filtration of model EPS solutions**, *Journal of Membrane Science*, **264**, pp. 190-199
- Zhang, K., Cui, Z. and Field, R.W. (2009), **Effect of bubble size and frequency on mass transfer in flat sheet MBR**, *Journal of Membrane Science*, **332**, pp. 30-37

Addendum A

Model foulant preparation

A.1 Introduction

A model foulant is an artificial wastewater feed which is exclusively used as a standard fouling agent to investigate the fouling behaviour for a specific membrane system. The main advantage of preparing and using a model foulant in membrane fouling experiments, as opposed to an acquired real life wastewater feed, is the possible elimination of variations in the chemical and physical properties. The consistency of such a prepared foulant reduces unknown factors and enables membrane fouling results to be explained by known factors which are set by the experimenter. The tailoring of these known factors to measure and compare the effect they have on membrane fouling forms the basis of membrane fouling experiments.

Besides consistency, other considerations, such as cost, safety, availability and practicality, may favour the use of a model foulant to a real life foulant. At least in the initial phases of fouling experiments in the development of a membrane system, the use of a model foulant is preferred to obtain an understanding of the membrane fouling dynamics. Thereafter the real life wastewater feed, which is ultimately to be treated by the membrane system, can be used for optimisation studies.

A.2 Model foulant selection

An appropriate model foulant should conform to meet certain requirements, namely:

- the foulant must behave reproducibly and therefore have the same properties in repeated preparations and experiments;
- the foulant must have industrial relevance and should simulate the fouling behaviour of the concerning wastewater to be treated as far as possible;
- the foulant's sizes and size distribution must be in accordance with the employed membrane's pore sizes;
- the foulant must exhibit a propensity to significantly foul the employed membrane;
- the foulant must be readily available for other researchers to reproduce the results; and
- should be known in the literature.

The technology developed in this project will ultimately be applied to the build of a membrane bioreactor for the treatment of wastewater with a high organic loading. It was therefore originally considered to use a prepared organic solution as a modelled wastewater for a membrane bioreactor [Ye et al., 2005]. Micro-organisms would have been inoculated into the solution and left to consume the nutrients for cell growth, as well as cell production, while the membrane would serve as barrier between the bio-phase and the permeate. Unfortunately the probable long start-up times and the complex behaviour of microbial growth, which would influence the properties of the wastewater, made the option of an organic solution as model foulant less favourable. Other factors, such as the risk of pathogenic contraction and the requirement for a more intense cleaning regime to remove biofouling from the membranes at the end of experiments, altogether led to the rejection of an organic solution as a model foulant.

The objective of this study was never to model biofouling in a membrane bioreactor, but to investigate the fouling dynamics for an immersed membrane system. So, for this study, regardless of the model foulant used and the resulting type of fouling, any fouling tendencies that could be identified, would aid in the design of the reactor and membrane module configurations of the future membrane bioreactor. Therefore, to eliminate biofouling for the sake of simplicity and reproducibility and only allow physico-chemical fouling mechanisms, it was decided to use a particulate suspension as model foulant.

A commercially available clay, bentonite (Ocean Bentonite, G&W Base & Industrial Minerals, South Africa), suspended in water, was selected as the model foulant for this study. Bentonite is an

attractive choice for a model foulant since it is relatively cheap, safe and allows for reproducibility. Bentonite particle sizes usually range from 0.5 to 10 μm [Gourgues et al., 1992; Van der Merwe, 2004] and thereby provide possible size distributions suited for both microfiltration and ultrafiltration membrane fouling experiments. The bentonite used in this study was however of a much coarser nature. The particle size distribution was measured with a Malvern Mastersizer and found to have a particle diameter of 18.53 μm at the 50th percentile. The particle size distribution of the bentonite used is shown in Figure A.1.

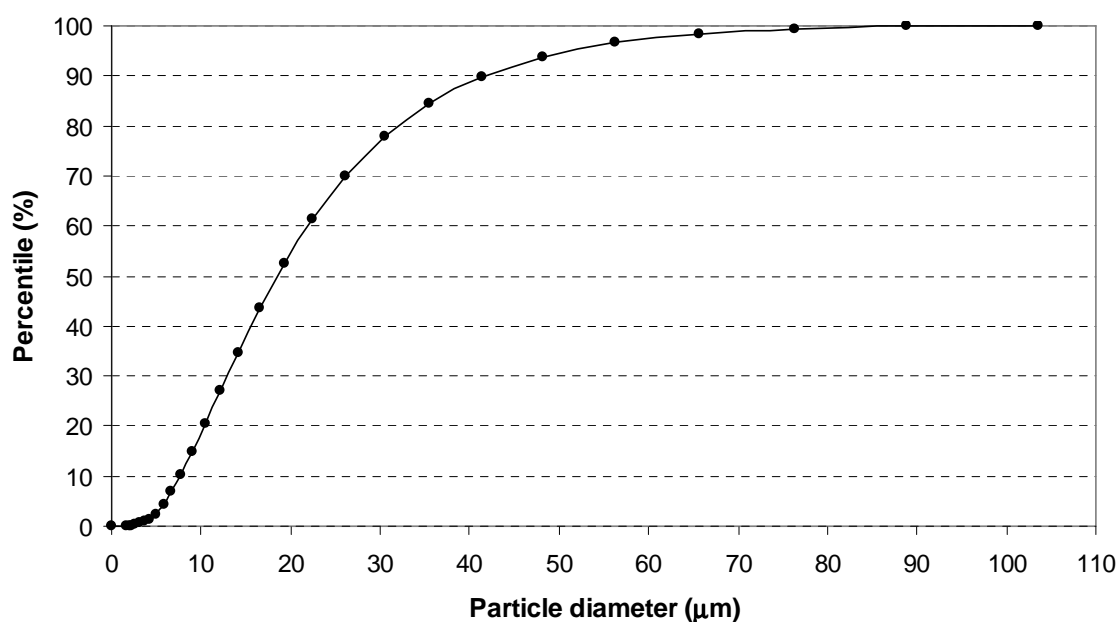


Figure A.1: Particle size distribution of the bentonite used in this study.

A bentonite particle is a thin lamella with the other dimensions approximately one hundred times larger than the thickness [Bacchin et al., 1996]. Bentonite therefore behaves as an excellent fouling agent, because when dispersed bentonite particles are deposited on the membrane surface, they collapse with their flat sides parallel to the membrane surface to form a densely layered and highly impermeable cake [Van der Merwe, 2003].

The use of bentonite as a model foulant has been widely documented for microfiltration and ultrafiltration membrane fouling experiments to investigate fundamental concepts of fouling [Gourgues et al., 1992; Bacchin et al., 1996; Vassilieff et al., 1996; Hamachi et al., 1999; Hamachi and Mietton-Peuchot, 1999, 2002; Seminario et al., 2002], to compare the efficiency of various fouling amelioration techniques [Milisic and Bersillon, 1986; Héran and Elmaleh, 2000; Guibert et al., 2002] and to measure the performance of membrane systems [Swart et al., 1994].

A.3 Suspension preparation

In preparing the model foulant, bentonite clay solids were required to disperse in reverse osmosis product water with a turbidity of less than 0.1 NTU. However, it was found that bentonite granules do not disperse easily in water since the bentonite particles in contact with the water swell and effectively seal the underlying particles from the water. The swelling phenomenon can be ascribed to the dominant mineral in bentonite, montmorillonite, which absorbs water in its interlayer crystal structure [Stewart et al., 2003]. Inadequate dispersing of the bentonite particles in water leads to the formation of a cloggy slurry.

Swart [1993] also experienced difficulty in dispersing bentonite in water, but reported that reproducible and dispersed suspensions could be prepared by applying high shear mixing and heat. Swart [1993] was able to disperse 1:1 mass proportions of the clays bentonite and kaolin in batches of 15 to 240 g in 1.5 L tap water by mixing it for 12 hours using a laboratory stirrer. This suspension was then added to a tank where it was diluted with tap water to the desired solids concentration. The resulting suspension was subjected to further stirring for 2 hours while heated to maintain a temperature of 30 °C.

A similar procedure was followed to prepare the model foulant bentonite suspensions in this study. Batch bentonite suspensions were prepared by adding 60 to 225 g of bentonite to approximately 1.5 L of reverse osmosis product water and stirring it overnight at a constant temperature of 30 °C. The combined mixing and heating of the bentonite suspensions seemed to effectively detach the particles from their aggregated state to become fully hydrated and dispersed. Although the suspensions appeared to be well dispersed after only a few hours of stirring and heating, no minimum mixing time was identified. Once a well dispersed suspension was prepared, it was added to the relevant tank and diluted to the correct solids concentration with reverse osmosis product water to create the model foulant for the specific fouling experiment.

It was considered to add a disinfectant to the model foulant to avoid micro-organisms from inhabiting the tank and biofouling the immersed membranes. The use of a standard disinfectant such as sodium azide [Maartens et al., 2002] would eventually work out too costly for the numerous and relative large volume experiments that were planned. Sodium azide is also very toxic and using it would require extra safety precautions and proper waste disposal protocols. The addition of a commercial swimming pool disinfectant (hth, Olin, South Africa), with calcium hypochlorite as active ingredient, was found to decrease the model foulant's pH and change the colloidal state of the bentonite particles to form aggregates with a reduced fouling propensity.

Consequently, it was decided to omit disinfection on the basis that the experimental treatments are too short to provide for any significant biological growth.

A.4 Turbidity calibration

A calibration curve was developed to correlate the concentration of the suspended bentonite with its turbidity. The calibration curve (Figure A.2) enabled the quick determination of the suspended bentonite concentration with the measurement of the turbidity of the suspension using a HACH 2100 turbidity meter. This technique to determine suspended concentrations has been used elsewhere by Gourgues et al. [1992] for bentonite suspensions and by Swart [1993] for kaolin and bentonite suspensions. Although this technique does not provide accurate suspended solids concentration values, it was found to provide acceptable indications for the studied bentonite suspensions.

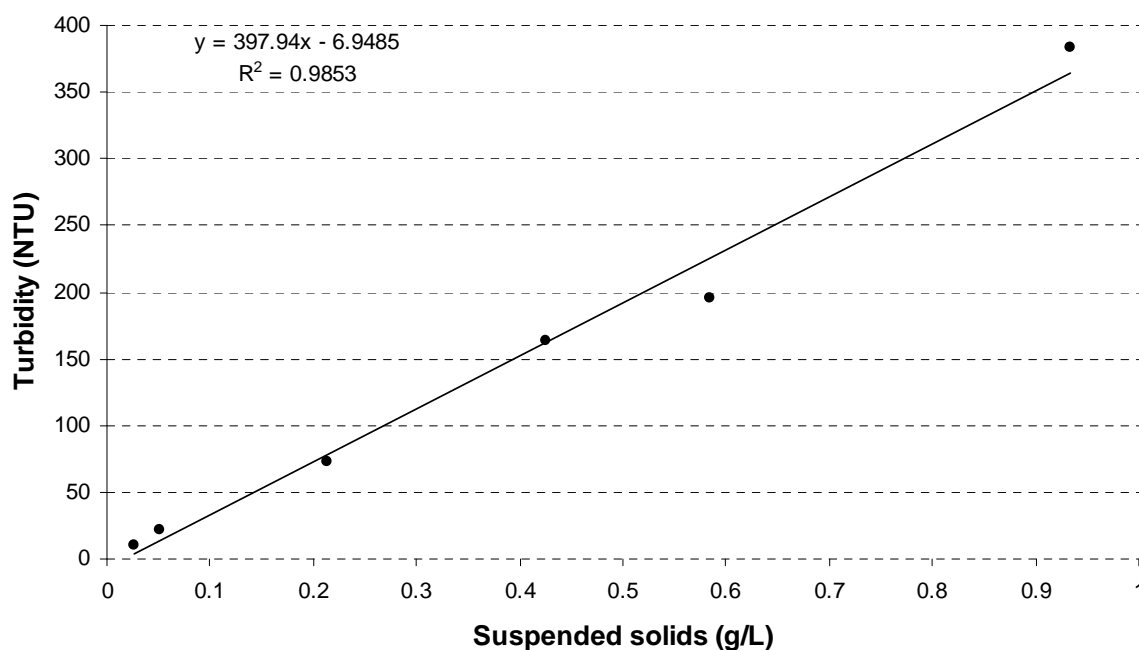


Figure A.2: Regressed calibration curve for bentonite suspensions.

Addendum B

Membrane element construction

B.1 Introduction

Membrane elements are the fundamental components of a membrane system capable of filtration. A collection of membrane elements are housed together in a membrane module. A number of membrane modules may be arranged to form a single membrane unit. Finally, a membrane system may comprise more than one membrane unit.

As a first approach, fouling behaviour was only studied on single immersed membrane elements. Results obtained from the studied membrane elements will ultimately provide guidelines to reduce membrane fouling in more complex membrane arrangements such as membrane modules and units.

For this study, a generic range of flat-sheet membrane elements were engineered by the same membrane material and production techniques. In a given experiment, the membrane elements that were employed only differed in their respective active filtration areas. The restriction of the constructional variables of the membrane elements to the active filtration area reduced the unknown factors, and thereby simplified data interpretation and enabled comparison of membrane fouling results.

B.2 Membrane material

A fabric of woven polyester was used as the membrane material. The obtained fabric consists of two layers that are interwoven in a manner to produce a series of separate tubes which provide for fluid flow channels. Similar tubular cloths were employed in cross-flow microfiltration studies by Pillay [1991], Swart [1993] and Swart et al. [1994], but whereas they studied pressurised inside-out filtration, the fabric had to facilitate outside-in filtration in this study. For outside-in filtration it is imperative to insert a spacer material in the filter tubes to keep them from collapsing and impeding fluid flow inside the tubes. In this study strips of woven stainless steel mesh were inserted in the tubes of the membrane material to act as spacer material. These spacer material strips were cut to have the same width as the membrane material tubes.

The woven fabric has a relative open weave and on its own may not be able to remove small particles in a filtration process to produce permeate of an acceptable quality. However, with the commencement of cake layer formation on the membrane surface, a dynamic membrane is created which reduces the effective pore sizes and enables the membrane to achieve higher permeate qualities [Pillay, 1991; Liu et al., 2009]. Alavi Moghaddam et al. [2001]; Chang et al. [2007] and Ngo et al. [2008] made use of non-woven coarse-pore filters as immersed membranes and highlighted the advantages of coarse-pore filtration, which are also gained by using the woven fabric of this study. They are:

- capable of high permeate fluxes;
- more energy efficient, since a TMP driving force as low as 2 to 3 kPa may be adequate for permeation;
- lower capital costs; and
- lower operating costs.

B.3 Membrane element production

The membrane elements for this study were fabricated in a casting procedure which was specially developed to produce physical resistant elements to ensure constructional integrity even after multiple fouling experiments and consequent harsh cleaning operations. The aim was not to optimise the membrane element design, but rather to produce elements of a standard format with reliable and repeatable performances in the shortest amount of time. With the employed casting procedure a membrane element could be manufactured in two days. Figure B.1 shows a photograph of three membrane elements under construction.



Figure B.1: A photograph of three membrane elements under construction.

Figure B.2 explains the casting techniques that were developed to produce a flat-sheet woven membrane element. Firstly, a membrane curtain is cut from the membrane material to include the required filtration area and an added 50 mm in length to compromise for the filtration area which will become inactive during the casting process (Figure B.2(a)). Since the membrane material comprises of a series of adjacent filter tubes, the width of the active membrane can only be selected in discrete quantities of filter tube widths of 39 mm. In addition the cut out membrane curtain also contains inactive tube remains on its sides (Figure B.2(b)).

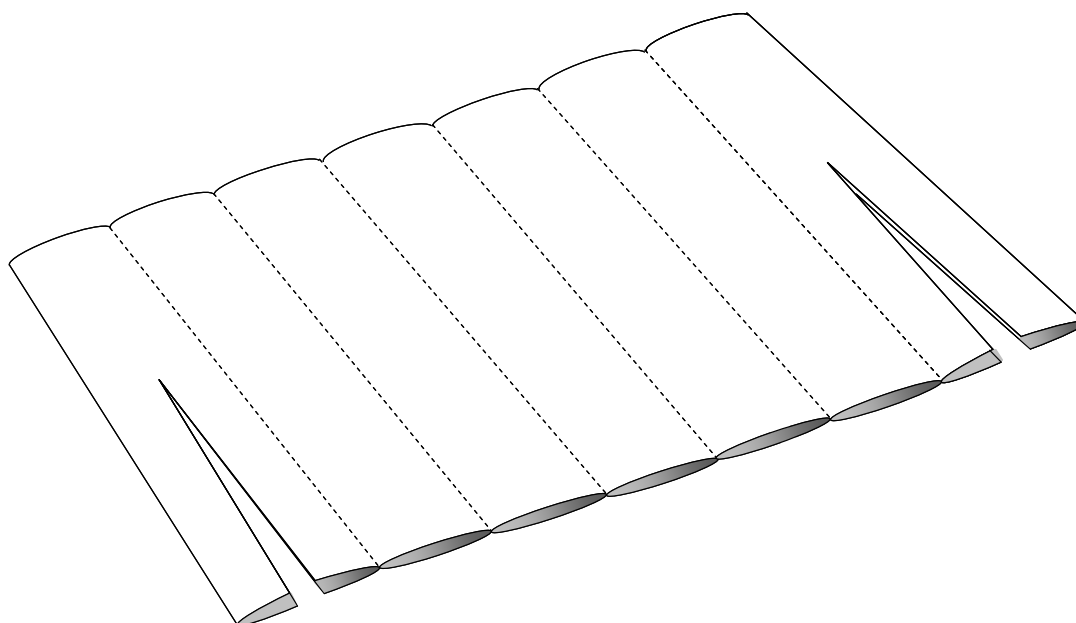


Figure B.2(a): Membrane curtain is cut from the membrane material.

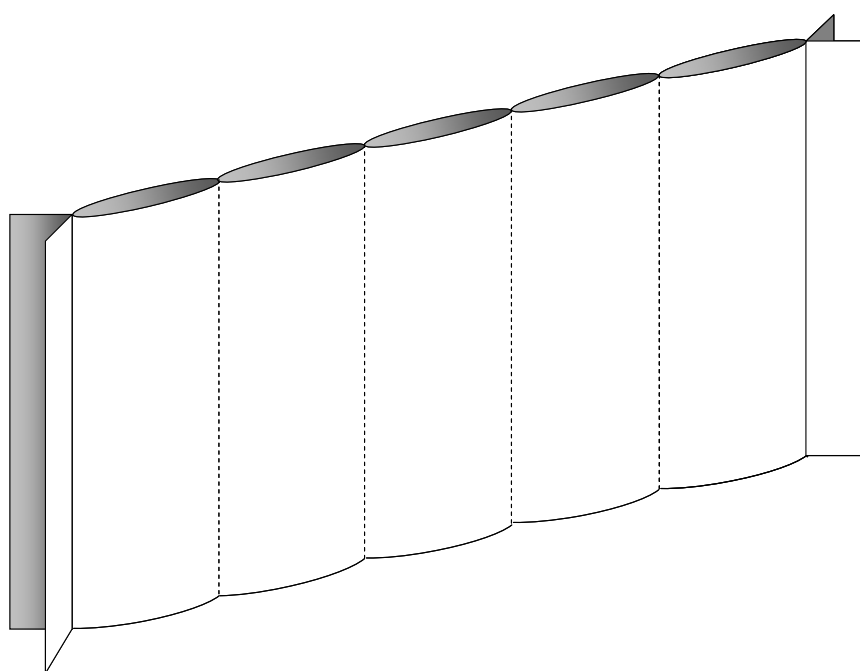


Figure B.2(b): Membrane curtain contains the selected number of filter tubes and the inactive tube remains on the sides

The stainless steel mesh spacer material strips, approximately 10 mm longer than the filter tubes' length, are inserted into the filter tubes (Figure B.2(c)). The membrane curtain, containing the spacer material strips, is now slotted into a 20 mm outer diameter PVC pipe with a slit the length of the cut membrane width, therefore including the tube remains on the membrane curtain's sides. These tube remains are glued together and sealed off from the adjacent filter tubes with any

commercially available silicon rubber sealant. Sealing off the tube remains fortifies the edges of the membrane curtain and avoid pinholing along the length of the seams, as experienced by Pillay [1991] and Swart [1993], to occur. Pinholing results in a loss of membrane integrity, since the seams move apart when subjected to a TMP to create holes through which larger particles can enter to reduce the quality of the permeate. The sides of the pipe are now closed off, taping proofed to be sufficient, and the first casting is ready to commence. Epoxy resin is introduced with a syringe through enlargements made on the ends of the slit in the pipe. The pipe is filled with the resin and left overnight to set, and effectively seal off the bottom end of the membrane curtain (Figure B.2(d)).

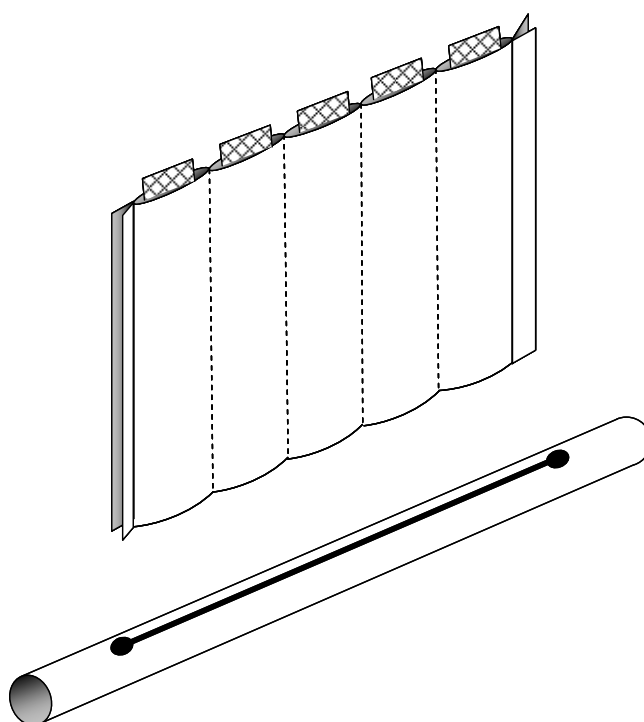


Figure B.2(c): Stainless steel mesh strips are inserted into the filter tubes to act as spacer material. The membrane curtain is then slotted inside a slit cut into a PVC pipe.

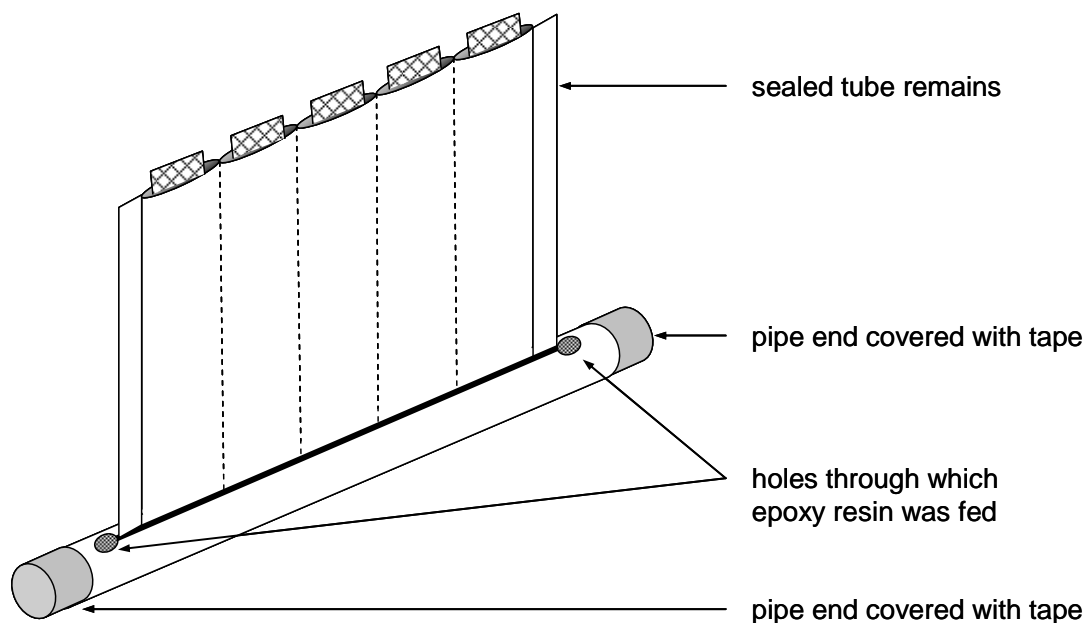


Figure B.2(d): Bottom end of membrane element sealed off.

The sealed off membrane curtain is turned around and this time the side with the protruding (approximately 10 mm) stainless steel mesh spacer material strips is slotted into a 20 mm outer diameter PVC pipe with a slit the length of the membrane curtain width. This pipe is to form part of the permeate collector of the membrane curtain's filter tubes. The pipe must have a length of 510 mm to fit into the mould which is to be used in the next casting step (see Figure B.3). A hole is drilled in line with the pipe's slit close to the edge on each end. Silicon rubber sealant is used to fashion plugs on the inside of the pipe behind the respective drilled holes (Figure B.2(e)). The slit containing the slotted membrane curtain's open end is sealed by applying silicon rubber sealant all around the membrane curtain entrance at the slit. The silicon rubber sealing at the membrane curtain entrance also helps to secure the membrane curtain's position (Figure B.2(f)).

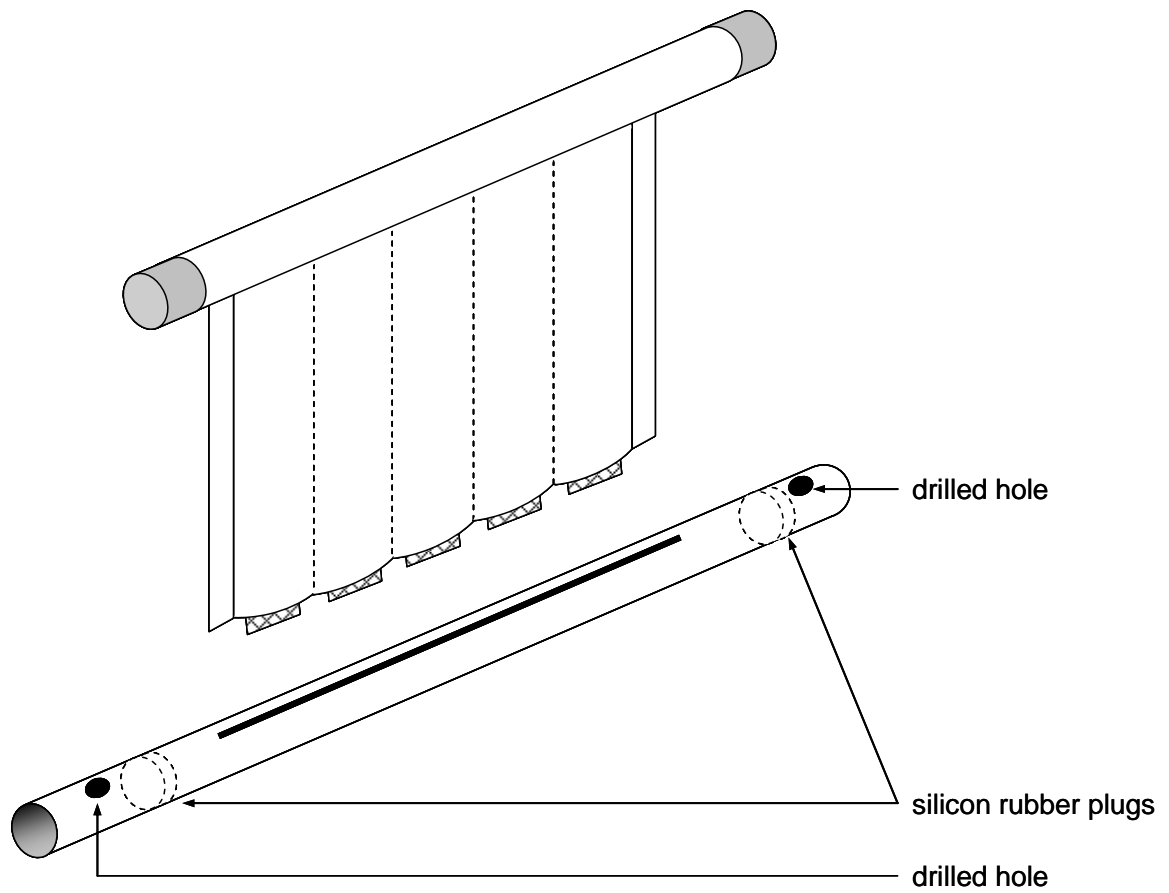


Figure B.2(e): Construction of the permeate collector.

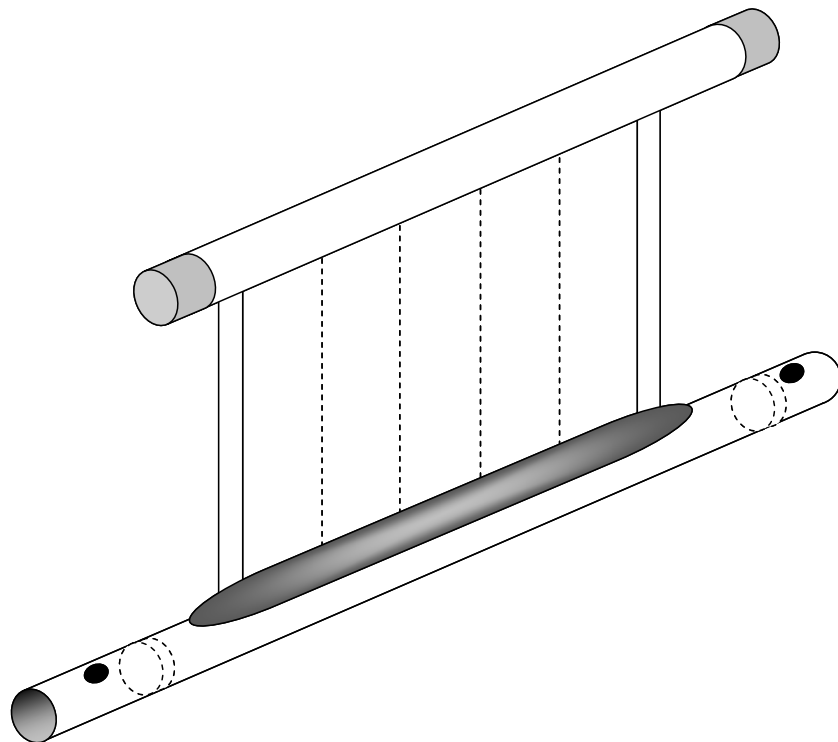


Figure B.2(f): Sealing of membrane curtain entrance at permeate collector.

The pipe housing the open end of the membrane curtain is positioned in a polyethylene mould comprising of four parts: two A blocks enclosing the respective ends of the pipe, and two B blocks enclosing the length of the pipe (Figure B.2(g)). A detail drawing of the mould is shown in Figure B.3. Epoxy resin is injected with a syringe into the housed pipe via tubes entering each A block (Figure B.2(h)). Inside the pipe the resin flow is however stopped by the silicon plugs and is consequently forced to exit the pipe through the drilled holes and encompass the length of the pipe and a fraction of the membrane curtain inside blocks B. The mould is filled with resin and left overnight to set. This casting technique enables the sealing of the pipe ends and the further securing of the membrane curtain with the permeate collector in a single step (Figure B.2(i)).

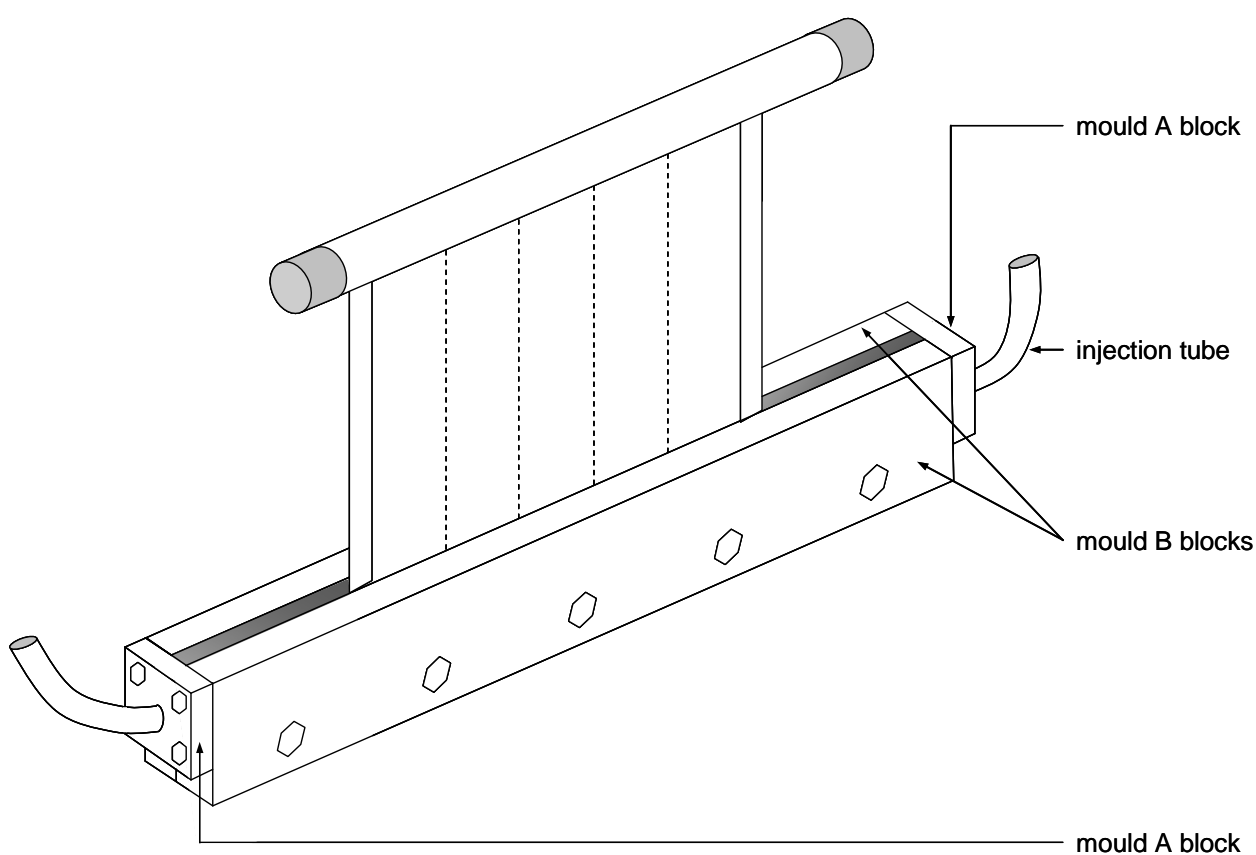


Figure B.2(g): The mould set-up around the permeate collector.

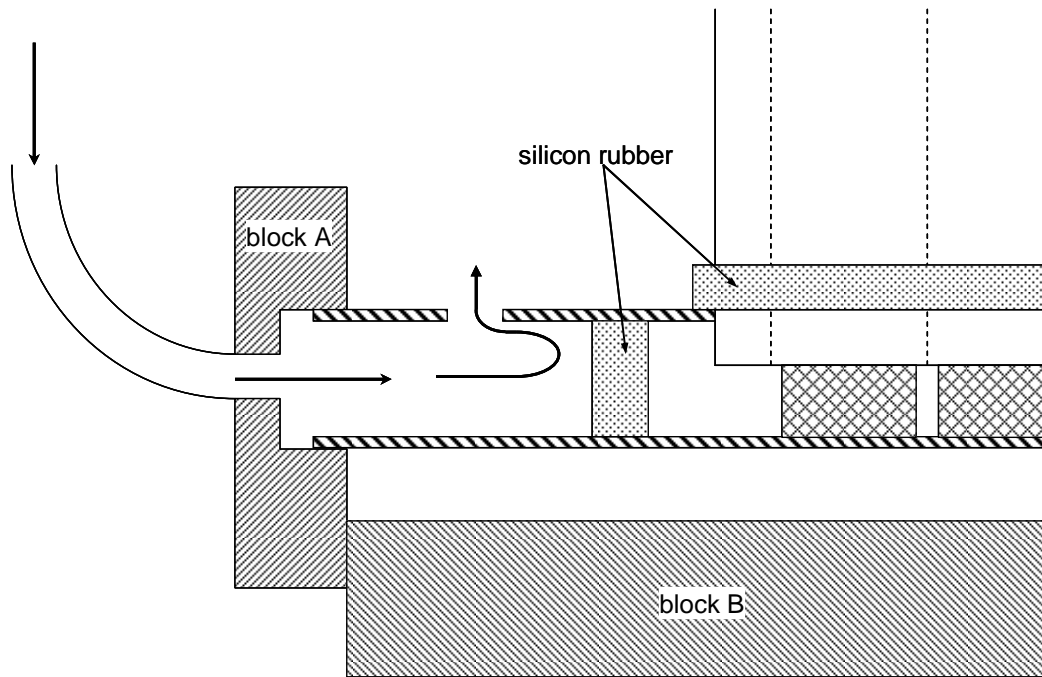


Figure B.2(h): The flow of the injected resin through the injection tube, into the PVC pipe and around the permeate collector.

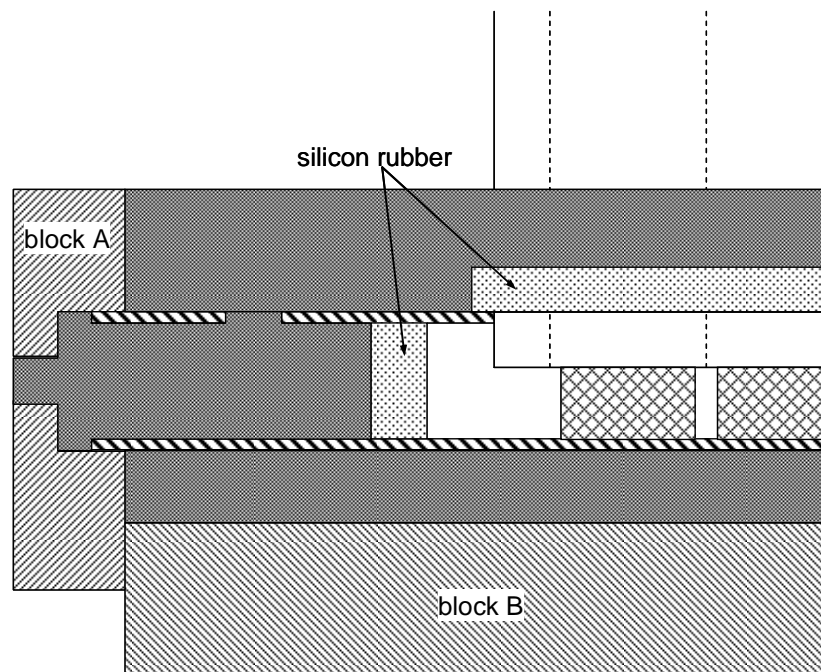


Figure B.2(i): The set resin around the permeate collector. Note how the silicon rubber plug and the silicon rubber sealing at the membrane curtain entrance keeps the permeate collector empty.

The polyethylene mould does not bind to the resin and may be removed once the resin has set to be used again in the production of a next membrane element. The undesired resin-filled pipes of the membrane element may be sawn off. A hole is drilled into the permeate collector and a tube fitting inserted and sealed with silicon rubber sealant (Figure B.2(j)). The permeate collection tube is connected to the tube fitting and the membrane element is ready for filtration. Figure B.2(k) shows a cross-section through the middle of the membrane element.

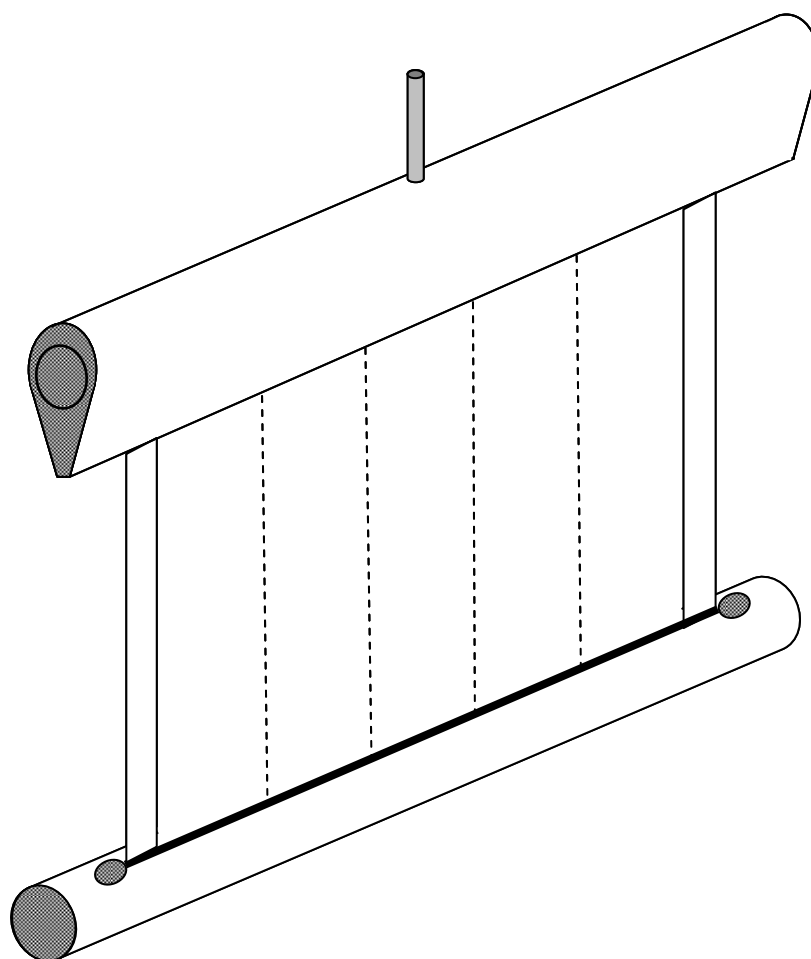


Figure B.2(j): The finished membrane element product. The resin filled parts of the bottom sealed pipe and the top permeate collector have been sawn off.

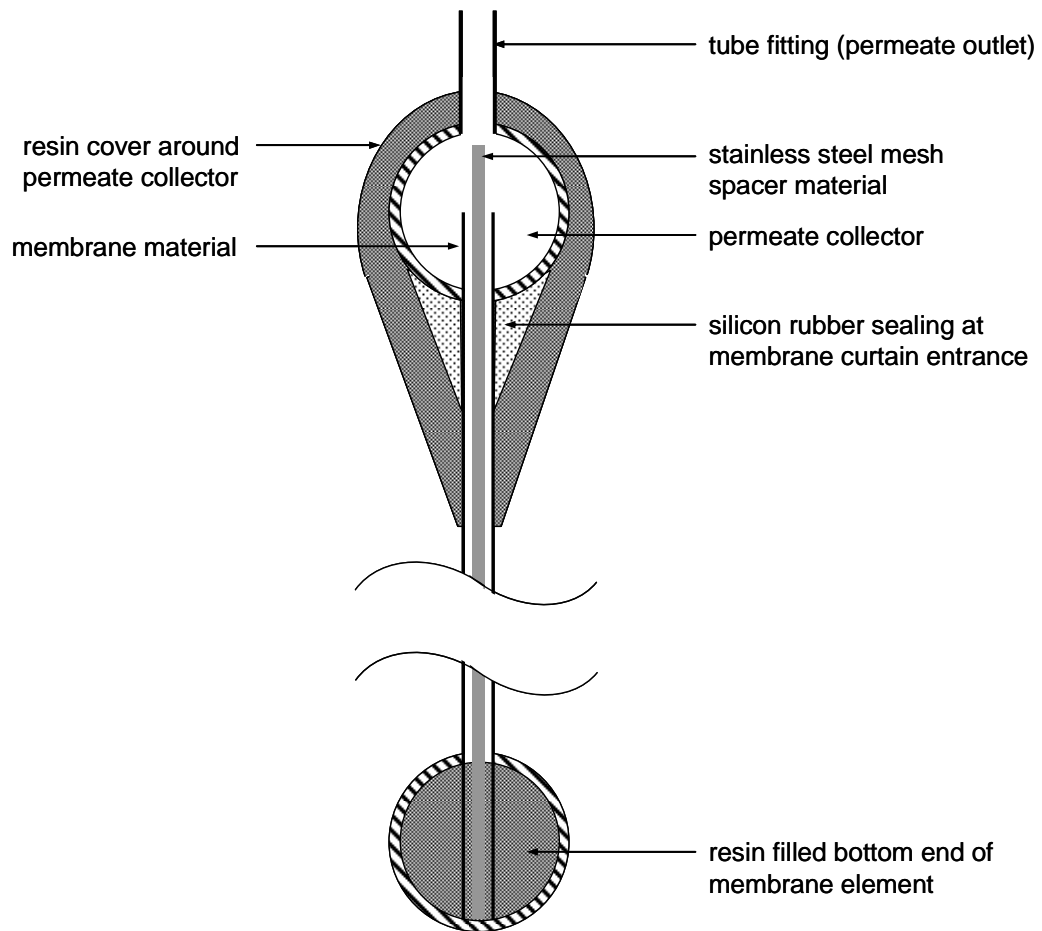


Figure B.2(k): Cross-section through the middle of a completed membrane element.

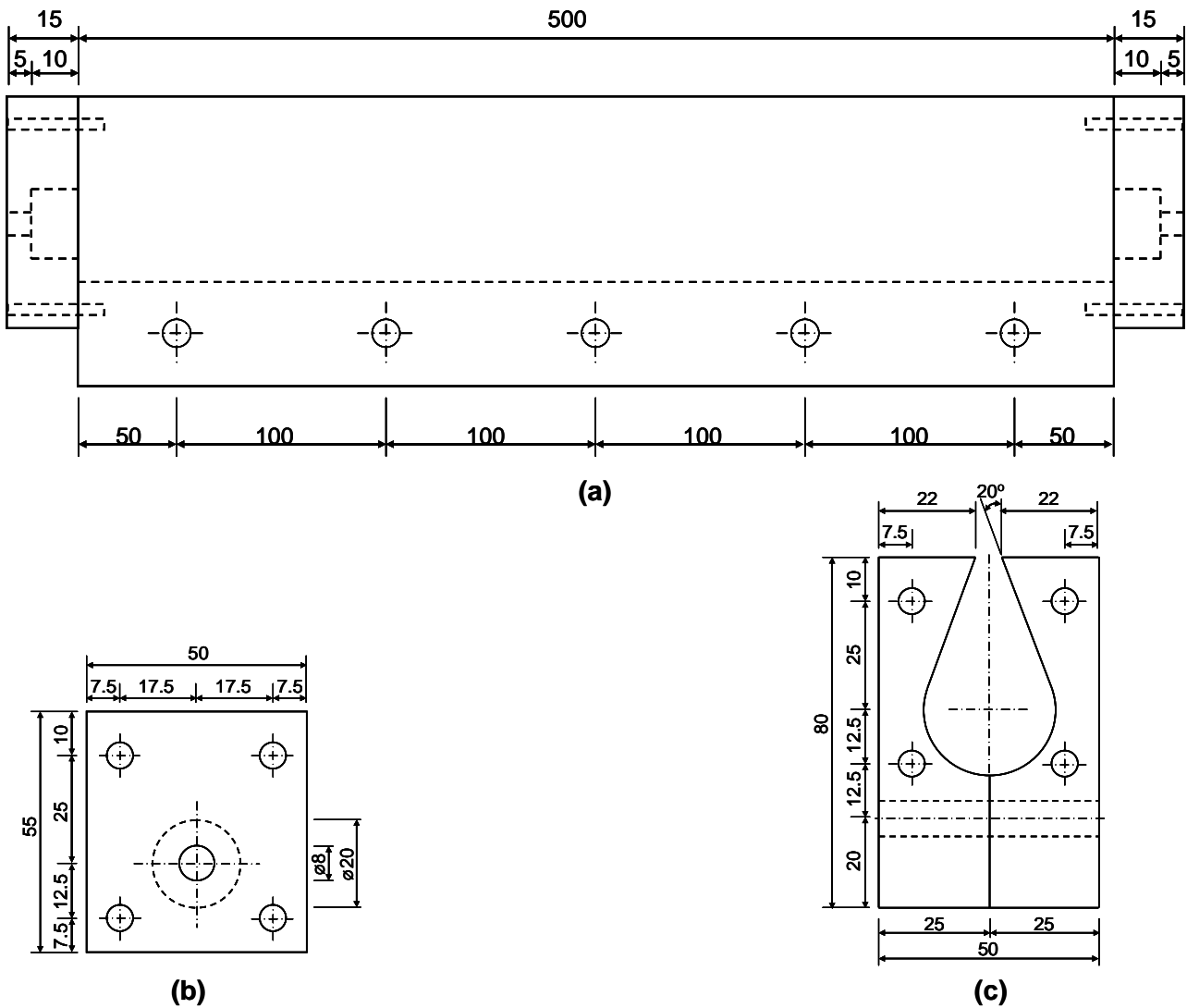


Figure B.3: Detail measurements of the polyethylene mould blocks: (a) blocks A and B connected to form the total mould; (b) one block A; and (c) both blocks B. Note that drawings are not to scale and that measurements are given in millimetres.

Addendum C

Flux-step experimental data

Flux-step experimental data at low aeration intensity (110 L/m².min) - Trial 2

Time (min)	Temperature (°C)	Nominal permeate flux (L/m ² . h)	Actual permeate flux (L/m ² . h)	dP (mm H ₂ O)
0	22.0	5	5.1	34
20	22.0	5	5.1	60
40	22.0	5	5.0	85
60	21.5	5	5.1	90
80	21.0	5	5.0	93
100	21.0	5	5.0	95
120	21.0	5	5.0	95
120	21.0	10	9.7	148
140	21.0	10	9.4	165
160	21.0	10	9.2	176
180	21.0	10	9.5	179
200	21.0	10	9.3	184
220	21.0	10	9.2	186
240	21.0	10	9.2	189
240	21.0	15	14.9	272
260	20.5	15	14.9	311
280	20.0	15	14.9	330
300	20.0	15	14.9	338
320	20.0	15	14.9	351
340	20.0	15	14.9	363
360	20.0	15	14.9	372
360	20.0	20	19.5	456
380	20.0	20	19.5	531
400	20.0	20	19.2	556
420	19.5	20	19.5	587
440	19.5	20	19.2	612
460	19.0	20	19.5	632
480	19.0	20	19.5	654
480	19.0	25	24.2	772
500	19.0	25	24.2	936
520	19.0	25	24.6	1041
540	19.0	25	25.0	1102
560	19.0	25	24.2	1165
580	19.0	25	24.2	1237
600	19.0	25	24.2	1307

Flux-step experimental data at low aeration intensity (110 L/m².min) - Trial 8

Time (min)	Temperature (°C)	Nominal permeate flux (L/m ² . h)	Actual permeate flux (L/m ² . h)	dP (mm H ₂ O)
0	22.5	5	4.9	28
20	22.5	5	5.1	55
40	22.5	5	5.1	79
60	22.5	5	5.1	86
80	22.0	5	5.1	88
100	22.0	5	5.0	89
120	22.0	5	5.0	89
120	22.0	10	10.0	136
140	22.0	10	10.0	159
160	22.0	10	10.0	163
180	22.0	10	10.0	165
200	22.0	10	9.8	169
220	22.0	10	9.8	172
240	22.0	10	9.8	177
240	22.0	15	15.2	255
260	21.5	15	15.2	290
280	21.5	15	15.2	314
300	21.5	15	15.0	329
320	21.5	15	15.2	348
340	21.5	15	15.2	354
360	21.5	15	15.2	364
360	21.5	20	19.5	439
380	21.5	20	19.7	508
400	21.5	20	19.7	542
420	21.5	20	19.7	567
440	21.0	20	19.7	586
460	21.0	20	20.3	604
480	21.0	20	20.3	632
480	21.0	25	25.4	761
500	21.0	25	25.4	894
520	21.0	25	25.0	986
540	21.0	25	25.0	1065
560	21.0	25	25.0	1120
580	21.0	25	25.4	1169
600	21.0	25	25.0	1236

Flux-step experimental data at intermediate aeration intensity (580 L/m².min) - Trial 3

Time (min)	Temperature (°C)	Nominal permeate flux (L/m ² . h)	Actual permeate flux (L/m ² . h)	dP (mm H ₂ O)
0	23.0	5	5.2	25
20	23.0	5	5.1	36
40	23.0	5	5.1	40
60	23.0	5	5.1	48
80	23.0	5	5.2	53
100	23.0	5	5.2	55
120	23.0	5	5.2	55
120	23.0	10	10.2	95
140	23.0	10	10.0	123
160	23.0	10	10.0	140
180	22.5	10	10.0	151
200	22.5	10	10.0	164
220	22.5	10	10.0	169
240	22.5	10	10.0	172
240	22.5	15	15.2	252
260	22.5	15	15.0	263
280	22.5	15	14.9	277
300	22.5	15	14.9	290
320	22.5	15	15.0	299
340	22.5	15	14.9	306
360	22.5	15	14.9	312
360	22.5	20	19.7	406
380	22.5	20	19.7	427
400	22.5	20	19.5	449
420	22.0	20	19.5	466
440	22.0	20	19.5	484
460	22.0	20	19.5	499
480	22.0	20	19.5	516
480	22.0	25	24.2	607
500	21.5	25	24.2	718
520	21.5	25	24.2	773
540	21.5	25	24.2	819
560	21.5	25	24.2	862
580	21.5	25	24.2	882
600	21.0	25	24.2	924

Flux-step experimental data at intermediate aeration intensity (580 L/m².min) - Trial 4

Time (min)	Temperature (°C)	Nominal permeate flux (L/m ² . h)	Actual permeate flux (L/m ² . h)	dP (mm H ₂ O)
0	21.5	5	4.9	32
20	21.5	5	4.9	44
40	21.5	5	5.0	46
60	21.5	5	5.1	50
80	21.5	5	5.0	50
100	21.5	5	5.1	50
120	21.0	5	5.1	50
120	21.0	10	9.8	115
140	21.0	10	9.8	132
160	21.0	10	9.8	160
180	21.0	10	9.8	169
200	21.0	10	9.7	171
220	21.0	10	9.7	174
240	21.0	10	9.7	176
240	21.0	15	14.7	230
260	21.0	15	14.9	249
280	21.0	15	14.9	258
300	21.0	15	14.9	273
320	20.5	15	14.7	284
340	20.5	15	14.9	292
360	20.5	15	14.9	299
360	20.5	20	20.0	375
380	20.5	20	20.0	403
400	20.5	20	20.3	418
420	20.0	20	19.7	432
440	20.0	20	19.7	448
460	20.0	20	20.0	463
480	20.0	20	19.7	469
480	20.0	25	24.6	546
500	20.0	25	24.6	654
520	20.0	25	24.6	706
540	20.0	25	24.6	760
560	20.0	25	24.6	793
580	19.5	25	25.0	817
600	19.5	25	25.0	846

Flux-step experimental data at high aeration intensity (1 100 L/m².min) - Trial 6

Time (min)	Temperature (°C)	Nominal permeate flux (L/m ² . h)	Actual permeate flux (L/m ² . h)	dP (mm H ₂ O)
0	20.0	5	5.3	23
20	20.0	5	5.1	43
40	20.0	5	5.1	76
60	20.0	5	5.1	82
80	20.0	5	5.0	85
100	20.0	5	5.1	89
120	20.0	5	5.0	89
120	20.0	10	9.8	133
140	20.0	10	10.0	178
160	20.0	10	9.8	185
180	20.0	10	10.0	192
200	20.0	10	10.2	197
220	20.0	10	10.0	202
240	20.0	10	10.0	206
240	20.0	15	15.2	300
260	19.5	15	15.2	332
280	19.5	15	15.2	353
300	19.5	15	15.0	365
320	19.5	15	15.0	378
340	19.5	15	15.2	391
360	19.0	15	15.2	423
360	19.0	20	19.5	516
380	19.0	20	19.2	556
400	19.0	20	19.2	584
420	19.0	20	19.2	607
440	19.0	20	19.5	646
460	19.0	20	19.2	683
480	19.0	20	19.2	711
480	19.0	25	24.2	929
500	19.0	25	25.0	1058
520	18.5	25	24.2	1156
540	18.5	25	24.2	1251
560	18.5	25	24.2	1343
580	18.5	25	24.2	1412
600	18.5	25	24.2	1496

Flux-step experimental data at high aeration intensity (1 100 L/m².min) - Trial 9

Time (min)	Temperature (°C)	Nominal permeate flux (L/m². h)	Actual permeate flux (L/m². h)	dP (mm H₂O)
0	22.0	5	5.0	28
20	22.0	5	5.0	40
40	22.0	5	5.0	66
60	22.0	5	5.0	82
80	22.0	5	5.0	89
100	22.0	5	4.9	92
120	22.0	5	5.0	94
120	22.0	10	9.7	144
140	21.5	10	9.7	191
160	21.5	10	9.7	207
180	21.5	10	9.8	217
200	21.5	10	9.7	222
220	21.5	10	10.0	228
240	21.5	10	9.7	233
240	21.5	15	15.2	327
260	21.5	15	15.2	374
280	21.5	15	15.2	388
300	21.0	15	15.2	396
320	21.0	15	15.2	409
340	21.0	15	15.0	421
360	20.5	15	15.0	435
360	20.5	20	20.3	543
380	20.5	20	20.0	601
400	20.5	20	20.0	629
420	20.5	20	20.0	652
440	20.0	20	20.0	688
460	20.0	20	20.0	717
480	20.0	20	20.0	743
480	20.0	25	24.6	984
500	20.0	25	24.6	1116
520	20.0	25	24.2	1190
540	20.0	25	24.6	1279
560	20.0	25	24.2	1361
580	20.0	25	24.2	1468
600	20.0	25	24.6	1551

Addendum *D*

UTDR experimental data

Determining speed of sound in bentonite cake layer

The weight ratio of bentonite to water in a bentonite cake layer was assumed to be 1:1 and the density of a bentonite cake layer was therefore assumed to be 2 g/cm³ (between the density of water at 1 g/cm³ and the density of bentonite at 3 g/cm³).

A bentonite clay of 1 g bentonite per cm³ water was prepared and used to fill a glass cell with an interspace distance of 10 mm. The same Panametrics Videoscanner V120-RB transducer was used as described in Section 4.4.2 for the UTDR experiment, but this time to measure the time delay between the reflected energy from the two glass sheets of the clay filled cell. The time delay was measured as 7.06 μs. From Equation 4.4:

$$c = \frac{2\Delta S}{\Delta t}$$

where c = speed of sound in the fouling layer (m/s)

ΔS = fouling layer thickness (m)

Δt = arrival time difference (s)

Therefore:

$$c = \frac{2 \times 0.010}{7.06 \times 10^{-6}} \approx 2800 \text{ m/s}$$

Addendum *E*

Screening design experimental data

Plackett-Burman design for area under velocity profile

BASE								Y ₁	Y ₂	Average Y	S ²
Treatment	A _g /A _r	H _r	H _B	Air	Depth	Diffuser	?				
1	+	-	-	+	-	+	+	0.6656	0.6401	0.6529	0.000325
2	+	+	-	-	+	-	+	0.9696	1.0226	0.9961	0.001405
3	+	+	+	-	-	+	-	0.7275	0.6665	0.6970	0.001861
4	-	+	+	+	-	-	+	0.2684	0.3174	0.2929	0.001201
5	+	-	+	+	+	-	-	0.8711	1.1573	1.0142	0.040955
6	-	+	-	+	+	+	-	0.3777	0.4281	0.4029	0.001270
7	-	-	+	-	+	+	+	0.5996	0.6552	0.6274	0.001546
8	-	-	-	-	-	-	-	0.6503	0.6761	0.6632	0.000333
HY_r	3.3602	2.3889	2.6315	2.3629	3.0406	2.3802	2.5693				
HY_B	1.9864	2.9577	2.7151	2.9837	2.3060	2.9664	2.7773				
Average Y_r	0.8400	0.5972	0.6579	0.5907	0.7602	0.5950	0.6423				
Average Y_B	0.4966	0.7394	0.6788	0.7459	0.5765	0.7416	0.6943				
Effect	0.3434	-0.1422	-0.0209	-0.1552	0.1837	-0.1466	-0.0520				
Average S_r²	0.011136	0.001434	0.011139	0.010938	0.011294	0.00125	0.001119				
Average S_B²	0.001087	0.01079	0.000833	0.001286	0.00093	0.010973	0.011105				
F	10.24248	7.524757	13.67189	8.506061	12.14739	8.776177	9.924163				
Absolute effect	0.3434	0.1422	0.0209	0.1552	0.1837	0.1466	0.0520				

REFLECTION								Y ₁	Y ₂	Average Y	S ²
Treatment	A _g /A _r	H _r	H _B	Air	Depth	Diffuser	?				
9	-	+	+	-	+	-	-	0.5807	0.6075	0.5941	0.000359
10	-	-	+	+	-	+	-	0.5271	0.5718	0.5495	0.000999
11	-	-	-	+	+	-	+	0.4598	0.5058	0.4828	0.001058
12	+	-	-	-	+	+	-	0.8195	0.5160	0.6678	0.046056
13	-	+	-	-	-	+	+	0.6141	0.5963	0.6052	0.000158
14	+	-	+	-	-	-	+	0.3938	0.3749	0.3844	0.000179
15	+	+	-	+	-	-	-	1.0319	0.9878	1.0099	0.000972
16	+	+	+	+	+	+	+	1.0076	0.9554	0.9815	0.001362
HY_r	3.0435	3.1907	2.5094	3.0236	2.7262	2.8039	2.4539				
HY_B	2.2316	2.0844	2.7656	2.2514	2.5489	2.4711	2.8212				
Average Y_r	0.7609	0.7977	0.6274	0.7559	0.6815	0.7010	0.6135				
Average Y_B	0.5579	0.5211	0.6914	0.5629	0.6372	0.6178	0.7053				
Effect	0.2030	0.2766	-0.0640	0.1931	0.0443	0.0832	-0.0918				
Average S_r²	0.012142	0.000713	0.000725	0.001098	0.012209	0.012144	0.000689				
Average S_B²	0.000379	0.012073	0.012061	0.011688	0.000577	0.000642	0.012097				
F	32.02561	16.93043	16.64084	10.64519	21.15495	18.91493	17.54766				
Absolute effect	0.2030	0.2766	0.0640	0.1931	0.0443	0.0832	0.0918				

Average effect	0.2732	0.0672	-0.0425	0.0189	0.1140	-0.0317	-0.0719	→ Main effects
Difference effect	-0.0702	0.2094	-0.0216	0.1741	-0.0697	0.1149	-0.0199	→ Confounded interactions

BD	AD	AG	AB	AF	AE	AC
CG	CE	BE	CF	BC	BG	BF
EF	FG	DF	EG	DG	CD	DE

Plackett-Burman design for average gradient of velocity profile

BASE								Y ₁	Y ₂	Average Y	S ²
Treatment	A _g /A _r	H _T	H _B	Air	Depth	Diffuser	?				
1	+	-	-	+	-	+	+	-0.0758	-0.0389	-0.0574	0.000681
2	+	+	-	-	+	-	+	0.0082	0.0195	0.0139	6.38E-05
3	+	+	+	-	-	+	-	-0.0028	-0.0104	-0.0066	2.89E-05
4	-	+	+	+	-	-	+	0.0833	0.0912	0.0873	3.12E-05
5	+	-	+	+	+	-	-	0.1129	0.0893	0.1011	0.000278
6	-	+	-	+	+	+	-	-0.0186	-0.0177	-0.0182	4.05E-07
7	-	-	+	-	+	+	+	-0.0752	-0.0952	-0.0852	0.0002
8	-	-	-	-	-	-	-	-0.0212	-0.0233	-0.0223	2.21E-06
HY₊	0.0510	0.0764	0.0966	0.1129	0.0116	-0.1673	0.0010				
HY₋	-0.0384	-0.0637	-0.0839	-0.1002	0.0011	0.1800	0.0003				
Average Y₊	0.0128	0.0191	0.0241	0.0282	0.0029	-0.0418	0.0002				
Average Y₋	-0.0096	-0.0159	-0.0210	-0.0251	0.0003	0.0450	0.0001				
Effect	0.0223	0.0350	0.0451	0.0533	0.0026	-0.0868	0.0002				
Average S₊²	0.000263	3.11E-05	0.000135	0.000248	0.000136	0.000228	0.000244				
Average S₋²	5.85E-05	0.00029	0.000187	7.37E-05	0.000186	9.39E-05	7.75E-05				
F	4.499326	9.341617	0.72072	3.359763	0.730364	0.412855	0.317639				
Absolute effect	0.0223	0.0350	0.0451	0.0533	0.0026	0.0868	0.0002				

REFLECTION								Y ₁	Y ₂	Average Y	S ²
Treatment	A _g /A _r	H _T	H _B	Air	Depth	Diffuser	?				
9	-	+	+	-	+	-	-	0.1442	0.1484	0.1463	8.82E-06
10	-	-	+	+	-	+	-	-0.0828	-0.0844	-0.0836	1.28E-06
11	-	-	-	+	+	-	+	0.0124	0.0255	0.0190	8.58E-05
12	+	-	-	-	+	+	-	-0.0422	-0.0344	-0.0383	3.04E-05
13	-	+	-	-	-	+	+	-0.0738	-0.0410	-0.0574	0.000538
14	+	-	+	-	-	-	+	0.1429	0.1267	0.1348	0.000131
15	+	+	-	+	-	-	-	-0.0481	-0.0415	-0.0448	2.18E-05
16	+	+	+	+	+	+	+	0.0113	-0.0266	-0.0077	0.000718
HY₊	0.0441	0.0365	0.1899	-0.1171	0.1193	-0.1870	0.0887				
HY₋	0.0243	0.0319	-0.1216	0.1854	-0.0510	0.2553	-0.0204				
Average Y₊	0.0110	0.0091	0.0475	-0.0293	0.0298	-0.0467	0.0222				
Average Y₋	0.0061	0.0080	-0.0304	0.0464	-0.0128	0.0638	-0.0051				
Effect	0.0050	0.0012	0.0779	-0.0756	0.0426	-0.1106	0.0273				
Average S₊²	0.000225	0.000322	0.000215	0.000207	0.000211	0.000322	0.000368				
Average S₋²	0.000137	6.22E-05	0.000169	0.000177	0.000173	6.19E-05	1.56E-05				
F	1.645241	0.193301	1.271628	0.856493	0.820872	5.200707	23.64607				
Absolute effect	0.0050	0.0012	0.0779	0.0756	0.0426	0.1106	0.0273				

Average effect	0.0136	0.0181	0.0615	-0.0112	0.0226	-0.0987	0.0137
Difference effect	-0.0087	-0.0169	0.0164	-0.0644	0.0200	-0.0119	0.0136

→ Main effects
 → Confounded interactions

BD	AD	AG	AB	AF	AE	AC
CG	CE	BE	CF	BC	BG	BF
EF	FG	DF	EG	DG	CD	DE

Treatment 1

	1		2		3		4	
1	1.75	1.37	2.12	4.49	2.35	2.23	5.04	2.30
2	1.61	2.54	1.97	3.78	2.06	2.09	6.83	5.38
3	3.15	2.55	1.46	3.26	2.46	2.11	6.93	7.36
4	1.35	3.22	2.27	1.84	7.19	3.46	4.63	4.88
5	2.81	1.64	3.11	2.18	2.62	1.67	9.37	4.17
6	1.45	3.76	2.13	1.75	1.09	2.35	8.21	3.42
7	1.74	0.96	2.56	2.15	5.11	3.62	7.44	4.84
8	1.56	2.52	3.10	3.20	1.60	4.66	5.68	5.04
9	1.42	2.23	2.03	1.97	2.98	2.34	6.79	4.14
10	1.67	2.41	2.65	2.48	3.14	3.08	4.68	4.51

Downcomer/riser 2 +
 Top clearance (m) 0.1 -
 Bottom clearance (m) 0.03 -
 Aeration intensity (L/m².min) 1350 +
 Depth (m) 1.1 -
 Diffuser position Riser +

Average times (s):

1.851	2.320	2.340	2.710	3.060	2.761	6.560	4.604
-------	-------	-------	-------	-------	-------	-------	-------

Distance (m): 0.6

Average rise velocities (m/s):

0.324	0.259	0.256	0.221	0.196	0.217	0.091	0.130
-------	-------	-------	-------	-------	-------	-------	-------

1	0.324	0.259
2	0.256	0.221
3	0.196	0.217
4	0.091	0.130

Area under graph:

0.6656	0.6401
Average:	0.6529
S ² :	0.000325

Residual area:

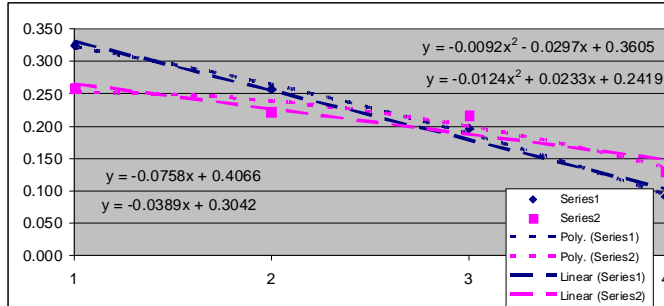
0.2992	0.1183
Average:	0.2088
S ² :	0.016362

Differential area:

0.3664	0.5218
Average:	0.4441
S ² :	0.0121

Average gradient:

-0.0758	-0.0389
Average:	-0.0574
S ² :	0.0007



Treatment 2

	1		2		3		4	
1	2.39	2.81	2.18	2.25	2.40	2.24	1.62	1.82
2	1.89	3.14	2.18	2.61	2.11	1.92	2.97	2.01
3	2.70	2.69	2.15	2.21	2.02	2.54	2.00	2.14
4	2.69	2.33	3.33	2.70	3.07	2.14	2.40	2.65
5	2.23	2.09	3.42	2.09	2.46	2.79	2.36	2.06
6	2.41	2.76	2.44	3.17	2.72	1.81	1.58	2.08
7	2.26	2.30	2.78	2.14	2.15	2.37	2.16	2.47
8	2.12	2.15	2.33	1.94	2.90	2.59	2.82	2.41
9	2.82	2.54	2.37	2.27	2.23	2.20	2.29	1.94
10	2.29	2.63	3.50	2.68	1.94	2.43	2.50	1.79

Downcomer/riser 2 +
 Top clearance (m) 0.2 +
 Bottom clearance (m) 0.03 -
 Aeration intensity (L/m².min) 800 -
 Depth (m) 1.4 +
 Diffuser position Bottom -

Average times (s):

2.380	2.544	2.668	2.406	2.400	2.303	2.270	2.137
-------	-------	-------	-------	-------	-------	-------	-------

Distance (m): 0.8

Average rise velocities (m/s):

0.336	0.314	0.300	0.333	0.333	0.347	0.352	0.374
-------	-------	-------	-------	-------	-------	-------	-------

1	0.336	0.314
2	0.300	0.333
3	0.333	0.347
4	0.352	0.374

Area under graph:

0.9696	1.0226
Average:	0.9961
S ² :	0.001405

Residual area:

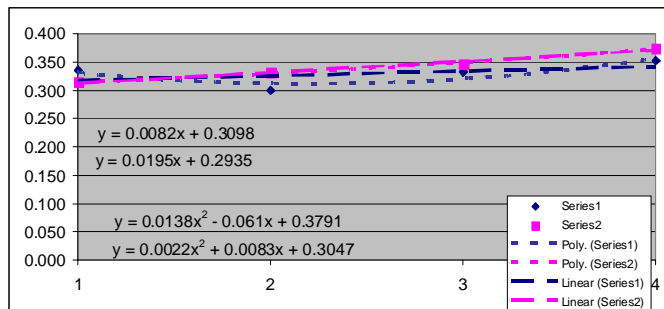
0.0981	0.0967
Average:	0.0974
S ² :	0.000001

Differential area:

0.8715	0.9259
Average:	0.8987
S ² :	0.0015

Average gradient:

0.0082	0.0195
Average:	0.0139
S ² :	0.0001



Treatment 3

	1		2		3		4	
1	1.51	1.73	2.09	2.70	1.18	2.18	1.61	1.90
2	3.31	2.62	2.01	2.39	1.53	2.54	3.47	2.86
3	1.71	1.87	3.23	2.17	2.19	2.23	3.03	2.57
4	1.69	2.17	2.13	2.62	1.57	2.08	1.65	3.13
5	2.14	1.81	2.51	2.48	2.10	2.62	2.72	2.87
6	2.09	1.98	2.44	2.07	1.62	2.22	2.96	2.26
7	1.84	2.16	2.94	2.26	1.83	1.97	2.53	2.05
8	2.33	1.76	2.71	1.85	2.11	2.20	1.92	1.86
9	2.15	2.00	1.98	2.43	1.27	1.84	2.33	1.59
10	1.78	2.11	2.39	2.02	1.74	2.57	2.18	2.61

Downcomer/riser 2 +
 Top clearance (m) 0.2 +
 Bottom clearance (m) 0.1 +
 Aeration intensity (L/m².min) 800 -
 Depth (m) 1.1 -
 Diffuser position Riser +

Average times (s):

2.055	2.021	2.443	2.299	1.714	2.245	2.440	2.370
-------	-------	-------	-------	-------	-------	-------	-------

Distance (m): 0.5

Average rise velocities (m/s):

0.243	0.247	0.205	0.217	0.292	0.223	0.205	0.211
-------	-------	-------	-------	-------	-------	-------	-------

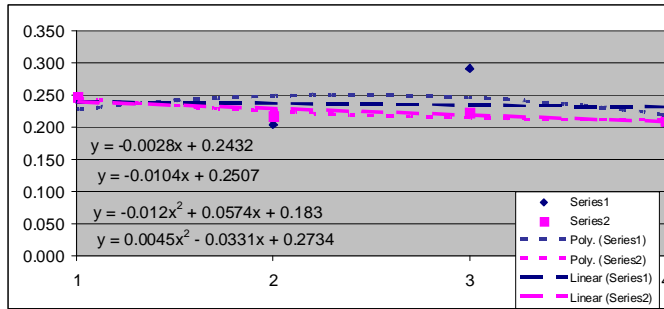
1	0.243	0.247
2	0.205	0.217
3	0.292	0.223
4	0.205	0.211

Area under graph:	0.7275	0.6665
Average:	0.6970	
S²:	0.001861	

Residual area:	0.0274	0.0679
Average:	0.0477	
S²:	0.000820	

Differential area:	0.7001	0.5986
Average:	0.6494	
S²:	0.0052	

Average gradient:	-0.0028	-0.0104
Average:	-0.0066	
S²:	0.0000	



Treatment 4

	1		2		3		4	
1	-	-	-	-	5.14	1.93	1.20	1.24
2	-	-	-	-	1.93	2.68	2.00	1.57
3	-	-	-	-	3.93	3.24	2.89	1.87
4	-	-	-	-	3.99	1.07	2.82	2.29
5	-	-	-	-	2.37	1.62	1.82	3.33
6	-	-	-	-	2.55	3.43	2.00	1.49
7	-	-	-	-	2.43	3.47	1.62	1.47
8	-	-	-	-	3.17	2.12	1.85	1.71
9	-	-	-	-	2.05	1.08	3.09	1.88
10	-	-	-	-	3.02	3.92	3.13	4.33

Downcomer/riser 0.5 -
 Top clearance (m) 0.2 +
 Bottom clearance (m) 0.1 +
 Aeration intensity (L/m².min) 1350 +
 Depth (m) 1.1 -
 Diffuser position Bottom -

Average times (s):

-	-	-	-	3.058	2.456	2.242	2.118
---	---	---	---	-------	-------	-------	-------

Distance (m): 0.5

Average rise velocities (m/s):

0.000	0.000	0.000	0.000	0.164	0.204	0.223	0.236
-------	-------	-------	-------	-------	-------	-------	-------

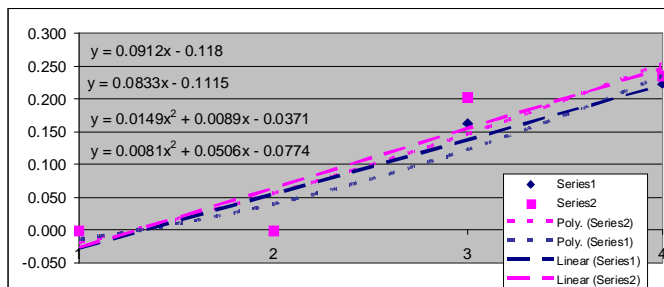
1	0.000	0.000
2	0.000	0.000
3	0.164	0.204
4	0.223	0.236

Area under graph:	0.2684	0.3174
Average:	0.2929	
S²:	0.001201	

Residual area:	0.4423	0.4464
Average:	0.4444	
S²:	0.000008	

Differential area:	-0.1739	-0.1290
Average:	-0.1515	
S²:	0.0010	

Average gradient:	0.0833	0.0912
Average:	0.0873	
S²:	0.0000	



Treatment 5

	1		2		3		4	
1	13.30	2.90	14.87	1.43	1.62	1.33	2.48	1.58
2	6.27	3.28	6.90	3.03	2.12	2.18	2.48	3.29
3	4.13	7.35	6.77	2.37	1.86	2.43	1.96	1.42
4	3.99	10.14	4.31	2.49	1.87	2.35	3.10	1.99
5	7.22	6.21	6.46	2.68	2.22	2.28	1.52	1.68
6	9.27	3.60	2.79	1.87	1.73	2.10	1.74	2.13
7	8.04	5.04	10.12	2.52	2.02	2.02	2.17	2.57
8	6.48	4.27	7.25	2.16	1.77	1.87	2.86	2.19
9	5.21	8.30	4.07	2.60	1.71	1.53	2.51	1.63
10	6.19	3.94	6.62	2.85	2.11	1.71	2.26	2.22

Downcomer/riser 2 +
 Top clearance (m) 0.1 -
 Bottom clearance (m) 0.1 +
 Aeration intensity (L/m².min) 1350 +
 Depth (m) 1.4 +
 Diffuser position Bottom -

Average times (s):

7.010	5.503	7.016	2.400	1.903	1.980	2.308	2.070
-------	-------	-------	-------	-------	-------	-------	-------

Distance (m): 0.9

Average rise velocities (m/s):

0.128	0.164	0.128	0.375	0.473	0.455	0.390	0.435
-------	-------	-------	-------	-------	-------	-------	-------

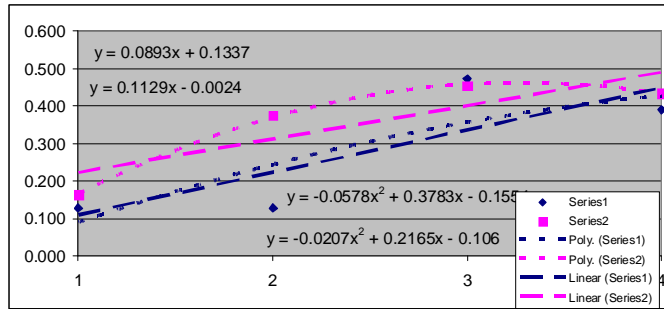
1	0.128	0.164
2	0.128	0.375
3	0.473	0.455
4	0.390	0.435

Area under graph:	0.8711	1.1573
Average:	1.0142	
S²:	0.040955	

Residual area:	0.4153	0.2335
Average:	0.3244	
S²:	0.016526	

Differential area:	0.4558	0.9238
Average:	0.6898	
S²:	0.1095	

Average gradient:	0.1129	0.0893
Average:	0.1011	
S²:	0.0003	



Treatment 6

	1		2		3		4	
1	5.17	4.93	5.27	7.87	7.09	4.56	6.68	6.12
2	5.13	3.85	6.78	5.44	3.09	3.81	3.25	3.71
3	3.85	5.96	8.07	4.73	7.07	6.13	5.59	10.37
4	2.47	4.23	7.07	4.32	1.99	4.95	11.17	6.40
5	8.05	4.77	5.84	7.64	7.83	7.88	5.37	4.87
6	3.86	3.61	6.95	4.22	9.63	6.54	17.03	7.33
7	4.71	4.12	7.21	5.93	4.39	5.99	8.96	3.64
8	7.13	3.87	6.36	4.04	8.17	8.05	10.14	4.09
9	4.46	6.17	5.59	6.30	5.63	4.43	4.85	11.64
10	4.51	3.45	7.93	5.06	6.28	6.33	9.89	7.64

Downcomer/riser 0.5 -
 Top clearance (m) 0.2 +
 Bottom clearance (m) 0.03 -
 Aeration intensity (L/m².min) 1350 +
 Depth (m) 1.4 +
 Diffuser position Riser +

Average times (s):

4.934	4.496	6.707	5.555	6.117	5.867	8.293	6.581
-------	-------	-------	-------	-------	-------	-------	-------

Distance (m): 0.8

Average rise velocities (m/s):

0.162	0.178	0.119	0.144	0.131	0.136	0.096	0.122
-------	-------	-------	-------	-------	-------	-------	-------

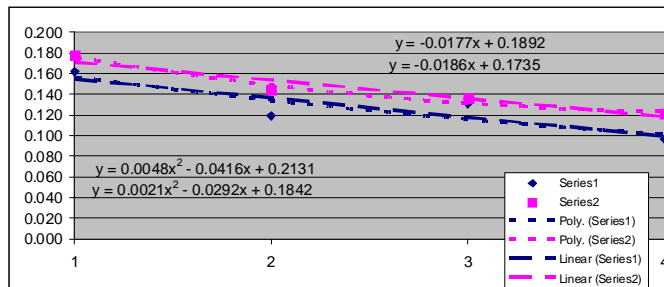
1	0.162	0.178
2	0.119	0.144
3	0.131	0.136
4	0.096	0.122

Area under graph:	0.3777	0.4281
Average:	0.4029	
S²:	0.001270	

Residual area:	0.0936	0.1206
Average:	0.1071	
S²:	0.000365	

Differential area:	0.2841	0.3075
Average:	0.2958	
S²:	0.0003	

Average gradient:	-0.0186	-0.0177
Average:	-0.0182	
S²:	0.0000	



Treatment 7

	1		2		3		4	
1	4.97	2.58	4.77	3.05	5.20	6.04	20.98	4.99
2	3.25	2.57	4.13	3.75	4.25	3.67	10.98	26.53
3	1.93	3.14	1.77	3.17	6.83	5.57	10.89	15.61
4	2.86	2.01	3.58	2.89	7.23	6.10	19.62	4.57
5	3.97	2.77	3.19	3.16	6.58	5.26	11.49	14.93
6	3.57	3.32	2.88	3.16	4.79	5.83	15.38	22.19
7	4.13	3.43	4.34	2.35	3.92	7.88	12.85	10.72
8	1.81	2.09	3.32	3.19	5.14	6.02	9.82	18.03
9	3.63	2.13	2.91	3.91	4.52	5.67	17.41	14.14
10	1.73	2.93	4.68	2.22	5.81	4.46	18.50	16.89

Downcomer/riser 0.5 -
 Top clearance (m) 0.1 -
 Bottom clearance (m) 0.1 +
 Aeration intensity (L/m².min) 800 -
 Depth (m) 1.4 +
 Diffuser position Riser +

Average times (s):

3.185	2.697	3.557	3.085	5.427	5.650	14.792	14.860
-------	-------	-------	-------	-------	-------	--------	--------

Distance (m): 0.9

Average rise velocities (m/s):

0.283	0.334	0.253	0.292	0.166	0.159	0.061	0.061
-------	-------	-------	-------	-------	-------	-------	-------

1	0.283	0.334
2	0.253	0.292
3	0.166	0.159
4	0.061	0.061

Area under graph:

0.5996	0.6552
Average:	0.6274
S ² :	0.001546

Residual area:

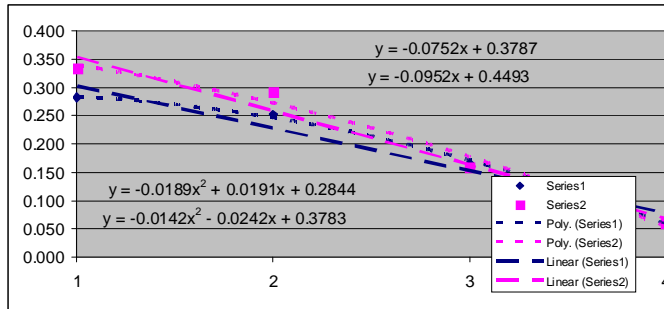
0.2542	0.3645
Average:	0.3094
S ² :	0.006083

Differential area:

0.3454	0.2907
Average:	0.3181
S ² :	0.0015

Average gradient:

-0.0752	-0.0952
Average:	-0.0852
S ² :	0.0002



Treatment 8

	1		2		3		4	
1	1.95	2.31	2.84	3.07	4.99	2.38	2.14	3.70
2	2.30	2.33	1.76	2.82	1.97	3.17	2.45	2.56
3	2.01	2.39	2.80	2.46	3.83	2.41	3.28	3.26
4	3.12	2.62	3.27	2.83	3.78	2.32	2.42	2.82
5	2.04	2.03	1.73	2.33	2.37	2.71	1.88	3.52
6	2.73	2.47	2.38	1.89	2.83	2.11	2.09	3.69
7	2.11	2.29	2.00	2.35	2.98	2.48	2.74	3.71
8	2.28	2.10	2.57	2.24	4.26	3.32	3.43	3.46
9	2.19	2.95	2.49	2.66	3.70	2.94	5.16	2.89
10	2.11	2.16	2.96	2.95	3.17	3.20	2.51	3.69

Downcomer/riser 0.5 -
 Top clearance (m) 0.1 -
 Bottom clearance (m) 0.03 -
 Aeration intensity (L/m².min) 800 -
 Depth (m) 1.1 -
 Diffuser position Bottom -

Average times (s):

2.284	2.365	2.480	2.560	3.388	2.704	2.810	3.330
-------	-------	-------	-------	-------	-------	-------	-------

Distance (m): 0.6

Average rise velocities (m/s):

0.263	0.254	0.242	0.234	0.177	0.222	0.214	0.180
-------	-------	-------	-------	-------	-------	-------	-------

1	0.263	0.254
2	0.242	0.234
3	0.177	0.222
4	0.214	0.180

Area under graph:

0.6503	0.6761
Average:	0.6632
S ² :	0.000333

Residual area:

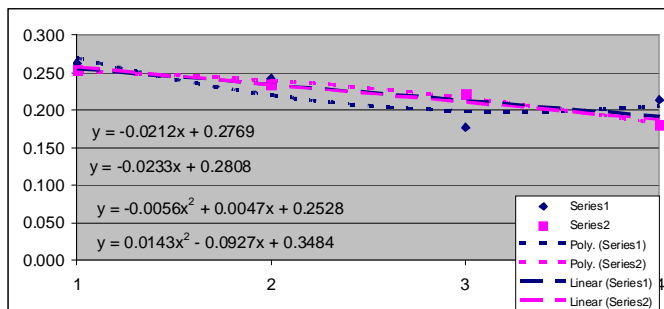
0.1597	0.0796
Average:	0.1197
S ² :	0.003208

Differential area:

0.4906	0.5965
Average:	0.5436
S ² :	0.0056

Average gradient:

-0.0212	-0.0233
Average:	-0.0223
S ² :	0.0000



Treatment 9

	1	2	3	4
1	-	-	2.83	1.77
2	-	-	1.47	2.34
3	-	-	1.17	1.29
4	-	-	3.07	2.01
5	-	-	1.89	1.49
6	-	-	2.04	1.63
7	-	-	1.76	2.15
8	-	-	1.70	1.86
9	-	-	1.55	2.57
10	-	-	2.49	1.84

Downcomer/riser 0.5 -
 Top clearance (m) 0.2 +
 Bottom clearance (m) 0.1 +
 Aeration intensity (L/m².min) 800 -
 Depth (m) 1.4 +
 Diffuser position Bottom -

Average times (s):

-	-	-	-	1.997	1.895	2.305	2.261
---	---	---	---	-------	-------	-------	-------

Distance (m):

Average rise velocities (m/s):

0.000	0.000	0.000	0.000	0.401	0.422	0.347	0.354
-------	-------	-------	-------	-------	-------	-------	-------

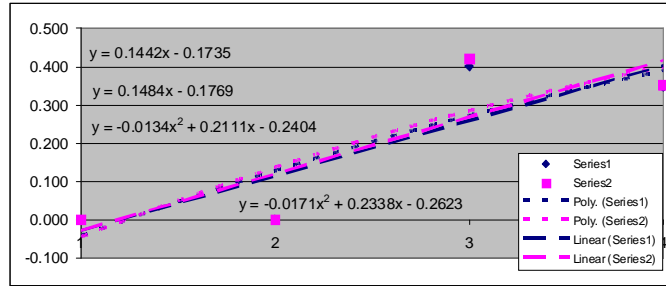
1	0.000	0.000
2	0.000	0.000
3	0.401	0.422
4	0.347	0.354

Area under graph:	0.5807	0.6075
Average:	0.5941	
S ² :	0.000359	

Residual area:	0.5881	0.5904
Average:	0.5893	
S ² :	0.000003	

Differential area:	-0.0074	0.0171
Average:	0.0049	
S ² :	0.0003	

Average gradient:	0.1442	0.1484
Average:	0.1463	
S ² :	0.0000	



Treatment 10

	1	2	3	4
1	1.30	1.77	1.44	2.36
2	3.20	1.59	2.82	5.67
3	2.53	2.17	2.17	2.48
4	2.35	1.53	4.36	1.55
5	2.08	1.90	2.73	1.43
6	2.97	1.85	1.87	2.87
7	0.99	1.68	3.17	3.21
8	1.55	1.56	1.49	1.94
9	1.96	2.13	3.12	3.97
10	2.28	1.74	2.48	2.48

Downcomer/riser 0.5 -
 Top clearance (m) 0.1 -
 Bottom clearance (m) 0.1 +
 Aeration intensity (L/m².min) 1350 +
 Depth (m) 1.1 -
 Diffuser position Riser +

Average times (s):

2.121	1.792	2.565	2.796	4.800	3.790	13.926	8.323
-------	-------	-------	-------	-------	-------	--------	-------

Distance (m):

Average rise velocities (m/s):

0.28	0.33	0.23	0.21	0.13	0.16	0.04	0.07
------	------	------	------	------	------	------	------

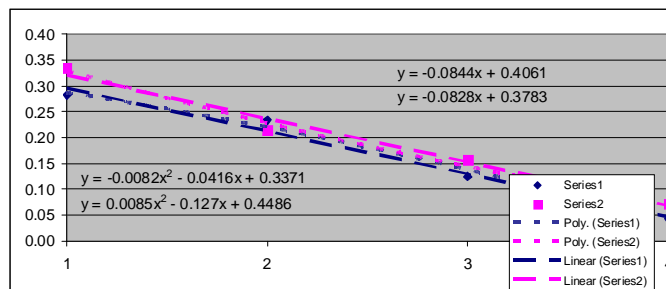
1	0.28	0.33
2	0.23	0.21
3	0.13	0.16
4	0.04	0.07

Area under graph:	0.5271	0.5718
Average:	0.5495	
S ² :	0.000999	

Residual area:	0.3348	0.4185
Average:	0.3767	
S ² :	0.003503	

Differential area:	0.1923	0.1533
Average:	0.1728	
S ² :	0.0008	

Average gradient:	-0.0828	-0.0844
Average:	-0.0836	
S ² :	0.0000	



Treatment 11

	1		2		3		4	
1	20.40	8.11	4.23	4.68	3.99	5.18	7.65	5.26
2	9.74	6.57	3.27	4.17	3.05	3.73	8.51	4.83
3	6.77	14.36	6.73	4.60	6.56	4.14	4.38	5.74
4	15.72	15.68	7.05	4.39	2.66	3.62	6.37	4.88
5	23.93	12.77	7.47	7.02	10.65	3.87	5.62	5.81
6	8.14	9.03	3.11	4.95	3.60	5.45	7.82	6.52
7	8.76	19.83	3.82	5.74	4.81	7.32	8.83	8.56
8	12.30	9.44	5.45	6.51	5.44	3.95	8.12	4.47
9	10.04	7.27	4.88	4.90	5.71	3.31	10.22	6.55
10	7.23	6.52	4.96	6.43	7.35	4.16	8.98	4.92

Downcomer/riser 0.5 -
 Top clearance (m) 0.1 -
 Bottom clearance (m) 0.03 -
 Aeration intensity (L/m².min) 1350 +
 Depth (m) 1.4 +
 Diffuser position Bottom -

Average times (s):

12.303	10.958	5.097	5.339	5.382	4.473	7.650	5.754
--------	--------	-------	-------	-------	-------	-------	-------

Distance (m): 0.9

Average rise velocities (m/s):

0.073	0.082	0.177	0.169	0.167	0.201	0.118	0.156
-------	-------	-------	-------	-------	-------	-------	-------

1	0.073	0.082
2	0.177	0.169
3	0.167	0.201
4	0.118	0.156

Area under graph:

0.4598	0.5058
Average: 0.4828	
S ² : 0.001058	

Residual area:

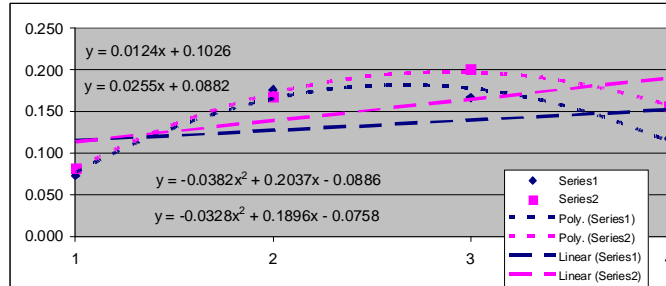
0.0891	0.0888
Average: 0.0890	
S ² : 0.000000	

Differential area:

0.3707	0.4170
Average: 0.3939	
S ² : 0.0011	

Average gradient:

0.0124	0.0255
Average: 0.0190	
S ² : 0.0001	



Treatment 12

	1		2		3		4	
1	2.66	2.33	1.80	2.22	6.13	3.97	6.04	7.06
2	2.43	2.33	1.84	4.33	2.41	5.31	2.58	8.05
3	3.82	3.67	3.75	4.73	5.51	4.45	4.57	5.77
4	3.71	3.77	2.75	4.45	3.11	7.63	5.59	7.32
5	2.77	3.12	2.63	5.74	3.96	6.67	3.24	4.09
6	2.57	2.59	2.83	2.70	5.38	5.30	2.86	6.78
7	3.68	6.94	3.47	13.07	3.73	6.42	5.15	7.23
8	2.84	4.81	2.90	2.31	4.32	4.91	4.80	7.93
9	2.48	3.03	1.92	7.69	3.92	6.28	6.04	6.11
10	2.97	3.94	2.11	4.72	3.77	6.36	3.17	5.34

Downcomer/riser 2 +
 Top clearance (m) 0.1 -
 Bottom clearance (m) 0.03 -
 Aeration intensity (L/m².min) 800 -
 Depth (m) 1.4 +
 Diffuser position Riser +

Average times (s):

2.993	3.653	2.600	5.196	4.224	5.730	4.404	6.568
-------	-------	-------	-------	-------	-------	-------	-------

Distance (m): 0.9

Average rise velocities (m/s):

0.301	0.246	0.346	0.173	0.213	0.157	0.204	0.137
-------	-------	-------	-------	-------	-------	-------	-------

1	0.301	0.246
2	0.346	0.173
3	0.213	0.157
4	0.204	0.137

Area under graph:

0.8195	0.5160
Average: 0.6678	
S ² : 0.046056	

Residual area:

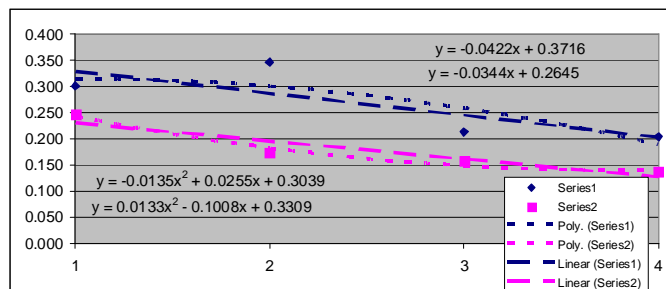
0.1282	0.2142
Average: 0.1712	
S ² : 0.003698	

Differential area:

0.6913	0.3018
Average: 0.4966	
S ² : 0.0759	

Average gradient:

-0.0422	-0.0344
Average: -0.0383	
S ² : 0.0000	



Treatment 13

	1		2		3		4	
1	1.21	2.33	1.55	1.89	4.86	3.47	3.93	2.99
2	1.87	2.37	2.13	1.91	4.08	1.32	4.67	2.08
3	1.83	1.88	3.59	3.26	2.55	1.47	8.21	3.29
4	1.53	1.96	1.43	1.77	3.56	2.17	3.70	4.57
5	1.49	1.78	1.46	2.29	2.43	4.39	5.43	3.33
6	1.37	1.84	2.24	2.07	2.75	2.93	6.74	5.74
7	1.76	2.17	1.70	2.33	3.43	4.36	3.38	4.12
8	1.55	1.42	2.38	2.86	2.21	2.25	3.66	2.83
9	1.18	2.33	2.33	1.84	2.90	3.37	5.89	4.92
10	2.07	1.59	1.51	2.02	2.24	2.77	5.67	3.44

Downcomer/riser 0.5 -
 Top clearance (m) 0.2 +
 Bottom clearance (m) 0.03 -
 Aeration intensity (L/m².min) 800 -
 Depth (m) 1.1 -
 Diffuser position Riser +

Average times (s):

1.586	1.967	2.032	2.224	3.101	2.850	5.128	3.731
-------	-------	-------	-------	-------	-------	-------	-------

Distance (m): 0.5

Average rise velocities (m/s):

0.315	0.254	0.246	0.225	0.161	0.175	0.098	0.134
-------	-------	-------	-------	-------	-------	-------	-------

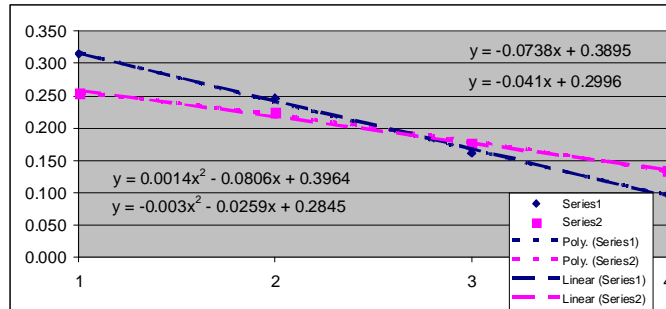
1	0.315	0.254
2	0.246	0.225
3	0.161	0.175
4	0.098	0.134

Area under graph:	0.6141	0.5963
Average:	0.6052	
S²:	0.000158	

Residual area:	0.3375	0.1706
Average:	0.2541	
S²:	0.013928	

Differential area:	0.2766	0.4257
Average:	0.3512	
S²:	0.0111	

Average gradient:	-0.0738	-0.0410
Average:	-0.0574	
S²:	0.0005	



Treatment 14

	1		2		3		4	
1	-	-	11.41	6.58	4.18	1.09	1.35	1.05
2	-	-	4.82	3.26	10.24	14.02	1.21	1.19
3	-	-	2.19	2.13	1.49	1.15	0.87	1.58
4	-	-	8.37	7.91	5.02	1.49	1.26	1.80
5	-	-	12.08	5.24	1.31	3.24	1.70	1.46
6	-	-	3.28	3.21	11.15	6.10	1.57	1.33
7	-	-	4.82	8.43	6.23	13.14	1.43	1.77
8	-	-	9.12	10.11	9.51	2.90	1.01	1.08
9	-	-	6.93	4.78	2.88	21.40	1.06	1.12
10	-	-	7.51	6.80	3.64	3.12	1.34	1.67

Downcomer/riser 2 +
 Top clearance (m) 0.1 -
 Bottom clearance (m) 0.1 +
 Aeration intensity (L/m².min) 800 -
 Depth (m) 1.1 -
 Diffuser position Bottom -

Average times (s):

-	-	7.053	5.845	5.565	6.765	1.280	1.405
---	---	-------	-------	-------	-------	-------	-------

Distance (m): 0.6

Average rise velocities (m/s):

0.000	0.000	0.085	0.103	0.108	0.089	0.469	0.427
-------	-------	-------	-------	-------	-------	-------	-------

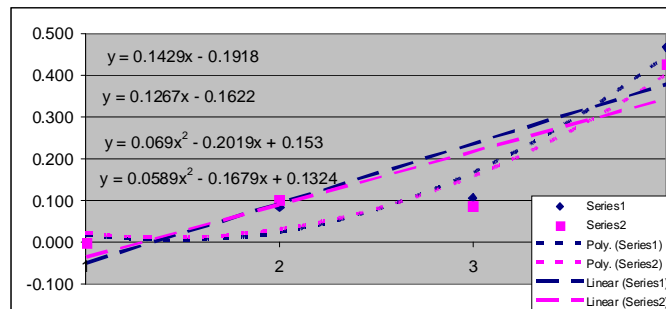
1	0.000	0.000
2	0.085	0.103
3	0.108	0.089
4	0.469	0.427

Area under graph:	0.3938	0.3749
Average:	0.3844	
S²:	0.000179	

Residual area:	0.9544	0.8347
Average:	0.8946	
S²:	0.007164	

Differential area:	-0.5606	-0.4598
Average:	-0.5102	
S²:	0.0051	

Average gradient:	0.1429	0.1267
Average:	0.1348	
S²:	0.0001	



Treatment 15

	1		2		3		4	
1	1.83	1.43	0.90	1.43	1.34	1.03	2.69	1.72
2	1.91	1.06	1.59	1.25	1.47	1.29	1.05	1.00
3	0.96	1.29	1.03	1.19	1.14	3.03	1.90	1.57
4	1.19	1.29	0.93	1.27	1.47	2.38	1.11	1.07
5	1.50	2.06	1.25	1.31	1.70	0.88	2.21	1.67
6	1.50	1.14	1.27	1.50	1.46	1.17	3.04	2.69
7	1.94	1.83	1.62	1.37	1.83	2.89	1.79	1.91
8	1.04	1.16	1.10	0.89	2.29	1.13	3.71	2.26
9	1.38	1.51	1.07	1.44	2.86	1.28	2.11	3.31
10	1.57	1.49	0.86	1.20	1.00	2.17	3.14	3.17

Downcomer/riser 2 +
 Top clearance (m) 0.2 +
 Bottom clearance (m) 0.03 -
 Aeration intensity (L/m².min) 1350 +
 Depth (m) 1.1 -
 Diffuser position Bottom -

Average times (s):

1.482	1.426	1.162	1.285	1.656	1.725	2.275	2.037
-------	-------	-------	-------	-------	-------	-------	-------

Distance (m): 0.5

Average rise velocities (m/s):

0.337	0.351	0.430	0.389	0.302	0.290	0.220	0.245
-------	-------	-------	-------	-------	-------	-------	-------

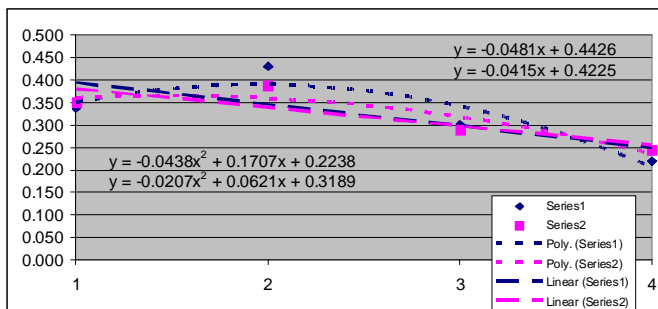
1	0.337	0.351
2	0.430	0.389
3	0.302	0.290
4	0.220	0.245

Area under graph:	1.0319	0.9878
Average:	1.0099	
S²:	0.000972	

Residual area:	0.1384	0.1086
Average:	0.1235	
S²:	0.000444	

Differential area:	0.8935	0.8792
Average:	0.8864	
S²:	0.0001	

Average gradient:	-0.0481	-0.0415
Average:	-0.0448	
S²:	0.0000	



Treatment 16

	1		2		3		4	
1	2.11	3.65	3.23	3.40	2.23	2.69	1.87	2.57
2	2.18	1.80	3.03	2.82	2.35	2.31	2.18	4.29
3	1.96	2.29	1.42	1.99	1.97	2.59	2.16	2.97
4	1.96	2.98	2.23	2.88	2.77	2.63	2.59	2.70
5	2.14	1.79	2.37	2.25	3.16	2.13	2.12	2.49
6	2.94	1.49	2.28	2.71	1.55	2.26	1.89	2.75
7	2.46	1.69	2.91	2.18	3.25	2.72	1.50	3.74
8	2.27	2.02	2.77	2.40	2.49	2.42	2.21	3.32
9	1.99	2.36	2.17	2.89	2.81	2.29	1.64	3.06
10	2.63	2.34	1.86	2.30	2.65	1.95	2.09	2.84

Downcomer/riser 2 +
 Top clearance (m) 0.2 +
 Bottom clearance (m) 0.1 +
 Aeration intensity (L/m².min) 1350 +
 Depth (m) 1.4 +
 Diffuser position Riser +

Average times (s):

2.264	2.241	2.427	2.582	2.523	2.399	2.025	3.073
-------	-------	-------	-------	-------	-------	-------	-------

Distance (m): 0.8

Average rise velocities (m/s):

0.353	0.357	0.330	0.310	0.317	0.333	0.395	0.260
-------	-------	-------	-------	-------	-------	-------	-------

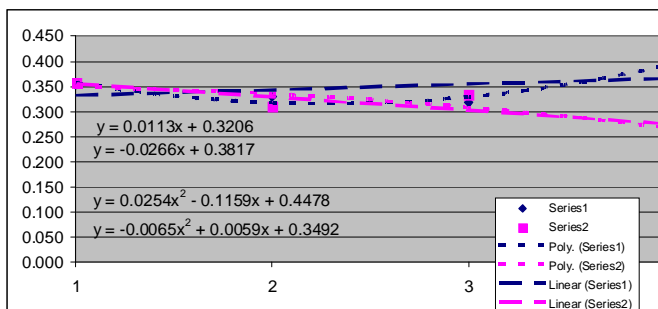
1	0.353	0.357
2	0.330	0.310
3	0.317	0.333
4	0.395	0.260

Area under graph:	1.0076	0.9554
Average:	0.9815	
S²:	0.001362	

Residual area:	0.1642	0.0904
Average:	0.1273	
S²:	0.002723	

Differential area:	0.8434	0.8650
Average:	0.8542	
S²:	0.0002	

Average gradient:	0.0113	-0.0266
Average:	-0.0077	
S²:	0.0007	



Treatment 17

	1		2		3		4	
1	1.93	2.71	3.87	3.04	3.02	3.83	7.47	4.70
2	2.13	2.58	2.50	3.67	6.21	4.56	3.78	3.55
3	2.23	3.13	2.38	2.84	5.91	4.41	4.02	4.13
4	2.72	1.79	2.89	2.42	3.59	3.50	2.82	2.89
5	1.87	2.21	3.35	3.28	4.12	5.61	2.54	4.21
6	3.11	2.53	3.18	2.51	4.93	4.85	3.31	3.76
7	2.49	2.88	2.71	4.28	3.33	6.72	4.61	7.83
8	1.90	3.15	2.46	2.43	3.62	4.78	7.06	4.27
9	2.09	2.94	2.93	3.17	3.63	7.26	3.46	4.52
10	2.06	3.47	2.83	4.25	4.31	4.16	5.44	4.17

Downcomer/riser 0.5 -
 Top clearance (m) 0.1 -
 Bottom clearance (m) 0.03 -
 Aeration intensity (L/m².min) 800 -
 Depth (m) 1.1 -
 Diffuser position Riser +

Average times (s):

2.253	2.739	2.910	3.189	4.267	4.968	4.451	4.403
-------	-------	-------	-------	-------	-------	-------	-------

Distance (m): 0.6

Average rise velocities (m/s):

0.266	0.219	0.206	0.188	0.141	0.121	0.135	0.136
-------	-------	-------	-------	-------	-------	-------	-------

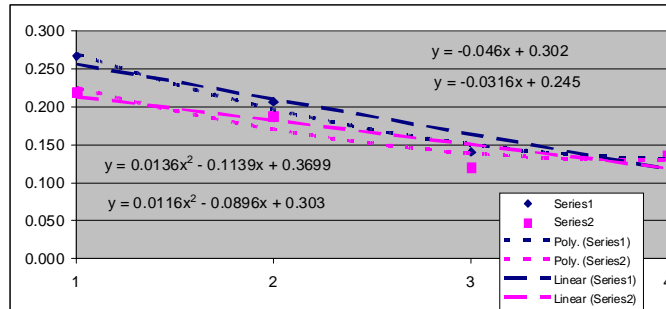
1	0.266	0.219
2	0.206	0.188
3	0.141	0.121
4	0.135	0.136

Area under graph:	0.5411	0.4806
Average:	0.5109	
S ² :	0.001830	

Residual area:	0.2678	0.1944
Average:	0.2311	
S ² :	0.002694	

Differential area:	0.2733	0.2862
Average:	0.2798	
S ² :	0.0001	

Average gradient:	-0.0460	-0.0316
Average:	-0.0388	
S ² :	0.0001	



Treatment 18

	1		2		3		4	
1	2.08	1.43	1.27	2.45	5.09	4.73	5.40	9.22
2	1.57	1.46	2.09	2.74	5.47	4.56	7.95	6.83
3	1.59	1.81	1.52	2.18	3.45	4.83	14.77	9.32
4	1.60	1.86	1.83	2.35	2.18	5.66	2.50	19.74
5	1.29	1.54	2.20	1.78	4.18	4.53	8.23	6.51
6	1.55	1.60	1.30	1.59	3.67	3.85	23.02	8.63
7	2.04	1.38	2.38	2.10	4.16	4.09	8.42	12.37
8	1.48	1.47	1.49	1.64	4.62	3.62	11.47	16.48
9	1.71	1.42	1.23	2.83	4.84	4.26	15.18	9.06
10	1.35	1.26	1.47	2.03	3.08	4.69	6.18	17.65

Downcomer/riser 0.5 -
 Top clearance (m) 0.1 -
 Bottom clearance (m) 0.03 -
 Aeration intensity (L/m².min) 1350 +
 Depth (m) 1.1 -
 Diffuser position Riser +

Average times (s):

1.626	1.523	1.678	2.169	4.074	4.482	10.312	11.581
-------	-------	-------	-------	-------	-------	--------	--------

Distance (m): 0.6

Average rise velocities (m/s):

0.369	0.394	0.358	0.277	0.147	0.134	0.058	0.052
-------	-------	-------	-------	-------	-------	-------	-------

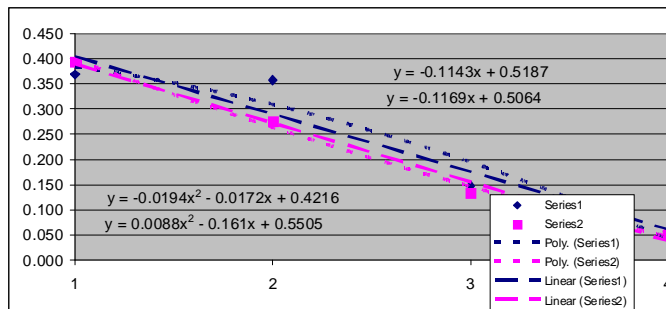
1	0.369	0.394
2	0.358	0.277
3	0.147	0.134
4	0.058	0.052

Area under graph:	0.7284	0.6288
Average:	0.6786	
S ² :	0.004960	

Residual area:	0.4266	0.5661
Average:	0.4964	
S ² :	0.009730	

Differential area:	0.3018	0.0627
Average:	0.1823	
S ² :	0.0286	

Average gradient:	-0.1143	-0.1169
Average:	-0.1156	
S ² :	0.0000	



Treatment 19

	1		2		3		4	
1	1.75	2.61	1.52	2.85	4.85	5.10	11.62	9.15
2	1.53	1.53	4.27	3.46	3.27	3.86	7.49	15.42
3	2.34	2.43	2.16	3.00	4.96	3.58	13.19	10.66
4	1.92	2.26	3.13	3.57	4.23	5.47	9.13	5.87
5	2.38	1.40	2.53	4.12	5.14	5.75	6.37	7.62
6	1.86	1.59	3.07	3.29	4.19	3.11	8.22	18.47
7	1.67	2.28	3.41	3.58	4.33	5.21	10.94	14.02
8	1.25	1.65	1.86	2.76	3.83	4.42	7.58	7.31
9	1.38	2.12	2.58	3.05	3.55	4.96	12.24	10.23
10	1.58	2.34	2.69	3.91	4.93	3.54	8.82	9.57

Downcomer/riser 0.5 -
 Top clearance (m) 0.1 -
 Bottom clearance (m) 0.1 +
 Aeration intensity (L/m².min) 800 -
 Depth (m) 1.1 -
 Diffuser position Riser +

Average times (s):

1.766	2.021	2.722	3.359	4.328	4.500	9.560	10.832
-------	-------	-------	-------	-------	-------	-------	--------

Distance (m): 0.6

Average rise velocities (m/s):

0.340	0.297	0.220	0.179	0.139	0.133	0.063	0.055
-------	-------	-------	-------	-------	-------	-------	-------

1	0.340	0.297
2	0.220	0.179
3	0.139	0.133
4	0.063	0.055

Area under graph:

0.5556	0.4833
Average:	0.5195
S ² :	0.002614

Residual area:

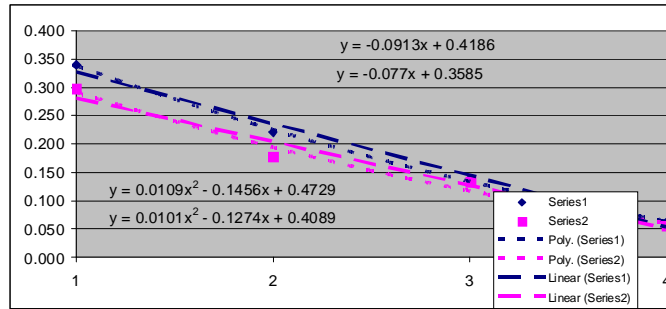
0.4590	0.3915
Average:	0.4253
S ² :	0.002278

Differential area:

0.0966	0.0918
Average:	0.0942
S ² :	0.0000

Average gradient:

-0.0913	-0.0770
Average:	-0.0842
S ² :	0.0001



Treatment 20

	1		2		3		4	
1	1.79	1.52	2.25	2.08	10.03	4.55	4.66	7.42
2	1.15	1.67	2.62	2.64	1.88	3.26	7.76	5.61
3	1.52	2.13	1.73	2.71	5.04	3.75	9.29	3.64
4	1.69	1.23	2.44	2.93	3.04	6.06	6.96	9.83
5	1.58	1.87	1.53	2.17	6.73	3.74	11.71	7.54
6	1.36	2.35	1.25	2.69	6.84	3.42	1.33	13.92
7	1.82	1.64	2.29	2.34	6.87	5.19	5.66	8.65
8	0.82	1.74	1.97	1.90	8.15	4.01	4.37	11.43
9	2.01	1.49	1.98	2.82	3.81	3.57	7.88	4.28
10	1.53	1.77	1.64	2.97	5.37	5.61	9.90	14.18

Downcomer/riser 0.5 -
 Top clearance (m) 0.2 +
 Bottom clearance (m) 0.1 +
 Aeration intensity (L/m².min) 800 -
 Depth (m) 1.1 -
 Diffuser position Riser +

Average times (s):

1.527	1.741	1.970	2.525	5.776	4.316	6.952	8.650
-------	-------	-------	-------	-------	-------	-------	-------

Distance (m): 0.5

Average rise velocities (m/s):

0.327	0.287	0.254	0.198	0.087	0.116	0.072	0.058
-------	-------	-------	-------	-------	-------	-------	-------

1	0.327	0.287
2	0.254	0.198
3	0.087	0.116
4	0.072	0.058

Area under graph:

0.5318	0.4832
Average:	0.5075
S ² :	0.001181

Residual area:

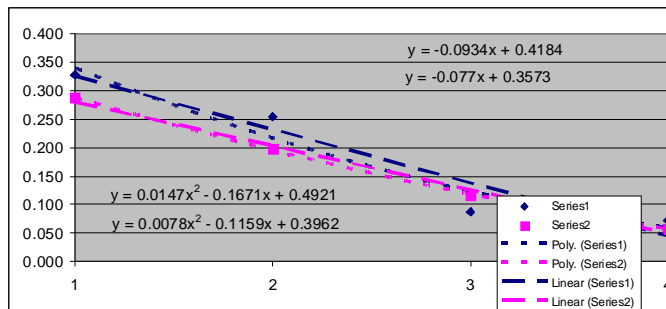
0.4874	0.3812
Average:	0.4343
S ² :	0.005639

Differential area:

0.0444	0.1020
Average:	0.0732
S ² :	0.0017

Average gradient:

-0.0934	-0.0770
Average:	-0.0852
S ² :	0.0001



Treatment 21

	1		2		3		4	
1	-	-	1.98	3.93	1.55	1.59	1.70	1.95
2	-	-	2.23	2.85	1.71	1.56	2.53	2.54
3	-	-	2.59	2.26	2.42	2.13	2.40	2.34
4	-	-	2.56	3.70	1.87	1.62	1.73	1.87
5	-	-	1.17	3.15	1.48	1.54	2.23	1.69
6	-	-	1.93	4.07	1.86	1.74	2.69	1.93
7	-	-	2.23	3.87	2.17	1.69	2.14	2.02
8	-	-	3.47	2.37	1.72	1.83	2.63	2.21
9	-	-	2.34	3.43	1.60	2.11	2.87	1.93
10	-	-	2.16	3.50	1.77	1.62	1.80	1.64

Downcomer/riser	0.5	-
Top clearance (m)	0.1	-
Bottom clearance (m)	0.1	+
Aeration intensity (L/m ² .min)	800	-
Depth (m)	1.1	-
Diffuser position	Bottom	-

Average times (s):

-	-	2.266	3.313	1.815	1.743	2.272	2.012
---	---	-------	-------	-------	-------	-------	-------

Distance (m):

Average rise velocities (m/s):

0.000	0.000	0.265	0.181	0.331	0.344	0.264	0.298
-------	-------	-------	-------	-------	-------	-------	-------

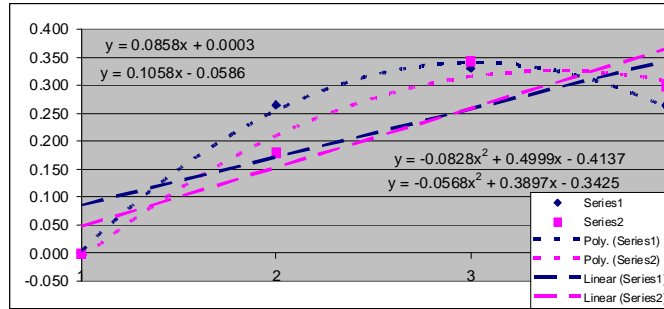
1	0.000	0.000
2	0.265	0.181
3	0.331	0.344
4	0.264	0.298

Area under graph:	0.7694	0.7025
Average:	0.7360	
S ² :	0.002238	

Residual area:	0.2531	0.2752
Average:	0.2642	
S ² :	0.000244	

Differential area:	0.5163	0.4273
Average:	0.4718	
S ² :	0.0040	

Average gradient:	0.0858	0.1058
Average:	0.0958	
S ² :	0.0002	



Treatment 22

	1		2		3		4	
1	3.68	5.47	7.20	3.83	1.93	2.15	2.80	2.34
2	7.92	6.91	7.93	4.28	6.27	2.26	2.09	1.51
3	4.20	7.32	2.49	4.36	6.32	3.14	1.33	1.82
4	11.30	4.58	2.92	4.29	3.15	4.83	2.76	2.01
5	6.56	4.74	4.85	5.81	4.30	3.72	2.47	1.25
6	8.81	8.17	4.73	3.06	3.31	2.59	1.45	2.47
7	4.80	3.37	3.85	3.87	2.88	3.02	1.41	3.06
8	6.47	4.14	6.13	4.00	4.40	3.12	1.85	2.72
9	5.89	3.78	5.79	6.45	3.11	2.43	1.65	2.15
10	7.90	3.29	4.31	4.46	4.56	3.07	2.08	0.98

Downcomer/riser	0.5	-
Top clearance (m)	0.1	-
Bottom clearance (m)	0.03	-
Aeration intensity (L/m ² .min)	1350	+
Depth (m)	1.1	-
Diffuser position	Bottom	-

Average times (s):

6.753	5.177	5.020	4.441	4.023	3.033	1.989	2.031
-------	-------	-------	-------	-------	-------	-------	-------

Distance (m):

Average rise velocities (m/s):

0.089	0.116	0.120	0.135	0.149	0.198	0.302	0.295
-------	-------	-------	-------	-------	-------	-------	-------

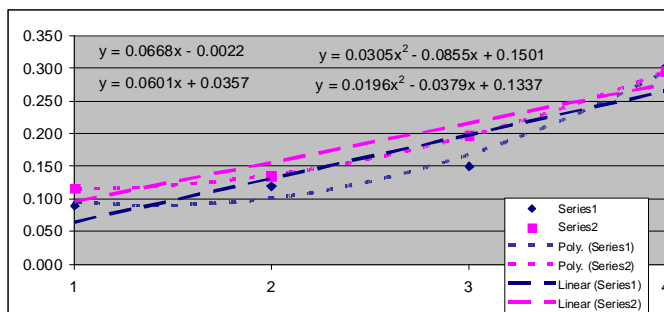
1	0.089	0.116
2	0.120	0.135
3	0.149	0.198
4	0.302	0.295

Area under graph:	0.4496	0.5285
Average:	0.4891	
S ² :	0.003113	

Residual area:	0.4388	0.3586
Average:	0.3987	
S ² :	0.003216	

Differential area:	0.0108	0.1699
Average:	0.0904	
S ² :	0.0127	

Average gradient:	0.0668	0.0601
Average:	0.0635	
S ² :	0.0000	



Treatment 23

	1		2		3		4	
1	1.69	4.68	4.85	2.82	4.00	3.45	4.13	1.58
2	4.96	4.15	3.08	2.76	2.28	3.32	2.33	1.39
3	4.15	4.83	1.78	2.13	2.03	3.57	1.49	1.70
4	4.78	3.97	2.14	3.34	2.10	3.42	2.32	1.64
5	4.42	3.39	2.80	4.11	3.15	2.88	1.47	1.47
6	3.95	4.41	2.26	3.75	2.85	3.02	1.63	2.20
7	3.12	3.60	1.84	3.09	3.74	4.17	1.97	1.74
8	3.78	3.86	2.76	2.63	2.31	3.28	1.67	1.29
9	4.44	4.92	4.20	3.82	2.68	3.51	1.09	1.88
10	2.51	4.23	2.57	3.73	1.93	3.05	1.76	1.72

Downcomer/riser 0.5 -
 Top clearance (m) 0.2 +
 Bottom clearance (m) 0.03 -
 Aeration intensity (L/m².min) 800 -
 Depth (m) 1.1 -
 Diffuser position Bottom -

Average times (s):

3.780	4.204	2.828	3.218	2.707	3.367	1.986	1.661
-------	-------	-------	-------	-------	-------	-------	-------

Distance (m): 0.5

Average rise velocities (m/s):

0.132	0.119	0.177	0.155	0.185	0.149	0.252	0.301
-------	-------	-------	-------	-------	-------	-------	-------

1	0.132	0.119
2	0.177	0.155
3	0.185	0.149
4	0.252	0.301

Area under graph:

0.5504	0.4986
Average:	0.5245
S ² :	0.001342

Residual area:

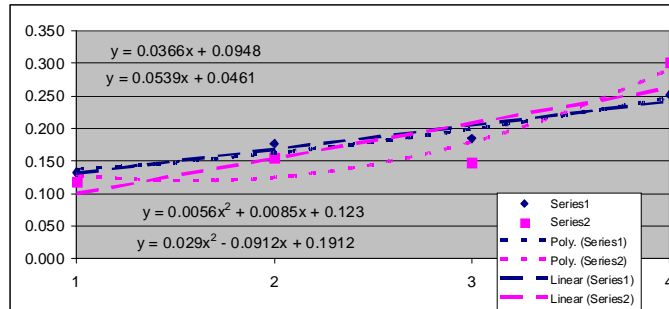
0.1895	0.3726
Average:	0.2811
S ² :	0.016763

Differential area:

0.3609	0.1260
Average:	0.2435
S ² :	0.0276

Average gradient:

0.0366	0.0539
Average:	0.0453
S ² :	0.0001



Treatment 24

	1		2		3		4	
1	3.92	1.99	4.07	2.48	2.96	5.37	7.05	3.60
2	3.60	2.18	2.02	2.06	8.28	2.14	5.07	4.27
3	1.01	1.98	1.55	1.89	3.17	2.27	5.02	6.77
4	7.97	2.18	2.44	8.76	3.13	3.93	5.56	3.66
5	3.59	1.89	2.81	6.69	3.11	2.02	7.32	6.69
6	1.57	1.21	3.16	5.59	14.83	6.11	6.19	7.12
7	4.46	2.05	1.97	2.94	5.14	2.67	4.84	3.94
8	1.61	2.20	2.76	2.99	6.52	5.11	6.58	5.37
9	1.90	1.57	3.43	2.14	4.29	3.54	6.73	3.97
10	1.45	1.80	2.54	1.17	3.93	4.30	5.68	4.59

Downcomer/riser 2 +
 Top clearance (m) 0.1 -
 Bottom clearance (m) 0.03 -
 Aeration intensity (L/m².min) 800 -
 Depth (m) 1.1 -
 Diffuser position Riser +

Average times (s):

3.108	1.905	2.675	3.671	5.536	3.746	6.004	4.998
-------	-------	-------	-------	-------	-------	-------	-------

Distance (m): 0.6

Average rise velocities (m/s):

0.193	0.315	0.224	0.163	0.108	0.160	0.100	0.120
-------	-------	-------	-------	-------	-------	-------	-------

1	0.193	0.315
2	0.224	0.163
3	0.108	0.160
4	0.100	0.120

Area under graph:

0.4847	0.5265
Average:	0.5056
S ² :	0.000874

Residual area:

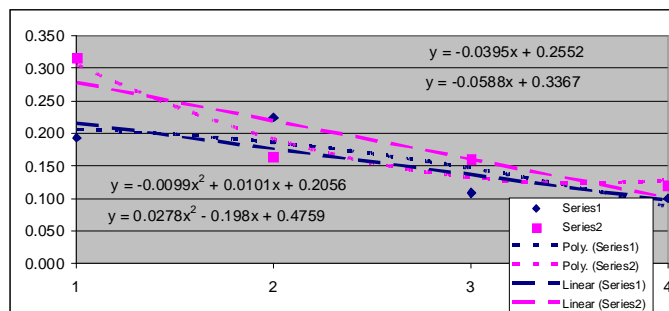
0.1328	0.3906
Average:	0.2617
S ² :	0.033230

Differential area:

0.3519	0.1359
Average:	0.2439
S ² :	0.0233

Average gradient:

-0.0395	-0.0588
Average:	-0.0492
S ² :	0.0002



Treatment 25

	1		2		3		4	
1	1.77	3.47	1.69	2.19	4.40	1.83	1.97	2.97
2	1.26	2.97	1.15	1.93	3.49	2.42	3.81	2.07
3	1.89	1.36	1.69	2.79	1.65	1.50	7.90	2.76
4	4.90	2.17	1.09	2.28	2.04	1.81	2.19	7.00
5	1.28	1.94	3.74	1.29	1.19	2.32	1.44	4.26
6	1.93	2.77	3.36	2.32	3.13	8.02	4.43	5.99
7	1.32	2.19	1.75	2.04	1.83	1.49	3.64	3.22
8	1.66	1.99	2.19	2.59	1.33	1.47	5.47	2.86
9	2.06	2.52	2.11	1.66	1.38	1.18	2.79	4.13
10	1.93	2.20	2.43	2.24	3.48	2.03	2.59	6.49

Downcomer/riser 2 +
 Top clearance (m) 0.2 +
 Bottom clearance (m) 0.03 -
 Aeration intensity (L/m².min) 800 -
 Depth (m) 1.1 -
 Diffuser position Riser +

Average times (s):

2.000	2.358	2.120	2.133	2.392	2.407	3.623	4.175
-------	-------	-------	-------	-------	-------	-------	-------

Distance (m): 0.5

Average rise velocities (m/s):

0.250	0.212	0.236	0.234	0.209	0.208	0.138	0.120
-------	-------	-------	-------	-------	-------	-------	-------

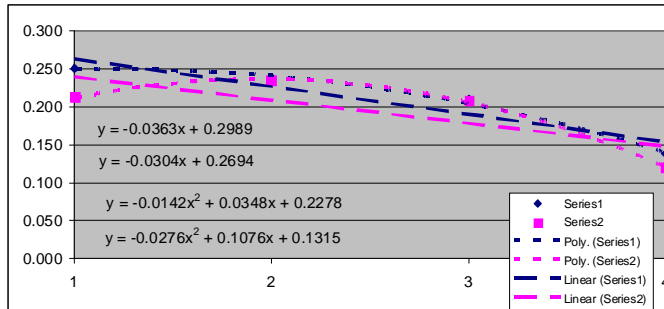
1	0.250	0.212
2	0.236	0.234
3	0.209	0.208
4	0.138	0.120

Area under graph:	0.6462	0.6219
Average:	0.6341	
S²:	0.000295	

Residual area:	0.1012	0.0872
Average:	0.0942	
S²:	0.000098	

Differential area:	0.5450	0.5347
Average:	0.5399	
S²:	0.0001	

Average gradient:	-0.0363	-0.0304
Average:	-0.0334	
S²:	0.0000	



Treatment 26

	1		2		3		4	
1	1.67	2.03	2.94	3.78	4.23	3.81	7.73	4.38
2	3.04	1.92	5.03	4.17	5.26	4.15	3.38	5.42
3	2.23	2.31	3.21	3.77	4.26	4.57	2.44	8.23
4	1.66	1.96	2.79	2.68	3.18	5.86	2.29	6.14
5	2.56	1.48	2.45	2.34	6.06	5.41	1.57	4.89
6	3.26	2.45	2.04	2.81	3.72	4.07	4.53	3.28
7	2.13	1.87	2.97	3.53	4.55	5.73	11.95	6.31
8	2.59	2.11	3.40	4.46	3.60	4.13	4.79	8.57
9	2.26	2.25	2.13	3.61	4.22	6.47	6.52	4.54
10	2.61	2.42	2.17	2.84	3.30	4.93	5.36	3.79

Downcomer/riser 2 +
 Top clearance (m) 0.1 -
 Bottom clearance (m) 0.1 +
 Aeration intensity (L/m².min) 800 -
 Depth (m) 1.1 -
 Diffuser position Riser +

Average times (s):

2.401	2.080	2.913	3.399	4.238	4.913	5.056	5.555
-------	-------	-------	-------	-------	-------	-------	-------

Distance (m): 0.6

Average rise velocities (m/s):

0.250	0.288	0.206	0.177	0.142	0.122	0.119	0.108
-------	-------	-------	-------	-------	-------	-------	-------

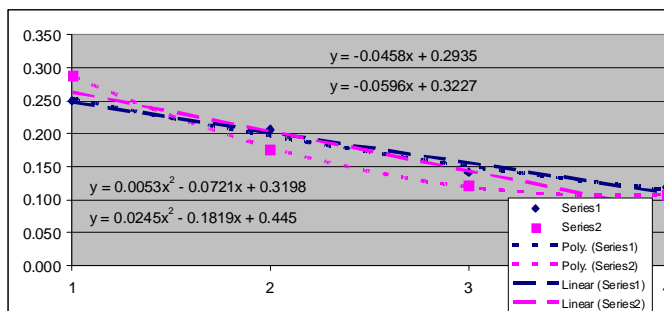
1	0.250	0.288
2	0.206	0.177
3	0.142	0.122
4	0.119	0.108

Area under graph:	0.5300	0.4853
Average:	0.5077	
S²:	0.000999	

Residual area:	0.2291	0.3775
Average:	0.3033	
S²:	0.011011	

Differential area:	0.3009	0.1078
Average:	0.2044	
S²:	0.0186	

Average gradient:	-0.0458	-0.0596
Average:	-0.0527	
S²:	0.0001	



Treatment 27

	1		2		3		4	
1	2.65	3.73	5.96	5.21	5.11	7.32	17.99	12.35
2	3.39	3.02	3.27	3.97	4.52	5.82	6.53	8.76
3	2.86	2.70	2.40	4.50	3.54	6.14	7.10	8.49
4	4.07	3.41	6.79	6.10	6.37	3.49	7.04	16.72
5	3.10	3.30	3.07	6.33	7.97	4.17	16.70	9.82
6	3.39	3.06	3.34	5.19	3.45	7.53	21.71	13.04
7	3.20	2.83	4.81	4.55	5.03	5.06	8.13	7.90
8	3.23	3.24	3.85	7.15	2.19	8.90	13.97	6.87
9	2.96	3.15	4.57	4.27	9.79	5.38	16.94	7.93
10	4.31	2.68	4.28	4.67	3.22	6.56	10.96	6.82

Downcomer/riser 0.5 -
 Top clearance (m) 0.1 -
 Bottom clearance (m) 0.03 -
 Aeration intensity (L/m².min) 800 -
 Depth (m) 1.4 +
 Diffuser position Riser +

Average times (s):

3.316	3.112	4.234	5.194	5.119	6.037	12.707	9.870
-------	-------	-------	-------	-------	-------	--------	-------

Distance (m): 0.9

Average rise velocities (m/s):

0.271	0.289	0.213	0.173	0.176	0.149	0.071	0.091
-------	-------	-------	-------	-------	-------	-------	-------

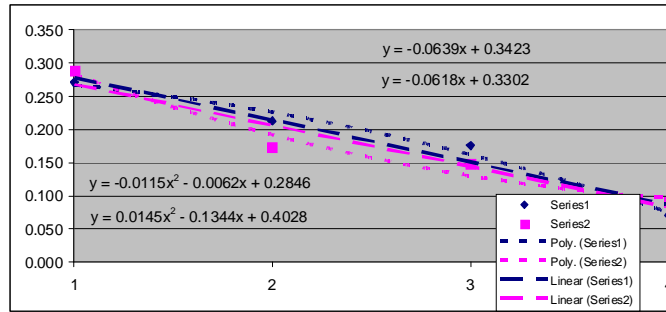
1	0.271	0.289
2	0.213	0.173
3	0.176	0.149
4	0.071	0.091

Area under graph:	0.5658	0.5049
Average:	0.5354	
S ² :	0.001854	

Residual area:	0.2349	0.3438
Average:	0.2894	
S ² :	0.005930	

Differential area:	0.3309	0.1611
Average:	0.2460	
S ² :	0.0144	

Average gradient:	-0.0639	-0.0618
Average:	-0.0629	
S ² :	0.0000	



Treatment 28

	1		2		3		4	
1	3.17	3.27	3.26	6.78	7.26	3.79	8.89	6.43
2	2.67	1.82	9.37	4.55	5.12	7.26	8.41	16.70
3	1.83	4.08	16.37	3.65	2.53	10.76	6.57	11.09
4	7.11	2.47	4.76	8.92	21.13	6.97	9.14	5.41
5	3.92	2.23	3.79	4.17	7.89	4.19	16.27	7.79
6	3.61	2.78	5.29	3.57	7.48	12.33	4.92	6.46
7	5.23	5.21	5.03	6.73	3.19	15.64	4.28	6.74
8	4.37	3.47	6.70	3.42	2.99	5.63	7.95	9.01
9	5.72	1.78	9.71	3.98	13.46	9.81	7.08	12.28
10	2.10	2.42	6.28	4.84	4.49	3.48	7.91	9.94

Downcomer/riser 0.5 -
 Top clearance (m) 0.2 +
 Bottom clearance (m) 0.03 -
 Aeration intensity (L/m².min) 800 -
 Depth (m) 1.4 +
 Diffuser position Riser +

Average times (s):

3.973	2.953	7.056	5.061	7.554	7.986	8.142	9.185
-------	-------	-------	-------	-------	-------	-------	-------

Distance (m): 0.8

Average rise velocities (m/s):

0.201	0.271	0.113	0.158	0.106	0.100	0.098	0.087
-------	-------	-------	-------	-------	-------	-------	-------

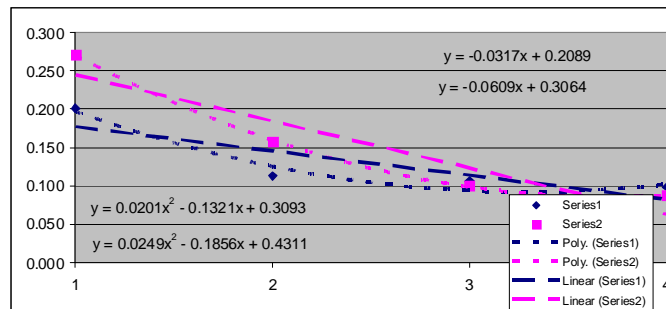
1	0.201	0.271
2	0.113	0.158
3	0.106	0.100
4	0.098	0.087

Area under graph:	0.3593	0.4242
Average:	0.3918	
S ² :	0.002106	

Residual area:	0.2327	0.3870
Average:	0.3099	
S ² :	0.011904	

Differential area:	0.1266	0.0372
Average:	0.0819	
S ² :	0.0040	

Average gradient:	-0.0317	-0.0609
Average:	-0.0463	
S ² :	0.0004	



Treatment 29

	1		2		3		4	
1	2.29	3.60	4.70	5.83	5.86	12.64	18.74	6.96
2	2.89	3.03	4.13	9.89	8.22	9.92	8.10	6.26
3	2.96	2.67	4.02	5.97	16.07	9.64	12.22	5.82
4	3.33	3.14	8.89	9.51	6.29	3.79	7.77	8.35
5	3.85	2.29	3.58	3.01	4.10	5.00	4.94	7.85
6	4.63	6.29	4.03	5.20	9.43	7.57	5.34	8.82
7	3.45	2.87	5.87	7.47	10.61	2.70	10.81	9.43
8	2.19	4.27	4.91	6.55	5.35	4.32	8.79	14.99
9	4.30	2.43	4.19	6.20	14.52	4.86	15.32	3.83
10	3.48	2.20	3.16	4.12	11.47	2.29	4.81	2.74

Downcomer/riser 0.5 -
 Top clearance (m) 0.1 -
 Bottom clearance (m) 0.03 -
 Aeration intensity (L/m².min) 1350 +
 Depth (m) 1.4 +
 Diffuser position Riser +

Average times (s):

3.337	3.279	4.748	6.375	9.192	6.273	9.684	7.505
-------	-------	-------	-------	-------	-------	-------	-------

Distance (m): 0.9

Average rise velocities (m/s):

0.270	0.274	0.190	0.141	0.098	0.143	0.093	0.120
-------	-------	-------	-------	-------	-------	-------	-------

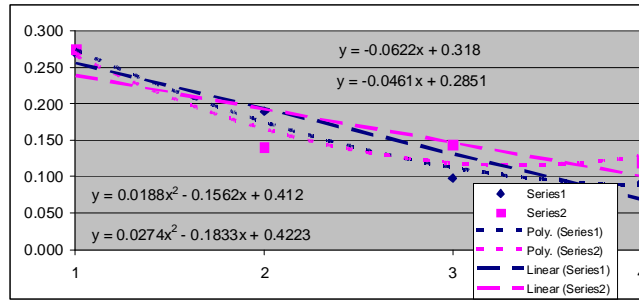
1	0.270	0.274
2	0.190	0.141
3	0.098	0.143
4	0.093	0.120

Area under graph:	0.4593	0.4676
Average:	0.4635	
S²:	0.000034	

Residual area:	0.3645	0.3317
Average:	0.3481	
S²:	0.000538	

Differential area:	0.0948	0.1359
Average:	0.1154	
S²:	0.0008	

Average gradient:	-0.0622	-0.0461
Average:	-0.0542	
S²:	0.0001	



Treatment 30

	1		2		3		4	
1	3.01	3.24	1.68	3.88	1.43	6.21	2.47	6.79
2	1.94	2.80	3.35	4.07	2.23	2.66	2.17	3.78
3	2.23	1.59	3.09	3.21	8.65	3.26	3.88	6.01
4	2.71	2.36	2.49	4.74	2.81	4.23	4.71	4.33
5	2.89	2.07	3.67	4.69	4.07	3.93	1.68	2.94
6	1.22	2.20	2.17	5.82	3.27	4.53	3.21	5.28
7	2.23	2.83	3.93	4.12	1.41	7.98	2.33	5.64
8	2.48	3.14	5.74	4.30	8.84	2.85	5.83	8.39
9	1.73	2.95	5.15	3.98	4.61	7.17	3.32	4.12
10	2.71	2.66	4.22	3.54	1.86	4.62	6.19	3.89

Downcomer/riser 2 +
 Top clearance (m) 0.1 -
 Bottom clearance (m) 0.03 -
 Aeration intensity (L/m².min) 800 -
 Depth (m) 1.1 -
 Diffuser position Bottom -

Average times (s):

2.315	2.584	3.549	4.235	3.918	4.744	3.579	5.117
-------	-------	-------	-------	-------	-------	-------	-------

Distance (m): 0.6

Average rise velocities (m/s):

0.259	0.232	0.169	0.142	0.153	0.126	0.168	0.117
-------	-------	-------	-------	-------	-------	-------	-------

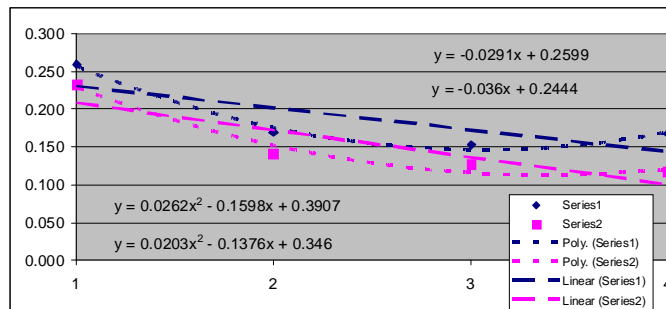
1	0.259	0.232
2	0.169	0.142
3	0.153	0.126
4	0.168	0.117

Area under graph:	0.5238	0.4323
Average:	0.4781	
S²:	0.004186	

Residual area:	0.2475	0.2538
Average:	0.2507	
S²:	0.000020	

Differential area:	0.2763	0.1785
Average:	0.2274	
S²:	0.0048	

Average gradient:	-0.0291	-0.0360
Average:	-0.0326	
S²:	0.0000	



Treatment 31

	1		2		3		4	
1	1.30	1.48	1.76	2.81	4.09	3.97	2.73	6.81
2	2.98	2.62	1.24	1.61	2.35	1.32	5.16	3.88
3	1.87	1.13	1.97	2.00	6.63	3.97	4.42	2.75
4	2.17	1.69	1.64	2.03	3.74	4.12	2.94	1.92
5	1.34	2.12	2.71	1.50	4.55	1.53	2.72	3.86
6	1.82	1.73	2.66	1.58	4.21	4.83	2.46	2.86
7	1.65	4.17	1.82	1.35	4.22	2.98	3.42	1.83
8	2.05	1.25	2.16	0.84	4.65	8.37	5.63	1.72
9	1.00	1.39	2.73	1.79	6.12	3.54	10.29	2.99
10	2.09	2.42	1.19	1.49	1.77	2.90	2.09	3.72

Downcomer/riser 0.5 -
 Top clearance (m) 0.2 +
 Bottom clearance (m) 0.03 -
 Aeration intensity (L/m².min) 1350 +
 Depth (m) 1.1 -
 Diffuser position Riser +

Average times (s):

1.827	2.000	1.988	1.700	4.233	3.753	4.186	3.234
-------	-------	-------	-------	-------	-------	-------	-------

Distance (m): 0.5

Average rise velocities (m/s):

0.274	0.250	0.252	0.294	0.118	0.133	0.119	0.155
-------	-------	-------	-------	-------	-------	-------	-------

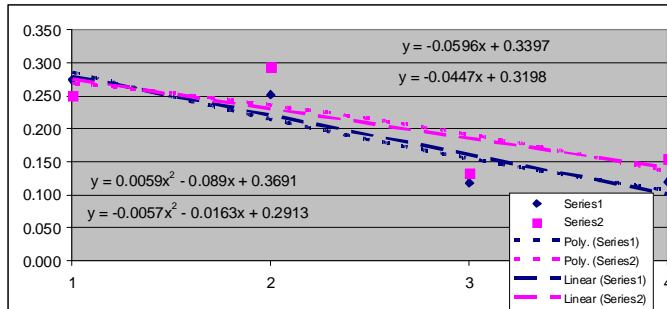
1	0.274	0.250
2	0.252	0.294
3	0.118	0.133
4	0.119	0.155

Area under graph:	0.5637	0.6320
Average:	0.5979	
S²:	0.002332	

Residual area:	0.2943	0.1760
Average:	0.2352	
S²:	0.006997	

Differential area:	0.2694	0.4560
Average:	0.3627	
S²:	0.0174	

Average gradient:	-0.0596	-0.0447
Average:	-0.0522	
S²:	0.0001	



Treatment 32

	1		2		3		4	
1	2.29	4.98	14.29	4.18	3.62	6.59	2.00	2.27
2	5.37	4.76	3.01	4.93	4.12	7.29	3.53	4.63
3	4.09	7.36	5.96	3.71	7.15	3.67	6.15	3.38
4	4.73	7.64	6.38	4.97	7.94	3.48	2.23	3.25
5	3.40	6.71	9.31	4.73	12.12	2.95	2.78	5.72
6	4.97	9.61	4.45	4.35	5.97	3.54	1.61	3.07
7	5.04	4.55	3.97	3.68	2.89	7.70	4.23	4.37
8	13.10	8.00	10.56	5.81	6.78	13.53	5.84	6.17
9	11.70	8.96	6.01	3.36	3.98	3.32	1.82	3.49
10	5.99	7.13	4.66	3.04	7.82	3.83	3.25	3.05

Downcomer/riser 0.5 -
 Top clearance (m) 0.1 -
 Bottom clearance (m) 0.03 -
 Aeration intensity (L/m².min) 800 -
 Depth (m) 1.1 -
 Diffuser position Bottom -

Average times (s):

6.068	6.970	6.860	4.276	6.239	5.590	3.344	3.940
-------	-------	-------	-------	-------	-------	-------	-------

Distance (m): 0.9

Average rise velocities (m/s):

0.148	0.129	0.131	0.210	0.144	0.161	0.269	0.228
-------	-------	-------	-------	-------	-------	-------	-------

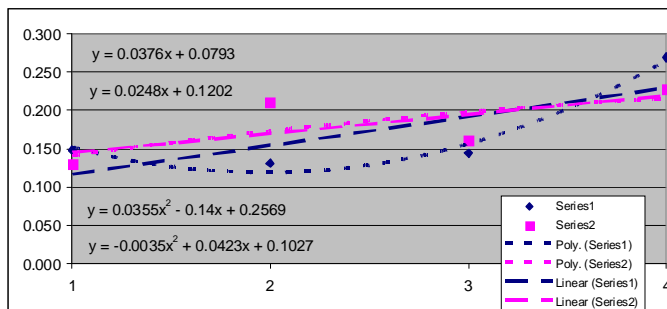
1	0.148	0.129
2	0.131	0.210
3	0.144	0.161
4	0.269	0.228

Area under graph:	0.4662	0.5519
Average:	0.5091	
S²:	0.003672	

Residual area:	0.3285	0.0959
Average:	0.2122	
S²:	0.027051	

Differential area:	0.1377	0.4560
Average:	0.2969	
S²:	0.0507	

Average gradient:	0.0376	0.0248
Average:	0.0312	
S²:	0.0001	



Addendum *F*

Model validation experimental data

Configuration 1

A	B	C	D	E	F
1	1	-1	-1	-1	1

Treatment 7			Treatment 10		
Time (min)	Flux (L/m ² .h)	TMP (mm H ₂ O)	Time (min)	Flux (L/m ² .h)	TMP (mm H ₂ O)
0	4	151	0	4	140
5	4	173	5	4	145
10	4	173	10	4	150
15	4	175	15	4	153
20	4	177	20	4	153
25	4	176	25	4	153
30	4	176	30	4	153
35	8	185	35	8	158
40	8	189	40	8	160
45	8	190	45	8	160
50	8	196	50	8	162
55	8	196	55	8	163
60	8	196	60	8	162
65	8	196	65	8	162
70	12	222	70	12	226
75	12	233	75	12	235
80	12	238	80	12	248
85	12	238	85	12	248
90	12	239	90	12	250
95	12	239	95	12	249
100	12	240	100	12	250
105	16	265	105	16	297
110	16	279	110	16	302
115	16	299	115	16	310
120	16	301	120	16	317
125	16	301	125	16	318
130	16	302	130	16	320
135	16	301	135	16	320
140	20	341	140	20	333
145	20	350	145	20	342
150	20	360	150	20	361
155	20	366	155	20	375
160	20	370	160	20	382
165	20	375	165	20	387
170	20	379	170	20	392
175	24	437	175	24	438
180	24	446	180	24	465
185	24	460	185	24	479
190	24	466	190	24	490
195	24	474	195	24	499
200	24	481	200	24	508
205	24	488	205	24	516
210	28	501	210	28	584
215	28	520	215	28	608
220	28	546	220	28	633
225	28	571	225	28	660
230	28	586	230	28	677
235	28	598	235	28	689
240	28	609	240	28	702
245	32	706	245	32	820
250	32	753	250	32	860
255	32	818	255	32	897
260	32	875	260	32	931
265	32	901	265	32	953
270	32	927	270	32	972
275	32	952	275	32	991

Configuration 2

A	B	C	D	E	F
1	-1	1	-1	1	-1

Treatment 3			Treatment 5		
Time (min)	Flux (L/m ² .h)	TMP (mm H ₂ O)	Time (min)	Flux (L/m ² .h)	TMP (mm H ₂ O)
0	4	175	0	4	151
5	4	175	5	4	151
10	4		10	4	152
15	4	178	15	4	152
20	4		20	4	152
25	4	181	25	4	152
30	4	182	30	4	152
35	8	196	35	8	156
40	8	204	40	8	158
45	8	206	45	8	158
50	8		50	8	
55	8	209	55	8	160
60	8	212	60	8	161
65	8	215	65	8	168
70	12	234	70	12	174
75	12	254	75	12	190
80	12	268	80	12	212
85	12		85	12	228
90	12	281	90	12	238
95	12	287	95	12	246
100	12	289	100	12	253
105	16	316	105	16	270
110	16	355	110	16	299
115	16	367	115	16	313
120	16	377	120	16	321
125	16	383	125	16	328
130	16	388	130	16	333
135	16	392	135	16	337
140	20	446	140	20	363
145	20	480	145	20	401
150	20	504	150	20	422
155	20	516	155	20	439
160	20	527	160	20	452
165	20	535	165	20	466
170	20	543	170	20	472
175	24	600	175	24	518
180	24	672	180	24	587
185	24	692	185	24	611
190	24	719	190	24	627
195	24	734	195	24	643
200	24	751	200	24	654
205	24	764	205	24	666
210	28	816	210	28	738
215	28	897	215	28	806
220	28	934	220	28	839
225	28	970	225	28	865
230	28	1001	230	28	891
235	28	1027	235	28	908
240	28	1052	240	28	929
245	32	1130	245	32	1008
250	32	1250	250	32	1118
255	32	1348	255	32	1185
260	32	1415	260	32	1234
265	32	1478	265	32	1293
			270	32	1335
			275	32	1373

Configuration 3

A	B	C	D	E	F
1	-1	-1	-1	-1	1

Treatment 4			Treatment 6		
Time (min)	Flux (L/m ² .h)	TMP (mm H ₂ O)	Time (min)	Flux (L/m ² .h)	TMP (mm H ₂ O)
0	4	165	0	4	148
5	4	249	5	4	148
10	4	249	10	4	148
15	4	251	15	4	149
20	4	250	20	4	149
25	4	250	25	4	149
30	4	251	30	4	149
35	8	256	35	8	153
40	8	264	40	8	153
45	8	272	45	8	153
50	8	281	50	8	160
55	8	286	55	8	171
60	8	290	60	8	176
65	8	294	65	8	181
70	12	313	70	12	190
75	12	362	75	12	210
80	12	384	80	12	220
85	12	401	85	12	228
90	12	415	90	12	234
95	12	425	95	12	244
100	12	434	100	12	251
105	16	465	105	16	275
110	16	519	110	16	315
115	16	539	115	16	329
120	16	556	120	16	339
125	16	565	125	16	349
130	16	571	130	16	354
135	16	577	135	16	359
140	20	610	140	20	395
145	20	693	145	20	437
150	20	723	150	20	466
155	20	744	155	20	485
160	20	763	160	20	496
165	20	779	165	20	509
170	20	793	170	20	519
175	24	850	175	24	555
180	24	910	180	24	603
185	24	944	185	24	627
190	24	968	190	24	641
195	24	993	195	24	655
200	24	1010	200	24	661
205	24	1031	205	24	673
210	28	1135	210	28	725
215	28	1195	215	28	798
220	28	1249	220	28	815
225	28	1272	225	28	838
230	28	1315	230	28	850
235	28		235	28	870
240	28	1359	240	28	880
			245	32	960
			250	32	1099
			255	32	1127
			260	32	1157
			265	32	1193
			270	32	1225
			275	32	1255

Configuration 4

A	B	C	D	E	F
-1	-1	1	1	-1	1

Treatment 8			Treatment 9		
Time (min)	Flux (L/m ² .h)	TMP (mm H ₂ O)	Time (min)	Flux (L/m ² .h)	TMP (mm H ₂ O)
0	4	147	0	4	167
5	4	147	5	4	168
10	4	148	10	4	168
15	4	147	15	4	169
20	4	146	20	4	169
25	4	147	25	4	169
30	4	146	30	4	169
35	8	150	35	8	175
40	8	151	40	8	177
45	8	153	45	8	178
50	8	153	50	8	184
55	8	157	55	8	190
60	8	172	60	8	193
65	8	185	65	8	195
70	12	196	70	12	201
75	12	233	75	12	214
80	12	259	80	12	222
85	12	278	85	12	228
90	12	293	90	12	231
95	12	302	95	12	232
100	12	311	100	12	233
105	16	332	105	16	246
110	16	375	110	16	259
115	16		115	16	269
120	16		120	16	275
125	16		125	16	281
130	16	432	130	16	286
135	16	436	135	16	290
140	20	478	140	20	325
145	20	514	145	20	354
150	20	526	150	20	366
155	20	535	155	20	376
160	20	545	160	20	383
165	20	551	165	20	390
170	20	560	170	20	397
175	24	591	175	24	425
180	24	650	180	24	464
185	24	671	185	24	483
190	24	688	190	24	497
195	24	702	195	24	508
200	24	711	200	24	516
205	24	722	205	24	524
210	28	775	210	28	578
215	28	824	215	28	633
220	28	849	220	28	658
225	28	876	225	28	674
230	28	893	230	28	690
235	28	910	235	28	706
240	28	927	240	28	720
245	32	1020	245	32	795
250	32	1088	250	32	848
255	32	1142	255	32	880
260	32	1170	260	32	904
265	32	1213	265	32	931
270	32	1228	270	32	954
275	32	1261	275	32	977

SYSTEM HYDRODYNAMICS TO REDUCE FOULING OF AIR-SPARGED IMMERSED FLAT-SHEET MICROFILTRATION MEMBRANES

by

Martin Louis Hamann

*Thesis submitted in partial fulfilment
of the requirements for the Degree*

of

MASTER OF SCIENCE IN ENGINEERING
(CHEMICAL ENGINEERING)

in the Department of Process Engineering
at the University of Stellenbosch

Supervised by

Prof Steven Bradshaw
Prof Ed Jacobs

STELLENBOSCH

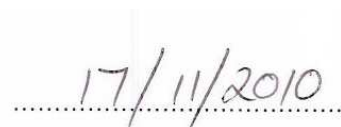
DECEMBER 2010

Declaration

I, the undersigned, hereby declare that the work contained in this thesis is my own original work and that I have not previously in its entirety or in part submitted it at any university for a degree.

A handwritten signature in black ink, appearing to read 'M. M. M.', written over a horizontal dotted line.

Signature

A handwritten date '17/11/2010' in black ink, written over a horizontal dotted line.

Date

Abstract

Immersed membrane systems hold many operational and environmental advantages in biological treatment of wastewater. However, immersed membrane filtration have only found application in niche markets to date because of higher capital and operating costs associated with membrane fouling. But with capital costs on the decline as membranes become less expensive, immersed membrane systems are increasingly considered as an attractive alternative to conventional treatment processes. Operating costs remain high however, since energy intensive techniques such as air-sparging are required to limit membrane fouling. Improving the air-scouring efficiency of air-sparged immersed membranes can significantly reduce operating costs and unlock the immersed membrane system technology to wider application.

The aim of this study was to identify factors that will improve air-scouring efficiency in order to produce guidelines that will help in the development of an immersed microfiltration membrane system with a resulting lower operating cost. Although, the research was done on a flat-sheet microfiltration membrane, the guidelines obtained can be used for the development of any immersed microfiltration membrane arrangement.

An airlift reactor set-up was chosen for this study. Six system hydrodynamic factors were evaluated in a factorial design to determine their effects on the cross-flow velocity profile. They were the downcomer area to riser area ratio, top clearance distance, bottom clearance distance, aeration intensity, water depth and air sparger location. It was found that the air-scouring efficiency was increased by generating a cross-flow velocity profile with increased magnitude and uniformity, but absolute uniformity of the cross-flow velocity profile was found to be a prerequisite for optimisation of air-scouring efficiency. Downcomer area to riser area ratio was found to be 99.9% significant in determining the magnitude of the cross-flow velocity profile.

Two models were developed to respectively predict the relative magnitude and uniformity of the cross-flow velocity profile. By using these two models, a methodology was developed to design an airlift reactor set-up that would produce system hydrodynamics with an improved air-scouring efficiency.

Opsomming

Gesonke membraanstelsels beskik oor talle bedryfs- en omgewingsvoordele in biologiese behandeling van afvalwater. Maar weens die hoër kapitaal- en bedryfskoste wat gepaardgaan met membraanbevuiling, kon gesonke membraanstelsels tot op hede nog net toepassing in nismarkte vind. Maar soos kapitaalkoste daal met al hoe goedkoper membrane beskikbaar, word gesonke membraanstelsels al hoe aanlokliker as 'n alternatief vir konvensionele behandelingsprosesse. Bedryfskoste bly egter hoog aangesien energie-intensiewe tegnieke soos lugborreling benodig word om membraanbevuiling te vertraag. Deur die effektiwiteit van die skropaksie wat lugborreling aan gesonke membrane bied te verbeter, kan 'n beduidende besparing in bedryfskoste teweeggebring word om sodoende die uitgebreide toepassing van gesonke membraanstelsel tegnologie moontlik te maak.

Hierdie studie het ten doel gehad die identifisering van faktore wat lugskropaksie effektiwiteit kan verbeter en om riglyne op te stel vir die ontwikkeling van 'n gesonke mikrofiltrasie membraanstelsel met gevolglik laer bedryfskoste. Alhoewel hierdie navorsing 'n plat-blad mikrofiltrasie membraan gebruik het, kan die riglyne steeds vir enige gesonke mikrofiltrasie membraanuitleg gebruik word.

Daar is besluit op 'n lugligter-reaktor opstelling vir hierdie studie. Ses stelselhidrodinamika faktore is geëvalueer in 'n faktoriale ontwerp om hul effekte op die kruisvloeiselheidsprofiel te bepaal. Hulle was die afvloe-area tot opvloe-area verhouding, topruimte-afstand, bodemuimte-afstand, belugtingsintensiteit, waterdiepte en belugterligging. Daar is bevind dat die lugskropaksie effektiwiteit verhoog word wanneer 'n kruisvloeiselheidsprofiel geskep word met 'n verhoogde grootte en gelykvormigheid, maar die absolute gelykvormigheid van die kruisvloeiselheidsprofiel is gevind om 'n voorvereiste te wees vir optimale effektiwiteit. Afvloe-area tot opvloe-area verhouding is gevind om 99.9% beduidend te wees in die bepaling van die selheidsprofiel se grootte.

Twee modelle is ontwikkel om afsonderlik die relatiewe grootte en gelykvormigheid van die kruisvloeiselheidsprofiel te voorspel. Die modelle is in 'n metodologie vervat vir die ontwerp van 'n lugligter opstelling met stelselhidrodinamika wat verbeterde lugskropaksie effektiwiteit sal skep.

Acknowledgements

I thank the Lord for the insight and strength He gave me to finish this study when completion seemed impossible. I also wish to express my sincere gratitude and appreciation to the following people for their contributions towards the successful completion of this study:

- My supervisor, Ed Jacobs, for the opportunity to be part of the MBR research programme. Without his guidance and motivation this thesis would never have seen the light of day.
 - My supervisor, Steven Bradshaw, for his continued belief in me and his willingness to help.
 - Minnaar Pienaar, for enrolling me yet one more time.
 - Deon Koen (University of Stellenbosch, Department of Chemistry and Polymer Science), for his assistance and advice in the workshop and laboratory.
 - Helen Divey (University of Cape Town, Department of Chemical Engineering), for measuring the bentonite particle size distribution.
 - Jianxin Li (University of Stellenbosch, Department of Chemistry and Polymer Science), for lending me his ultrasonic equipment and helping me with the UTDR data interpretation.
 - Joos van der Merwe (University of Stellenbosch, Department of Geology), for helping me develop a suitable bentonite suspension preparation method.
 - All my Sasol colleagues for their interest and continued encouragement, especially to Ronél Augustyn, Michael van Niekerk, Doep Du Plessis, Estelle Marais and Deon Nieuwenhuis.
 - Alan Anderson, my spiritual brother. Thank you for all the support. I regret not attending your wedding because of this thesis.
 - My parents for their countless sacrifices.
 - My wife, Jolene, for her unconditional love and support through all these years and to my daughter, Annika, for lighting up my day with a single smile.
-

Table of contents

DECLARATION	I
ABSTRACT	II
OPSOMMING	III
ACKNOWLEDGEMENTS	IV
TABLE OF CONTENTS	V
LIST OF FIGURES	VIII
LIST OF TABLES	XI
LIST OF ABBREVIATIONS	XII
INTRODUCTION	1
1.1 Background.....	1
1.2 Aim of study.....	4
1.3 Layout of thesis.....	5
MEMBRANE FOULING BACKGROUND	6
2.1 Introduction	6
2.2 Mass transport	7
2.2.1 Concentration polarisation.....	8
2.2.2 Back-transport	9
Brownian diffusion.....	10
Shear-induced diffusion	11
Inertial lift.....	12
Surface transport.....	13
2.3 Membrane fouling mechanisms.....	14
2.3.1 Physico-chemical fouling mechanisms	14
2.3.2 Biofouling mechanisms	16

2.3.3	Membrane fouling modelling	17
2.4	Membrane fouling amelioration	22
2.4.1	Feed pretreatment	22
2.4.2	Membrane material selection	23
2.4.3	Back-transport promotion	23
	Surface hydrodynamics	23
	Permeate flux destabilisation	23
	Sub-critical flux operation	24
AIR-SCOURING OF IMMERSSED MEMBRANES		27
3.1	Introduction	27
3.2	Scouring action of rising bubbles	28
3.3	Airlift reactors	30
3.3.1	Liquid velocity	31
3.3.2	Airlift reactor application for immersed membrane fouling control	32
FOULING QUANTIFICATION FOR AIR-SCOURING EVALUATION		33
4.1	Introduction	33
4.2	Fouling quantification methods	35
4.3	Flux-step method for indirect fouling quantification	37
4.3.1	Background	37
4.3.2	Experimental set-up	40
4.3.3	Method	42
4.3.4	Results	44
4.4	Ultrasound for direct fouling quantification	49
4.4.1	Background	49
4.4.2	Experimental set-up	55
	Ultrasonic measurement system	55
	A_d/A_r ratios	60
	Constant aeration intensity	60
	Constant permeate flux	61
4.4.3	Method	61
4.4.4	Results	62
	Reflected waveforms	62
	Membrane fouling	66
SYSTEM HYDRODYNAMIC EFFECTS OF AIRLIFT REACTOR FACTORS		68
5.1	Introduction	68
5.2	Design of experiments	71
5.2.1	Full factorial designs	73
5.2.2	Screening designs	73
5.3	Screening of system hydrodynamic factors	75
5.3.1	Experimental set-up	75
5.3.2	Method	77
	Linear liquid velocity measurement	77
	Response calculation	78

Design of experiment	80
Effects calculation	84
Significance of effects	85
5.3.3 Results.....	86
Area under the velocity profile	86
Average gradient of the velocity profile.....	86
5.4 Validation of system hydrodynamic factors	88
5.4.1 Experimental set-up	88
5.4.2 Method.....	88
5.4.3 Results.....	90
CONCLUSIONS	92
6.1 Introduction	92
6.2 Air-scouring efficiency.....	93
6.3 System hydrodynamic factors	94
REFERENCES	95
MODEL FOULANT PREPARATION.....	110
A.1 Introduction	110
A.2 Model foulant selection	111
A.3 Suspension preparation.....	113
A.4 Turbidity calibration.....	114
MEMBRANE ELEMENT CONSTRUCTION.....	115
B.1 Introduction	115
B.2 Membrane material.....	116
B.3 Membrane element production	117
FLUX-STEP EXPERIMENTAL DATA	127
UTDR EXPERIMENTAL DATA.....	133
Determining speed of sound in bentonite cake layer	133
SCREENING DESIGN EXPERIMENTAL DATA.....	134
MODEL VALIDATION EXPERIMENTAL DATA	152

List of figures

Figure 1.1: Equivalent wastewater treatment processes: (a) conventional activated sludge process and (b) MBR process replacing all the conventional process steps in one treatment step.....	3
Figure 1.2: The two MBR process configurations for solids/liquid separation: (a) sidestream operation and (b) immersed operation.	3
Figure 1.3: Thesis flow diagram indicating the logical unfolding of information and results necessary to reach sensible conclusions.	5
Figure 2.1 Mass transport operations for pressure-driven cross-flow membrane filtration.	8
Figure 2.2: Illustration of the particle size dependency of membrane fouling. A minimum back-diffusivity exists with deposition of material at a relative low TMP.	12
Figure 2.3: Physico-chemical fouling mechanisms [Belfort et al., 1993].	15
Figure 2.4: Stages of biofilm growth on a clean membrane.	16
Figure 2.5: Contribution of each hydraulic resistance to the TMP for a hypothetical microfiltration process at constant permeate flux where the feed could be changed from pure water to a particulate suspension.	21
Figure 2.6: Critical flux hypothesis for microfiltration: (a) strong form and (b) weak form. Above the critical flux in both cases TMP continuous to increase at constant permeate flux and displays TMP hysteresis when permeate flux is reduced to below the critical flux.	25
Figure 2.7: Hypothetical TMP profile of incremented constant permeate fluxes from sub-critical to above critical fluxes.	26
Figure 2.8: Hypothetical TMP profiles of constant permeate fluxes when the feed was switched from pure water to a particulate suspension. Above critical flux cake layer formation commences and continues at a constant rate.	26
Figure 3.1: Aeration regimes inside a tube: (a) bubble flow; (b) slug flow; (c) churn flow; (d) annular flow; and (e) mist flow [Judd et al., 2001].	28
Figure 3.2: Slug flow inside an inside-out tubular membrane. A rising air slug scours the membrane surface by first subjecting it to a negative shear stress ($\tau_{L\text{Film}}$) and then by a positive shear stress ($\tau_{L\text{Slug}}$) [Laborie et al., 1998; Cabassud et al., 2001].	29
Figure 3.3: Air-sparging of immersed outside-in flat-sheet membranes.	29
Figure 3.4: Liquid flow patterns: (a) chaotic liquid circulation cells in a bubble column; (b) clearly defined liquid flow in an airlift reactor: upwards in the gassed riser and downwards in the ungassed downcomers [Chisti and Moo-Young, 1987; Choi et al., 1996].	30
Figure 4.1: The typical TMP profile of a flux-step experiment where the permeate flux was incremented five times with an arbitrary chosen permeate flux J from below critical flux to above critical flux at a time increment of t . In this case a permeate flux of $2J$ was still below the critical flux, whereas a permeate flux of $3J$ was above the critical flux with a resulting continued increase in TMP.	38
Figure 4.2: The rates of stabilised TMP increase of each permeate flux increment as derived from the typical TMP profile of a flux-step experiment as shown in Figure 4.1. The critical flux is found where $d\text{TMP}/dt$ changes from zero to a positive value,	

	which in this case, lies between the flux-step experiment's second and third permeate flux increment.	40
Figure 4.3:	Set-up for the flux-step experiment: (a) main equipment and (b) detail of airlift reactor.	41
Figure 4.4:	The presence of a region of stagnant bubbles in the riser section during aeration. This region promotes localised fouling where it crosses the immersed membrane.	45
Figure 4.5:	Membrane fouling rate at different aeration intensities. The intermediate aeration intensity (580 L/(m ² ·min)) produced the highest scouring ability. Between an aeration intensity of 580 and 1 100 L/(m ² ·min) the region of stagnant bubbles develop to cross the immersed membrane and promote localised fouling.....	47
Figure 4.6:	Membrane fouling rate at different permeate fluxes. An increase in the permeate flux will lead to an increase in the fouling rate (dTMP/dt), if above the critical flux. However, at the correct aeration intensity the fouling rate at any permeate flux can be greatly reduced. Under and over aeration may accelerate the fouling rate as is shown in this graph.....	47
Figure 4.7:	Reflection of wave energy at media interfaces. Two cases are shown here: (a) material 2 has a higher acoustic impedance than material 1, but the difference is slight to produce a low energy reflected wave in phase with the incident wave; (b) material 2 has a lower acoustic impedance than material 1 and the difference is significant to produce a high energy reflected wave out of phase with the incident wave.....	51
Figure 4.8:	Hypothetical oscilloscope waveforms to explain UTDR for fouling quantification. (Notice that only one side of the immersed membrane was considered here.).....	54
Figure 4.9:	The experimental set-up for the UTDR experiment for the direct fouling quantification of immersed membrane fouling. Besides the ultrasonic equipment, the equipment set-up is identical to the equipment set-up described in Section 4.3.2 for the flux-step experiment.....	56
Figure 4.10:	A photograph of one of the membrane elements that were used in the ultrasound experiment with its membrane spacer material and the Panametrics Videoscan V120-RB transducer.	57
Figure 4.11:	Section of the side view of the riser section to show the location of the immersed ultrasonic transducer. The transducer was positioned halfway the depth of the membrane element's flat-sheet surface.	59
Figure 4.12(a):	Typical waveform translation of a clean membrane.....	63
Figure 4.12(b):	Typical waveform translation of internal fouling.	64
Figure 4.12(c):	Typical waveform translation of cake layer formation.	65
Figure 4.13:	The arrival time differences at the relative positions after 20 hours of membrane filtration in a 1.0 g/L bentonite suspension.	67
Figure 5.1:	Typical hydrodynamic field patterns that were observed in the riser section of an airlift reactor: (a) fast rising liquid and bubbles in the middle with churning liquid and stagnant bubbles on the sides; (b) uniformly fast rising liquid and bubbles across the riser section; and (c) fast rising liquid and bubbles on the sides with churning liquid and stagnant bubbles in the middle.....	68
Figure 5.2:	The six aspects of airlift reactor design that were investigated to determine their influences on the velocity profile in the riser section.....	70
Figure 5.3:	A basic explanation of DOE for a hypothetical system. (a) Three factors, A, B and C, were identified as possibly having an impact on the response and needed to be investigated. An experimental error is present in the system and contributes to the value of the response. (b) Two levels were chosen for each factor, which are the only values where the factors are maintained during the designed experiment. Note that the levels of factor C are attributes. Each factor's high level is indicated by "+1" and their corresponding low level is indicated by "-1". (c) Factors A and B, as well as their interaction AB, were found to have a significant effect on the response, since they managed to change the response value to	

	outside of its inherent variation. Factor C and all other interactions are insignificant and can be ignored in future optimisation studies.	72
Figure 5.4:	Experimental set-up for the screening of system hydrodynamic factors: (a) PVC tank with one half of the front containing a clear PVC sheet and (b) the baffle plate framework which could be changed to create different airlift reactor configurations when slotted inside the PVC tank.....	76
Figure 5.5:	Velocity profile quantification: (a) hypothetical pathways of PP pieces when entering the riser section in the different subsections and (b) hypothetical plotted average linear liquid velocities calculated for each subsection to compile a velocity profile across the riser section. The magnitude of the velocity profile is indicated by the area under the profile and the uniformity is indicated by the average gradient of the profile.	79
Figure 5.6:	Average membrane fouling rates for the different configurations. Although not shown for the sake of clarity, the variability in the fouling rate increased with an increase in absolute velocity profile gradient and was therefore the highest for configuration 4.	91
Figure A.1:	Particle size distribution of the bentonite used in this study.....	112
Figure A.2:	Regressed calibration curve for bentonite suspensions.	114
Figure B.1:	A photograph of three membrane elements under construction.	117
Figure B.2(a):	Membrane curtain is cut from the membrane material.	118
Figure B.2(b):	Membrane curtain contains the selected number of filter tubes and the inactive tube remains on the sides.....	118
Figure B.2(c):	Stainless steel mesh strips are inserted into the filter tubes to act as spacer material. The membrane curtain is then slotted inside a slit cut into a PVC pipe. ...	119
Figure B.2(d):	Bottom end of membrane element sealed off.	120
Figure B.2(e):	Construction of the permeate collector.	121
Figure B.2(f):	Sealing of membrane curtain entrance at permeate collector.	121
Figure B.2(g):	The mould set-up around the permeate collector.....	122
Figure B.2(h):	The flow of the injected resin through the injection tube, into the PVC pipe and around the permeate collector.	123
Figure B.2(i):	The set resin around the permeate collector. Note how the silicon rubber plug and the silicon rubber sealing at the membrane curtain entrance keeps the permeate collector empty.....	123
Figure B.2(j):	The finished membrane element product. The resin filled parts of the bottom sealed pipe and the top permeate collector have been sawn off.	124
Figure B.2(k):	Cross-section through the middle of a completed membrane element.....	125
Figure B.3:	Detail measurements of the polyethylene mould blocks: (a) blocks A and B connected to form the total mould; (b) one block A; and (c) both blocks B. Note that drawings are not to scale and that measurements are given in millimetres.	126

List of tables

Table 4.1:	The three chosen aeration intensities for the flux-step experiment. (Notice the relative large deviation in the compressor's air flow rate to achieve the high aeration intensity.)	43
Table 4.2:	The random order in which the trials were conducted to minimise the risk of unknown influences on the results.	43
Table 4.3:	Panametrics Videoscan ultrasonic transducers that were evaluated for the monitoring of fouling layer formation [Koen, 2000b]	57
Table 4.4:	The three airlift reactor geometries and the flat-sheet membrane sizes used in the UTDR experiment.	60
Table 5.1:	Plackett-Burman design for 7 factors (factors A, B, C, D, E, F and G) and 8 treatments. Each factor is completely confounded with three interactions, but is opposite in sign. The "+" and "-" signs in each treatment indicate the required high or low level of the corresponding factor for the specific treatment.	74
Table 5.2:	Values of the levels at which each factor was evaluated.....	80
Table 5.3:	The treatments for the experimental design of the base, reflection and full factorial treatments. The "+" and "-" signs indicate the setting of the levels. The order indicates the randomisation of the treatments and their replicates. The shaded treatments indicate treatments that were already covered in the base and reflection treatments.	82
Table 5.4:	The treatments (from the full factorial section of Table 5.3) used in the full factorial designs to determine the effects of the interactions. The "+" and "-" signs indicate the levels of the respective factors in the same order as the name of the interaction. The numbers of the shown treatments refer to numbers 1 to 22 mentioned in the full factorial section of Table 5.3.....	83
Table 5.5:	The decision limits for the significance of effects.....	85
Table 5.6:	Different airlift reactor configurations chosen to validate their predicted velocity profile areas and gradients as predicted by Equations 5.7 and 5.8. The "+1" and "-1" indicate the respective high and low levels of the specific factor as is explained in Table 5.2. Configuration 1 represents the configuration with the most uniform velocity profile and configuration 2 represents the configuration with the highest velocity profile area.....	89
Table 5.7:	The random order in which the treatments were conducted to minimise the risk of unknown influences on the results. The configuration numbers correlate with the configurations listed in Table 5.6.....	90

List of abbreviations

A_d/A_r	total downcomer cross-sectional area to riser cross-sectional area ratio
CSV	comma separated value (Microsoft Excel file format)
df	degrees of freedom
DL	decision limits
DOE	design of experiments
EPS	extracellular polymeric substances
MBR	membrane bioreactor
OD	outer diameter
PP	polypropylene
PVC	polyvinyl chloride
TMP	transmembrane pressure
UTDR	ultrasonic time-domain reflectometry

Chapter 1

Introduction

1.1 Background

In biological treatment of wastewater, membranes provide absolute separation of solids and liquids [Günder and Krauth, 1998]. This ability offers membrane systems a superior operating envelope compared to conventional treatment systems that have to rely on clarification for solids/liquid separation. Since the hydraulic retention time is completely decoupled from the sludge retention time in a membrane system, the sludge age can be set to any value by the operator, the system can be operated at very high mixed liquor suspended solids concentrations, slow-growing microorganisms such as nitrifying bacteria can be accommodated and waste sludge production can be reduced [Judd, 2008]. Besides improved operability, membrane systems, by the nature of the exclusivity of their solids/liquid separation, can produce on-specification treated water in a single process step; thereby eliminating conventional downstream treatment steps to reduce plant footprint [Günder and Krauth, 1998; Gander et al., 2000]. The most widely used membrane system for solids/liquid separation in wastewater treatment processes is the membrane bioreactor (MBR) [Stephenson et al., 2000a]. Figure 1.1 illustrates the simplification that an MBR system introduces to a wastewater treatment process to achieve similar, or even better, product results when compared to a conventional activated sludge system.

However, membrane fouling [Meng et al., 2009] still remains the main obstacle for the wider application of MBR technology, since membrane fouling is responsible for considerable capital cost and operating cost components. For the two different MBR configurations, sidestream and immersed [Gander et al., 2000; Van't Oever, 2005; Pearce, 2008] shown in Figure 1.2, there is a trade-off between cost and performance to address membrane fouling. In a sidestream configuration the membranes are external to the bioreactor and the wastewater is pumped across the membranes at high cross-flow velocities to reduce fouling. The cross-flow pumping results in high operating costs, but the membranes can be allowed to operate at high permeate flows. In an immersed configuration the membranes are immersed in the wastewater and only a moderate cross-flow can be induced across the membranes by vigorously aerating the water beneath the membranes. Also, immersed membranes have to revert to much lower permeate flows to reduce

membrane fouling and therefore require larger membrane surfaces to produce the same permeate rate than a sidestream configuration. Gander et al. [2000] have found that the sidestream configuration has a higher total energy cost, up to two orders of magnitude higher, than the total energy cost of operating an immersed configuration.

With a continued decrease in membrane cost over the last two decades [Churchouse and Wildgoose, 1999; Judd, 2008] and with lower energy requirements than sidestream configurations, immersed MBRs have become the most popular MBR configuration for solids/liquids separation in wastewater treatment processes. With environmental regulations becoming increasingly more stringent and demand for additional hydraulic capacity increases on existing conventional activated sludge processes, the opportunity exists to retrofit these wastewater treatment plants with immersed MBRs [Ahn et al., 1999; Tiranuntakul et al., 2005].

Although an immersed MBR usually has a lower operating cost than a sidestream MBR, the major portion of the immersed MBR's operating cost is for coarse bubble aeration to limit fouling of the immersed membranes [Gander et al., 2000; Judd, 2008]. In the view of rising energy prices, it is therefore imperative that immersed MBRs, and especially those for retrofitted systems, are designed and operated as optimally as possible to improve their fouling behaviour and reduce the operating cost of aeration [Verrecht et al., 2008].

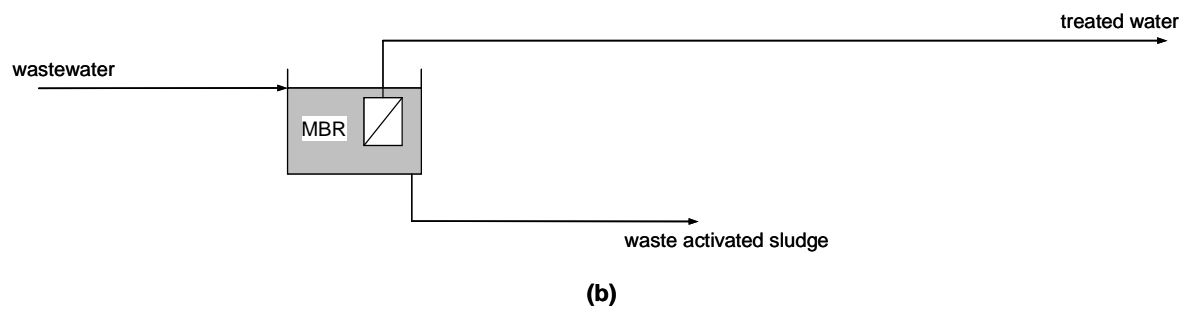
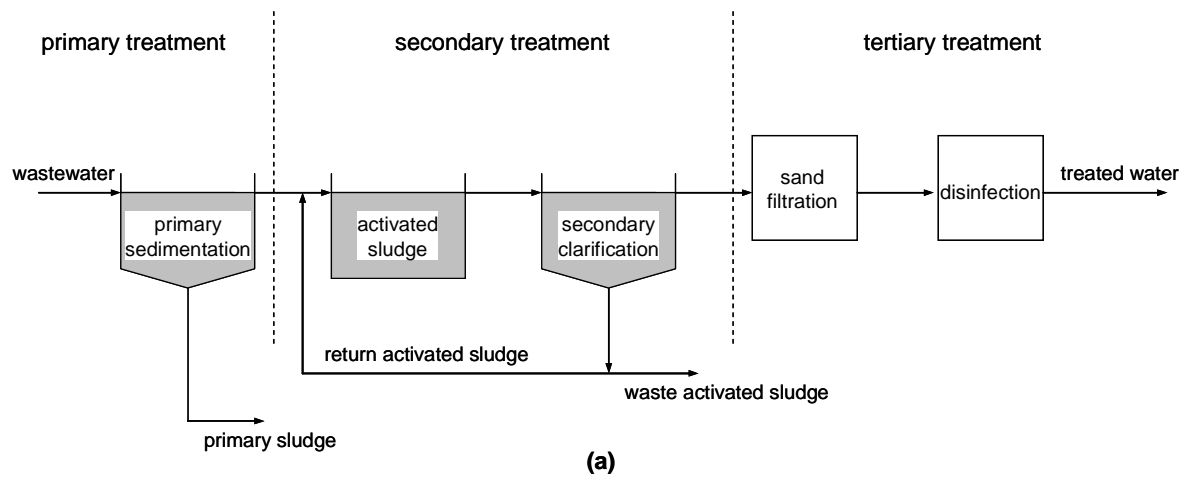


Figure 1.1: Equivalent wastewater treatment processes: (a) conventional activated sludge process and (b) MBR process replacing all the conventional process steps in one treatment step.

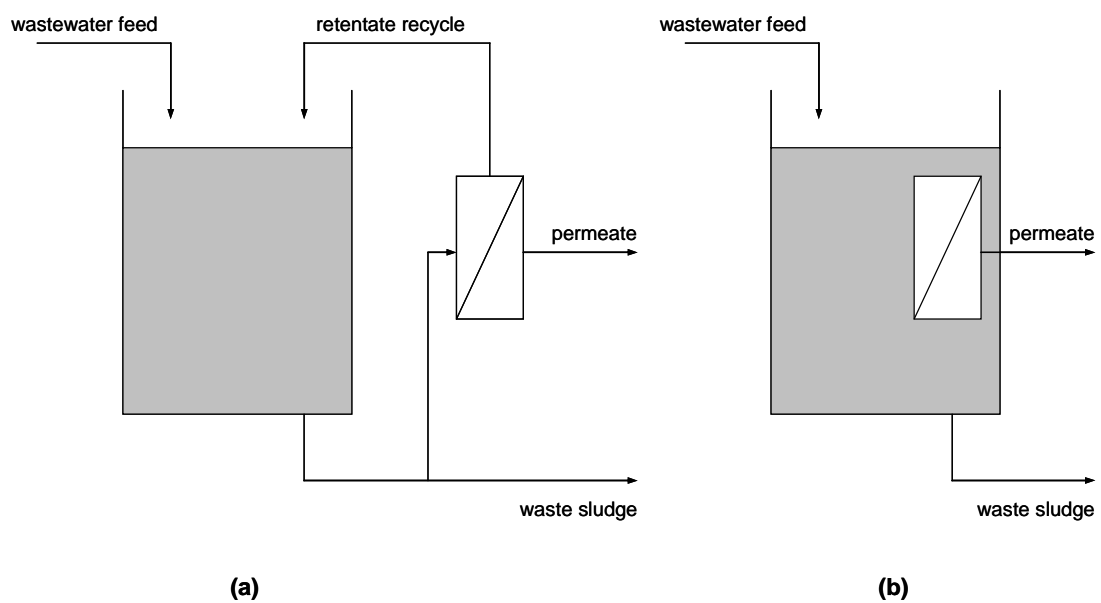


Figure 1.2: The two MBR process configurations for solids/liquid separation: (a) sidestream operation and (b) immersed operation.

1.2 Aim of study

Immersed MBR systems hold very promising opportunities, but their widespread application is still hindered by their high operating and capital costs as a result of membrane fouling. With membrane costs declining, the capital cost of immersed MBR systems will eventually compare better with conventional activated sludge systems. But with increasing energy prices, immersed MBR systems will remain unfavourable because of their air-scouring (or other abatement techniques) requirements, unless this can be improved. There is consequently an incentive to improve on the air-scouring efficiencies of immersed MBR systems.

The aim of this study is to identify factors that will improve air-scouring efficiency of an immersed microfiltration membrane and to suggest the directions for further optimisation. Optimisation of these factors, physical parameters and operating parameters is beyond the scope of this study and should be addressed in future optimisation studies.

1.3 Layout of thesis

This thesis covers many different fields of science and information is therefore required to be unfolded in a logical manner. Results in one chapter are used as inputs in the next chapters. All the results of the previous chapters are discussed in Chapter 6 for a holistic approach.

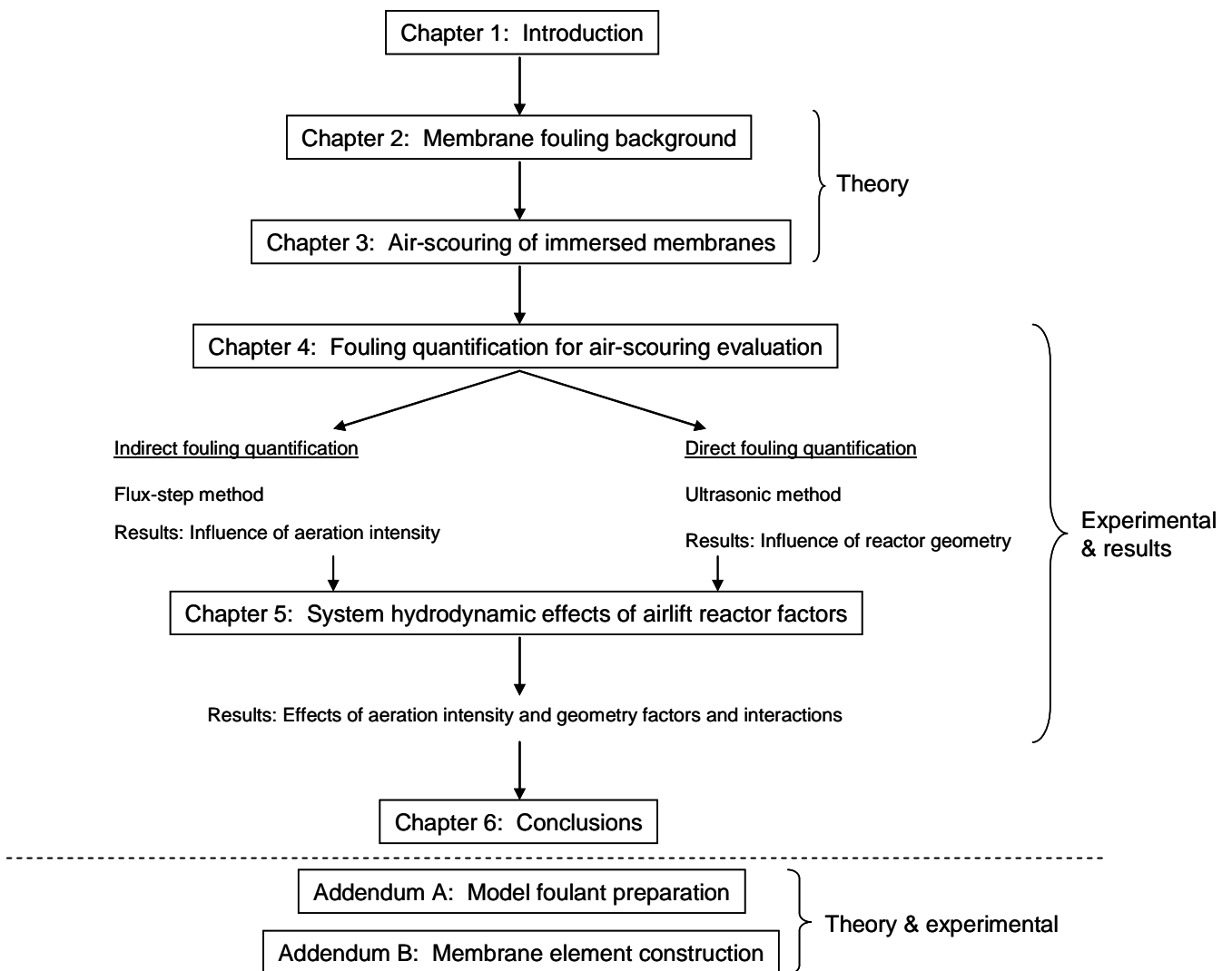


Figure 1.3: Thesis flow diagram indicating the logical unfolding of information and results necessary to reach sensible conclusions.

Chapter 2

Membrane fouling background

2.1 Introduction

Membrane fouling refers to the collective processes responsible for the undesirable accumulation of deposit on the membrane surface and inside the membrane pores to increase the hydraulic resistance to mass transport through the membrane during filtration operations. While the immediate manifestation of membrane fouling is a declining specific permeate flux (unit permeate flux per unit driving force), the long term results may include irreversible fouling and membrane damage to shorten membrane lifetime [Al-Ahmad et al., 2000]. Membrane fouling is the single most important impediment to the widespread large-scale application of membrane filtration for wastewater treatment, since large capital investments and high operating costs are necessitated to reduce fouling or to treat its detrimental consequences in order to maintain an adequate throughput.

Membrane fouling forms a mechanistic part of membrane filtration and can never be completely eliminated. It is therefore important to understand the causes of membrane fouling and the conditions that will suppress it to enable the design and operation of a membrane system with a more favourable fouling behaviour; and therefore with a more viable water treatment production. This chapter will focus on the membrane fouling encountered in microfiltration for wastewater treatment applications.

2.2 Mass transport

During microfiltration the driving force for mass transport through the membrane is an applied pressure differential across the membrane which is known as the transmembrane pressure (TMP) [Belfort et al. (1994)]. The TMP can either be created by applying a vacuum on the permeate side of the membrane or by increasing the pressure on the feed side.

Figure 2.1 illustrates the mass transport operations for pressure-driven cross-flow membrane filtration. The TMP driving force creates a convective fluid flow which follows the pressure gradient from the high pressure at the bulk of the feed stream to the low pressure on the permeate side of the membrane. Any other material present in the fluid is consequently also carried to the membrane where the membrane pore size differentiates the larger material, which is retained on the high pressure side of the membrane, from the smaller material passing through the membrane. Close to the membrane surface the cross-flow may be assumed to be laminar, but because of wall friction the cross-flow velocity is zero at the membrane surface. A velocity boundary layer is therefore created to form a relative stagnant film across the membrane surface in which back-transport is limited to diffusion, a relatively slow mass transport process. With the consequent accumulation of rejected material near the membrane surface a concentration boundary layer develops in the stagnant film with an increased concentration of this material near the membrane surface compared to the lower uniform concentration in the bulk; a phenomenon known as concentration polarisation. Back-transport mechanisms facilitate the removal of retained material from near the membrane surface back to the bulk, but if the convective permeation flux is greater than the back-transport flux, the material is likely to be deposited on the membrane surface. Conversely, with a back-transport flux greater than the permeation flux, the likelihood of material deposition is limited.

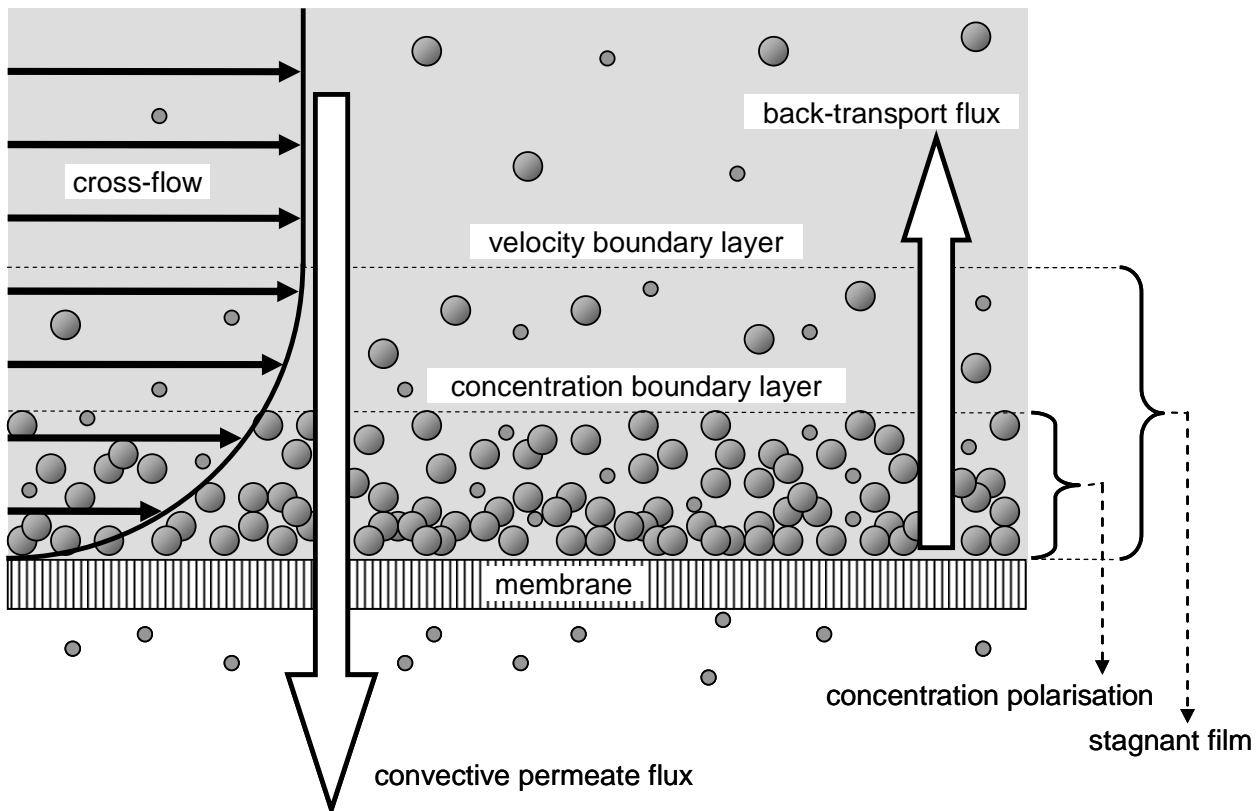


Figure 2.1 Mass transport operations for pressure-driven cross-flow membrane filtration.

Because microfiltration is based on size exclusion at the membrane surface, the accumulation of material near the membrane is an inevitable result of this separation process. Arguably, it can be viewed therefore that concentration polarisation and the relative size of the back-transport flux to the permeation flux determines the extent of membrane fouling.

2.2.1 Concentration polarisation

Concentration polarisation describes the tendency of material to accumulate at the membrane surface and can be ascribed to two phenomena associated with membrane filtration: permselectivity of membranes and the existence of a stagnant film near the membrane surface in cross-flow operations [Matthiasson and Sivik, 1980].

Concentration polarisation itself usually represents a resistance against permeate flux, since the osmotic pressure of the retained material reduces the effective TMP driving force [Belfort et al., 1994]. However, for microfiltration operations the resistance induced by concentration polarisation is negligible, since the retained particles are relatively large with small osmotic pressures [Bai and

Leow, 2002]. But even though it may act as an additional resistance against permeation, it is important to note that concentration polarisation is not a fouling mechanism, since it is a reversible result of membrane separation and will disappear once membrane filtration is stopped. However, concentration polarisation provides the conditions in which fouling can occur.

The transition from concentration polarisation to membrane fouling may be quite different and complex for reverse osmosis, ultrafiltration and microfiltration operations, but in each filtration operation concentration polarisation ultimately leads to an increase in TMP at constant permeate flux operation or decrease in permeate flux at constant TMP operation. For reverse osmosis the presence of a concentration boundary layer at the membrane surface increases the propensity for scaling [Lee and Lueptow, 2003]. In ultrafiltration operations, concentration polarisation promotes the precipitation of slightly soluble solutes and particle-particle interactions to form a gel layer on the membrane [Chen et al., 1997; Bacchin et al., 2002]. The effect of concentration polarisation to promote membrane fouling tends to be severe for microfiltration operations, since the permeate fluxes are usually high, while the diffusive back-transport is slow for particles [Wakeman and Williams; 2002]. Consequently, the close proximity of the retained particles to the membrane surface leads to the formation of a cake layer.

Since material retention will always occur in microfiltration operations, concentration polarisation can never be completely removed. The extent of concentration polarisation should therefore be kept to a minimum to limit membrane fouling by operating at low permeate fluxes to reduce the driving force and improving turbulence on the feed side of the membrane to enhance back-transport.

2.2.2 Back-transport

Particle back-transport mechanisms can be divided into two classes: diffusive and convective hydrodynamic shear forces [Silva et al., 2000]. Most of the proposed models in the literature for back-transport are primarily based on diffusion mechanisms, but in microfiltration and ultrafiltration systems with hydrodynamic shear forces at the membrane surface the back-transport of particles are predominantly caused by these convective forces and the effect of diffusion may be neglected [Shulz et al., 1989; Sayed Razavi et al., 1996]. The proposed models for diffusive back-transport include Brownian diffusion and shear-induced diffusion, whereas convective hydrodynamic back-transport mechanisms may be explained by inertial lift and surface transport [Belfort et al., 1994; Tardieu et al., 1998].

Brownian diffusion

Consider the cross-flow membrane filtration of a fluid containing only true solutes. Initially the rate at which solute species are introduced to the stagnant film is determined by the convective permeation flux and the degree of solute retention of the membrane. Diffusion is the only mechanism for back-transport in the stagnant film and the back-diffusion of solute to the bulk will increase with the increase of solute in the stagnant film. At steady-state operation the build-up of solute in the stagnant film is counteracted by a Brownian diffusive flux of solute away from the membrane.

When assuming a 100% retention of solute by the membrane and a constant stagnant film thickness, Brownian back-diffusion for steady-state membrane filtration can be defined by the film model as [Stephenson et al., 2000b]:

$$J = k \ln\left(\frac{C_m}{C_b}\right) \quad (2.1)$$

with $k = \frac{D_B}{\delta}$ (2.2)

where J = permeate flux (m/s)
 D_B = Brownian diffusion coefficient (m²/s)
 δ = stagnant film thickness (m)
 C_m = solute concentration at membrane surface (volume fraction)
 C_b = solute concentration in bulk (volume fraction)
 k = mass transfer coefficient (m/s)

The Brownian diffusion coefficient for solutes can be estimated from the Stokes-Einstein equation [Field, 1993]:

$$D_B = \frac{\kappa T}{6\pi\mu r_p} \quad (2.3)$$

where κ = Boltzmann constant = 1.380×10^{-23} (J/K)
 T = absolute temperature (K)
 μ = absolute viscosity (Pa.s)
 r_p = particle or solute radius (m)

It is evident from Equation 2.1 that the film model predicts the permeate flux to be mass transfer limited and independent of TMP under steady-state conditions. The permeate flux therefore

benefits from improved back-transport which is obtained by a higher mass transfer coefficient (Equation 2.2) and an increased concentration driving force from the membrane surface to the bulk. Equation 2.3 shows the inverse relationship between a solute's radius and its Brownian diffusion coefficient and explains why larger Brownian diffusion coefficients are exhibited by solutes of smaller radii to increase back-transport from the membrane surface. In addition, as is shown by Equation 2.2, back-transport is enhanced by a thinner stagnant film. The stagnant film thickness again is dependent on the system hydrodynamics, and any technique to increase the fluid shear rate at the membrane surface will decrease the stagnant film's thickness to increase back-transport and maintain the system at a higher permeate flux [Porter, 1972; Reed and Belfort, 1982].

Although film theory provides acceptable permeate flux predictions when true solutes accumulate near the membrane surface, it was found, however, that the predictions for colloidal and particulate suspensions were 1 to 2 orders of magnitude smaller than the experimental permeate fluxes [Porter, 1972; Reed and Belfort, 1982]. This gross under-prediction of the permeate flux, the so-called flux paradox [Green and Belfort, 1980], can be explained by the small Brownian diffusivity of larger materials. The inaccuracy of the film model to predict the permeate fluxes for the ultrafiltration of colloids and the microfiltration of particles, suggests that other back-transport mechanisms also play a role during these operations.

Shear-induced diffusion

Unlike Brownian diffusion, a perikinetic effect, where diffusion is facilitated by the random bombarding motion of fluid molecules, shear-induced diffusion is an orthokinetic effect, meaning that the diffusion is caused by velocity gradients. When considering a particle in a suspension which is subjected to a shear flow, the particle will interact with other particles to cause a succession of displacements across the fluid streamlines. The particle displacement of the resulting random behaviour will, however, in the absence of a concentration gradient, have a zero mean. In the presence of a concentration gradient, the particle will experience more interactions from the high concentration side, compared to the low concentration side, and a resulting force will consequently displace the particle to streamlines down the concentration gradient [Eckstein et al., 1977; Leighton and Acrivos, 1987; Davis and Leighton, 1987]. Following on the early work of Eckstein et al. [1977], Leighton and Acrivos [1986] estimated shear-induced diffusivities from:

$$D_s = \frac{1}{3} r_p^2 \gamma \varphi^2 \left(1 + \frac{1}{2} e^{8.8\varphi} \right) \quad \text{for } \varphi < 0.5 \quad (2.4)$$

where D_s = shear-induced diffusion coefficient (m^2/s)
 r_p = particle radius (m)
 γ = fluid shear rate (s^{-1})
 φ = volumetric particle concentration (dimensionless)

Equation 2.4 shows the direct proportionality between the shear-induced diffusion coefficient and the square of the particle diameter and the shear rate. Brownian diffusion, on the other hand, is inversely proportional to the particle diameter and independent of shear rate (Equation 2.3). As a result, Brownian diffusion is the dominant back-diffusion mechanism for sub-micrometre particles in a low shear field, whereas shear-induced diffusion is important in typical cross-flow microfiltration operations to remove micrometre-size and larger particles from the membrane surface [Howell, 1995]. From the particle size dependency of these two back-diffusion mechanisms, it can be shown that a minimum back-diffusivity exists, as shown in Figure 2.2.

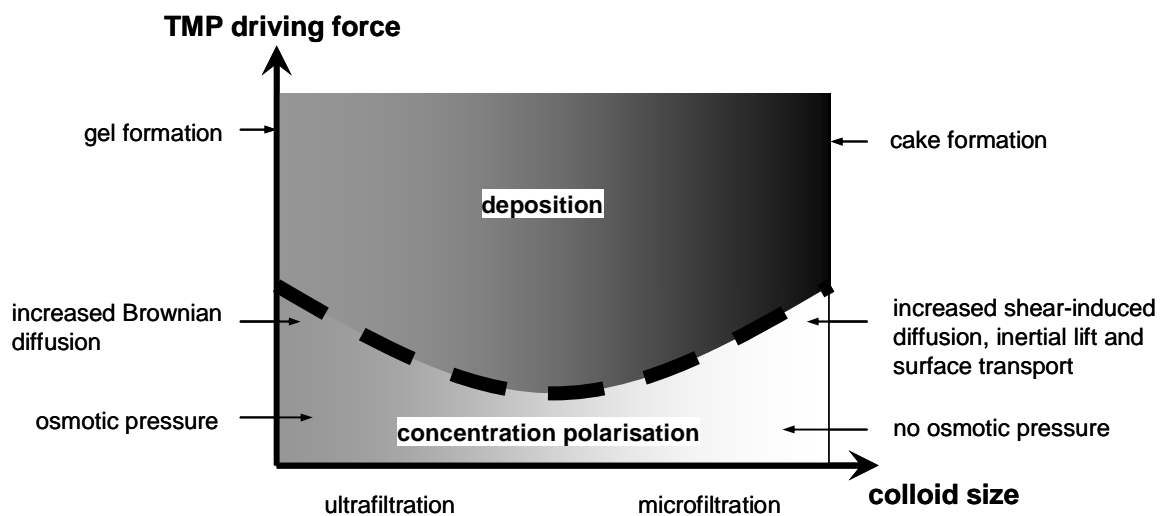


Figure 2.2: Illustration of the particle size dependency of membrane fouling. A minimum back-diffusivity exists with deposition of material at a relative low TMP.

Inertial lift

For tubular membranes the inertial lift model describes that, under lift and drag forces, neutrally buoyant particles in a laminar flow field will move away from both the membrane tube wall and the tube axis to reach equilibrium at a radial position [Green and Belfort, 1980; Belfort, 1989]. This phenomenon is also known in the literature as the tubular pinch effect [Porter, 1972]. Inertial lift

was first observed and published by Segré and Silberberg [1961] who worked with dilute suspensions of rigid spheres. Although a number of studies followed to investigate inertial lift, it was not until Porter [1972] first suggested that inertial lift could explain the flux paradox with Brownian diffusion as back-transport model, that inertial lift was investigated as an augmenting back-transport mechanism in tubular membranes. The study of inertial lift has also been extended to membrane systems containing slits [Altena and Belfort, 1984; Otis et al., 1986; Drew et al., 1991].

The lift forces, such as slip-spin and slip-shear forces [Porter, 1972], arise from nonlinear interactions of particles with the surrounding flow field. When these lift forces are stronger than the permeation drag force, it is proposed that the particles will not deposit on the membrane surface, but will migrate away from the membrane wall. Numerous models have been developed to determine the corresponding lift velocity of a particle in a given system, which must exceed the permeate velocity if the particle is to be carried away from the membrane [Cox and Brenner, 1968; Ho and Leal, 1974; Vasseur and Cox, 1976]. The derived expression for the lift velocity varies from system to system, but summarised, for both a tube and a slit, it applies that the lift velocity is increased for suspensions with larger particles at high cross-flow velocities [Green and Belfort, 1980; Altena and Belfort, 1984].

Surface transport

Surface transport models consider the possibility of particles deposited on the membrane surface to slide or roll tangentially across the membrane surface with the cross-flow. Surface transport can be described by two approaches: continuum and single-particle models.

In the continuum approach [Leonard and Vassilieff, 1984; Davis and Birdsell, 1987; Romero and Davis, 1988, 1990] particles retained at the membrane surface either remain as a stagnant cake layer on the membrane surface or they may, at high enough shear rates, move along the membrane surface in a flowing cake layer.

Single particle models consider the forces acting on a single spherical particle on the membrane or the stagnant cake surface to determine if the particle will adhere to the surface or be transported along the surface [Lu and Ju, 1989; Stamatakis and Tien, 1993].

Quantitative predictions of surface transport are difficult, but like shear-induced diffusion and inertial lift, surface transport is promoted by increases in the cross-flow velocity and the particle sizes.

2.3 Membrane fouling mechanisms

Depending on the concentration polarisation and back-transport conditions, the fouling behaviour of microfiltration membranes differs from system to system. The parameters that determine the concentration polarisation and back-transport are: particles' sizes, surface charges and concentrations; membrane material and its pore size distribution; hydrodynamic conditions at the membrane surface; temperature; pH and TMP driving force [Kawakatsu et al., 1993; Hwang et al., 1996; Bowen and Sharif, 1998; Bai and Leow, 2002; Le-Clech et al., 2003b; Trussell et al., 2007].

2.3.1 Physico-chemical fouling mechanisms

A polarised particle that is not being back-transported to the bulk has one of several destinations. Firstly, the particle may permeate through the membrane, given that the particle is smaller than the membrane pore size and that no attractive forces between the particle and the membrane material exist. In this scenario the particle leaves the membrane unimpeded, but other possibilities exist in which the particle can foul the membrane to reduce its permeability and thereby increase the hydraulic resistance to permeation. Depending on the relative sizes of the particle and available membrane pore, as well as prevailing surface charges, possible physico-chemical fouling mechanisms are adsorption, pore-blocking and cake layer formation [Belfort et al., 1993; Kawakatsu et al., 1993]. These three fouling mechanisms and their possible effects on the pore size distribution and the TMP versus permeate flux relation are shown schematically in Figure 2.3 for a membrane with a typical pore size distribution.

In the presence of attractive forces between the particle and the membrane, the particle may interact with the membrane through adsorption. The particle can adsorb to the membrane surface (the upstream side of the membrane) or, when small enough, adsorb to the membrane on the inside of an accessible pore to constrict it (Figure 2.3(a)). Continued adsorption of other particles inside the pores will result in a loss of pores from the pore size distribution to reduce the cross-sectional area available for permeation. The TMP therefore has to compensate for the reduced permeability and is consequently higher, compared to pure water filtration, when a constant permeate flux is required.

If the particle approaches a membrane pore of similar size, pore-blocking may occur when entering it to bridge the pore's entrance partially or even completely (Figure 2.3(b)). Pore-blocking affects

the pore size distribution and the TMP versus permeate flux relation in a similar way as adsorption, perhaps more severe, since a single particle suffices to completely block a membrane pore.

The surface filtration mechanism of sieving occurs when the particle is too large to enter a membrane pore (Figure 2.3(c)). The subsequent deposition of large particles on the membrane surface or other already deposited material forms a growing cake layer. The deposited cake layer acts as an additional filter, or so-called dynamic membrane, and reduces the effective pore sizes. The cake continues to acquire higher hydraulic resistances as the cake layer grows and the effective pore sizes decline with filtration time and TMP through particle compaction, particle rearrangement and deposition of smaller particles in the pores of the cake. The permeate flux is observed to change, with increased cake hydraulic resistance, from being pressure-controlled to being mass transfer-controlled, independent of TMP, as is shown in Figure 2.3(c) [Belfort et al., 1993; Hwang et al., 1996].

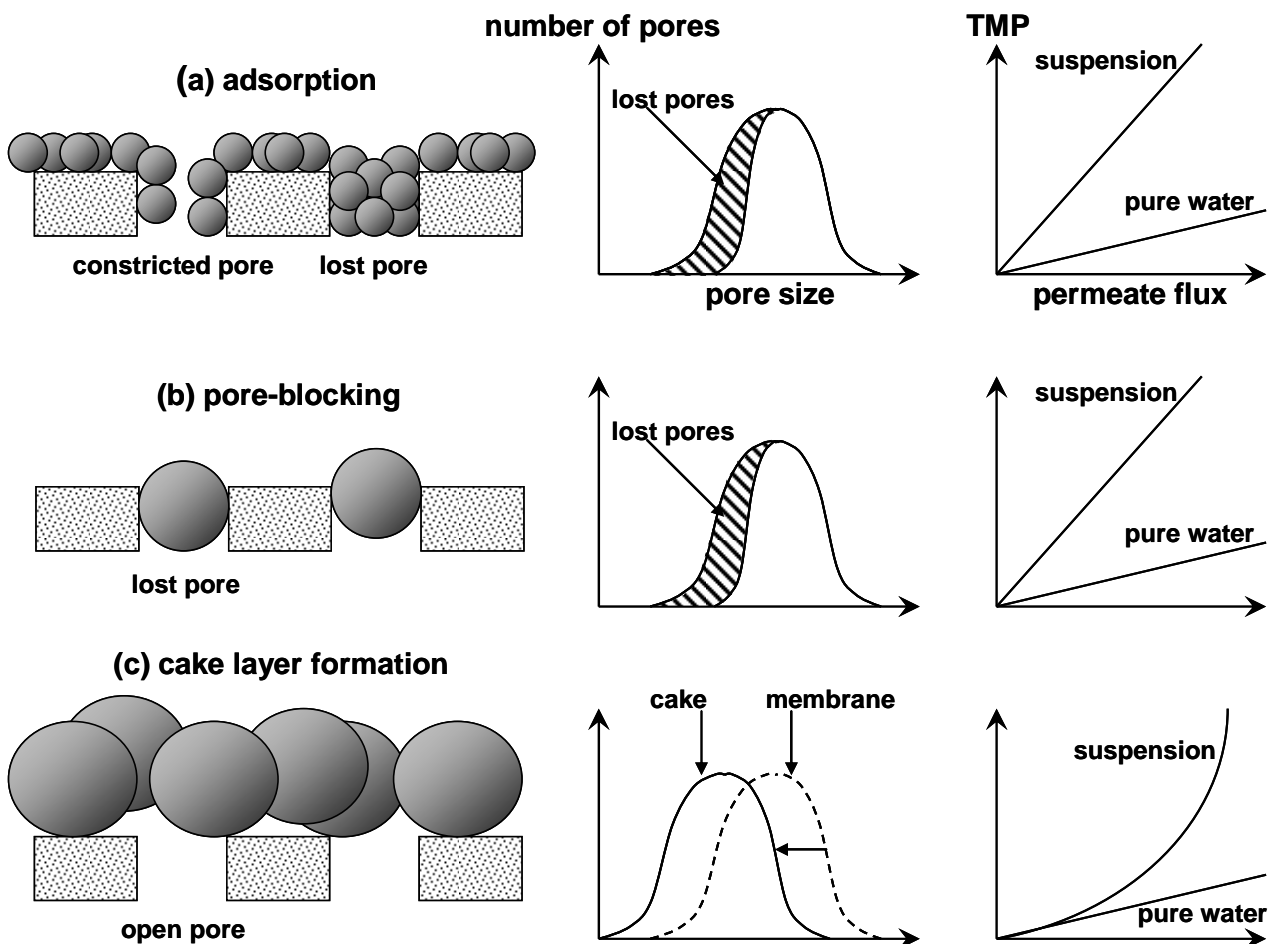


Figure 2.3: Physico-chemical fouling mechanisms [Belfort et al., 1993].

2.3.2 Biofouling mechanisms

Membrane biofouling arises from biofilm formation [Jacobs et al., 1996] on the surface and in the pores of the membrane to impose an extra hydraulic resistance [McDonogh et al., 1994; Aryal et al., 2009]. Biofilm comprises microbial cells embedded in a highly hydrated matrix of excreted extracellular polymeric substances (EPS) [Baker and Dudley, 1998]. It is widely documented that EPS mainly constitutes biofouling [Hodgson et al., 1993; Baker and Dudley, 1998; Nagaoka et al., 1998, 2000]. EPS serves as a binding material for the adhesion of the micro-organisms to the membrane surface and the cohesion of the biofilm [Flemming et al., 1997], thereby significantly increasing the energy requirement for biofilm removal. Complex biofilms, typical to industrial membrane operations, are often closely associated with entrapped particles [Al-Ahmad et al., 2000]. These deposits can even be more detrimental to membrane operation, since they may form more rapidly and be more tightly bound than biofilm on its own [Characklis, 1990].

The process of biofilm formation on a clean membrane surface is postulated to follow a number of steps [Flemming and Schaule, 1988; Lynch and Edyvean, 1988; Marshall and Blainey, 1991] and are shown in Figure 2.4:

1. Immediately upon immersion of the clean membrane in a bio-phase, dissolved organic material is adsorbed onto the membrane surface to form a conditioned layer.
2. Microbial cells transported to the membrane surface attach to the conditioned layer.
3. Growth and metabolism (start of EPS production) of the attached micro-organisms.
4. Limitation of biofilm growth by fluid shear forces and nutrient limitation at the base of the biofilm to attain a steady-state thickness.

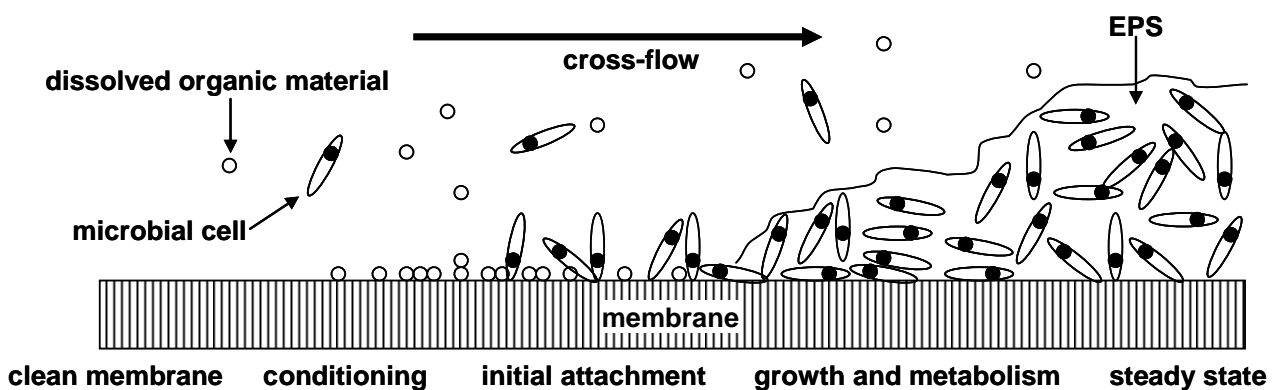


Figure 2.4: Stages of biofilm growth on a clean membrane.

Membrane biofouling, although inherently different from the physico-chemical attachment mechanisms of non-living particles, is nevertheless also considered to foul membranes by

constricting and blocking pores; and the formation of a cake layer on the membrane surface [Shimizu et al., 1997; Lim and Bai, 2003].

2.3.3 Membrane fouling modelling

Resistance models offer the simplest way to account for membrane fouling in the dynamic modelling of membrane performances [Kawakatsu et al., 1993; Piron et al., 1995; Chen et al., 1997; Tansel et al., 2000; Ghosh, 2002]. The starting point in the development of these models follows Darcy's law which can be written as:

$$J = \frac{\Delta P - \sigma \Delta \Pi}{\mu R_t} \quad (2.5)$$

where J = permeate flux (m/s)
 ΔP = transmembrane pressure (TMP) (Pa)
 σ = osmotic reflection coefficient (dimensionless)
 $\Delta \Pi$ = transmembrane osmotic pressure (Pa)
 μ = absolute viscosity of the fluid (Pa.s)
 R_t = total hydraulic resistance (m⁻¹)

In Equation 2.5 the driving force for permeation is the effective TMP which is the applied TMP, ΔP , minus the resulting transmembrane osmotic pressure, $\sigma \Delta \Pi$. The osmotic reflection coefficient, σ , is a measure of the leakiness of the membrane to the osmotic components and varies from one for a fully retentive membrane to zero for a fully permeable membrane. The transmembrane osmotic pressure, $\Delta \Pi$, resembles a pressure resistance that has to be overcome for permeation to occur and results from the difference in osmotic potential on both sides of the membrane during concentration polarisation as mentioned in Section 2.2.1.

The total hydraulic resistance, R_t , is defined as the sum of a series of resistances:

$$R_t = R_m + R_i + R_c \quad (2.6)$$

where R_m = membrane resistance (m⁻¹)
 R_i = internal fouling (adsorption and pore-blocking) resistance (m⁻¹)
 R_c = cake resistance (m⁻¹)

The membrane resistance states the intrinsic resistance of an unfouled membrane and is the benchmark for the minimum in the total hydraulic resistance. During membrane operation, fouling mechanisms will increase this minimum hydraulic resistance by depositing material internally

through adsorption and pore-blocking and externally through cake layer formation. Adsorption and pore-blocking resistances are usually lumped together as internal fouling resistance since it is very hard to quantitatively and qualitatively tell the resulting fouling apart. Instead of distinguishing between internal fouling and cake resistances, some sources refer to the fouling resistances as either being reversible or irreversible [Field et al., 1995; Krstić et al., 2002; Vyas et al., 2002]. This distinction is made on a quantitative basis for a specific cleaning process after a certain membrane operation time by comparing the calculated total hydraulic resistance values from Equation 2.5 at the start of operation, at the end of operation and after subsequent cleaning as follows:

$$R_{irre} = (R_t)_{clean} - R_m \quad (2.7)$$

$$R_{re} = (R_t)_{end} - (R_t)_{clean} \quad (2.8)$$

where R_{irre} = irreversible fouling resistance (m^{-1})

$(R_t)_{clean}$ = total hydraulic resistance after cleaning (m^{-1})

R_m = membrane resistance and equal to R_t for an unfouled membrane (m^{-1})

R_{re} = reversible fouling resistance (m^{-1})

$(R_t)_{end}$ = total hydraulic resistance at the end of membrane operation (m^{-1})

The specific cleaning process is therefore only able to remove the reversible fouling resistance, but by improving the cleaning process for the same membrane operation, the ratio of R_{re} to R_{irre} may be increased. Generally the removal of the cake layer requires considerably less energy compared to the removal of internal fouling, hence cake layer formation is often reversible, while internal fouling is usually irreversible [Wakeman and Williams, 2002].

Particles and large colloids exhibit negligible osmotic pressures and can be ignored in MF operations. Therefore, when substituting Equation 2.6 into Equation 2.5, the resistance model for microfiltration becomes:

$$J = \frac{\Delta P}{\mu (R_m + R_i + R_c)} \quad (2.9)$$

and when microfiltration is operated at a constant flux and the fluid viscosity assumed to be constant, the required TMP to compensate for an increasing total hydraulic resistance can be calculated from:

$$\Delta P(t) = J\mu [R_m(t) + R_i(t) + R_c(t)] \quad (2.10)$$

Although the membrane resistance, R_m , is usually considered as a constant, a time dependency was included for the term in Equation 2.10, since membrane compaction or a loss of integrity may increase or decrease the membrane resistance respectively with time.

As indicated in Equation 2.10, the evolution of the TMP increase is the result of various resistances working together, but the relative importance of each of the resistances may change with time. When constant flux permeation is started with an unfouled membrane, the initial TMP only depends on R_m , since R_i and R_c are zero. Since it is possible that membrane pores can be completely blocked by the first particles to reach the membrane, the subsequent internal fouling can be a very quick process to cause a rapid TMP increase [Bai and Leow, 2002]. Internal fouling can however be ignored if the suspended particles are larger than the membrane pores. As more particles are deposited on the membrane surface, a cake layer starts to form which offers an additional growing resistance, R_c , and, for a flat membrane, it can be calculated from [Belfort et al., 1994]:

$$R_c = \hat{R}_c \delta_c \quad (2.11)$$

where \hat{R}_c = specific cake resistance per unit cake thickness (m^{-2})

δ_c = cake thickness (m)

The initial impact of cake layer formation on the total hydraulic resistance does not seem to be as drastic, compared with internal fouling [Lim and Bai, 2003]. This may be explained by the relative permeability of a cake layer, as opposed to pore-blocking, and the fact that the cake layer thickness is limited by the prevailing shear stress at the cake surface [Benkahla et al., 1995]. After a steady-state cake thickness is attained, the further gradual increase in R_c can mainly be ascribed, as is evident from Equation 2.11, to the increase in the specific cake resistance of the cake layer. According to Porter [1977] the specific cake resistance can be described by:

$$\hat{R}_c = \alpha_o (\Delta P)^s \rho_s \Phi_c \quad (2.12)$$

where α_o = constant dependent on the size and shape of the cake particles

s = compressibility exponent of the cake

ρ_s = mass density of solids in the cake (kg/m^3)

Φ_c = solid volume fraction in the cake

The constant, α_o , increases with a decrease in particle size; and the solid volume fraction, Φ_c , increases as smaller particles are entrapped in the cake. It has been documented elsewhere that a cake layer of smaller particles or a cake layer capturing smaller particles exhibits increased

specific cake resistances [Bai and Leow, 2002; Lim and Bai, 2003]. Cake layers may also be compressed with increasing TMP to raise the specific cake resistance [Kawakatsu et al., 1993]. The compressibility exponent, s , varies from zero for a perfectly incompressible cake to one for a perfectly compressible cake. In practice the compressibility of cakes usually ranges between 0.1 and 0.8 [Porter, 1977].

In general, microfiltration can initially be characterised by a membrane resistance limited, followed by an internal fouling resistance limited and eventually a cake resistance limited process [Lim and Bai, 2003]. Although filtration models have been developed for each resistance limited process [Suki et al., 1986; Belfort et al., 1993; Silva et al., 2000], the exact behaviour of each resistance remains very system specific and must be empirically determined.

Consider the TMP-time profile of a hypothetical cross-flow microfiltration process in Figure 2.5 showing the contributions of each resistance limited process on the TMP required to produce a constant permeate flux. No fouling occurs while pure water is filtrated and the hydraulic resistance remains the constant resistance imposed by the membrane. In this process the feed is instantaneously switched from pure water to a particulate suspension capable of fouling the membrane internally and depositing a cake layer externally. With the onset of suspension filtration, internal fouling is the resistance limited process and the TMP initially rises rapidly, where after the gradient decreases as cake layer formation becomes the resistance limited process. Cake layer thickening and specific cake resistance behaviour will determine the rate of cake resistance increase, which tends to be linear at a constant permeate flux [Tardieu et al., 1998, 1999; Ghosh, 2002; Guibert et al., 2002]. Although the rate by which internal fouling increases the hydraulic resistance is usually much more rapid than that of cake layer formation, the latter is the resistance limited process for most of the microfiltration time and is therefore eventually responsible for the majority of the total hydraulic resistance and the resulting TMP increase. Filtration at higher constant permeate fluxes will accelerate both the rates of internal fouling resistance and cake layer resistance increases.

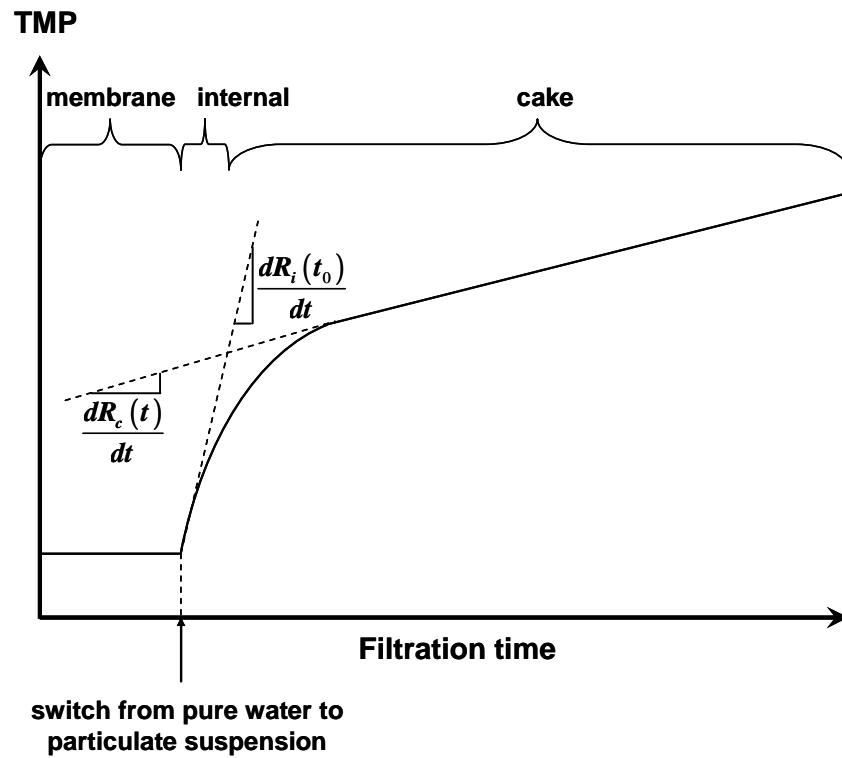


Figure 2.5: Contribution of each hydraulic resistance to the TMP for a hypothetical microfiltration process at constant permeate flux where the feed could be changed from pure water to a particulate suspension.

2.4 Membrane fouling amelioration

Membrane fouling manifests as an increasing TMP during constant permeate flux operations or as a decreasing permeate flux during constant TMP operations. In both cases a critical point will be reached where membrane operation becomes uneconomical; either because of too high operating costs to maintain an escalating TMP in the former case or because of inadequate throughput in the latter case. Also, for certain systems, the resulting high TMP and bio-deterioration of bio-susceptible membranes when biofouling is present, can cause severe membrane damage. These undesirable situations necessitate a disruption of membrane operation to perform a membrane cleaning or replacement operation, depending on the irreversibility of the fouling and the integrity of the membranes. Clearly the frequency and the extent of these membrane cleaning and replacement operations have to be minimised for reduced downtime, operating (cleaning chemicals) and capital (replaced membranes) costs. Although the prevention of fouling can probably never be achieved, the viability of a membrane process will ultimately be determined by its ability to limit fouling to:

- extend the period of economical membrane operation and thereby reduce the frequency of membrane cleaning and replacement;
- reduce membrane damage and increase membrane lifespan;
- require a less severe cleaning regime with resulting cost savings and an extended membrane lifespan; and
- reduce product water consumption for cleaning or backwashing of membranes.

Membrane fouling amelioration strategies during membrane operation can be grouped into three approaches [Ridgway and Safarik, 1991; Fane et al., 2000; Wakeman and Williams, 2002; Leiknes, 2003]:

- feed pretreatment;
- membrane material selection; and
- back-transport promotion.

2.4.1 Feed pretreatment

In feed pretreatment the foulants are either removed or treated to prevent them from reaching and depositing on the membrane surface. Physical processes include prefiltration, centrifugation and heating followed by settling, while chemical processes include precipitation, coagulation and flocculation [Mietton and Ben Aim, 1992], or dosing of proprietary chemicals as anti-scalants or disinfectants.

2.4.2 Membrane material selection

For systems where surface chemistry plays a significant part in membrane fouling, the choice of membrane material may greatly determine the extent of fouling during operation and the ability to remove foulants during cleaning [Matthiasson, 1983; Ma et al., 2001]. Physical membrane properties that may also be important are porosity and surface roughness [Ridgway and Safarik, 1991; Sadr Ghayeni et al., 1998; Pasmore et al., 2001; Vrijenhoek et al., 2001].

2.4.3 Back-transport promotion

Back-transport of material from the membrane to the bulk may be improved by the hydrodynamic conditions at the membrane surface, destabilisation of the permeate flux and by limiting the transport of foulants to the membrane by operating at a sub-critical flux.

Surface hydrodynamics

By applying a cross-flow, and thereby exerting a shear stress, a thin concentration boundary layer is maintained across the membrane surface on the feed side to increase back-transport of fouling material to the bulk. Increased shear stress is obtained at higher cross-flow velocities. The shear stress may also be created by relative movement of the membrane to the fluid [Engler and Wiesner, 2000; Fyles and Lycon, 2000; Lee and Lueptow, 2003].

When the applied shear is coupled with fluid instabilities to induce turbulence, the concentration and velocity boundary layers at the membrane surface are disturbed to convectively augment back-transport through a scouring action [Winzeler and Belfort, 1993]. Various methods are employed to generate turbulence: placing inserts in flow channels [Gupta et al., 1995; Schwinge et al., 2000; Krstic et al., 2002], air or gas sparging [Cui and Wright, 1994; Cabassud et al., 1997, 2001; Mercier et al., 1997; Laborie et al., 1998; Li et al., 1998b; Serra et al., 1999; Mercier-Bonin et al., 2001; Chang and Judd, 2002], pulsatile feed flow [Finnigan and Howell, 1989; Mackley and Sherman, 1994] and vibration of the membrane [Bian et al., 2000; Al Akoum et al., 2002].

Permeate flux destabilisation

Destabilisation strategies strive to overcome the binding energy of adsorbed material and to destroy cake layer structures and thereby leaving the detached material at the disposal of back-transport mechanisms.

In permeate flux destabilisation the TMP is switched in cycles between a positive and negative value to change the direction of permeation through the membrane from forward filtration (production stage) to reverse filtration (cleaning stage) respectively. Optimal values for the frequency, duration, flow rate and negative TMP for flow reversal will depend on the system and type of flow reversal, such as backwashing [Serra et al., 1999; Hwang et al., 2009] or a more rapid backpulsing [Redkar et al., 1996; Jones et al., 1999; Héran and Elmaleh, 2000; Mores et al., 2000; Ma et al., 2001].

In a strategy called relaxation or crossflushing [Ma et al., 2001; Wu et al., 2008a], the TMP, and therefore permeation, is stopped intermittently, while cross-flow is continued across the membrane. In the absence of the TMP driving force the cake layer decompresses, and may even detach from the membrane surface to be sheared off by the cross-flow.

Sub-critical flux operation

For a certain cross-flow velocity it can be concluded from the back-transport models described in Section 2.2.2 and the force models proposed by Lu and Ju [1989], Bacchin et al. [1995] and Vigneswaran et al. [2000] that the net force on a particle, normal to the membrane surface, will depend on the particle's size. Shear-induced diffusion, inertial lift and surface transport back-transport mechanisms are amplified as particle size increases in the micrometre range. The stronger back-transport force on a larger particle must at least be balanced out by a higher convective permeate flux in order for the particle to reach the membrane surface for possible deposition. The permeate flux with a drag force equal to the back-transport force for a certain particle is the critical flux for that particle. Therefore, for given hydrodynamics, the permeate flux will determine which particle sizes will be deposited - incrementing the permeate flux will lead to the successive deposition of increasing particle sizes [Howell, 1995; Tardieu et al., 1998]. On the other hand, by improving the surface hydrodynamics, with an increased cross-flow velocity for example, the particle back-transport is augmented to consequently raise the critical flux needed for each particle size to reach the membrane surface. Ultimately, it is therefore theoretically possible, when operating a membrane system below its lowest particle critical flux, to experience no membrane fouling. Although the consequent lower permeate fluxes of sub-critical flux operation may necessitate a larger membrane area, it provides a possible solution for long-term non-fouling membrane operation. Pollice et al. [2005] have however still found biofouling to occur at sub-critical fluxes.

The critical flux concept was introduced by Field et al. [1995] and the existence of the critical flux has since been experimentally confirmed by other researchers [Chen et al., 1997; Li et al., 1998a;

Defrance and Jaffrin, 1999a, 1999b; Fradin and Field, 1999; Wu et al., 1999; Kwon et al., 2000; Vigneswaran et al., 2000; Vyas et al., 2002]. Translated for constant permeate flux operation, Field et al. [1995] hypothesised that for microfiltration there exists a critical permeate flux on start-up below which no increase in TMP with time is observed, but above this permeate flux fouling occurs with a consequent continuous increase in TMP.

Defrance and Jaffrin [1999a] described stable TMP operation at sub-critical fluxes for their system with pore-blocking, adsorption and concentration polarisation as quasi-steady resistance values. However, when the critical flux for the system is exceeded, cake formation commences and the TMP rises rapidly without stabilisation. These findings explain the expansion of the critical flux concept to include a weak and strong form of the critical flux hypothesis for microfiltration [Fradin and Field, 1999; Ognier et al., 2004] and is explained in Figure 2.6. In its strong form the sub-critical flux of a membrane operation is equivalent to the pure water permeate flux and requires the same TMP, since no fouling has occurred and no additional hydraulic resistance has to be overcome. However, in its weak form the sub-critical flux has to account for internal fouling and requires a slightly higher TMP than the TMP for the same pure water permeate flux. In both cases the sub-critical flux varies linearly with the corresponding TMP without any hysteresis. In reality this will only strictly be applicable to completely reversible fouling, whereas irreversible fouling will always demonstrate some degree of hysteresis. Nevertheless, above the critical flux the TMP exhibits a significant hysteresis when the permeate flux is reduced, even when reduced to below the critical flux.

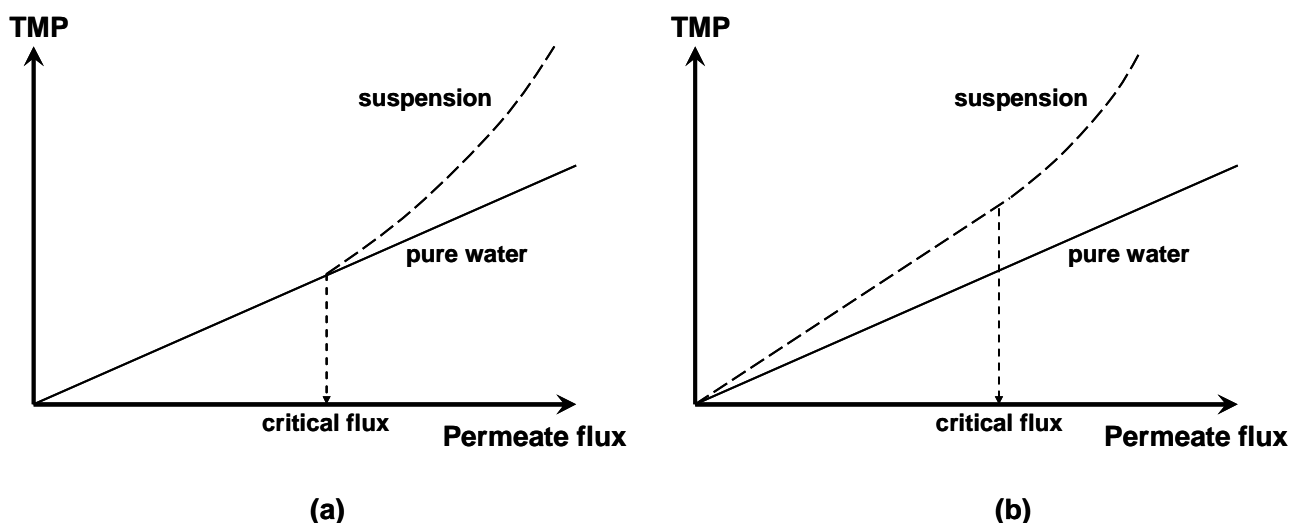


Figure 2.6: Critical flux hypothesis for microfiltration: (a) strong form and (b) weak form. Above the critical flux in both cases TMP continues to increase at constant permeate flux and displays TMP hysteresis when permeate flux is reduced to below the critical flux.

Figure 2.7 shows the hypothetical TMP profile when a permeate flux is incremented from A to E which is from sub-critical to above critical. Figure 2.8 shows the TMP profiles of these constant permeate fluxes A to E for a hypothetical microfiltration process where the feed could be switched from pure water to a particulate suspension capable of internal fouling and cake layer formation.

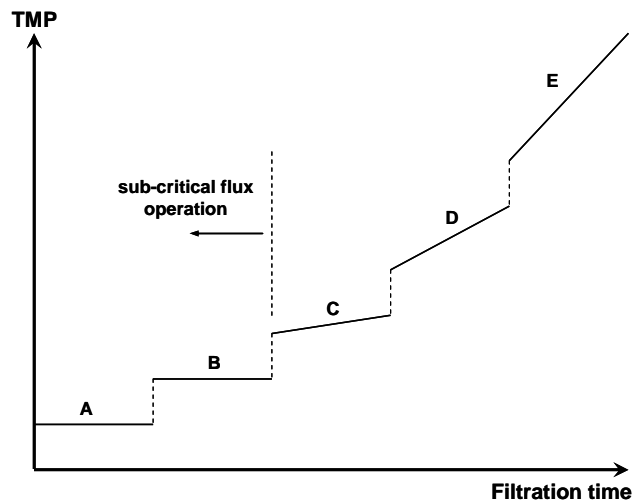


Figure 2.7: Hypothetical TMP profile of incremented constant permeate fluxes from sub-critical to above critical fluxes.

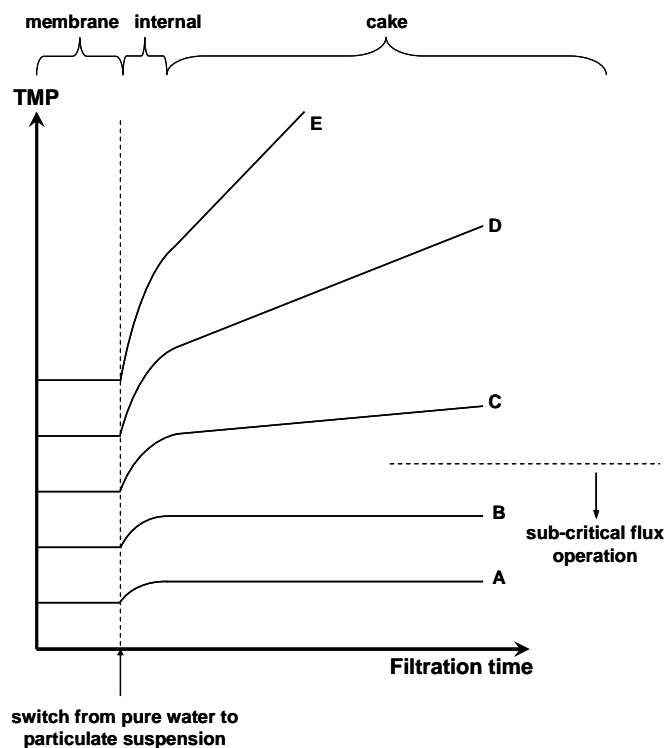


Figure 2.8: Hypothetical TMP profiles of constant permeate fluxes when the feed was switched from pure water to a particulate suspension. Above critical flux cake layer formation commences and continues at a constant rate.

Chapter 3

Air-scouring of immersed membranes

3.1 Introduction

Improved surface hydrodynamics, as mentioned in Section 2.4.3, provide a means to arrest membrane fouling. When a cross-flow is applied across the membrane, the shear stresses exerted at the membrane surface should limit concentration polarisation and restrict particle deposition by improving back-transport. The side-stream membrane configuration especially lends itself to the utilisation of a high shear rate cross-flow, since the feed is pumped at high velocities through an external unit across the membrane surfaces. The shear rate at the membrane surface may even be further increased by the introduction of turbulence promoters in the external unit [Krstić et al., 2002]. For immersed membrane systems, however, the physical design usually rules out the possibility for the feed to be pumped across the membrane surfaces and immersed membranes consequently have to rely on other methods to generate cross-flow.

A popular technique to provide flow across the surface of immersed MBR membranes is to sparge the membranes with gas, usually air, from a diffuser located at the bottom of the reactor. Besides fine-bubble aeration for the respiratory support of biomass in aerobic MBRs, coarse-bubble aeration is also typically employed in an attempt to control membrane fouling [Gander et al., 2000; Chang and Judd, 2002]. The rising bubbles induce a moderate cross-flow and, when intimately in contact with the membranes, are able to scour the membrane surfaces [Bouhabila et al., 1998]. Depending on the membrane configuration, it is even possible to shake the membranes [Ueda et al., 1997; Günder and Krauth, 1998; Suda et al., 1998; Wicaksana et al., 2006] to loosen and remove deposited material.

3.2 Scouring action of rising bubbles

The ability of air, when introduced on the feed side of inside-out tubular membranes, to remove deposited material from the membrane surface has been investigated by Judd et al. [2001], Cabassud et al. [1997, 2001], Mercier et al. [1997] and Laborie et al. [1998]. A number of aeration regimes, depending on the supplied air flow rate, can be produced inside a tube, ranging from fine bubbles, in which the liquid is the continuous medium, to mist, in which the air is the continuous medium (Figure 3.1).

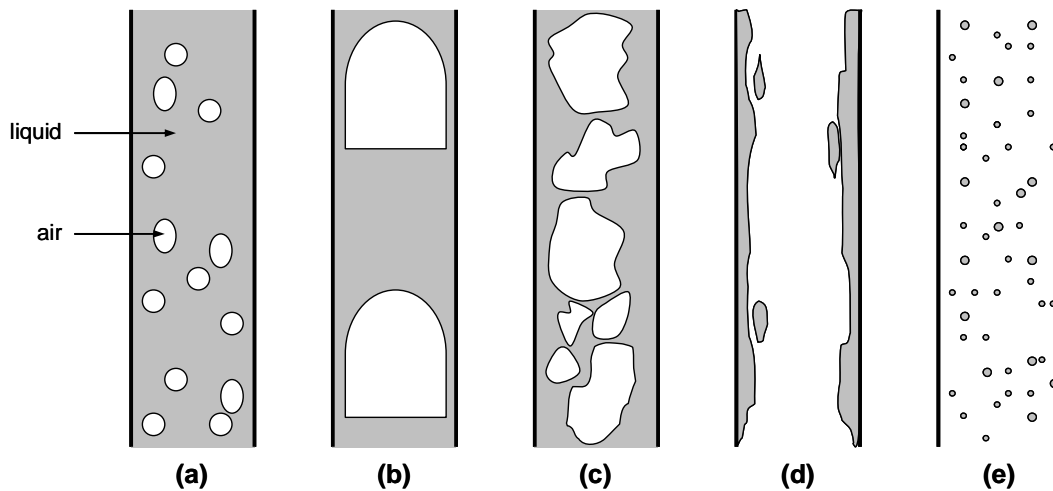


Figure 3.1: Aeration regimes inside a tube: (a) bubble flow; (b) slug flow; (c) churn flow; (d) annular flow; and (e) mist flow [Judd et al., 2001].

In the slug flow aeration regime, an intermediate state where the flow can be described as successively moving pockets of air and liquid, the scouring action of the air was found to be the most effective. The key to this pronounced effect of slug flow lies in the rapid alternation of shear stresses at the membrane surface. An air slug is an almost cylindrical air bubble which occupies most of the cross-sectional tube area with only a thin liquid film separating it from the membrane wall. As an air slug rises the liquid ahead of the air slug is forced down into the liquid film where it accelerates as it moves downwards. The liquid is then injected into the relative stagnant liquid slug behind the air slug to create a highly agitated mixing zone in the air slug's wake. Consequently, with the passing of an air slug, a point on the membrane surface is first subjected to a negative shear stress ($\tau_{L\text{Film}}$), induced by the liquid film around the air slug, to be followed by a positive shear stress ($\tau_{L\text{Slug}}$), induced by the liquid slug (Figure 3.2). This exposure to a fast falling liquid film and a changing shear rate at the membrane surface is responsible for the superior scouring action and

the consequent reduced fouling observed in inside-out vertically installed tubular membranes operating with slug flow aeration regimes.

Mercier-Bonin et al. [2000] have shown that the successes of slug flow in inside-out tubular membranes to reduce fouling can be repeated to a certain degree by injecting air together with the feed when operating inside-out flat-sheet membranes. It is therefore conceivable that the scouring performance of air bubbles inside inside-out membranes may be emulated between immersed outside-in flat-sheet membranes; provided that they are closely packed to allow the bubble diameters to be comparable to the channel widths between the membranes [Zhang et al., 2009] as shown in Figure 3.3.

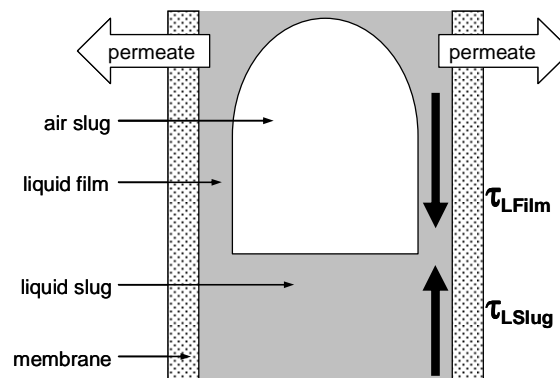


Figure 3.2: Slug flow inside an inside-out tubular membrane. A rising air slug scours the membrane surface by first subjecting it to a negative shear stress (τ_{LFilm}) and then by a positive shear stress (τ_{LSlug}) [Laborie et al., 1998; Cabassud et al., 2001].

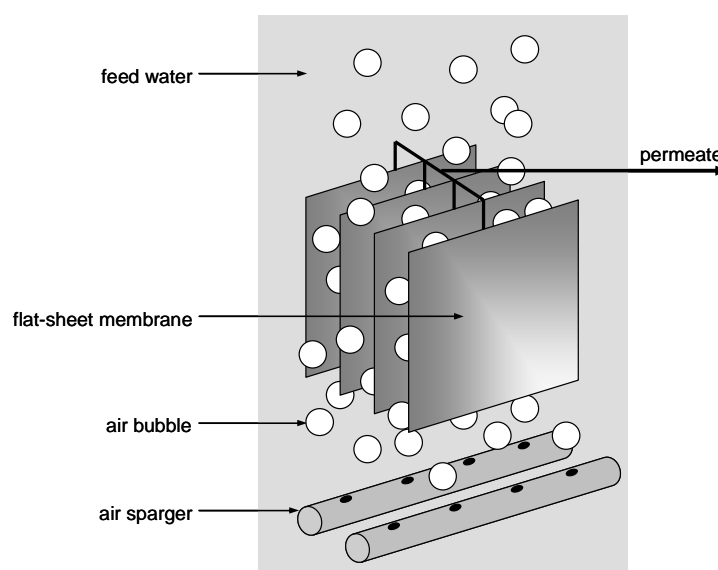


Figure 3.3: Air-sparging of immersed outside-in flat-sheet membranes.

3.3 Airlift reactors

An airlift reactor is a pneumatic agitator in which bubbling gas, usually air, produces the required mixing of the contained suspension. Airlift reactors are therefore ideal for gas-liquid-solid-contact bioprocesses, since these processes demand constant and mild shear throughout the reactor, as well as aseptic operation – all aspects which cannot be guaranteed by the intrusion of mechanical stirring [Chisti and Moo-Young, 1987; Chisti, 1989a]. Unlike a bubble column (Figure 3.4(a)), which is simply an air-sparged tank, an airlift reactor (Figure 3.4(b)) is divided into two distinct, but connected, zones of which one is sparged with air. The subsequent difference in gas hold-ups, and therefore the difference in bulk densities, between the two regions, generates liquid motion between the zones. The denser liquid in the ungasged zone (the downcomer) flows downwards to displace the less dense liquid in the gassed zone (the riser) upwards. Because of these regions of different liquid densities, airlift reactors, as opposed to bubble columns, display a more clearly defined liquid flow with higher linear liquid velocities for the same sparging energy input [Choi et al., 1996].

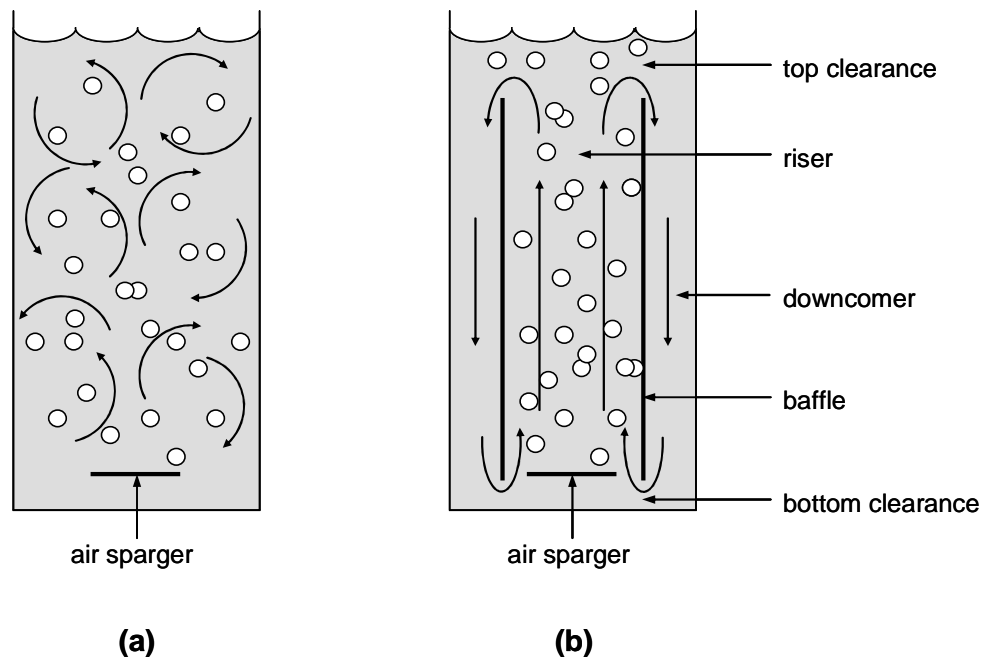


Figure 3.4: Liquid flow patterns: (a) chaotic liquid circulation cells in a bubble column; (b) clearly defined liquid flow in an airlift reactor: upwards in the gassed riser and downwards in the ungasged downcomers [Chisti and Moo-Young, 1987; Choi et al., 1996].

3.3.1 Liquid velocity

The gas-induced liquid circulation velocity is one of the most important characteristic parameters of airlift reactor design and determines the gas hold-up behaviour, mass and heat transfer, extent of mixing and the ability of the reactor to suspend solids [Chisti and Moo-Young, 1993; Contreras et al., 1998]. Nevertheless, the accurate extrapolation of riser and downcomer liquid velocities from studied airlift reactors to any other airlift reactor system, in terms of geometry and operating conditions, has eluded researchers up to now [Chisti, 1989b; Livingston and Zhang, 1993; Merchuk and Berzin, 1995; García-Calvo and Letón, 1996; Al-Masry and Abasaeed, 1998; Couvert et al., 2001]. Numerous empirical correlations have been proposed for the estimation of liquid velocities, but their applicability tends to be restricted to the systems they were derived from. On the other hand, over-simplified assumptions have rendered developed models, based on energy [Chisti and Moo-Young, 1988; Merchuk and Berzin, 1995; García-Calvo and Letón, 1996; Hwang and Cheng, 1997] and momentum balances [Siegel et al., 1986; Dhaouadi et al., 1996; Couvert et al., 2001; Van Baten et al., 2003], incomplete and unable to predict liquid velocities over the full range of airlift reactor geometries and scales. Also, most of the published work on liquid velocities in airlift reactors has been focussed on simple two-phase air-water systems.

Despite these shortcomings in attaining a liquid velocity prediction method relevant to any airlift reactor system, the observed trends are invaluable for the design of airlift reactors that require an enhanced liquid circulation. Unfortunately however, airlift reactor parameters seem to form intricate interactions to affect the circulation velocity equivocally [Siegel et al., 1986; Livingston and Zhang, 1993; Lu et al., 2000], and the influence of system parameters in isolation should therefore be regarded with discretion.

Increasing the sparging rate of gas in the riser causes the riser liquid velocity to increase, although a limit seems to exist beyond which an increase in the sparging rate does not effect the riser liquid velocity [Siegel et al., 1986; Livingston and Zhang, 1993; Hwang and Cheng, 1997; Al-Masry and Abasaeed, 1998; Lu et al., 2000; Couvert et al., 2001]. Like gas sparging, the ratio of the total cross-sectional areas of the downcomer sections to the riser sections, has been found to have a significant effect on the riser liquid velocity [Siegel et al., 1986; Chisti et al., 1988; Livingston and Zhang, 1993; Al-Masry and Abasaeed, 1998; Lu et al., 2000]. An increase in this ratio reduces the downcomer liquid velocity relative to the riser liquid velocity, enabling more gas to escape the downward drag in the downcomer, and thereby effectively increasing the bulk density difference between the downcomer and riser regions for enhanced riser liquid velocity. The size and nature of the top [Siegel et al., 1986; Chisti and Moo-Young, 1993; Livingston and Zhang, 1993; Couvert et al., 1999] and bottom clearances [Chisti et al., 1988; Livingston and Zhang, 1993; Merchuk and

Berzin, 1995; Choi et al., 1996; Couvert et al., 1999], interconnecting the riser and downcomer sections, not only determine the degree of resistance presented against liquid circulation, but, in the case of the top clearance, also the extent of gas separation to provide ungasged fluid to the downcomer for increased liquid circulation, as mentioned before. The riser liquid velocity also seems to benefit from an increase in the riser height [Siegel et al., 1986; Chisti et al., 1988; Chisti and Moo-Young, 1993; Livingston and Zhang, 1993; Lu et al., 1995; Hwang and Cheng, 1997; Lu et al., 2000].

3.3.2 Airlift reactor application for immersed membrane fouling control

The scouring action that a rising bubble exerts on nearby surfaces, as explained in Section 3.2, is enhanced when superimposed on the rising liquid cross-flow, since both the shear stresses and the rate of shear stress reversal at the surfaces are increased. This technique has been successfully applied for fouling control of immersed membranes installed in the riser sections of airlift reactors [Churchouse and Wildgoose, 1999; Liu et al., 2000, 2003; Chang and Judd, 2002; Guibert et al., 2002; Shim et al., 2002].

Increasing the riser liquid velocity will therefore also increase the rising bubbles' ability to scour the immersed membranes and remove deposited material from the membrane surfaces. Experimental results of membranes immersed in risers of airlift bioreactors have indeed shown that the riser liquid velocity could be increased, as discussed in Section 3.3.1, by adopting airlift reactor geometries with higher ratios of downcomer to riser cross-sectional areas, larger bottom clearances, increased liquid depths and by intensifying air sparging in the riser; and that these increased cross-flow velocities led to decreased membrane fouling rates [Liu et al., 2000, 2003; Shim et al., 2002]. Optimised airlift reactors to generate fast riser velocities for increased bubble scouring are therefore ideal to be used in the control of immersed membrane fouling.

Chapter 4

Fouling quantification for air-scouring evaluation

4.1 Introduction

In Chapter 3 the scouring action of air bubbles rising close to membrane surfaces and the viability of sparged air as a method to control immersed membrane fouling were described and explained. Indeed, the application of air-sparging to successfully limit fouling in immersed membrane systems has been extensively documented [Shimizu et al., 1996; Ueda et al., 1997; Bouhabila et al., 1998; Ozaki and Yamamoto, 2001; Chang and Judd, 2002; Guibert et al., 2002; Cui et al., 2003; Le-Clech et al., 2003b]. Despite these numerous accounts, however, the quantitative influence of the applied air on the fouling dynamics has remained unclear.

As explained in Chapter 3, air-scouring is enhanced when more and faster rising bubbles sweep the membrane surface. It therefore seems logical to hypothesise that an increase in the sparged air flow rate will increase the supplied air's ability to scour and reduce immersed membrane fouling. Bouhabila et al. [2001] have confirmed this hypothesis and reported to have found that an increase in the air flow rate has enabled their MBR to operate stably at higher constant fluxes, because of reduced fouling.

Ueda et al. [1997], Silva et al. [2000], Chang and Fane [2001] however, have found that, for a given system, a critical aeration value exists after which an increase in the air flow rate had no effect on the air's scouring ability. Scouring efficiency is defined as the amount of deposited material removed from the membrane surface per volume supplied sparged air in a given time. Therefore, operating at a higher sparged air flow rate than a system's critical aeration value will reduce the sparged air's scouring efficiency, since the increased aeration does not benefit further material removal from the membrane surface. A lower scouring efficiency consequently translates into higher operating costs. Nonetheless, without increasing the air flow rate, Ueda et al. [1997] found that when aeration was intensified from fewer diffusers and the membranes rearranged, the scouring efficiency was increased. Chang and Fane [2001] managed to show that less densely

spaced hollow fibre membranes with smaller diameters positioned in wider channels are less prone to foul than high density hollow fibre membranes with larger diameters in smaller channels at the same air flow rate.

The above-mentioned findings conclude that the hypothesis of increased air-scouring with an increased air flow rate has to be rejected. Although the hypothesis may appear to be true in certain cases, air flow rate is not necessarily the only factor that governs the scouring ability of the sparged air, but geometrical factors also seem to play a significant role. Studies of membranes immersed in airlift reactors have confirmed the importance of geometrical factors to provide ideal system hydrodynamics for efficient air-scouring [Liu et al., 2000, 2003; Shim et al., 2002].

Since membrane air-scouring dominates the operating costs of immersed membrane processes, typically more than 90% for MBRs [Gander et al., 2000], a drive exists to optimise reactor design for higher air-scouring efficiencies [Liu et al., 2000]. In order to evaluate the air-scouring efficiencies of different reactor designs it is necessary to measure some tangible and comparable process output. If the membrane fouling can be quantified, it can be used as a tool to indicate the immersed membrane process's air-scouring efficiency.

4.2 Fouling quantification methods

Methods to quantify membrane fouling may either be direct or indirect. With direct fouling quantification an aspect of the fouling condition on the membrane is measured, whereas indirect fouling quantification refers to the measurement of a membrane fouling consequent as an indicator of the actual fouling behaviour. Naturally, direct fouling quantification is able to provide a membrane fouling diagnosis of far greater accuracy than indirect fouling quantification, but unfortunately the implementation thereof is usually limited by its costly, localised, invasive and sometimes even destructive nature. With indirect fouling quantification methods, on the other hand, it may be possible to obtain a fairly reliable, but inexpensive, indication of the fouling process as a whole in real-time without interfering in the filtration process. Accordingly, indirect fouling quantification is widely favoured as the method for long-term, continuous and holistic monitoring of membrane fouling.

Direct fouling quantification methods include the measurement of the cake layer thickness with light adsorption [Hamachi and Mietton-Peuchot, 1999, 2002], visual techniques [Chang et al., 2002] and ultrasound [Li et al., 2003], as well as the measurement of the cake layer mass by gathering and weighing cake after filtration experiments [Fradin and Field, 1999] or during membrane autopsies [Fane et al., 2000; Vrouwenvelder and Van der Kooij, 2001] and the use of thermogravimetric techniques [Tay et al., 2003].

For indirect fouling quantification researchers have mainly relied on the Darcian resistance model equation, as explained in Section 2.3.3, to predict the membrane fouling resistance [Kwon et al., 2000]. By using Equations 2.6 and 2.9, the microfiltration resistance model equation can be simplified to:

$$J = \frac{\Delta P}{\mu R_t} \quad (4.1)$$

where J = permeate flux (m/s)
 ΔP = transmembrane pressure (TMP) (Pa)
 μ = absolute viscosity of the fluid (Pa.s)
 R_t = total hydraulic resistance (m⁻¹)

Assuming the absolute viscosity of the fluid to be a constant, it is possible, by using Equation 4.1, to estimate the total hydraulic resistance from a single process variable. By setting the filtration

process at a constant permeate flux and measuring the TMP or filtrating at a constant TMP and measuring the permeate flux, the total hydraulic resistance, now the only unknown, can be calculated. The fouling hydraulic resistance is found by subtracting the clean membrane hydraulic resistance from the calculated process total hydraulic resistance (Section 2.3.3). Both TMP and permeate flux are easily measurable variables, hence the popularity of this fouling quantification technique.

Other indirect membrane fouling quantification techniques include the measuring of the decline in the feed's solids concentration [Kwon et al., 2000; McCarthy et al., 2002] and the use of fouling indices to indicate the membrane fouling potential [Rabie et al., 2001].

4.3 Flux-step method for indirect fouling quantification

In Section 4.1 it was hypothesised that an increase in the sparged air flow rate will increase the scouring ability of the air, thereby enabling the immersed membranes to filtrate at a low fouling rate. Although evidence exist in the literature that an increase in the air flow rate may not always affect the air's scouring ability (Section 4.1), and effectively reduce the air-scouring efficiency, it was decided to investigate the influence of an increasing air flow rate on an immersed flat-sheet membrane's fouling rate. As a first approach the indirect fouling quantification technique, the flux-step method, was used for its simplicity and holistic fouling indication. In addition, the flux-step method has been widely used and is regarded as a reliable technique to quantify membrane fouling propensity [Bouhabila et al., 1998; Defrance and Jaffrin, 1999a; Tardieu et al., 1999; Guibert et al., 2002; Le-Clech et al., 2003a, 2003b; Wu et al., 2008b].

4.3.1 Background

The flux-step method uses Equation 4.1 and the critical flux concept, as explained in Section 2.4.3, to characterise a membrane system's ability to resist fouling. The membrane system's permeate flux is incremented with an arbitrary chosen constant at constant time intervals while the resulting TMP is recorded as an indication of the change in the total hydraulic resistance. Figure 4.1 shows the typical TMP results of a flux-step experiment where the permeate flux was incremented from below critical flux to above critical flux.

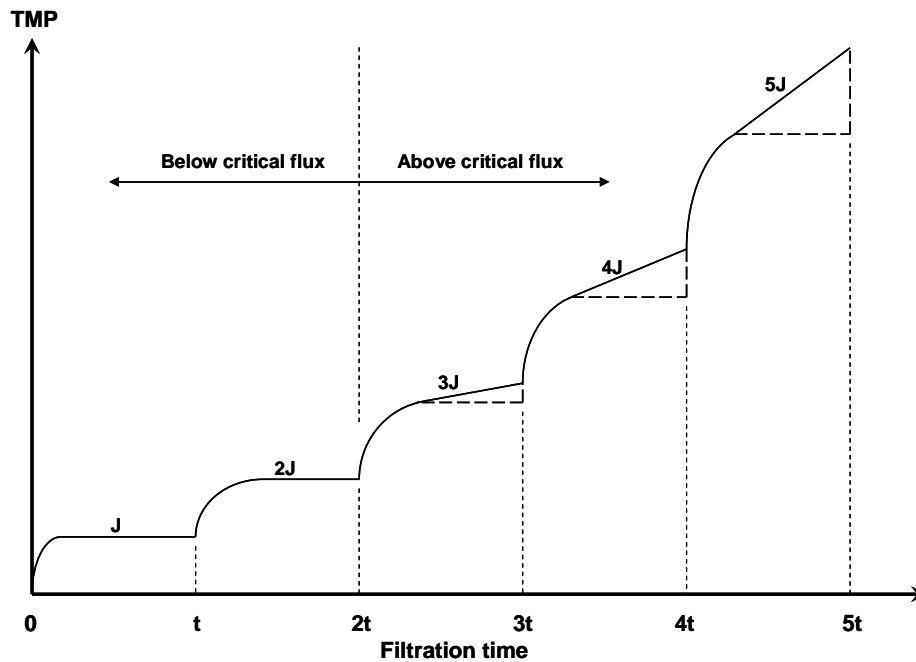


Figure 4.1: The typical TMP profile of a flux-step experiment where the permeate flux was incremented five times with an arbitrary chosen permeate flux J from below critical flux to above critical flux at a time increment of t . In this case a permeate flux of $2J$ was still below the critical flux, whereas a permeate flux of $3J$ was above the critical flux with a resulting continued increase in TMP.

Internal fouling is the only possible fouling mechanism if the initial permeate fluxes are below the critical flux and the total hydraulic resistance will therefore rise sharply, but quickly attain an equilibrium value after the permeate flux is stepped up each time. The TMP will concomitantly exhibit the same behaviour as predicted by Equation 4.1 for constant permeate flux filtration and stabilise at a constant value. However, when the permeate flux is incremented to a value above the critical flux for the system, cake layer formation commences and continues to increase the total hydraulic resistance (Section 2.3). To achieve a constant permeate flux, the compensating TMP also has to increase continuously at a constant rate [Tardieu et al., 1998, 1999; Ghosh, 2002; Guibert et al., 2002].

From Figure 4.1 it can also be seen that the successive permeate fluxes above the critical flux reveals increasing rates of TMP growth. Stabilised TMP growth is obtained once the TMP rate of change has reached a constant value and occurs when cake layer formation becomes the resistance limited process (Section 2.3.3). Mathematically the stabilised TMP profile for Figure 5.1 can be explained as:

$$\left(\frac{\partial TMP}{\partial t}\right)_J = \left(\frac{\partial TMP}{\partial t}\right)_{2J} = 0 \quad \text{for the sub-critical fluxes } J \text{ and } 2J; \text{ and as}$$

$$0 < \left(\frac{\partial TMP}{\partial t}\right)_{3J} < \left(\frac{\partial TMP}{\partial t}\right)_{4J} < \left(\frac{\partial TMP}{\partial t}\right)_{5J} \quad \text{for permeate fluxes of } 3J, 4J \text{ and } 5J.$$

The critical flux of a membrane system can be estimated from a graph of the stabilised rates of TMP increase plotted against the associated permeate fluxes. The permeate flux at which the stabilised rate of TMP increase changes from zero to a positive value indicates the critical flux. See Figure 4.2, which uses the hypothetical stabilised rates of TMP increase derived from Figure 4.1 to estimate the critical flux.

The smaller the permeate flux increments the more accurate the critical flux estimation. It is also important to keep the periods between permeate flux increments long enough to ensure that internal fouling has stabilised, thereby eliminating its influence on the rate of TMP increase.

Once the critical fluxes for different sparged immersed membrane systems have been determined, they can be compared to establish which system is better designed or operated to achieve superior air-scouring of the membrane surfaces. The higher the critical flux of a membrane system, the better the air-scouring for improved back-transport and the less susceptible the membrane is to membrane fouling.

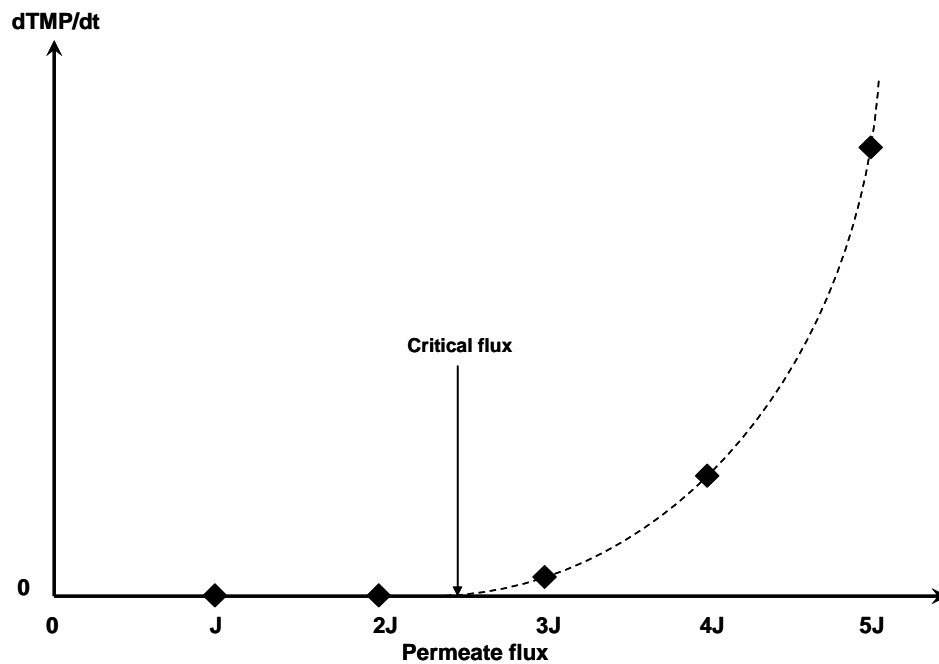


Figure 4.2: The rates of stabilised TMP increase of each permeate flux increment as derived from the typical TMP profile of a flux-step experiment as shown in Figure 4.1. The critical flux is found where $dTMP/dt$ changes from zero to a positive value, which in this case, lies between the flux-step experiment's second and third permeate flux increment.

4.3.2 Experimental set-up

An airlift reactor design, as explained in Section 3.3, was adopted for this flux-step study to determine the effect of air flow rate on the sparged air's ability to scour immersed membranes. Only a single flat-sheet membrane element was immersed and studied in the airlift reactor. With the reactor walls close to the membrane element the set-up represented the basic unit of a membrane module consisting of several flat-sheets [Ozaki and Yamamoto, 2001]. The air-scouring and fouling behaviours observed on the flat-sheet will therefore predict the behaviours found in a module of similar flat-sheet membranes immersed in a scaled-up airlift reactor. The experimental set-up for the flux-step experiment is shown in Figure 4.3.

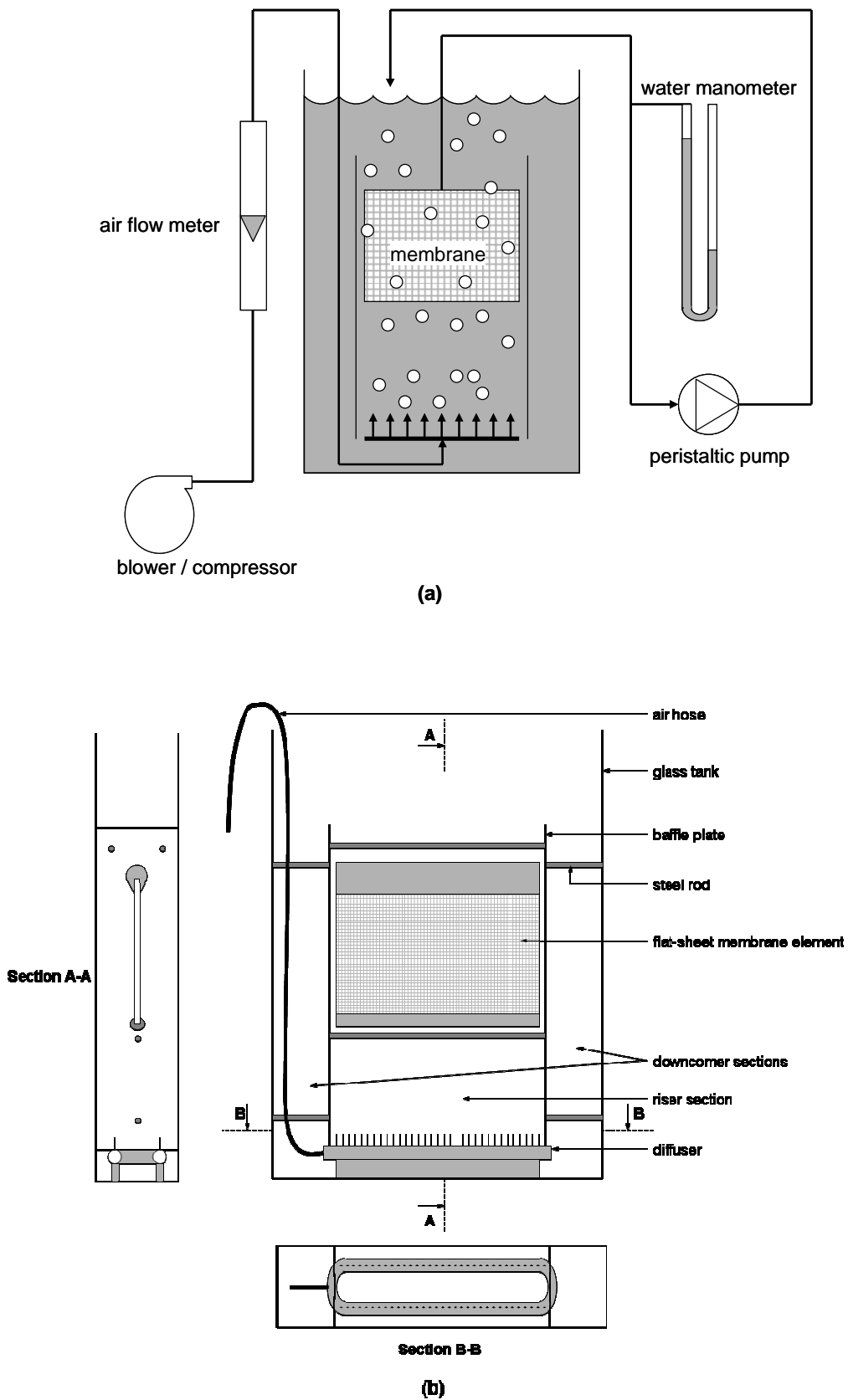


Figure 4.3: Set-up for the flux-step experiment: (a) main equipment and (b) detail of airlift reactor.

The flat-sheet membrane element used in this study was fabricated according to the method explained in Addendum B and had a total active surface area of 0.12 m². The membrane element was firmly secured inside a framework of two Perspex baffle-plates and seven steel rods. The framework, containing the membrane element, fitted tightly into a rectangular glass tank, and the baffle-plates divided the tank into a riser and two downcomer sections. The resulting airlift reactor had a cross-sectional downcomer area to riser area (A_d/A_r) ratio of 0.31. The membrane element was located in the riser and occupied the width of the riser. A double-pipe diffuser was located at the bottom of the tank and stretched the width of the riser. With the baffle-plates resting on the diffuser, it was unable to move during operation and could therefore provide a stable hydrodynamic field for the duration of an experimental trial. Equal size bubbles were obtained by fitting the diffuser with 0.6 mm inner diameter capillary membrane stubs from where the air could escape.

The airlift reactor was filled with a model foulant of ocean bentonite suspended in RO water. For each trial a fresh batch of 60 L suspension was prepared, as explained in Addendum A, with a bentonite concentration of 1.0 g/L.

A very steady air flow was fed to the diffuser at the bottom of the airlift reactor by a blower for relative low air flow rates. Unfortunately the blower was unable to deliver the required higher air flow rates at this high static head of 870 mm water and a compressor, although providing a fluctuating air flow, had to be used. The supplied air flow rate was measured with an air flow meter. A variable speed peristaltic pump, connected to the immersed flat-sheet membrane element, produced the necessary constant permeate flux. The TMP created was measured with a water-filled manometer. Pressure fluctuations caused by the operation of the peristaltic pump was assumed to be negligible in destabilising the concentration boundary layer at the membrane surface, since the deviation was less than 1% of the measured TMP. The permeate was pumped back to the tank to operate at a bentonite concentration which was assumed to remain constant.

4.3.3 Method

The influence of the sparged air flow rate on the scouring ability was studied at three different aeration intensities in the riser. Aeration intensity is defined as the supplied air flow rate per cross-sectional riser area. The lowest aeration intensity was chosen where the supplied air flow rate was just sufficient to provide bubbling along the full length of the diffuser. The highest aeration intensity was set at a value that compares well and even exceeds the maximum aeration intensities used in similar studies by other researchers (Ueda et al. [1997] used 612 L/(m²·min); Liu et al. [2000] used 926 L/(m²·min); Bouhabila et al. [2001] used 60 L/(m²·min); and Shim et al. [2002] used

1 136 L/(m²·min)). An intermediate air flow rate was chosen for an intermediate aeration intensity. A summary of the three chosen aeration intensities is given in Table 4.1.

Table 4.1: The three chosen aeration intensities for the flux-step experiment. (Notice the relative large deviation in the compressor's air flow rate to achieve the high aeration intensity.)

	Equipment	Air flow rate (L/min)	Cross-sectional riser area (m ²)	Aeration intensity (L/(m ² ·min))
Low aeration intensity	Blower	6.0 ± 0.5	0.0516	110 ± 10
Intermediate aeration intensity	Blower	30.0 ± 0.5	0.0516	580 ± 10
High aeration intensity	Compressor	58.0 ± 8.0	0.0516	1 100 ± 160

These three aeration intensities were respectively used in three treatments, filtrating RO water only, as well as in three treatments with replication, filtrating the bentonite suspension. The experiment to quantify fouling at different air flow rates with the flux-step method therefore consisted of nine trials. These nine trials were conducted in a random order, as shown in Table 4.2, to reduce experimental error. No need existed to replicate the three treatments with RO water filtration, since, regardless of the aeration intensity, no fouling should occur and were therefore replicates per se.

Table 4.2: The random order in which the trials were conducted to minimise the risk of unknown influences on the results.

	RO water	Bentonite suspension (1.0 g/L)
Low aeration intensity	1	2, 8
Intermediate aeration intensity	7	3, 4
High aeration intensity	5	6, 9

For each treatment, subjected to a certain aeration intensity, the permeate flux was incremented with 5 L/(m²·h) from an initial permeate flux of 5 L/(m²·h) to a permeate flux of 25 L/(m²·h). Each permeate flux was maintained for a period of two hours to ensure that internal fouling has

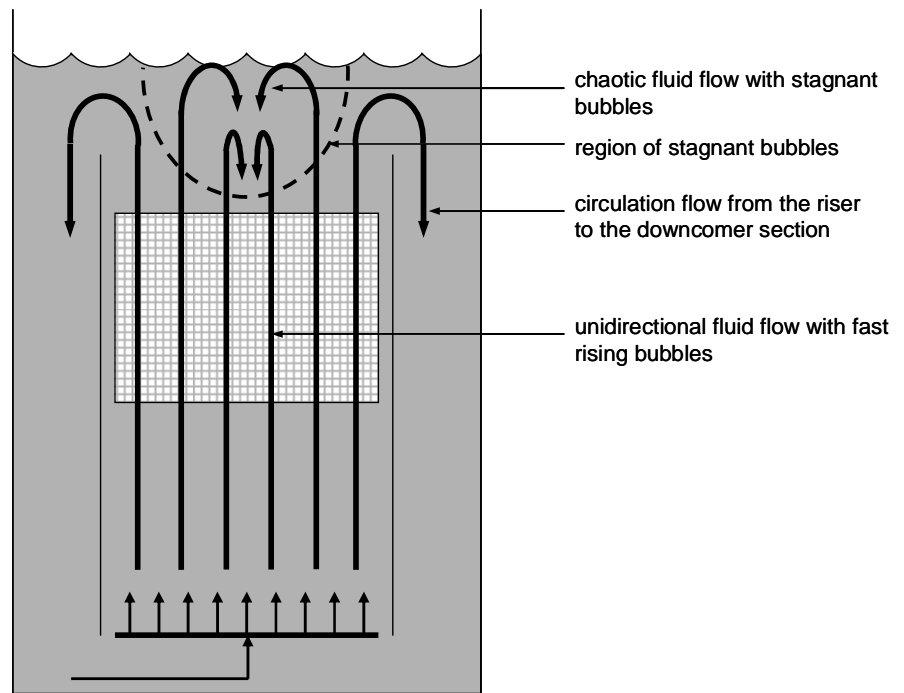
stabilised and that any subsequent fouling could be attributed to cake layer formation alone. During these two hour periods the TMP was regularly recorded and the permeate flux, air flow rate and suspension temperature measured to confirm they stay relatively constant. The permeate flux did not vary more than $0.8 \text{ L}/(\text{m}^2 \cdot \text{h})$ from the intended permeate flux and the treatments were conducted at suspension temperatures of $20 \pm 3^\circ\text{C}$.

A simple backwash procedure, prior to an experimental trial, proved to be adequate in restoring the original hydraulic resistance of the membrane, therefore removing all particles within, as well as on the membrane surface.

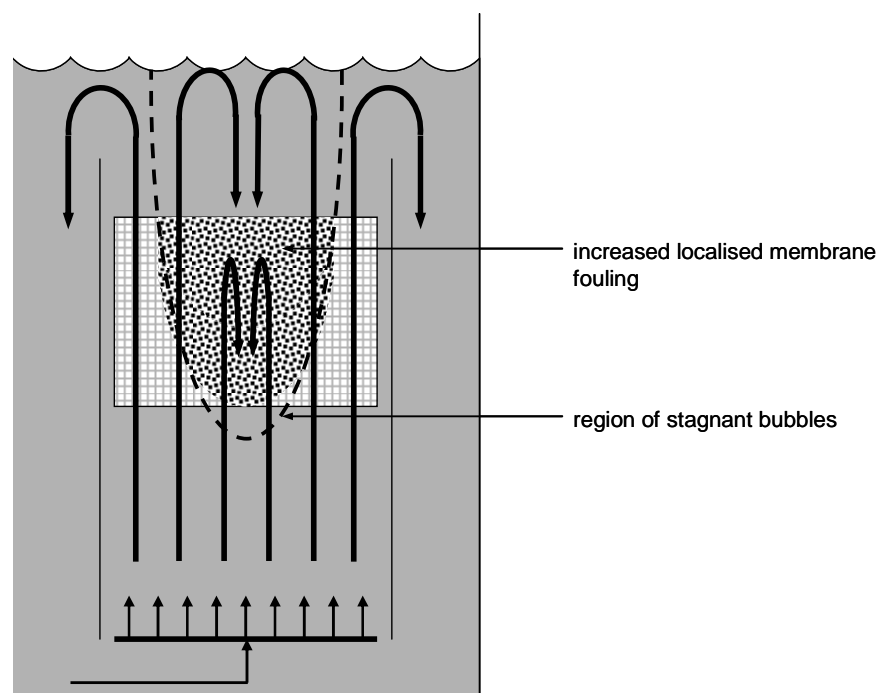
4.3.4 Results

An interesting visual observation was made from the three treatments in the flux-step experiment. With each treatment a region of trapped air bubbles was observed in the riser section. The bubbles trapped in this region moved in short erratic distances and were therefore not truly stagnant, but compared to the fast and unidirectional rising of the bubbles outside of this region, they appeared very stagnant. In the treatment with the low aeration intensity this region of fairly stagnant bubbles was located at the top of the riser section, but as the aeration intensity was increased, the region grew towards the bottom of the riser section. This phenomenon is depicted in Figure 4.4.

As described in Section 3.3, an increase in the air flow will lead to an increased air holdup in the riser section and therefore an increased difference in density between the riser and the downcomer sections with a consequent higher liquid circulation velocity. But as the liquid circulation velocity increases, more air bubbles are entrained into the downcomer sections, and when the downward liquid velocity exceeds the rise velocity of the air bubbles in the downcomers, the air holdup in the downcomer sections starts to increase. At this critical circulation velocity the difference in density between the riser and downcomer sections, the driving force for the circulation, starts to diminish to the extent that any further increases in the air supplied to the riser section will lead to very little to no increases in the induced liquid circulation velocity [Couvert et al., 1999, 2001]. But except for the induced circulation, water is also transported to the top of the riser section through the drag of the rising air bubbles. Therefore, at high air flow rates supplied to the riser section and a consequent relative low liquid circulation velocity, the resistance for the water to enter the downcomer sections becomes too high and a portion of the water starts to circulate from the top towards the bottom of the riser section. This downward flow of circulating water in the riser section force balances the rising bubbles – therefore the visual effect of a region of trapped and stagnant bubbles in the riser section.



(a) Relative low aeration intensity



(b) Relative high aeration intensity

Figure 4.4: The presence of a region of stagnant bubbles in the riser section during aeration. This region promotes localised fouling where it crosses the immersed membrane.

For the low and intermediate aeration intensity treatments of this experiment the region of stagnant bubbles was located above the immersed membrane in the riser section (Figure 4.4(a)). The fluid flow across the membrane surface was unaffected by the circulation of water inside the riser section and was therefore fast and unidirectional. This improved the scouring ability of the sparged air and allowed for uniform membrane fouling.

However, for the high aeration intensity the region of stagnant bubbles grew towards the bottom of the riser section as a result of increased circulation inside the riser section (Figure 4.4(b)). The region even crossed the immersed membrane and therefore affected the fluid flow behaviour across the membrane surface. Across the edges of the membrane the fluid flow was very fast and unidirectional, but across the middle, which was situated in the region of stagnant bubbles, the fluid flow was slow and chaotic. The scouring ability of the slow moving bubbles in this region was very poor, since, visually it seemed as if all the membrane fouling occurred where the region of stagnant bubbles crossed the membrane surface. With the whole membrane surface subjected to a constant permeate flux, the region of stagnant bubbles, unable to remove particles from the membrane surface, will actually promote localised membrane fouling.

In the flux-step experiment the rate of membrane fouling is manifested in the increase of TMP with time ($dTMP/dt$). During the flux-step experiment, the TMP data of only the last hour of each two hour permeate flux period was used to determine the fouling rates. This was to ensure that the calculated fouling rates accounted for cake layer formation only. The TMP increase for each permeate flux at each of the three aeration intensities was therefore found to be a linear function with time, since fouling rate is a constant when cake layer formation is the only fouling mechanism. These derived fouling rates are represented in two ways in Figures 4.5 and 4.6. The three aeration intensity treatments were replicated and the deviation shown in Figures 4.5 and 4.6. Experimental data can be found in Addendum C.

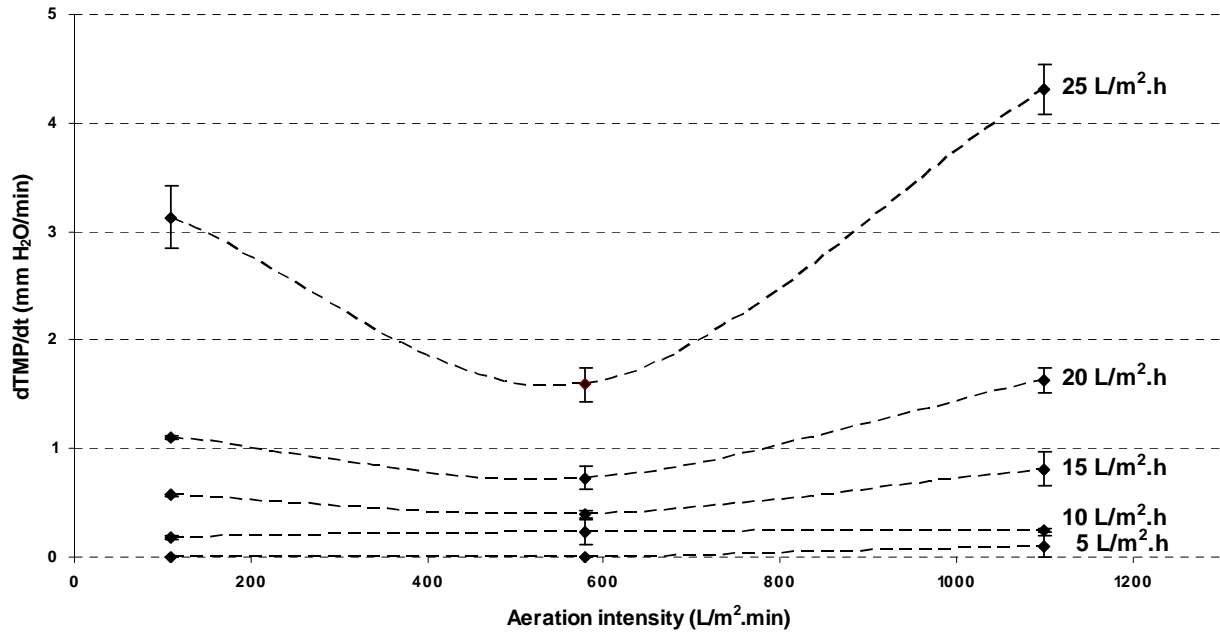


Figure 4.5: Membrane fouling rate at different aeration intensities. The intermediate aeration intensity (580 L/(m².min)) produced the highest scouring ability. Between an aeration intensity of 580 and 1 100 L/(m².min) the region of stagnant bubbles develop to cross the immersed membrane and promote localised fouling.

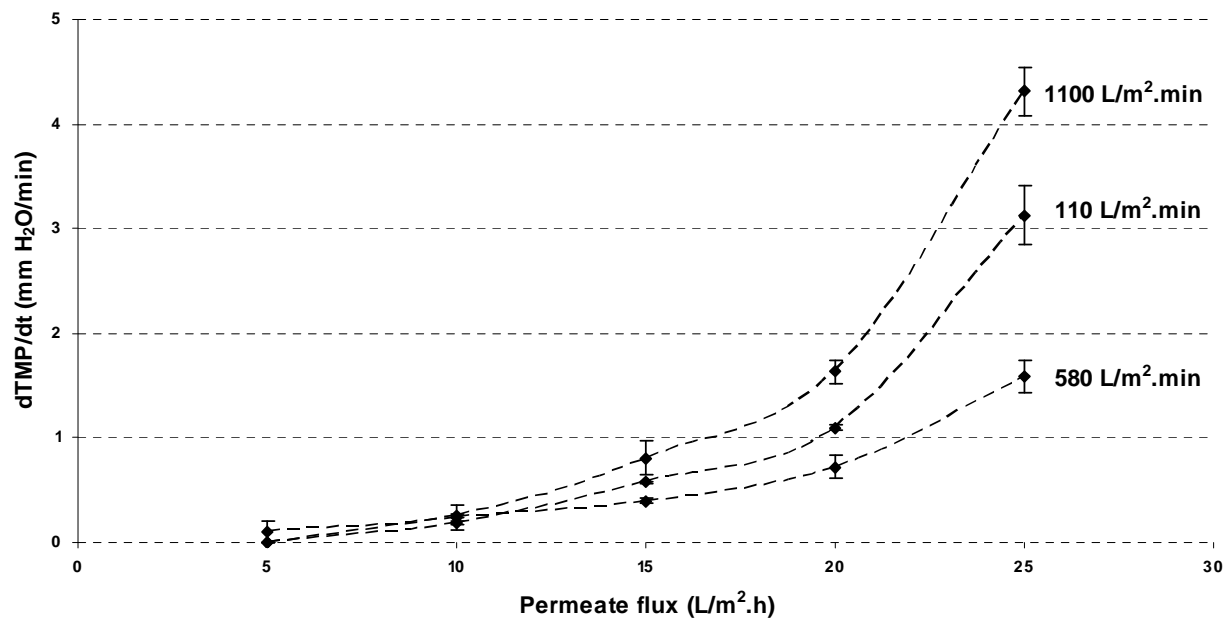


Figure 4.6: Membrane fouling rate at different permeate fluxes. An increase in the permeate flux will lead to an increase in the fouling rate (dTMP/dt), if above the critical flux. However, at the correct aeration intensity the fouling rate at any permeate flux can be greatly reduced. Under and over aeration may accelerate the fouling rate as is shown in this graph.

For the configuration used in this flux-step experiment, it can be seen from Figures 4.5 and 4.6 that an increase in the aeration intensity from 110 L/(m²·min) to 580 L/(m²·min) increased the scouring ability of the sparged air and reduced the fouling rate. It is also evident that sub-critical flux operation was achieved for this configuration at a permeate flux of 5 L/(m²·h) at aeration intensities of 110 L/(m²·min) and 580 L/(m²·min). However, when the aeration intensity was increased from 580 L/(m²·min) to 1 100 L/(m²·min), the fouling rate for each flux increased. Even the critical flux was reduced to a value below 5 L/(m²·h). This paradoxical decrease in scouring ability with an increase in aeration intensity can be explained by the formation of a region of stagnant bubbles that encompassed a significant portion of the immersed membrane.

4.4 Ultrasound for direct fouling quantification

In Section 4.3.4 it was showed that by increasing the aeration intensity, in an attempt to improve the scouring ability of the sparged air, that, on the contrary, the membrane fouling rate might be increased. In this case the increased aeration intensity produced a hydrodynamic stagnant region in the riser section of the airlift reactor which promoted localised fouling where it crossed the membrane element. It is therefore important to understand the system hydrodynamics in an airlift reactor, since this will dictate the scouring ability of the sparged air and the consequent fouling behaviour of the immersed membrane system. Section 3.3.1 lists that both sparged air flow rate (aeration intensity) and reactor geometry determine the system hydrodynamics in an airlift reactor.

The flux-step method used in Section 4.3 indicated the effect of aeration intensity on the overall membrane fouling rate, but being an indirect fouling quantification method, was not able to correlate the aeration intensity with the visually observed localised bentonite deposition. However, realising the presence of complex hydrodynamic fields in an airlift reactor from this experiment, it was felt that the use of a direct fouling quantification method would add more value if the influence of reactor geometry on the membrane fouling behaviour was also investigated. A direct fouling quantification method would be able to measure the fouling profile across the membrane surface, which would describe the reigning system hydrodynamics as created by the reactor geometry.

It was decided to use an ultrasonic technique, ultrasonic time-domain reflectometry (UTDR), as the direct fouling quantification method to investigate the influence of the airlift reactor geometry on the fouling of an immersed membrane. UTDR enables the measurement of fouling layer thickness in real-time, in a non-destructive and non-invasive manner [Peterson et al., 1998; Mairal et al., 1999; 2000; Xu et al., 2009]. These qualities made UTDR very favourable, compared to other direct fouling quantification methods, since it allowed for the monitoring of fouling layer growth during membrane filtration and the repeated use of the same membrane. Unfortunately the technique is limited by its localised nature and therefore requires several trials at different locations to provide for a fouling profile.

4.4.1 Background

When ultrasonic wave energy propagates through a composite structure of material layers with different acoustic impedances, a portion of the energy will be reflected and the remaining energy

will be transmitted at each successive media interface. The acoustic impedance of a medium is defined as [Li et al., 2003]:

$$W = V_m \rho \quad (4.2)$$

where W = acoustic impedance (kg/s.m²)
 V_m = sound velocity in medium (m/s)
 ρ = medium's density (kg/m³)

The proportioning of the reflected and transmitted wave energy at each interface will be dependent on the relative acoustic impedances of the media at the interface. Consider from material 1 an incident ultrasonic wave normal to the interface between material 1 and material 2. The ratio of the reflected wave amplitude to the incident wave amplitude is then given as [Koen, 2000a]:

$$C_r = \frac{W_2 - W_1}{W_2 + W_1} \quad (4.3)$$

where C_r = ratio of reflected wave amplitude to incident wave amplitude
 W_1 = acoustic impedance of material 1 with incident wave (kg/s.m²)
 W_2 = acoustic impedance of material 2 with transmitted wave (kg/s.m²)

Therefore, if material 2 has a greater acoustic impedance than material 1, the ratio C_r will be positive, indicating that the reflected wave will be in phase with the incident wave. Conversely, if the acoustic impedance of material 2 is less than the acoustic impedance of material 1, the consequent negative value of C_r indicates that the reflected wave is out of phase with the incident wave. Important though, is to realise that the larger the difference in the acoustic impedances of the two materials, the higher the proportion of reflected energy at the interface will be, regardless of being in or out of phase with the incident wave.

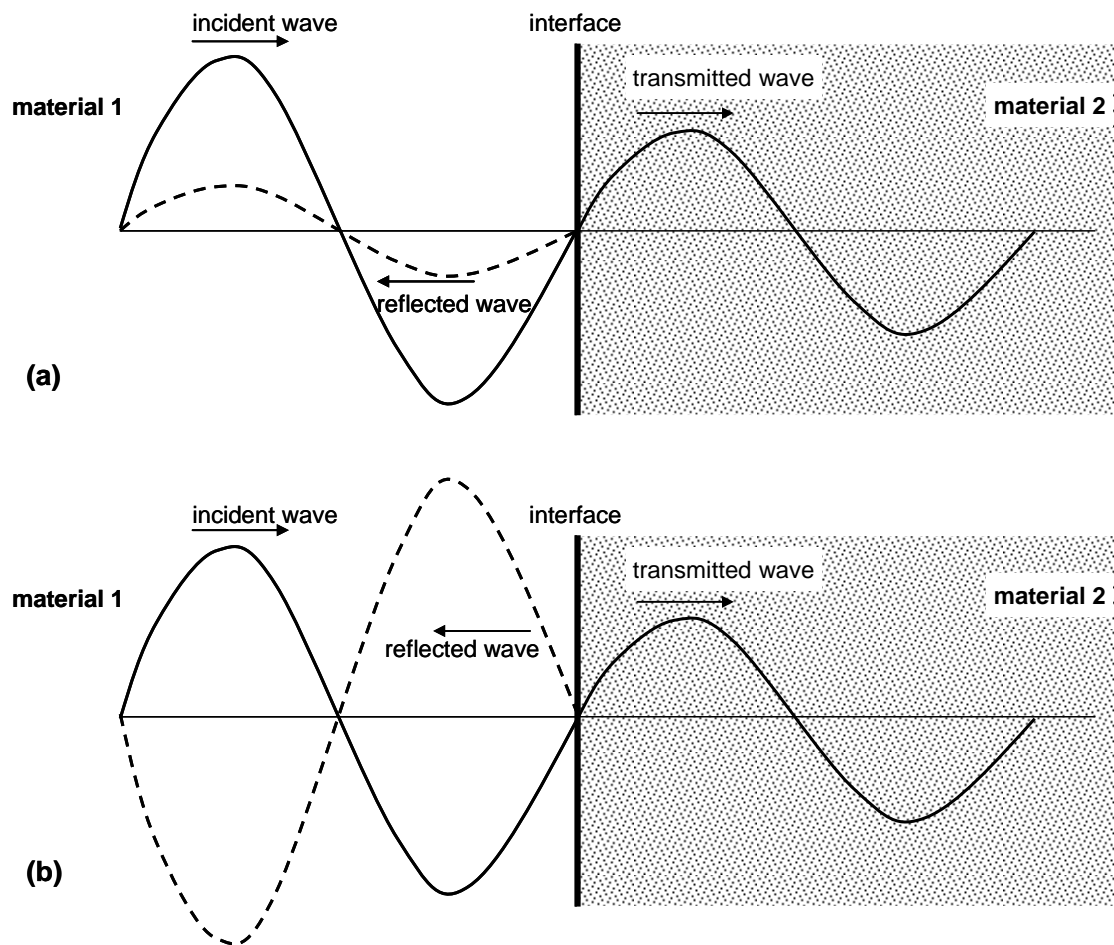


Figure 4.7: Reflection of wave energy at media interfaces. Two cases are shown here: (a) material 2 has a higher acoustic impedance than material 1, but the difference is slight to produce a low energy reflected wave in phase with the incident wave; (b) material 2 has a lower acoustic impedance than material 1 and the difference is significant to produce a high energy reflected wave out of phase with the incident wave.

Equation 4.3 only applies for the case when an ultrasonic wave arrives normal to an absolutely perfect media interface without any scattering, attenuation or any other form of energy dissipation at the interface. Accordingly, Equation 4.3 cannot be used for an accurate prediction of the reflected wave energy, but was given here to highlight the role of an acoustic impedance difference at a media interface on the reflection of wave energy.

The technique of UTDR relies on this phenomenon of wave energy reflection at interfaces of acoustic impedance changes to measure material thicknesses and to differentiate between media along the propagation direction in a composite system. With UTDR it is possible to detect the commencement of a fouling layer on the membrane surface when ultrasonic wave energy is reflected at the surface of the new fouling layer – a new media interface. The fouling layer growth

is measured with the increase in travelling time between the reflected wave energy from the fouling layer surface interface and the reflected wave energy from the fouling layer/membrane surface interface. The utilisation of UTDR to detect and measure the fouling layer thickness on an immersed membrane is explained in Figure 4.8.

As shown in Figure 4.8, a transducer is used to convert a generated electrical signal into an ultrasonic pressure signal and to emit the ultrasonic waves onto the immersed membrane. The reflected ultrasonic waves are also received by the transducer and converted into an electric signal which can be displayed on an oscilloscope. The interpreted electric signal is represented as a waveform of amplitudes against their arrival times. This indicates the amount of wave energy that is reflected at each media interface and the total travel time of the ultrasonic waves from the transducer to the respective interfaces and back to the transducer.

Consider Figure 4.8(a), showing a clean immersed membrane before filtration has started. Ultrasonic waves propagate from the transducer through the water in which the membrane is immersed to meet the clean membrane, the first difference in media density, at the water/membrane interface, A. A fraction of the sent energy is reflected from the interface, received again by the transducer, converted and displayed as peak A of a waveform on the oscilloscope. The remainder of the energy continues to propagate through the membrane to meet the membrane/water interface B where, again, a certain fraction of the energy of incidence is reflected to produce peak B of the displayed waveform. In this case, although the change in impedance at the two interfaces is the same, the difference in amplitude value between peaks A and B is ascribed to the difference in the available incidence energy at each interface.

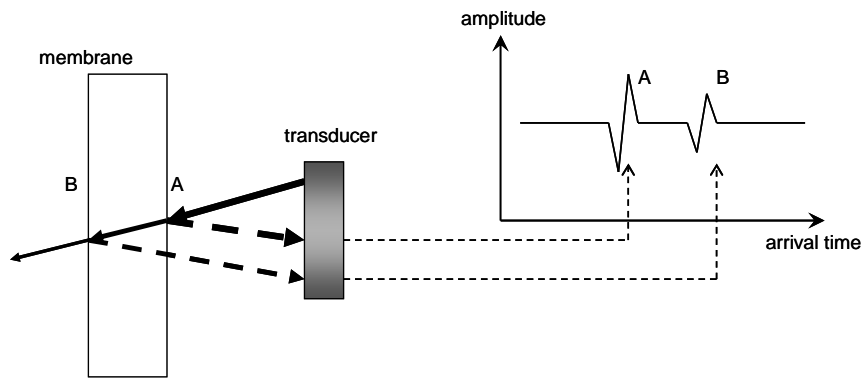
In Figure 4.8(b) the filtration was started and particles have just started to group on the membrane surface to form the first traces of a cake layer. But, as mentioned in Section 2.3, internal fouling is a rapid fouling mechanism and dominates in the early stages of filtration. Therefore, before the proper commencement of a cake layer has started, internal fouling has already impregnated the outer layers of the membrane to solidify it to a certain extent and made it denser as well as smoother. Hence, as internal fouling leads to cake layer formation, the denser membrane surface represents an interface (A') of greater acoustic impedance change with a greater proportion of the incidence energy reflected. Also, the smoother surface means that less of the reflected waves are lost through scattering, but rather reflected back to the transducer. The increase in the reflected wave energy from this interface to the transducer is manifested in the amplitude increase at the arrival time correlating with interface A'. Since more wave energy is reflected at interface A', the transmitted wave energy is reduced and consequently the amount of wave energy to be reflected

at interface B' is also reduced. Therefore the decrease in the amplitude at the arrival time that correlates with interface B'.

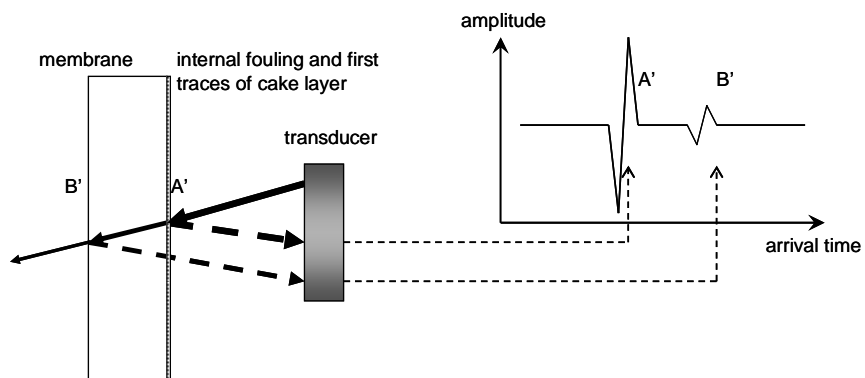
In Figure 4.8(c) membrane filtration has occurred for a significant time and a well established cake layer has formed on the membrane surface. Comparing the displayed waveforms of Figures 4.8(a) and 4.8(c), it can be seen that the presence of the cake layer has resulted in the appearance of a new peak C in the waveform with an earlier arrival time than the water/membrane surface interface A. Peak C represents the energy that is reflected from the new water/cake layer surface interface. The portion of the incident energy that is reflected from this new interface, and therefore the amplitude of peak C, will be determined by the density and the texture of the cake layer surface. The denser the cake layer and the smoother the cake layer surface the greater the portion of the incident wave energy that will be reflected at the water/cake layer surface interface [Koen, 2000b; Li et al., 2002b]. Again, as was the case with cake layer commencement shown in Figure 4.8(b), the subsequent interfaces will receive a reduction in incident wave energy, thereby reducing the wave energy that is reflected at each interface and consequently also the amplitudes of the waveform of the reflected energy. The new water/cake layer interface is closer to the transducer and hence the earlier arrival time of peak C. If the immersed membrane is static the time-domain positions of peaks A'' and B'' will stay unchanged, but the consequent growth in the cake layer will manifest in the movement of peak C to an earlier arrival time. The measured arrival time difference, Δt , between peaks C and A'' will therefore increase as the cake layer thickness increases. Given that the speed of sound through the cake layer is known, the measured arrival time difference between peaks C and A'' can be used to calculate the cake layer thickness with [Li et al., 2002a]:

$$\Delta S = \frac{1}{2} c \Delta t \quad (4.4)$$

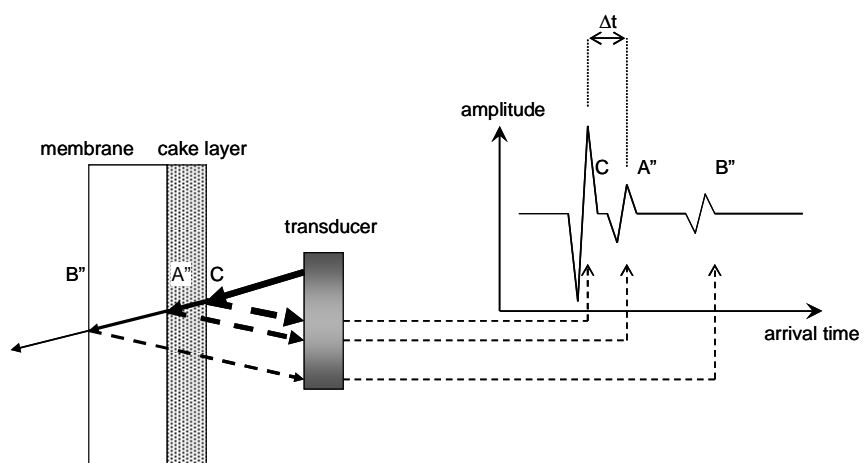
where ΔS = fouling layer thickness (m)
 c = speed of sound in the fouling layer (m/s)
 Δt = arrival time difference (s)



(a) clean membrane



(b) cake layer commencement



(c) cake layer growth

Figure 4.8: Hypothetical oscilloscope waveforms to explain UTDR for fouling quantification. (Notice that only one side of the immersed membrane was considered here.)

Although Figure 4.8 presents oversimplified and hypothetical waveforms, it serves to explain how the technique of UTDR is employed to measure fouling layer thicknesses. UTDR and its application to measure cake layer thickness were discussed here in a very concise and superficial manner; in just enough detail to allow for the comprehension of the experimental work to follow. The technique of UTDR to monitor membrane fouling is described in much greater detail elsewhere [Koen, 2000b; Li, 2002].

4.4.2 Experimental set-up

The experimental set-up for the direct quantification of immersed membrane fouling with UTDR was similar to the experimental set-up for the indirect fouling quantification as described in Section 4.3.2 and shown in Figure 4.3. The only differences were the addition of the ultrasonic measurement system, the study of airlift reactor geometries at three A_d/A_r ratios and the aeration intensity, as well as the permeate flux, set to constants of $1\,100 \pm 160 \text{ L}/(\text{m}^2 \cdot \text{min})$ and $15 \pm 0.4 \text{ L}/(\text{m}^2 \cdot \text{h})$ respectively.

Ultrasonic measurement system

The ultrasonic measurement system was the only new equipment that was added to the experimental set-up described in Section 4.3.2, and comprised of an ultrasonic transducer, a pulser/receiver, an oscilloscope, a computer and the connecting cables (Figure 4.9).

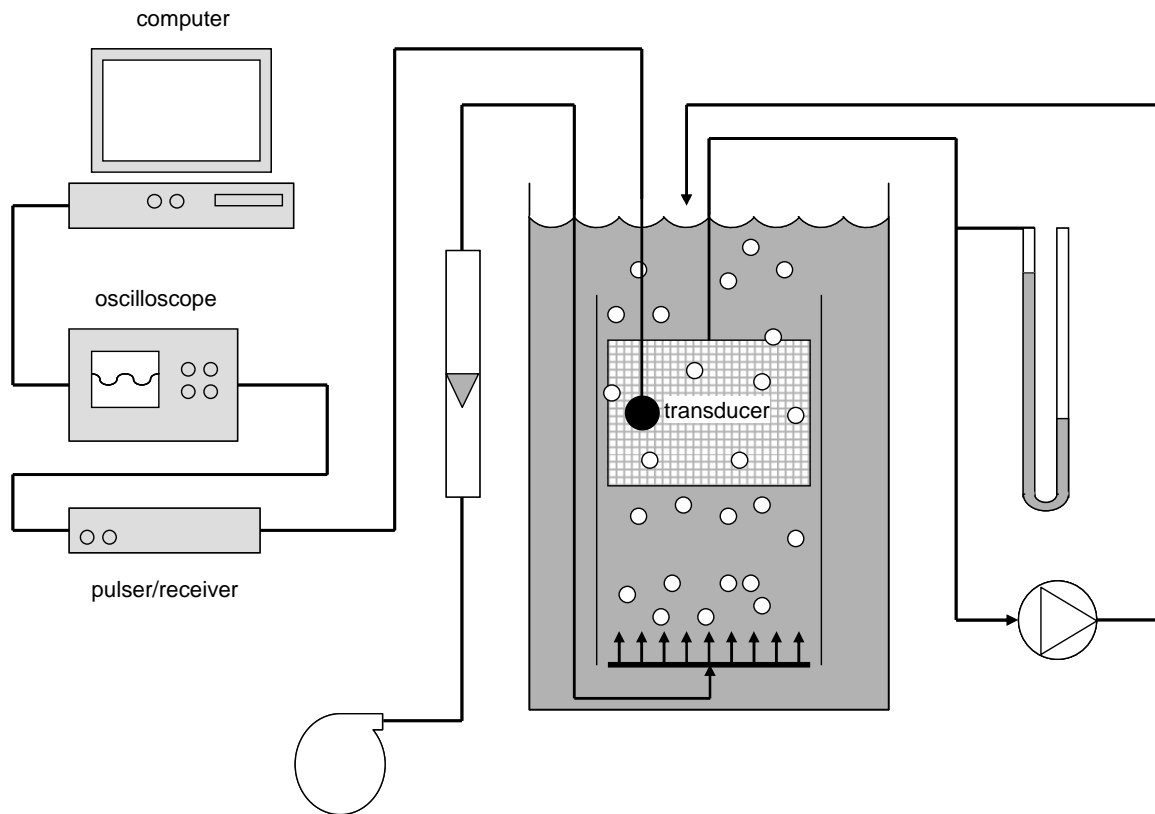


Figure 4.9: The experimental set-up for the UTDR experiment for the direct fouling quantification of immersed membrane fouling. Besides the ultrasonic equipment, the equipment set-up is identical to the equipment set-up described in Section 4.3.2 for the flux-step experiment.

In this study a Panametrics Videoscan ultrasonic transducer was used. The type of transducer to be used must be selected for its application. The transducer can either be selected to enhance the sensitivity or the resolution of the system [Koen, 2000b]. Low ultrasonic frequency transducers enhance the sensitivity of the system to enable it to detect density changes at various depths of the test material, as opposed to high ultrasonic frequency transducers that enhance the resolution of the system to enable it to finely discriminate between density changes near the surface of the test material. Therefore, the higher the frequency of the transducer, the better is the resolution, but with a decrease in penetration depth. For this study of fouling layer monitoring a set of ultrasonic transducers were evaluated, as shown in Table 4.3. The V120-RB 7.5 MHz transducer was found to be the best suited for this application, because it is capable of fairly high resolution at the membrane surface and with adequate sensitivity for the detection of density differences just beneath the membrane surface. The theoretical resolution of the V120-RB transducer in water is given as 48 μm . This is an indication of the smallest detail that can be detected by the transducer in water. The bentonite particle size distribution was measured, as shown in Addendum A, and it

was found that approximately 6% of the particles were larger than 48 μm with the 90th percentile of the particle size distribution at 41.78 μm . It was found that the relative small amount of particles larger than 48 μm did not add significant noise to the reflected energy.

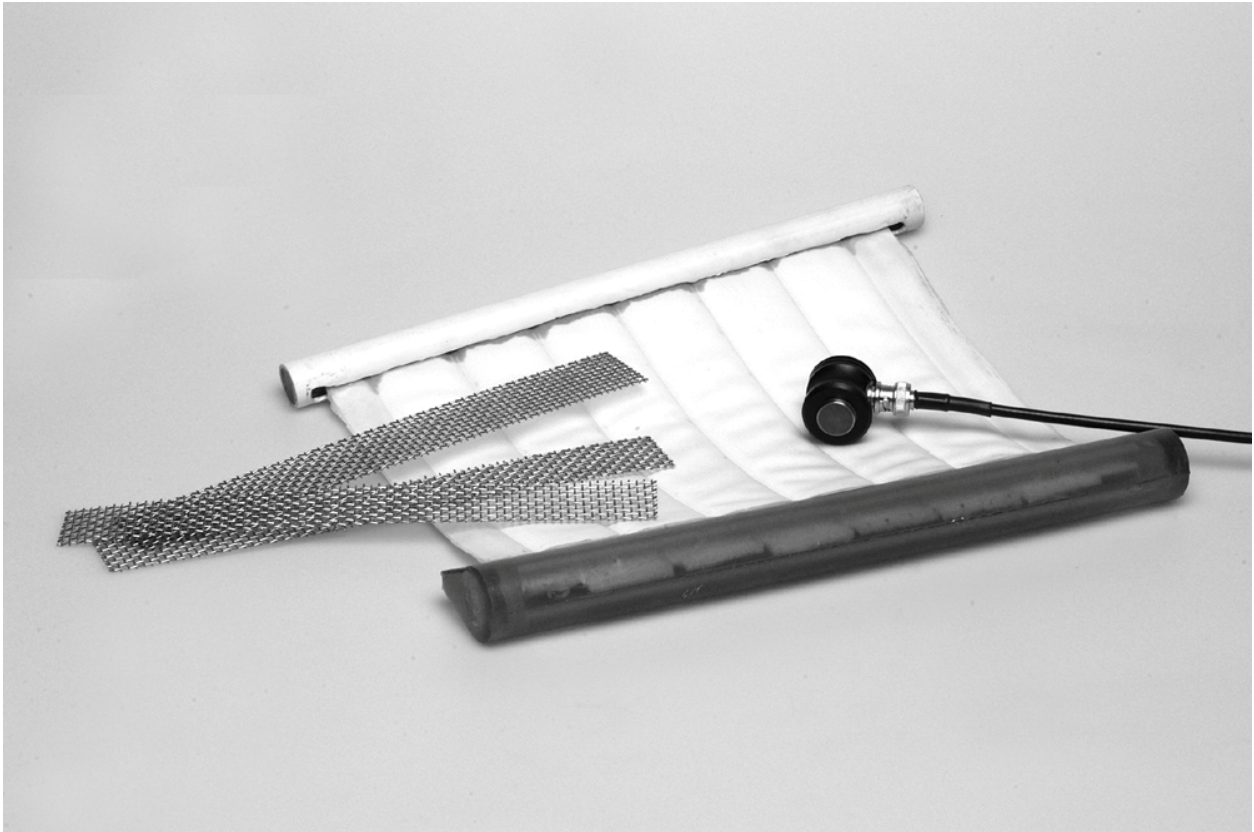


Figure 4.10: A photograph of one of the membrane elements that were used in the ultrasound experiment with its membrane spacer material and the Panametrics Videoscan V120-RB transducer.

Table 4.3: Panametrics Videoscan ultrasonic transducers that were evaluated for the monitoring of fouling layer formation [Koen, 2000b]

Transducer type	Frequency (MHz)	Resolution (μm)
V106-RB	2.25	159
V182-RB	3.5	102
V109-RB	5	72
V120-RB	7.5	48
V111-RB	10	36

The 7.5 MHz ultrasonic transducer was placed inside the riser section of the airlift reactor, as shown in Figure 4.11, so that the bentonite suspension was the only medium between the transducer and the membrane surface. The transducer was positioned to face the one side of the membrane element at halfway the depth of the flat-sheet membrane surface. The different membrane elements used in the experiment only differed with regards to their widths and were placed at the same depth in every trial to ensure that they were subjected to the same water head range (bottom to top of flat-sheet membrane surface). Consequently, the local TMP of the membrane surfaces monitored by the transducer all experienced the same water head contribution. The transducer and the membrane element were tightly secured to remain immovable during aeration. This enabled the transducer to detect the fouling process accurately with UTDR. The transducer was placed at a distance of between 20 mm and 30 mm from the membrane surface so as not to disturb the fluid-flow behaviour near the membrane surface. There was no need to ensure that the distance between the transducer and the membrane surface is the same for all the experimental trials; however, the distance between the transducer and the membrane surface had to remain constant for the duration of an experimental trial.

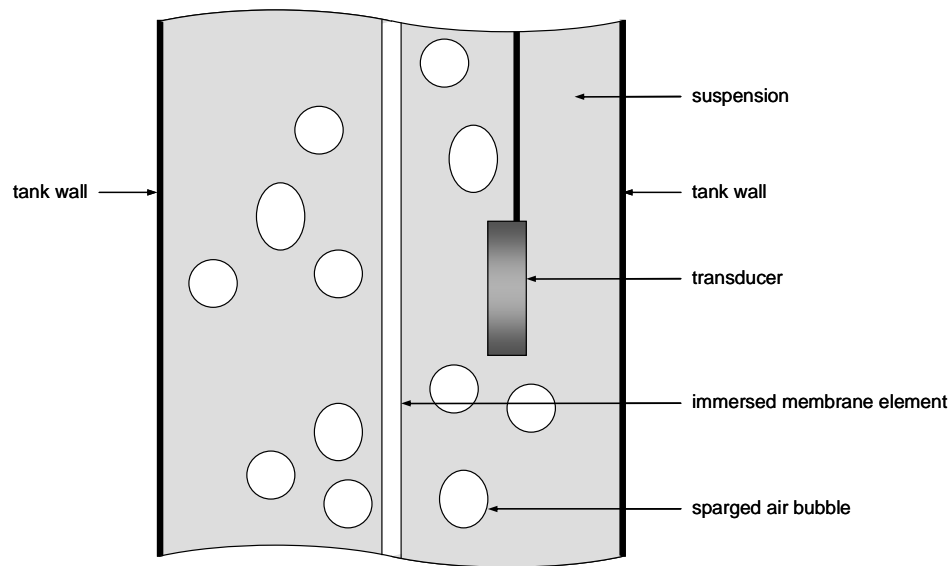


Figure 4.11: Section of the side view of the riser section to show the location of the immersed ultrasonic transducer. The transducer was positioned halfway the depth of the membrane element's flat-sheet surface.

The transducer was connected to a pulser-receiver (Panametrics 5058PR). The pulser-receiver is responsible for generating the high frequency signal, as well as receiving the converted reflected signal from the transducer. An oscilloscope (Hewlett Packard 54602B) was used to observe the reflected signal as a waveform which could be captured as 2 000 time-amplitude value pairs (4 000 data points) and stored on a computer's hard drive. The waveform data was saved in comma-separated (.CSV) form and could be opened in Microsoft Excel for further data processing.

Numerous experiments, together with the chosen 7.5 MHz ultrasonic transducer, were performed to determine the operating settings of the pulser-receiver which would provide for the most sensible visualisation of the reflected waveform on the oscilloscope.

The optimum operating settings of the pulser-receiver was found to be:

- an excitation pulse of 400 V;
- a pulse damping of 50 Ω ;
- with the internal trigger set at a repetition rate of 200 MHz;
- a receiver gain of 40 dB;
- a receiver attenuation of 25 dB;
- with echo pulses selected as normal (0°); and
- with the use of the 0.1 MHz high pass filter.

A_d/A_r ratios

The framework of two Perspex baffle-plates and seven steel rods, as mentioned in Section 4.3.2, could be adjusted by sliding the baffle-plates on the steel rods to create different A_d/A_r ratios inside the airlift reactor. Three A_d/A_r ratios of 0.31, 0.71 and 1.45 were created for this direct fouling quantification study. Since the flat-sheet membrane elements had to stretch the widths of the respective riser sections, a membrane element had to be fabricated for each A_d/A_r ratio airlift reactor, as explained in Addendum B. Except for the differences in the respective membrane elements' widths, the membrane elements all had the same dimensions. The riser and downcomer cross-sectional dimensions, as well as the dimensions of the active membrane area of the membrane element used for each A_d/A_r ratio are given in Table 4.4. Note that the active flat-sheet membrane widths are smaller than the respective occupied riser section widths. This is because the inactive tubes remain on the membrane elements' sides and the permeate collector (see Addendum B) require the remaining space in the riser sections. For each configuration a double-pipe diffuser, with 0.6 mm holes, was located at the bottom of the tank and stretched the width of the respective riser.

Table 4.4: The three airlift reactor geometries and the flat-sheet membrane sizes used in the UTDR experiment.

A_d/A_r ratio	Cross-sectional riser dimensions (mm)	Cross-sectional downcomer dimensions (mm)	Active flat-sheet membrane dimensions (mm)	Total active membrane area (m ²)
0.31	430 x 120	67 x 120	351 x 170	0.12
0.71	330 x 120	117 x 120	234 x 170	0.080
1.45	230 x 120	167 x 120	156 x 170	0.053

Constant aeration intensity

As discussed before, the system hydrodynamics are a function of the aeration intensity and the reactor geometry. A constant aeration intensity, therefore, had to be chosen if the influence of reactor geometry at different A_d/A_r ratios, as the only variable, on the system hydrodynamics were to be investigated. The aeration intensity was set to the highest value that was used in Section 4.3, namely 1 100 L/(m²·min). Although any arbitrary value could have been used for this experiment, this relative high aeration intensity was chosen to establish if the lower than expected scouring efficiency, as was observed in Section 4.3, could be improved by changing the airlift reactor geometry. Depending on the geometry that was investigated, either a compressor or a

blower was used to supply the necessary airflow. A compressor was used when the A_d/A_r ratio of 0.31 was investigated and a blower was used when A_d/A_r ratios of 0.71 and 1.45 were investigated. As explained in Section 4.3.2, the blower was unable to provide the relative high airflow needed to maintain the required aeration intensity at the given head for the large cross-sectional area of the riser section when an A_d/A_r of 0.31 was investigated. A compressor was consequently used with a fairly high deviation of 160 L/m²/min in the resulting aeration intensity. The blower was, however, quite capable of providing the necessary airflow to the smaller riser section geometries to maintain aeration intensities within 10 L/m²/min from the desired 1 100 L/m²/min.

Constant permeate flux

The reigning system hydrodynamics in an airlift reactor determine the scouring ability of the sparged air in the riser section as it sweeps across the immersed membrane surface. In other words, the system hydrodynamics influence the rate of back-transport of retained material from the membrane surface to the bulk. Conversely, the permeate flux determines the rate of material transported to the membrane surface. The net force is therefore manifested as the fouling behaviour of the membrane, and if the fouling behaviour is to be related to the geometry of the airlift reactor, it is imperative that the overall permeate flux is kept constant for comparison sake. The permeate flux was arbitrarily set to 15 ± 0.4 L/(m²·h), an intermediate value used in the flux-step experiment, as described in Section 4.3.

4.4.3 Method

The fouling profiles of the membrane elements used in each of the three airlift reactor geometries were generated by measuring the fouling with the UTDR technique at three locations across the membrane surface. The transducer was positioned to measure the fouling on the one side of the far left, middle and far right filter tubes of each membrane element. The experiment to directly quantify fouling in different airlift reactor geometries with the UTDR technique therefore consisted of nine trials. Each trial lasted 20 hours to ensure sufficient cake layer formation that could provide a sensible fouling profile across the membrane surface.

A simple backwash procedure, prior to an experimental trial, proved to be adequate in restoring the original hydraulic resistance of the membrane, therefore removing all particles within, as well as on the membrane surface. The clean backwashed membrane element was then fitted into a glass tank in the same manner as explained in Section 4.3.2 and the ultrasonic transducer located in the correct position as described in Section 4.4.2. The tank was then filled with RO water and permeation started at the constant flux of 15 ± 0.4 L/(m²·h), but without any aeration. This was

done in order to collapse the filter tubes to present a compressed and steady membrane element to the transducer; providing the reference state of the membrane surface before membrane fouling has commenced. With the membrane element compressed, the transducer was slowly rotated in the horizontal to find the position where it received the strongest reflected signal as viewed on the oscilloscope. The transducer would be tightly set once the point of maximum wave energy reflection has been found. In this position the transducer's surface would be parallel to the compressed membrane surface. The received waveform was saved on the computer hard drive as the reference signal to which the signal of the fouled membrane would be compared.

When the permeation was stopped, the membrane element's filter tubes would relax and slowly expand to a fraction of its original volume before permeation, but on re-commencement of permeation the membrane would quickly assume the stable compressed form and reproduce the reference waveform on the oscilloscope. With permeation still stopped, the fouling agent, a suspension of bentonite in RO water, was then added to the tank to create a particulate suspension. For each trial a fresh batch of 60 L suspension was prepared, as explained in Addendum A, with a bentonite concentration of 1.0 g/L. Aeration of the tank at the chosen constant aeration intensity was subsequently started to ensure a homogeneous suspension. The preparation for a UTDR trial was completed now and permeation could recommence.

Permeation was maintained at $15 \pm 0.4 \text{ L}/(\text{m}^2 \cdot \text{h})$ for all trials, while air was supplied to the specific geometry to produce an aeration intensity of $1\ 100 \pm 160 \text{ L}/(\text{m}^2 \cdot \text{min})$. When sampling the reflected ultrasonic signal from the membrane surface, the aeration was momentarily stopped (less than 10 s), while permeation was allowed to continue. Without the interference of the bubbles the transducer was able to receive a clear reflected ultrasonic signal. If the permeation were stopped during the sampling process the membrane would relax, creating an uneven surface with increased scattering of the reflected signal, thereby complicating data interpretation. It was assumed that the increased fouling in the brief absence of aeration was negligible. Sampling was conducted at suspension temperatures of $25 \pm 2^\circ\text{C}$.

4.4.4 Results

Reflected waveforms

In this UTDR investigation the fouling layer was not found to be a clearly defined layer on the membrane surface with a uniform density, but rather a transition from concentration polarisation to an external cake layer to internal fouling. A differential waveform, which is the difference between the test waveform and the initial reference waveform, was therefore employed to highlight any

density changes [Li et al., 2002a]. These density changes could again indicate the fouling mechanisms that were occurring. In Figure 4.12 real and typical waveforms obtained during the study are shown.

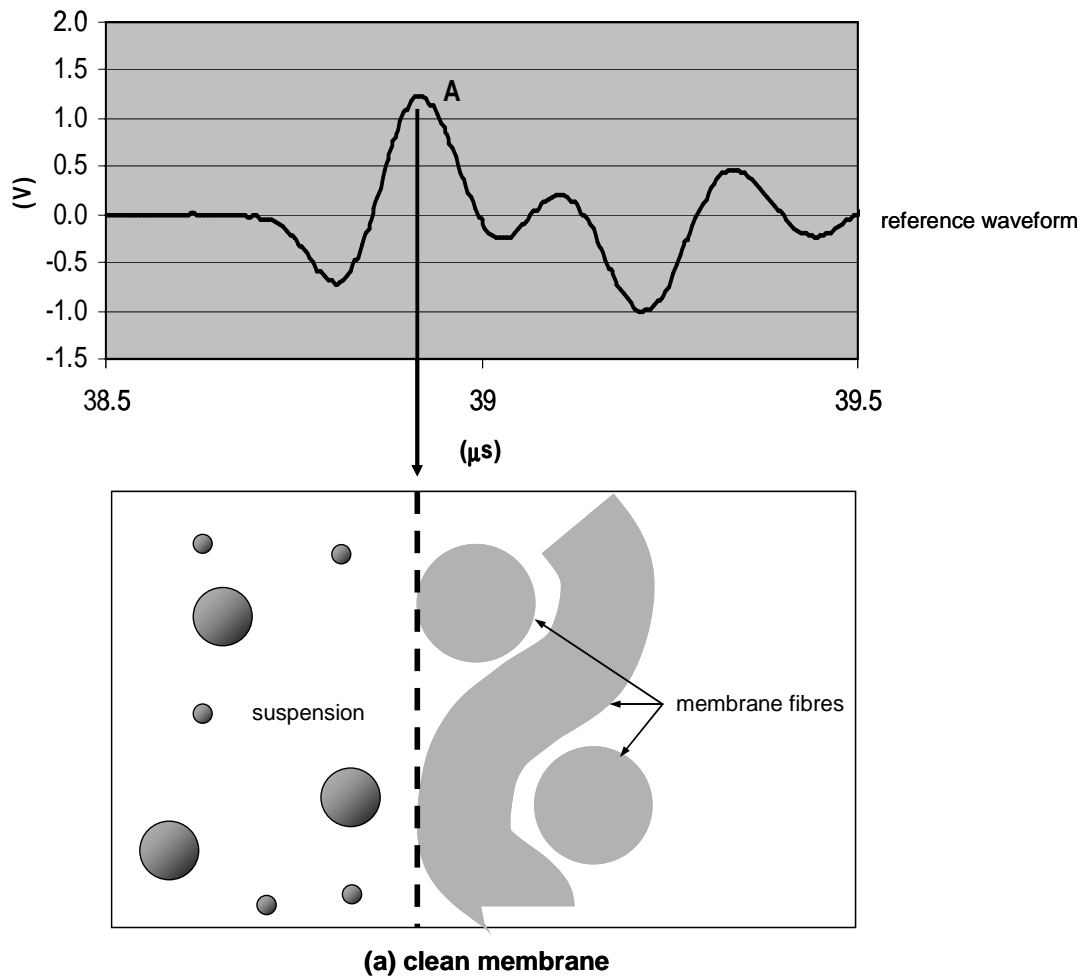


Figure 4.12(a): Typical waveform translation of a clean membrane.

Figure 4.12(a) shows a reflected waveform from a clean membrane at the start of filtration. Peak A represents the membrane surface. This waveform is saved on a computer's hard drive as the reference waveform.

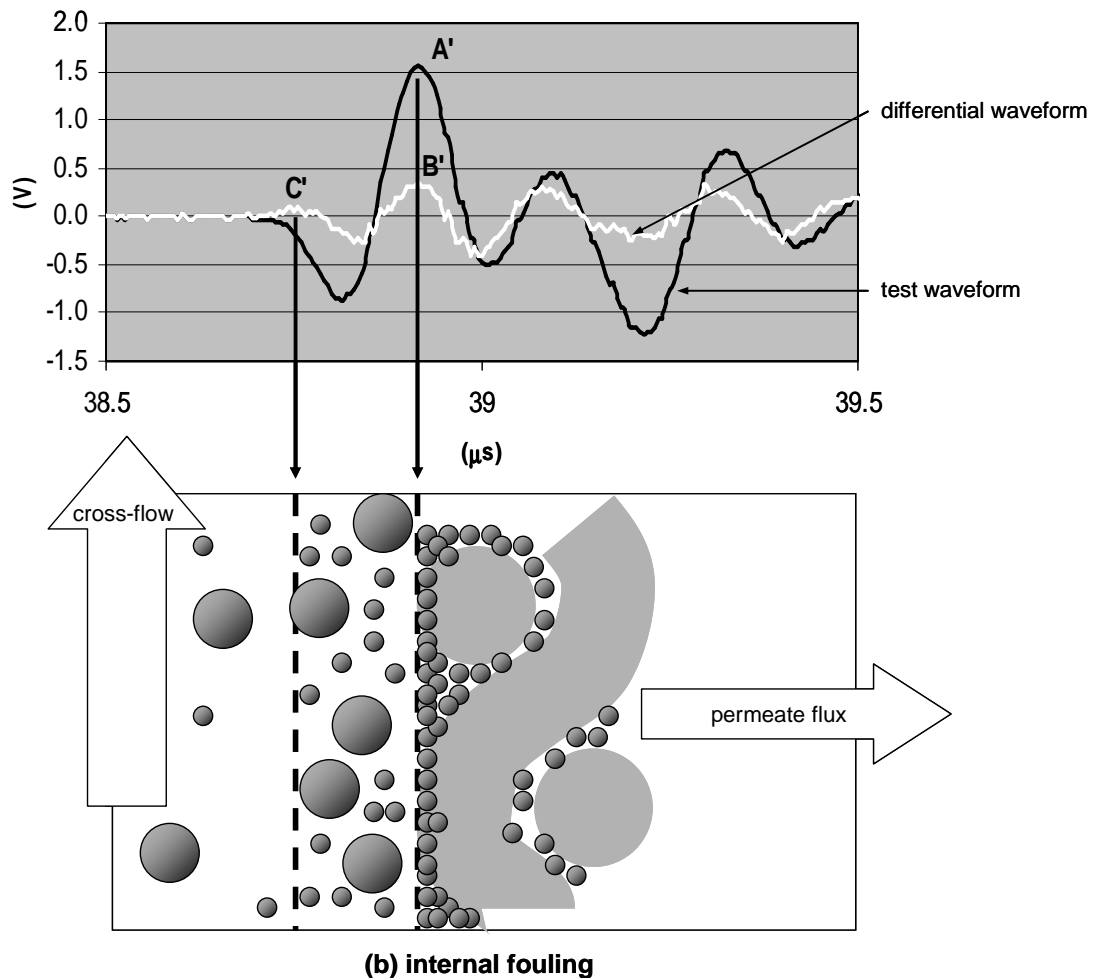


Figure 4.12(b): Typical waveform translation of internal fouling.

When permeation is started, small particles are drawn into the relatively open membrane matrix where they adsorb onto the material and plug the pores (passages between the individual fibres and weave). The membrane quickly densifies with resulting higher acoustic impedance and increased reflection of wave energy. This is depicted in the sudden increase of peak A to form peak A' (Figure 4.12(b)) one minute after start-up. At this stage the differential waveform indicates a difference in density of the membrane surface with peak B' and the existence of concentration polarisation with the appearance of peak C'.

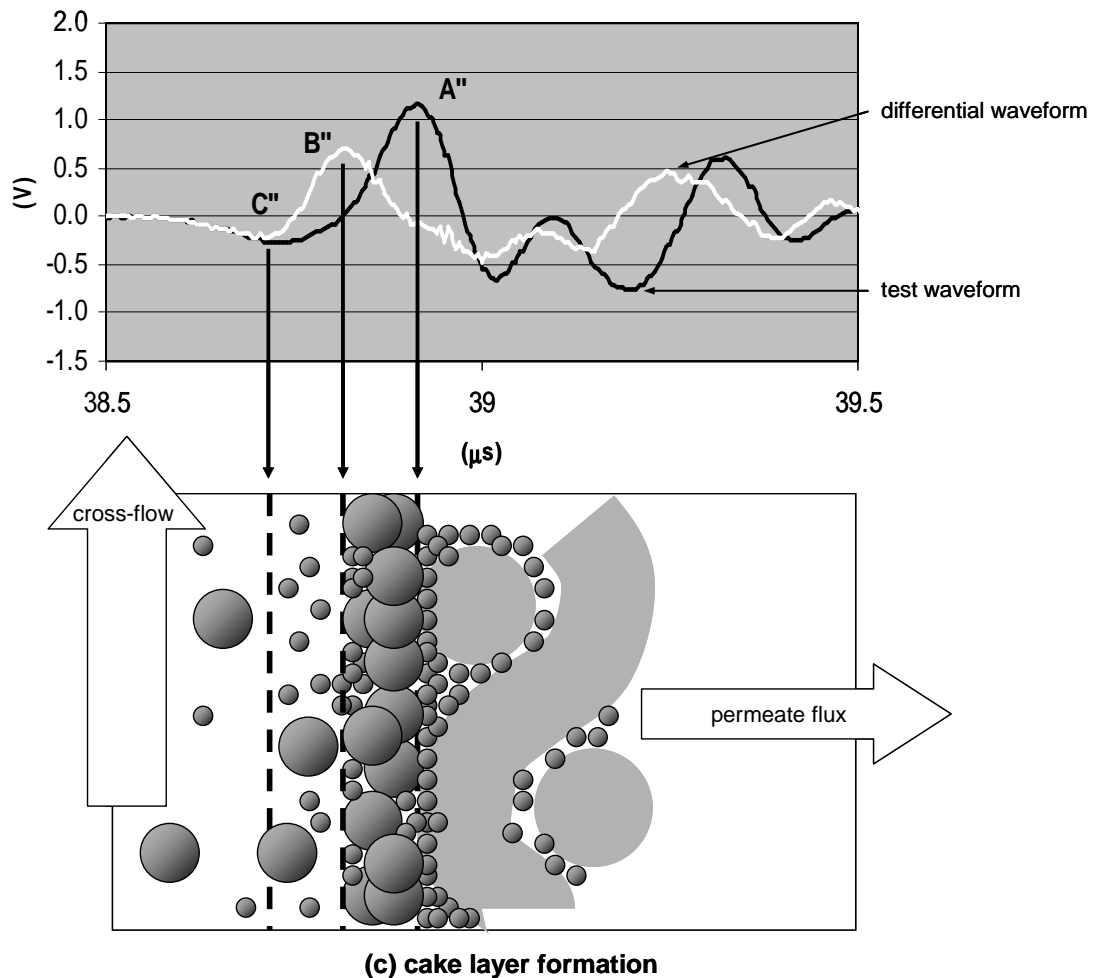


Figure 4.12(c): Typical waveform translation of cake layer formation.

After the initial internal fouling, another fouling mode starts to dominate, namely external fouling where particles are deposited onto the membrane surface to form a cake layer. This cake layer shelters the membrane from the transducer, causing a decrease in peak A'' as the effective reflected energy from the membrane is reduced, as is shown in Figure 4.12(c) which was sampled 25 minutes after start-up. The existence of polarised particles, a cake layer and internal fouling complicated the fouling interpretation of the test waveform, but with the use of the differential waveform the state of fouling inside and on the membrane surface could be determined. The time-domain shift of peak B'' from the membrane surface at peak B' (Figure 4.12(b)) indicates that deposition has occurred. C'' indicates the time-domain position of the concentration boundary

layer (concentration polarisation) where the accumulation of material is responsible for energy reflection.

Membrane fouling

In the configuration with an A_d/A_r ratio of 0.31, it was observed that very high riser cross-flow velocities occurred on the sides, just next to the dividing baffle plates, compared to the very slow, almost stagnant, cross-flow that occurred in the remaining middle of the riser. As the A_d/A_r ratio was increased, the variance in the cross-flow velocity seemed to decrease. Assuming that the density of the cake layer is approximately 2 g/cm^3 (between the density of water of 1 g/cm^3 and the density of bentonite of 3 g/cm^3), velocity of sound in the cake layer was measured to be 2800 m/s (Addendum D). After 20 h of operation the fouling layers in the middle on the membranes had arrival time differences of 90 ns, 105 ns and 130 ns for the airlift reactor configurations with A_d/A_r ratios of 1.45, 0.71 and 0.31 respectively. By using Equation 4.4 these arrival times equate to fouling layer thicknesses of 0.126 mm, 0.147 mm and 0.182 mm respectively. Figure 4.13 shows the calculated fouling layer thickness after 20 h of operation at the various relative positions for the configurations investigated. The thicker fouling layer on the right side (relative position of +1) of the large membrane ($A_d/A_r = 0.31$) can be ascribed to the positioning of the manifold outlet on the right with a significant pressure loss from right to left to produce higher local TMP values on the right side than, for example, the left side (relative position of -1).

By comparing the evolution of the relative height of peak A in each experiment, it was found that for a low A_d/A_r ratio such as 0.31, cake layer formation mainly occurred in the middle of the membrane with internal fouling mainly on the sides. For the higher A_d/A_r ratios the fouling behaviour was more uniform across the whole membrane.

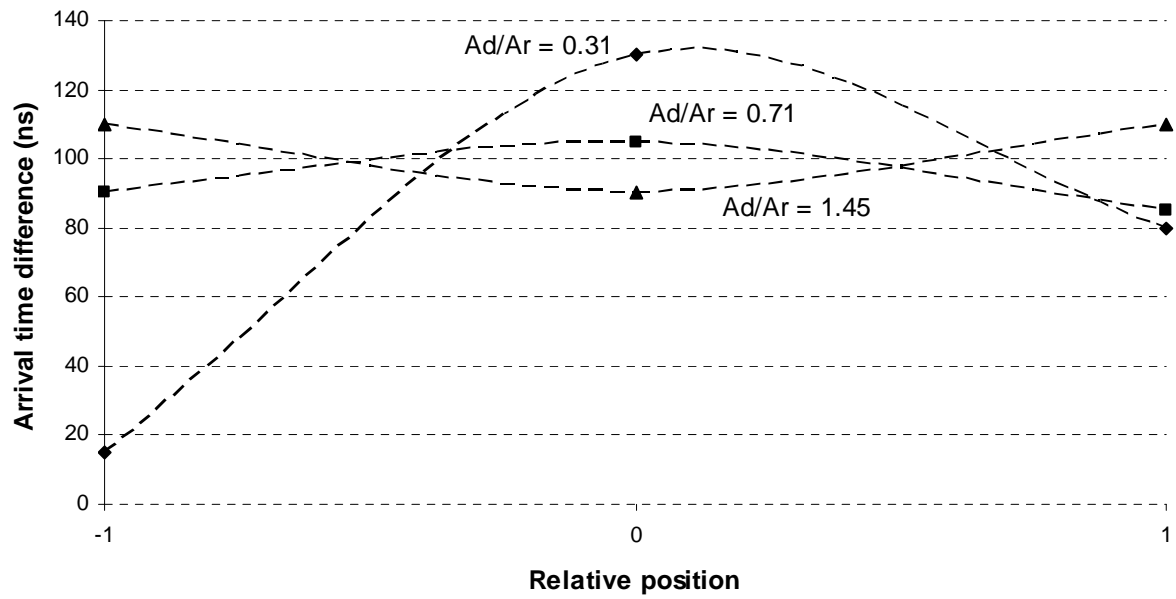


Figure 4.13: The arrival time differences at the relative positions after 20 hours of membrane filtration in a 1.0 g/L bentonite suspension.

Chapter 5

System hydrodynamic effects of airlift reactor factors

5.1 Introduction

The system hydrodynamics of an airlift reactor refer to all the intricate gas-liquid interactions in the various sections of an airlift reactor to create the governing circulation fluid flow. The behaviour of this resulting fluid flow in the riser section of the airlift reactor becomes particularly important if the fast rising liquid and gas bubbles are utilised to limit membrane fouling as was described in Chapter 3. In Chapter 4 it was determined that both the aeration intensity and the geometric configuration of an airlift reactor influence the system hydrodynamics, and are therefore responsible for the fluid flow behaviour that is induced in the riser section. The fluid flow behaviour in the riser section can be described as a hydrodynamic field consisting of fluid flow vectors. The sum of all these fluid flow vectors produces a resultant flow with a velocity profile across the riser section. As was previously observed, typical hydrodynamic fields in airlift reactor riser sections with their respective velocity profiles are shown in Figure 5.1.

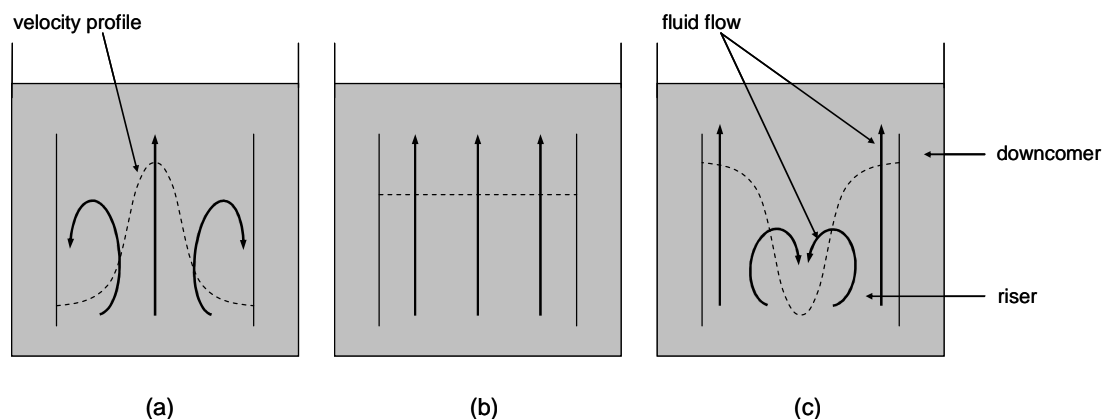


Figure 5.1: Typical hydrodynamic field patterns that were observed in the riser section of an airlift reactor: (a) fast rising liquid and bubbles in the middle with churning liquid and stagnant bubbles on the sides; (b) uniformly fast rising liquid and bubbles across the riser section; and (c) fast rising liquid and bubbles on the sides with churning liquid and stagnant bubbles in the middle.

Because of the two-phase operation of an airlift reactor, there are in reality two velocity profiles in the riser section: the liquid velocity profile and the gas bubble velocity profile superimposed onto the liquid velocity profile. In this study, however, only the liquid velocity profile was investigated since it governs the gas bubble velocity profile. Any further mention of the velocity profile will refer to the liquid velocity profile in the riser section of the airlift reactor.

The presence of a velocity profile in the riser section of the airlift reactor was discussed in Chapter 4. From the findings in Chapter 4 it can be postulated that if an airlift reactor riser section were to be utilised to limit fouling of immersed membranes, the optimal airlift reactor arrangement would be where the aeration intensity and the reactor configuration provide system hydrodynamics such that the velocity profile of the hydrodynamic field in the riser section is maximised and perfectly uniform. The optimised case would be akin to the hydrodynamic field and velocity profile depicted in Figure 5.1(b).

In Section 3.1.1 it was noted that for an airlift reactor the aeration intensity, the ratio of the total cross-sectional areas of the downcomer sections to the riser sections (A_d/A_r), the top clearance distance, the bottom clearance distance and riser section height all seem to influence the liquid velocity in the riser section. In other words, all of these aspects can influence the magnitude of the velocity profile and can be arranged in such a way as to maximise the velocity profile. But if these aspects could also be arranged to simultaneously satisfy the requirement of an uniform velocity profile, then the optimum airlift reactor design for immersed membrane scouring in the riser section would be found. The five airlift reactor aspects mentioned above must therefore be investigated to determine their influences on the velocity profile. Since the top clearance and bottom clearance distances are already considered, it was decided to rather evaluate the influence of the airlift reactor water depth as opposed to the riser section height, since it is related and much simpler to execute during the experiment. Also, it was thought that the air sparger and its introduction of air bubbles at the very bottom of the riser section might contribute to the resistance to the circulation flow in the interconnecting zone from the downcomer section to the riser section. Moving the air sparger to inside the riser section could potentially improve the velocity profile in the riser section.

Bubble size was not considered. In Section 3.2 it was explained how the scouring action of rising bubbles is increased when the bubbles move closer to the membrane surfaces. It was therefore assumed that the optimal bubble size diameter would be equal to the channel width of immersed flat-sheet membranes. The channel width between membrane surfaces was again thought to form part of future optimisation studies and not relevant to this study.

Consequently six aspects of airlift reactor design were identified which could influence the velocity profile. These relationships must be uncovered to enable the design and operation of an airlift reactor with improved system hydrodynamics for a higher scouring efficiency of immersed membranes. The six aspects of airlift reactor design that were investigated are listed and indicated in Figure 5.2.

- 1) downcomer area to riser area ratio (A_d/A_r)
- 2) top clearance distance
- 3) bottom clearance distance
- 4) aeration intensity
- 5) water depth
- 6) air sparger location

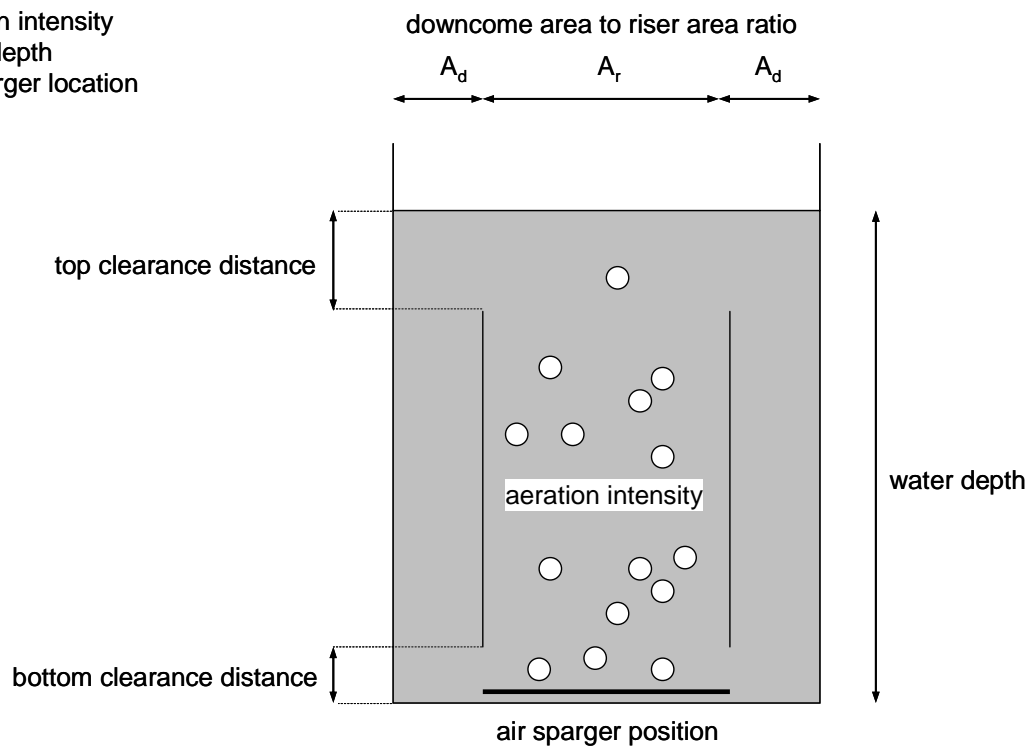


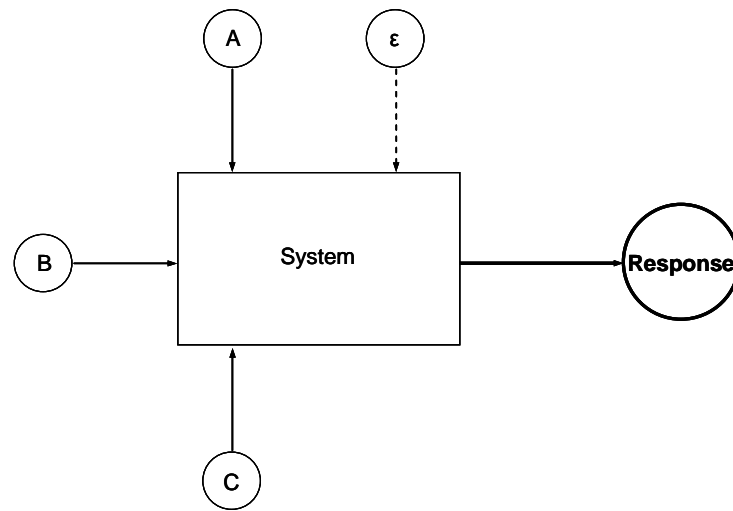
Figure 5.2: The six aspects of airlift reactor design that were investigated to determine their influences on the velocity profile in the riser section.

5.2 Design of experiments

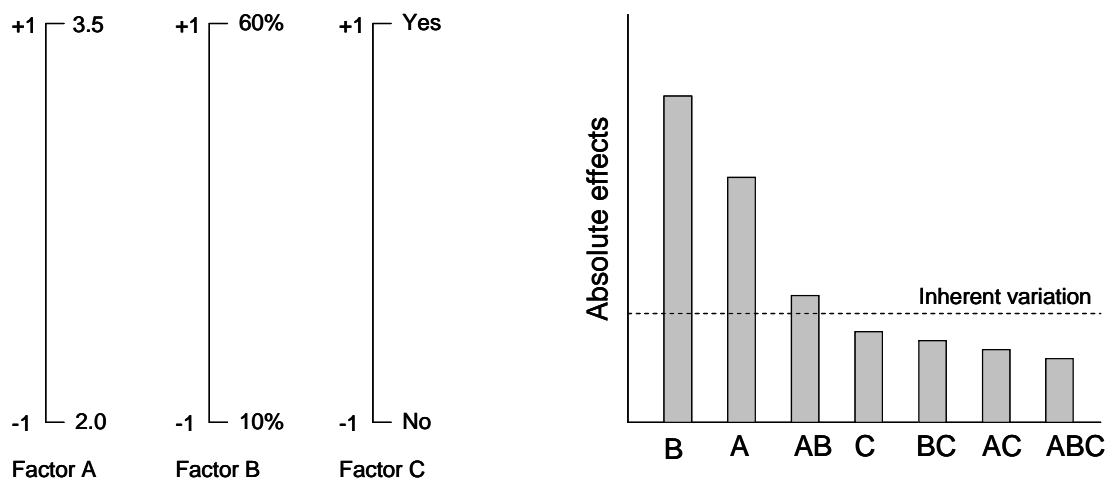
This section only gives a very basic account of design of experiments (DOE) to explain the experimental work and the results that were obtained. Barrentine [1999] provides a good introduction to DOE, but a more fundamental explanation can be found in most statistics textbooks. DOE is a methodology to simultaneously study various system inputs and their interactions with each other to determine their respective effects on a single target output. This is a much more time efficient approach as opposed to testing one system input at a time. Also, by testing system inputs one at a time, the possibility exists that the existence of potential interactions might be overlooked. DOE is therefore ideally suited to investigate multi-factorial systems with potential interactions as a first round tool to optimise these systems.

In DOE the independent system inputs or variables are referred to as factors. For the designed experiment the factors are set at predetermined values which are referred to as levels. Levels do not have to be numeric values, but can also be attributes, i.e. continuous or discrete. In its simplest form a DOE contain factors that are evaluated at only two levels, thereby assuming that the relationships between the factors and the target output are of a linear kind. Factors can be evaluated at more than two levels to capture the potential existence of nonlinear relationships. Sometimes two or more factors together can form an interaction which can influence the target output differently than these factors would individually. The target output in DOE is referred to as the response and it is the result of all the actions of the factors. The impact of a change in a factor or an interaction on the value of the response is referred to as the effect on the response.

In every system there is a certain degree of inherent variation of the response. In other words, if a designed experiment were to be repeated with all the identified factors at the exact same levels, then the response will demonstrate a deviation from the previous experimental trial. The smaller the deviation, the smaller is the experimental error and the more reproducible is the system. The experimental error is a combination of the variation of the factors, the variation of unknown factors and the variation of the response measurement to produce inherent variation of the response. To reduce the impact of experimental error the unique settings of the factor levels, called treatments, must be performed in a randomised fashion. It is therefore important to determine the inherent variation of the response to confirm the significance of factors. If the effect of a factor is indeed higher than the inherent variation of the response, then the factor is regarded to have a significant effect on the response and does not form part of the normal process noise. Figure 5.3 captures the abovementioned concepts for a hypothetical system where DOE was used to determine the effects of all the identified factors and their potential interactions on the system response.



(a)



(b)

(c)

Figure 5.3: A basic explanation of DOE for a hypothetical system. (a) Three factors, A, B and C, were identified as possibly having an impact on the response and needed to be investigated. An experimental error is present in the system and contributes to the value of the response. (b) Two levels were chosen for each factor, which are the only values where the factors are maintained during the designed experiment. Note that the levels of factor C are attributes. Each factor's high level is indicated by "+1" and their corresponding low level is indicated by "-1". (c) Factors A and B, as well as their interaction AB, were found to have a significant effect on the response, since they managed to change the response value to outside of its inherent variation. Factor C and all other interactions are insignificant and can be ignored in future optimisation studies.

The six aspects of airlift reactor design that were identified in Section 5.1 will be used as six factors in the DOE study to establish their effects on the response, the velocity profile in the riser section of the airlift reactor.

5.2.1 Full factorial designs

In full factorial design experiments all the factors are completely considered. The experiment is carried out by studying all possible unique treatments to evaluate all the factors at all their required levels. With a full factorial design experiment the effects of all factors and all interactions can be determined. Also, if factors are evaluated at more than two levels, a full factorial design experiment can tell if the effects on the response are linear or nonlinear. The number of treatments required to perform a full factorial design experiment is calculated by:

$$n = L^f \quad (5.1)$$

where n = number of treatments required
 L = number of levels per factor
 f = number of factors

It is clear that the size of a full factorial design can become enormous with the addition of every extra factor to be considered; even more so if the factors are to be evaluated at many levels. If many factors need to be investigated, it is advisable to first screen the factors and only use the significant factors in subsequent full factorial design experiments with more than two levels for further optimisation.

5.2.2 Screening designs

Screening designs are types of fractional factorial designs which can investigate the same number of factors, but with far less treatments compared to a full factorial design. Unfortunately some of the information is lost when opting for a screening design, but the trade-off in time saved, makes screening designs the recommended starting place when a system with many factors need to be investigated. Subsequent full factorial design experiments can be performed on the screened factors for further optimisation.

With a screening design experiment the factors are evaluated at two levels, and as a result can therefore not give any indication whether the effects are linear or nonlinear. Also, although scarce, the existence of three-factor and higher interactions cannot be detected with screening design experiments. But the main disadvantage of screening designs however, is the confusion of effects

that is created by the confounding of factors and interactions, where the same effect is calculated for factors and interactions. Confounded effects are called aliases and can be between a factor and an interaction or between an interaction and another interaction.

Plackett-Burman designs [Wang et al., 2009] are screening designs that can be used to study $n-1$ factors with n treatments in which n is divisible by four. For example, 7 factors can be studied with 8 treatments. If n is also a power of two, like in the case with 7 factors and 8 treatments, the design is said to be geometric. In geometric designs the confounding of the effects is complete, meaning that they are identical in size, but possibly opposite in sign. Designs are nongeometric if n is divisible by four, but is not a power of two, like in the case with 11 factors and 12 treatments. In nongeometric designs each factor is partially confounded with all interactions that do not contain the factor. The Plackett-Burman design for 7 factors and 8 treatments are shown in Table 5.1. Table 5.1 also shows the aliases, and since this is a geometric design, the confounding is complete. For example, in the case of factor A:

$$E(A) = -E(BD) = -E(CG) = -E(EF)$$

where $E(A)$ = effect of factor A

$E(BD)$ = effect of interaction BD

$E(CG)$ = effect of interaction CG

$E(EF)$ = effect of interaction EF

Table 5.1: Plackett-Burman design for 7 factors (factors A, B, C, D, E, F and G) and 8 treatments. Each factor is completely confounded with three interactions, but is opposite in sign. The “+” and “-” signs in each treatment indicate the required high or low level of the corresponding factor for the specific treatment.

Treatment	A	B	C	D	E	F	G
1	+	-	-	+	-	+	+
2	+	+	-	-	+	-	+
3	+	+	+	-	-	+	-
4	-	+	+	+	-	-	+
5	+	-	+	+	+	-	-
6	-	+	-	+	+	+	-
7	-	-	+	-	+	+	+
8	-	-	-	-	-	-	-
	-BD	-AD	-AG	-AB	-AF	-AE	-AC
	-CG	-CE	-BE	-CF	-BC	-BG	-BF
	-EF	-FG	-DF	-EG	-DG	-CD	-DE

5.3 Screening of system hydrodynamic factors

The six system hydrodynamic factors identified in Section 5.1, with potential effects on the velocity profile in the riser section of an airlift reactor, will be screened in a screening design experiment to determine all the significant factors and two-factor interactions.

5.3.1 Experimental set-up

The configuration of the experimental set-up needed to be flexible to accommodate all the combinations of factor levels that were required for the different treatments of the screening design. Since many treatments needed to be performed, it was important that changing the configuration from one treatment to the next treatment was done in a swift manner to save time. At the same time these changes needed to be accurate to ensure that the correct levels were maintained throughout the experiment. For these reasons an experimental set-up was devised that consisted of many interchangeable parts that could be quickly fitted together and then slotted into the correct positions.

An airlift reactor was constructed within a PVC tank. PVC sheet baffle plates were inserted in the tank to divide it into riser and downcomer sections. The tank contained slots which guided the baffle plates when inserted into the tank, provided stability for the baffle plates during aeration and kept the baffle plates in the correct positions to ensure that the ratio of the downcomer to riser cross-sectional area remained at the right levels. The baffle plates were connected with steel rods for increased stability and to allow for the baffle plates to be easily slid into the correct position to create the required ratio of the downcomer to riser cross-sectional area. Additional PVC sheets could also be fitted on top of these baffle plates, when required, to change the top clearance distance. The baffle plates were supported by steel rod feet, which could also be adjusted, when required, to change the bottom clearance distance. Two air spargers were used in this experiment to fit the two riser sections widths that were created as a result of the two levels of the downcomer to riser ratio factor. The air spargers were identical in design, except for their lengths. Each air sparger was fabricated from a 15 mm (OD) PVC pipe that stretched from baffle plate to baffle plate; containing a single line of 2 mm holes, spaced 50 mm apart, on the top. The baffle plates could support the air sparger at two positions: 200 mm above the bottom of the baffle plates inside the riser section or at the bottom of the tank at the baffle plates' steel rod feet. The relative large holes of the air spargers reduced the pressure drops across them and enabled a blower, even at the relative deep water depths of this experiment, to supply air at constant rates. The air flow rate

was measured with a flow meter and maintained at constant flows to produce the required levels of aeration intensities in the riser section. Tap water was used to fill the airlift reactor. The correct water depth was achieved by making up with tap water or draining the airlift reactor; both which could be done quickly.

The tank housing the airlift reactor was made from grey PVC sheets, but one half of the front side contained a clear PVC sheet to enable visual observation of the hydrodynamic behaviour inside the tank. The use of the clear PVC sheet was restricted to only half of the one side, since the clear PVC sheet had a thickness of 6 mm compared to the grey PVC sheet thickness of 10 mm that consequently limited the ability of the clear PVC sheet to sufficiently withstand the water pressure. Figure 5.4 shows the PVC tank construction and the baffle plate framework that was slotted inside the PVC tank to create the different airlift reactor configurations.

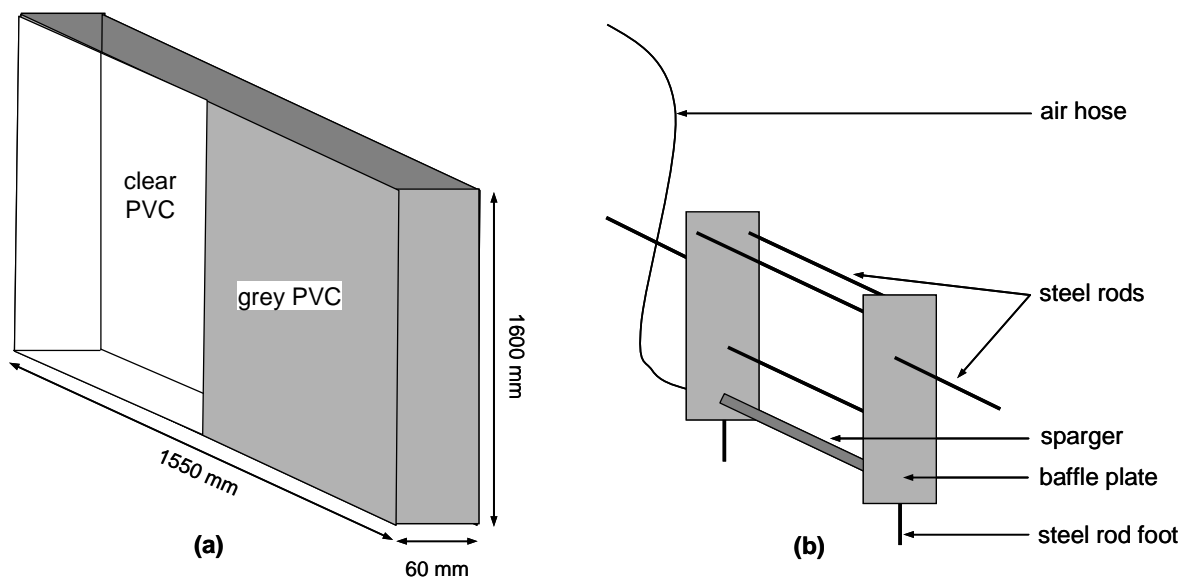


Figure 5.4: Experimental set-up for the screening of system hydrodynamic factors: (a) PVC tank with one half of the front containing a clear PVC sheet and (b) the baffle plate framework which could be changed to create different airlift reactor configurations when slotted inside the PVC tank.

5.3.2 Method

Eventually two facets of the response, the velocity profile in the riser section, must be optimised simultaneously to find the best values of the system hydrodynamic factors for optimised scouring efficiency: magnitude and uniformity. Both these facets can be assessed by measuring the linear liquid velocities across the width of the riser section.

Linear liquid velocity measurement

Linear liquid velocity is a critical operating parameter of airlift reactors and considerable attention has been given to its measurement. However, since the liquid flow behaviour tends to be very complex, it is difficult to measure it directly and usually requires some form of tracer measurement. The tracer is introduced somewhere in the circulation fluid flow path of an airlift reactor and a certain unique property of the tracer is used to detect its arrival some time later downstream in the circulation fluid flow path. The linear liquid velocity can therefore be deduced from the known path distance and the measured travel time of the tracer. Typical tracer measurements include measuring the conductance increase after a salt injection [Hwang and Cheng, 1997; Couvert et al., 1999; Lu et al., 2000]; visually observing colour after a dye injection [Chisty and Moo-Young, 1987; Wongsuchoto et al., 2003]; measuring the pH change after an acid or base injection [Chisty et al., 1988; Livingston and Zhang, 1993; Choi et al., 1996; Couvert et al., 2001]; and measuring the temperature change after a cold or hot stream injection [Dhaouadi et al., 1996].

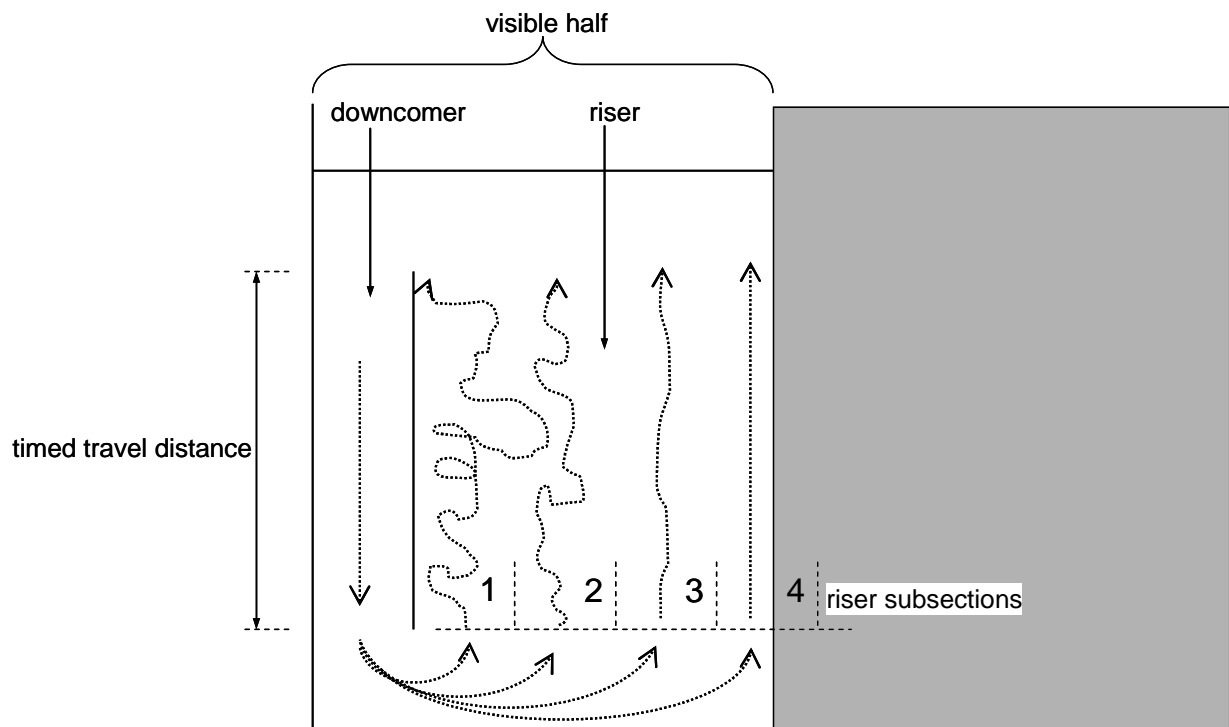
The abovementioned techniques for linear liquid velocity measurement would be impractical, unsafe and expensive in a screening design where numerous measurements would have to be taken in quick succession. Since the relative values, rather than the actual values, of the velocity profiles in the screening design is of importance, it was decided therefore to rather use an indication of the linear liquid velocities to compile velocity profiles. A similar approach was taken by Liu et al. [2003] where the observed velocity of the mixed liquor was assumed as the actual liquid velocity. In this study clearly visible grey polypropylene (PP) pieces of approximately 1 cm^3 with a measured density of 0.97 g/cm^3 that were dragged with the circulation fluid flow were found to work well in this regard.

The PP pieces were added with the tap water in the tank and used as visual tracers to indicate the liquid velocity. With the airlift reactor in operation, the circulation flow would drag the PP pieces down the downcomer sections and again up in the riser section. The PP pieces were well distributed below the riser section to rise up across the whole riser section. The times it took the PP pieces to travel the distance from the bottom of the baffle plate to the top of the baffle plate in

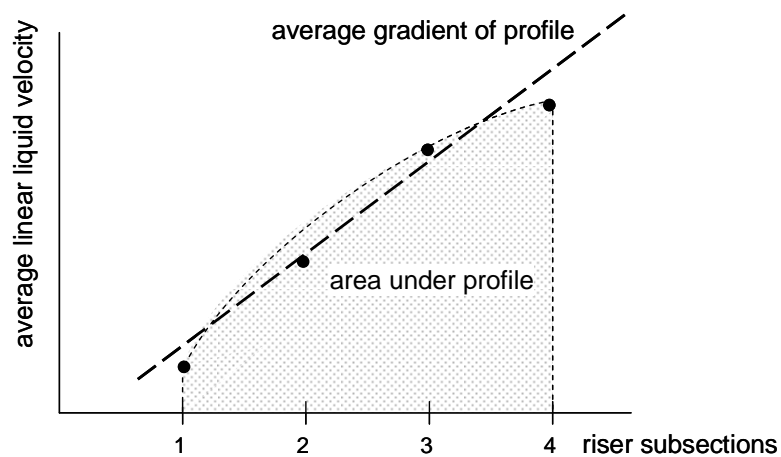
the riser section were measured and converted to linear velocities. This was an inexpensive velocity measurement technique and could be quickly repeated for any number of trials. Although this may not be an accurate measurement of the linear liquid velocities, because of the slight buoyancy of the PP pieces, this technique still produced comparable indications from which the effects of the factors on the hydrodynamics of the system could be calculated.

Response calculation

The baffle plate frameworks that were slotted in the tank were symmetrical - each time creating the riser section in the middle with the downcomer sections on the sides. As a result, one downcomer and exactly one half of the riser section could be seen through the clear PVC sheet that made up one half of the tank's front side. It was assumed that, since the geometry is symmetrical, the hydrodynamic field pattern in the riser section would also be symmetrical and that it would only be necessary to attain a velocity profile of the visible half of the riser section. The width of the entire riser section was divided into seven subsections, stretching from the bottom to the top, with three and a half subsections therefore located in the visible part of the riser section. The calculated linear liquid velocities of the PP pieces were allocated to the specific visible subsection where they entered the riser section, as is explained in Figure 5.5(a). For each subsection an average linear liquid velocity was calculated from 10 measurements. Therefore, 40 measurements were required for each experimental treatment to calculate four average linear liquid velocities from which a velocity profile could be compiled. From the velocity profile, the area under the profile, as well as the average gradient of the profile were calculated as outputs for the effects on velocity profile magnitude and velocity profile uniformity respectively. Figure 5.5 explains this velocity profile quantification procedure. For the velocity profile magnitude in the riser section to be optimised, the area of the integrated velocity profile in the riser section must be maximised, and for the velocity profile uniformity to be optimised, the gradient of the velocity profile in the riser section must be equal to zero. Although the velocity profile was only determined for one half of the riser section, it was assumed that, since the geometry is symmetrical, that the velocity profile magnitude will be exactly the same in the other half and that the velocity uniformity will be the same in the other half, but with an average gradient opposite in sign. Since the riser subsections represent normalised distance to enable comparison of the two riser section widths, the velocity profile area and gradient do not have units and only indicate relative values for the same system.



(a)



(b)

Figure 5.5: Velocity profile quantification: (a) hypothetical pathways of PP pieces when entering the riser section in the different subsections and (b) hypothetical plotted average linear liquid velocities calculated for each subsection to compile a velocity profile across the riser section. The magnitude of the velocity profile is indicated by the area under the profile and the uniformity is indicated by the average gradient of the profile.

Design of experiment

The six factors in the experiment that controls the system hydrodynamics will most probably exhibit nonlinear behaviours, but to reduce the experimental work of the factorial design experiment, the factors were assumed to be linear and that evaluation at two levels would provide for adequate estimations of their effects. Table 5.2 shows the different levels at which each factor were evaluated. The “+1” indicates the high level and the “-1” indicates the low level of the factor. The values of these levels were determined by the physical limitations of the experimental set-up, ease of measuring and practicality for continuously changing the baffle plate framework for the various geometrical arrangements. For simplification the six factors will be referred to by the symbols A to F as is indicated in Table 5.2.

Table 5.2: Values of the levels at which each factor was evaluated.

Factors	Levels	
	- 1	+ 1
A: A_d/A_r	0.5	2
B: Top clearance distance	100 mm	200 mm
C: Bottom clearance distance	30 mm	100 mm
D: Aeration intensity	800 L/(m ² ·min)	1 350 L/(m ² ·min)
E: Water depth	1 100 mm	1 400 mm
F: Air sparger position	Bottom (very bottom of tank below riser section)	Riser section (200 mm above bottom of baffle plates)

From Equation 5.1, a full factorial design of these six factors at two levels would require 64 (2^6) independent experimental treatments, and when replication is included to determine the experimental error, a total amount of 128 ($2^6 + 2^6$) independent experimental treatments would be required. A full factorial design would therefore have consumed a lot of experimental time, and it was decided that a screening design, an 8 treatment Plackett-Burman design with 7 factors [Clauhan et al., 2007; Vatanara et al., 2007; Mukherjee et al., 2008; Dejaegher et al., 2009; Oita et al., 2009], as was shown in Table 5.1, would be utilised. In this case the 7th factor was a so-called dummy factor, since it did not represent any process parameter. Unfortunately, in a screening design the effects could be confounded with each other and is an additional reflection required to

determine the main factor effects. A reflection treatment is an inverse of a base treatment where the factors are evaluated at opposite levels as compared to the levels they were evaluated at in the base treatment. In this case the base and reflection treatments would require 16 independent experimental treatments, and including replication to determine the experimental error, a total of 32 treatments would be required to determine the effects of the factors. These treatments had to be performed in a random order to reduce the experimental error by eliminating the effects of potential unknown factors such as changing water temperature.

It was expected that numerous two-factor interactions would also exist and that their effects should also be determined. Each two-factor interaction was investigated in a two-factor two-level (2^2) full factorial design by only changing the levels of the factors investigated and leaving the other factors unchanged in the six-factor treatment configurations. After carefully examining the unique treatments required to capture all two-factor interactions in the six-factor treatment configurations, it was found that 22 unique six-factor treatment configurations would be required. However, six of these treatments were already captured in the base and reflection treatments to determine the factor effects. Therefore, 16 additional treatments were required, and with replication to determine the experimental error, 32 independent treatments were required to determine the interaction effects. These treatments also had to be randomised to reduce the experimental error. Since only two factors are investigated at a time in these treatments, the levels of the factors not considered were set at the levels which were the easiest to set-up to save time. For this reason factor F, the sparger position, was kept at the "+1" level when not investigated, since it could be quickly installed and removed from the riser section. Similarly, factor E, the water depth, was kept at the "-1" level when not investigated, since a lower water depth made the insertion and removal of the baffle plate framework in and out of the PVC tank much more easier.

Consequently, the total factorial design experiment consisted of 32 independent experimental treatments with 32 replicate treatments; each treatment providing a value for the integrated area under the velocity profile and a value for the average gradient of the velocity profile. Since the same system with the same six-factor configurations were used for all the treatments, it was decided to perform the whole experiment of base, reflection, full factorial and all replication treatments in one randomised experiment to determine the experimental error for all 32 treatments and evaluate all the calculated effects against the same standard error of the effect. For these 32 treatments the degrees of freedom were 32, and for evaluating the effects at a 95% significant level, the tabular t-value of 2.04 from statistical tables was used to determine the experimental errors for both the integrated area under the velocity profile and the average gradient of the velocity profile outputs. The treatments of the whole experimental design are shown in Table 5.3 and the treatments used to perform the full factorial designs are shown in Table 5.4.

Table 5.3: The treatments for the experimental design of the base, reflection and full factorial treatments. The “+” and “-“ signs indicate the setting of the levels. The order indicates the randomisation of the treatments and their replicates. The shaded treatments indicate treatments that were already covered in the base and reflection treatments.

	Treatment	A	B	C	D	E	F	Order
Base	1	+	-	-	+	-	+	4, 18
	2	+	+	-	-	+	-	16, 30
	3	+	+	+	-	-	+	54, 55
	4	-	+	+	+	-	-	6, 9
	5	+	-	+	+	+	-	41, 43
	6	-	+	-	+	+	+	53, 56
	7	-	-	+	-	+	+	7, 8
	8	-	-	-	-	-	-	42, 45
Reflection	9	-	+	+	-	+	-	44, 59
	10	-	-	+	+	-	+	46, 57
	11	-	-	-	+	+	-	1, 31
	12	+	-	-	-	+	+	47, 52
	13	-	+	-	-	-	+	19, 20
	14	+	-	+	-	-	-	3, 17
	15	+	+	-	+	-	-	39, 40
	16	+	+	+	+	+	+	2, 5
Full factorial	17 (1)	-	-	-	-	-	+	10, 24
	(13) (2)	-	+	-	-	-	+	
	18 (3)	-	-	-	+	-	+	12, 25
	19 (4)	-	-	+	-	-	+	13, 15
	20 (5)	-	+	+	-	-	+	11, 14
	(10) (6)	-	-	+	+	-	+	
	21 (7)	-	-	+	-	-	-	26, 51
	22 (8)	-	-	-	+	-	-	27, 58
	23 (9)	-	+	-	-	-	-	28, 64
	24(10)	+	-	-	-	-	+	21, 36
	25(11)	+	+	-	-	-	+	32, 48
	26(12)	+	-	+	-	-	+	33, 37
	(1)(13)	+	-	-	+	-	+	
	(12)(14)	+	-	-	-	+	+	
	27(15)	-	-	-	-	+	+	34, 60
	28(16)	-	+	-	-	+	+	35, 61
29(17)	-	-	-	+	+	+	23, 62	
(7)(18)	-	-	+	-	+	+		
30(19)	+	-	-	-	-	-	29, 49	
(8)(20)	-	-	-	-	-	-		
31(21)	-	+	-	+	-	+	22, 38	
32(22)	-	-	-	-	+	-	50, 63	

Table 5.4: The treatments (from the full factorial section of Table 5.3) used in the full factorial designs to determine the effects of the interactions. The “+” and “-“ signs indicate the levels of the respective factors in the same order as the name of the interaction. The numbers of the shown treatments refer to numbers 1 to 22 mentioned in the full factorial section of Table 5.3.

Interaction	++	+-	-+	--
AB	11	10	2	1
AC	12	10	4	1
AD	13	10	3	1
AE	14	10	15	1
AF	10	19	1	20
BC	5	2	4	1
BD	21	2	3	1
BE	16	2	15	1
BF	2	9	1	20
CD	6	4	3	1
CE	18	4	15	1
CF	4	7	1	20
DE	17	3	15	1
DF	3	8	1	20
EF	15	22	1	20

Effects calculation

A main effect is defined as the difference between the average of all the responses when a factor is evaluated at its high level and the average of all the responses when the same factor is evaluated at its low level. The main effect of factor X is calculated as [Barrentine,1999]:

$$E(X_i) = \bar{Y}_{X_{i+}} - \bar{Y}_{X_{i-}} = \frac{\sum Y_{X_{i+}} - \sum Y_{X_{i-}}}{N} \quad (5.2)$$

where $E(X_i)$ = main effect of factor X_i

$\bar{Y}_{X_{i+}}$ = average of the responses when factor X is at its high level

$\bar{Y}_{X_{i-}}$ = average of the responses when factor X is at its low level

$Y_{X_{i+}}$ = response when factor X is at its high level

$Y_{X_{i-}}$ = response when factor X is at its low level

N = number of treatments per level evaluation

An interaction is defined as one half the difference of the effect of a factor at another factor's high level and this other factor's low level. The interaction effect is calculated as [Barrentine, 1999]:

$$E(X_i X_j) = \frac{1}{2} \left[(\bar{Y}_{X_{i+}} - \bar{Y}_{X_{i-}})_{X_{j+}} - (\bar{Y}_{X_{i+}} - \bar{Y}_{X_{i-}})_{X_{j-}} \right] \quad (5.3)$$

where $E(X_i X_j)$ = effect of interaction $X_i X_j$ between factors X_i and X_j

X_{i+} = condition of factor X_i at its high level

X_{i-} = condition of factor X_i at its low level

X_{j+} = condition of factor X_j at its high level

X_{j-} = condition of factor X_j at its low level

With the main effects and the interaction effects known, a model can be created to calculate and predict the response for any arrangement of factor levels [Barrentime, 1999]:

$$Y = \bar{Y} + \frac{1}{2} \sum E(X_i) X_i + \frac{1}{2} \sum E(X_i X_j) X_i X_j \quad (5.4)$$

where Y = the calculated response

\bar{Y} = the average of all responses of data

X_i = the level of factor X_i (like -1 or +1)

$X_i X_j$ = the product of the levels of interaction $X_i X_j$ constituent factors (like -1 x -1 = +1)

Significance of effects

The variance for a unique factor treatment was calculated by using the observed responses:

$$S_i^2 = \frac{\sum (Y_i - \bar{Y})^2}{n-1} \quad (5.5)$$

where S_i^2 = variance of the treatment

Y_i = independent response

\bar{Y} = average response for the treatment

n = number of independent treatments performed

The average standard deviation for the effects is calculated by:

$$S_e = \sqrt{\frac{\sum S_i^2}{k}} \quad (5.6)$$

where S_e = average standard deviation for the effects

k = number of unique treatments in the experiment

S_e for the 32 treatments were calculated as

For this experiment the degrees of freedom (df) are calculated by:

$$\begin{aligned} \text{df} &= (\text{number of observations per treatment} - 1) \times (\text{number of treatments}) \\ &= (2 - 1) \times 32 = 32 \end{aligned}$$

For degrees of freedom of 32 the tabular t-value from statistical tables for a significant level of 95% is 2.04. Therefore, the absolute decision limits (DL) for the significance of effects in this experiment is shown in Table 5.5.

Table 5.5: The decision limits for the significance of effects.

	Velocity profile area	Velocity profile gradient
df	32	32
S_e	0.0646	0.0120
DL	0.1318	0.0245

5.3.3 Results

Area under the velocity profile

Factor A and interaction DF were found to be 99.9% and 95% significant respectively in determining the area under the velocity profile. The model to predict the area under the velocity profile includes the average of all the treatments' responses, the determined effects of all the significant factors and interactions, as well as the determined effects of the factors of the significant interactions (hierarchy rule states that the main factors of all significant interaction effects must be included). Using Equation 5.4, the 95% significant model for the prediction of the area under the velocity profile can therefore be written as:

$$Y_{area} = \bar{Y}_{area} + \frac{E(A)}{2}A + \frac{E(D)}{2}D + \frac{E(F)}{2}F + \frac{E(DF)}{2}DF$$

When including the average value of all the treatments' responses and the effects on the area under the velocity profile, as was determined in this experiment, the model can be written as:

$$Y_{area} = 0.6003 + \frac{0.2732}{2}A + \frac{0.0189}{2}D + \frac{-0.0317}{2}F + \frac{0.1710}{2}DF \quad (5.7)$$

Consequently, if Y_{area} has to be maximised for improved fluid flow velocity in the riser section, and considering the +1 and -1 levels of this experiment, A and DF must both be equal to 1. For DF to be equal to 1, the product of D and F must be equal to 1. To counter factor F 's negative effect, F must be equal to -1, and consequently D too. Therefore, only considering the chosen levels, as shown in Table 5.2, the airlift reactor arrangement which would have the highest fluid flow velocity in the riser section would have an A_d/A_r ratio of 2, be operated with an aeration intensity of 800 L/(m²·min) and have the sparger positioned at the bottom of the tank. The other factors did not seem to influence the fluid flow velocity in the riser section. Experimental data can be found in Addendum E.

Average gradient of the velocity profile

Factors C and F , and interactions CF and DF , were found to be 99.9% significant. Interactions AD , BD , BF , CD , DE and EF were found to be 99% significant. As with the area under the velocity profile, using the average of all the treatments' responses and the determined effects on the

average gradients of the velocity profiles, the same procedure can be followed to arrive at the 95% significant model for the prediction of the average gradient of the velocity profile:

$$\begin{aligned}
 Y_{gradient} = & -0.0122 + \frac{0.0136}{2}A + \frac{0.0181}{2}B + \frac{0.0615}{2}C + \frac{-0.0112}{2}D + \frac{0.0226}{2}E + \\
 & \frac{-0.0987}{2}F + \frac{0.0343}{2}AD + \frac{0.0410}{2}BD + \frac{-0.0431}{2}BF + \frac{0.0387}{2}CD + \frac{-0.0817}{2}CF + \\
 & \frac{0.0428}{2}DE + \frac{-0.0813}{2}DF + \frac{-0.0388}{2}EF
 \end{aligned} \tag{5.8}$$

To optimise the uniformity of the fluid flow in the riser section, the average gradient of the velocity profile $Y_{gradient}$ needs to be equal to zero. Using the solver function of Microsoft's Excel, and considering the +1 and -1 levels of this experiment, an optimised average gradient of the velocity profile could be achieved by evaluating the factors at the following levels:

A → +1

B → +1

C → -1

D → -1

E → -1

F → +1

Therefore, only considering the chosen levels, as shown in Table 5.2, the airlift reactor arrangement which would have the most uniform fluid flow in the riser section would have an A_d/A_r ratio of 2, have a top clearance distance of 200 mm, have a bottom clearance distance of 30 mm, be operated with an aeration intensity of 800 L/(m²·min), have a water depth of 1 100 mm and have the sparger positioned inside the riser section (200 mm above the bottom of the baffle plates). Experimental data can be found in Addendum E.

5.4 Validation of system hydrodynamic factors

The models that were developed for calculating the responses on the velocity profile in the riser section (see Section 5.3.3) for the experimental set-up of Section 5.3.1 must be validated.

5.4.1 Experimental set-up

The experimental set-up for validating the effects of the system hydrodynamic factors was the same as the experimental set-up described in Section 5.3.1, but instead of tap water, the PVC tank was filled with a particulate suspension of bentonite. The bentonite suspension of approximately 0.3 g/L was prepared as described in Addendum A. Also, a flat-sheet membrane element was installed in the riser section and was fabricated as explained in Addendum B with an active area of 0.335 m². The membrane element was tightly secured within the baffle plate framework and was located right in the middle of the riser section width. The active membrane area had a width of 429 mm and was wide enough to be exposed to a nonuniform velocity profile in all studied configurations. The water head above the immersed membrane element was kept constant throughout the experiment at 250 mm to ensure that all TMP changes could only be ascribed to membrane fouling. Similar to the flux-step experiment described in Section 4.3.2, a peristaltic pump withdrew permeate and returned it to the tank while a water manometer measured the increase in TMP across the membrane.

5.4.2 Method

Levels for the six factors were chosen to produce four airlift reactor configurations in such a way that the one configuration would produce the maximum velocity profile area according to the prediction of Equation 5.7, one configuration would produce the most uniform velocity profile according to Equation 5.8 and the other two would produce poor velocity profile areas and gradients according to Equations 5.7 and 5.8. The levels were maintained at the same values as explained in Table 5.2.

The flux-step approach, as was applied in Section 4.3, was used to compare the different configurations' abilities to scour the immersed membrane to limit membrane fouling. Two pure water flux treatments were conducted at permeate fluxes incremented by 4 L/(m²·h) from 4 L/(m²·h) to 40 L/(m²·h) to determine the membrane resistance. Thereafter the configurations were evaluated in independent bentonite suspension treatments by incrementing the permeate flux

by 4 L/(m²·h) from 4 L/(m²·h) to 28 L/(m²·h). Each constant permeate flux was maintained for 30 minutes to ensure that internal fouling has stabilised and that any subsequent fouling could be attributed to cake layer formation alone. During these 30 minute periods the TMP was regularly recorded and the permeate flux, air flow rate and suspension temperature measured to confirm they stay relatively constant. The permeate flux did not vary more than 0.4 L/(m²·h) from the intended permeate flux and the treatments were conducted at suspension temperatures of 20 ± 3°C. Table 5.7 shows the order in which the treatments were performed.

The PVC tank in the experiment was much larger than the tank used in the fouling experiments described in Chapter 4 and with the much larger downcomer sections when evaluating the A_d/A_r ratio at 2 (at its +1 level), bentonite would settle in the dead zones of the downcomer sections to reduce the concentration of suspended bentonite. In order to maintain the suspended bentonite at a constant concentration to enable the sensible comparison of membrane fouling data, it was decided to operate at a much lower bentonite concentration of approximately 0.3 g/L (compared to 1.0 g/L in the fouling experiments of Chapter 4) and continuously add bentonite during the experiment. As explained in Addendum A, a suspended bentonite calibration curve was compiled which correlates suspended bentonite concentration with turbidity measured in NTU. From the calibration curve the turbidity of the suspension was maintained at 128 ± 11 NTU by continuously adding small amounts of dry bentonite to ensure that the suspended bentonite concentration remained between 0.31 g/L and 0.37 g/L throughout the experiment.

A simple backwash procedure, prior to an experimental treatment, proved to be adequate in restoring the original hydraulic resistance of the membrane, therefore removing all particles within, as well as on the membrane surface.

Table 5.6: Different airlift reactor configurations chosen to validate their predicted velocity profile areas and gradients as predicted by Equations 5.7 and 5.8. The “+1” and “-1” indicate the respective high and low levels of the specific factor as is explained in Table 5.2. Configuration 1 represents the configuration with the most uniform velocity profile and configuration 2 represents the configuration with the highest velocity profile area.

Configuration	A	B	C	D	E	F	Predicted velocity profile area	Predicted velocity profile gradient
1	+1	+1	-1	-1	-1	+1	0.6261	0.0003
2	+1	-1	+1	-1	+1	-1	0.8288	0.0432
3	+1	-1	-1	-1	-1	+1	0.6261	0.0663
4	-1	-1	+1	+1	-1	+1	0.5428	-0.1438

Table 5.7: The random order in which the treatments were conducted to minimise the risk of unknown influences on the results. The configuration numbers correlate with the configurations listed in Table 5.6.

	Tap water	Bentonite suspension (0.3 g/L)
Configuration 1 (without aeration)	1, 2	
Configuration 1		7, 10
Configuration 2		3, 5
Configuration 3		4, 6
Configuration 4		8, 9

5.4.3 Results

The average stabilised membrane fouling rates for each configuration at each permeate flux is shown in Figure 5.6. Configuration 1 with the predicted most uniform velocity profile had the lowest membrane fouling rate at any of the permeate fluxes and displayed sub-critical flux operation up to a permeate flux of $16 \text{ L}/(\text{m}^2 \cdot \text{h})$. Configuration 2 with the highest velocity profile area performed worse than configuration 1, but better than the other at lower permeate fluxes. Experimental data can be found in Addendum F.

From Figure 5.6 it was estimated, using the technique explained in Figure 4.2, that the critical flux in the different configurations was:

Configuration 1 $\rightarrow 16 \text{ L}/(\text{m}^2 \cdot \text{h})$

Configuration 2 $\rightarrow 11 \text{ L}/(\text{m}^2 \cdot \text{h})$

Configuration 3 $\rightarrow 6 \text{ L}/(\text{m}^2 \cdot \text{h})$

Configuration 4 $\rightarrow 4 \text{ L}/(\text{m}^2 \cdot \text{h})$

When considering the critical fluxes of the different configurations, there seems to be an increase in critical flux with an increase in the predicted uniformity of the velocity profile as calculated by Equation 5.8. An increase in the predicted velocity profile area also seems to reduce the membrane fouling rate, especially at lower permeate fluxes. Both Equations 5.7 and 5.8 therefore seems to give a correct indication of the velocity profile and its effect in reducing membrane fouling. The velocity profile uniformity seems to have a much greater impact on the velocity profile's ability to scour the membrane surface, than the velocity profile area.

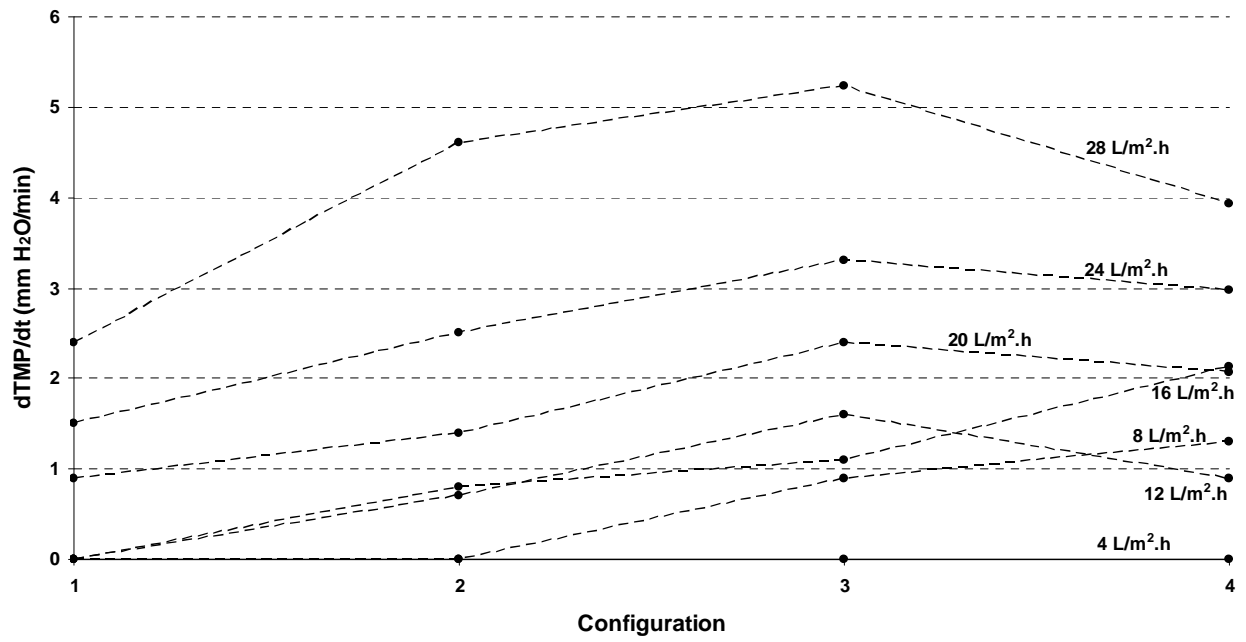


Figure 5.6: Average membrane fouling rates for the different configurations. Although not shown for the sake of clarity, the variability in the fouling rate increased with an increase in absolute velocity profile gradient and was therefore the highest for configuration 4.

Chapter 6

Conclusions

6.1 Introduction

Immersed membrane systems hold many operational and environmental advantages over conventional activated sludge systems, and even sidestream membrane systems. However, except for certain niche applications, immersed membrane systems cannot compete with conventional activated sludge systems when comparing for lowest capital and operating costs. The higher costs associated with immersed membrane systems, as a result of membrane fouling, have made them fairly unattractive in the wastewater treatment field to date. However, the capital layout required for immersed membrane systems has been steadily decreasing over the last two decades, relative to conventional systems, and because of ever-increasingly stringent environmental legislation, immersed membrane systems are more and more considered for new wastewater treatment projects. Retrofitting of existing conventional activated sludge systems with immersed membranes is also becoming more prominent.

Unfortunately operating costs remain high for immersed membrane systems with the largest portion by far dedicated to coarse bubble aeration of the membranes to reduce fouling. In the current climate of worldwide rising energy prices an incentive exists to optimise immersed membrane operation, especially by increasing the air-scouring efficiency. In achieving this, and therefore reducing unit operating cost, immersed membrane systems will develop into a relevant wastewater treatment technology with very unique solutions – perfectly positioned in the global showdown for greener living.

From this study it turned out that air-scouring is not as trivial a matter as was previously believed and that great care must be taken to ensure that the immersed membrane system as a whole is conducive for improved system hydrodynamics for increased air-scouring. Failure to consider system hydrodynamics can promote membrane fouling, even when aeration is increased or intensified.

6.2 Air-scouring efficiency

By nature membrane filtration will always result in membrane fouling, but the fouling rate can be reduced by increasing the efficacy of back-transport mechanisms to remove material from the membrane surface. Air-scouring is usually applied in immersed membrane systems to induce flow across the membrane surfaces to enhance back-transport.

Contrary to what was previously believed, it was found in this study that increasing the air flow rate for an increase in aeration intensity does not necessarily translate to an increase in scouring ability to remove more material from the membrane surfaces. In certain instances an increase in aeration intensity has no effect on the air-scouring ability and could even promote localised fouling. Consequently, by operating immersed membrane systems at increased aeration intensities the resulting low air-scouring efficiencies can seriously jeopardise operating costs of incorrectly designed membrane reactors.

It was found that the air-scouring efficiency is increased by ensuring a uniform cross-flow velocity profile across the membrane surfaces. With a uniform cross-flow velocity profile across the membrane surfaces the same air-scouring ability can be achieved at much lower aeration intensities to significantly increase air-scouring efficiency. A uniform cross-flow velocity profile eliminates localised critical fluxes and selective fouling as permeate flux is increased. With the onset of localised fouling the effective permeate flux for the remaining membrane surface is increased to exceed local critical fluxes and initiate cake layer formation. This vicious cycle is continuously repeated across the whole membrane surface to result in high observed fouling rates. In other words, if localised fouling can be avoided by maintaining a uniform cross-flow velocity profile across the membrane surface, then the membrane will experience only internal fouling until steady state is reached for sub-critical fluxes and slow even cake layer formation for permeate fluxes above the critical flux.

6.3 System hydrodynamic factors

This study highlighted the importance of immersed membranes located in the riser section of an airlift reactor as opposed to simply immerse membranes in bubble reactors. Airlift reactors are capable of providing fast rising and unidirectional bubbles to scour membrane surfaces. Bubble reactors, on the other hand, display chaotic bubble patterns which are less efficient in scouring membrane surfaces.

With the introduction of airlift reactor geometry, the system hydrodynamics of the airlift reactor must be considered if the cross-flow velocity profile in the riser section, and therefore across the membrane surfaces, were to be improved. Six system hydrodynamic factors were investigated in this study and the most important factor identified was the ratio of the total downcomer to riser cross-sectional areas (A_d/A_r). The higher the value of A_d/A_r , the faster is the velocity profile in the riser section.

When designing an airlift reactor with the purpose of air-scouring immersed membranes, the following methodology must be considered to improve air-scouring efficiency:

- choose A_d/A_r as high as physically allowed in the design (higher than the “+1” level used in this study) ;
- opt for placing the air sparger at the very bottom of the tank below the riser section (similar to the “-1” level used in this study); and
- rather operate at lower aeration intensities (similar to the “-1” level used in this study) to also improve air-scouring efficiency.

These steps, according to Equation 5.7 developed in Chapter 5, will provide a fast velocity profile, but not necessarily a uniform velocity profile. As was proven in this study, the uniformity of the velocity profile is critical in avoiding localised membrane fouling with severe fouling rates at higher permeate fluxes. With the values of the three abovementioned system hydrodynamic factors set, the levels of the remaining three factors (top clearance distance, bottom clearance distance and water depth) can be tailored by using Equation 5.8 to achieve a velocity profile with the lowest absolute gradient. The levels can also be extrapolated and evaluated outside of the “-1” to “+1” range.

References

- Ahn, K.-H., Cha, H.-Y. and Song, K.-G. (1999), **Retrofitting municipal sewage treatment plants using an innovative membrane-bioreactor system**, *Desalination*, **124**, pp. 279-286
- Al-Ahmad, M., Abdul Aleem, F.A., Mutiri, A. and Ubaisy, A. (2000), **Biofouling in RO membrane systems part 1: fundamentals and control**, *Desalination*, **132**, pp. 173-179
- Al Akoum, O., Jaffrin, M.Y., Ding, L., Paullier, P. and Vanhoutte, C. (2002), **An hydrodynamic investigation of microfiltration and ultrafiltration in a vibrating membrane module**, *Journal of Membrane Science*, **197**, pp. 37-52
- Alavi Moghaddam, M.R., Satoh, H. and Mino, T. (2001), **Effect of important operation parameters on the performance of coarse pore filtration activated sludge process**, IWA Conference on Water and Wastewater Management in Developing Countries, Kuala Lumpur, Malaysia
- Al-Masry, W.A. and Abasaeed, A.E. (1998), **On the scale-up of external loop airlift reactors: Newtonian systems**, *Chemical Engineering Science*, **53**(24), pp. 4085-4094
- Altena, F.W. and Belfort, G. (1984), **Lateral migration of spherical particles in porous flow channels: application to membrane filtration**, *Chemical Engineering Science*, **39**(2), pp. 343-355
- Aryal, R., Lebegue, J., Vigneswaran, S., Kandasamy, J. and Grasmick, A. (2009), **Identification and characterisation of biofilm formed on membrane bio-reactor**, *Separation and Purification Technology*, **67**, pp. 86-94
- Bacchin, P., Aimar, P. and Sanchez, V. (1995), **Model for colloidal fouling of membranes**, *AIChE Journal*, **41**(2), pp. 368-376
- Bacchin, P., Aimar, P. and Sanchez, V. (1996), **Influence of surface interaction on transfer during colloid ultrafiltration**, *Journal of Membrane Science*, **115**, pp. 49-63
- Bacchin, P., Si-Hassen, D., Starov, V., Clifton, M.J. and Aimar, P. (2002), **A unifying model for concentration polarization, gel-layer formation and particle deposition in cross-flow membrane filtration of colloidal suspensions**, *Chemical Engineering Science*, **57**, pp. 77-91

-
- Bai, R. and Leow, H.F. (2002), **Microfiltration of activated sludge wastewater – the effect of system operation parameters**, *Separation and Purification Technology*, **29**, pp. 189-198
- Baker, J.S. and Dudley, L.Y. (1998), **Biofouling in membrane systems – a review**, *Desalination*, **118**, pp. 81-90
- Barrentine, L.B. (1999), **An Introduction to Design of Experiments**, ASQ Quality Press, Milwaukee, Wisconsin
- Belfort, G. (1989), **Fluid mechanics in membrane filtration: recent developments**, *Journal of Membrane Science*, **40**, pp. 123-147
- Belfort, G., Pimbley, J.M., Greiner, A. and Chung, K.Y. (1993), **Diagnosis of membrane fouling using a rotating annular filter. 1. Cell culture media**, *Journal of Membrane Science*, **77**, pp. 1-22
- Belfort, G., Davis, R.H. and Zydney, A.L. (1994), **Review – The behavior of suspensions and macromolecular solutions in crossflow microfiltration**, *Journal of Membrane Science*, **96**, pp. 1-58
- Benkahla, Y.K., Ould-Dris, A., Jaffrin, M.Y. and Si-Hassen, D. (1995), **Cake growth mechanism in cross-flow microfiltration of mineral suspensions**, *Journal of Membrane Science*, **98**, pp. 107-117
- Bian, R., Yamamoto, K. and Watanabe, Y. (2000), **The effect of shear rate on controlling the concentration polarization and membrane fouling**, *Desalination*, **131**, pp. 225-236
- Bouhabila, E.H., Ben Aïm, R. and Buisson, H. (1998), **Microfiltration of activated sludge using submerged membrane with air bubbling (application to wastewater treatment)**, *Desalination*, **118**, pp. 315-322
- Bouhabila, E.H., Ben Aïm, R. and Buisson, H. (2001), **Fouling characterisation in membrane bioreactors**, *Separation and Purification Technology*, **22-23**, pp. 123-132
- Bowen, W.R. and Sharif, A.O. (1998), **Hydrodynamic and colloidal interactions effects on the rejection of a particle larger than a pore in microfiltration and ultrafiltration membranes**, *Chemical Engineering Science*, **53**(5), pp. 879-890
- Cabassud, C., Laborie, S., Durand-Bourlier, L. and Lainé, J.M. (2001), **Air sparging in ultrafiltration hollow fibres: relationship between flux enhancement, cake characteristics and hydrodynamic parameters**, *Journal of Membrane Science*, **181**, pp. 57-69
- Cabassud, C., Laborie, S. and Lainé, J.M. (1997), **How slug flow can improve ultrafiltration flux in organic hollow fibres**, *Journal of Membrane Science*, **128**, pp. 93-101
- Cauhan, K., Trivedi, U. and Patel, K.C. (2007), **Statistical screening of medium components by Plackett-Burman design for lactic acid production by *Lactobacillus* sp. KCP01 using date juice**, *Bioresource Technology*, **98**, pp. 98-103

-
- Chang, I.-S. and Judd, S.J (2002), **Air sparging of a submerged MBR for municipal wastewater treatment**, *Process Biochemistry*, **37**, pp. 915-920
- Chang, S. and Fane, A.G. (2001), **The effect of fibre diameter on filtration and flux distribution – relevance to submerged hollow fibre modules**, *Journal of Membrane Science*, **184**, pp. 221-231
- Chang, S., Fane, A.G. and Vigneswaran, S. (2002), **Experimental assessment of filtration of biomass with transverse and axial fibres**, *Chemical Engineering Journal*, **87**, pp. 121-127
- Chang, W.-K., Hu, A., Horng, R.-Y. and Tzou, W.-Y. (2007), **Membrane bioreactor with nonwoven fabrics as solid-liquid separation media for wastewater treatment**, *Desalination*, **202**, pp. 122-128
- Characklis, W.G. (1991), **Biofouling: effects and control**, in: Flemming, H.-C. and Geesey, G.G. (eds.), *Biofouling and Biocorrosion in Industrial Water Systems*, Springer-Verlag, Berlin, pp. 7-27
- Chen, V., Fane, A.G., Madaeni, S. and Wenten, I.G. (1997), **Particle deposition during membrane filtration of colloids: transition between concentration polarization and cake formation**, *Journal of Membrane Science*, **125**, pp. 109-122
- Chisti, M.Y. (1989a), **Airlift Bioreactors**, Elsevier Science Publishing Ltd, New York, pp. 1-8
- Chisti, M.Y. (1989b), **Airlift Bioreactors**, Elsevier Science Publishing Ltd, New York, pp. 53-57
- Chisti, M.Y., Halard, B. and Moo-Young, M. (1988), **Liquid circulation in airlift reactors**, *Chemical Engineering Science*, **43**(3), pp. 451-457
- Chisti, M.Y. and Moo-Young, M. (1987), **Airlift reactors: characteristics, applications and design considerations**, *Chemical Engineering Communications*, **60**, pp. 195-242
- Chisti, Y. and Moo-Young, M. (1988), **Prediction of liquid circulation velocity in airlift reactors with biological media**, *Journal of Chemical Technology and Biotechnology*, **42**, pp 211-219
- Chisti, Y. and Moo-Young, M. (1993), **Improve the performance of airlift reactors**, *Chemical Engineering Progress*, **89**(6), pp. 38-45
- Choi, K.H., Chisti, Y. and Moo-Young, M. (1996), **Comparative evaluation of hydrodynamic and gas-liquid mass transfer characteristics in bubble column and airlift slurry reactors**, *Chemical Engineering Journal*, **62**, pp. 223-229
- Churchouse, S. and Wildgoose, D. (1999), **Membrane bioreactors hit the big time – from lab to full-scale application**, 2nd Symposium on Membrane Bioreactors for Wastewater Treatment, Cranfield University, Cranfield, UK

- Contreras, A., Chisti, M. and Molina, E. (1998), **A reassessment of relationship between riser and downcomer gas holdups in airlift reactors**, *Chemical Engineering Science*, **53**(24), pp. 4151-4154
- Couvert, A., Bastoul, D., Roustan, M., Line, A. and Chatellier, P. (2001), **Prediction of liquid velocity and gas hold-up in rectangular air-lift reactors of different scales**, *Chemical Engineering and Processing*, **40**, pp. 113-119
- Couvert, A., Roustan, M. and Chatellier, P. (1999), **Two-phase hydrodynamic study of a rectangular air-lift loop reactor with an internal baffle**, *Chemical Engineering Science*, **54**, pp. 5245-5252
- Cox, R.G. and Brenner, H. (1968), **The lateral migration of solid particles in Poiseuille flow – I Theory**, *Chemical Engineering Science*, **23**, pp. 147-173
- Cui, Z.F. and Wright, K.I.T. (1994), **Gas-liquid two-phase cross-flow ultrafiltration of BSA and dextran solutions**, *Journal of Membrane Science*, **90**, pp. 183-189
- Cui, Z.F., Chang, S. and Fane, A.G. (2003), **The use of gas bubbling to enhance membrane processes**, *Journal of Membrane Science*, **221**, pp. 1-35
- Davis, R.H. and Birdsell, S.A. (1987), **Hydrodynamic model and experiments for crossflow microfiltration**, *Chemical Engineering Communications*, **49**, pp. 217-234
- Davis, R.H. and Leighton, D.T. (1987), **Shear-induced transport of a particle layer along a porous wall**, *Chemical Engineering Science*, **42**(2), pp. 275-281
- Defrance, L. and Jaffrin, M.Y. (1999a), **Comparison between filtrations at fixed transmembrane pressure and fixed permeate flux: application to a membrane bioreactor used for wastewater treatment**, *Journal of Membrane Science*, **152**, pp. 203-210
- Defrance, L. and Jaffrin, M.Y. (1999b), **Reversibility of fouling formed in activated sludge filtration**, *Journal of Membrane Science*, **157**, pp. 73-84
- Dejaegher, B., Durand, A. and Vander Heyden, Y. (2009), **Identification of significant effects from an experimental screening design in the absence of effect sparsity**, *Journal of Chromatography B*, **877**(23), pp. 2252-2261
- Dhaouadi, H., Poncin, S., Hornut, J.M., Wild, G. and Oinas, P. (1996), **Hydrodynamics of an airlift reactor: experiments and modeling**, *Chemical Engineering Science*, **51**(11), pp. 2625-2630
- Drew, D.A., Schonberg, J.A. and Belfort, G. (1991), **Lateral inertial migration of a small sphere in fast laminar flow through a membrane duct**, *Chemical Engineering Science*, **46**(12), pp. 3219-3224
- Eckstein, E.C., Bailey, D.G. and Shapiro, A.H. (1977), **Self-diffusion of particles in shear flow of a suspension**, *Journal of Fluid Mechanics*, **79**, pp. 191-208

-
- Engler, J. and Wiesner, M.R. (2000), **Particle fouling of a rotating membrane disk**, *Water Research*, **34**(2), pp. 557-565
- Fane, A.G., Beatson, P. and Li, H. (2000), **Membrane fouling and its control in environmental applications**, *Water Science and Technology*, **41**(10-11), pp. 303-308
- Field, R.W. (1993), **Transport processes in membrane systems**, in: Howell, J.A., Sanchez, V. and Field, R.W. (eds.), *Membranes in Bioprocessing: Theory and Applications*, Chapman & Hall, Cambridge, p. 67
- Field, R.W., Wu, D., Howell, J.A. and Gupta, B.B. (1995), **Critical flux concept for microfiltration fouling**, *Journal of Membrane Science*, **100**, pp. 259-272
- Finnigan, S.M. and Howell, J.A. (1989), **The effect of pulsatile flow on ultrafiltration fluxes in a baffled tubular membrane system**, *Chemical Engineering Research and Design*, **67**, pp. 278-282
- Flemming, H.-C. and Schaule, G. (1988), **Biofouling on membranes – a microbiological approach**, *Desalination*, **70**, pp. 95-119
- Flemming, H.-C., Schaule, G., Griebe, T., Schmitt, J. and Tamachkiarowa, A. (1997), **Biofouling – the Achilles heel of membrane processes**, *Desalination*, **113**, pp. 215-225
- Fradin, B. and Field, R.W. (1999), **Crossflow microfiltration of magnesium hydroxide suspensions: determination of critical fluxes, measurement and modelling of fouling**, *Separation and Purification Technology*, **16**, pp. 25-45
- Fyles, T.M. and Lycon, D.S. (2000), **Fouling reduction using centrifugal membrane separation**, *Journal of Membrane Science*, **176**, pp. 267-276
- Gander, M., Jefferson, B. and Judd, S. (2000), **Aerobic MBRs for domestic wastewater treatment: a review with cost considerations**, *Separation and Purification Technology*, **18**, pp. 119-130
- García-Calvo, E. and Letón, P. (1996), **Prediction of gas hold-up and liquid velocity in airlift reactors using two-phase flow friction coefficients**, *Journal of Chemical Technology and Biotechnology*, **67**, pp. 388-396
- Ghosh, R. (2002), **Study of membrane fouling by BSA using pulsed injection technique**, *Journal of Membrane Science*, **195**, pp. 115-123
- Gourgues, C., Aimar, P. and Sanchez, V. (1992), **Ultrafiltration of bentonite suspensions with hollow fibre membranes**, *Journal of Membrane Science*, **74**, pp. 51-69
- Green, G. and Belfort, G. (1980), **Fouling of ultrafiltration membranes: lateral migration and the particle trajectory model**, *Desalination*, **35**, pp. 129-147
- Guibert, D., Ben Aim, R., Rabie, H. and Côté, P. (2002), **Aeration performance of immersed hollow-fibre membranes in a bentonite suspension**, *Desalination*, **148**, pp. 395-400

- Günder, B. and Krauth, K. (1998), **Replacement of secondary clarification by membrane separation – results with plate and hollow fibre modules**, *Water Science and Technology*, **38**(4-5), pp. 383-393
- Gupta, B.B., Howell, J.A., Wu, D. and Field, R.W. (1995), **A helical baffle for crossflow microfiltration**, *Journal of Membrane Science*, **102**, pp. 31-42
- Hamachi, M., Cabassud, M., Davin, A. and Mietton-Peuchot, M. (1999), **Dynamic modelling of crossflow microfiltration of bentonite suspension using recurrent neural networks**, *Chemical Engineering and Processing*, **38**, pp. 203-210
- Hamachi, M. and Mietton-Peuchot, M. (1999), **Experimental investigations of cake characteristics in crossflow microfiltration**, *Chemical Engineering Science*, **54**, pp. 4023-4030
- Hamachi, M. and Mietton-Peuchot, M. (2002), **Analysis of deposit behaviour in crossflow microfiltration by means of thickness measurement**, *Chemical Engineering Journal*, **86**, pp. 251-257
- Héran, M. and Elmaleh, S. (2000), **Cross-flow microfiltration with high frequency reverse flow**, *Water Science and Technology*, **41**(10-11), pp. 337-343
- Ho, B.P. and Leal, L.G. (1974), **Inertial migration of rigid spheres in two-dimensional unidirectional flows**, *Journal of Fluid Mechanics*, **65**, pp. 365-400
- Hodgson, P.H., Leslie, G.L., Schneider, R.P., Fane, A.G., Fell, C.J.D. and Marshall, K.C. (1993), **Cake resistance and solute rejection in bacterial microfiltration: the role of the extracellular matrix**, *Journal of Membrane Science*, **79**, pp. 35-53
- Howell, J.A. (1995), **Sub-critical flux operation of microfiltration**, *Journal of Membrane Science*, **107**, pp. 165-171
- Hwang, K.-J., Chan, C.-S. and Tung, K.-L. (2009), **Effect of backwash on the performance of submerged membrane filtration**, *Journal of Membrane Science*, **330**, pp. 349-356
- Hwang, S.-J., Chang, D.-J. and Chen, C.-H. (1996), **Steady state permeate flux for particle cross-flow filtration**, *Chemical Engineering Journal*, **61**, pp. 171-178
- Hwang, S.-J. and Cheng, Y.-L. (1997), **Gas holdup and liquid velocity in three-phase internal-loop airlift reactors**, *Chemical Engineering Science*, **52**(21/22), pp. 3949-3960
- Jacobs, L., De Bruyn, E.E. and Cloete, T.E. (1996), **The use of biodispersants available for biofouling control in industrial water systems**, WRC Project No. 592/1/97, Water Research Commission of South Africa, South Africa
- Jones, W.F., Valentine, R.L. and Rodgers, V.G.J. (1999), **Removal of suspended clay from water using transmembrane pressure pulsed microfiltration**, *Journal of Membrane Science*, **157**, pp. 199-210

-
- Judd, S. (2008), **The status of membrane bioreactor technology**, *Trends in Biotechnology*, **26**(2), pp. 109-116
- Judd, S.J., Le-Clech, P., Taha, T. and Cui, Z.F. (2001), **Theoretical and experimental representation of a submerged membrane bio-reactor system**, *Membrane Technology*, **135**, pp. 4-9
- Kawakatsu, T., Nakao, S. and Kimura, S. (1993), **Effects of size and compressibility of suspended particles and surface pore size of membrane on flux in crossflow filtration**, *Journal of Membrane Science*, **81**, pp. 173-190
- Koen, L.J. (2000a), **Ultrasonic-time-domain-reflectometry as a real time non-destructive visualisation technique of concentration polarisation and fouling on reverse osmosis membranes**, Master thesis, University of Stellenbosch, Stellenbosch, South Africa, pp. 2-22 – 2-23
- Koen, L.J. (2000b), **Ultrasonic-time-domain-reflectometry as a real time non-destructive visualisation technique of concentration polarisation and fouling on reverse osmosis membranes**, Master thesis, University of Stellenbosch, Stellenbosch, South Africa
- Krstić, D.M., Tekić, M.N., Carić, M.Đ. and Milanović, S.D. (2002), **The effect of turbulence promoter on cross-flow microfiltration of skim milk**, *Journal of Membrane Science*, **208**, pp. 303-314
- Kwon, D.Y., Vigneswaran, S., Fane, A.G. and Ben Aim, R. (2000), **Experimental determination of critical flux in cross-flow microfiltration**, *Separation and Purification Technology*, **19**, pp. 169-181
- Laborie, S., Cabassud, C., Durand-Bourlier, L. and Lainé, J.M. (1998), **Fouling control by air sparging inside hollow fibre membranes – effects on energy consumption**, *Desalination*, **118**, pp. 189-196
- Le-Clech, P., Jefferson, B., Chang, I.S. and Judd, S.J. (2003a), **Critical flux determination by the flux-step method in a submerged membrane bioreactor**, *Journal of Membrane Science*, **227**, pp. 81-93
- Le-Clech, P., Jefferson, B. and Judd, S.J. (2003b), **Impact of aeration, solids concentration and membrane characteristics on the hydraulic performance of a membrane bioreactor**, *Journal of Membrane Science*, **218**, pp. 117-129
- Lee, S. and Lueptow, R.M. (2003), **Control of scale formation in reverse osmosis by membrane rotation**, *Desalination*, **155**, pp. 131-139
- Leighton, D. and Acrivos, A. (1986), **Viscous resuspension**, *Chemical Engineering Science*, **41**(6), pp. 1377-1384
- Leighton, D. and Acrivos, A. (1987), **Measurement of shear-induced self-diffusion in concentrated suspensions of spheres**, *Journal of Fluid Mechanics*, **177**, pp. 109-131

- Leiknes, T. (2003), **Low pressure membrane systems for water and wastewater treatment - emphasis on submerged membrane technology**, 5th WISA-MTD Symposium, Vereeniging, South Africa
- Leonard, E.F. and Vassilieff, C.S. (1984), **The deposition of rejected matter in membrane separation processes**, *Chemical Engineering Communications*, **30**, pp. 209-217
- Li, H., Fane, A.G., Coster, H.G.L. and Vigneswaran, S. (1998a), **Direct observation of particle deposition on the membrane surface during crossflow microfiltration**, *Journal of Membrane Science*, **149**, pp. 83-97
- Li, J. (2002), **Real-time investigation of fouling phenomena in membrane filtrations by a non-invasive ultrasonic technique**, Doctoral thesis, University of Stellenbosch, Stellenbosch, South Africa
- Li, J., Hallbauer, D.K. and Sanderson, R.D. (2003), **Direct monitoring of membrane fouling and cleaning during ultrafiltration using a non-invasive ultrasonic technique**, *Journal of Membrane Science*, **215**, pp. 33-52
- Li, J., Sanderson, R.D., Hallbauer, D.K. and Hallbauer-Zadorozhnaya, V.Y. (2002a), **Measurement and modelling of organic fouling deposition in ultrafiltration by ultrasonic transfer signals and reflections**, *Desalination*, **146**, pp. 177-185
- Li, J., Sanderson, R.D. and Jacobs, E.P. (2002b), **Non-invasive visualization of the fouling of microfiltration membranes by ultrasonic time-domain reflectometry**, *Journal of Membrane Science*, **201**, pp. 17-29
- Li, Q.Y., Ghosh, R., Bellara, S.R., Cui, Z.F. and Pepper, D.S. (1998b), **Enhancement of ultrafiltration by gas sparging with flat sheet membrane modules**, *Separation and Purification Technology*, **14**, pp. 79-83
- Lim, A.L. and Bai, R. (2003), **Membrane fouling and cleaning in microfiltration of activated sludge wastewater**, *Journal of Membrane Science*, **216**, pp. 279-290
- Liu, H., Yang, C., Pu, W. and Zhang, J. (2009), **Formation mechanism and structure of dynamic membrane in the dynamic membrane bioreactor**, *Chemical Engineering Journal*, **148**, pp. 290-295
- Liu, R., Huang, X., Sun, Y.F. and Qian, Y. (2003), **Hydrodynamic effect on sludge accumulation over membrane surfaces in a submerged membrane bioreactor**, *Process Biochemistry*, **39**, pp. 157-163
- Liu, R., Huang, X., Wang, C., Chen, L. and Qian, Y. (2000), **Study on hydraulic characteristics in a submerged membrane bioreactor process**, *Process Biochemistry*, **36**, pp. 249-254
- Livingston, A.G. and Zhang, S.F. (1993), **Hydrodynamic behaviour of three-phase (gas-liquid-solid) airlift reactors**, *Chemical Engineering Science*, **48**(9), pp. 1641-1654

-
- Lu, W.-J., Hwang, S.-J. and Chang, C.-M. (1995), **Liquid velocity and gas holdup in three-phase internal loop airlift reactors with low-density particles**, *Chemical Engineering Science*, **50**(8), pp. 1301-1310
- Lu, W.-M. and Ju, S.-C. (1989), **Selective particle deposition in crossflow filtration**, *Separation Science and Technology*, **24**, pp. 512-540
- Lu, X., Ding, J., Wang, Y. and Shi, J. (2000), **Comparison of the hydrodynamics and mass transfer characteristics of a modified square airlift reactor with common airlift reactors**, *Chemical Engineering Science*, **55**, pp. 2257-2263
- Lynch, J.L. and Edyvean, R.G.J. (1988), **Biofouling in oilfield water systems – a review**, *Biofouling*, **1**, pp. 147-162
- Ma, H., Hakim, L.F., Bowman, C.N. and Davis, R.H. (2001), **Factors affecting membrane fouling reduction by surface modification and backpulsing**, *Journal of Membrane Science*, **189**, pp. 255-270
- Maartens, A., Jacobs, E.P. and Swart, P. (2002), **UF of pulp and paper effluent: membrane fouling prevention and cleaning**, *Journal of Membrane Science*, **209**, pp. 81-92
- Mackley, M.R. and Sherman, N.E. (1994), **Cross-flow filtration with and without cake formation**, *Chemical Engineering Science*, **49**(2), pp. 171-178
- Mairal, A.P., Greenberg, A.R. and Krantz, W.B. (2000), **Investigation of membrane fouling and cleaning using ultrasonic time-domain reflectometry**, *Desalination*, **130**, pp. 45-60
- Mairal, A.P., Greenberg, A.R., Krantz, W.B. and Bond, L.J. (1999), **Real-time measurement of inorganic fouling of RO desalination membranes using ultrasonic time-domain reflectometry**, *Journal of Membrane Science*, **159**, pp. 185-196
- Marshall, K.C. and Blainey, B.L. (1991), **Role of bacterial adhesion in biofilm formation and biocorrosion**, in: Flemming, H.-C. and Geesey, G.G. (eds.), *Biofouling and Biocorrosion in Industrial Water Systems*, Springer-Verlag, Berlin, pp. 29-46
- Matthiasson, E. (1983), **The role of macromolecular adsorption in fouling of ultrafiltration membranes**, *Journal of Membrane Science*, **16**, pp. 23-36
- Matthiasson, E. and Sivik, B. (1980), **Concentration polarisation and fouling**, *Desalination*, **35**, pp. 59-103
- McCarthy, A.A., Walsh, P.K. and Foley, G. (2002), **Experimental techniques for quantifying the cake mass, the cake and membrane resistances and the specific cake resistance during crossflow filtration of microbial suspensions**, *Journal of Membrane Science*, **201**, pp. 31-45
- McDonogh, R., Schaule, G. and Flemming, H.-C. (1994), **The permeability of biofouling layers on membranes**, *Journal of Membrane Science*, **87**, pp. 199-217
-

-
- Meng, F., Chae, S.-R., Drews, A., Kraume, M., Shin, H.-S. and Yang, F. (2009), **Review – Recent advances in membrane bioreactors (MBRs): Membrane fouling and membrane material**, *Water Research*, **43**, pp. 1489-1512
- Merchuk, J.C. and Berzin, I. (1995), **Distribution of energy dissipation in airlift reactors**, *Chemical Engineering Science*, **50**(14), pp 2225-2233
- Mercier, M., Fonade, C. and Lafforgue-Delorme, C. (1997), **How slug flow can enhance the ultrafiltration flux in mineral tubular membranes**, *Journal of Membrane Science*, **128**, pp 103-113
- Mercier-Bonin, M., Daubert, I., Léonard, D., Maranges, C., Fonade, C. and Lafforgue, C. (2001), **How unsteady filtration conditions can improve the process efficiency during cell cultures in membrane bioreactors**, *Separation and Purification Technology*, **22-23**, pp. 601-615
- Mercier-Bonin, M., Lagane, C. and Fonade, C. (2000), **Influence of a gas/liquid two-phase flow on the ultrafiltration and microfiltration performances: case of a ceramic flat sheet membrane**, *Journal of Membrane Science*, **180**, pp. 93-102
- Mietton, M. and Ben Aim, R. (1992), **Improvement of crossflow microfiltration performances with flocculation**, *Journal of Membrane Science*, **68**, pp. 241-248
- Milicic, V. and Bersillon, J.L. (1986), **Anti-fouling techniques in cross-flow microfiltration**, *Filtration and Separation*, **23**, pp. 347-349
- Mores, W.D., Bowman, C.N. and Davis, R.H. (2000), **Theoretical and experimental flux maximization by optimization of backpulsing**, *Journal of Membrane Science*, **165**, pp. 225-236
- Mukherjee, S., Das, P., Sivapathasekaran, C. and Sen, R. (2008), **Enhanced production of biosurfactant by a marine bacterium on statistical screening of nutritional parameters**, *Biochemical Engineering Journal*, **42**, pp. 254-260
- Nagaoka, H., Yamanishi, S. and Miya, A. (1998), **Modeling of biofouling by extracellular polymers in a membrane separation activated sludge system**, *Water Science and Technology*, **38**(4-5), pp. 497-504
- Nagaoka, H., Kono, S., Yamanishi, S. and Miya, A. (2000), **Influence of organic loading rate on membrane fouling in membrane separation activated sludge process**, *Water Science and Technology*, **41**(10-11), pp. 355-362
- Ngo, H.-H., Guo, W. and Xing, W. (2008), **Evaluation of a novel sponge-submerged membrane bioreactor (SSMBR) for sustainable water reclamation**, *Bioresource Technology*, **99**, pp. 2429-2435
- Ognier, S., Wisniewski, C. and Grasmick, A. (2004), **Membrane bioreactor fouling in sub-critical filtration conditions: a local critical flux concept**, *Journal of Membrane Science*, **229**, pp. 171-177

-
- Oita, I., Halewyck, H., Pieters, S., Dejaegher, B., Thys, B., Rombaut, B. and Vander Heyden, Y. (2009), **Improving the capillary electrophoretic analysis of poliovirus using a Plackett-Burman design**, *Journal of Pharmaceutical and Biomedical Analysis*, **50**(4), pp. 655-663
- Otis, J.R., Altena, F.W., Mahar, J.T. and Belfort, G. (1986), **Measurements of single spherical particle trajectories with lateral migration in a slit with one porous wall under laminar flow conditions**, *Experiments in Fluids*, **4**, pp. 1-10
- Ozaki, N. and Yamamoto, K. (2001), **Hydraulic effects on sludge accumulation on membrane surface in crossflow filtration**, *Water Research*, **35**(13), pp. 3137-3146
- Pasmore, M., Todd, P., Smith, S., Baker, D., Silverstein, J., Coons, D. and Bowman, C.N. (2001), **Effects of ultrafiltration membrane surface properties on *Pseudomonas aeruginosa* biofilm initiation for the purpose of reducing biofouling**, *Journal of Membrane Science*, **194**, pp. 15-32
- Pearce, G. (2008), **Introduction to membranes – MBRs: Manufacturers' comparison: part 1**, *Filtration & Separation*, **45**(2), pp. 28-31
- Peterson, R.A., Greenberg, A.R., Bond, L.J. and Krantz, W.B. (1998), **Use of ultrasonic TDR for real-time noninvasive measurement of compressive strain during membrane compaction**, *Desalination*, **116**, pp. 115-122
- Pillay, V.L. (1991), **Modelling of turbulent cross-flow microfiltration of particulate suspensions**, Ph.D. thesis, University of Natal, South Africa
- Piron, E., René, F. and Latrille, E. (1995), **A cross-flow microfiltration model based on integration of the mass transport equation**, *Journal of Membrane Science*, **108**, pp. 57-70
- Pollice, A., Brookes, A., Jefferson, B. and Judd, S. (2005), **Sub-critical flux fouling in membrane bioreactors – a review of recent literature**, *Desalination*, **174**, pp. 221-230
- Porter, M.C. (1972), **Concentration polarization with membrane ultrafiltration**, *Industrial and Engineering Chemistry, Product Research and Development*, **11**(3), pp. 234-248
- Porter, M.C. (1977), **What, when and why of membranes – MF, UF and RO**, *AIChE Symposium Series*, **73**(171), pp. 83-103
- Rabie, H.R., Côté, P. and Adams, N. (2001), **A method for assessing membrane fouling in pilot- and full-scale systems**, *Desalination*, **141**, pp. 237-243
- Redkar, S., Kuberkar, V. and Davis, R.H. (1996), **Modelling of concentration polarization and depolarization with high-frequency backpulsing**, *Journal of Membrane Science*, **121**, pp. 229-242

-
- Reed, R.H. and Belfort, G. (1982), **Characterization of fouling potential for pressure-driven membrane processes: a new simulated flow cell**, *Water Science and Technology*, **14**, pp. 499-522
- Ridgway, H.F. and Safarik, J. (1991), **Biofouling of reverse osmosis membranes**, in: Flemming, H.-C. and Geesey, G.G. (eds.), *Biofouling and Biocorrosion in Industrial Water Systems*, Springer-Verlag, Berlin, pp. 81-111
- Romero, C.A. and Davis, R.H. (1988), **Global model of crossflow microfiltration based on hydrodynamic particle diffusion**, *Journal of Membrane Science*, **39**, pp. 157-185
- Romero, C.A. and Davis, R.H. (1990), **Transient model of crossflow microfiltration**, *Chemical Engineering Science*, **45**(1), pp. 13-25
- Sadr Ghayeni, S.B., Beatson, P.J., Schneider, R.P. and Fane, A.G. (1998), **Adhesion of waste water bacteria to reverse osmosis membranes**, *Journal of Membrane Science*, **138**, pp. 29-42
- Sayed Razavi, S.K. and Harris, J.L. (1996), **Shear controlled model of the ultrafiltration of soy suspensions**, *Journal of Membrane Science*, **118**, pp. 279-288
- Schwinge, J., Wiley, D.E., Fane, A.G. and Guenther, R. (2000), **Characterization of a zigzag spacer for ultrafiltration**, *Journal of Membrane Science*, **172**, pp. 19-31
- Segré, G. and Silberberg, A. (1961), **Radial particle displacements in Poiseuille flow of suspensions**, *Nature*, **189**, pp. 209-210
- Seminario, L., Rozas, R., Bórques, R. and Toledo, P.G. (2002), **Pore blocking and permeability reduction in cross-flow microfiltration**, *Journal of Membrane Science*, **209**, pp. 121-142
- Serra, C., Durand-Bourlier, L., Clifton, M.J., Moulin, P., Rouch, J.-C. and Aptel, P. (1999), **Use of air sparging to improve backwash efficiency in hollow-fibre modules**, *Journal of Membrane Science*, **161**, pp. 95-113
- Shim, J.K., Yoo, I.-K. and Lee, Y.M. (2002), **Design and operation considerations for wastewater treatment using a flat submerged membrane bioreactor**, *Process Biochemistry*, **38**, pp. 279-285
- Shimizu, Y., Uryu, K., Okuno, Y.-I., Ohtubo, S. and Watanabe, A. (1997), **Effect of particle size distributions of activated sludges on cross-flow microfiltration flux for submerged membranes**, *Journal of Fermentation and Bioengineering*, **83**(6), pp. 583-589
- Shimizu, Y., Uryu, K., Okuno, Y.-I. and Watanabe, A. (1996), **Cross-flow microfiltration of activated sludge using submerged membrane with air bubbling**, *Journal of Fermentation and Bioengineering*, **81**(1), pp. 55-60
- Shulz, G. and Ripperger, S. (1989), **Concentration polarization in crossflow microfiltration**, *Journal of Membrane Science*, **40**, pp. 173-187

- Siegel, M.H., Merchuk, J.C. and Schugerl, K. (1986), **Air-lift reactor analysis: interrelationships between riser, downcomer, and gas-liquid separator behavior, including gas recirculation effects**, *AIChE Journal*, **32**(10), pp. 1585-1596
- Silva, C.M., Reeve, D.W., Husain, H., Rabie, H.R. and Woodhouse, K.A. (2000), **Model for flux prediction in high-shear microfiltration systems**, *Journal of Membrane Science*, **173**, pp. 87-98
- Stamatakis, K. and Tien, C. (1993), **A simple model of cross-flow filtration based on particle adhesion**, *AIChE Journal*, **39**(8), pp. 1292-1302
- Stephenson, T., Judd, S., Jefferson, B. and Brindle, K. (2000a), **Membrane bioreactors for wastewater treatment**, IWA Publishing, London
- Stephenson, T., Judd, S., Jefferson, B. and Brindle, K. (2000b), **Membrane bioreactors for wastewater treatment**, IWA Publishing, London, p. 32
- Stewart, D.I., Studds, P.G. and Cousens, T.W. (2003), **The factors controlling the engineering properties of bentonite-enhanced sand**, *Applied Clay Science*, **23**, pp. 97-110
- Suda, K., Shibuya, S., Itoh, Y. and Kohno, T. (1998), **Development of a tank-submerged type membrane filtration system**, *Desalination*, **119**, pp. 151-158
- Suki, A., Fane, A.G. and Fell, C.J.D. (1986), **Modelling fouling mechanisms in protein ultrafiltration**, *Journal of Membrane Science*, **27**, pp. 181-193
- Swart, A.F. (1993), **Considerations in the selection of the operating regimes for microfiltration**, M.Sc.Eng. thesis, University of Natal, South Africa
- Swart, A.F., Brouckaert, C.J. and Buckley, C.A. (1994), **Criteria for selecting the operating regime of the crossflow microfilter or the tubular filter press for clarification of turbid waters**, *Journal of Membrane Science*, **87**, pp. 57-69
- Tansel, B., Bao, W.Y. and Tansel, I.N. (2000), **Characterization of fouling kinetics in ultrafiltration systems by resistances in series model**, *Desalination*, **129**, pp. 7-14
- Tardieu, E., Grasmick, A., Geaugey, V. and Manem, J. (1998), **Hydrodynamic control of bioparticle deposition in a MBR applied to wastewater treatment**, *Journal of Membrane Science*, **147**, pp. 1-12
- Tardieu, E., Grasmick, A., Geaugey, V. and Manem, J. (1999), **Influence of hydrodynamics on fouling velocity in a recirculated MBR for wastewater treatment**, *Journal of Membrane Science*, **156**, pp. 131-140
- Tay, J.-H., Liu, J. and Sun, D.D. (2003), **Quantification of membrane fouling using thermogravimetric method**, *Journal of Membrane Science*, **217**, pp. 17-28

-
- Tiranuntakul, M., Jegatheesan, V., Schneider, P.A. and Fracchia, H.L. (2005), **Performance of an oxidation ditch retrofitted with a membrane bioreactor during the start-up**, *Desalination*, **183**, pp. 417-424
- Trussell, R.S., Merlo, R.P., Hermanowicz, S.W. and Jenkins, D. (2007), **Influence of mixed liquor properties and aeration intensity on membrane fouling in a submerged membrane bioreactor at high mixed liquor suspended solids concentrations**, *Water Research*, **41**, pp. 947-958
- Ueda, T., Hata, K., Kikuoka, Y. and Seino, O. (1997), **Effects of aeration on suction pressure in a submerged membrane bioreactor**, *Water Research*, **31**(3), pp. 489-494
- Van Baten, J.M., Ellenberger, J. and Krishna, R. (2003), **Hydrodynamics of internal air-lift reactors: experiments versus CFD simulations**, *Chemical Engineering and Processing*, **42**, pp. 733-742
- Van der Merwe, J.J. (2003), Personal communication, Department of Geology, University of Stellenbosch, Stellenbosch, South Africa
- Van der Merwe, J.J. (2004), **Parameters affecting accuracy and reproducibility of sedigraph particle size analysis of clays**, Master thesis, University of Stellenbosch, Stellenbosch, South Africa
- Van't Oever, R. (2005), **MBR focus: is submerged best?**, *Filtration & Separation*, **42**(5), pp. 24-27
- Vasseur, P. and Cox, R.G. (1976), **The lateral migration of a spherical particle in two-dimensional shear flows**, *Journal of Fluid Mechanics*, **78**, pp. 385-413
- Vassilieff, C.S., Doneva, T.A. and Ljutov, L.G. (1996), Cross-flow microfiltration of bentonite-in-water dispersions: initial transient effects at low concentration, *Journal of Membrane Science*, **119**, pp. 65-80
- Vatanara, A., Najafabadi, A.R., Gilani, K., Asgharian, R., Darabi, M. and Rafiee-Tehrani, M. (2007), **A Plackett-Burman design for screening of the operation variables in the formation of salbutamol sulphate particles by supercritical antisolvent**, *Journal of Supercritical Fluids*, **40**, pp. 111-116
- Verrecht, B., Judd, S., Guglielmi, G., Brepols, C. and Mulder, J.W. (2008), **An aeration energy model for an immersed membrane bioreactor**, *Water Research*, **42**, pp. 4761-4770
- Vigneswaran, S., Kwon, D.Y., Ngo, H.H. and Hu, J.Y. (2000), **Improvement of microfiltration performance in water treatment: is critical flux a viable solution?**, *Water Science Technology*, **41**(10-11), pp. 309-315
- Vrijenhoek, E.M., Hong, S. and Elimelech, M. (2001), **Influence of membrane surface properties on initial rate of colloidal fouling of reverse osmosis and nanofiltration membranes**, *Journal of Membrane Science*, **188**, pp. 115-128

- Vrouwenvelder, J.S. and Van der Kooij, D. (2001), **Diagnosis, prediction and prevention of biofouling of NF and RO membranes**, *Desalination*, **139**, pp. 65-71
- Vyas, H.K., Bennett, R.J. and Marshall, A.D. (2002), **Performance of crossflow microfiltration during constant transmembrane pressure and constant flux operations**, *International Dairy Journal*, **12**, pp. 473-479
- Wakeman, R.J. and Williams, C.J. (2002), **Additional techniques to improve microfiltration**, *Separation and Purification Technology*, **26**, pp. 3-18
- Wang, J. and Wan, W. (2009), **Experimental design methods for fermentative hydrogen production: A review**, *International Journal of Hydrogen Energy*, **34**, pp. 235-244
- Wicaksana, F., Fane, A.G. and Chen, V. (2006), **Fibre movement induced by bubbling using submerged hollow fibre membranes**, *Journal of Membrane Science*, **271**, pp. 186-195
- Winzeler, H.B. and Belfort, G. (1993), **Enhanced performance for pressure-driven membrane processes: the argument for fluid instabilities**, *Journal of Membrane Science*, **80**, pp. 35-47
- Wongsuchoto, P., Charinpanitkul, T. and Pavasant, P. (2003), **Bubble size distribution and gas-liquid mass transfer in airlift contactors**, *Chemical Engineering Journal*, **92**, pp. 81-90
- Wu, D., Howell, J.A. and Field, R.W. (1999), **Critical flux measurement for model colloids**, *Journal of Membrane Science*, **152**, pp. 89-98
- Wu, J., Le-Clech, P., Stuetz, R.M., Fane, A.G. and Chen, V. (2008a), **Effects of relaxation and backwashing conditions on fouling in membrane bioreactor**, *Journal of Membrane Science*, **324**, pp. 26-32
- Wu, Z., Wang, Z., Huang, S., Mai, S., Yang, C., Wang, X. and Zhou, Z. (2008b), **Effects of various factors on critical flux in submerged membrane bioreactors for municipal wastewater treatment**, *Separation and Purification Technology*, **62**, pp. 56-63
- Xu, X., Li, J., Li, H., Cai, Y., Cao, Y., He, B. and Zhang, Y. (2009), **Non-invasive monitoring of fouling in hollow fibre membrane via UTDR**, *Journal of Membrane Science*, **326**, pp. 103-110
- Ye, Y., Le Clech, P., Chen, V. and Fane, A.G. (2005), **Evolution of fouling during crossflow filtration of model EPS solutions**, *Journal of Membrane Science*, **264**, pp. 190-199
- Zhang, K., Cui, Z. and Field, R.W. (2009), **Effect of bubble size and frequency on mass transfer in flat sheet MBR**, *Journal of Membrane Science*, **332**, pp. 30-37

Addendum A

Model foulant preparation

A.1 Introduction

A model foulant is an artificial wastewater feed which is exclusively used as a standard fouling agent to investigate the fouling behaviour for a specific membrane system. The main advantage of preparing and using a model foulant in membrane fouling experiments, as opposed to an acquired real life wastewater feed, is the possible elimination of variations in the chemical and physical properties. The consistency of such a prepared foulant reduces unknown factors and enables membrane fouling results to be explained by known factors which are set by the experimenter. The tailoring of these known factors to measure and compare the effect they have on membrane fouling forms the basis of membrane fouling experiments.

Besides consistency, other considerations, such as cost, safety, availability and practicality, may favour the use of a model foulant to a real life foulant. At least in the initial phases of fouling experiments in the development of a membrane system, the use of a model foulant is preferred to obtain an understanding of the membrane fouling dynamics. Thereafter the real life wastewater feed, which is ultimately to be treated by the membrane system, can be used for optimisation studies.

A.2 Model foulant selection

An appropriate model foulant should conform to meet certain requirements, namely:

- the foulant must behave reproducibly and therefore have the same properties in repeated preparations and experiments;
- the foulant must have industrial relevance and should simulate the fouling behaviour of the concerning wastewater to be treated as far as possible;
- the foulant's sizes and size distribution must be in accordance with the employed membrane's pore sizes;
- the foulant must exhibit a propensity to significantly foul the employed membrane;
- the foulant must be readily available for other researchers to reproduce the results; and
- should be known in the literature.

The technology developed in this project will ultimately be applied to the build of a membrane bioreactor for the treatment of wastewater with a high organic loading. It was therefore originally considered to use a prepared organic solution as a modelled wastewater for a membrane bioreactor [Ye et al., 2005]. Micro-organisms would have been inoculated into the solution and left to consume the nutrients for cell growth, as well as cell production, while the membrane would serve as barrier between the bio-phase and the permeate. Unfortunately the probable long start-up times and the complex behaviour of microbial growth, which would influence the properties of the wastewater, made the option of an organic solution as model foulant less favourable. Other factors, such as the risk of pathogenic contraction and the requirement for a more intense cleaning regime to remove biofouling from the membranes at the end of experiments, altogether led to the rejection of an organic solution as a model foulant.

The objective of this study was never to model biofouling in a membrane bioreactor, but to investigate the fouling dynamics for an immersed membrane system. So, for this study, regardless of the model foulant used and the resulting type of fouling, any fouling tendencies that could be identified, would aid in the design of the reactor and membrane module configurations of the future membrane bioreactor. Therefore, to eliminate biofouling for the sake of simplicity and reproducibility and only allow physico-chemical fouling mechanisms, it was decided to use a particulate suspension as model foulant.

A commercially available clay, bentonite (Ocean Bentonite, G&W Base & Industrial Minerals, South Africa), suspended in water, was selected as the model foulant for this study. Bentonite is an

attractive choice for a model foulant since it is relatively cheap, safe and allows for reproducibility. Bentonite particle sizes usually range from 0.5 to 10 μm [Gourgues et al., 1992; Van der Merwe, 2004] and thereby provide possible size distributions suited for both microfiltration and ultrafiltration membrane fouling experiments. The bentonite used in this study was however of a much coarser nature. The particle size distribution was measured with a Malvern Mastersizer and found to have a particle diameter of 18.53 μm at the 50th percentile. The particle size distribution of the bentonite used is shown in Figure A.1.

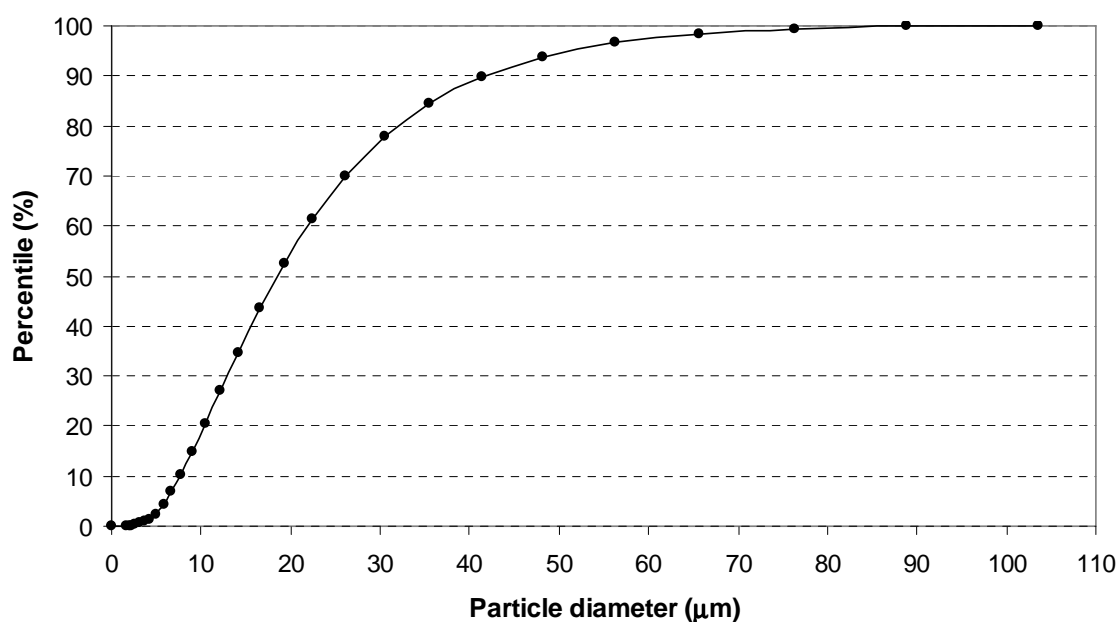


Figure A.1: Particle size distribution of the bentonite used in this study.

A bentonite particle is a thin lamella with the other dimensions approximately one hundred times larger than the thickness [Bacchin et al., 1996]. Bentonite therefore behaves as an excellent fouling agent, because when dispersed bentonite particles are deposited on the membrane surface, they collapse with their flat sides parallel to the membrane surface to form a densely layered and highly impermeable cake [Van der Merwe, 2003].

The use of bentonite as a model foulant has been widely documented for microfiltration and ultrafiltration membrane fouling experiments to investigate fundamental concepts of fouling [Gourgues et al., 1992; Bacchin et al., 1996; Vassiliev et al., 1996; Hamachi et al., 1999; Hamachi and Mietton-Peuchot, 1999, 2002; Seminario et al., 2002], to compare the efficiency of various fouling amelioration techniques [Milisic and Bersillon, 1986; Héran and Elmaleh, 2000; Guibert et al., 2002] and to measure the performance of membrane systems [Swart et al., 1994].

A.3 Suspension preparation

In preparing the model foulant, bentonite clay solids were required to disperse in reverse osmosis product water with a turbidity of less than 0.1 NTU. However, it was found that bentonite granules do not disperse easily in water since the bentonite particles in contact with the water swell and effectively seal the underlying particles from the water. The swelling phenomenon can be ascribed to the dominant mineral in bentonite, montmorillonite, which absorbs water in its interlayer crystal structure [Stewart et al., 2003]. Inadequate dispersing of the bentonite particles in water leads to the formation of a cloggy slurry.

Swart [1993] also experienced difficulty in dispersing bentonite in water, but reported that reproducible and dispersed suspensions could be prepared by applying high shear mixing and heat. Swart [1993] was able to disperse 1:1 mass proportions of the clays bentonite and kaolin in batches of 15 to 240 g in 1.5 L tap water by mixing it for 12 hours using a laboratory stirrer. This suspension was then added to a tank where it was diluted with tap water to the desired solids concentration. The resulting suspension was subjected to further stirring for 2 hours while heated to maintain a temperature of 30 °C.

A similar procedure was followed to prepare the model foulant bentonite suspensions in this study. Batch bentonite suspensions were prepared by adding 60 to 225 g of bentonite to approximately 1.5 L of reverse osmosis product water and stirring it overnight at a constant temperature of 30 °C. The combined mixing and heating of the bentonite suspensions seemed to effectively detach the particles from their aggregated state to become fully hydrated and dispersed. Although the suspensions appeared to be well dispersed after only a few hours of stirring and heating, no minimum mixing time was identified. Once a well dispersed suspension was prepared, it was added to the relevant tank and diluted to the correct solids concentration with reverse osmosis product water to create the model foulant for the specific fouling experiment.

It was considered to add a disinfectant to the model foulant to avoid micro-organisms from inhabiting the tank and biofouling the immersed membranes. The use of a standard disinfectant such as sodium azide [Maartens et al., 2002] would eventually work out too costly for the numerous and relative large volume experiments that were planned. Sodium azide is also very toxic and using it would require extra safety precautions and proper waste disposal protocols. The addition of a commercial swimming pool disinfectant (hth, Olin, South Africa), with calcium hypochlorite as active ingredient, was found to decrease the model foulant's pH and change the colloidal state of the bentonite particles to form aggregates with a reduced fouling propensity.

Consequently, it was decided to omit disinfection on the basis that the experimental treatments are too short to provide for any significant biological growth.

A.4 Turbidity calibration

A calibration curve was developed to correlate the concentration of the suspended bentonite with its turbidity. The calibration curve (Figure A.2) enabled the quick determination of the suspended bentonite concentration with the measurement of the turbidity of the suspension using a HACH 2100 turbidity meter. This technique to determine suspended concentrations has been used elsewhere by Gourgues et al. [1992] for bentonite suspensions and by Swart [1993] for kaolin and bentonite suspensions. Although this technique does not provide accurate suspended solids concentration values, it was found to provide acceptable indications for the studied bentonite suspensions.

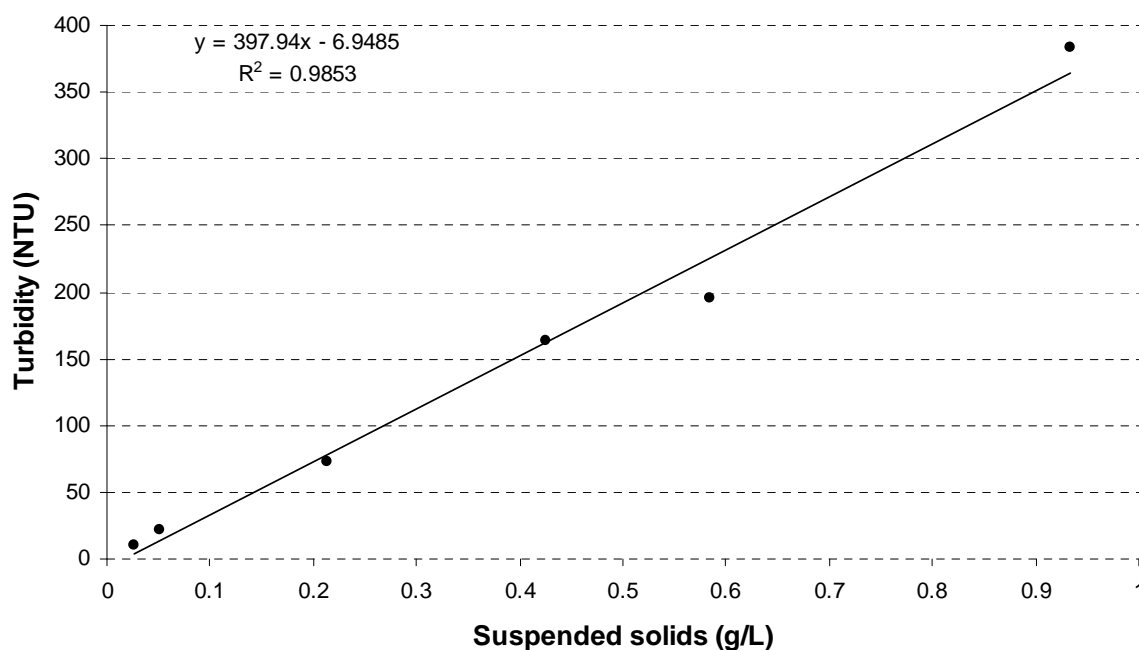


Figure A.2: Regressed calibration curve for bentonite suspensions.

Addendum B

Membrane element construction

B.1 Introduction

Membrane elements are the fundamental components of a membrane system capable of filtration. A collection of membrane elements are housed together in a membrane module. A number of membrane modules may be arranged to form a single membrane unit. Finally, a membrane system may comprise more than one membrane unit.

As a first approach, fouling behaviour was only studied on single immersed membrane elements. Results obtained from the studied membrane elements will ultimately provide guidelines to reduce membrane fouling in more complex membrane arrangements such as membrane modules and units.

For this study, a generic range of flat-sheet membrane elements were engineered by the same membrane material and production techniques. In a given experiment, the membrane elements that were employed only differed in their respective active filtration areas. The restriction of the constructional variables of the membrane elements to the active filtration area reduced the unknown factors, and thereby simplified data interpretation and enabled comparison of membrane fouling results.

B.2 Membrane material

A fabric of woven polyester was used as the membrane material. The obtained fabric consists of two layers that are interwoven in a manner to produce a series of separate tubes which provide for fluid flow channels. Similar tubular cloths were employed in cross-flow microfiltration studies by Pillay [1991], Swart [1993] and Swart et al. [1994], but whereas they studied pressurised inside-out filtration, the fabric had to facilitate outside-in filtration in this study. For outside-in filtration it is imperative to insert a spacer material in the filter tubes to keep them from collapsing and impeding fluid flow inside the tubes. In this study strips of woven stainless steel mesh were inserted in the tubes of the membrane material to act as spacer material. These spacer material strips were cut to have the same width as the membrane material tubes.

The woven fabric has a relative open weave and on its own may not be able to remove small particles in a filtration process to produce permeate of an acceptable quality. However, with the commencement of cake layer formation on the membrane surface, a dynamic membrane is created which reduces the effective pore sizes and enables the membrane to achieve higher permeate qualities [Pillay, 1991; Liu et al., 2009]. Alavi Moghaddam et al. [2001]; Chang et al. [2007] and Ngo et al. [2008] made use of non-woven coarse-pore filters as immersed membranes and highlighted the advantages of coarse-pore filtration, which are also gained by using the woven fabric of this study. They are:

- capable of high permeate fluxes;
- more energy efficient, since a TMP driving force as low as 2 to 3 kPa may be adequate for permeation;
- lower capital costs; and
- lower operating costs.

B.3 Membrane element production

The membrane elements for this study were fabricated in a casting procedure which was specially developed to produce physical resistant elements to ensure constructional integrity even after multiple fouling experiments and consequent harsh cleaning operations. The aim was not to optimise the membrane element design, but rather to produce elements of a standard format with reliable and repeatable performances in the shortest amount of time. With the employed casting procedure a membrane element could be manufactured in two days. Figure B.1 shows a photograph of three membrane elements under construction.



Figure B.1: A photograph of three membrane elements under construction.

Figure B.2 explains the casting techniques that were developed to produce a flat-sheet woven membrane element. Firstly, a membrane curtain is cut from the membrane material to include the required filtration area and an added 50 mm in length to compromise for the filtration area which will become inactive during the casting process (Figure B.2(a)). Since the membrane material comprises of a series of adjacent filter tubes, the width of the active membrane can only be selected in discrete quantities of filter tube widths of 39 mm. In addition the cut out membrane curtain also contains inactive tube remains on its sides (Figure B.2(b)).

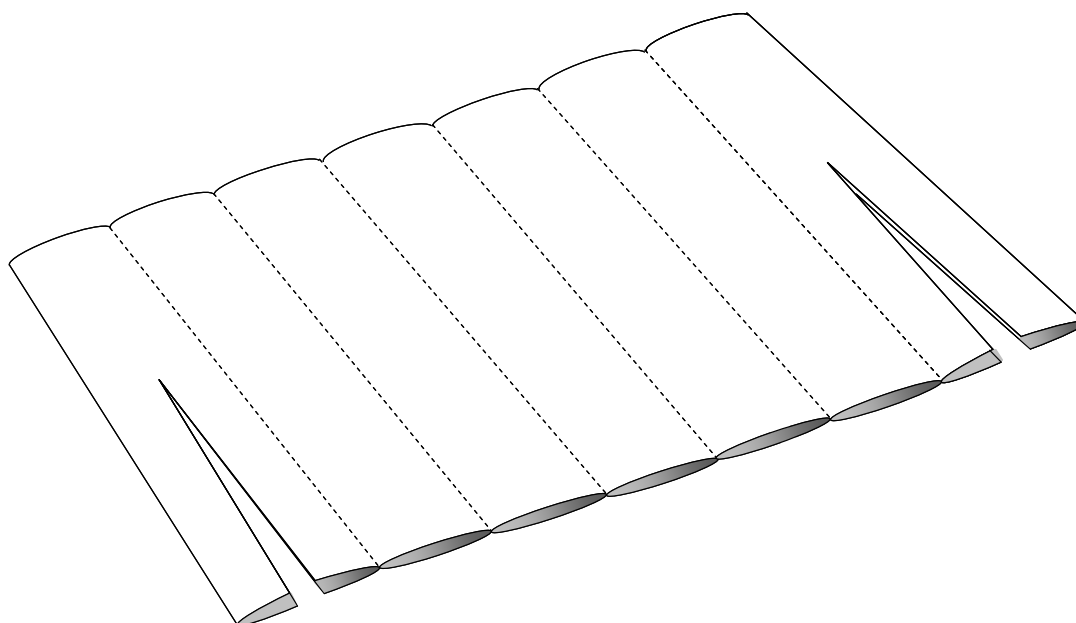


Figure B.2(a): Membrane curtain is cut from the membrane material.

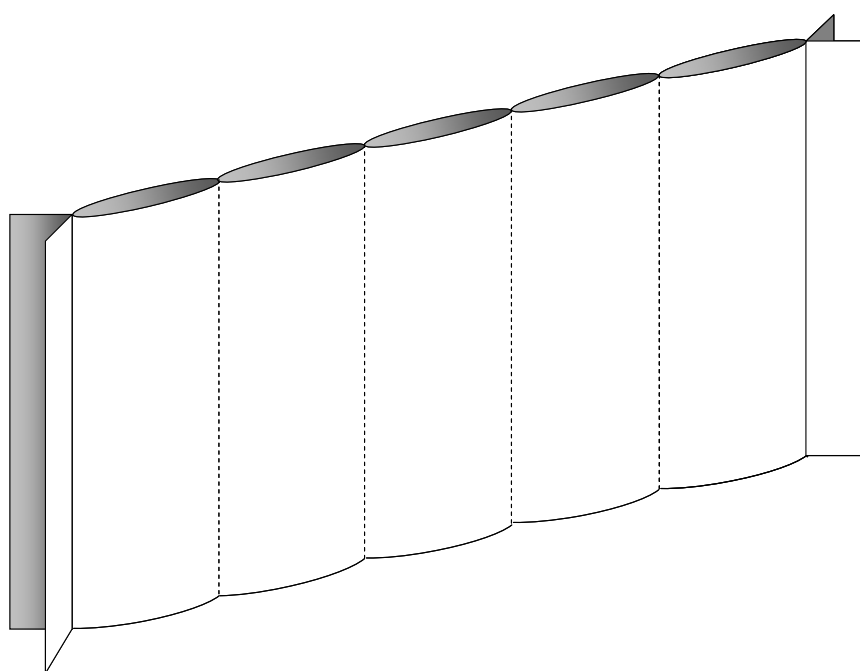


Figure B.2(b): Membrane curtain contains the selected number of filter tubes and the inactive tube remains on the sides

The stainless steel mesh spacer material strips, approximately 10 mm longer than the filter tubes' length, are inserted into the filter tubes (Figure B.2(c)). The membrane curtain, containing the spacer material strips, is now slotted into a 20 mm outer diameter PVC pipe with a slit the length of the cut membrane width, therefore including the tube remains on the membrane curtain's sides. These tube remains are glued together and sealed off from the adjacent filter tubes with any

commercially available silicon rubber sealant. Sealing off the tube remains fortifies the edges of the membrane curtain and avoid pinholing along the length of the seams, as experienced by Pillay [1991] and Swart [1993], to occur. Pinholing results in a loss of membrane integrity, since the seams move apart when subjected to a TMP to create holes through which larger particles can enter to reduce the quality of the permeate. The sides of the pipe are now closed off, taping proofed to be sufficient, and the first casting is ready to commence. Epoxy resin is introduced with a syringe through enlargements made on the ends of the slit in the pipe. The pipe is filled with the resin and left overnight to set, and effectively seal off the bottom end of the membrane curtain (Figure B.2(d)).

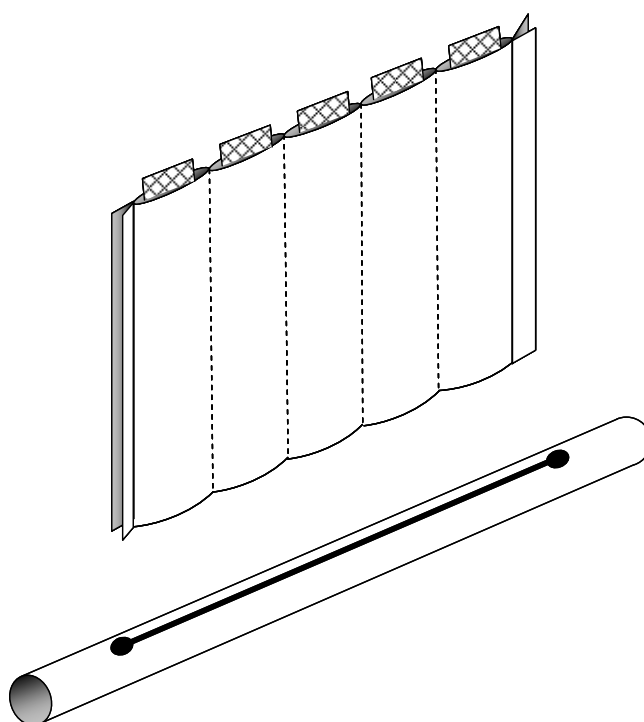


Figure B.2(c): Stainless steel mesh strips are inserted into the filter tubes to act as spacer material. The membrane curtain is then slotted inside a slit cut into a PVC pipe.

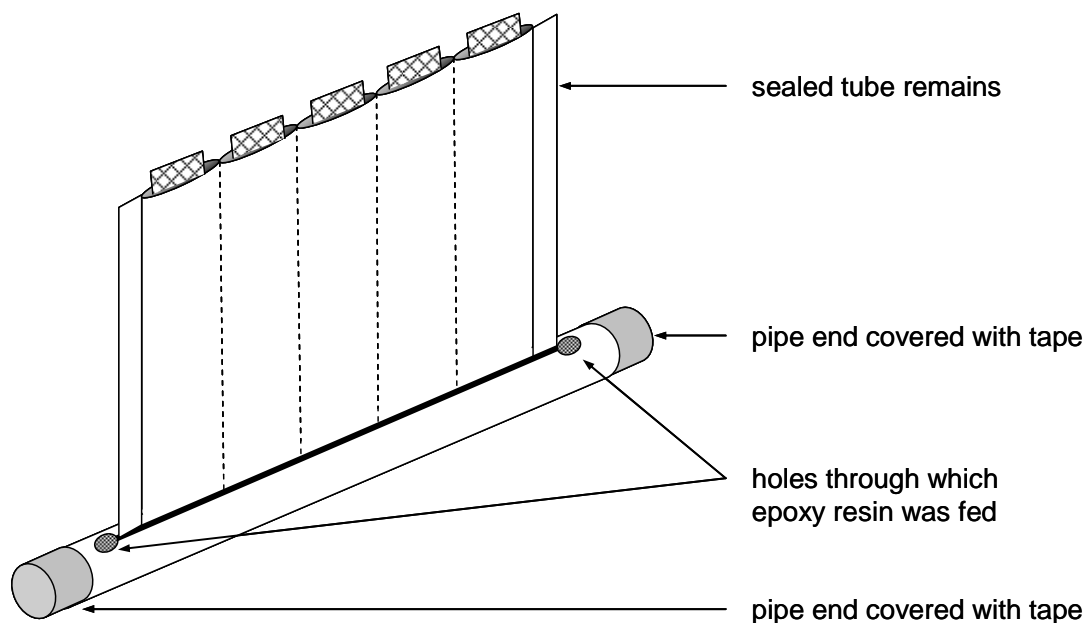


Figure B.2(d): Bottom end of membrane element sealed off.

The sealed off membrane curtain is turned around and this time the side with the protruding (approximately 10 mm) stainless steel mesh spacer material strips is slotted into a 20 mm outer diameter PVC pipe with a slit the length of the membrane curtain width. This pipe is to form part of the permeate collector of the membrane curtain's filter tubes. The pipe must have a length of 510 mm to fit into the mould which is to be used in the next casting step (see Figure B.3). A hole is drilled in line with the pipe's slit close to the edge on each end. Silicon rubber sealant is used to fashion plugs on the inside of the pipe behind the respective drilled holes (Figure B.2(e)). The slit containing the slotted membrane curtain's open end is sealed by applying silicon rubber sealant all around the membrane curtain entrance at the slit. The silicon rubber sealing at the membrane curtain entrance also helps to secure the membrane curtain's position (Figure B.2(f)).

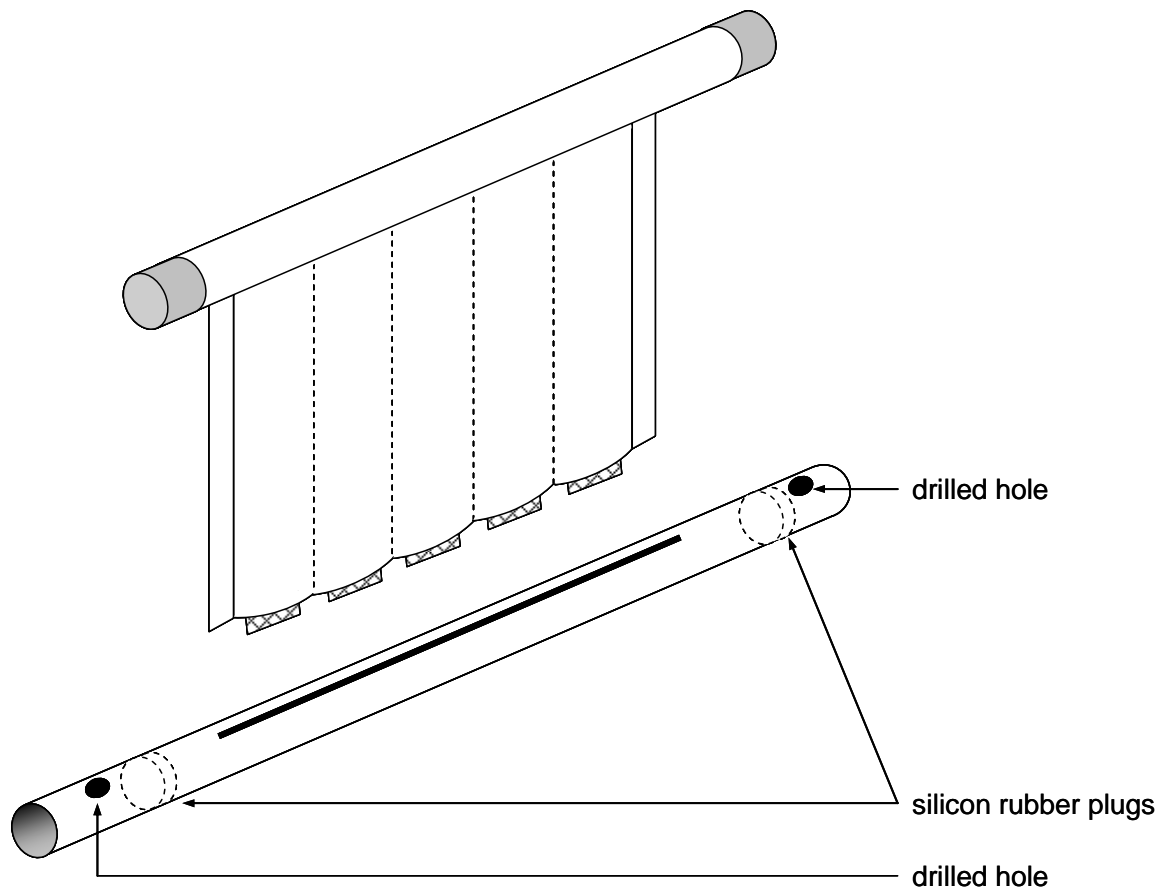


Figure B.2(e): Construction of the permeate collector.

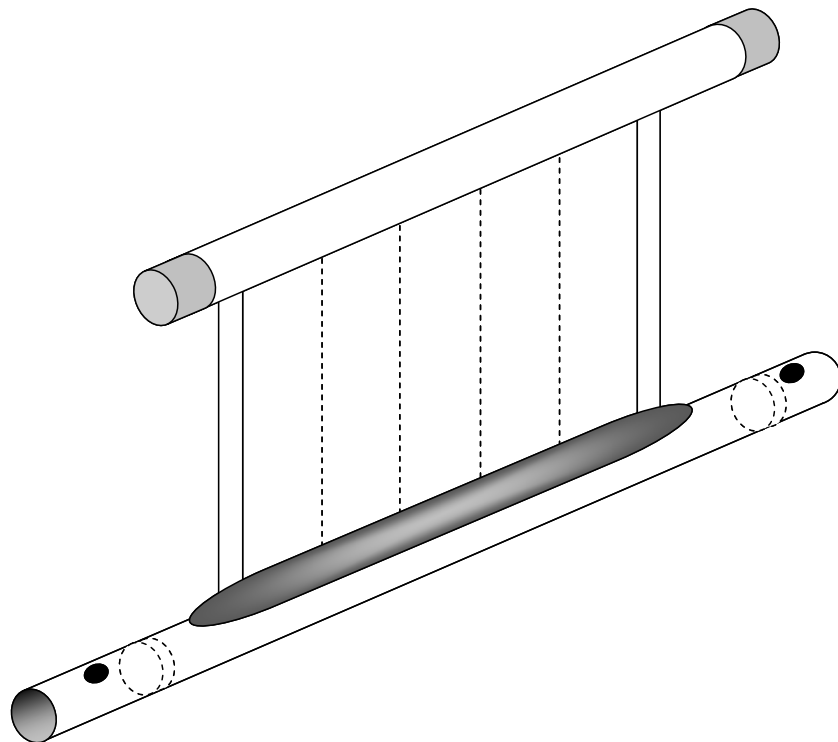


Figure B.2(f): Sealing of membrane curtain entrance at permeate collector.

The pipe housing the open end of the membrane curtain is positioned in a polyethylene mould comprising of four parts: two A blocks enclosing the respective ends of the pipe, and two B blocks enclosing the length of the pipe (Figure B.2(g)). A detail drawing of the mould is shown in Figure B.3. Epoxy resin is injected with a syringe into the housed pipe via tubes entering each A block (Figure B.2(h)). Inside the pipe the resin flow is however stopped by the silicon plugs and is consequently forced to exit the pipe through the drilled holes and encompass the length of the pipe and a fraction of the membrane curtain inside blocks B. The mould is filled with resin and left overnight to set. This casting technique enables the sealing of the pipe ends and the further securing of the membrane curtain with the permeate collector in a single step (Figure B.2(i)).

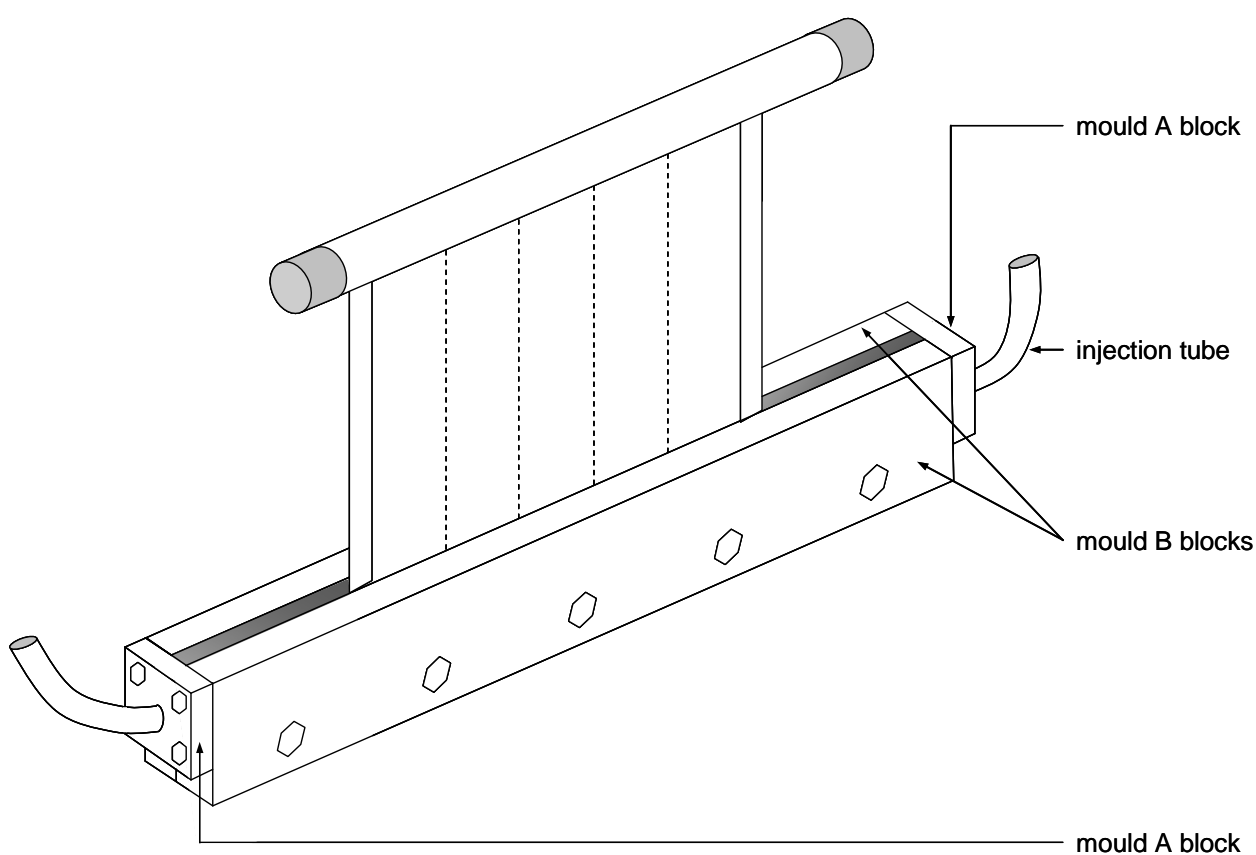


Figure B.2(g): The mould set-up around the permeate collector.

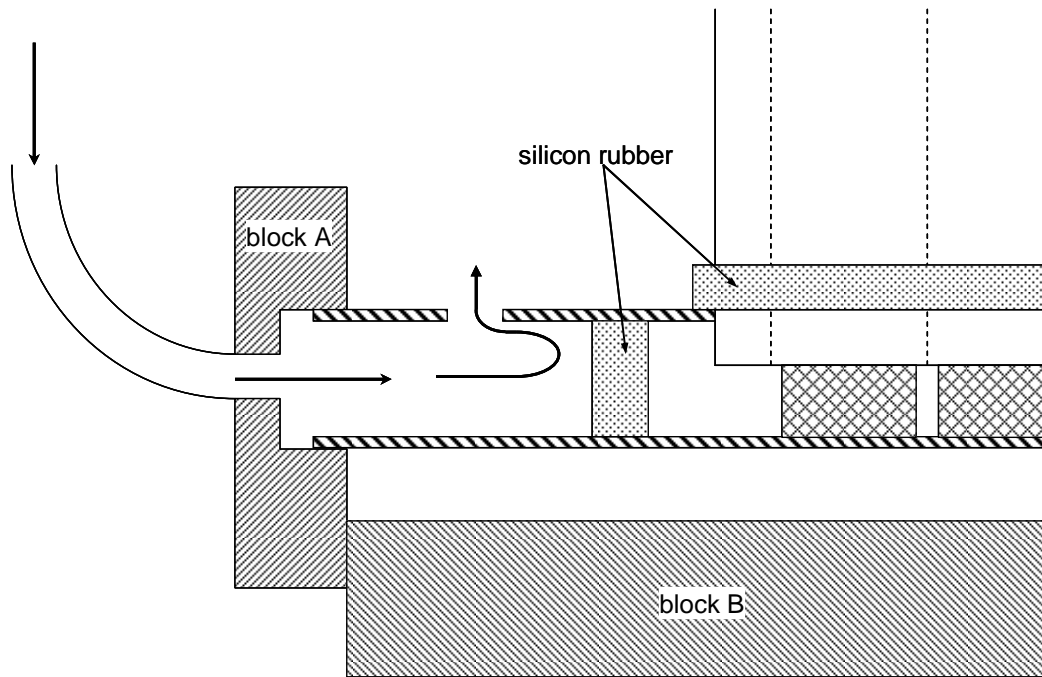


Figure B.2(h): The flow of the injected resin through the injection tube, into the PVC pipe and around the permeate collector.

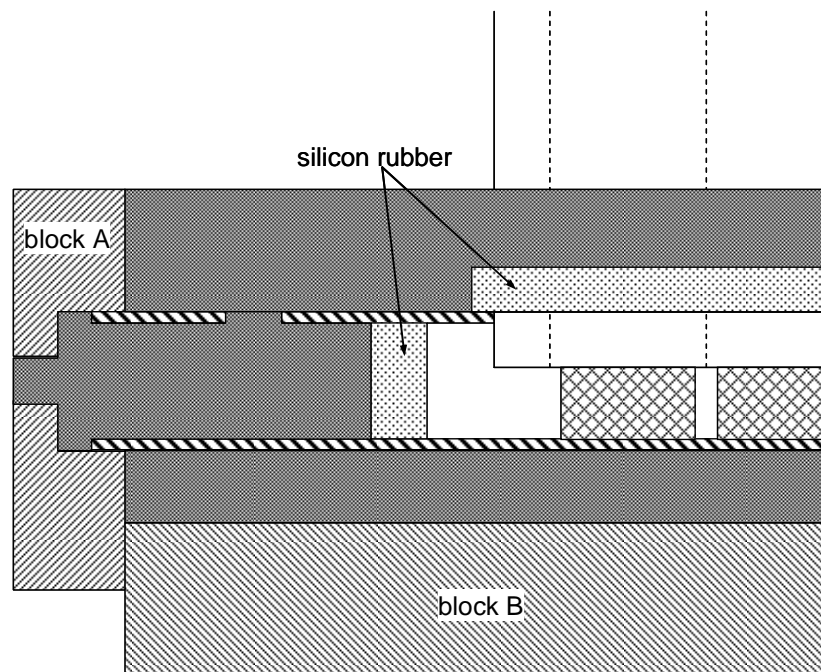


Figure B.2(i): The set resin around the permeate collector. Note how the silicon rubber plug and the silicon rubber sealing at the membrane curtain entrance keeps the permeate collector empty.

The polyethylene mould does not bind to the resin and may be removed once the resin has set to be used again in the production of a next membrane element. The undesired resin-filled pipes of the membrane element may be sawn off. A hole is drilled into the permeate collector and a tube fitting inserted and sealed with silicon rubber sealant (Figure B.2(j)). The permeate collection tube is connected to the tube fitting and the membrane element is ready for filtration. Figure B.2(k) shows a cross-section through the middle of the membrane element.

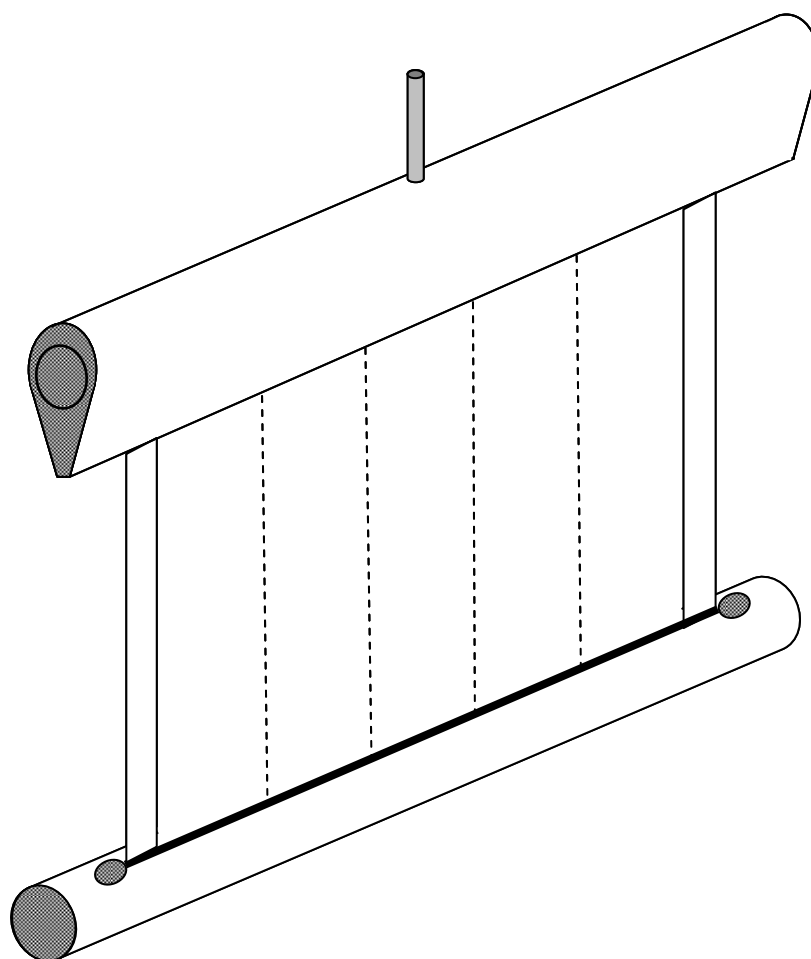


Figure B.2(j): The finished membrane element product. The resin filled parts of the bottom sealed pipe and the top permeate collector have been sawn off.

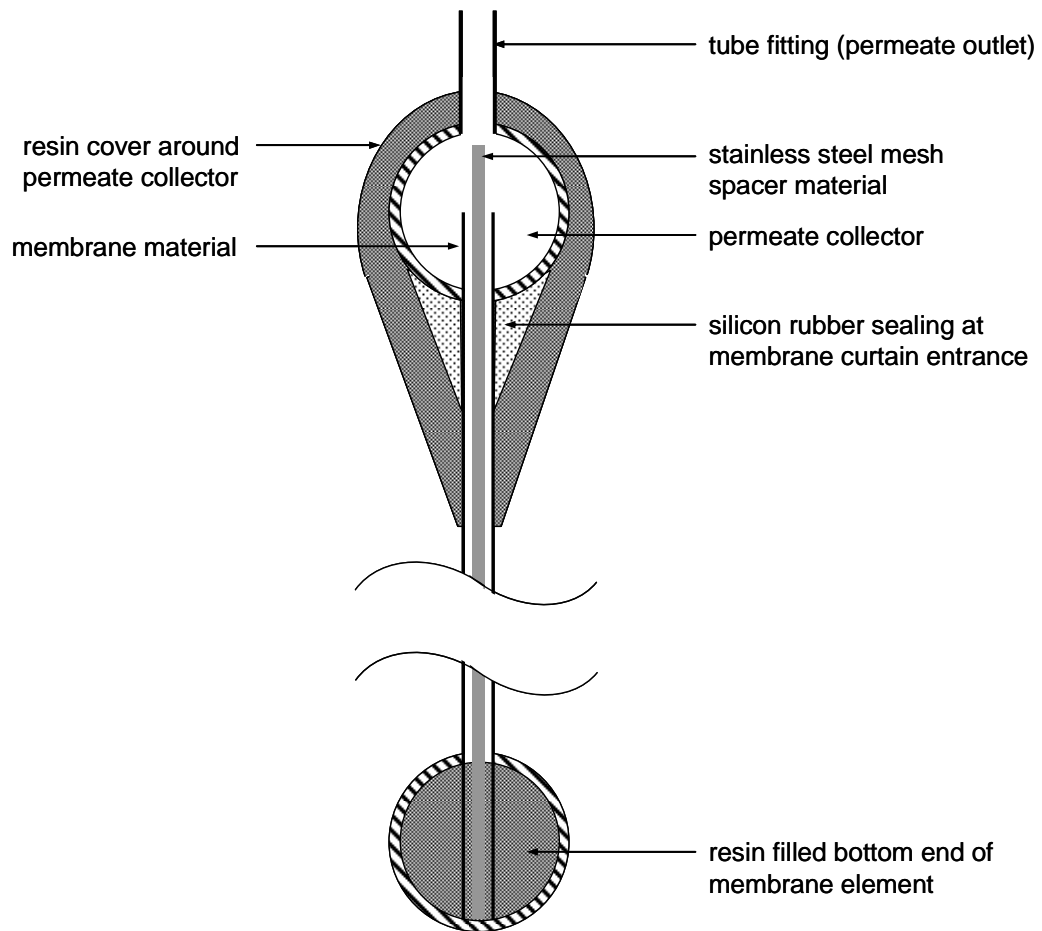


Figure B.2(k): Cross-section through the middle of a completed membrane element.

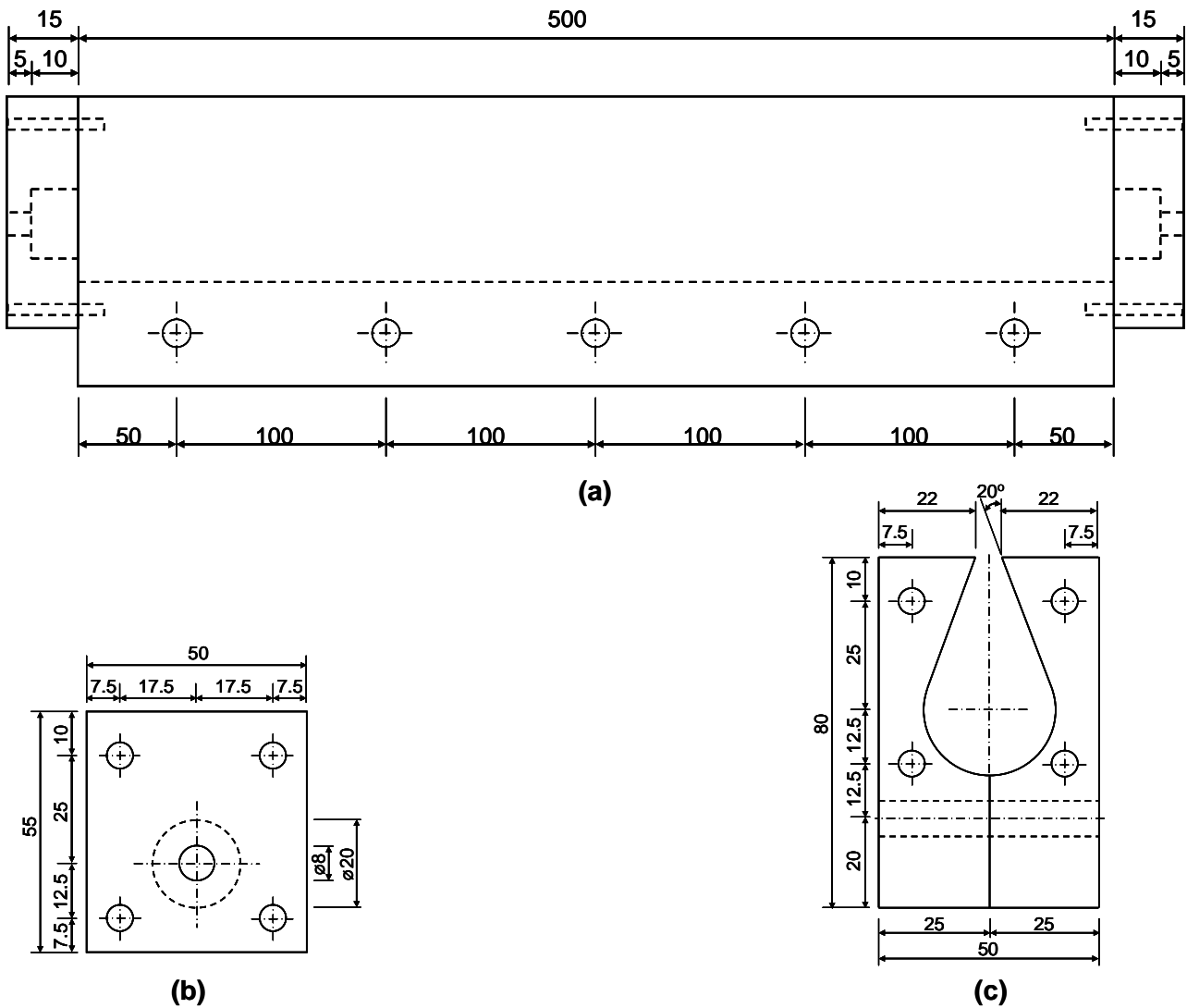


Figure B.3: Detail measurements of the polyethylene mould blocks: (a) blocks A and B connected to form the total mould; (b) one block A; and (c) both blocks B. Note that drawings are not to scale and that measurements are given in millimetres.

Addendum C

Flux-step experimental data

Flux-step experimental data at low aeration intensity (110 L/m².min) - Trial 2

Time (min)	Temperature (°C)	Nominal permeate flux (L/m ² . h)	Actual permeate flux (L/m ² . h)	dP (mm H ₂ O)
0	22.0	5	5.1	34
20	22.0	5	5.1	60
40	22.0	5	5.0	85
60	21.5	5	5.1	90
80	21.0	5	5.0	93
100	21.0	5	5.0	95
120	21.0	5	5.0	95
120	21.0	10	9.7	148
140	21.0	10	9.4	165
160	21.0	10	9.2	176
180	21.0	10	9.5	179
200	21.0	10	9.3	184
220	21.0	10	9.2	186
240	21.0	10	9.2	189
240	21.0	15	14.9	272
260	20.5	15	14.9	311
280	20.0	15	14.9	330
300	20.0	15	14.9	338
320	20.0	15	14.9	351
340	20.0	15	14.9	363
360	20.0	15	14.9	372
360	20.0	20	19.5	456
380	20.0	20	19.5	531
400	20.0	20	19.2	556
420	19.5	20	19.5	587
440	19.5	20	19.2	612
460	19.0	20	19.5	632
480	19.0	20	19.5	654
480	19.0	25	24.2	772
500	19.0	25	24.2	936
520	19.0	25	24.6	1041
540	19.0	25	25.0	1102
560	19.0	25	24.2	1165
580	19.0	25	24.2	1237
600	19.0	25	24.2	1307

Flux-step experimental data at low aeration intensity (110 L/m².min) - Trial 8

Time (min)	Temperature (°C)	Nominal permeate flux (L/m ² . h)	Actual permeate flux (L/m ² . h)	dP (mm H ₂ O)
0	22.5	5	4.9	28
20	22.5	5	5.1	55
40	22.5	5	5.1	79
60	22.5	5	5.1	86
80	22.0	5	5.1	88
100	22.0	5	5.0	89
120	22.0	5	5.0	89
120	22.0	10	10.0	136
140	22.0	10	10.0	159
160	22.0	10	10.0	163
180	22.0	10	10.0	165
200	22.0	10	9.8	169
220	22.0	10	9.8	172
240	22.0	10	9.8	177
240	22.0	15	15.2	255
260	21.5	15	15.2	290
280	21.5	15	15.2	314
300	21.5	15	15.0	329
320	21.5	15	15.2	348
340	21.5	15	15.2	354
360	21.5	15	15.2	364
360	21.5	20	19.5	439
380	21.5	20	19.7	508
400	21.5	20	19.7	542
420	21.5	20	19.7	567
440	21.0	20	19.7	586
460	21.0	20	20.3	604
480	21.0	20	20.3	632
480	21.0	25	25.4	761
500	21.0	25	25.4	894
520	21.0	25	25.0	986
540	21.0	25	25.0	1065
560	21.0	25	25.0	1120
580	21.0	25	25.4	1169
600	21.0	25	25.0	1236

Flux-step experimental data at intermediate aeration intensity (580 L/m².min) - Trial 3

Time (min)	Temperature (°C)	Nominal permeate flux (L/m ² . h)	Actual permeate flux (L/m ² . h)	dP (mm H ₂ O)
0	23.0	5	5.2	25
20	23.0	5	5.1	36
40	23.0	5	5.1	40
60	23.0	5	5.1	48
80	23.0	5	5.2	53
100	23.0	5	5.2	55
120	23.0	5	5.2	55
120	23.0	10	10.2	95
140	23.0	10	10.0	123
160	23.0	10	10.0	140
180	22.5	10	10.0	151
200	22.5	10	10.0	164
220	22.5	10	10.0	169
240	22.5	10	10.0	172
240	22.5	15	15.2	252
260	22.5	15	15.0	263
280	22.5	15	14.9	277
300	22.5	15	14.9	290
320	22.5	15	15.0	299
340	22.5	15	14.9	306
360	22.5	15	14.9	312
360	22.5	20	19.7	406
380	22.5	20	19.7	427
400	22.5	20	19.5	449
420	22.0	20	19.5	466
440	22.0	20	19.5	484
460	22.0	20	19.5	499
480	22.0	20	19.5	516
480	22.0	25	24.2	607
500	21.5	25	24.2	718
520	21.5	25	24.2	773
540	21.5	25	24.2	819
560	21.5	25	24.2	862
580	21.5	25	24.2	882
600	21.0	25	24.2	924

Flux-step experimental data at intermediate aeration intensity (580 L/m².min) - Trial 4

Time (min)	Temperature (°C)	Nominal permeate flux (L/m ² . h)	Actual permeate flux (L/m ² . h)	dP (mm H ₂ O)
0	21.5	5	4.9	32
20	21.5	5	4.9	44
40	21.5	5	5.0	46
60	21.5	5	5.1	50
80	21.5	5	5.0	50
100	21.5	5	5.1	50
120	21.0	5	5.1	50
120	21.0	10	9.8	115
140	21.0	10	9.8	132
160	21.0	10	9.8	160
180	21.0	10	9.8	169
200	21.0	10	9.7	171
220	21.0	10	9.7	174
240	21.0	10	9.7	176
240	21.0	15	14.7	230
260	21.0	15	14.9	249
280	21.0	15	14.9	258
300	21.0	15	14.9	273
320	20.5	15	14.7	284
340	20.5	15	14.9	292
360	20.5	15	14.9	299
360	20.5	20	20.0	375
380	20.5	20	20.0	403
400	20.5	20	20.3	418
420	20.0	20	19.7	432
440	20.0	20	19.7	448
460	20.0	20	20.0	463
480	20.0	20	19.7	469
480	20.0	25	24.6	546
500	20.0	25	24.6	654
520	20.0	25	24.6	706
540	20.0	25	24.6	760
560	20.0	25	24.6	793
580	19.5	25	25.0	817
600	19.5	25	25.0	846

Flux-step experimental data at high aeration intensity (1 100 L/m².min) - Trial 6

Time (min)	Temperature (°C)	Nominal permeate flux (L/m². h)	Actual permeate flux (L/m². h)	dP (mm H₂O)
0	20.0	5	5.3	23
20	20.0	5	5.1	43
40	20.0	5	5.1	76
60	20.0	5	5.1	82
80	20.0	5	5.0	85
100	20.0	5	5.1	89
120	20.0	5	5.0	89
120	20.0	10	9.8	133
140	20.0	10	10.0	178
160	20.0	10	9.8	185
180	20.0	10	10.0	192
200	20.0	10	10.2	197
220	20.0	10	10.0	202
240	20.0	10	10.0	206
240	20.0	15	15.2	300
260	19.5	15	15.2	332
280	19.5	15	15.2	353
300	19.5	15	15.0	365
320	19.5	15	15.0	378
340	19.5	15	15.2	391
360	19.0	15	15.2	423
360	19.0	20	19.5	516
380	19.0	20	19.2	556
400	19.0	20	19.2	584
420	19.0	20	19.2	607
440	19.0	20	19.5	646
460	19.0	20	19.2	683
480	19.0	20	19.2	711
480	19.0	25	24.2	929
500	19.0	25	25.0	1058
520	18.5	25	24.2	1156
540	18.5	25	24.2	1251
560	18.5	25	24.2	1343
580	18.5	25	24.2	1412
600	18.5	25	24.2	1496

Flux-step experimental data at high aeration intensity (1 100 L/m².min) - Trial 9

Time (min)	Temperature (°C)	Nominal permeate flux (L/m². h)	Actual permeate flux (L/m². h)	dP (mm H₂O)
0	22.0	5	5.0	28
20	22.0	5	5.0	40
40	22.0	5	5.0	66
60	22.0	5	5.0	82
80	22.0	5	5.0	89
100	22.0	5	4.9	92
120	22.0	5	5.0	94
120	22.0	10	9.7	144
140	21.5	10	9.7	191
160	21.5	10	9.7	207
180	21.5	10	9.8	217
200	21.5	10	9.7	222
220	21.5	10	10.0	228
240	21.5	10	9.7	233
240	21.5	15	15.2	327
260	21.5	15	15.2	374
280	21.5	15	15.2	388
300	21.0	15	15.2	396
320	21.0	15	15.2	409
340	21.0	15	15.0	421
360	20.5	15	15.0	435
360	20.5	20	20.3	543
380	20.5	20	20.0	601
400	20.5	20	20.0	629
420	20.5	20	20.0	652
440	20.0	20	20.0	688
460	20.0	20	20.0	717
480	20.0	20	20.0	743
480	20.0	25	24.6	984
500	20.0	25	24.6	1116
520	20.0	25	24.2	1190
540	20.0	25	24.6	1279
560	20.0	25	24.2	1361
580	20.0	25	24.2	1468
600	20.0	25	24.6	1551

Addendum *D*

UTDR experimental data

Determining speed of sound in bentonite cake layer

The weight ratio of bentonite to water in a bentonite cake layer was assumed to be 1:1 and the density of a bentonite cake layer was therefore assumed to be 2 g/cm³ (between the density of water at 1 g/cm³ and the density of bentonite at 3 g/cm³).

A bentonite clay of 1 g bentonite per cm³ water was prepared and used to fill a glass cell with an interspace distance of 10 mm. The same Panametrics Videoscanner V120-RB transducer was used as described in Section 4.4.2 for the UTDR experiment, but this time to measure the time delay between the reflected energy from the two glass sheets of the clay filled cell. The time delay was measured as 7.06 μs. From Equation 4.4:

$$c = \frac{2\Delta S}{\Delta t}$$

where c = speed of sound in the fouling layer (m/s)

ΔS = fouling layer thickness (m)

Δt = arrival time difference (s)

Therefore:

$$c = \frac{2 \times 0.010}{7.06 \times 10^{-6}} \approx 2800 \text{ m/s}$$

Addendum E

Screening design experimental data

Plackett-Burman design for area under velocity profile

BASE								Y ₁	Y ₂	Average Y	S ²
Treatment	A _g /A _r	H _r	H _B	Air	Depth	Diffuser	?				
1	+	-	-	+	-	+	+	0.6656	0.6401	0.6529	0.000325
2	+	+	-	-	+	-	+	0.9696	1.0226	0.9961	0.001405
3	+	+	+	-	-	+	-	0.7275	0.6665	0.6970	0.001861
4	-	+	+	+	-	-	+	0.2684	0.3174	0.2929	0.001201
5	+	-	+	+	+	-	-	0.8711	1.1573	1.0142	0.040955
6	-	+	-	+	+	+	-	0.3777	0.4281	0.4029	0.001270
7	-	-	+	-	+	+	+	0.5996	0.6552	0.6274	0.001546
8	-	-	-	-	-	-	-	0.6503	0.6761	0.6632	0.000333
HY_r	3.3602	2.3889	2.6315	2.3629	3.0406	2.3802	2.5693				
HY_B	1.9864	2.9577	2.7151	2.9837	2.3060	2.9664	2.7773				
Average Y_r	0.8400	0.5972	0.6579	0.5907	0.7602	0.5950	0.6423				
Average Y_B	0.4966	0.7394	0.6788	0.7459	0.5765	0.7416	0.6943				
Effect	0.3434	-0.1422	-0.0209	-0.1552	0.1837	-0.1466	-0.0520				
Average S_r²	0.011136	0.001434	0.011139	0.010938	0.011294	0.00125	0.001119				
Average S_B²	0.001087	0.01079	0.000833	0.001286	0.00093	0.010973	0.011105				
F	10.24248	7.524757	13.67189	8.506061	12.14739	8.776177	9.924163				
Absolute effect	0.3434	0.1422	0.0209	0.1552	0.1837	0.1466	0.0520				

REFLECTION								Y ₁	Y ₂	Average Y	S ²
Treatment	A _g /A _r	H _r	H _B	Air	Depth	Diffuser	?				
9	-	+	+	-	+	-	-	0.5807	0.6075	0.5941	0.000359
10	-	-	+	+	-	+	-	0.5271	0.5718	0.5495	0.000999
11	-	-	-	+	+	-	+	0.4598	0.5058	0.4828	0.001058
12	+	-	-	-	+	+	-	0.8195	0.5160	0.6678	0.046056
13	-	+	-	-	-	+	+	0.6141	0.5963	0.6052	0.000158
14	+	-	+	-	-	-	+	0.3938	0.3749	0.3844	0.000179
15	+	+	-	+	-	-	-	1.0319	0.9878	1.0099	0.000972
16	+	+	+	+	+	+	+	1.0076	0.9554	0.9815	0.001362
HY_r	3.0435	3.1907	2.5094	3.0236	2.7262	2.8039	2.4539				
HY_B	2.2316	2.0844	2.7656	2.2514	2.5489	2.4711	2.8212				
Average Y_r	0.7609	0.7977	0.6274	0.7559	0.6815	0.7010	0.6135				
Average Y_B	0.5579	0.5211	0.6914	0.5629	0.6372	0.6178	0.7053				
Effect	0.2030	0.2766	-0.0640	0.1931	0.0443	0.0832	-0.0918				
Average S_r²	0.012142	0.000713	0.000725	0.001098	0.012209	0.012144	0.000689				
Average S_B²	0.000379	0.012073	0.012061	0.011688	0.000577	0.000642	0.012097				
F	32.02561	16.93043	16.64084	10.64519	21.15495	18.91493	17.54766				
Absolute effect	0.2030	0.2766	0.0640	0.1931	0.0443	0.0832	0.0918				

Average effect	0.2732	0.0672	-0.0425	0.0189	0.1140	-0.0317	-0.0719	→ Main effects
Difference effect	-0.0702	0.2094	-0.0216	0.1741	-0.0697	0.1149	-0.0199	→ Confounded interactions

BD	AD	AG	AB	AF	AE	AC
CG	CE	BE	CF	BC	BG	BF
EF	FG	DF	EG	DG	CD	DE

Plackett-Burman design for average gradient of velocity profile

BASE								Y ₁	Y ₂	Average Y	S ²
Treatment	A _g /A _r	H _T	H _B	Air	Depth	Diffuser	?				
1	+	-	-	+	-	+	+	-0.0758	-0.0389	-0.0574	0.000681
2	+	+	-	-	+	-	+	0.0082	0.0195	0.0139	6.38E-05
3	+	+	+	-	-	+	-	-0.0028	-0.0104	-0.0066	2.89E-05
4	-	+	+	+	-	-	+	0.0833	0.0912	0.0873	3.12E-05
5	+	-	+	+	+	-	-	0.1129	0.0893	0.1011	0.000278
6	-	+	-	+	+	+	-	-0.0186	-0.0177	-0.0182	4.05E-07
7	-	-	+	-	+	+	+	-0.0752	-0.0952	-0.0852	0.0002
8	-	-	-	-	-	-	-	-0.0212	-0.0233	-0.0223	2.21E-06
HY₊	0.0510	0.0764	0.0966	0.1129	0.0116	-0.1673	0.0010				
HY₋	-0.0384	-0.0637	-0.0839	-0.1002	0.0011	0.1800	0.0003				
Average Y₊	0.0128	0.0191	0.0241	0.0282	0.0029	-0.0418	0.0002				
Average Y₋	-0.0096	-0.0159	-0.0210	-0.0251	0.0003	0.0450	0.0001				
Effect	0.0223	0.0350	0.0451	0.0533	0.0026	-0.0868	0.0002				
Average S₊²	0.000263	3.11E-05	0.000135	0.000248	0.000136	0.000228	0.000244				
Average S₋²	5.85E-05	0.00029	0.000187	7.37E-05	0.000186	9.39E-05	7.75E-05				
F	4.499326	9.341617	0.72072	3.359763	0.730364	0.412855	0.317639				
Absolute effect	0.0223	0.0350	0.0451	0.0533	0.0026	0.0868	0.0002				

REFLECTION								Y ₁	Y ₂	Average Y	S ²
Treatment	A _g /A _r	H _T	H _B	Air	Depth	Diffuser	?				
9	-	+	+	-	+	-	-	0.1442	0.1484	0.1463	8.82E-06
10	-	-	+	+	-	+	-	-0.0828	-0.0844	-0.0836	1.28E-06
11	-	-	-	+	+	-	+	0.0124	0.0255	0.0190	8.58E-05
12	+	-	-	-	+	+	-	-0.0422	-0.0344	-0.0383	3.04E-05
13	-	+	-	-	-	+	+	-0.0738	-0.0410	-0.0574	0.000538
14	+	-	+	-	-	-	+	0.1429	0.1267	0.1348	0.000131
15	+	+	-	+	-	-	-	-0.0481	-0.0415	-0.0448	2.18E-05
16	+	+	+	+	+	+	+	0.0113	-0.0266	-0.0077	0.000718
HY₊	0.0441	0.0365	0.1899	-0.1171	0.1193	-0.1870	0.0887				
HY₋	0.0243	0.0319	-0.1216	0.1854	-0.0510	0.2553	-0.0204				
Average Y₊	0.0110	0.0091	0.0475	-0.0293	0.0298	-0.0467	0.0222				
Average Y₋	0.0061	0.0080	-0.0304	0.0464	-0.0128	0.0638	-0.0051				
Effect	0.0050	0.0012	0.0779	-0.0756	0.0426	-0.1106	0.0273				
Average S₊²	0.000225	0.000322	0.000215	0.000207	0.000211	0.000322	0.000368				
Average S₋²	0.000137	6.22E-05	0.000169	0.000177	0.000173	6.19E-05	1.56E-05				
F	1.645241	0.193301	1.271628	0.856493	0.820872	5.200707	23.64607				
Absolute effect	0.0050	0.0012	0.0779	0.0756	0.0426	0.1106	0.0273				

Average effect	0.0136	0.0181	0.0615	-0.0112	0.0226	-0.0987	0.0137
Difference effect	-0.0087	-0.0169	0.0164	-0.0644	0.0200	-0.0119	0.0136

→ Main effects
 → Confounded interactions

BD	AD	AG	AB	AF	AE	AC
CG	CE	BE	CF	BC	BG	BF
EF	FG	DF	EG	DG	CD	DE

Treatment 1

	1		2		3		4	
1	1.75	1.37	2.12	4.49	2.35	2.23	5.04	2.30
2	1.61	2.54	1.97	3.78	2.06	2.09	6.83	5.38
3	3.15	2.55	1.46	3.26	2.46	2.11	6.93	7.36
4	1.35	3.22	2.27	1.84	7.19	3.46	4.63	4.88
5	2.81	1.64	3.11	2.18	2.62	1.67	9.37	4.17
6	1.45	3.76	2.13	1.75	1.09	2.35	8.21	3.42
7	1.74	0.96	2.56	2.15	5.11	3.62	7.44	4.84
8	1.56	2.52	3.10	3.20	1.60	4.66	5.68	5.04
9	1.42	2.23	2.03	1.97	2.98	2.34	6.79	4.14
10	1.67	2.41	2.65	2.48	3.14	3.08	4.68	4.51

Downcomer/riser 2 +
 Top clearance (m) 0.1 -
 Bottom clearance (m) 0.03 -
 Aeration intensity (L/m².min) 1350 +
 Depth (m) 1.1 -
 Diffuser position Riser +

Average times (s):

1.851	2.320	2.340	2.710	3.060	2.761	6.560	4.604
-------	-------	-------	-------	-------	-------	-------	-------

Distance (m): 0.6

Average rise velocities (m/s):

0.324	0.259	0.256	0.221	0.196	0.217	0.091	0.130
-------	-------	-------	-------	-------	-------	-------	-------

1	0.324	0.259
2	0.256	0.221
3	0.196	0.217
4	0.091	0.130

Area under graph:

0.6656	0.6401
Average:	0.6529
S ² :	0.000325

Residual area:

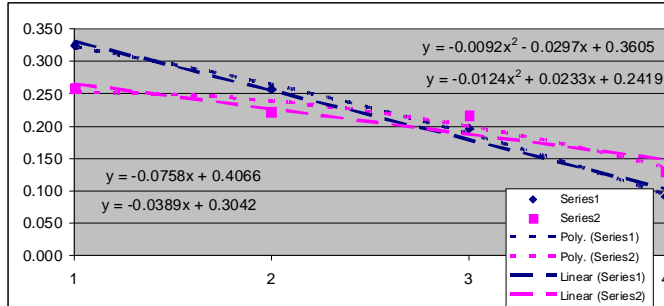
0.2992	0.1183
Average:	0.2088
S ² :	0.016362

Differential area:

0.3664	0.5218
Average:	0.4441
S ² :	0.0121

Average gradient:

-0.0758	-0.0389
Average:	-0.0574
S ² :	0.0007



Treatment 2

	1		2		3		4	
1	2.39	2.81	2.18	2.25	2.40	2.24	1.62	1.82
2	1.89	3.14	2.18	2.61	2.11	1.92	2.97	2.01
3	2.70	2.69	2.15	2.21	2.02	2.54	2.00	2.14
4	2.69	2.33	3.33	2.70	3.07	2.14	2.40	2.65
5	2.23	2.09	3.42	2.09	2.46	2.79	2.36	2.06
6	2.41	2.76	2.44	3.17	2.72	1.81	1.58	2.08
7	2.26	2.30	2.78	2.14	2.15	2.37	2.16	2.47
8	2.12	2.15	2.33	1.94	2.90	2.59	2.82	2.41
9	2.82	2.54	2.37	2.27	2.23	2.20	2.29	1.94
10	2.29	2.63	3.50	2.68	1.94	2.43	2.50	1.79

Downcomer/riser 2 +
 Top clearance (m) 0.2 +
 Bottom clearance (m) 0.03 -
 Aeration intensity (L/m².min) 800 -
 Depth (m) 1.4 +
 Diffuser position Bottom -

Average times (s):

2.380	2.544	2.668	2.406	2.400	2.303	2.270	2.137
-------	-------	-------	-------	-------	-------	-------	-------

Distance (m): 0.8

Average rise velocities (m/s):

0.336	0.314	0.300	0.333	0.333	0.347	0.352	0.374
-------	-------	-------	-------	-------	-------	-------	-------

1	0.336	0.314
2	0.300	0.333
3	0.333	0.347
4	0.352	0.374

Area under graph:

0.9696	1.0226
Average:	0.9961
S ² :	0.001405

Residual area:

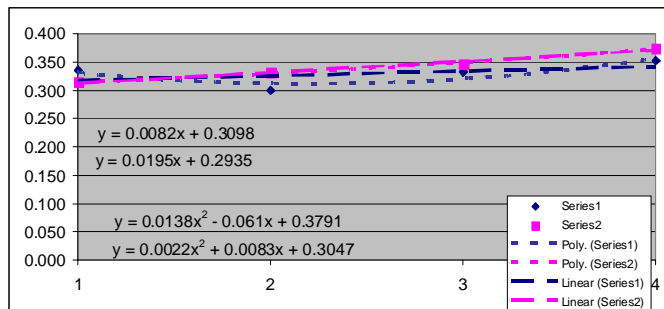
0.0981	0.0967
Average:	0.0974
S ² :	0.000001

Differential area:

0.8715	0.9259
Average:	0.8987
S ² :	0.0015

Average gradient:

0.0082	0.0195
Average:	0.0139
S ² :	0.0001



Treatment 3

	1		2		3		4	
1	1.51	1.73	2.09	2.70	1.18	2.18	1.61	1.90
2	3.31	2.62	2.01	2.39	1.53	2.54	3.47	2.86
3	1.71	1.87	3.23	2.17	2.19	2.23	3.03	2.57
4	1.69	2.17	2.13	2.62	1.57	2.08	1.65	3.13
5	2.14	1.81	2.51	2.48	2.10	2.62	2.72	2.87
6	2.09	1.98	2.44	2.07	1.62	2.22	2.96	2.26
7	1.84	2.16	2.94	2.26	1.83	1.97	2.53	2.05
8	2.33	1.76	2.71	1.85	2.11	2.20	1.92	1.86
9	2.15	2.00	1.98	2.43	1.27	1.84	2.33	1.59
10	1.78	2.11	2.39	2.02	1.74	2.57	2.18	2.61

Downcomer/riser 2 +
 Top clearance (m) 0.2 +
 Bottom clearance (m) 0.1 +
 Aeration intensity (L/m².min) 800 -
 Depth (m) 1.1 -
 Diffuser position Riser +

Average times (s):

2.055	2.021	2.443	2.299	1.714	2.245	2.440	2.370
-------	-------	-------	-------	-------	-------	-------	-------

Distance (m): 0.5

Average rise velocities (m/s):

0.243	0.247	0.205	0.217	0.292	0.223	0.205	0.211
-------	-------	-------	-------	-------	-------	-------	-------

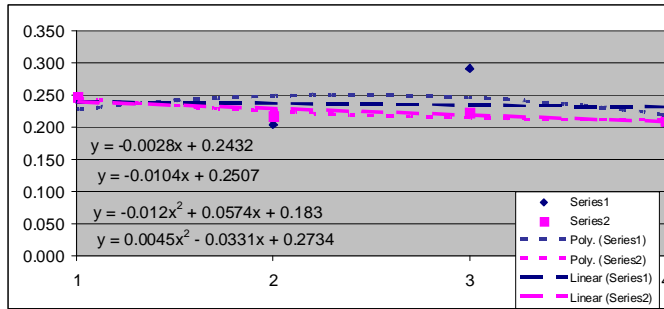
1	0.243	0.247
2	0.205	0.217
3	0.292	0.223
4	0.205	0.211

Area under graph:	0.7275	0.6665
Average:	0.6970	
S²:	0.001861	

Residual area:	0.0274	0.0679
Average:	0.0477	
S²:	0.000820	

Differential area:	0.7001	0.5986
Average:	0.6494	
S²:	0.0052	

Average gradient:	-0.0028	-0.0104
Average:	-0.0066	
S²:	0.0000	



Treatment 4

	1		2		3		4	
1	-	-	-	-	5.14	1.93	1.20	1.24
2	-	-	-	-	1.93	2.68	2.00	1.57
3	-	-	-	-	3.93	3.24	2.89	1.87
4	-	-	-	-	3.99	1.07	2.82	2.29
5	-	-	-	-	2.37	1.62	1.82	3.33
6	-	-	-	-	2.55	3.43	2.00	1.49
7	-	-	-	-	2.43	3.47	1.62	1.47
8	-	-	-	-	3.17	2.12	1.85	1.71
9	-	-	-	-	2.05	1.08	3.09	1.88
10	-	-	-	-	3.02	3.92	3.13	4.33

Downcomer/riser 0.5 -
 Top clearance (m) 0.2 +
 Bottom clearance (m) 0.1 +
 Aeration intensity (L/m².min) 1350 +
 Depth (m) 1.1 -
 Diffuser position Bottom -

Average times (s):

-	-	-	-	3.058	2.456	2.242	2.118
---	---	---	---	-------	-------	-------	-------

Distance (m): 0.5

Average rise velocities (m/s):

0.000	0.000	0.000	0.000	0.164	0.204	0.223	0.236
-------	-------	-------	-------	-------	-------	-------	-------

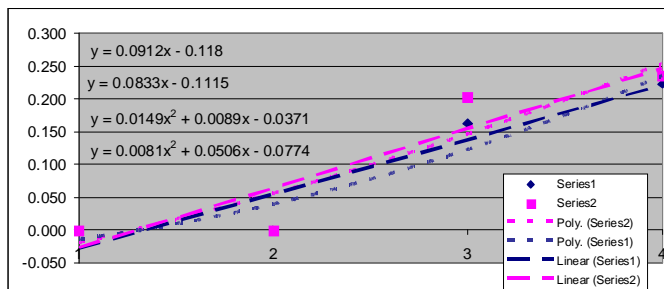
1	0.000	0.000
2	0.000	0.000
3	0.164	0.204
4	0.223	0.236

Area under graph:	0.2684	0.3174
Average:	0.2929	
S²:	0.001201	

Residual area:	0.4423	0.4464
Average:	0.4444	
S²:	0.000008	

Differential area:	-0.1739	-0.1290
Average:	-0.1515	
S²:	0.0010	

Average gradient:	0.0833	0.0912
Average:	0.0873	
S²:	0.0000	



Treatment 5

	1		2		3		4	
1	13.30	2.90	14.87	1.43	1.62	1.33	2.48	1.58
2	6.27	3.28	6.90	3.03	2.12	2.18	2.48	3.29
3	4.13	7.35	6.77	2.37	1.86	2.43	1.96	1.42
4	3.99	10.14	4.31	2.49	1.87	2.35	3.10	1.99
5	7.22	6.21	6.46	2.68	2.22	2.28	1.52	1.68
6	9.27	3.60	2.79	1.87	1.73	2.10	1.74	2.13
7	8.04	5.04	10.12	2.52	2.02	2.02	2.17	2.57
8	6.48	4.27	7.25	2.16	1.77	1.87	2.86	2.19
9	5.21	8.30	4.07	2.60	1.71	1.53	2.51	1.63
10	6.19	3.94	6.62	2.85	2.11	1.71	2.26	2.22

Downcomer/riser 2 +
 Top clearance (m) 0.1 -
 Bottom clearance (m) 0.1 +
 Aeration intensity (L/m².min) 1350 +
 Depth (m) 1.4 +
 Diffuser position Bottom -

Average times (s):

7.010	5.503	7.016	2.400	1.903	1.980	2.308	2.070
-------	-------	-------	-------	-------	-------	-------	-------

Distance (m): 0.9

Average rise velocities (m/s):

0.128	0.164	0.128	0.375	0.473	0.455	0.390	0.435
-------	-------	-------	-------	-------	-------	-------	-------

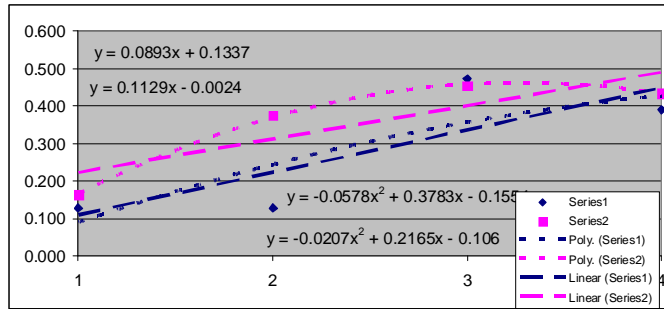
1	0.128	0.164
2	0.128	0.375
3	0.473	0.455
4	0.390	0.435

Area under graph:	0.8711	1.1573
Average:	1.0142	
S²:	0.040955	

Residual area:	0.4153	0.2335
Average:	0.3244	
S²:	0.016526	

Differential area:	0.4558	0.9238
Average:	0.6898	
S²:	0.1095	

Average gradient:	0.1129	0.0893
Average:	0.1011	
S²:	0.0003	



Treatment 6

	1		2		3		4	
1	5.17	4.93	5.27	7.87	7.09	4.56	6.68	6.12
2	5.13	3.85	6.78	5.44	3.09	3.81	3.25	3.71
3	3.85	5.96	8.07	4.73	7.07	6.13	5.59	10.37
4	2.47	4.23	7.07	4.32	1.99	4.95	11.17	6.40
5	8.05	4.77	5.84	7.64	7.83	7.88	5.37	4.87
6	3.86	3.61	6.95	4.22	9.63	6.54	17.03	7.33
7	4.71	4.12	7.21	5.93	4.39	5.99	8.96	3.64
8	7.13	3.87	6.36	4.04	8.17	8.05	10.14	4.09
9	4.46	6.17	5.59	6.30	5.63	4.43	4.85	11.64
10	4.51	3.45	7.93	5.06	6.28	6.33	9.89	7.64

Downcomer/riser 0.5 -
 Top clearance (m) 0.2 +
 Bottom clearance (m) 0.03 -
 Aeration intensity (L/m².min) 1350 +
 Depth (m) 1.4 +
 Diffuser position Riser +

Average times (s):

4.934	4.496	6.707	5.555	6.117	5.867	8.293	6.581
-------	-------	-------	-------	-------	-------	-------	-------

Distance (m): 0.8

Average rise velocities (m/s):

0.162	0.178	0.119	0.144	0.131	0.136	0.096	0.122
-------	-------	-------	-------	-------	-------	-------	-------

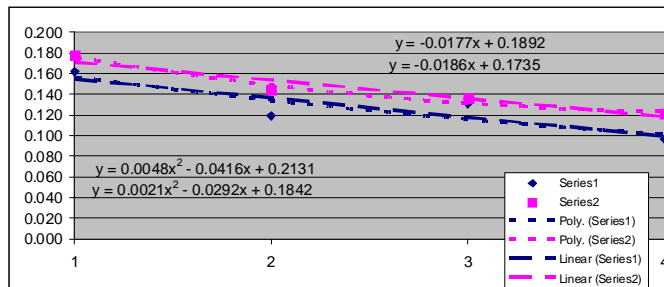
1	0.162	0.178
2	0.119	0.144
3	0.131	0.136
4	0.096	0.122

Area under graph:	0.3777	0.4281
Average:	0.4029	
S²:	0.001270	

Residual area:	0.0936	0.1206
Average:	0.1071	
S²:	0.000365	

Differential area:	0.2841	0.3075
Average:	0.2958	
S²:	0.0003	

Average gradient:	-0.0186	-0.0177
Average:	-0.0182	
S²:	0.0000	



Treatment 7

	1		2		3		4	
1	4.97	2.58	4.77	3.05	5.20	6.04	20.98	4.99
2	3.25	2.57	4.13	3.75	4.25	3.67	10.98	26.53
3	1.93	3.14	1.77	3.17	6.83	5.57	10.89	15.61
4	2.86	2.01	3.58	2.89	7.23	6.10	19.62	4.57
5	3.97	2.77	3.19	3.16	6.58	5.26	11.49	14.93
6	3.57	3.32	2.88	3.16	4.79	5.83	15.38	22.19
7	4.13	3.43	4.34	2.35	3.92	7.88	12.85	10.72
8	1.81	2.09	3.32	3.19	5.14	6.02	9.82	18.03
9	3.63	2.13	2.91	3.91	4.52	5.67	17.41	14.14
10	1.73	2.93	4.68	2.22	5.81	4.46	18.50	16.89

Downcomer/riser 0.5 -
 Top clearance (m) 0.1 -
 Bottom clearance (m) 0.1 +
 Aeration intensity (L/m².min) 800 -
 Depth (m) 1.4 +
 Diffuser position Riser +

Average times (s):

3.185	2.697	3.557	3.085	5.427	5.650	14.792	14.860
-------	-------	-------	-------	-------	-------	--------	--------

Distance (m): 0.9

Average rise velocities (m/s):

0.283	0.334	0.253	0.292	0.166	0.159	0.061	0.061
-------	-------	-------	-------	-------	-------	-------	-------

1	0.283	0.334
2	0.253	0.292
3	0.166	0.159
4	0.061	0.061

Area under graph:

0.5996	0.6552
Average:	0.6274
S ² :	0.001546

Residual area:

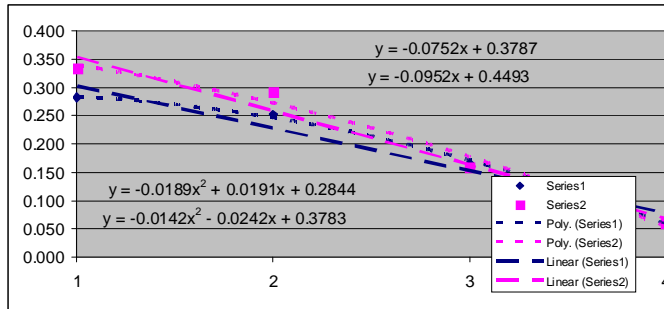
0.2542	0.3645
Average:	0.3094
S ² :	0.006083

Differential area:

0.3454	0.2907
Average:	0.3181
S ² :	0.0015

Average gradient:

-0.0752	-0.0952
Average:	-0.0852
S ² :	0.0002



Treatment 8

	1		2		3		4	
1	1.95	2.31	2.84	3.07	4.99	2.38	2.14	3.70
2	2.30	2.33	1.76	2.82	1.97	3.17	2.45	2.56
3	2.01	2.39	2.80	2.46	3.83	2.41	3.28	3.26
4	3.12	2.62	3.27	2.83	3.78	2.32	2.42	2.82
5	2.04	2.03	1.73	2.33	2.37	2.71	1.88	3.52
6	2.73	2.47	2.38	1.89	2.83	2.11	2.09	3.69
7	2.11	2.29	2.00	2.35	2.98	2.48	2.74	3.71
8	2.28	2.10	2.57	2.24	4.26	3.32	3.43	3.46
9	2.19	2.95	2.49	2.66	3.70	2.94	5.16	2.89
10	2.11	2.16	2.96	2.95	3.17	3.20	2.51	3.69

Downcomer/riser 0.5 -
 Top clearance (m) 0.1 -
 Bottom clearance (m) 0.03 -
 Aeration intensity (L/m².min) 800 -
 Depth (m) 1.1 -
 Diffuser position Bottom -

Average times (s):

2.284	2.365	2.480	2.560	3.388	2.704	2.810	3.330
-------	-------	-------	-------	-------	-------	-------	-------

Distance (m): 0.6

Average rise velocities (m/s):

0.263	0.254	0.242	0.234	0.177	0.222	0.214	0.180
-------	-------	-------	-------	-------	-------	-------	-------

1	0.263	0.254
2	0.242	0.234
3	0.177	0.222
4	0.214	0.180

Area under graph:

0.6503	0.6761
Average:	0.6632
S ² :	0.000333

Residual area:

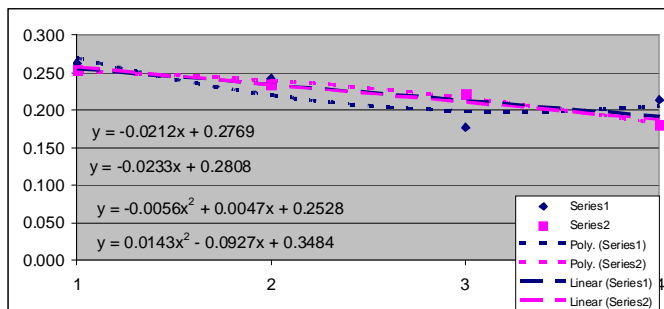
0.1597	0.0796
Average:	0.1197
S ² :	0.003208

Differential area:

0.4906	0.5965
Average:	0.5436
S ² :	0.0056

Average gradient:

-0.0212	-0.0233
Average:	-0.0223
S ² :	0.0000



Treatment 9

	1	2	3	4
1	-	-	2.83	1.77
2	-	-	1.47	2.34
3	-	-	1.17	1.29
4	-	-	3.07	2.01
5	-	-	1.89	1.49
6	-	-	2.04	1.63
7	-	-	1.76	2.15
8	-	-	1.70	1.86
9	-	-	1.55	2.57
10	-	-	2.49	1.84

Downcomer/riser 0.5 -
 Top clearance (m) 0.2 +
 Bottom clearance (m) 0.1 +
 Aeration intensity (L/m².min) 800 -
 Depth (m) 1.4 +
 Diffuser position Bottom -

Average times (s):

-	-	-	-	1.997	1.895	2.305	2.261
---	---	---	---	-------	-------	-------	-------

Distance (m):

Average rise velocities (m/s):

0.000	0.000	0.000	0.000	0.401	0.422	0.347	0.354
-------	-------	-------	-------	-------	-------	-------	-------

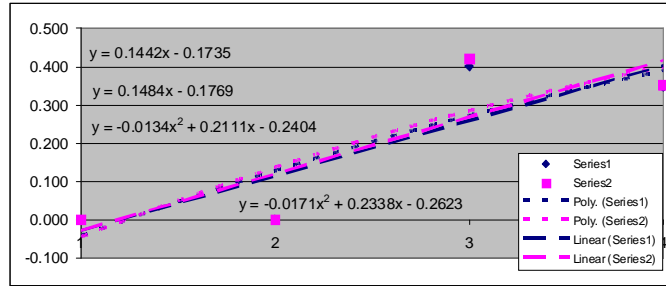
1	0.000	0.000
2	0.000	0.000
3	0.401	0.422
4	0.347	0.354

Area under graph:	0.5807	0.6075
Average:	0.5941	
S ² :	0.000359	

Residual area:	0.5881	0.5904
Average:	0.5893	
S ² :	0.000003	

Differential area:	-0.0074	0.0171
Average:	0.0049	
S ² :	0.0003	

Average gradient:	0.1442	0.1484
Average:	0.1463	
S ² :	0.0000	



Treatment 10

	1	2	3	4
1	1.30	1.77	1.44	2.36
2	3.20	1.59	2.82	5.67
3	2.53	2.17	2.17	2.48
4	2.35	1.53	4.36	1.55
5	2.08	1.90	2.73	1.43
6	2.97	1.85	1.87	2.87
7	0.99	1.68	3.17	3.21
8	1.55	1.56	1.49	1.94
9	1.96	2.13	3.12	3.97
10	2.28	1.74	2.48	2.48

Downcomer/riser 0.5 -
 Top clearance (m) 0.1 -
 Bottom clearance (m) 0.1 +
 Aeration intensity (L/m².min) 1350 +
 Depth (m) 1.1 -
 Diffuser position Riser +

Average times (s):

2.121	1.792	2.565	2.796	4.800	3.790	13.926	8.323
-------	-------	-------	-------	-------	-------	--------	-------

Distance (m):

Average rise velocities (m/s):

0.28	0.33	0.23	0.21	0.13	0.16	0.04	0.07
------	------	------	------	------	------	------	------

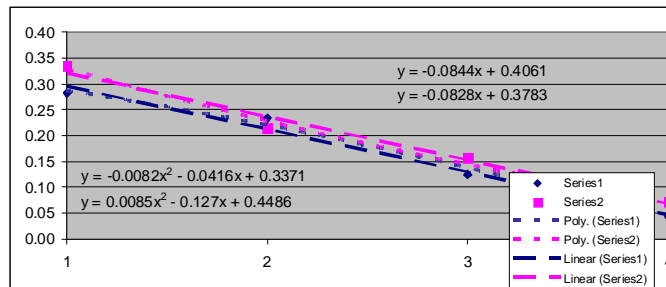
1	0.28	0.33
2	0.23	0.21
3	0.13	0.16
4	0.04	0.07

Area under graph:	0.5271	0.5718
Average:	0.5495	
S ² :	0.000999	

Residual area:	0.3348	0.4185
Average:	0.3767	
S ² :	0.003503	

Differential area:	0.1923	0.1533
Average:	0.1728	
S ² :	0.0008	

Average gradient:	-0.0828	-0.0844
Average:	-0.0836	
S ² :	0.0000	



Treatment 11

	1		2		3		4	
1	20.40	8.11	4.23	4.68	3.99	5.18	7.65	5.26
2	9.74	6.57	3.27	4.17	3.05	3.73	8.51	4.83
3	6.77	14.36	6.73	4.60	6.56	4.14	4.38	5.74
4	15.72	15.68	7.05	4.39	2.66	3.62	6.37	4.88
5	23.93	12.77	7.47	7.02	10.65	3.87	5.62	5.81
6	8.14	9.03	3.11	4.95	3.60	5.45	7.82	6.52
7	8.76	19.83	3.82	5.74	4.81	7.32	8.83	8.56
8	12.30	9.44	5.45	6.51	5.44	3.95	8.12	4.47
9	10.04	7.27	4.88	4.90	5.71	3.31	10.22	6.55
10	7.23	6.52	4.96	6.43	7.35	4.16	8.98	4.92

Downcomer/riser 0.5 -
 Top clearance (m) 0.1 -
 Bottom clearance (m) 0.03 -
 Aeration intensity (L/m².min) 1350 +
 Depth (m) 1.4 +
 Diffuser position Bottom -

Average times (s):

12.303	10.958	5.097	5.339	5.382	4.473	7.650	5.754
--------	--------	-------	-------	-------	-------	-------	-------

Distance (m): 0.9

Average rise velocities (m/s):

0.073	0.082	0.177	0.169	0.167	0.201	0.118	0.156
-------	-------	-------	-------	-------	-------	-------	-------

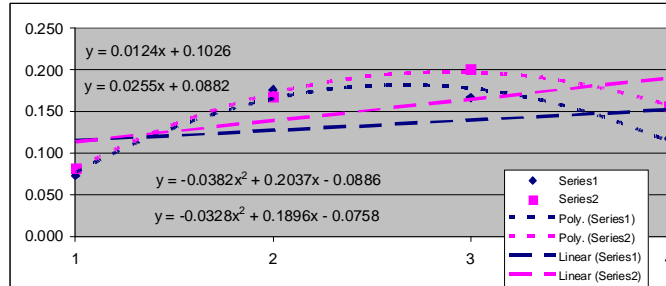
1	0.073	0.082
2	0.177	0.169
3	0.167	0.201
4	0.118	0.156

Area under graph:	0.4598	0.5058
Average:	0.4828	
S²:	0.001058	

Residual area:	0.0891	0.0888
Average:	0.0890	
S²:	0.000000	

Differential area:	0.3707	0.4170
Average:	0.3939	
S²:	0.0011	

Average gradient:	0.0124	0.0255
Average:	0.0190	
S²:	0.0001	



Treatment 12

	1		2		3		4	
1	2.66	2.33	1.80	2.22	6.13	3.97	6.04	7.06
2	2.43	2.33	1.84	4.33	2.41	5.31	2.58	8.05
3	3.82	3.67	3.75	4.73	5.51	4.45	4.57	5.77
4	3.71	3.77	2.75	4.45	3.11	7.63	5.59	7.32
5	2.77	3.12	2.63	5.74	3.96	6.67	3.24	4.09
6	2.57	2.59	2.83	2.70	5.38	5.30	2.86	6.78
7	3.68	6.94	3.47	13.07	3.73	6.42	5.15	7.23
8	2.84	4.81	2.90	2.31	4.32	4.91	4.80	7.93
9	2.48	3.03	1.92	7.69	3.92	6.28	6.04	6.11
10	2.97	3.94	2.11	4.72	3.77	6.36	3.17	5.34

Downcomer/riser 2 +
 Top clearance (m) 0.1 -
 Bottom clearance (m) 0.03 -
 Aeration intensity (L/m².min) 800 -
 Depth (m) 1.4 +
 Diffuser position Riser +

Average times (s):

2.993	3.653	2.600	5.196	4.224	5.730	4.404	6.568
-------	-------	-------	-------	-------	-------	-------	-------

Distance (m): 0.9

Average rise velocities (m/s):

0.301	0.246	0.346	0.173	0.213	0.157	0.204	0.137
-------	-------	-------	-------	-------	-------	-------	-------

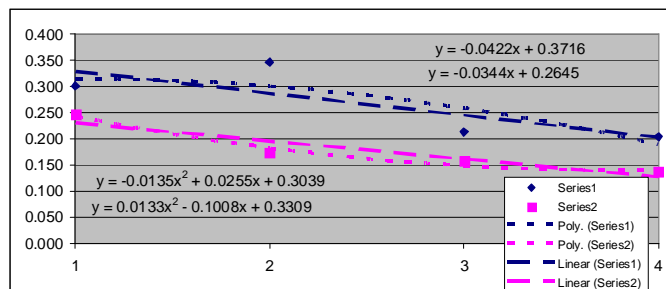
1	0.301	0.246
2	0.346	0.173
3	0.213	0.157
4	0.204	0.137

Area under graph:	0.8195	0.5160
Average:	0.6678	
S²:	0.046056	

Residual area:	0.1282	0.2142
Average:	0.1712	
S²:	0.003698	

Differential area:	0.6913	0.3018
Average:	0.4966	
S²:	0.0759	

Average gradient:	-0.0422	-0.0344
Average:	-0.0383	
S²:	0.0000	



Treatment 13

	1		2		3		4	
1	1.21	2.33	1.55	1.89	4.86	3.47	3.93	2.99
2	1.87	2.37	2.13	1.91	4.08	1.32	4.67	2.08
3	1.83	1.88	3.59	3.26	2.55	1.47	8.21	3.29
4	1.53	1.96	1.43	1.77	3.56	2.17	3.70	4.57
5	1.49	1.78	1.46	2.29	2.43	4.39	5.43	3.33
6	1.37	1.84	2.24	2.07	2.75	2.93	6.74	5.74
7	1.76	2.17	1.70	2.33	3.43	4.36	3.38	4.12
8	1.55	1.42	2.38	2.86	2.21	2.25	3.66	2.83
9	1.18	2.33	2.33	1.84	2.90	3.37	5.89	4.92
10	2.07	1.59	1.51	2.02	2.24	2.77	5.67	3.44

Downcomer/riser 0.5 -
 Top clearance (m) 0.2 +
 Bottom clearance (m) 0.03 -
 Aeration intensity (L/m².min) 800 -
 Depth (m) 1.1 -
 Diffuser position Riser +

Average times (s):

1.586	1.967	2.032	2.224	3.101	2.850	5.128	3.731
-------	-------	-------	-------	-------	-------	-------	-------

Distance (m): 0.5

Average rise velocities (m/s):

0.315	0.254	0.246	0.225	0.161	0.175	0.098	0.134
-------	-------	-------	-------	-------	-------	-------	-------

1	0.315	0.254
2	0.246	0.225
3	0.161	0.175
4	0.098	0.134

Area under graph:

0.6141	0.5963
Average:	0.6052
S ² :	0.000158

Residual area:

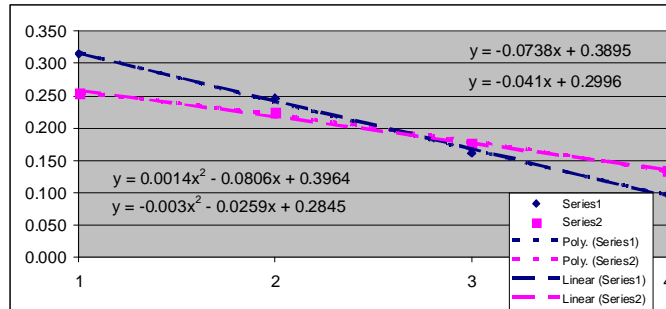
0.3375	0.1706
Average:	0.2541
S ² :	0.013928

Differential area:

0.2766	0.4257
Average:	0.3512
S ² :	0.0111

Average gradient:

-0.0738	-0.0410
Average:	-0.0574
S ² :	0.0005



Treatment 14

	1		2		3		4	
1	-	-	11.41	6.58	4.18	1.09	1.35	1.05
2	-	-	4.82	3.26	10.24	14.02	1.21	1.19
3	-	-	2.19	2.13	1.49	1.15	0.87	1.58
4	-	-	8.37	7.91	5.02	1.49	1.26	1.80
5	-	-	12.08	5.24	1.31	3.24	1.70	1.46
6	-	-	3.28	3.21	11.15	6.10	1.57	1.33
7	-	-	4.82	8.43	6.23	13.14	1.43	1.77
8	-	-	9.12	10.11	9.51	2.90	1.01	1.08
9	-	-	6.93	4.78	2.88	21.40	1.06	1.12
10	-	-	7.51	6.80	3.64	3.12	1.34	1.67

Downcomer/riser 2 +
 Top clearance (m) 0.1 -
 Bottom clearance (m) 0.1 +
 Aeration intensity (L/m².min) 800 -
 Depth (m) 1.1 -
 Diffuser position Bottom -

Average times (s):

-	-	7.053	5.845	5.565	6.765	1.280	1.405
---	---	-------	-------	-------	-------	-------	-------

Distance (m): 0.6

Average rise velocities (m/s):

0.000	0.000	0.085	0.103	0.108	0.089	0.469	0.427
-------	-------	-------	-------	-------	-------	-------	-------

1	0.000	0.000
2	0.085	0.103
3	0.108	0.089
4	0.469	0.427

Area under graph:

0.3938	0.3749
Average:	0.3844
S ² :	0.000179

Residual area:

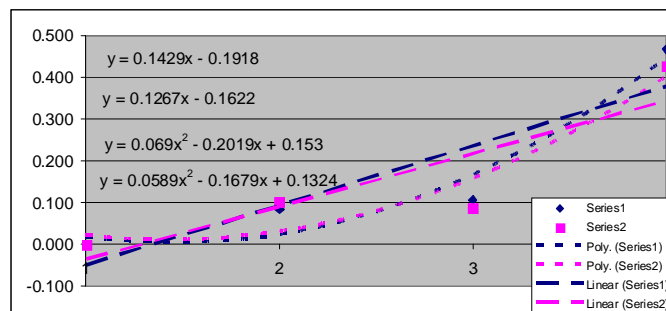
0.9544	0.8347
Average:	0.8946
S ² :	0.007164

Differential area:

-0.5606	-0.4598
Average:	-0.5102
S ² :	0.0051

Average gradient:

0.1429	0.1267
Average:	0.1348
S ² :	0.0001



Treatment 15

	1		2		3		4	
1	1.83	1.43	0.90	1.43	1.34	1.03	2.69	1.72
2	1.91	1.06	1.59	1.25	1.47	1.29	1.05	1.00
3	0.96	1.29	1.03	1.19	1.14	3.03	1.90	1.57
4	1.19	1.29	0.93	1.27	1.47	2.38	1.11	1.07
5	1.50	2.06	1.25	1.31	1.70	0.88	2.21	1.67
6	1.50	1.14	1.27	1.50	1.46	1.17	3.04	2.69
7	1.94	1.83	1.62	1.37	1.83	2.89	1.79	1.91
8	1.04	1.16	1.10	0.89	2.29	1.13	3.71	2.26
9	1.38	1.51	1.07	1.44	2.86	1.28	2.11	3.31
10	1.57	1.49	0.86	1.20	1.00	2.17	3.14	3.17

Downcomer/riser 2 +
 Top clearance (m) 0.2 +
 Bottom clearance (m) 0.03 -
 Aeration intensity (L/m².min) 1350 +
 Depth (m) 1.1 -
 Diffuser position Bottom -

Average times (s):

1.482	1.426	1.162	1.285	1.656	1.725	2.275	2.037
-------	-------	-------	-------	-------	-------	-------	-------

Distance (m): 0.5

Average rise velocities (m/s):

0.337	0.351	0.430	0.389	0.302	0.290	0.220	0.245
-------	-------	-------	-------	-------	-------	-------	-------

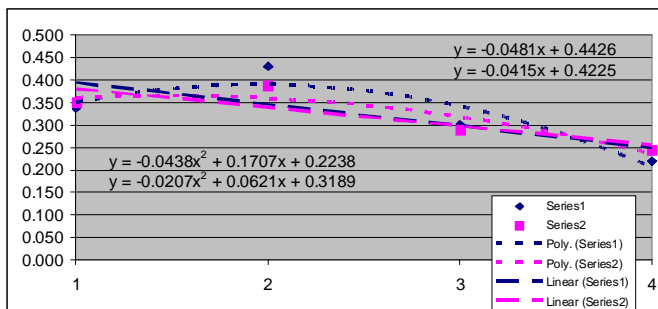
1	0.337	0.351
2	0.430	0.389
3	0.302	0.290
4	0.220	0.245

Area under graph:	1.0319	0.9878
Average:	1.0099	
S²:	0.000972	

Residual area:	0.1384	0.1086
Average:	0.1235	
S²:	0.000444	

Differential area:	0.8935	0.8792
Average:	0.8864	
S²:	0.0001	

Average gradient:	-0.0481	-0.0415
Average:	-0.0448	
S²:	0.0000	



Treatment 16

	1		2		3		4	
1	2.11	3.65	3.23	3.40	2.23	2.69	1.87	2.57
2	2.18	1.80	3.03	2.82	2.35	2.31	2.18	4.29
3	1.96	2.29	1.42	1.99	1.97	2.59	2.16	2.97
4	1.96	2.98	2.23	2.88	2.77	2.63	2.59	2.70
5	2.14	1.79	2.37	2.25	3.16	2.13	2.12	2.49
6	2.94	1.49	2.28	2.71	1.55	2.26	1.89	2.75
7	2.46	1.69	2.91	2.18	3.25	2.72	1.50	3.74
8	2.27	2.02	2.77	2.40	2.49	2.42	2.21	3.32
9	1.99	2.36	2.17	2.89	2.81	2.29	1.64	3.06
10	2.63	2.34	1.86	2.30	2.65	1.95	2.09	2.84

Downcomer/riser 2 +
 Top clearance (m) 0.2 +
 Bottom clearance (m) 0.1 +
 Aeration intensity (L/m².min) 1350 +
 Depth (m) 1.4 +
 Diffuser position Riser +

Average times (s):

2.264	2.241	2.427	2.582	2.523	2.399	2.025	3.073
-------	-------	-------	-------	-------	-------	-------	-------

Distance (m): 0.8

Average rise velocities (m/s):

0.353	0.357	0.330	0.310	0.317	0.333	0.395	0.260
-------	-------	-------	-------	-------	-------	-------	-------

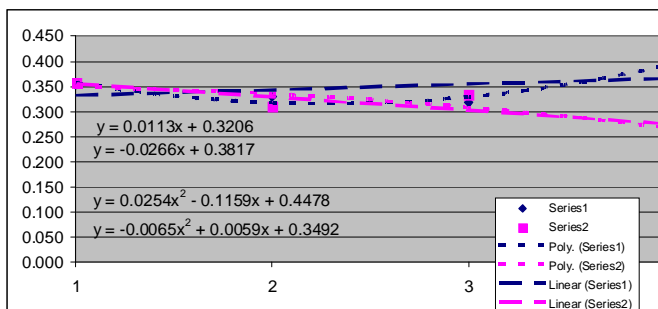
1	0.353	0.357
2	0.330	0.310
3	0.317	0.333
4	0.395	0.260

Area under graph:	1.0076	0.9554
Average:	0.9815	
S²:	0.001362	

Residual area:	0.1642	0.0904
Average:	0.1273	
S²:	0.002723	

Differential area:	0.8434	0.8650
Average:	0.8542	
S²:	0.0002	

Average gradient:	0.0113	-0.0266
Average:	-0.0077	
S²:	0.0007	



Treatment 17

	1		2		3		4	
1	1.93	2.71	3.87	3.04	3.02	3.83	7.47	4.70
2	2.13	2.58	2.50	3.67	6.21	4.56	3.78	3.55
3	2.23	3.13	2.38	2.84	5.91	4.41	4.02	4.13
4	2.72	1.79	2.89	2.42	3.59	3.50	2.82	2.89
5	1.87	2.21	3.35	3.28	4.12	5.61	2.54	4.21
6	3.11	2.53	3.18	2.51	4.93	4.85	3.31	3.76
7	2.49	2.88	2.71	4.28	3.33	6.72	4.61	7.83
8	1.90	3.15	2.46	2.43	3.62	4.78	7.06	4.27
9	2.09	2.94	2.93	3.17	3.63	7.26	3.46	4.52
10	2.06	3.47	2.83	4.25	4.31	4.16	5.44	4.17

Downcomer/riser 0.5 -
 Top clearance (m) 0.1 -
 Bottom clearance (m) 0.03 -
 Aeration intensity (L/m².min) 800 -
 Depth (m) 1.1 -
 Diffuser position Riser +

Average times (s):

2.253	2.739	2.910	3.189	4.267	4.968	4.451	4.403
-------	-------	-------	-------	-------	-------	-------	-------

Distance (m): 0.6

Average rise velocities (m/s):

0.266	0.219	0.206	0.188	0.141	0.121	0.135	0.136
-------	-------	-------	-------	-------	-------	-------	-------

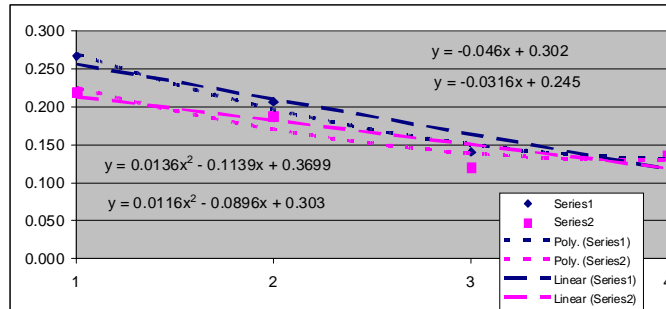
1	0.266	0.219
2	0.206	0.188
3	0.141	0.121
4	0.135	0.136

Area under graph:	0.5411	0.4806
Average:	0.5109	
S ² :	0.001830	

Residual area:	0.2678	0.1944
Average:	0.2311	
S ² :	0.002694	

Differential area:	0.2733	0.2862
Average:	0.2798	
S ² :	0.0001	

Average gradient:	-0.0460	-0.0316
Average:	-0.0388	
S ² :	0.0001	



Treatment 18

	1		2		3		4	
1	2.08	1.43	1.27	2.45	5.09	4.73	5.40	9.22
2	1.57	1.46	2.09	2.74	5.47	4.56	7.95	6.83
3	1.59	1.81	1.52	2.18	3.45	4.83	14.77	9.32
4	1.60	1.86	1.83	2.35	2.18	5.66	2.50	19.74
5	1.29	1.54	2.20	1.78	4.18	4.53	8.23	6.51
6	1.55	1.60	1.30	1.59	3.67	3.85	23.02	8.63
7	2.04	1.38	2.38	2.10	4.16	4.09	8.42	12.37
8	1.48	1.47	1.49	1.64	4.62	3.62	11.47	16.48
9	1.71	1.42	1.23	2.83	4.84	4.26	15.18	9.06
10	1.35	1.26	1.47	2.03	3.08	4.69	6.18	17.65

Downcomer/riser 0.5 -
 Top clearance (m) 0.1 -
 Bottom clearance (m) 0.03 -
 Aeration intensity (L/m².min) 1350 +
 Depth (m) 1.1 -
 Diffuser position Riser +

Average times (s):

1.626	1.523	1.678	2.169	4.074	4.482	10.312	11.581
-------	-------	-------	-------	-------	-------	--------	--------

Distance (m): 0.6

Average rise velocities (m/s):

0.369	0.394	0.358	0.277	0.147	0.134	0.058	0.052
-------	-------	-------	-------	-------	-------	-------	-------

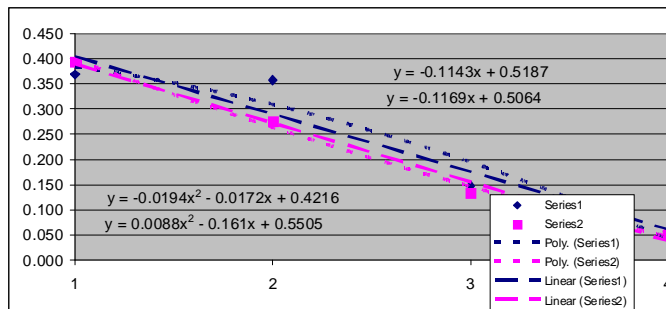
1	0.369	0.394
2	0.358	0.277
3	0.147	0.134
4	0.058	0.052

Area under graph:	0.7284	0.6288
Average:	0.6786	
S ² :	0.004960	

Residual area:	0.4266	0.5661
Average:	0.4964	
S ² :	0.009730	

Differential area:	0.3018	0.0627
Average:	0.1823	
S ² :	0.0286	

Average gradient:	-0.1143	-0.1169
Average:	-0.1156	
S ² :	0.0000	



Treatment 19

	1		2		3		4	
1	1.75	2.61	1.52	2.85	4.85	5.10	11.62	9.15
2	1.53	1.53	4.27	3.46	3.27	3.86	7.49	15.42
3	2.34	2.43	2.16	3.00	4.96	3.58	13.19	10.66
4	1.92	2.26	3.13	3.57	4.23	5.47	9.13	5.87
5	2.38	1.40	2.53	4.12	5.14	5.75	6.37	7.62
6	1.86	1.59	3.07	3.29	4.19	3.11	8.22	18.47
7	1.67	2.28	3.41	3.58	4.33	5.21	10.94	14.02
8	1.25	1.65	1.86	2.76	3.83	4.42	7.58	7.31
9	1.38	2.12	2.58	3.05	3.55	4.96	12.24	10.23
10	1.58	2.34	2.69	3.91	4.93	3.54	8.82	9.57

Downcomer/riser 0.5 -
 Top clearance (m) 0.1 -
 Bottom clearance (m) 0.1 +
 Aeration intensity (L/m².min) 800 -
 Depth (m) 1.1 -
 Diffuser position Riser +

Average times (s):

1.766	2.021	2.722	3.359	4.328	4.500	9.560	10.832
-------	-------	-------	-------	-------	-------	-------	--------

Distance (m): 0.6

Average rise velocities (m/s):

0.340	0.297	0.220	0.179	0.139	0.133	0.063	0.055
-------	-------	-------	-------	-------	-------	-------	-------

1	0.340	0.297
2	0.220	0.179
3	0.139	0.133
4	0.063	0.055

Area under graph:

0.5556	0.4833
Average:	0.5195
S ² :	0.002614

Residual area:

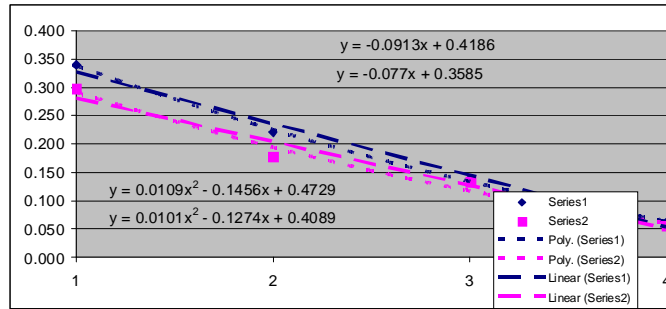
0.4590	0.3915
Average:	0.4253
S ² :	0.002278

Differential area:

0.0966	0.0918
Average:	0.0942
S ² :	0.0000

Average gradient:

-0.0913	-0.0770
Average:	-0.0842
S ² :	0.0001



Treatment 20

	1		2		3		4	
1	1.79	1.52	2.25	2.08	10.03	4.55	4.66	7.42
2	1.15	1.67	2.62	2.64	1.88	3.26	7.76	5.61
3	1.52	2.13	1.73	2.71	5.04	3.75	9.29	3.64
4	1.69	1.23	2.44	2.93	3.04	6.06	6.96	9.83
5	1.58	1.87	1.53	2.17	6.73	3.74	11.71	7.54
6	1.36	2.35	1.25	2.69	6.84	3.42	1.33	13.92
7	1.82	1.64	2.29	2.34	6.87	5.19	5.66	8.65
8	0.82	1.74	1.97	1.90	8.15	4.01	4.37	11.43
9	2.01	1.49	1.98	2.82	3.81	3.57	7.88	4.28
10	1.53	1.77	1.64	2.97	5.37	5.61	9.90	14.18

Downcomer/riser 0.5 -
 Top clearance (m) 0.2 +
 Bottom clearance (m) 0.1 +
 Aeration intensity (L/m².min) 800 -
 Depth (m) 1.1 -
 Diffuser position Riser +

Average times (s):

1.527	1.741	1.970	2.525	5.776	4.316	6.952	8.650
-------	-------	-------	-------	-------	-------	-------	-------

Distance (m): 0.5

Average rise velocities (m/s):

0.327	0.287	0.254	0.198	0.087	0.116	0.072	0.058
-------	-------	-------	-------	-------	-------	-------	-------

1	0.327	0.287
2	0.254	0.198
3	0.087	0.116
4	0.072	0.058

Area under graph:

0.5318	0.4832
Average:	0.5075
S ² :	0.001181

Residual area:

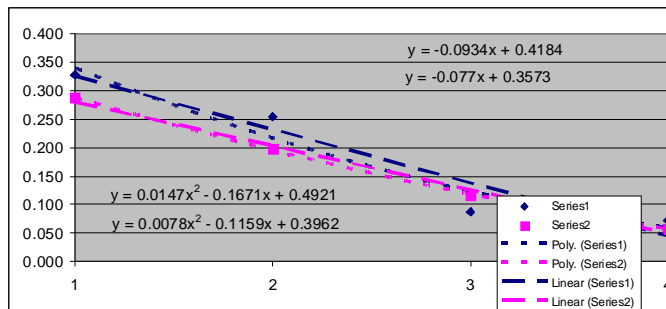
0.4874	0.3812
Average:	0.4343
S ² :	0.005639

Differential area:

0.0444	0.1020
Average:	0.0732
S ² :	0.0017

Average gradient:

-0.0934	-0.0770
Average:	-0.0852
S ² :	0.0001



Treatment 21

	1		2		3		4	
1	-	-	1.98	3.93	1.55	1.59	1.70	1.95
2	-	-	2.23	2.85	1.71	1.56	2.53	2.54
3	-	-	2.59	2.26	2.42	2.13	2.40	2.34
4	-	-	2.56	3.70	1.87	1.62	1.73	1.87
5	-	-	1.17	3.15	1.48	1.54	2.23	1.69
6	-	-	1.93	4.07	1.86	1.74	2.69	1.93
7	-	-	2.23	3.87	2.17	1.69	2.14	2.02
8	-	-	3.47	2.37	1.72	1.83	2.63	2.21
9	-	-	2.34	3.43	1.60	2.11	2.87	1.93
10	-	-	2.16	3.50	1.77	1.62	1.80	1.64

Downcomer/riser	0.5	-
Top clearance (m)	0.1	-
Bottom clearance (m)	0.1	+
Aeration intensity (L/m ² .min)	800	-
Depth (m)	1.1	-
Diffuser position	Bottom	-

Average times (s):

-	-	2.266	3.313	1.815	1.743	2.272	2.012
---	---	-------	-------	-------	-------	-------	-------

Distance (m):

Average rise velocities (m/s):

0.000	0.000	0.265	0.181	0.331	0.344	0.264	0.298
-------	-------	-------	-------	-------	-------	-------	-------

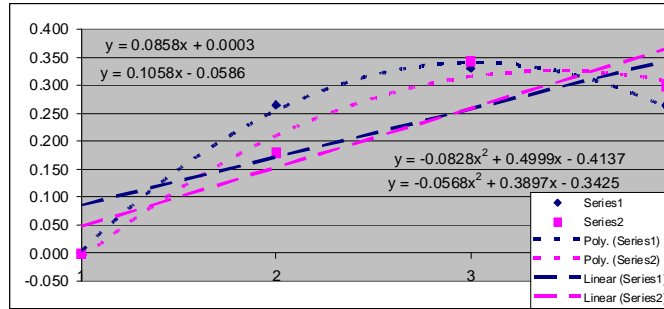
1	0.000	0.000
2	0.265	0.181
3	0.331	0.344
4	0.264	0.298

Area under graph:	0.7694	0.7025
Average:	0.7360	
S²:	0.002238	

Residual area:	0.2531	0.2752
Average:	0.2642	
S²:	0.000244	

Differential area:	0.5163	0.4273
Average:	0.4718	
S²:	0.0040	

Average gradient:	0.0858	0.1058
Average:	0.0958	
S²:	0.0002	



Treatment 22

	1		2		3		4	
1	3.68	5.47	7.20	3.83	1.93	2.15	2.80	2.34
2	7.92	6.91	7.93	4.28	6.27	2.26	2.09	1.51
3	4.20	7.32	2.49	4.36	6.32	3.14	1.33	1.82
4	11.30	4.58	2.92	4.29	3.15	4.83	2.76	2.01
5	6.56	4.74	4.85	5.81	4.30	3.72	2.47	1.25
6	8.81	8.17	4.73	3.06	3.31	2.59	1.45	2.47
7	4.80	3.37	3.85	3.87	2.88	3.02	1.41	3.06
8	6.47	4.14	6.13	4.00	4.40	3.12	1.85	2.72
9	5.89	3.78	5.79	6.45	3.11	2.43	1.65	2.15
10	7.90	3.29	4.31	4.46	4.56	3.07	2.08	0.98

Downcomer/riser	0.5	-
Top clearance (m)	0.1	-
Bottom clearance (m)	0.03	-
Aeration intensity (L/m ² .min)	1350	+
Depth (m)	1.1	-
Diffuser position	Bottom	-

Average times (s):

6.753	5.177	5.020	4.441	4.023	3.033	1.989	2.031
-------	-------	-------	-------	-------	-------	-------	-------

Distance (m):

Average rise velocities (m/s):

0.089	0.116	0.120	0.135	0.149	0.198	0.302	0.295
-------	-------	-------	-------	-------	-------	-------	-------

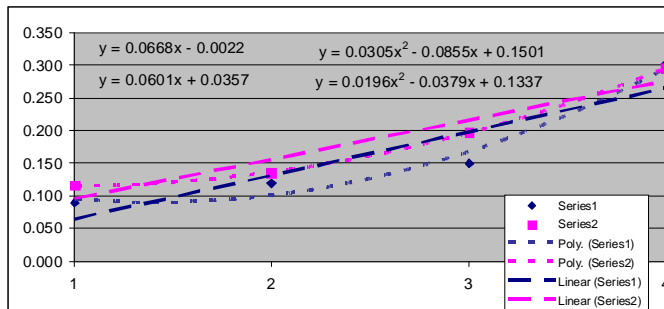
1	0.089	0.116
2	0.120	0.135
3	0.149	0.198
4	0.302	0.295

Area under graph:	0.4496	0.5285
Average:	0.4891	
S²:	0.003113	

Residual area:	0.4388	0.3586
Average:	0.3987	
S²:	0.003216	

Differential area:	0.0108	0.1699
Average:	0.0904	
S²:	0.0127	

Average gradient:	0.0668	0.0601
Average:	0.0635	
S²:	0.0000	



Treatment 23

	1		2		3		4	
1	1.69	4.68	4.85	2.82	4.00	3.45	4.13	1.58
2	4.96	4.15	3.08	2.76	2.28	3.32	2.33	1.39
3	4.15	4.83	1.78	2.13	2.03	3.57	1.49	1.70
4	4.78	3.97	2.14	3.34	2.10	3.42	2.32	1.64
5	4.42	3.39	2.80	4.11	3.15	2.88	1.47	1.47
6	3.95	4.41	2.26	3.75	2.85	3.02	1.63	2.20
7	3.12	3.60	1.84	3.09	3.74	4.17	1.97	1.74
8	3.78	3.86	2.76	2.63	2.31	3.28	1.67	1.29
9	4.44	4.92	4.20	3.82	2.68	3.51	1.09	1.88
10	2.51	4.23	2.57	3.73	1.93	3.05	1.76	1.72

Downcomer/riser 0.5 -
 Top clearance (m) 0.2 +
 Bottom clearance (m) 0.03 -
 Aeration intensity (L/m².min) 800 -
 Depth (m) 1.1 -
 Diffuser position Bottom -

Average times (s):

3.780	4.204	2.828	3.218	2.707	3.367	1.986	1.661
-------	-------	-------	-------	-------	-------	-------	-------

Distance (m): 0.5

Average rise velocities (m/s):

0.132	0.119	0.177	0.155	0.185	0.149	0.252	0.301
-------	-------	-------	-------	-------	-------	-------	-------

1	0.132	0.119
2	0.177	0.155
3	0.185	0.149
4	0.252	0.301

Area under graph:

0.5504	0.4986
Average:	0.5245
S ² :	0.001342

Residual area:

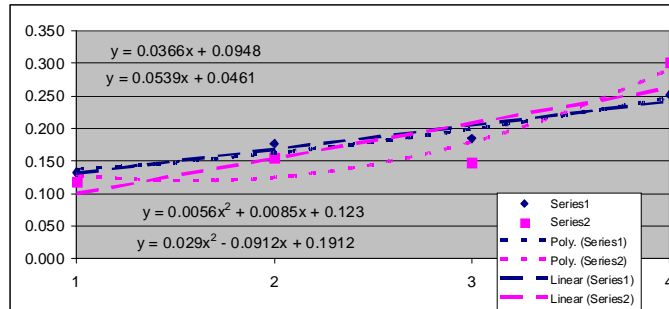
0.1895	0.3726
Average:	0.2811
S ² :	0.016763

Differential area:

0.3609	0.1260
Average:	0.2435
S ² :	0.0276

Average gradient:

0.0366	0.0539
Average:	0.0453
S ² :	0.0001



Treatment 24

	1		2		3		4	
1	3.92	1.99	4.07	2.48	2.96	5.37	7.05	3.60
2	3.60	2.18	2.02	2.06	8.28	2.14	5.07	4.27
3	1.01	1.98	1.55	1.89	3.17	2.27	5.02	6.77
4	7.97	2.18	2.44	8.76	3.13	3.93	5.56	3.66
5	3.59	1.89	2.81	6.69	3.11	2.02	7.32	6.69
6	1.57	1.21	3.16	5.59	14.83	6.11	6.19	7.12
7	4.46	2.05	1.97	2.94	5.14	2.67	4.84	3.94
8	1.61	2.20	2.76	2.99	6.52	5.11	6.58	5.37
9	1.90	1.57	3.43	2.14	4.29	3.54	6.73	3.97
10	1.45	1.80	2.54	1.17	3.93	4.30	5.68	4.59

Downcomer/riser 2 +
 Top clearance (m) 0.1 -
 Bottom clearance (m) 0.03 -
 Aeration intensity (L/m².min) 800 -
 Depth (m) 1.1 -
 Diffuser position Riser +

Average times (s):

3.108	1.905	2.675	3.671	5.536	3.746	6.004	4.998
-------	-------	-------	-------	-------	-------	-------	-------

Distance (m): 0.6

Average rise velocities (m/s):

0.193	0.315	0.224	0.163	0.108	0.160	0.100	0.120
-------	-------	-------	-------	-------	-------	-------	-------

1	0.193	0.315
2	0.224	0.163
3	0.108	0.160
4	0.100	0.120

Area under graph:

0.4847	0.5265
Average:	0.5056
S ² :	0.000874

Residual area:

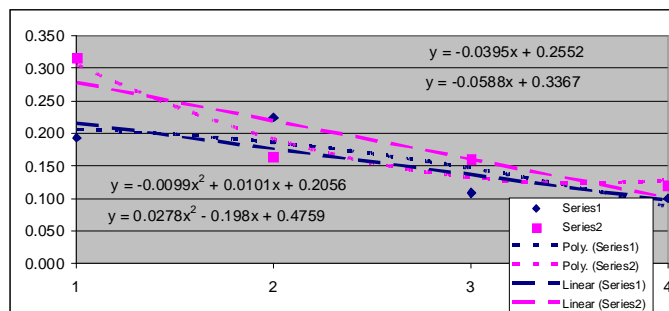
0.1328	0.3906
Average:	0.2617
S ² :	0.033230

Differential area:

0.3519	0.1359
Average:	0.2439
S ² :	0.0233

Average gradient:

-0.0395	-0.0588
Average:	-0.0492
S ² :	0.0002



Treatment 25

	1		2		3		4	
1	1.77	3.47	1.69	2.19	4.40	1.83	1.97	2.97
2	1.26	2.97	1.15	1.93	3.49	2.42	3.81	2.07
3	1.89	1.36	1.69	2.79	1.65	1.50	7.90	2.76
4	4.90	2.17	1.09	2.28	2.04	1.81	2.19	7.00
5	1.28	1.94	3.74	1.29	1.19	2.32	1.44	4.26
6	1.93	2.77	3.36	2.32	3.13	8.02	4.43	5.99
7	1.32	2.19	1.75	2.04	1.83	1.49	3.64	3.22
8	1.66	1.99	2.19	2.59	1.33	1.47	5.47	2.86
9	2.06	2.52	2.11	1.66	1.38	1.18	2.79	4.13
10	1.93	2.20	2.43	2.24	3.48	2.03	2.59	6.49

Downcomer/riser 2 +
 Top clearance (m) 0.2 +
 Bottom clearance (m) 0.03 -
 Aeration intensity (L/m².min) 800 -
 Depth (m) 1.1 -
 Diffuser position Riser +

Average times (s):

2.000	2.358	2.120	2.133	2.392	2.407	3.623	4.175
-------	-------	-------	-------	-------	-------	-------	-------

Distance (m): 0.5

Average rise velocities (m/s):

0.250	0.212	0.236	0.234	0.209	0.208	0.138	0.120
-------	-------	-------	-------	-------	-------	-------	-------

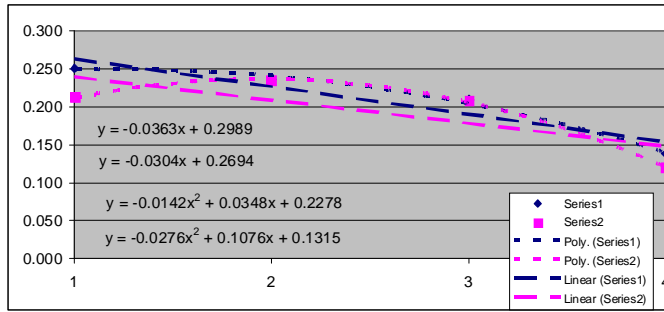
1	0.250	0.212
2	0.236	0.234
3	0.209	0.208
4	0.138	0.120

Area under graph:	0.6462	0.6219
Average:	0.6341	
S²:	0.000295	

Residual area:	0.1012	0.0872
Average:	0.0942	
S²:	0.000098	

Differential area:	0.5450	0.5347
Average:	0.5399	
S²:	0.0001	

Average gradient:	-0.0363	-0.0304
Average:	-0.0334	
S²:	0.0000	



Treatment 26

	1		2		3		4	
1	1.67	2.03	2.94	3.78	4.23	3.81	7.73	4.38
2	3.04	1.92	5.03	4.17	5.26	4.15	3.38	5.42
3	2.23	2.31	3.21	3.77	4.26	4.57	2.44	8.23
4	1.66	1.96	2.79	2.68	3.18	5.86	2.29	6.14
5	2.56	1.48	2.45	2.34	6.06	5.41	1.57	4.89
6	3.26	2.45	2.04	2.81	3.72	4.07	4.53	3.28
7	2.13	1.87	2.97	3.53	4.55	5.73	11.95	6.31
8	2.59	2.11	3.40	4.46	3.60	4.13	4.79	8.57
9	2.26	2.25	2.13	3.61	4.22	6.47	6.52	4.54
10	2.61	2.42	2.17	2.84	3.30	4.93	5.36	3.79

Downcomer/riser 2 +
 Top clearance (m) 0.1 -
 Bottom clearance (m) 0.1 +
 Aeration intensity (L/m².min) 800 -
 Depth (m) 1.1 -
 Diffuser position Riser +

Average times (s):

2.401	2.080	2.913	3.399	4.238	4.913	5.056	5.555
-------	-------	-------	-------	-------	-------	-------	-------

Distance (m): 0.6

Average rise velocities (m/s):

0.250	0.288	0.206	0.177	0.142	0.122	0.119	0.108
-------	-------	-------	-------	-------	-------	-------	-------

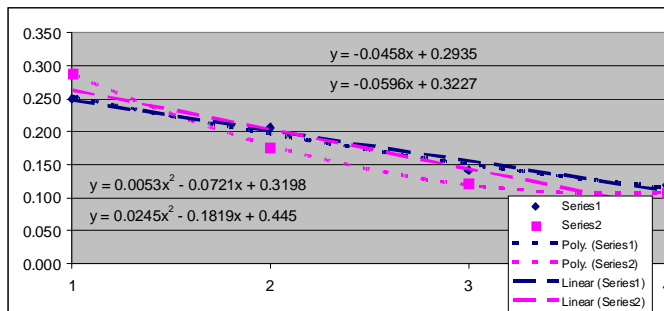
1	0.250	0.288
2	0.206	0.177
3	0.142	0.122
4	0.119	0.108

Area under graph:	0.5300	0.4853
Average:	0.5077	
S²:	0.000999	

Residual area:	0.2291	0.3775
Average:	0.3033	
S²:	0.011011	

Differential area:	0.3009	0.1078
Average:	0.2044	
S²:	0.0186	

Average gradient:	-0.0458	-0.0596
Average:	-0.0527	
S²:	0.0001	



Treatment 27

	1		2		3		4	
1	2.65	3.73	5.96	5.21	5.11	7.32	17.99	12.35
2	3.39	3.02	3.27	3.97	4.52	5.82	6.53	8.76
3	2.86	2.70	2.40	4.50	3.54	6.14	7.10	8.49
4	4.07	3.41	6.79	6.10	6.37	3.49	7.04	16.72
5	3.10	3.30	3.07	6.33	7.97	4.17	16.70	9.82
6	3.39	3.06	3.34	5.19	3.45	7.53	21.71	13.04
7	3.20	2.83	4.81	4.55	5.03	5.06	8.13	7.90
8	3.23	3.24	3.85	7.15	2.19	8.90	13.97	6.87
9	2.96	3.15	4.57	4.27	9.79	5.38	16.94	7.93
10	4.31	2.68	4.28	4.67	3.22	6.56	10.96	6.82

Downcomer/riser 0.5 -
 Top clearance (m) 0.1 -
 Bottom clearance (m) 0.03 -
 Aeration intensity (L/m².min) 800 -
 Depth (m) 1.4 +
 Diffuser position Riser +

Average times (s):

3.316	3.112	4.234	5.194	5.119	6.037	12.707	9.870
-------	-------	-------	-------	-------	-------	--------	-------

Distance (m): 0.9

Average rise velocities (m/s):

0.271	0.289	0.213	0.173	0.176	0.149	0.071	0.091
-------	-------	-------	-------	-------	-------	-------	-------

1	0.271	0.289
2	0.213	0.173
3	0.176	0.149
4	0.071	0.091

Area under graph:

0.5658	0.5049
Average:	0.5354
S ² :	0.001854

Residual area:

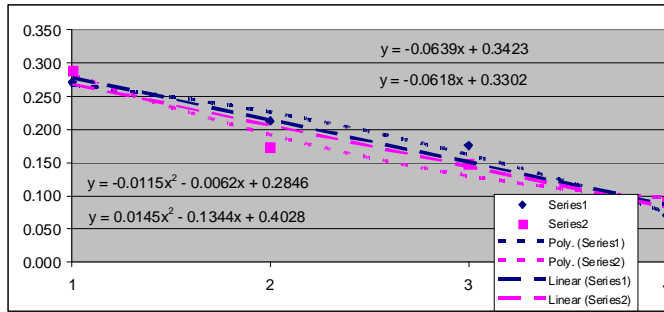
0.2349	0.3438
Average:	0.2894
S ² :	0.005930

Differential area:

0.3309	0.1611
Average:	0.2460
S ² :	0.0144

Average gradient:

-0.0639	-0.0618
Average:	-0.0629
S ² :	0.0000



Treatment 28

	1		2		3		4	
1	3.17	3.27	3.26	6.78	7.26	3.79	8.89	6.43
2	2.67	1.82	9.37	4.55	5.12	7.26	8.41	16.70
3	1.83	4.08	16.37	3.65	2.53	10.76	6.57	11.09
4	7.11	2.47	4.76	8.92	21.13	6.97	9.14	5.41
5	3.92	2.23	3.79	4.17	7.89	4.19	16.27	7.79
6	3.61	2.78	5.29	3.57	7.48	12.33	4.92	6.46
7	5.23	5.21	5.03	6.73	3.19	15.64	4.28	6.74
8	4.37	3.47	6.70	3.42	2.99	5.63	7.95	9.01
9	5.72	1.78	9.71	3.98	13.46	9.81	7.08	12.28
10	2.10	2.42	6.28	4.84	4.49	3.48	7.91	9.94

Downcomer/riser 0.5 -
 Top clearance (m) 0.2 +
 Bottom clearance (m) 0.03 -
 Aeration intensity (L/m².min) 800 -
 Depth (m) 1.4 +
 Diffuser position Riser +

Average times (s):

3.973	2.953	7.056	5.061	7.554	7.986	8.142	9.185
-------	-------	-------	-------	-------	-------	-------	-------

Distance (m): 0.8

Average rise velocities (m/s):

0.201	0.271	0.113	0.158	0.106	0.100	0.098	0.087
-------	-------	-------	-------	-------	-------	-------	-------

1	0.201	0.271
2	0.113	0.158
3	0.106	0.100
4	0.098	0.087

Area under graph:

0.3593	0.4242
Average:	0.3918
S ² :	0.002106

Residual area:

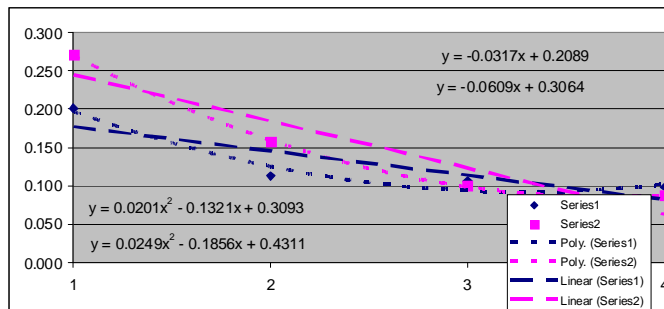
0.2327	0.3870
Average:	0.3099
S ² :	0.011904

Differential area:

0.1266	0.0372
Average:	0.0819
S ² :	0.0040

Average gradient:

-0.0317	-0.0609
Average:	-0.0463
S ² :	0.0004



Treatment 29

	1		2		3		4	
1	2.29	3.60	4.70	5.83	5.86	12.64	18.74	6.96
2	2.89	3.03	4.13	9.89	8.22	9.92	8.10	6.26
3	2.96	2.67	4.02	5.97	16.07	9.64	12.22	5.82
4	3.33	3.14	8.89	9.51	6.29	3.79	7.77	8.35
5	3.85	2.29	3.58	3.01	4.10	5.00	4.94	7.85
6	4.63	6.29	4.03	5.20	9.43	7.57	5.34	8.82
7	3.45	2.87	5.87	7.47	10.61	2.70	10.81	9.43
8	2.19	4.27	4.91	6.55	5.35	4.32	8.79	14.99
9	4.30	2.43	4.19	6.20	14.52	4.86	15.32	3.83
10	3.48	2.20	3.16	4.12	11.47	2.29	4.81	2.74

Downcomer/riser 0.5 -
 Top clearance (m) 0.1 -
 Bottom clearance (m) 0.03 -
 Aeration intensity (L/m².min) 1350 +
 Depth (m) 1.4 +
 Diffuser position Riser +

Average times (s):

3.337	3.279	4.748	6.375	9.192	6.273	9.684	7.505
-------	-------	-------	-------	-------	-------	-------	-------

Distance (m): 0.9

Average rise velocities (m/s):

0.270	0.274	0.190	0.141	0.098	0.143	0.093	0.120
-------	-------	-------	-------	-------	-------	-------	-------

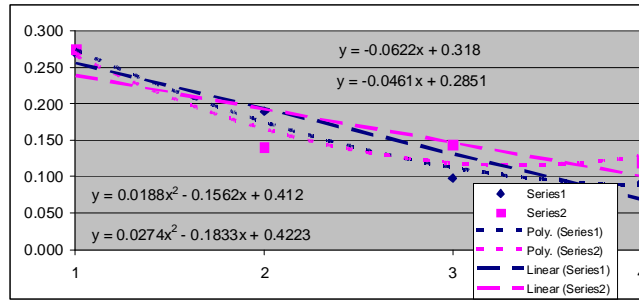
1	0.270	0.274
2	0.190	0.141
3	0.098	0.143
4	0.093	0.120

Area under graph:	0.4593	0.4676
Average:	0.4635	
S²:	0.000034	

Residual area:	0.3645	0.3317
Average:	0.3481	
S²:	0.000538	

Differential area:	0.0948	0.1359
Average:	0.1154	
S²:	0.0008	

Average gradient:	-0.0622	-0.0461
Average:	-0.0542	
S²:	0.0001	



Treatment 30

	1		2		3		4	
1	3.01	3.24	1.68	3.88	1.43	6.21	2.47	6.79
2	1.94	2.80	3.35	4.07	2.23	2.66	2.17	3.78
3	2.23	1.59	3.09	3.21	8.65	3.26	3.88	6.01
4	2.71	2.36	2.49	4.74	2.81	4.23	4.71	4.33
5	2.89	2.07	3.67	4.69	4.07	3.93	1.68	2.94
6	1.22	2.20	2.17	5.82	3.27	4.53	3.21	5.28
7	2.23	2.83	3.93	4.12	1.41	7.98	2.33	5.64
8	2.48	3.14	5.74	4.30	8.84	2.85	5.83	8.39
9	1.73	2.95	5.15	3.98	4.61	7.17	3.32	4.12
10	2.71	2.66	4.22	3.54	1.86	4.62	6.19	3.89

Downcomer/riser 2 +
 Top clearance (m) 0.1 -
 Bottom clearance (m) 0.03 -
 Aeration intensity (L/m².min) 800 -
 Depth (m) 1.1 -
 Diffuser position Bottom -

Average times (s):

2.315	2.584	3.549	4.235	3.918	4.744	3.579	5.117
-------	-------	-------	-------	-------	-------	-------	-------

Distance (m): 0.6

Average rise velocities (m/s):

0.259	0.232	0.169	0.142	0.153	0.126	0.168	0.117
-------	-------	-------	-------	-------	-------	-------	-------

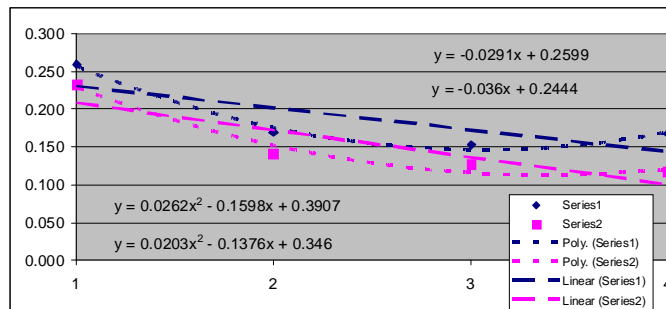
1	0.259	0.232
2	0.169	0.142
3	0.153	0.126
4	0.168	0.117

Area under graph:	0.5238	0.4323
Average:	0.4781	
S²:	0.004186	

Residual area:	0.2475	0.2538
Average:	0.2507	
S²:	0.000020	

Differential area:	0.2763	0.1785
Average:	0.2274	
S²:	0.0048	

Average gradient:	-0.0291	-0.0360
Average:	-0.0326	
S²:	0.0000	



Treatment 31

	1		2		3		4	
1	1.30	1.48	1.76	2.81	4.09	3.97	2.73	6.81
2	2.98	2.62	1.24	1.61	2.35	1.32	5.16	3.88
3	1.87	1.13	1.97	2.00	6.63	3.97	4.42	2.75
4	2.17	1.69	1.64	2.03	3.74	4.12	2.94	1.92
5	1.34	2.12	2.71	1.50	4.55	1.53	2.72	3.86
6	1.82	1.73	2.66	1.58	4.21	4.83	2.46	2.86
7	1.65	4.17	1.82	1.35	4.22	2.98	3.42	1.83
8	2.05	1.25	2.16	0.84	4.65	8.37	5.63	1.72
9	1.00	1.39	2.73	1.79	6.12	3.54	10.29	2.99
10	2.09	2.42	1.19	1.49	1.77	2.90	2.09	3.72

Downcomer/riser 0.5 -
 Top clearance (m) 0.2 +
 Bottom clearance (m) 0.03 -
 Aeration intensity (L/m².min) 1350 +
 Depth (m) 1.1 -
 Diffuser position Riser +

Average times (s):

1.827	2.000	1.988	1.700	4.233	3.753	4.186	3.234
-------	-------	-------	-------	-------	-------	-------	-------

Distance (m): 0.5

Average rise velocities (m/s):

0.274	0.250	0.252	0.294	0.118	0.133	0.119	0.155
-------	-------	-------	-------	-------	-------	-------	-------

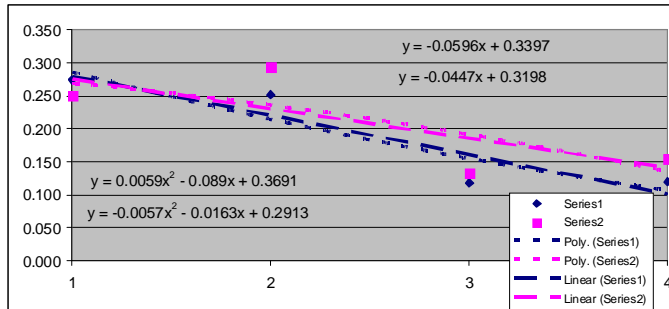
1	0.274	0.250
2	0.252	0.294
3	0.118	0.133
4	0.119	0.155

Area under graph:	0.5637	0.6320
Average:	0.5979	
S²:	0.002332	

Residual area:	0.2943	0.1760
Average:	0.2352	
S²:	0.006997	

Differential area:	0.2694	0.4560
Average:	0.3627	
S²:	0.0174	

Average gradient:	-0.0596	-0.0447
Average:	-0.0522	
S²:	0.0001	



Treatment 32

	1		2		3		4	
1	2.29	4.98	14.29	4.18	3.62	6.59	2.00	2.27
2	5.37	4.76	3.01	4.93	4.12	7.29	3.53	4.63
3	4.09	7.36	5.96	3.71	7.15	3.67	6.15	3.38
4	4.73	7.64	6.38	4.97	7.94	3.48	2.23	3.25
5	3.40	6.71	9.31	4.73	12.12	2.95	2.78	5.72
6	4.97	9.61	4.45	4.35	5.97	3.54	1.61	3.07
7	5.04	4.55	3.97	3.68	2.89	7.70	4.23	4.37
8	13.10	8.00	10.56	5.81	6.78	13.53	5.84	6.17
9	11.70	8.96	6.01	3.36	3.98	3.32	1.82	3.49
10	5.99	7.13	4.66	3.04	7.82	3.83	3.25	3.05

Downcomer/riser 0.5 -
 Top clearance (m) 0.1 -
 Bottom clearance (m) 0.03 -
 Aeration intensity (L/m².min) 800 -
 Depth (m) 1.1 -
 Diffuser position Bottom -

Average times (s):

6.068	6.970	6.860	4.276	6.239	5.590	3.344	3.940
-------	-------	-------	-------	-------	-------	-------	-------

Distance (m): 0.9

Average rise velocities (m/s):

0.148	0.129	0.131	0.210	0.144	0.161	0.269	0.228
-------	-------	-------	-------	-------	-------	-------	-------

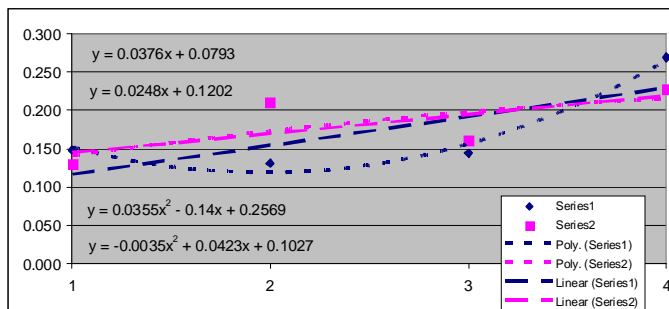
1	0.148	0.129
2	0.131	0.210
3	0.144	0.161
4	0.269	0.228

Area under graph:	0.4662	0.5519
Average:	0.5091	
S²:	0.003672	

Residual area:	0.3285	0.0959
Average:	0.2122	
S²:	0.027051	

Differential area:	0.1377	0.4560
Average:	0.2969	
S²:	0.0507	

Average gradient:	0.0376	0.0248
Average:	0.0312	
S²:	0.0001	



Addendum *F*

Model validation experimental data

Configuration 1

A	B	C	D	E	F
1	1	-1	-1	-1	1

Treatment 7			Treatment 10		
Time (min)	Flux (L/m ² .h)	TMP (mm H ₂ O)	Time (min)	Flux (L/m ² .h)	TMP (mm H ₂ O)
0	4	151	0	4	140
5	4	173	5	4	145
10	4	173	10	4	150
15	4	175	15	4	153
20	4	177	20	4	153
25	4	176	25	4	153
30	4	176	30	4	153
35	8	185	35	8	158
40	8	189	40	8	160
45	8	190	45	8	160
50	8	196	50	8	162
55	8	196	55	8	163
60	8	196	60	8	162
65	8	196	65	8	162
70	12	222	70	12	226
75	12	233	75	12	235
80	12	238	80	12	248
85	12	238	85	12	248
90	12	239	90	12	250
95	12	239	95	12	249
100	12	240	100	12	250
105	16	265	105	16	297
110	16	279	110	16	302
115	16	299	115	16	310
120	16	301	120	16	317
125	16	301	125	16	318
130	16	302	130	16	320
135	16	301	135	16	320
140	20	341	140	20	333
145	20	350	145	20	342
150	20	360	150	20	361
155	20	366	155	20	375
160	20	370	160	20	382
165	20	375	165	20	387
170	20	379	170	20	392
175	24	437	175	24	438
180	24	446	180	24	465
185	24	460	185	24	479
190	24	466	190	24	490
195	24	474	195	24	499
200	24	481	200	24	508
205	24	488	205	24	516
210	28	501	210	28	584
215	28	520	215	28	608
220	28	546	220	28	633
225	28	571	225	28	660
230	28	586	230	28	677
235	28	598	235	28	689
240	28	609	240	28	702
245	32	706	245	32	820
250	32	753	250	32	860
255	32	818	255	32	897
260	32	875	260	32	931
265	32	901	265	32	953
270	32	927	270	32	972
275	32	952	275	32	991

Configuration 2

A	B	C	D	E	F
1	-1	1	-1	1	-1

Treatment 3			Treatment 5		
Time (min)	Flux (L/m ² .h)	TMP (mm H ₂ O)	Time (min)	Flux (L/m ² .h)	TMP (mm H ₂ O)
0	4	175	0	4	151
5	4	175	5	4	151
10	4		10	4	152
15	4	178	15	4	152
20	4		20	4	152
25	4	181	25	4	152
30	4	182	30	4	152
35	8	196	35	8	156
40	8	204	40	8	158
45	8	206	45	8	158
50	8		50	8	
55	8	209	55	8	160
60	8	212	60	8	161
65	8	215	65	8	168
70	12	234	70	12	174
75	12	254	75	12	190
80	12	268	80	12	212
85	12		85	12	228
90	12	281	90	12	238
95	12	287	95	12	246
100	12	289	100	12	253
105	16	316	105	16	270
110	16	355	110	16	299
115	16	367	115	16	313
120	16	377	120	16	321
125	16	383	125	16	328
130	16	388	130	16	333
135	16	392	135	16	337
140	20	446	140	20	363
145	20	480	145	20	401
150	20	504	150	20	422
155	20	516	155	20	439
160	20	527	160	20	452
165	20	535	165	20	466
170	20	543	170	20	472
175	24	600	175	24	518
180	24	672	180	24	587
185	24	692	185	24	611
190	24	719	190	24	627
195	24	734	195	24	643
200	24	751	200	24	654
205	24	764	205	24	666
210	28	816	210	28	738
215	28	897	215	28	806
220	28	934	220	28	839
225	28	970	225	28	865
230	28	1001	230	28	891
235	28	1027	235	28	908
240	28	1052	240	28	929
245	32	1130	245	32	1008
250	32	1250	250	32	1118
255	32	1348	255	32	1185
260	32	1415	260	32	1234
265	32	1478	265	32	1293
			270	32	1335
			275	32	1373

Configuration 3

A	B	C	D	E	F
1	-1	-1	-1	-1	1

Treatment 4			Treatment 6		
Time (min)	Flux (L/m ² .h)	TMP (mm H ₂ O)	Time (min)	Flux (L/m ² .h)	TMP (mm H ₂ O)
0	4	165	0	4	148
5	4	249	5	4	148
10	4	249	10	4	148
15	4	251	15	4	149
20	4	250	20	4	149
25	4	250	25	4	149
30	4	251	30	4	149
35	8	256	35	8	153
40	8	264	40	8	153
45	8	272	45	8	153
50	8	281	50	8	160
55	8	286	55	8	171
60	8	290	60	8	176
65	8	294	65	8	181
70	12	313	70	12	190
75	12	362	75	12	210
80	12	384	80	12	220
85	12	401	85	12	228
90	12	415	90	12	234
95	12	425	95	12	244
100	12	434	100	12	251
105	16	465	105	16	275
110	16	519	110	16	315
115	16	539	115	16	329
120	16	556	120	16	339
125	16	565	125	16	349
130	16	571	130	16	354
135	16	577	135	16	359
140	20	610	140	20	395
145	20	693	145	20	437
150	20	723	150	20	466
155	20	744	155	20	485
160	20	763	160	20	496
165	20	779	165	20	509
170	20	793	170	20	519
175	24	850	175	24	555
180	24	910	180	24	603
185	24	944	185	24	627
190	24	968	190	24	641
195	24	993	195	24	655
200	24	1010	200	24	661
205	24	1031	205	24	673
210	28	1135	210	28	725
215	28	1195	215	28	798
220	28	1249	220	28	815
225	28	1272	225	28	838
230	28	1315	230	28	850
235	28		235	28	870
240	28	1359	240	28	880
			245	32	960
			250	32	1099
			255	32	1127
			260	32	1157
			265	32	1193
			270	32	1225
			275	32	1255

Configuration 4

A	B	C	D	E	F
-1	-1	1	1	-1	1

Treatment 8			Treatment 9		
Time (min)	Flux (L/m ² .h)	TMP (mm H ₂ O)	Time (min)	Flux (L/m ² .h)	TMP (mm H ₂ O)
0	4	147	0	4	167
5	4	147	5	4	168
10	4	148	10	4	168
15	4	147	15	4	169
20	4	146	20	4	169
25	4	147	25	4	169
30	4	146	30	4	169
35	8	150	35	8	175
40	8	151	40	8	177
45	8	153	45	8	178
50	8	153	50	8	184
55	8	157	55	8	190
60	8	172	60	8	193
65	8	185	65	8	195
70	12	196	70	12	201
75	12	233	75	12	214
80	12	259	80	12	222
85	12	278	85	12	228
90	12	293	90	12	231
95	12	302	95	12	232
100	12	311	100	12	233
105	16	332	105	16	246
110	16	375	110	16	259
115	16		115	16	269
120	16		120	16	275
125	16		125	16	281
130	16	432	130	16	286
135	16	436	135	16	290
140	20	478	140	20	325
145	20	514	145	20	354
150	20	526	150	20	366
155	20	535	155	20	376
160	20	545	160	20	383
165	20	551	165	20	390
170	20	560	170	20	397
175	24	591	175	24	425
180	24	650	180	24	464
185	24	671	185	24	483
190	24	688	190	24	497
195	24	702	195	24	508
200	24	711	200	24	516
205	24	722	205	24	524
210	28	775	210	28	578
215	28	824	215	28	633
220	28	849	220	28	658
225	28	876	225	28	674
230	28	893	230	28	690
235	28	910	235	28	706
240	28	927	240	28	720
245	32	1020	245	32	795
250	32	1088	250	32	848
255	32	1142	255	32	880
260	32	1170	260	32	904
265	32	1213	265	32	931
270	32	1228	270	32	954
275	32	1261	275	32	977